

1127-21  
146

# JOURNAL OF COLLOID SCIENCE

## EDITOR-IN-CHIEF

VICTOR K. LA MER  
*Columbia University, New York*

## ADVISORY BOARD

A. E. ALEXANDER	J. J. HERMANS	ROBERT SIMHA
STEPHEN BRUNAUER	L. G. LONGSWORTH	R. H. SMELLIE
J. A. CHRISTIANSEN	S. G. MASON	HARRY SOBOTKA
P. J. W. DEBYE	KAROL J. MYSELS	JACINTO STEINHARDT
B. DERJAGUIN	J. TH. G. OVERBEEK	TORSTEN TEORELL
D. G. DERVICHIAN	J. H. SCHULMAN	A. C. ZETTMLOYER
JOHN T. EDSALL	LEO SHEDLOVSKY	BRUNO H. ZIMM
I. FANKUCHEN	THEODORE SHEDLOVSKY	W. A. ZISMAN
JOHN D. FERRY		

Volume 15  
1960



ACADEMIC PRESS  
*New York and London*



## A THEORY AND METHOD FOR THE SPREADING OF PROTEIN MONOLAYERS\*<sup>1</sup>

H. J. Trurnit

*Research Institute for Advanced Study, Baltimore 12, Maryland*

*Received June 2, 1959*

### ABSTRACT

Protein monolayers, or true H-films, can be spread quickly and without loss on distilled water or dilute buffer solutions, if the protein solution before reaching the water surface of the film trough is spread out into a very thin layer around a glass rod. During the flow time along the glass rod the vast majority of all protein molecules diffuse to the water/air interface and spread, if flow rate, protein concentration, glass rod length, and diameter are chosen correctly. The influence of these parameters is investigated theoretically, and the theoretical predictions are compared with results from spreading experiments.

### INTRODUCTION

Monomolecular films of surface denatured proteins have been the subject of physiocochemical, biochemical and immunochemical studies for over 30 years. These monolayers, at low film pressure, ideally consist of completely unfolded, and therefore insoluble, protein molecules (polypeptide chains) at the water/air interface. The main chemical bonds between the amino acids are probably still intact in this state, but the secondary and tertiary bonds (hydrogen bonds, ionic bonds, dipole bonds) which are responsible for the shape of the native protein molecules, are presumably partially or completely broken and rearranged between adjacent polypeptide chains and between the polypeptide chains and the aqueous subphase. Quantitative data, obtained from these monolayer studies, depend in most cases on—among other things—an accurate value for the amount of protein per unit film area or surface concentration. Spreading without loss is therefore of prime importance, because the preparation of a monolayer of protein on a water surface is usually the first step in these experiments.

\* This paper is dedicated to Dr. Hans Netter, Professor of Physiological Chemistry, University of Kiel, Germany, on the occasion of his 60th birthday.

<sup>1</sup> A short outline of this paper has been incorporated into a handbook article on protein films (1). It was meant to be presented at the 1959 annual meeting of the Biophysical Society at Pittsburgh. The author, however, was not able to attend the meeting.



A distinction has been made between films which are spread by bringing the protein from the outside (air) to the interface, the water initially containing no protein in solution, and those which form spontaneously on the surface of every protein solution by diffusion of protein molecules towards the water/air interface. For the former Langmuir coined the name "H-films". The second type was called "D-films" by this author. These classifications refer actually to the location of the protein source with respect to the interface, rather than to the difference in film structure. But frequently it is erroneously assumed that an H-film has necessarily the properties of what we define below as a "true H-film".

Under normal conditions D-films, after reaching equilibrium, are more complex than H-films. They consist, probably, of an insoluble layer of completely unfolded surface denatured molecules mixed with partially unfolded ones. Attached to this layer by adsorption underneath is at least one layer of nondenatured molecules. The monolayer on top is formed by those molecules which reach the newly formed water/air interface first. We will not deal here with D-films of this type. See the extensive review of Neurath and Bull (2). However, one can easily see that a D-film will have identical properties with those of a true H-film (see below) if the protein concentration in a container of given geometry is small enough to permit every protein molecule in the solution to find space at the water/air interface in a fully unfolded state.<sup>2</sup> We will call an H-film of this origin a DH-film. In practice one cannot work, in the usual way, with these extremely small concentrations accurately because of unavoidable losses, by adsorption, on the container walls (up to  $5 \times 10^{-7}$  g./cm.<sup>2</sup>) and the time for diffusion of, say 99%, of the material towards the surface, even in very shallow containers, is very long.<sup>3</sup>

However, when the protein is brought to the water surface from the outside, a true H-film would be formed if this application of the protein could be accomplished without loss of protein molecules into the interior of the water. A "true H-film" may be defined as a protein monolayer on a water surface in which all molecules are unfolded to the same degree and to such an extent that they have become insoluble. The definition has to include the postulate that the substrate solution should not contain any protein—either dissolved or adsorbed underneath the monolayer. If during the deposition molecules in their soluble state escape into the water, they will eventually reach the surface again by diffusion and be adsorbed underneath the H-film. By definition, this combination is a D-film.

The efforts of most investigators have been directed towards making

<sup>2</sup> Taking the thickness of a fully unfolded H-film as 4.5 Å, the density of the film as 1.3, and a protein solution of 1 cm. depth in a container with perpendicular walls, this limiting concentration is  $5.8 \times 10^{-8}$  g./ml.

<sup>3</sup> For a solution of 1 cm. depth at 20°C., this time is about 500 hours, for a solution of 1 mm. depth it is 5 hours, if we take a molecular species with a diffusion coefficient  $D_{20} = 10 \times 10^{-7}$  cm.<sup>2</sup> sec.<sup>-1</sup>.



true H-films, by bringing the protein to the surface from the outside. It has been found to be very difficult, if not impossible, to make true H-films, that is, to spread directly without loss. The most satisfactory method from a theoretical point of view seems to be the one where a very small crystal of dry protein is brought in contact with the water surface. The spreading of film from the air/water/crystal boundary line takes place very rapidly and much faster than the dissolving of protein molecules into the aqueous phase at the crystal/water interface (3). The practical drawback of this technique is the difficulty in handling and weighing these small amounts, which are in the range of  $10$  to  $100 \times 10^{-6}$  g. It is also possible that small crystal lumps break off at the boundary line and float away on top of the film without ever spreading.

The technique most frequently used is the spreading of film from aqueous solutions of the protein by depositing drops of this solution "carefully" on the water surface. Considerable loss of protein into the trough solution is unavoidable with this type of spreading. Every investigator has searched for ways and means to minimize the loss. From Gorter's (4) work it is known that spreading on a substrate the pH of which is near the isoelectric point (IP) of the protein yields maximum areas rather quickly. Several authors (5, 6), realizing that these escaped molecules will eventually reach the surface of the trough solution by diffusion, recommend waiting periods up to 36 hours after spreading before the film is compressed on the trough. However, it is very difficult, if not impossible, to prevent spontaneous surface contamination over even 1 to 2 hours.

The loss during spreading and the possibility of surface contamination during a waiting period become critically important when the isotherms of protein films in the very low pressure region are used for the determination of molecular weights of proteins (7-9). The safest way is presumably to fill the tray not with water but with ammonium sulfate solution (5%-35%).<sup>4</sup>

To test for losses during spreading one can compare the film thickness, calculated from the specific area ( $\text{m}^2/\text{mg.}$ ) at a given pressure, with the interferometric thickness (ellipsometer) of the same film after deposition, under the same pressure, on a Langmuir-Blodgett slide. Or one can weigh the total film, after skimming it off the water surface, without loss, and drying it. A third procedure would be the use of radioactive protein and the measurement of the specific activity per unit area after transferring the film from the water surface onto a solid surface.<sup>5</sup> All these tests have their

<sup>4</sup> 0.1-0.01 N HCl solutions have also been used.

<sup>5</sup> It has been suggested to test for losses by comparing the specific areas from films spread with two different amounts of material. It was thought that identical specific areas indicated complete spreading. This is not a proper test: if the relative loss, during the deposition of the solution in droplet form, is the same in both cases, the specific area will also be the same—and too small. Since the relative loss depends on the mechanics of the deposition of the drops and on trough depth (which are both kept constant), chances are that the relative loss is identical in both cases.

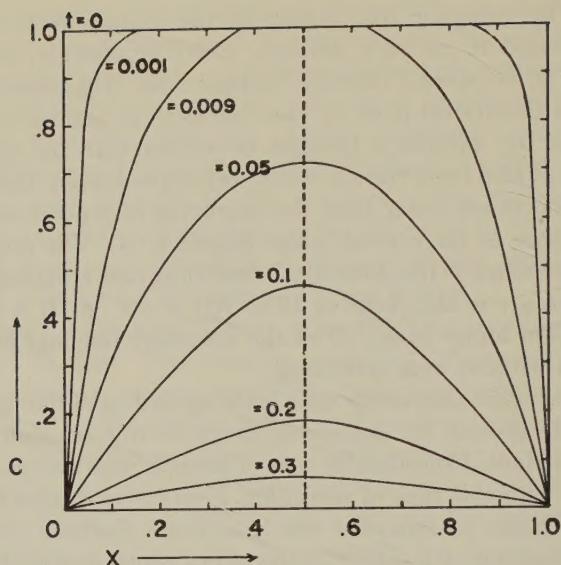


FIG. 1. Concentration curves for diffusion out of a slab with two "open" faces. They are calculated from Eq. [1] for  $D = 1.0$ ,  $d = 1.0$ , and  $c_0 = 1.0$ . The values for  $t$ , in seconds, indicate the time interval elapsed since the beginning of the diffusion process. The figure is taken from "Diffusion in Solids, Liquids and Gases," by W. Jost, Academic Press, New York, 1952. The original figure in Jost's book (page 36) has a printing error:  $t = 0.09$  should be corrected to  $t = 0.009$ .

intrinsic difficulties. At least one of them should be applied. But they do not suggest, as such, a rational method for spreading without loss. The spreading of proteins, so far, has been an empirical procedure.

This paper proposes a rational treatment of the problem based on simple diffusion theory. The approach is based on the belief that losses are unavoidable, especially if one wants to study protein film properties not only on some very specific substrates (such as concentrated ammonium sulfate solutions) but on any type of aqueous solution including distilled water. It will be shown that DH-films rather than H-films are the obvious solution. Experimental conditions will be evolved theoretically, for which a very high and known percentage of all the molecules reaches the water surface in a reasonably short time to form a DH-film.

### THEORY

For diffusion out of a slab (see Fig. 1) diffusion theory (10) gives the following equation for a system which has constant initial concentration and for which the concentration at both faces is kept zero at all times:



$$c_{t,x} = \frac{4c_0}{\pi} \sum_{n=0}^{\infty} \frac{1}{2n+1} \times \sin \frac{(2n+1)\pi x}{d'} \times \exp \left[ -\left( \frac{(2n+1)\pi}{d'} \right)^2 Dt \right], \quad [1]$$

where  $c_{t,x}$  = concentration after time  $t$  at distance  $x$  from one slab face;

$c_0$  = initial concentration;

$d'$  = is the thickness of the slab;

$D$  = coefficient of diffusion; and

$n = 0, 1, 2, \dots$

Then the average concentration  $\bar{c}$  in the slab after time  $t$  is

$$\bar{c} = \frac{8c_0}{\pi^2} \sum_{n=0}^{\infty} \frac{1}{(2n+1)^2} \times \exp \left[ -\left( \frac{(2n+1)\pi}{d'} \right)^2 Dt \right]. \quad [2]$$

These equations will still hold if we insert an infinitely thin impermeable barrier (dotted line in Fig. 1) parallel to the faces at  $x = d'/2$ , provided this barrier is an ideal reflector, that is, does not adsorb solute or interact chemically with it. Then the equation for unilateral diffusion out of either side of the slab with one face "open" and one face "closed"<sup>6</sup> becomes

$$\bar{c} = \frac{8c_0}{\pi^2} \sum_{n=0}^{\infty} \frac{1}{(2n+1)^2} \times \exp \left[ -\left( \frac{(2n+1)\pi}{2d} \right)^2 Dt \right], \quad [3]$$

where  $d$  is now the thickness of each half of the slab or  $d'/2$ . If  $c_0$  and  $D$  are known,  $\bar{c}$  is a function of  $d$  and  $t$ . Equation [3] shows that the time  $t$  required to reduce  $\bar{c}$  to a given fraction of  $c_0$  is proportional to  $d^2$ .

Consider now the case that a solution moves "en block" downward through the slab, in other words that the velocity  $v$  of each small volume is independent of  $x$ . Equation [3] will still hold. In a real situation, where the barrier at  $x = d$  is a solid surface, a downward motion of a thin layer of liquid will be of the laminar flow type, that is:  $v = f(x)$  with  $v = 0$  for  $x = d$ . Since the direction of diffusion ( $x$ ) is perpendicular to the direction of flow, Eq. [3] will still apply.

## METHOD

The preceding treatment of unilateral diffusion out of a slab suggests the following experimental arrangement for the spreading of DH-films:

Consider a cylindrical glass rod of diameter  $a$  and length  $l$  (see Fig. 2). It stands in a vertical position in a shallow film trough. Its upper end is hemispherical. The protein solution is delivered to the top of the rod from a pipette at constant flow rate  $f$  (ml./min.). The solution on leaving the pipette tip will spread out to form a thin layer of thickness  $d$  which runs

<sup>6</sup> In order to keep the  $x$  direction positive, we consider the left half of Fig. 1.



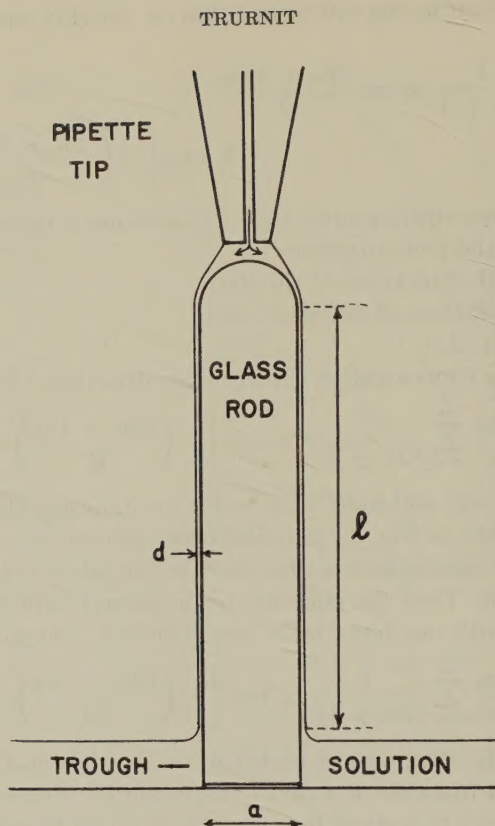


FIG. 2. Experimental arrangement for the spreading of protein films. For explanation see text. The proportions of rod length  $l$ , rod diameter  $a$ , water layer thickness  $d$ , and trough depth used in this figure are not those used in an actual experiment. They were chosen for a clear demonstration of the principle involved.

down the glass rod. This layer, along the rod, has a glass/water interface and an air/water interface. Any small section of this layer (for  $d \ll a$ ) is represented by the left half of Fig. 1. Protein molecules which are accidentally in the molecular vicinity of the water/air interface when the solution leaves the pipette tip will unfold at the interface to form a new phase outside the solution, a film. They will "spread." This "leaving the aqueous phase" will reduce the protein concentration very near the interface to zero. This in turn sets up a diffusion gradient which will cause further protein molecules to diffuse towards the interface.<sup>7</sup>

The thickness  $d$  of the water film is a function of the flow rate  $f$ , the radius of the glass rod, and the viscosity  $\eta$  of the liquid. The average vertical velocity  $\bar{v}$  (cm./sec.) of the water layer along the glass rod is also a function

<sup>7</sup> This is the same mechanism which is operative in forming a D-film on any protein solutions which have a water/air interface.

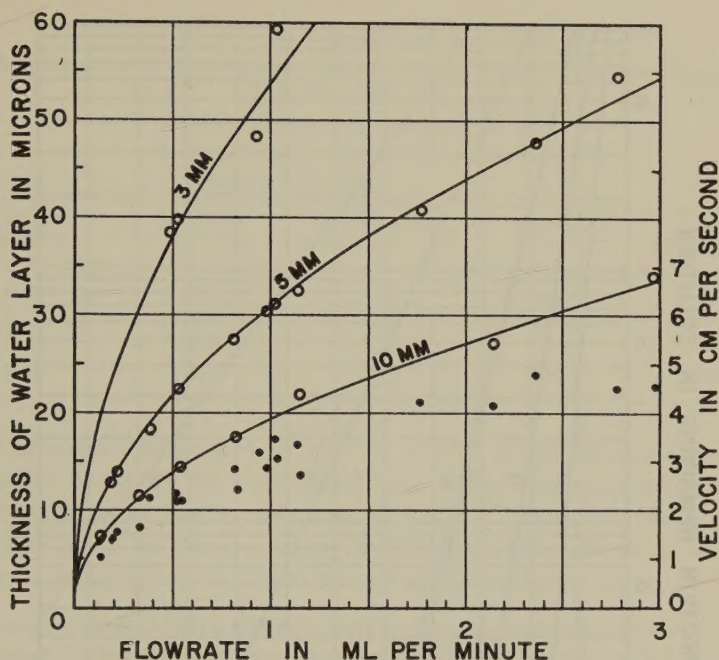


FIG. 3. Thickness of water layer  $d$  and average velocity  $\bar{v}$  as a function of flow rate  $f$ . The mm. values in the diagram indicate the diameter  $a$  of the glass rod used. The circles are experimental points for  $d$  (left ordinate). The drawn-out curves are "best fitting" parabola segments calculated from one experimental point from each glass rod series. It is not implied that there is a theoretical justification for this parabolic function. The theory of flow in "open" systems has not been worked out yet. The curves may be regarded merely as guide lines for extrapolation. The dots indicate the average vertical velocity  $\bar{v}$  of the water layer (right-hand ordinate). At any given flow rate  $\bar{v}$  is slightly lower for larger  $a$  values than for smaller ones.

of  $f$ ,  $a$ , and  $\eta$ . These functions can be determined experimentally. The velocity  $\bar{v}$  together with the length  $l$  of the glass rod determines the flow time, that is, the time  $t$  (in Eq. [3]) during which each volume element within the water layer is exposed to the conditions for which Eq. [3] holds. *The water layer around the glass rod is the site of diffusion and spreading of the protein film.*

Figure 3 shows the results of such experiments. If the initial concentration  $c_0$  in the pipette and the coefficient of diffusion  $D$  of the protein are known, a flow rate  $f$ , a glass rod radius  $a$ , and length  $l$  can be specified for which the average concentration  $\bar{c}$  of the protein solution on arrival at the lower end of the glass rod (after time  $t$ ) has become so small (e.g., 0.1% or any desired value) that the amount of protein remaining in solution, and thereby lost into the trough solution, becomes negligible.

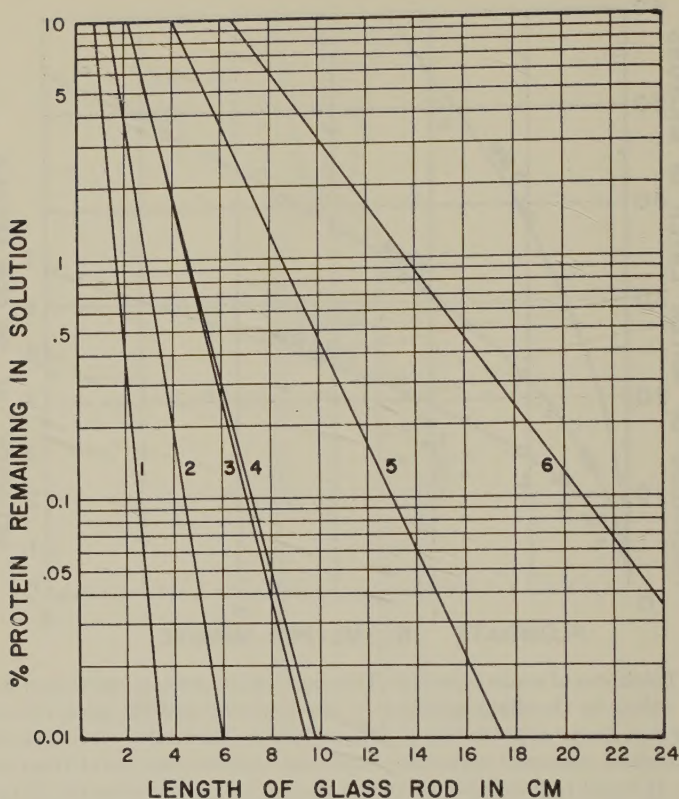


FIG. 4. Loss of protein, given in per cent of initial concentration, as a function of glass rod length, for rods of 5 mm. diameter. The six lines are obtained by solving Eq. [3] for three different values of the coefficient of diffusion  $D$  and for two different values of layer thickness  $d$ . Each value of  $d$  in Fig. 3 corresponds to a value for flow rate  $f$  and an average velocity  $\bar{v}$ ,  $\bar{v}$  and  $l$  determining the value of  $t$  needed to solve Eq. [3]. Lines 1, 2, and 3 are calculated for  $f = 0.1$  ml./min.,  $d = 10\mu$ ,  $\bar{v} = 1$  cm./sec. with  $D_{20} = 10.95 \times 10^{-7}$  cm.<sup>2</sup>/sec. (trypsin),  $6.10 \times 10^{-7}$  cm.<sup>2</sup>/sec. (human serum albumin), and  $3.84 \times 10^{-7}$  cm.<sup>2</sup>/sec. (human serum gamma globulin), respectively. Lines 4, 5, and 6 are for the same  $D_{20}$  values, in the same sequence, but for:  $f = 0.2$  ml./min.,  $d = 14\mu$ , and  $\bar{v} = 1.5$  cm./sec.

Figure 4 gives data for the fraction of unspread protein as a function of glass rod length.

As pointed out previously a DH-film will form in the course of a diffusion process only if the total number of molecules in the solution is sufficiently small so that each molecule in a layer of given depth finds space at the water/air interface in a completely unfolded state: The maximal permissible protein concentration is a function of the water layer thickness  $d$ . For layers of solution 10 microns and 14 microns deep (Fig. 4) the upper



TABLE I

*The Determination of Water Layer Thickness  $d$  and Average Vertical Velocity  $\bar{v}$  from Resistance Measurements*

HCl solution:  $\rho = 326 \text{ ohms} \times \text{cm.}$

Glass rod:  $l = 12.0 \text{ cm.}$ ,  $a = 5.0 \text{ mm.}$

Temperature:  $20^\circ\text{C.}$

Flow rate (ml./min.)	Resistance $R \cdot 10^{-2}$ (ohms)	Water layer cross section $q$ ( $\text{cm.}^2 \cdot 10^3$ )	Thickness $d$ $\mu$	Average vertical velocity $\bar{v}$ (cm./sec.)
0.19	1935	2.02	12.9	1.56
0.21	1750	2.24	14.2	1.57
0.39	1335	2.93	18.6	2.22
1.02	800	4.89	31.2	3.47

limits of concentration are 58 and  $41 \times 10^{-6} \text{ g./ml.}$ , respectively. These figures are based on the assumption that a fully expanded protein film at very low pressure has a thickness of 4.5 AU.<sup>8</sup> However, since the film molecules in this case are still close to each other, it is safer to use somewhat smaller concentrations in actual spreading experiments.

The experiments for determining  $d$  and  $\bar{v}$  as a function of  $f$  (Fig. 3) were carried out as follows: A glass rod of known length and diameter was thoroughly cleaned and mounted in a vertical position in a wider glass tubing, wet on the inside, to prevent evaporation from the glass rod. A Mariotte bottle filled with dilute KCl or HCl solution was mounted above the glass rod in such a way that the solution from the Mariotte bottle passed down a rubber tubing and was delivered to the top of the glass rod through a pipette orifice. A hose clamp permitted the adjustment of the flow rate  $f$ . The electrical resistance  $R$  of the solution layer, covering the glass rod, was measured with an A.C. conductivity bridge. One electrode made contact with the solution between the pipette tip and the upper end of the glass rod. The other electrode was an insulated metal clamp at the lower end of the glass rod.

Nine different glass rods of 3, 5, and 10 mm. diameter and of 10, 30, and 60 cm. length were used. The specific resistance,  $\rho$ , of the solutions were in the range of 300–400 ohms  $\times$  cm. An example of one of these experiments is given in Table I.

Measurements with a Höppler viscosimeter indicated that the viscosities of the solutions were so close to that of distilled water that correction could be neglected. Likewise, the viscosities of the protein solutions of concentrations below the upper critical limit, mentioned above, were practically those of distilled water.

The flow rate  $f$  was determined by collecting the solution, which dropped off the lower end of the glass rod, in a small graduated cylinder during a measured number of minutes.

Flow rate  $f$  and resistance  $R$  yield the thickness  $d$  of the water layer and the average vertical velocity  $\bar{v}$ :

$$d = \frac{\rho l}{Ra\pi}; \quad \bar{v} = \frac{f}{60q},$$

where  $q = a\pi d$ .

<sup>8</sup> The shorter of the two interchain separations in  $\beta$ -keratin is 4.65 Å.

Figure 3 indicates that the thickness  $d$  of the water layer is a function of rod diameter  $a$  and that it is a square-root function of  $f$ . For small flow rates (below 5 ml./min.) it is independent of length  $l$ . The average velocity  $\bar{v}$ , however, changes only little with the rod diameter. This would indicate that  $q$ , the cross section of the water layer, is independent of  $a$  at any given flow rate. This is borne out by the data with a reasonable degree of accuracy. Simple arithmetic shows that  $\bar{v}$  should be a linear function of  $f$ , if  $d$  is proportional to the square root of  $f$ . It is not clear why the experimental data are nonlinear for small flow rates.

The results from experiments with the 10 mm. diameter glass rods were not quite as consistent as those with the 5 mm. and 3 mm. glass rods. A glass ring around the upper end of the 10 mm. rod was used to insure a more even distribution of the water around the rod. In all experiments care was taken to avoid nonlaminar flow. At high flow rates (above 5 ml./min.) with 60 cm. glass rods "ripples" were observed at the lower end of the rod. The temperature during these experiments was  $20^\circ \pm 1^\circ\text{C}$ .

#### DISCUSSION

The value of the preceding theoretical treatment is limited by the assumptions and boundary conditions entering into it. For example image forces near the interface, which might slow down diffusion, are not taken into account. The theory does not necessarily predict in detail the actual behavior of protein solutions exposed to this spreading technique. However, it provides a framework of reference for a rational discussion of the results of actual spreading experiments. A study of films from different proteins is now under way (jointly with G. Colmano), using the new spreading technique, and will be published at a later date. Table II may serve as an example at this time to demonstrate the practical value of the new method as well as the existing differences, with regards to quantitative detail, between theory and experiment. It shows the specific areas obtained by spreading bovine plasma albumin (Armour Co.) films with the conventional "drop delivery" technique and with the glass rod technique. It should be emphasized that the protein was dissolved in distilled water and was spread on distilled water.

Table II shows that the highest value for the specific area obtained with the glass rod technique on distilled water ( $0.83 \text{ m.}^2/\text{mg.}$ ) is very close to the areas published for films of various proteins at 5 dynes/cm. spread on concentrated ammonium sulfate solutions or on 0.1  $N$  HCl ( $0.9 \text{ m.}^2/\text{mg.}$ ). It also shows that loss occurs when the flow rate is too high. And most drastically it shows that the droplet method even with a 90 min. waiting period is completely insufficient for quantitative work on pure water and highly dilute salt or buffer solutions. The data indicate that there is an *initial* loss of more than half of the total protein (60%) with the droplet technique.

TABLE II

*Specific Areas of Films of Bovine Plasma Albumin (Armour and Co.) Spread with the Glass Rod Technique and with the Droplet Technique*

Concentration:  $43.5 \cdot 10^{-6}$  g. protein per ml. distilled water.  
Glass rod diameter: 5.0 mm.  
Volume delivered in both cases: 1.00 ml.  
Trough (3 mm. deep) filled with distilled water ( $\rho = 8 \times 10^5$  ohms  $\times$  cm.).  
Temperature 20°-21°C.  
The droplets were carefully deposited from about 2 mm. height and evenly distributed over the water surface.  
Compression rate:  $\sim 0.7$  mm./sec. Compression of "glass rod films" was started immediately after spreading.  
Surface contamination: 30 min. after cleaning less than 0.5 dynes/cm. after an area reduction to 7% of the maximal area.

Glass rod spreading	Rod length (cm.)	Specific area ( $m.^2/mg.$ at 5 dynes/cm.)	% lost, assuming complete spreading for highest value
Flow rate in ml./min.	2	0.83	0
	5 <sup>a</sup>	0.82	1
0.2	12	0.73	12
2.0	2	0.74	11
	5	0.73	12
	12	0.70	16
Droplet spreading			
5 min. interval between spreading and compression		0.33	60
90 min. interval		0.47	43

<sup>a</sup> A bovine plasma albumin film, spread under the same conditions, was deposited on a Langmuir-Blodgett slide at a pressure of 10 dynes/cm. Its thickness, measured in the ellipsometer, was 10.3 Å. The theoretical value is 10.4 Å.

Comparison of the data from Table II with the theoretical predictions of Fig. 4 shows that for a flow rate of 0.2 ml./min. the predicted loss is much higher than 10% for a 2 cm. glass rod and about 6% for a 5 cm. glass rod, whereas the actual loss with these two glass rods is probably negligible. This discrepancy suggests that one or several promoting conditions or mechanisms exist which are not accounted for by the theory. On the other hand, the 12 cm. glass rod, which according to Fig. 4 should reduce the loss to less than 0.2% at a flow rate of 0.2 ml./min., causes a loss of 12%.

The increase in efficiency above the theoretical value may, in part, be due to a mechanism which was suggested by Langmuir (11):

"When an aqueous solution of a protein is injected just below the surface of water in a tray, some of the protein molecules diffuse to the surface, they generate a surface pressure which causes the film to flow radially outward, dragging with it a thin film of underlying water. To supply the water for this radial outflow near the surface there



must be an upflow of water under the point from which the protein spreads. Under favorable conditions this upflow may bring all the protein molecules to the surface and prevent any loss of protein by diffusion downward.<sup>9</sup>

The radial symmetry of the glass rod is an ideal configuration to promote this mechanism. The "injection of protein solution just below the surface of the water" is in our case the arrival, from above, of a thin cylindrical layer of *protein solution* at the water surface of the trough. With the shorter glass rods the solution has not yet been exhausted by diffusion. In our case film comes already down along the surface of the vertical cylinder and spreads out radially over the water surface, and thereby starts the Langmuir mechanism immediately. The "favorable conditions," which Langmuir envisioned, are incidentally included in the glass rod method.

The reason for the failure of the longer glass rod to perform according to theory (it should yield the highest specific film area) is not yet understood. Evaporation of water from the rod<sup>10</sup> would cause  $d$  to become smaller and thereby make the diffusion processes even more efficient. The theory does not take into account accelerated flow, which for longer rods may well occur. Acceleration along the rod would cause a "pinching" of the cross section in a downward direction and make  $d$  so small that some unknown effect might disturb the diffusion process. It is well known that liquids, and especially water, change their bulk properties in the immediate vicinity of a solid.

Acceleration may also be responsible for the fact that  $\bar{v}$  is not a linear function of  $f$  (see above under "Method"), or that  $d$  appears to be a square-root function of  $f$  instead of cube-root function, as predicted by theory.<sup>11</sup>

It should be mentioned that the glass rod technique permits spreading proteins from one solution A (in the pipette) and studying the film properties on another solution B (the trough solution) where A and B may have different temperature, pH, and ionic composition. The small local contamination of B by A (ratio  $\sim 1000:1$ ) may be negligible in many cases.

Finally, the glass rod technique can be used to spread a protein film at a water/oil interface, provided the glass rod is water-wet when it is inserted through the interface. The quantitative relationships (Fig. 3) will be different.

The improvement in the spreading of protein films offered by the glass rod technique will permit an experimental re-evaluation and possibly a refinement of molecular weight determinations based on film isotherms, which

<sup>9</sup> Langmuir, by his reasoning, is led not to the main mechanism postulated in this paper (concentration near interface = zero, owing to loss of molecules into another phase, therefore concentration gradient and diffusion towards the interface) but to an auxiliary mechanism only, even if he mentions diffusion.

<sup>10</sup> A protective cylinder around the rod was not employed in these experiments.

<sup>11</sup> According to Dr. George Hall, of RIAS.

the author considers still to be a controversial subject. For instrumental improvements towards this goal see (12).

#### ACKNOWLEDGMENTS

Dr. Germille Colmano and Mrs. M. J. Russo participated in the experimental work. Drs. Ruth Aranow and George Hall have helped with advice on the theoretical part. I am very grateful to all of them.

This work was in part supported by a research grant (C-3370) of the U. S. Public Health Service.

#### REFERENCES

1. SOBOTKA, H., AND TRURNIT, J. H., "Unimolecular layers in protein analysis," in R. J. Block and P. Alexander, eds., "A Laboratory Manual of Analytical Methods of Protein Chemistry." Pergamon Press, Ltd., London, in press.
2. NEURATH, H., AND BULL, H. B., *Chem. Revs.* **23**, 391, (1938).
3. HUGHES, A., AND RIDEAL, E. K., *Proc. Roy. Soc. (London)* **A137**, 62 (1932).
4. GORTER, E., *Proc. Roy. Acad. (Amsterdam)* **37**, 788 (1934).
5. MITCHELL, J. S., *Trans. Faraday Soc.* **33**, 1129 (1937).
6. COCKBAIN, E. G., AND SCHULMAN, J. H., *Trans. Faraday Soc.* **35**, 1266 (1939).
7. BULL, H. B., *Advances in Protein Chem.* **3**, 95 (1947).
8. MISHUCK, E., AND EIRICH, F., in H. Sobotka, ed., "Monomolecular Layers," a publication of the American Association for the Advancement of Science, Washington, D. C., 1954.
9. GUASTALLA, J., *Compt. rend.* **208**, 1087 (1939).
10. JOST, W., "Diffusion in Solids, Liquids, Gases." Academic Press, New York, 1952.
11. LANGMUIR, I., *Cold Spring Harbor Symposia Quant. Biol.* **6**, 171 (1938), on page 172.
12. TRURNIT, H. J., AND LAUER, W., *Rev. Sci. Instruments* **30**, 975 (1959).

## A TEST OF THE BECKER-DOERING THEORY OF NUCLEATION KINETICS<sup>1, 2</sup>

W. I. Higuchi<sup>3</sup> and C. T. O'Konski

*Department of Chemistry, University of California, Berkeley, California<sup>4</sup>*

*Received May 25, 1959*

### ABSTRACT

Intensive consideration was given to the possibility of developing a method for studies of gas-phase nucleation which would be better than the usual cloud-chamber techniques. The method selected and developed involves steady-state production of nuclei in a turbulent jet where a dilute vapor issuing from a nozzle is rapidly quenched by a cooler annular gas stream. The nuclei are grown, and the resulting aerosol particles are electronically counted by means of light-scattering instrumentation. Equations are developed for the rate of production of nuclei in the jet under steady-state conditions. With their application, the pre-exponential and exponential factors of the Becker-Doering equation were separately determined from data on dibutyl phthalate (DBP), triethylene glycol (TEG), and *n*-octadecane (OCD). Heterogeneous nucleation was observed with DBP, OCD, and sulfur vapor. A critical résumé of the Becker-Doering theory is given. Large deviations from the theory observed with TEG are discussed in relation to the effects of hydrogen bonding on the structure of the critical nucleus.

### I. INTRODUCTION

It is of considerable interest to test the Becker-Doering theory (1-3) of nucleation kinetics, as this is the only treatment which leads to explicit expressions for the nucleation rate in terms of the experimental conditions and determinable properties of the system.

The theory, as developed for supersaturated vapors, is based upon a simple model. The gas is treated as a mixture of the monomeric vapor and clusters of varying sizes with concentrations computed from their free energies. A crucial step is the calculation of the free energy of a cluster of critical size, i.e., one which has equal probabilities of growing and evaporating when in contact with the supersaturated vapor under specified

<sup>1</sup> Presented before the Division of Colloid Chemistry at the 133rd Meeting of the American Chemical Society in San Francisco, April 13-18, 1958. Abstracts of papers, p. 3-1.

<sup>2</sup> Based upon the thesis submitted by W. I. Higuchi in partial fulfillment of the requirements for the Ph.D. in Chemistry, January, 1957. See also reference 17.

<sup>3</sup> Present address: School of Pharmacy, Univ. of Wisconsin.



conditions. This is done with the assumption that this cluster, or nucleation embryo, may be regarded as a small liquid droplet with the properties of the bulk phase. A contribution to the free energy of the embryo is computed from the surface tension. Further, it is considered that the rate of growth of embryos is calculable from the kinetic theory of gases, treating this as a diffusion problem. The final result is a rate equation of the form

$$J = A \exp(-\phi^*/kT). \quad [1]$$

Here  $\phi^*$  is the free energy of formation of the critical cluster from the supersaturated vapor,  $A$  is a kinetic factor,  $J$  is the number of droplets formed per cubic centimeter per second, and  $k$  and  $T$  have their usual meanings.

In order to evaluate  $\phi^*$ , it is assumed that the critical cluster is in equilibrium with the supersaturated vapor. Its free energy of formation from the supersaturated vapor may be expressed by the sum of two terms, a surface term  $4\pi r^{*2}\gamma$ , and the Kelvin term,

$$-g^* kT \ln \frac{p}{p_0} = -g^* \frac{2\gamma M}{N\rho r^*}. \quad [2]$$

Here  $r^*$  is the radius of the critical droplet,  $\gamma$  is the surface tension of the liquid,  $g^*$  is the number of molecules in the critical embryo,  $p$  is the vapor pressure,  $p_0$  is the vapor pressure of bulk liquid at temperature  $T$ ,  $\rho$  is the density of the liquid,  $M$  is the molecular weight, and  $N$  is Avogadro's number. The first term represents the free energy of formation of the critical embryo from bulk liquid ( $r = \infty$ ), and the second term is the free energy change in transferring  $g^*$  molecules from the supersaturated vapor to the bulk liquid; their sum is the free energy of formation of the critical embryo from the supersaturated vapor. Thus

$$\phi^* = 4\pi r^{*2}\gamma - 2g^*\gamma M/N\rho r^* = (4/3)\pi r^{*2}\gamma. \quad [3]$$

The Frenkel treatment (3) for the kinetic factor gives

$$A = aN^{3/2}(p/RT)^2(2M\gamma/\pi)^{1/2}/\rho. \quad [4]$$

Here  $a$  is the accommodation coefficient or "sticking probability" of vapor molecules on the embryos and  $R$  is the gas constant. Farley (4) has obtained the same equation assuming  $a = 1$ . As a result of a simplifying mathematical approximation, Becker and Doering (1) obtained a value for  $A$  greater by  $g^{*2/3}/\pi$ , which is numerically the order of ten. Barnard (5) obtained a more exact expression for  $A$ , viz.,

$$A = a(2m\gamma/\pi)^{1/2}(p/T)^2N^{3/2}(1/R^2\rho) \exp\{(\gamma M/\rho RT)(4\pi\rho N/3M)^{1/3} - \ln S - (2/3)\ln g^*\}. \quad [5]$$

To obtain an explicit expression for  $J$  in terms of experimental quantities, the Kelvin equation may be solved for  $r^*$  and combined with Eq. [3] and [1]. The results may be written

$$J = A \exp(-\alpha/T^3 \log^2 S), \quad [6]$$

where  $\alpha$  depends upon the properties of the liquid, and is defined by the equation

$$(2.303)^2 \alpha = 16\pi\gamma^3 M^2 / 3k\rho^2 R^2. \quad [7]$$

The supersaturation,  $S$ , is conventionally defined as the ratio of the pressure of supersaturated vapor to that of bulk liquid at the prevailing temperature; more precisely, it is the ratio of the fugacities.

The approximations in evaluating the pre-exponential factor,  $A$ , are generally regarded as being relatively free of criticism, in contrast to the assumptions involved in computing the exponential term. This is because the nucleation rate depends sensitively upon the terms in the exponential.

One of the criticisms of the theory is that the concepts of surface tension and density are not rigorously applicable to clusters of a few molecules. As Reiss (6) has pointed out, it is difficult to define thermodynamic quantities when the dimensions of one of the phases is comparable to the thickness of the transition layer. Equation [3] is clearly not adequate for computing the free energy of formation of small clusters. Various studies (7-11) show that surface tension and surface free energy are dependent on the curvature of the droplet. Also, the surface free energy, not the surface tension, is the quantity appropriate (12) to the Kelvin expression. However, the effects of droplet size are not readily calculable and therefore cannot be incorporated into the theory in a general way.

Because of many objections to the theory, it appears desirable to test it in a number of representative cases to ascertain its limitations and to attempt a correlation of any detectable deviations from the theory with known molecular properties. Previous studies, mainly with the expansion cloud chamber, were generally of a very low order of accuracy, possibly with uncertainties of the order of 100 in  $J$ , and the terms  $A$  and  $\alpha$  defined above were not independently determined. The results of cloud-chamber experiments with homogeneous vapors have been summarized in various reviews (5, 13-15). Results are confined to low molecular weight organic liquids because of limitations of the cloud-chamber technique. Higher molecular weight substances with different types of intermolecular forces, associating vapors, metals, and salts are among the interesting systems not yet studied.

In this research, several new methods for studying nucleation kinetics are considered and are evaluated briefly. The turbulent jet quenching technique was selected and developed for use with modern electronic light-

scattering instrumentation. Measurements over a wide range of nucleation rate were made on several compounds with various types of intermolecular forces. These are reported and evaluated by means of an extension of the theory to turbulent jets.

## II. CHOICE OF EXPERIMENTAL METHOD

To test the theory, it is required that supersaturation be produced under known conditions and that the rate of homogeneous production of nuclei be measured. A very sensitive and general method for observing small particles is light scattering; it was therefore decided to employ photometric or particle-counting techniques (16). Various ways of producing supersaturations were considered; these may be classified as (I) Chemical; (II) Photochemical; and (III) Physical.

A homogeneous chemical technique would require rapid means of uniformly mixing, decomposing, or polymerizing a gas to form a substance of lower vapor pressure. Observation times must be short compared to the time required for the supersaturated material to diffuse to the walls, to preclude difficulties from the condensation which generally occurs on surfaces at a lower degree of super-saturation than is required for homogeneous nucleation. The chemical reaction must be virtually complete in a time interval which is short compared to the duration of the nucleation process, in order that the supersaturation be accurately known during nucleation. Referring to Eq. [6] above, it can be seen that the nucleation rate,  $J$ , is very sensitive to the temperature. Since rapid decompositions or polymerizations generally involve temperature changes, accurate control of the degree of reaction would be necessary. No chemical reaction system could be found in which these requirements are met.

Photochemical reactions appeared to offer some important advantages. First, the reaction might be made exceedingly rapid by application of the well-known flash photolysis technique. In principle, this could be carried out in a homogeneous manner so that the entire system under observation would be exposed to the same conditions of supersaturation and temperature. Also, the degree of supersaturation might be conveniently controlled by varying the flash intensity. Accordingly, detailed consideration was given to various photochemical reactions, and some exploratory experiments were conducted by Dr. G. J. Doyle (17). Theoretical calculations were made of the expected nucleation rates, growth rates, and levels of detectability by means of light scattering under various experimental conditions. It was concluded that execution of this technique would be exceedingly difficult or impossible for the most favorable reactions which could be found.

Both the chemical and the photochemical methods suffer fundamental limitations. Chemical rate processes generally limit the rate of produc-

tion of supersaturation, so a complete and detailed knowledge of the chemical kinetics would be required to compute the degree of supersaturation. Also, interpretation of data is difficult when the supersaturation is time-dependent. Thus, physical methods for producing supersaturation appear the most promising.

The physical methods considered can be grouped into three classes of three subclasses each: (A) Cooling by expansion: (1) Wilson cloud chamber; (2) bursting diaphragm technique; (3) cyclic expansion and compression (standing sound wave or reciprocating piston). (B) Cooling by thermal conduction: (1) chimney, as in a condensation-type aerosol generator; (2) coaxial flow of a vapor into a cooler gas stream; (3) diffusion cloud chamber. (C) Cooling by rapid mixing of a vapor with a quenching gas: (1) junction of two flowing streams in a Y-tube; (2) turbulent jet into a static gas; (3) turbulent jet into a coaxial flowing stream.

Most of the experimental data on nucleation kinetics have been obtained with the Wilson expansion cloud chamber (18). As customarily employed (13, 14, 19-21), one measures the degree of expansion of a gas containing the vapor at a known pressure required to produce a cloud. The temperature and degree of supersaturation corresponding to this "critical expansion ratio" is then computed assuming that the expansion is adiabatic. Generally, only rough, visual estimates of the number of cloud droplets produced per cubic centimeter were made. The principal experimental difficulties are: Nucleation begins before the expansion ceases and continues after the final expansion is reached until the growth of the droplets by diffusion depletes the system to the extent that the rate becomes negligible. Thus the system is not homogeneous, as a result both of the depletion of vapor and of the heat released upon condensation. Mason (22) and Corner (23) have pointed out that the simplifying assumptions customarily applied are generally not valid. Other difficulties are that extraneous centers of condensation are difficult to detect and eliminate, and that a wide range of nucleation rates cannot be conveniently covered.

More rapid expansions than possible in the Wilson cloud chamber might be produced by application of the bursting diaphragm technique employed in shock tube experiments in chemical kinetics (24). However, unlike the shock wave front which is of importance in the chemical kinetics studies, the rarefaction front is not sharp. Furthermore, this technique would suffer from the difficulties mentioned for the Wilson cloud chamber.

If a gas containing a nearly saturated vapor is subjected to rapid compression and expansion, as in a reciprocating piston or a high-intensity standing sound wave, condensation nuclei might be formed during the expansion part of the cycle. With an appropriate optical and electronic system the variations of light scattering might be employed to follow the



vapor polymerization into the supersaturated region, and possibly to measure the production of critical embryos and their growth. An important advantage of this technique would be that the supersaturation could be produced at the expansion phase of the cycle, whereas the average conditions would correspond to undersaturation so condensation on the walls could be avoided. If nucleation did occur, it seems probable that difficulties would arise because of incomplete evaporation of the nuclei during the compression phase of the cycle. When a fog of spontaneous condensation is compressed in the Wilson cloud chamber and again expanded, it has been observed (25) that a dense fog appears at a relatively low supersaturation. The reason for the persistence of the nucleation embryos has never been satisfactorily explained. Furthermore, impurities present as condensation centers in the gas would be difficult to remove initially. Partly for these reasons and partly because of complexities in the interpretation, development of this method was not undertaken. With light-scattering (26, 27) observations, the cyclic expansion technique appears promising for studies of the thermodynamic properties of gases into the supersaturated region.

In any of the methods (*B*) involving cooling by thermal conduction, heat transport and mass transport occur simultaneously, and it would be required that one measure or establish values of the temperature and vapor concentration in the region while the rate of production of nuclei is being measured. Rates of diffusion and thermal conductivities under supersaturated conditions and as a function of temperature would be required correctly to interpret experiments of type *B*. Therefore, these methods are not as promising as the ones considered below. However, it should be noted that in at least one instance (28) the diffusion cloud chamber (29, 30) has been employed to obtain a value for the critical supersaturation (of methanol vapor). The flow methods, (*B1*) and (*B2*), appear less promising than the diffusion cloud chamber. Some preliminary experiments of nucleation kinetics in alkali halide vapors with method *B1* indicated great difficulties in applying that technique (17; see also footnote 2).

Perhaps the simplest method of quenching a vapor stream by mixing would involve the use of a Y-tube, method (*C1*), which has been employed in measurements of gas-phase chemical reactions. For the present application, this technique could not be applied unless construction materials could be found at which condensation of the vapor under study would not occur on the walls to any appreciable extent. Whereas this may be possible, as there are surfaces not readily wet by certain liquids, no suitable systems were known. A more generally applicable approach is to carry out the quenching in a turbulent jet, methods (*C2*) or (*C3*), and to design the apparatus and arrange the conditions so that the nucleation process

would occur in a region well removed from the walls. A full discussion of the method is given in Sections III and IV.

### III. NUCLEATION IN TURBULENT JETS: THEORETICAL

The problem of the condensation of vapors in a turbulent jet issuing into a stagnant quenching gas (method *C2* above) has been discussed by Amelin (31), who conducted some experiments on pure water vapor. Hottel (32) had previously considered this method for the generation of aerosols, but abandoned it because of difficulties connected with heat transfer which caused condensation of the vapor on the nozzle walls.

When a gas mixture at a temperature  $T_1$ , containing a vapor at a partial pressure  $p_1$ , mixes rapidly and adiabatically with another gas mixture at a temperature  $T_2$ , containing the same vapor at a partial pressure  $p_2$ , a heat and material balance shows (31) that for any element of volume in the mixing region:

$$T = (T_1 + T_2 an)/(1 + an) \quad [8]$$

and

$$p = (p_1 + p_2 bn)/(1 + bn), \quad [9]$$

where  $n = q_2/q_1$ ,  $a = c_2/c_1$ , and  $b = M_1/M_2$ . Here  $T$  is the absolute temperature,  $c$  is the specific heat,  $p$  is the vapor pressure,  $M$  is the molecular weight, and  $q$  is the quantity by weight. The subscripts 1 and 2 refer to the first and second gases, respectively. These equations refer to a constant total pressure mixing process and are applicable when eddy diffusion and heat transfer become rapid compared to the molecular transport rates.

From Eq. [9], it is seen that the supersaturation in any element of volume defined by  $n = q_2/q_1$  is

$$S = p/p_T = (p_1 + p_2 bn)/(1 + bn)p_T, \quad [10]$$

where  $p_T$  is the equilibrium vapor pressure of the material in question at temperature  $T$ .

In the entire mixing region of the two gas streams,  $n$  must vary from 0 to  $\infty$ . Then there may be a maximum value of  $S = S_m$  in the region at  $T = T_m$  for some  $n = n_m$  defined by

$$(\partial S/\partial n)_{T_1, T_2, p_1, p_2} = 0. \quad [11]$$

Amelin has applied Eq. [11] to the case of a turbulent jet of pure water vapor. He made the approximation that the  $S_m$  value at the point of cloud formation can be taken as the supersaturation at which nucleation occurs. It should be pointed out that Eq. [11] does not define the maximum nucleation rate in the jet. From the Becker-Doering equation [6] it can be

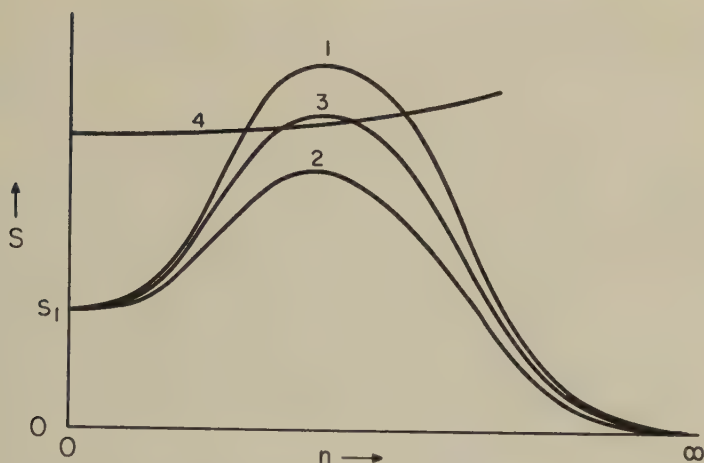


FIG. 1. Schematic representation of cloud formation in a turbulent jet (from Amelin (31)).

seen that the maximization should be for  $(T^3 \log^2 S)$  rather than  $S$  alone. Amelin's assumption may therefore lead to errors in interpreting the data.

In Fig. 1, Amelin's analysis is graphically presented. The nozzle conditions of the jet are  $n = 0$ ,  $T = T_1$ , and  $p = p_1$ ; and the unmixed surrounding air is defined by  $T = T_2$ ,  $p = p_2$ , and  $n = \infty$ . Curve 4 is the critical supersaturation curve. Curve 1 shows the case where  $T_2$  has such a value that  $S_m \gg S(\text{critical})$ . Curve 2 shows the case where  $T_2$  has such a value that  $S_m \ll S(\text{critical})$ . Amelin observed the condensation of water vapor issuing as a free jet into stagnant air (method C2). Keeping  $T_1$ ,  $p_1$ , and  $p_2$  constant he measured  $T_2$  at the point of appearance of a visible cloud (curve 3). He then increased  $T_2$  until the cloud disappeared. Using the mean value of  $T_2$  for the appearance and the disappearance of a cloud he calculated  $S_m = 2.74$  and  $T_m = 41^\circ\text{C}$ . This value agrees well with Volmer and Flood's (14) cloud-chamber value for the critical supersaturation, which was 2.78 (obtained by extrapolation assuming the Becker-Doering theory).

For the reason given above and for the following reasons, Amelin's agreement with Volmer and Flood's critical supersaturation value appears to be fortuitous. Amelin neglected the fact that there is a distribution of  $n$  values near  $n_m$ , i.e., he has assumed that all the nucleation is occurring at  $S = S_m$ . Hence, he has also neglected the volume dependence of  $n$ , illustrated in Fig. 2, which shows the structure of a turbulent jet taken from Hottel (32). Amelin did not discuss the effect of fluctuations in turbulence, but it appears that such effects could not be very important (see Section VI, Discussion). Amelin did not determine the droplet con-

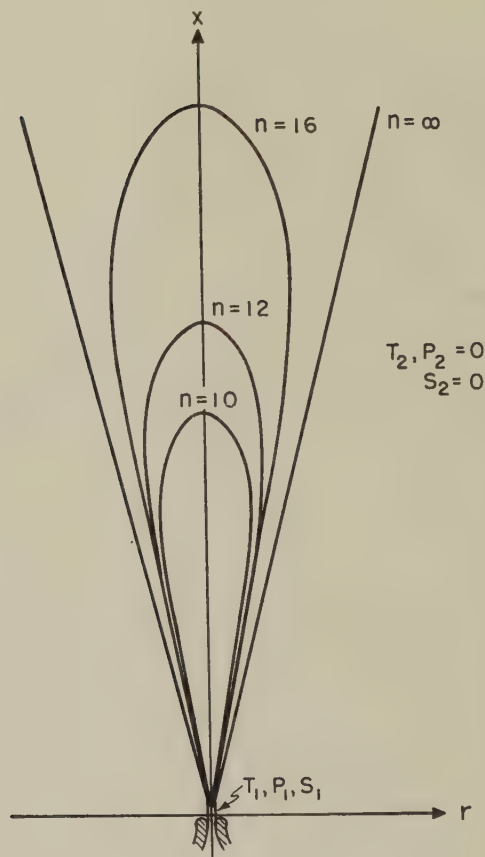


FIG. 2. Free jet profile.

centration required to obtain a visible cloud. The uncertainty in the estimated nucleation rate might be the order of 1000 for his experiments.

For this research an analysis is presented which includes an expression for the nucleation rate as a function of the coordinates in the jet. This can be used to calculate the total nucleation rate in the whole jet.

Since by using an aerosol counting method (16) the rate of nucleation can be measured accurately, the concept of a "critical" supersaturation was discarded and a study of the rates of nucleation as a function of supersaturation was made by adaptation of method C2 above. It will be seen that these studies facilitate a direct comparison of experiment with theory.

It is well known (33, 34) that current phenomenological theories of free turbulent jets do not describe quantitatively the experimental data. The difficulties lie in the lack of understanding of the phenomena of turbulent transfer of heat, mass, and momentum. Recently, Baron and Alexander



(34) have generalized Reichardt's hypothesis on the basis of a semiempirical approach. The key assumption in their treatment is that an error function expression

$$\overline{\psi u} = \{1/f_1(x)\} \exp \{-r/f_2(x)\}^2 \quad [12]$$

is a solution to the equations of motion in a free turbulent axially symmetric jet. Here  $\psi$  is the local instantaneous concentration of any quantity (heat, mass, or momentum),  $u$  is the local instantaneous axial component of the velocity,  $x$  is the distance along the axis of the jet from the nozzle, and  $r$  is the radial distance from the axis of the jet;  $\overline{\psi u}$  is the time-mean value of  $\psi u$ . The basis for this assumption is that experimental data (35, 36) on flux (mass, heat, and momentum) distributions in free jets are well correlated by Eq. [12]. With the added assumption that the flux profiles at successive sections through the jets are similar (this is supported by the experimental work of Corrsin and Uberroi) (35, 36), the constants  $f_1(x)$  and  $f_2(x)$  can be evaluated. Baron (37) then obtained for the steady-state time-mean value of the mass fraction,  $\chi_n = 1/(n + 1)$ , of the nozzle fluid at any point in the jet,

$$\chi_n = (\delta_0/\bar{\delta})^{1/2} (dC_m/2C^2x) \exp - (r/x)^2 (1/C^2 - 1/2C_m^2). \quad [13]$$

Here  $\delta_0$  is the density of the nozzle fluid,  $\bar{\delta}$  is the time-mean density in the jet at a point  $x$ ,  $r$  is the axial and radial coordinate, respectively,  $d$  is the nozzle diameter, and  $C$  and  $C_m$  are constants for any turbulent round jet. Baron suggested values of  $C = 0.0855$  and  $C_m = 0.075$  based on experimental data. Equation [13] with these constants leads to an expression for flame shapes which is identical, within the experimental error of the constants, with an expression proposed by Hawthorne, Weddel, and Hottel (38) and which agrees well with the experiments (37) on flames.

With the use of expression [13] it is now possible to examine the supersaturation as a function of the coordinates, and therefore the nucleation rate as a function of the coordinates. For the large ratios of the jet velocity to the mixing stream velocity as used in this research, recent studies (38, 39) show that the free jet expressions apply. Consider the structure of a jet (Fig. 2) and take a surface  $n = \text{constant}$ . In polar coordinates the volume enclosed by this surface is

$$V(n) = \int_0^{\pi/2} \int_0^R 2\pi R^2 \cos \theta \, d\theta \, dR. \quad [14]$$

Equation [13] may be rearranged to give

$$R = \{K(n + 1)/\sin \theta\} \exp (-k \cot^2 \theta), \quad [15]$$

where

$$K = (\delta_0/\bar{\delta})^{1/2} (dC_m/2C^2)$$

and

$$k = (1/C^2 - 1/2C_m^2).$$

Then the combining of [15] and [14] gives

$$V(n) = 2\pi K^3(n+1)^3(1/3) \int_0^{\pi/2} (\cos \theta / \sin^3 \theta) \exp(-3k \cot^2 \theta) d\theta. \quad [16]$$

Employing Baron's values (37) for  $C = 0.0855$  and  $C_m = 0.075$ , also taking  $\delta_0 = 0.808 \times 10^{-3}$  g. c.c.<sup>-1</sup> and  $\bar{\delta} = 1.06 \times 10^{-3}$  g. c.c.<sup>-1</sup>, and solving the integral in [16] one obtains

$$V(n) = W(n+1)^3 = 6.63 \times 10^{-4}(n+1)^3 \text{ c.c.} \quad [17]$$

The volume distribution function for  $n$  is obtained by differentiation of [17]:

$$(dV/dn) = 3W(n+1)^2. \quad [18]$$

It is assumed in obtaining Eq. [16] that  $\bar{\delta}$  is a constant. This is a reasonable assumption for this research since for large values of  $n$  and for small changes in  $n$ , encountered in this work,  $\bar{\delta}$  can vary only a few per cent.

The total rate of nuclei production in the whole jet in unit time is

$$I = \int_0^\infty J dV. \quad [19]$$

Employing [19], [18], and Eq. [6] of Section I, we obtain

$$I = \int_0^\infty J(dV/dn) dn; \quad [20]$$

$$I = 3W \int_0^\infty A(n+1)^2 \exp(-\alpha/T^3 \log^2 S) dn. \quad [21]$$

As  $T$ ,  $S$ , and  $A$  are all functions of  $n$ ,  $I$  is a very involved function of  $n$ . Attempts to solve [21] analytically proved fruitless. In this research, the Becker-Doering theory is tested in the form of Eq. [21], which may be solved graphically for the particular case.

Experimentally, the quantity  $I$  is determined as a function of the conditions. From the data,  $\alpha$  may be calculated and compared with the theoretical equation [7].

#### IV. THE TURBULENT JET TECHNIQUE: APPARATUS AND METHODS

##### A. Apparatus

It is possible to quench a vapor issuing from a nozzle with a cooler gas in such a manner that nucleation occurs at appreciable rates in a region entirely out of contact with the surfaces of a suitably designed apparatus and to grow the nuclei to large particles for the purpose of determining

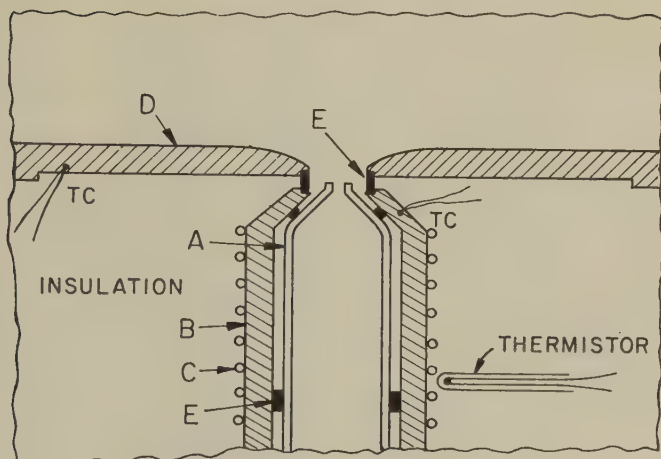


FIG. 3. Nozzle and thermal shields in the quenching region.

the rate of production of the nuclei (40). The principal design problem which was encountered in this work was the accurate knowledge of nozzle gas and quenching gas temperatures in the production of a jet. A sharp temperature drop from the nozzle region into the incoming quenching gas was necessary to avoid condensation in the nozzle. Figure 3 shows how these requirements were met. In the figure *A* was a pyrex nozzle through which the nozzle gas passed at a temperature  $T_1$ , and *B* was a heat-compensated copper thermal shield also at  $T_1$ . The quenching gas at a temperature  $T_2$  passed over the copper surface, *D*, also at  $T_2$ . The Teflon gasket, *E*, served as a thermal barrier between the two regions at different temperatures.

Figure 4 is a flow diagram of the apparatus. Regulators 2 and 3 were diaphragm-type pressure controllers. All filters were two sheets of asbestos filter paper,<sup>4</sup> each 0.5 mm. thick and 75 cm.<sup>2</sup> in area. The desiccant was anhydrous magnesium perchlorate. The deoxygenator for the carrier gas line consisted of a quartz tube filled with copper turnings placed in a furnace maintained at 750°C. The flow rates were measured by precision Fischer and Porter Flowrater units.<sup>5</sup> The source of the quenching gas was a 100 p.s.i. compressed air line.

Figure 5 is a scale drawing which shows the details of the evaporator and the mixer, *A* and *B*, respectively. The furnaces of *A* and *B* were constructed from nickel pipe evenly wound with number 16 B. and S. gauge Chromel A wire. The sensing elements for thermal regulation were the Western Electric type 14A thermistors, each of which formed one arm of

<sup>4</sup> Hollingsworth and Vose Company, East Walpole, Massachusetts.

<sup>5</sup> Fischer and Porter Company, Hatboro, Pennsylvania.



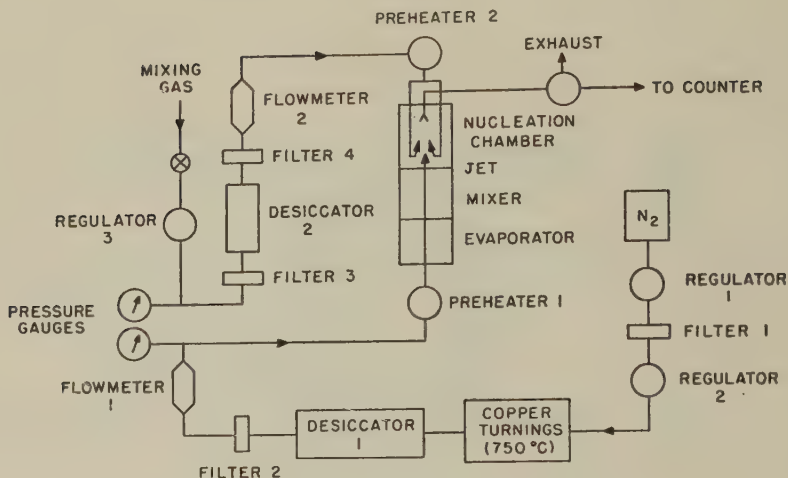


FIG. 4. Flow diagram of turbulent jet nucleation apparatus.

a Wheatstone Bridge from which the unbalanced signal activated a relay for the heaters. With this arrangement temperatures in *A* and *B* were maintained constant to within  $\pm 0.2^\circ\text{C}$ . for hours.

The preheater for the nitrogen gas was a 500-ml. pyrex flask enclosed in a heating mantle controlled by a variac. Preliminary experiments showed that at  $\sim 3$  l./min. the gas attained nearly the wall temperature about half way up *A*, even without the preheater, for wall temperatures  $\sim 220^\circ\text{C}$ . The cylindrical pyrex bucket was suspended coaxially with respect to the walls. Following this stage was a mixer (two 2-mm. jets striking each other) followed by another mixer about 25 cm. higher. The mixer *B* was of sufficient length to allow the flow stream to equilibrate thermally with the wall.

The glass nozzle, shown in Figs. 3, 5, and 6 narrowed to  $0.100 \pm 0.005$  cm. at the tip and was axially symmetric. The other end expanded to allow a union with the pyrex section of *B* below. The part of the copper nozzle jacket which was beyond the furnace of *B* and inside the nozzle section was close wound up to the nozzle tip region with a single layer of number 22 B. and S. insulated Nichrome wire. A thermistor was used (as shown) to regulate the temperature to about  $\pm 0.1^\circ\text{C}$ . The pyrex nozzle section was held snugly in the jacket by two Teflon spacers and by mechanical pressure from below. The spacers also served as a seal to prevent flow of gas out of the nucleation chamber.

When the whole section above the nozzle unit was lowered into position, the nucleation chamber was formed. The surfaces of contact were close fitting to aid thermal equilibrium between the two sections, and a silicone rubber O-ring sealed the chamber. On the outside of the heavy copper

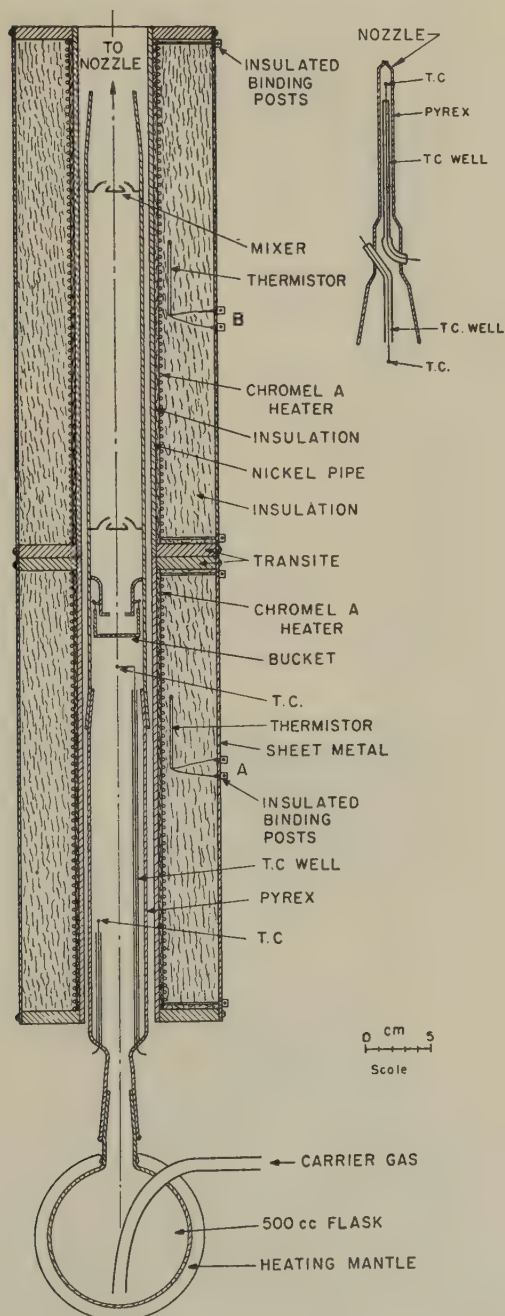


FIG. 5. Heater, vapor pickup section, mixer, and nozzle.

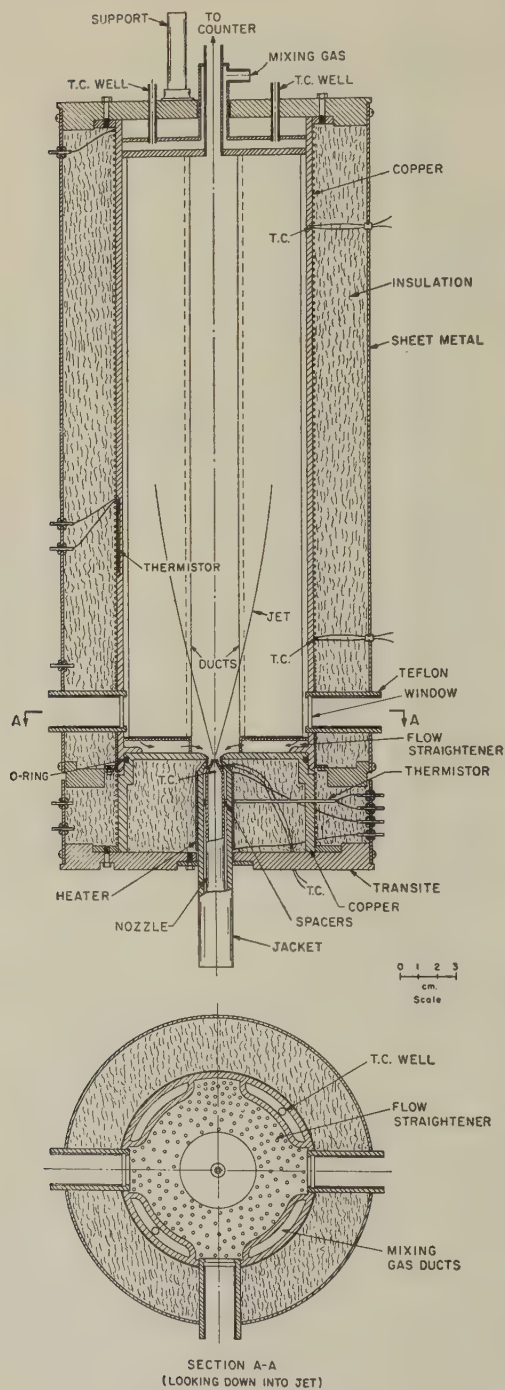


Fig. 6. Nucleation and growth chamber.



walls ( $\sim 4$  mm. thick), as well as around the walls of the nozzle unit, number 22 B. and S. Chromel A wire was wound for heating. A thermistor imbedded in the walls of the nucleation chamber served to regulate the chamber wall temperatures to  $\pm 0.02^\circ\text{C}$ . at around  $50^\circ\text{C}$ .

In Fig. 6, the cross-sectional view  $A - A$  shows the four ducts for the mixing gas. A wire gauze ( $\sim 400$  mesh per inch) in the mixing gas stream prevented recirculation. This flow straightener is shown schematically in Fig. 6 (both views).

Calibrated Chromel-Alumel thermocouples were liberally placed throughout the apparatus to measure the gas temperatures, to insure gas-wall temperature equilibration, and to maintain steady temperature conditions during a run.

To approximate the free jet, the nucleation chamber diameter was made as large as conveniently possible. The ratio of the chamber diameter to the nozzle diameter is about 90, and the studies of Alexander and coworkers (39, 41) show that the spreading of jet under this condition is essentially that of a free jet for the region of interest, i.e.,  $n < 30$ .

The extent of aerosol loss by sedimentation and diffusion in the nucleation chamber and in the conduit to the counter was estimated. If  $L$  is the fraction of the aerosol which passes the conduit, the concentration of the aerosol reaching the counter is

$$N = IL/F, \quad [22]$$

where  $F$  is the total flow rate of the aerosol stream leaving the nucleation chamber and  $I$  is given by Eq. [21]. Unless otherwise specified  $F = 7.0 \times 10^4$  c.c./min. for the experiments in this study.

Langstroth and Gillespie (42) have studied the overall effects of wall losses of ammonium chloride aerosols ( $0.3$ – $2.2 \mu$  diameter) in chambers of different sizes as a function of stirring velocity up to velocities of  $2\text{m./sec}$ . and obtained empirical first-order rate equations to describe these processes. For the rate of removal of particles,

$$-dn/dt = \beta n,$$

where  $n$  is the number of particles in a unit volume. It was found (41) that  $\beta$  is a linear function of velocity. The maximum value of the flow velocity encountered in our nucleation experiments was around  $10\text{ m./sec}$ . The  $\beta$  value of Langstroth and Gillespie for this velocity is  $\sim 0.1\text{ min.}^{-1} = 2 \times 10^{-3}\text{ sec.}^{-1}$  (extrapolated). The flow time constant in the nucleation experiments was the order of  $1\text{ sec.}$ ; therefore wall losses were estimated to be negligible. The horizontal time of flow was minimized by employing a vertical flow arrangement (16, *b*) through the counter cell.

*B. Experimental Considerations of the Jet*

In Section III it was assumed that molecular heat and mass transfer are negligible compared to eddy transfer. It is known qualitatively (43) that the ratio of turbulent diffusion to molecular diffusion becomes greater as the Reynolds' number  $R_e$  in the nozzle increases. Here  $R_e$  is defined as:

$$R_e = DV\rho/\eta,$$

where  $D$  is the diameter of conduit,  $V$  is the mean flow velocity, and  $\rho$  and  $\eta$  are the density and viscosity of the fluid, respectively. Hottel and co-workers investigated experimentally the axial concentration distribution in a jet as a function of  $R_e$ . They found (32) that for an isothermal jet of air, the axial distribution of the time-mean concentration becomes geometrically similar for all nozzle sizes at  $R_e \approx 3000$ . This dynamical similarity is interpreted to mean that as far as the mean mass transfer rate is concerned, the jet mixing is predominantly turbulent at  $R_e > 3000$ . Since other experiments (33) have shown that heat and mass diffuse at about the same rate under turbulent conditions, it appeared reasonable to expect that the mean temperature distribution in the jet would attain dynamical similarity at  $R_e \sim 3000$ . Corrsin (35, 36) has shown that density differences (due to temperature differences between the nozzle fluid and the ambient fluid) up to about a factor of two do not appreciably affect the dynamical similarity of the jet. On the basis of these considerations most experiments were carried out at about  $R_e = 3500$ . Early experiments with dibutyl phthalate at  $R_e = 3500$  and  $R_e = 4100$ , but under otherwise identical conditions, gave identical results within the experimental uncertainty, indicating that mixing was sufficiently rapid as far as these nucleation experiments were concerned and thus justifying the use of  $R_e \sim 3500$  for all experiments.

With the present apparatus, problems would arise if very much higher  $R_e$  were attempted. Already at  $R_e \sim 3500$ , the Mach number was  $\sim 0.20$ – $0.25$  with the present nozzle size of 1.0-mm. diameter. The cooling upon expansion would become an important correction if the velocity were increased very much more. On the other hand, if a larger nozzle were used, a much higher volume flow rate would be necessary and proper heat exchange would be more difficult to achieve.

"Choking" (41) will occur in the situation where the confined jet receives insufficient mixing gas. This is the phenomenon of back recirculation of the already mixed stream down the sides of the chamber where it is re-entrained in the jet. The effect was clearly observable through the viewing windows with dibutyl phthalate aerosols at low mixing gas flow rates. This was avoided in the experiments by an adequate supply of mixing gas. In the studies here, the nozzle flow was  $\sim 3$  l./min. and the mixing gas flow was about 67 l./min. Therefore choking was essentially absent up

to  $n \sim 22$ . For all experiments in this research, nucleation occurred at  $n \sim 10$ – $12$ , and at  $n \sim 20$  the nucleation rate was negligibly small. Hence, the effects of choking were believed to be negligible.

### C. Materials

There were a number of factors which determined the choice of materials. It was decided to limit the study to liquids since the theory is conveniently applicable to this case only. Furthermore, the following considerations were essential: (a) availability of vapor pressure, surface tension, and density data over the temperature range of interest; (b) stability of the material at about  $200^\circ\text{C}$ .; and (c) sufficiently low volatility so that the aerosol droplets would not evaporate before counting and so that the liquid level in the sample bucket would not change appreciably during the experiment. These limitations narrowed the number of suitable compounds to a few.

Dibutyl phthalate (DBP) was purified according to the procedure recommended by Riddick and Toops (44). Eastman DBP was shaken with water, then with  $0.1\text{ }M\text{ Na}_2\text{CO}_3$ , and several times again with water. The material was then dried, filtered, and distilled at about  $1\text{ mm. Hg}$ . The center cut of  $50\%$  was retained for this work. A spectrophotometric test indicated that the content of phthalic anhydride, which is a thermal decomposition product, was below  $0.02\%$ .

Triethylene glycol (TEG) used in this work was a sample of a specially purified TEG kindly donated by Carbide and Carbon Chemicals Company,<sup>6</sup> which also furnished the vapor pressure equation for TEG.

Octadecane (OCD) of  $99\%$  purity<sup>7</sup> was used directly in the studies. One experiment was carried out with an A.P.I. standard sample<sup>8</sup> of OCD with a  $0.10 \pm 0.08$  mole % impurity specifically to see whether the purity difference was important. Identical results were obtained with the A.P.I. sample and the  $99\%$  OCD within the uncertainty of the experimental error.

The sulfur sample was of commercial grade. Its impurity content was not known but probably  $\text{H}_2\text{O}$ ,  $\text{H}_2\text{SO}_4$ , and organic impurities were present (45).

### D. Procedure

Preliminary experiments established the general procedure which was followed in most cases. Figure 7 shows the light-scattering pulse height distribution curves for DBP and TEG as measured with the counter (16), also a calibrating curve for  $0.81\text{ }\mu$  diameter latex aerosols (16, a). The counter was operated at low aerosol flow rates (16) ( $3$ – $6\text{ c.c./min.}$ ) and was

<sup>6</sup> Carbide and Carbon Chemicals Company, South Charleston, West Virginia.

<sup>7</sup> Humphrey-Wilkenson, Inc., North Haven, Connecticut.

<sup>8</sup> Prepared by the A.P.I. Research Project 6, Carnegie Institute of Technology.



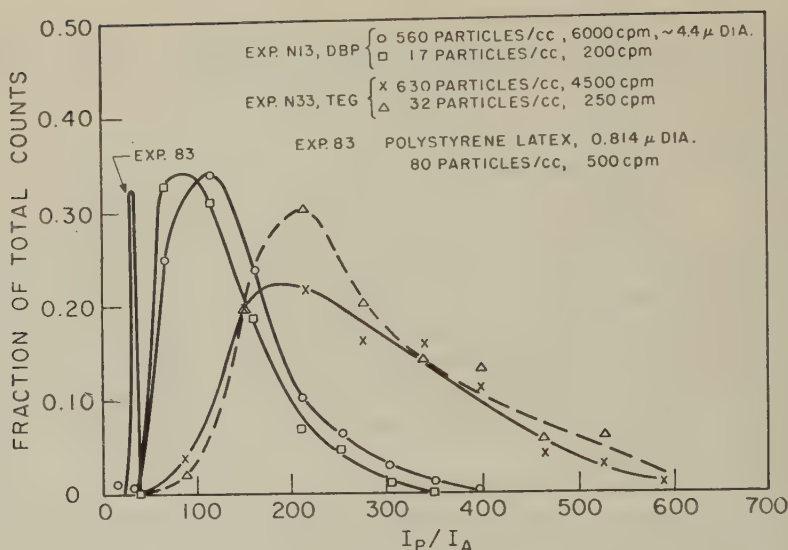


FIG. 7. Light-scattering pulse amplitude distribution. Window widths of  $I_P/I_A$  were 2.4 for Expt. 83, 63 for Expts. N13 and N33. See reference 16, *b* for explanation.

fitted with a low area entrance slit. This accounts for the high  $I_P/I_A$  values compared to the earlier results (16). The mean particle size ( $4 \mu$ ) for the DBP aerosol was determined in a settling apparatus. Because particles this size have appreciable settling rates, the previous counter cell (16, *a*) was remounted (16, *b*) to give a vertical aerosol flow. The two curves for each substance correspond to differing  $T_2$  values and hence to different rates of nucleation. It is clear that the particle signal distributions did not change much when the nucleation rates were changed by factors of about 20 (for TEG) to 30 (for DBP). The curves indicate that the growth did not vary much with nuclei concentration. This was anticipated, since vapor depletion in the nucleation chamber occurred mainly through wall condensation, as indicated by a mass balance calculation. The curves of Fig. 7 also demonstrated that, when the pulse height discriminator (16) was set sufficiently low, all droplets were counted.

A typical run was carried out as follows: With the sample in the bucket all furnaces and thermal regulation units were activated to their predetermined levels. This generally took about 30 min. The carrier nitrogen was then turned on followed by the mixing gas flow. The fluctuation in the  $N_2$  flow rate was about  $\pm 0.5\%$  while for the mixing air it was about 1%. Counting began when all temperatures and flow rates were again steady. The counts were recorded only after the counting rate itself also became steady. The bucket temperature, the nozzle temperature, and  $T_2$

were measured before and after each count. Following a satisfactory series of counts,  $T_2$  was measured at the base of the mixing gas duct where the mixing air entered the nucleation chamber.  $T_2$  was increased, and again after a steady  $T_2$  and a steady count rate were attained (about 5 min. after resetting the thermal regulator), the count rates and the corresponding temperatures were recorded. This was continued over a range of  $T_2$  with the nozzle temperature, the bucket temperature, and the flow rates kept as constant as possible. When the counting was completed, the mixing gas was turned off followed by the stopping of the nozzle flow. The duration of a run was generally about 2 hours. The value of  $p_1$  was calculated from the weight loss of the bucket assuming the perfect gas law. Since there were small variations in the bucket temperature during the experiments (about 0.1–0.2°C.) instantaneous  $p_1$  values were obtained by making a small correction to the mean values by means of a weight loss-bucket temperature calibration curve. An adiabatic correction (46) for the pressure change through the nozzle, amounting to about 4 degrees, was applied to the nozzle temperatures measured with the thermocouple. This corrected value was taken as  $T_1$ .

Evaporation and diffusion losses of the sample during the heating up and cooling down periods in the procedure amounted to less than 1% for the highest bucket temperatures in the DBP experiments. The effect of changes in liquid levels of the bucket on the nucleation rates was unobservable for DBP and TEG and was assumed negligible for the others.

## V. RESULTS AND TREATMENT OF DATA

Although it would have been most convenient to present the data in the form of curves of  $T_2$  versus  $N$ , small variations in  $T_1$  and  $p_1$  during the course of each run made the use of tables more appropriate. The results are presented in Tables I through IV. An experiment was also attempted with phenanthrene, but appreciable nucleation could not be observed under the most favorable conditions.

Four methods of treating the data are described below. The first two procedures for calculating the experimental  $\alpha$  values are of approximate nature. The third and fourth methods involve direct comparisons of Eq. [21] with the data but are somewhat more tedious and are therefore less desirable for examining the gross features of the results.

### A. Method 1

This involves application of Amelin's approximation that essentially all the nucleation is taking place at  $S = S_m$  given by Eq. [11]. Then Eq. [21] with  $A$  given by [4] becomes

$$I = G(p_1/T_m)^2 \exp(-\alpha/T_m^3 \log^2 S_m), \quad [23]$$

TABLE I  
*Dibutyl Phthalate*

Experiment N-25				Experiment N-26			
$T_1(^{\circ}\text{K.})$	$T_2(^{\circ}\text{K.})$	$p_1$ ( $\mu$ Hg)	$N$ (c.c. $^{-1}$ )	$T_1(^{\circ}\text{K.})$	$T_2(^{\circ}\text{K.})$	$p_1$ ( $\mu$ Hg)	$N$ (c.c. $^{-1}$ )
426.04	317.44	713	311	426.61	320.66	864	787
426.42	318.71	710	71.6	426.73	321.18	866	438
426.48	319.64	711	26.6	426.98	321.36	865	352
426.86	320.44	709	10.2	426.98	321.76	867	128
426.73	321.34	710	6.2	426.98	322.29	872	96.2
426.73	321.40	709	6.4	426.98	323.19	875	21.7
426.63	322.49	709	2.8	427.01	323.46	874	13.4
				427.23	324.21	873	4.5
				427.37	324.74	866	4.0
Experiment N-27				Experiment N-28			
$T_1(^{\circ}\text{K.})$	$T_2(^{\circ}\text{K.})$	$p_1$ ( $\mu$ Hg)	$N$ (c.c. $^{-1}$ )	$T_1(^{\circ}\text{K.})$	$T_2(^{\circ}\text{K.})$	$p_1$ ( $\mu$ Hg)	$N$ (c.c. $^{-1}$ )
426.61	320.26	874	1140	426.48	318.31	747	433
426.61	321.06	873	483	426.48	318.69	751	343
426.63	321.63	865	210	426.56	319.41	753	131
426.71	322.09	863	119	426.61	319.76	751	81.5
426.81	322.18	861	77	426.78	320.71	758	23.7
426.88	323.09	861	20.5	426.86	321.91	760	7.5
427.06	323.18	861	15.4	426.88	322.00	760	6.9
427.03	324.31	861	8.3				
427.01	324.54	867	6.8				
Experiment N-30							
$T_1(^{\circ}\text{K.})$	$T_2(^{\circ}\text{K.})$	$p_1$ ( $\mu$ Hg)	$N$ (c.c. $^{-1}$ )				
426.73	312.66	$581 \pm 2$	1350				
426.75	313.14	$581 \pm 2$	665				
426.73	313.79	$581 \pm 2$	272				
426.73	315.29	$581 \pm 2$	92				
426.88	316.29	$581 \pm 2$	32.3				
427.18	317.69	$581 \pm 2$	10.4				
427.11	317.76	$581 \pm 2$	11.5				
427.08	318.69	$581 \pm 2$	4.8				

where  $G$  is a constant. From Eq. [22]

$$N = G(L/F)(p_1/T_m)^2 \exp(-\alpha/T_m^3 \log^2 S_m); \quad [24]$$

$$\log N = \log(GL/F) + 2 \log(p_1/T_m) - \alpha/2.30T_m^3 \log^2 S_m. \quad [25]$$

If the quenching gas and vapor stream flow rates and their temperatures,  $T_2$  and  $T_1$ , are held constant while the vapor pressure  $p_1$  is allowed to



TABLE II  
*Triethylene Glycol*

Experiment N-34				Experiment N-38			
$T_1(^{\circ}\text{K.})$	$T_2(^{\circ}\text{K.})$	$\frac{p_1}{(\mu \text{ Hg})}$	$N \text{ (c.c.}^{-1}\text{)}$	$T_1(^{\circ}\text{K.})$	$T_2(^{\circ}\text{K.})$	$\frac{p_1}{(\mu \text{ Hg})}$	$N \text{ (c.c.}^{-1}\text{)}$
415.91	308.14	1761	338	418.43	311.52	1958	54.8
416.14	308.69	1761	272	418.48	312.38	1946	23.8
416.14	309.24	1766	190	418.58	313.36	1956	9.4
416.19	309.76	1780	182	418.46	314.09	1964	6.0
416.34	310.81	1773	40.2	418.46	314.86	1964	2.6
416.44	312.03	1763	12.6				
416.49	312.76	1766	3.8				
416.58	315.19	1768	0.8				

Experiment N-35				Experiment N-39			
$T_1(^{\circ}\text{K.})$	$T_2(^{\circ}\text{K.})$	$\frac{p_1}{(\mu \text{ Hg})}$	$N \text{ (c.c.}^{-1}\text{)}$	$T_1(^{\circ}\text{K.})$	$T_2(^{\circ}\text{K.})$	$\frac{p_1}{(\mu \text{ Hg})}$	$N \text{ (c.c.}^{-1}\text{)}$
416.51	311.54	2310	578	418.58	310.36	1456	1.9
416.55	312.23	2301	339	418.58	310.66	1469	1.8
416.60	313.00	2294	168	418.61	310.79	1483	1.24
416.65	313.99	2308	80.5				
416.93	315.14	2317	38.4				
416.88	316.04	2315	16				
416.80	317.26	2299	4.6				
416.78	318.46	2289	1.6				

change, maximum supersaturation will be achieved at a temperature  $T_m$  which is constant if the heat capacity of the vapor stream may be considered constant—a good assumption when the vapor concentration is low. Taking derivatives, we find

$$\partial(\log N)/\partial(T_m^3 \log^2 S_m)^{-1} = -T_m^3 \log^3 S_m - \alpha/2.30. \quad [26]$$

Thus  $\alpha$  can be obtained from the slope of the plot of  $\log N$  vs.  $(T_m^3 \log^2 S_m)^{-1}$ .

If the experiments are conducted over a range of  $T_2$  for various  $p_1$ , points of constant  $T_m$  on the constant  $p_1$  curves may be connected to yield curves appropriate to this analysis.

### B. Method 2

In this approximate method only a single experiment is necessary. Contrary to the previous method,  $p_1$  is constant in this case. Differentiating Eq. [25] with respect to  $(T_m^3 \log^2 S_m)^{-1}$ , with  $p_1$  constant,

$$\partial \log N / \partial (T_m^3 \log^2 S_m)^{-1} = -\alpha/2.30. \quad [27]$$

TABLE III  
*n-Octadecane*

Experiment N-45				Experiment N-46			
$T_1(^{\circ}\text{K.})$	$T_2(^{\circ}\text{K.})$	$p_1$ ( $\mu$ Hg)	$N$ (c.c. <sup>-1</sup> )	$T_1(^{\circ}\text{K.})$	$T_2(^{\circ}\text{K.})$	$p_1$ ( $\mu$ Hg)	$N$ (c.c. <sup>-1</sup> )
419.91	309.86	1247	117	420.14	310.56	1502	790
419.44	310.41	1242	34.3	420.04	310.76	1483	318
420.04	311.09	1253	7.0	420.14	310.99	1490	120
420.09	311.78	1260	4.5	420.14	311.63	1507	21.0
420.19	312.29	1256	4.5	420.14	311.98	1504	10.5
				420.14	312.38	1504	6.7
				420.14	313.00	1490	2.1
				420.14	313.56	1491	2.1

Experiment N-47			
$T_1(^{\circ}\text{K.})$	$T_2(^{\circ}\text{K.})$	$p_1$ ( $\mu$ Hg)	$N$ (c.c. <sup>-1</sup> )
420.06	308.39	1092	535
420.06	308.56	1090	244
420.24	308.96	1094	105
420.19	309.44	1090	34.1
420.19	309.89	1098	12.5
420.19	310.19	1098	5.0
420.09	310.84	1088	4.2
420.09	311.83	1105	3.9
420.19	311.94	1105	4.2

TABLE IV  
*Sulfur*

$T_1(^{\circ}\text{K.})$	$T_2(^{\circ}\text{K.})$	$p_1$ ( $\mu$ Hg)	$N$ (c.c. <sup>-1</sup> )
466.9	312.27	871	961
$\pm 0.2$	312.63	871	531
	313.09	865	129.5
	313.69	867	54.0
	314.19	866	44.7
	315.29	860	35.2
	316.56	860	35.5
	318.16	860	35.3
	320.34	862	28.6
	322.56	862	20.2
	325.09	862	11.0

$T_m$  in the third term of Eq. [25] is taken as constant. This is permissible since the term varies very little compared to the last term.

### C. Method 3

This is a more exact method of evaluating  $\alpha$ , and does not involve Amelin's approximation. Knowing the approximate value of  $\alpha$  determined

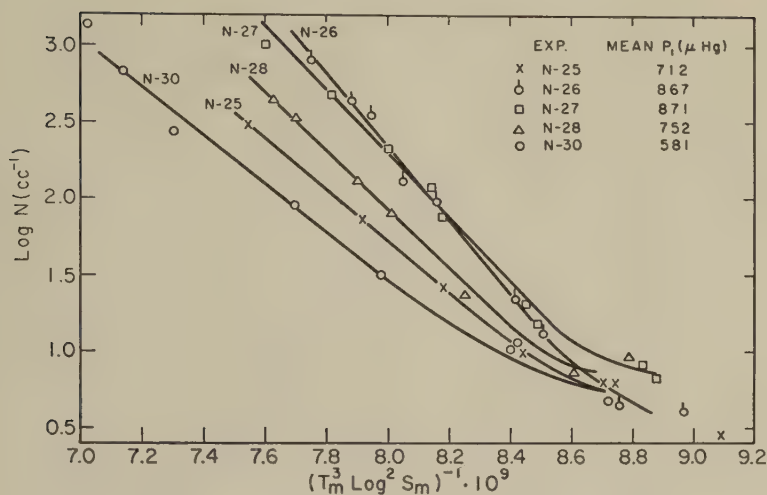


FIG. 8. Droplet concentration for dibutyl phthalate aerosol vs.  $1/T_m^3 \log^2 S_m$ .

by method 1, we can obtain a more exact value by using Eq. [21], the integrations being carried out graphically. The integration is carried out for two values of  $I$ , say  $I_A$  and  $I_B$ , for which  $T_1$  and  $T_2$  are the same but for which the  $p_1$  values are different. Different  $\alpha$  values near the  $\alpha$ 's determined by method 1 are tried until the experimental ratio  $I_A/I_B$  agrees with the calculated  $I_A/I_B$ . The only assumptions in applying this method are that Eq. [21] is applicable and that, over the range of  $T$  and  $S$  values of importance,  $\alpha$  is essentially constant. It can be estimated from the temperature coefficient of surface tension that  $\gamma$  changes around 1.0% over the region of interest so that  $\alpha$  should be constant to around 3% if the theory is applicable in its usual form. This method is more rigorous than methods 1 and 2 based upon Amelin's approximation. The results of method 3 can be used to appraise methods 1 and 2.

#### D. Method 4

All the previous three methods are relative in the sense that they involve the supersaturation *dependence* of the rate of nucleation. Such analyses obviate the use of assumed values for the accommodation coefficient,  $a$ , and the jet factor,  $W$ . Employing Eqs. [22] and [17], with  $W = 6.6 \times 10^{-4}$ , and  $F = 7.0 \times 10^4$  c.c./min., one may obtain an expression for further comparison with theory. By means of graphical integration  $\alpha$  values may be calculated assuming  $a = 1$ , or, conversely, values for  $a$  may be obtained employing the  $\alpha$ 's determined by method 3. Thus, method 4 is a test of the applicability of the theory on an absolute basis.

The data treated by the procedure indicated by methods 1 and 2 are



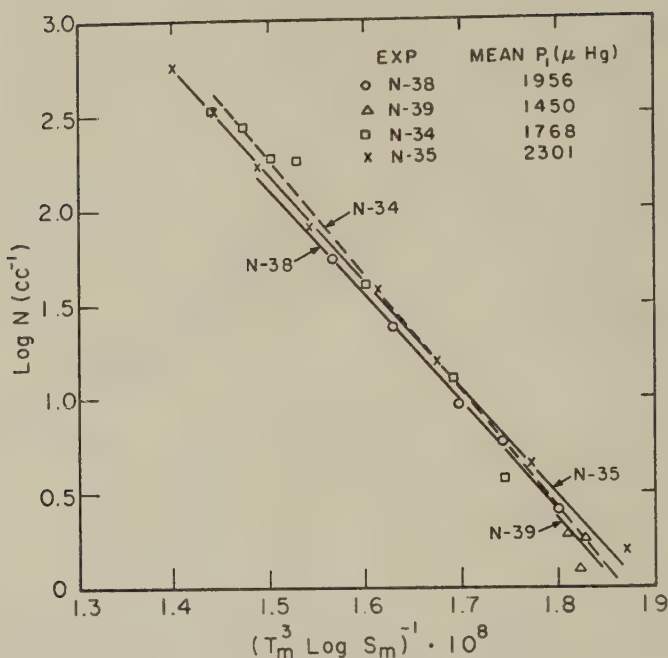


FIG. 9. Triethylene glycol aerosol concentration vs.  $1/T_m^3 \log^2 S_m$ .

plotted in Figs. 8-11. For the calculations,  $a = b = 0.97$ , and the following vapor pressure relations were employed:

For DBP (47),

$$\log P = 10.065 - 1666/T - 547,700/T^2.$$

For TEG<sup>6</sup>

$$\log P = 11.53287 - 2880.31/(T - 50.96).$$

For OCD (48),

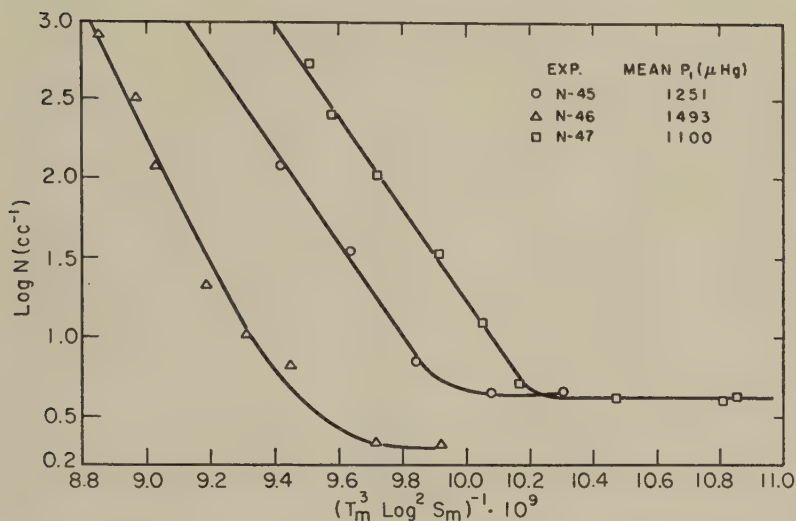
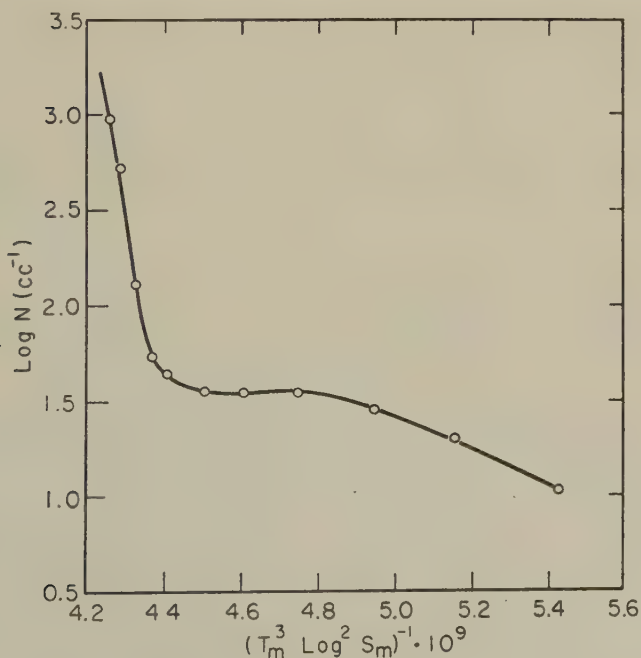
$$\log P = 15.036 - 4730/T.$$

For sulfur (49),

$$\log P = 11.70 - 4055/T.$$

In all cases  $P = \mu$  Hg and  $T = ^\circ\text{K}$ .

The curves for all experiments are practically linear for large  $N$  values consistent with the predictions of the analysis of method 2. In the cases of DBP and OCD the curves level off near the same  $N$  value, indicating condensation of the vapor on a fixed number of centers below the "critical supersaturation" condition. This phenomenon is absent in the case of TEG, suggesting that the heterogeneous nuclei are not active for this substance. On the other hand, in the sulfur experiment the plateau occurred at a much higher  $N$  value, indicating a much higher concentration of nucleating centers.

FIG. 10. *n*-Octadecane aerosol concentration vs.  $1/T_m^3 \log^2 S_m$ .FIG. 11. Sulfur aerosol concentration vs.  $1/T_m^3 \log^2 S_m$ .

In Table V are given  $\alpha$  values calculated by methods 1 and 2 with the data. Where method 1 was applied,  $\alpha$  values were calculated at a  $T_m$  value which was common to all experiments with the particular compound.

Agreement is satisfactory between the two methods for DBP and TEG,

TABLE V  
*Approximate Determination of  $\alpha$* 

Compound	Method	Expt.	$T_m$	$S_m$	$10^{-8} \alpha$
DBP	2 (at $\log N = 2.50$ )	N-25	326.7	89	38
		N-26	330.9	73	56
		N-27	330.9	74	48
		N-28	328.0	83	44
		N-30	322.7	89	37
DBP	1	All expts.	330.0	60-80	$55.5 \pm 2.7$
TEG	2 (at $\log N = 1.50$ )	N-38	323.0	23	13.1
		N-35	326.0	22	13.1
		N-34	321.9	23	14.2
TEG	1	All expts.	322.0	20-30	$11.5 \pm 0.7$
OCD	2 (at $\log N = 2.00$ )	N-45	319.2	64	67
		N-46	320.4	69	94
		N-47	318.3	61	67
OCD	1	All expts.	319	54-72	$37 \pm 9$
Sulfur	2 (at $\log N = 2.50$ )	N-51	324	400	300

although not for OCD. The basic experimental differences between method 1 and method 2 in their present application are that in the former  $S_m$  is varied at essentially constant  $T_m$  by varying  $P_m$ ; whereas in method 2,  $S_m$  is varied by changing  $T_m$  at constant  $P_1$ . Hence, method 1 relies on a change in an experimentally measured quantity whereas method 2 depends upon the accuracy of the temperature coefficient predicted by the particular vapor pressure relation employed. For this reason method 1 should in general be more acceptable. The apparent trend with temperature of  $\alpha$  for DBP determined by method 1 is too large to be explained by the variation in surface tension with temperature (see Eq. [4]). In view of the uncertainty in graphically determining the slopes in some of the experiments with DBP (see Fig. 8), this trend may not be real.

In Table VI the values for  $\alpha$  calculated by methods 3 and 4 are given. In all cases smoothed values of  $I$  taken from Figs. 8-11 were employed, thus avoiding the possibility of using a nonrepresentative set of points. In applying method 4, it was assumed that  $a = 1$  and the bulk liquid densities used in the calculations of  $A$  were those given in the fourth column. The  $T$  values given in the third column correspond to temperatures for the maximum rates in the jet at the particular conditions.  $S$  corresponds to the supersaturation for an appreciable rate. In the calculation of  $A$  for sulfur, the molecular weight of the octamer,  $S_8$ , was employed.

The results of the approximate method 1 (Table V, column 6) are in good agreement with those of method 3 (Table VI, column 7) in the cases of DBP and TEG. This justifies the application of Amelin's assumption (Eq. [11]) in treating nucleation data in turbulent jets.

TABLE VI  
*The  $\alpha$  Values Determined by Eq. [21]*

Compound	Method	$T(^{\circ}\text{K.})$	$\rho$	$S$	$10^{-8} \alpha$ by Eq. [5]	$10^{-8} \alpha$ by Eq. [4]
DBP	3	332	1.014 <sup>a</sup>	70	56	54
	4	332	1.014	70	60	45
TEG	3	324	1.100 <sup>b</sup>	25	12.2	12.0
	4	324	1.100	25	31	25
OCD	4	319	0.764 <sup>c</sup>	63	54	40
	4	324	1.861 <sup>d</sup>	420	92	70

<sup>a</sup> See Reference 50.<sup>b</sup> See Reference 51.<sup>c</sup> See Reference 52.<sup>d</sup> See Reference 53.

TABLE VII  
*Comparison of the Results with the Becker-Doering Theory*

Compound				A according to Eq. [4]				A according to Eq. [5]			
	$T(^{\circ}\text{K.})$	$S_{\text{av.}}$	$\gamma_0$	$\gamma_{\text{rel.}}$	$\gamma_{\text{abs.}}$	$\xi_{\text{rel.}}$	$\xi_{\text{abs.}}$	$\gamma_{\text{rel.}}$	$\gamma_{\text{abs.}}$	$\xi_{\text{rel.}}$	$\xi_{\text{abs.}}$
DBP	332	70	29.4 <sup>a</sup>	27.7 $\pm$ 1.1	26.0	19 $\pm$ 2	16	28.2 $\pm$ 1.1	28.8	19 $\pm$ 2	21
TEG	324	25	42.8 <sup>b</sup>	26.9 $\pm$ 0.8	33.9	11.4 $\pm$ 1	23	27.0 $\pm$ 0.8	36.8	11.6 $\pm$ 1	29
OCD	319	63	26.1 <sup>c</sup>	25 $\pm$ 4	22	27 $\pm$ 10	19	25 $\pm$ 4	24	27 $\pm$ 10	25
S <sub>8</sub>	325	420	67.6 <sup>d</sup>	78	49	43	11	79	54	43	14

<sup>a</sup> Extrapolation of room temperature value (at 24.9 $^{\circ}\text{C.}$ ,  $\gamma_0 = 32.9 \pm 0.2$ ) measured with the Cenco Tensiometer (Ring Method). The relation used was  $\gamma_0 \propto p^4$ .

<sup>b</sup> See reference 51.<sup>c</sup> See reference 52.<sup>d</sup> See reference 54.

## VI. DISCUSSION

### A. Comparison of Experimental Results with the Becker-Doering Theory

The experimental values of the exponential coefficient,  $\alpha$ , can be used to compute  $\gamma$ , the surface free energies of the condensation nuclei, by means of Eq. [7]. With the use of the bulk densities given in Table VI and the  $\alpha$  values given in Tables V and VI, the  $\gamma$ 's were calculated and are given in Table VII, along with the experimental bulk surface tension ( $\gamma_0$ ) values for the liquids. The numbers under the heading "Method" refer to the relative methods (1, 2, or 3) and the absolute method (4). Conservative estimates of the probable uncertainty are given with the  $\gamma_{\text{rel.}}$  values. Where method 3 was applied to obtain an  $\alpha$  (DBP and TEG), that value of  $\alpha$  was used to calculate  $\gamma_{\text{rel.}}$ . In the case of OCD  $\gamma_{\text{rel.}}$  was calculated from the average  $\alpha$  values of methods 1 and 2 (Table V). For sulfur  $\alpha_{\text{rel.}}$  was calculated by the  $\alpha$  determined only by method 2. Also



given in Table VII are the  $g$  values, i.e., the numbers of molecules in the critical nuclei, corresponding to the particular method of calculation;  $S_{av.}$  is the mean value of the supersaturation in the range over which  $\alpha$  was determined.

For DBP, where the greatest effort was made to obtain precise results, it can be seen that the agreement between all the  $\gamma$ 's and  $\gamma_0$  is satisfactory. It seems quite remarkable that with an aggregate of only around 20 molecules the surface free energy should fall so near the bulk value. This might be the result of the near cancellation of the free-energy increments associated with the enthalpy and entropy changes of the surface molecules in going from bulk liquid to the small cluster. At the highly curved interface, the enthalpy should be higher than in the surface of bulk liquid because of the decreased potential energy of interaction, and the entropy might be expected to be larger because of the increased freedom of motion, arising partly from the weakening of the attractive forces. The experimental results presented here are the only indication of surface free energy of small clusters, as it is impracticable to carry out measurements of surface tension by any known technique on droplets small enough to show a measurable change from the bulk value.

In the case of TEG, where the precision was comparable to that of DBP, both the  $\gamma_{rel.}$  and the  $\gamma_{abs.}$  values are below the bulk value by many times the probable error. This contrasts sharply with the relatively good agreement for DBP, and might reflect a fundamental difference with respect to the nucleation process of the hydrogen-bonding substances as compared to "normal" liquids, or it might be the result primarily of the lower number of molecules,  $g_{rel.}$ , in the condensation nucleus. Furthermore, the difference between  $\gamma_{rel.}$  and  $\gamma_{abs.}$  for TEG is much larger than the probable error. Free-energy considerations alone cannot explain these deviations.

As stated above, the precision was relatively poor for the OCD results. Although all the values of  $\gamma$  are close to  $\gamma_0$ , it can be said only that the surface free energy obtained from the nucleation experiments agrees with the bulk value within the estimated precision, which was 15%.

In the case of sulfur only one experiment was carried out. Computations were made considering the vapor as pure  $S_8$ , which is the predominant mole at 50°C. As seen in Table VII, the agreement with theory was reasonable. The species  $S_2$  and  $S_6$ , although they constitute only a few mole per cent (54) at the temperature of the experiment, may assume some importance in the nucleation process. Since the molecular weight appears to the second power in the exponential term (see Eq. [7]) of the Becker-Doering theory, the lower molecular weight species may be quite important even when their concentrations are relatively small. A further possible complication with this substance, as pointed out by Ford and LaMer (49), is that

TABLE VIII  
*Critical Supersaturation for Low Molecular Weight Vapors*

Vapor	$S = p_1/p_\infty$ (measured)	$p_1/p_\infty$ (calcd.)	No. of molecules in stable nucleus	Nucleus radius $r(\text{\AA})$
Water, 275.2°K.	$4.2 \pm 0.1$	4.2	80.0	8.9
Water, 261.0°K.	5.0	5.0	72.0	8.0
Methanol, 270.0°K.	3.0	1.8	32.0	7.9
Ethanol, 273.0°K.	2.3	2.3	128.0	14.2
1-Propanol, 270.0°K.	3.0	3.2	115.0	15.0
Isopropyl alcohol, 256.0°K.	2.8	2.9	119.0	15.2
<i>n</i> -Butyl alcohol, 270.0°K.	4.6	4.5	72.0	13.6
Nitromethane, 252.0°K.	6.0	6.2	66.0	11.0
Ethyl acetate, 242.0°K.	8.6-12.3	10.4	40.0	11.4

the vapor-to-crystal nucleation process may be important. More detailed consideration of the experimental data therefore appeared unjustified.

It has already been pointed out in the Introduction that there are serious theoretical reasons for expecting that the Becker-Doering equation will not be applicable where very small nuclei are involved. Nevertheless, the agreement has been quite good between supersaturation values calculated from the Becker-Doering theory and measured values obtained in cloud-chamber experiments. This is illustrated by the results summarized in Table VIII, which was taken from Pound, Madonna, and Sciulli (13). The agreement between experimental and calculated supersaturation values was good except for methanol, and in that instance good agreement was obtained with the Becker-Doering theory by Franck and Hertz in their recent work (28). However, since all the cloud-chamber results involve approximations for the pre-exponential factor, their agreement with theory may be considered fortuitous. In this research, where the exponential factor was obtained independently of such estimates, there was agreement with the Becker-Doering theory within experimental error for DBP, even though this compound has a higher molecular weight, a higher  $S$ , and a lower  $g$  than any substance in Table VIII. This lends support to the suggestion that the Becker-Doering equation is a useful approximation even when macroscopic values of  $\gamma$  are employed. It is interesting that reasonably good agreement with the theory was obtained in this study with DBP, which has a higher molecular weight, a higher  $S$ , and a lower  $g$  than any of the substances listed in Table VIII. This suggests that the agreement with the Becker-Doering theory is not purely fortuitous.

Thus, it appears that TEG is the only substance for which the nucleation rate is grossly different from that predicted by the Becker-Doering

theory. For this material the number of molecules  $g_{rel.} = 11.5 \pm 1$  appears to be the lowest ever reported for a critical nucleus. It seems quite reasonable that a change in the surface free energy of the order observed would be found where the critical nucleus consists of so few molecules. If we consider the nucleus to be 13 molecules, symmetrically disposed, then we may visualize it as a central molecule surrounded by 12 closely packed nearest neighbors. Here most of the molecules are in the surface, and one would certainly expect a significant departure from the macroscopic surface free energy.

Benson and Shuttleworth (55) have made some computations on the surface energy of a cluster of 13 molecules with van der Waals type interactions at 0°K. They found that the surface energy decreased about 15% or less from that of the infinite crystal. It is interesting that the calculation on the basis of so simple a model is roughly in accord with our experimental observations. Shuttleworth also found that the density of the cluster was about 6% less than that of the infinite crystal, mainly because of the decrease in density associated with the first layer. Since this density change is roughly the order of the decrease in density upon melting most crystalline substances, our use of bulk-liquid density should be a reasonably good approximation for the cluster.

Triethylene glycol (TEG) has a rather high surface energy (enthalpy) for an organic liquid. Its value of 72 ergs/cm.<sup>2</sup> at room temperature is much higher than the 54 ergs/cm.<sup>2</sup> reached in the fatty acid series or the 53 ergs/cm.<sup>2</sup> for *n*-octadecane (OCD). Gallaughier and Hibbert (51) suggest that this high value is due to the stronger and more specific nature of the interactions in TEG. They propose that the TEG molecule is probably oriented as an inverted U at the surface with the OH groups anchoring the molecule in the interior. They base this last statement on the observations that the surface energy of 72 ergs/cm.<sup>2</sup> becomes constant in the polyethylene glycol series at TEG, suggesting that only the ethylene oxide groups are at the surface and that the value of 72 ergs/cm.<sup>2</sup> is very close to the surface energies of ethylene oxide and 1,4-dioxane. This is a further indication that the small cluster observed with TEG cannot be regarded as a disordered aggregate of molecules resembling closely the properties of the bulk liquid.

There appear to be no estimates of surface entropies for small clusters. In addition to the configurational entropy of the surface molecules, it has been pointed out (56, 57) that one should include an entropy term due to the translational and rotational motions of the cluster as a whole. Rodebush (56, 57) showed that this term becomes more important as the size of a cluster decreases. At the present time it cannot be stated how important the gross motions of the cluster are compared to variation of the surface entropy with radius, and how large the entropy term may be in

comparison with the enthalpy term in determining the deviation of surface free energies of the condensation nuclei from bulk values.

Thermodynamic and statistical mechanical considerations (7-11, 58) suggest that the surface free energy should decrease with decreasing droplet radius. This is in accord with observations (see Table VII) for both DBP and TEG.

As stated earlier, it was assumed that the accommodation coefficient,  $a$ , was unity in calculating  $\alpha$  (and hence,  $\gamma_{\text{abs.}}$ ) by method 4. It therefore appears (see Table VII) that this assumption was essentially valid in the cases of DBP, OCD, and probably sulfur within the uncertainty of their respective probable experimental errors, as the agreement between  $\gamma_{\text{rel.}}$  and  $\gamma_{\text{abs.}}$  is satisfactory in these instances. In view of the fact that  $a$  cannot exceed unity, the  $A$  value given by the more exact equation [5] is more consistent with the results on DBP and OCD, although for the latter the uncertainty in the results is greater than the discrepancy between  $a = 1$  and the  $a$  value consistent with Eq. [4]. The better agreement of Eq. [5] with the results for DBP gives further support to kinetic aspects of the model underlying the theory.

The large discrepancy between  $\gamma_{\text{rel.}}$  and  $\gamma_{\text{abs.}}$  for TEG can be resolved by assuming a very small  $a$  value of ca.  $10^{-8}$  to ca.  $10^{-10}$ . Gallaughier and Hibbert (51) have postulated that TEG has a highly ordered surface structure. If the TEG molecules have to get into a very special arrangement on the surface to form hydrogen bonds with OH groups in the interior, one would expect the sticking probability to be low. Wyllie (59) has reported a value of 0.052 for the accommodation coefficient of glycerol, which is certainly a strongly hydrogen-bonding molecule, whereas it is known (59) that for most normal liquids the accommodation coefficient is about unity. Thus, it is possible that a very low accommodation coefficient may account for the results with TEG. The serious disagreement between  $\gamma_0$  and  $\gamma_{\text{rel.}}$  seems to reflect the inadequacy of the theory for TEG, apart from the anomalous value of the accommodation coefficient.

### *B. Heterogeneous Nucleation*

A very small amount of  $\text{H}_2\text{SO}_4$  vapor was found to affect tremendously the necessary conditions for DBP aerosol formation. When the carrier gas was passed over (not bubbled through) concentrated  $\text{H}_2\text{SO}_4$  in a flask (16), following the procedure of LaMer and Gordieyeff (60), Corbeil and Gendron (61), nucleation occurred at a low supersaturation value ( $S_m = 0.9 \pm 0.5$ ). This is to be compared with supersaturations between 60 and 80 which were necessary for DBP homogeneous nucleation. In view of this, one must consider possible sources of foreign nuclei in the experiments.

Foreign nuclei may originate in the flow system. These may be dust



particles in the flow line itself, natural ions, or impurities in the nitrogen and compressed air sources that have escaped the filters. It is believed that in the experiments on DBP and OCD (see Figs. 8 and 10) the plateaus observed at low  $N$  values ( $N < 10$ ) are caused by those nuclei originating somewhere in the flow system.

Foreign nuclei may also arise from impurities in the sample or from decomposition of the sample. The experiment on sulfur (Fig. 10) may provide an example of this type of heterogeneous nucleation. The plateau is very much higher than those in the DBP or OCD experiments. The gradual sloping off at lower supersaturation values suggests a spread or distribution of efficiencies of nuclei which might be associated with a distribution of sizes of very small nuclei.

It is interesting that TEG had no plateau (Fig. 8). The foreign nuclei that were effective in the cases of DBP and OCD may be insufficiently wetted by TEG, which has a much greater surface tension than the other two liquids. This might arise from the same hydrogen-bonding properties believed to be responsible for a low accommodation coefficient with TEG.

### *C. Some Additional Considerations of the Turbulent Jet Technique*

1. *Time Lag in Nucleation.* The axial jet velocity in the region of nucleation, i.e.,  $n \sim 10$ , is about 8 m. per second. From an examination of Fig. 2, which is to scale, it is calculated that from  $n = 10$  to  $n = 11$  the distance is about 0.5 cm. for a 1-mm. diameter nozzle. The jet then traverses a region  $\Delta n = 1$  in about  $6 \times 10^{-4}$  sec. Collins (62) has derived an approximate time-dependent nucleation rate expression following the Frenkel (3) formulation. He found an equation for the relaxation time,  $\tau$ , for the attainment of the steady-state distribution of clusters. Inserting numerical values for a representative case, DBP at  $T = 334^\circ\text{K}$ .,  $M = 278$ , density = 1.01 g./c.c.,  $\gamma = 28$ ,  $p_1 = 0.87$  mm. Hg, and  $g = 20$ , we found  $\tau = 9 \times 10^{-6}$  sec. Since this is short compared to the transit time obtained above, it appears that the steady-state nucleation rates were very closely approached in the jet.

2. *Depletion Effects.* Because in the jet the nuclei are removed rapidly from the region of nucleation, and the experiments were carried out at low particulate concentrations, in contrast to the expansion cloud-chamber methods, the concentration is practically unaffected in the region of appreciable nucleation rates. Thus, the above treatment required no corrections for depletion. Similarly, the temperature rise due to condensation was negligible. Under the conditions employed by Amelin (31), who obtained a dense cloud, a more complicated analysis might be necessary.

3. *Fluctuations in the Jet.* Baron (37) has discussed temperature fluctuations in jets in connection with the possibility of studying a chemical reaction. As quantitative data are not available on these fluctuations,

corrections cannot be applied. Experiments of Corrsin (35, 36) indicate that for  $n$  around 10, and under the conditions of the experiments of this research, the maximum high-frequency temperature fluctuations may be of the order of  $1^{\circ}\text{C}$ ., which correspond to supersaturation fluctuations of  $\pm 8\%$ . About 30% of this effect is offset by the  $T^3$  term in the nucleation rate expression. Fluctuations should increase the absolute rate of production of nuclei but should not greatly affect the values of  $\gamma$  obtained by the relative rate method.

#### ACKNOWLEDGMENTS

This research was supported by the Office of Naval Research, and in its later stages some additional support was obtained through a Grant-In-Aid of the California Research Corporation.

We are happy to acknowledge the collaboration of Dr. George J. Doyle and Dr. Moshe D. Bitron in preliminary work regarding the choice of experimental method; in particular, we wish to thank Dr. Bitron for calling Amelin's work to our attention and for assisting in the exploration of flow methods. We also wish to thank Dr. Sonya Krause for help in evaluation of the literature concerning the cloud-chamber method.

#### REFERENCES

1. BECKER, R., AND DOERING, W., *Ann. Physik* **24**, 719 (1935).
2. VOLMER, M., "Kinetik der Phasenbildung." Edwards Bros., Ann Arbor, Michigan, 1945.
3. FRENKEL, J., "Kinetic Theory of Liquids," Ch. 7. Dover Publications, New York, 1955.
4. FARLEY, F. J. M., *Proc. Roy. Soc. (London)* **A212**, 530 (1952).
5. BARNARD, A. J., *Proc. Roy. Soc. (London)* **A220**, 132 (1953).
6. REISS, H., *Ind. Eng. Chem.* **44**, 1284 (1952).
7. TOLMAN, R. C., *J. Chem. Phys.* **16**, 758 (1948); *ibid.* **17**, 333 (1949).
8. KIRKWOOD, J. G., AND BUFF, F. P., *J. Chem. Phys.* **17**, 338 (1949).
9. BUFF, F. P., *J. Chem. Phys.* **19**, 1591 (1951).
10. KOENIG, F. O., *J. Chem. Phys.* **18**, 449 (1950).
11. HILL, T. L., *J. Chem. Phys.* **20**, 141 (1952).
12. SHUTTLEWORTH, R., *Proc. Phys. Soc. (London)* **A63**, 44 (1950).
13. POUND, G. M., MADONNA, L. A., AND SCIULLI, C. M., "Proceedings of the Conference on Interfacial Phenomena and Nucleation," Vol. 1, p. 85. Office of Technical Services U. S. Dept. of Commerce (U. S. Air Research and Development Command) Cambridge, Massachusetts, 1955.
14. VOLMER, M., AND FLOOD, H., *Z. physik. Chem.* **A170**, 273 (1934).
15. BRADLEY, R. S., *Quart. Revs. (London)* **5**, 315 (1951).
16. (a) O'KONSKI, C. T., AND DOYLE, G. J., *Anal. Chem.* **27**, 694 (1955); (b) O'KONSKI, C. T., BITRON, M. D., AND HIGUCHI, W. I., *Proc. A.S.T.M. Symposium on Instrumentation*. Boston, June, 1958. In press.
17. O'KONSKI, C. T., Kinetics of Gas Phase Nucleation, Final Report, Office of Naval Research, Contract No. ONR 222-12, Proj. No. NR 051-302, Jan. 1, 1958. Department of Chemistry, University of California, Berkeley, California.
18. WILSON, C. T. R., *Phil. Trans. Roy. Soc.* **A189**, 265 (1897); *Proc. Roy. Soc. (London)* **A87**, 277 (1912).
19. SCHARER, L., *Ann. Physik* **35**, 617 (1939).

20. LABY, T. H., *Phil. Trans.* **A208**, 445 (1908).
21. POWELL, C. F., *Proc. Roy. Soc. (London)* **A119**, 553 (1928).
22. MASON, B. J., *Proc. Roy. Soc. (London)* **B64**, 773 (1951).
23. CORNER, J., *Proc. Roy. Soc. (London)* **A211**, 417 (1952).
24. BRITTON, D., DAVIDSON, N., AND SCHOTT, G., *Discussions Faraday Soc.* **17**, 58 (1954).
25. WILSON, J. G., "Principles of Cloud Chamber Technique." Cambridge University Press, London, 1951.
26. SINCLAIR, D., "Handbook on Aerosols," Ch. 6. U. S. Atomic Energy Commission, 1950.
27. VAN DE HULST, H. C., "Light Scattering by Small Particles." Wiley, New York, 1957.
28. FRANCK, J. P., AND HERTZ, H. G., *Z. Physik* **143**, 559 (1956).
29. LANGSDORF, A., *Ind. Eng. Chem.* **44**, 1298 (1952).
30. COWAN, E. W., *Rev. Sci. Instr.* **21**, 991 (1950).
31. AMELIN, A. G., *Kolloid. Zhur.* **10**, 169 (1948).
32. HOTTEL, H. C., "Production of Smoke of Controlled Size by the Use of Induction Nozzles." OSRD No. 468, January 12, 1942. Microfilm available U.S.D.A. library, Washington 25, D. C. See also reference 37.
33. PAI, S., "Fluid Dynamics of Jets." Van Nostrand, New York, 1954.
34. BARON, T., AND ALEXANDER, L. E., *Chem. Eng. Progr.* **47**, 181 (1951).
35. CORRSIN, S., AND UBERROI, M., N.A.C.A. Tech. Note No. 1865, April, 1949.
36. CORRSIN, S., AND UBERROI, M., N.A.C.A. Report 998, 1950.
37. BARON, T., *Chem. Eng. Progr.* **50**, 73 (1954).
38. HOTTEL, H. C., Fourth Symposium on Combustion, Paper No. 9. Williams and Wilkins, Baltimore, Maryland, 1953.
39. ALEXANDER, L. G., COMINGS, E. W., GRIMMETT, H. L., AND WHITE, E. A., *Chem. Eng. Progr. Symposium Ser.* **50**, 93 (1954).
40. O'KONSKI, C. T., AND HIGUCHI, W. I., *J. Phys. Chem.* **60**, 1598 (1956).
41. ALEXANDER, L. G., KIVNICK, A., COMING, E. W., AND HEINZE, E. D., *Am. Inst. Chem. Eng.* **1**, 74 (1955).
42. LANGSTROTH, G. O., AND GILLESPIE, T., *Can. J. Chem.* **29**, 201 (1951).
43. LEWIS, B., AND VON ELBE, G., "Combustion, Flames, and Explosions," p. 495. Academic Press, New York, 1951.
44. RIDDICK, J. A., AND TOOPS, E. E., JR., "Organic Solvents," 2nd ed., Vol. 7 of "Technique of Organic Chemistry," edited by A. Weissberger. Interscience Publishers, New York, 1955.
45. BACON, R. F., AND FANELLI, R., *J. Am. Chem. Soc.* **65**, 639 (1943).
46. KEENAN, J. H., AND KAYE, J., "Gas Tables." Wiley, New York, 1948.
47. SMALL, P. A., SMALL, K. W., AND COWLEY, P., *Trans. Faraday Soc.* **44**, 810 (1948).
48. BRADLEY, R. S., AND SHELLARD, A. D., *Proc. Roy. Soc. (London)* **A198**, 239 (1949).
49. FORD, G. P., AND LAMER, V. K., *J. Am. Chem. Soc.* **72**, 1959 (1950).
50. KEMPPINEN, A. I., AND GORKIEN, N. A., *J. Phys. Chem.* **60**, 126 (1956).
51. GALLAUGHER, A. F., AND HIBBERT, H., *J. Am. Chem. Soc.* **59**, 2515 (1937).
52. "Selected Values of Physical and Thermodynamic Properties of Hydrocarbons and Related Compounds," A.P.I. Project 44, p. 337. Carnegie Press, Pittsburgh, Pennsylvania, 1955.
53. KELLAS, A. M., *J. Am. Chem. Soc.* **113**, 903 (1918). Extrapolation of the data.
54. TULLER, W. N., "The Sulfur Data Book." McGraw-Hill, New York, 1954. Extrapolation of high-temperature data.
55. BENSON, G. C., AND SHUTTLEWORTH, R., *J. Chem. Phys.* **19**, 130 (1951).

56. RODEBUSH, W. H., *Proc. Natl. Acad. Sci. U.S.* **40**, 789 (1954).
57. RODEBUSH, W. H., *Ind. Eng. Chem.* **44**, 1289 (1952).
58. BUFF, F. P., *J. Chem. Phys.* **23**, 419 (1955); *ibid.* **25**, 146 (1956).
59. WYLLIE, G., *Proc. Roy. Soc. (London)* **A197**, 383 (1949).
60. LAMER, V. K., AND GORDIYEFF, V. A., Progress Report No. 3, Contract AF 19 (122)-164.
61. GENDRON, P. R., Contract AF 19 (122)-380, May 31, 1954.
62. COLLINS, F. C., "Proceedings on the Conference on Interfacial Phenomena and Nucleation," Vol. 1, p. 163. Office of Technical Services, U.S. Dept. of Commerce, (U.S. Air Research and Development Command) Cambridge, Massachusetts, 1955.



## DYNAMIC MECHANICAL AND CREEP PROPERTIES OF A 23% CELLULOSE NITRATE SOLUTION; ANDRADE CREEP IN POLYMERIC SYSTEMS

Donald J. Plazek<sup>1</sup>

*Department of Chemistry, University of Wisconsin, Madison, Wisconsin*

*Received January 7, 1959; revised May 15, 1959*

### INTRODUCTION

Although numerous studies have recently been made on the time-dependent mechanical properties of crystalline polymers, little information has been available on polymeric gels with a low degree of crystallinity (1-3); and in particular the changes in those properties as this type of system passes through the melting point have not been studied in detail. With this fact in mind the dynamic mechanical and creep properties of a 23% solution of cellulose nitrate in diethyl phthalate were extensively measured. Past experience and knowledge of solutions of cellulose derivatives suggested that this system would form a crystalline gel reasonably near room temperature. Since the degree of nitration of the polymer was not complete (there remained one hydroxyl residue for every three chain units), it was expected that the amount of crystallization would be small. It will be seen that the mechanical property results can be interpreted as reflecting a low degree of crystallinity at the lower temperatures of measurement, but that some other physical property measurements do not indicate the presence of crystallinity.

It has been pointed out (4) that many systems which are known to possess randomly distributed strong or weak centers deform under constant stress in a manner described by an equation originally proposed by Andrade (5, 6). Cellulose nitrate, which is well known to be polycrystalline, deforms in such a manner (7). The measurements being reported here not only show that the behavior of the solution of cellulose nitrate in diethyl phthalate is described by a form of the Andrade equation at the temperatures where crystallization is suspected, but also at higher temperatures, where the solution is completely amorphous.

### MATERIALS

Both the diethyl phthalate (DEP) and the cellulose nitrate (CN) were obtained from Allegany Ballistics Laboratory through the kind assistance

<sup>1</sup> Union Carbide and Carbon Fellow in Physical Chemistry, 1955-56. Present address: Mellon Institute, Pittsburgh, Pennsylvania.

of Dr. Seymour Newman. The DEP was used as received. The nitrogen content of the cellulose nitrate (lot X205) was reported to be 12.6%. A rough head-and-tail fractionation was carried out on the CN, primarily for purification. Precipitation from a 1 per cent acetone solution was accomplished with the dropwise addition of *n*-heptane. The center cut which was used in this study was then dried in a vacuum oven at 50°C. for 12 hours.

The intrinsic viscosity of the sample at the onset of the mechanical measurements was measured in ethyl acetate at 25.0°C. and was found<sup>2</sup> to be 3.7 dl./g. Two years later, just before the final series of measurements, a check on the intrinsic viscosity showed it to be 3.4 dl./g. with a Huggins constant of 0.34. Such a slight decrease was judged insufficient to appreciably affect the mechanical properties. Later, loss tangent results, which are independent of sample coefficient, bore out this conclusion. The number-average molecular weight was determined<sup>3</sup> from osmotic pressure measurements in ethyl acetate at 25.0°C. to be 94,000. The thermodynamic coefficient  $A_2$  was  $9.0 \times 10^{-4}$  cm.<sup>3</sup> mole g.<sup>-2</sup>, which is in the range previously reported for CN samples of higher nitrogen content (8, 9).

The solution of CN in DEP, 23.0% by weight of polymer, was mixed by slowly rotating a sealed flask, which contained the CN and DEP and a Teflon-covered stirring bar, between the poles of a large permanent magnet. During the mixing, which took about one week, the flask was heated to about 50°C. with an infrared lamp. This procedure was deemed safe because intrinsic viscosity measurements on a similar solution were the same before and after mixing. This stock solution was then stored at -5°C. to inhibit degradation.

The specific volume,  $\bar{v}$  (0.830 cm.<sup>3</sup>/g.), at 25.0°C. and the thermal expansion coefficient,  $\alpha$  ( $7.4 \times 10^{-4}$  deg.<sup>-1</sup>), above the glass temperature,  $T_g$ , used for the 23% solution were interpolated from dilatometric measurements on the CN-DEP system made in this laboratory by Dr. Marcel N. Vrancken (10) on the same original stock. An interpolated value of  $T_g$  was found to be -87°C., which is very near the minimum in the  $T_g$ -concentration curve.

## METHODS

The double transducer of Fitzgerald and Ferry (11) was used for measurements of the dynamic shear moduli at frequencies,  $\nu$ , between 10 and 2800 cycles/sec. at 14 temperatures from -47° to 35°C. Dynamic shear moduli were also measured in a freely damped torsion pendulum (12) from 0.06 to 11 cycles/sec. at 10 temperatures between -25° and 35°C. Torsional creep and recovery measurements were carried out in the above

<sup>2</sup> This measurement was made by David W. Carlson.

<sup>3</sup> The latter intrinsic viscosity measurement mentioned and the osmotic pressure measurements were carried out by Kazuhiko Ninomiya.

instrument by removing the inertial arms and imposing the stress on the sample by twisting the support wire through a known angle. Creep runs were made at 10 temperatures extending from  $-33^{\circ}$  to  $25^{\circ}\text{C.}$ , and the recovery was measured after the cessation of most of these runs.

## RESULTS

### *Double Transducer*

Three pairs of disc-shaped samples, 1, 2, and 3, with the approximate dimensions of  $1\frac{1}{16}$  in. diameter and  $\frac{1}{8}$  in. height, were measured in the double transducer. Most of the data in the region of the rubberlike to glasslike transition were obtained from samples 1; but upon their removal from the instrument it was obvious from their distorted appearance (caused by air which had been trapped at the sample-instrument interfaces) that the sample coefficient and hence the absolute magnitude of the data were incorrect. The yellow solution, the consistency of which at room temperature is reminiscent of a honey with a very high viscosity, is difficult to handle. Samples 2 also failed to maintain their shape. Finally results the absolute magnitude of which could be trusted were obtained from samples 3.

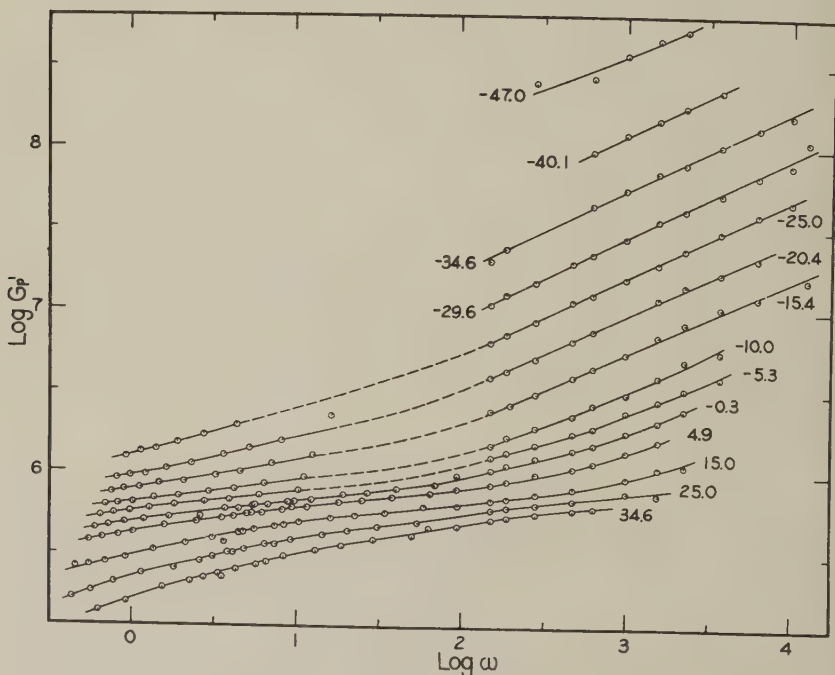


FIG. 1. Real part of the complex dynamic shear modulus plotted logarithmically against radial frequency, at 14 temperatures as indicated. Data at left, from torsion pendulum; at right, from transducer. The modulus (units dynes/cm.<sup>2</sup>) has been reduced by the factor  $T_{0\rho_0}/T\rho$  ( $T_0 = 298.2^{\circ}\text{K.}$ ).

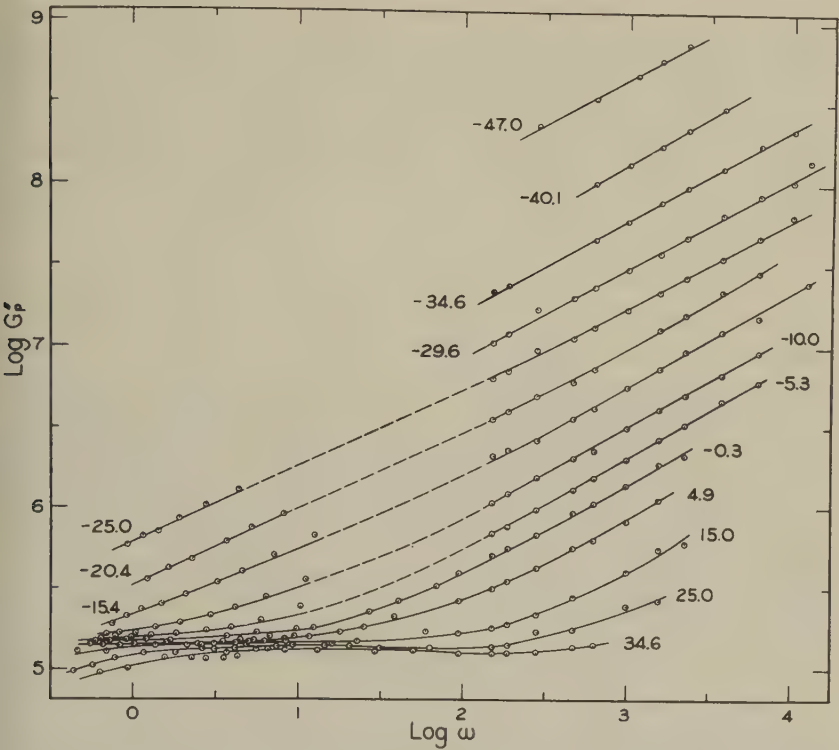


FIG. 2. Imaginary part of the complex dynamic shear modulus, reduced and plotted as in Fig. 1, at the temperatures indicated.

After the application of empirical correction coefficients to samples 1 and 2 of 18% and 11%, respectively, the results were averaged where temperatures were duplicated. The details of measurement and the establishment of the sample coefficients for these samples are given elsewhere (13). The averages in the form of the real component,  $G_p'$  (storage modulus), and the imaginary component,  $G_p''$  (loss modulus) of the complex dynamic rigidity,  $G_p^*$  (dynes/cm.<sup>2</sup>), are plotted logarithmically against the logarithm of the angular frequency,  $\omega$  (sec.<sup>-1</sup>,  $2\pi\nu$ ), in Figs. 1 and 2, respectively. The subscript  $p$  indicates that reduction to 25°C. has been made as follows:

$$G_p = (T_0\rho_0/T\rho)G, \tag{1}$$

where  $\rho_0$  is the density at the reference temperature  $T_0$  (298.2°K.) and  $\rho$  the density at the temperature of measurement,  $T$ . The measurements at the various temperatures describe the behavior of the system in the "rubbery plateau" and much of the glasslike to rubberlike transition. The highest moduli measured are still more than an order of magnitude less than the usual glassy modulus (about  $10^{10}$  dynes/cm.<sup>2</sup>).

Before the last of the mechanical measurements were made, another



pair of samples, 5, were measured in the transducer to ascertain further if appreciable degradation had occurred in the stock solution in the elapsed time of two years since its preparation. The loss tangents,  $G''/G'$ , obtained, which are molecular weight dependent at low frequencies, confirmed the conclusion drawn from the intrinsic viscosity measurements. They were indeed higher than the original measurements but only a shade beyond experimental error.

### *Torsion Pendulum, Dynamic*

The low-frequency dynamic data presented here were obtained from measurements on two samples, 6 and 7, in the torsion pendulum. Their approximate dimensions were: 6, diameter, 2 in. and height,  $\frac{1}{32}$  in.; 7, diameter,  $1\frac{1}{8}$  in. and height,  $\frac{5}{32}$  in. The calculated sample coefficient for sample 6 was not expected to be correct, because of its pancake shape. Hence the five runs made on sample 6 were empirically matched to the corresponding runs of sample 7, overlapping for  $\frac{1}{3}$  of a logarithmic decade. The shift was equivalent to a 30% increase in the moduli. A further increase of 20% was necessary to bring the combined curves of 6 and 7 into coincidence with the accepted averages of the double transducer results. Imperfect surface adhesion for sample 7 had been observed, and the shift though larger than expected is still reasonable. The resulting moduli are also plotted in the fashion as mentioned previously, in Figs. 1 and 2; the torsion pendulum data are shown at values of  $\log \omega$  less than 2.0. Temperatures are indicated and the pip direction serves as identification in later graphs.

### *Aging Study*

The first studies in the double transducer indicated that the measured mechanical properties of the 23% CN-DEP solution were independent of thermal history, i.e., there were no observable aging effects. Changes due to aging might have occurred in the first 2 to 3 hours that it took to attain thermal equilibrium, but thereafter the data were reproducible as measured in check runs above and below the estimated melting point. Since it was desired that characteristic quantities be measured and since the storage modulus of a cellulose nitrate-isophorone gel<sup>4</sup> was shown (9) to have increased linearly with time over 400% in the first 23 hours after cooling below the gel melting point, special check runs were made in the torsion pendulum at three temperatures below ( $-19^\circ$ ,  $-5^\circ$ , and  $0^\circ\text{C.}$ ), and one above ( $25^\circ\text{C.}$ ), the assuming melting point. Dynamic measurements were made soon after thermal equilibrium was established, after which the sample

<sup>4</sup> The polymer was appreciably closer to the trinitrate (nitrogen content = 13.8%) than the present sample and therefore the amount of crystallinity was certainly greater.

was allowed to remain at the fixed temperature for a period of from one to three days. The dynamic measurements were then repeated, and the logarithmic decrements and frequencies were found in all cases to check within experimental error. It is possible to detect and distinguish changes in sample character and shape because changes in the loss tangent, which is independent of the sample coefficient, reflect only changes in the sample character, such as degradation or aging, and the frequency changes reflect both. The dynamic check runs just mentioned and others before and after creep runs all indicate that the properties of the sample were fixed and unambiguous.

### *Analysis of Dynamic Results*

A necessary requirement that the time shifts,  $\log a_T$ , represent the temperature behavior of the mechanical properties of a system and the processes yielding such behavior is that the same shift reduce to a single composite curve any and all of the time-dependent mechanical property measurements (14, 15). Two examples of the kinds of systems that do not always adhere to established reduction principles are those which exhibit changes in thermodynamical character with temperature, e.g., occurrence of phase changes (16), and those in which processes having different temperature behaviors appreciably contribute in varying measurable degrees to the intensive property being investigated (17).

Since crystallization was expected at lower temperatures in the solution being studied, it was not surprising that reduction failed at  $-10^\circ\text{C}$ . and below, i.e., the necessary horizontal shifts to obtain superposition for the moduli in Figs. 1 and 2 were different. The deviation for  $-10^\circ\text{C}$ . is not serious since it is just outside the limits of experimental scatter. It will be seen later that the melting point is believed to be appreciably higher than  $-10^\circ\text{C}$ ., but since other crystalline gels in the past have proved to be amenable to reduction (the crystalline phase presumed to be small or at least constant with temperature), no conflict with the above statements need arise.

The following equation of WLF form (15) was established from the seven highest temperatures of measurement,  $T$  in  $^\circ\text{K}$ :

$$\log a_T = -\frac{8.48(T - 298.2)}{165.5 + (T - 298.2)} \quad [2]$$

Because further analysis and comparison will be made with the creep compliance curves, the data in Figs. 1 and 2 were first transformed into their complex reciprocals the real,  $J_p'$  ( $\text{cm}^2/\text{dyne}$ ), and imaginary,  $J_p''$ , components of the complex dynamic compliance,  $J_p^*$ , and their logarithms are plotted against the logarithm of the frequency reduced to  $25^\circ\text{C}$ .,  $\omega a_T$ , in Figs. 3 and 4.

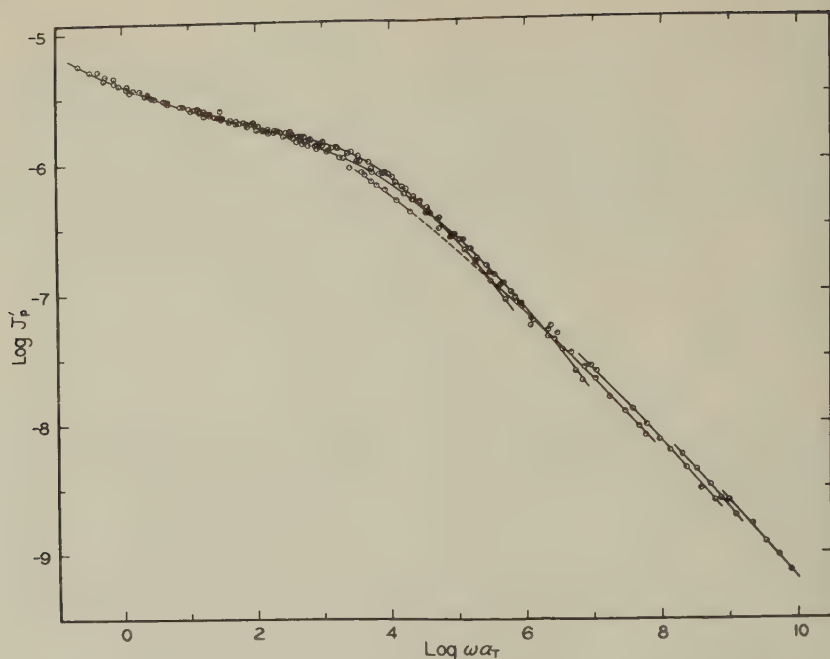


FIG. 3. Real part of the complex shear compliance (units  $\text{cm}^2/\text{dyne}$ ), reduced to  $25^\circ\text{C}$ . and plotted logarithmically against reduced frequency with shift factors calculated from the WLF equation. Temperature key to pips same as in Fig. 1.

It can be seen in Fig. 3 that the  $\log J'_p$  curves below  $-10^\circ\text{C}$ . do not fall on a single composite curve.<sup>5</sup> The deviations are such as to indicate that the glasslike to rubberlike transition is broadened in quite the same manner as has been observed in the past in systems having differing amounts of crystallinity (1, 2). Although the temperature range of successful superposition is not so large as usual, the fairly large frequency range (about four logarithmic decades) at each temperature enables the test of reduction to be a severe one and leaves little doubt about its correctness.

The same conclusions can be drawn from the  $\log J''_p$  data in Fig. 4, although the deviations from superposition appear to be much smaller, the broadening being only readily apparent for the lower temperature measurements which extend into the region of the peak. In this region the  $-25^\circ$  and  $-20^\circ\text{C}$ . results are represented by the dashed lines. The  $-15^\circ$  and  $-10^\circ\text{C}$ . curves (not shown) indicate the same but smaller deviations. The lower temperature results appear to reduce satisfactorily at high reduced frequency; this is certainly misleading and can be attributed to the much smaller frequency range available at the lowest temperatures; viz., Figs. 1 and 2.

<sup>5</sup> Several of the lower temperature curves have been omitted for the sake of clarity.

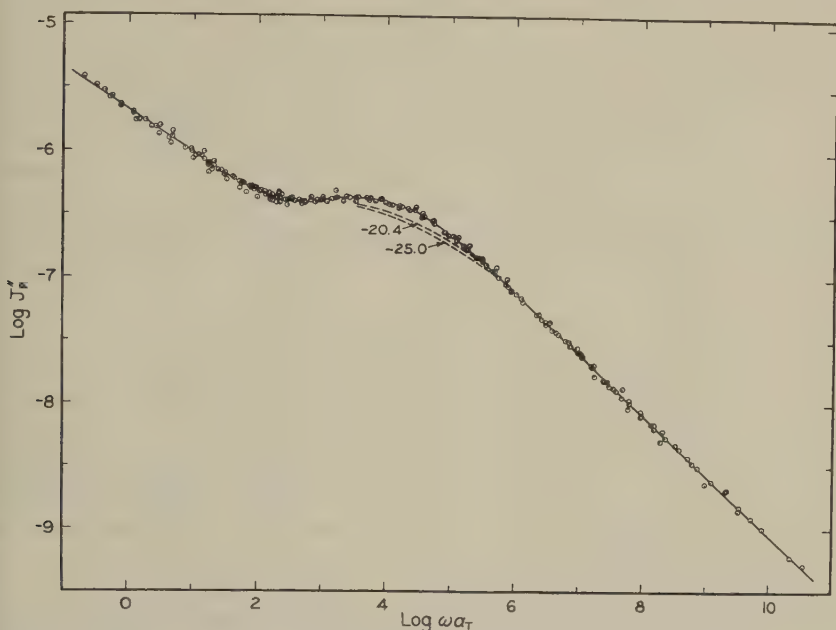


FIG. 4. Imaginary part of the complex shear compliance, reduced and plotted as in Fig. 3.

#### *Torsion Pendulum, Creep*

All but one of the creep runs reported here were made on sample 4 in the torsion pendulum instrument; the diameter of the sample was approximately  $1\frac{1}{8}$  in. and its height  $\frac{5}{16}$  in. Dynamic measurements were also made on this sample only to aid in assessing and analyzing the twelve creep runs. They indicated that the calculated sample coefficients gave results in essential agreement with the absolute magnitude of the moduli accepted from double transducer measurements. Discrepancies were within a few per cent, and it was gratifyingly unnecessary to apply any empirical corrections. To confirm this conclusion a short creep run was made on sample 7 at  $-25.0^\circ\text{C}$ ., and the result, as will be seen later, was in excellent agreement with measurements at neighboring temperatures on sample 4. The experimental conditions are given in Table I. The maximum stresses,  $\mathcal{T}_m$ , listed are those at the outer radius of the disc-shaped sample, and the peripheral strain,  $\gamma_m$ , is the maximum reached at the end of the creep portion of each run. Four separate creep runs, 3, 4, 9, and 10, were made at  $-4.5^\circ\text{C}$ . to confirm that the measurements were being made in the region of linear stress-strain behavior and also to check the precision of the method used. Runs 3 and 4 were carried out using a torque approximately  $11\frac{1}{2}$  times larger than used in runs 9 and 10. The experimental conditions for 3 and 4 were identical and the measured values for one fell within the



TABLE I  
Creep, Experimental Conditions

Run	$T(^{\circ}\text{C.})$	$\gamma_m \times 10^2$	$\tau_m \times 10^{-2}$ (dynes/cm. <sup>2</sup> )	Time of creep $\times 10^{-2}$ (sec.)	Time of recov- ery $\times 10^{-2}$ (sec.)	% $\gamma$ recov- ered
7	-33.2	1.64	46.4	200.0	250.0	69
8	-28.4	1.58	46.4	42.0	63.0	75
13	-25.0	3.75	108.0	4.6	—	—
6	-23.6	1.75	46.4	17.0	36.0	81
5	-14.3	4.94	46.6	78.0	130.0	75
12	-9.3	4.83	46.4	20.5	26.3	64
3	-4.5	4.64	46.9	8.5	21.5	83
10	-4.5	0.620	4.05	41.0	—	—
11	5.5	1.11	4.04	106.0	—	—
1 <sup>a</sup>	15.5	1.77	3.30	73.0	1,640.0	92
2 <sup>b</sup>	25.0	1.62	1.10	130.0	160.0	36

<sup>a</sup> 5% permanent loss.

<sup>b</sup> 29% permanent loss.

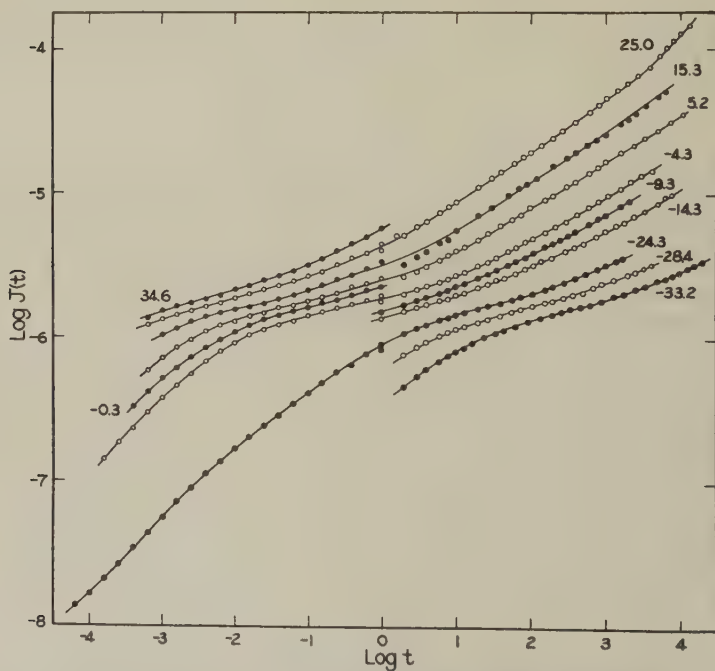


Fig. 5. Creep compliance (units cm.<sup>2</sup>/dyne) plotted logarithmically at 11 temperatures as indicated ( $t$  in seconds). For  $\log t > 0$ , measured directly; for  $\log t < 0$ , calculated from dynamic measurements by Eq. [3]. Where temperatures do not exactly match, average values are shown.

scatter of the other; the same statements are also true for 9 and 10. The precision and the reproducibility are therefore satisfactory, and since the results under the different applied stresses were found to differ only 4 % it can be concluded that all the work done was in the region of linearity. The creep results are shown in the right half, ( $\log t \geq 0$ ), of Fig. 5; a log-log plot of creep compliance,  $J(t)$  in  $\text{cm}^2/\text{dyne}$ , versus time,  $t$  in seconds.

The data in the left half of Fig. 5 are values of  $J(t)$  transformed from dynamic shear compliances. The approximation method of Ninomiya and Ferry (18),

$$J(t) = J'(\omega) + 0.40 J''(0.40\omega) - 0.014 J''(10\omega) \mid_{t=1/\omega} \quad [3]$$

was used on the dynamic results at those temperatures where reduction appeared to be successful,  $-5.3^\circ$  to  $34.6^\circ\text{C}.$ , and at one illustrative temperature,  $-24.0^\circ\text{C}.$ , where the crystallinity present appreciably affects the mechanical properties of the system. Where a curve encompasses both regions and the temperatures are close but do not match exactly, average temperatures are given. Measurements of recovery were made on most of the runs, the durations of which are also listed in Table I along with the per cent of the strain recovered during the time that the recovery was observed. It will be shown later that where there is no viscous deformation the recovery measurements, as far as they were measured, are compatible with an assumed 100 % recovery.

### *Analysis of Creep Compliance*

Values of  $\log a_T$  calculated from Eq. [2] were used in the reduction of the time scale to  $25.0^\circ\text{C}.$  for all the curves from Fig. 5. The resulting plot of  $\log J_p(t)$  as a function of  $\log t/a_T$  is shown in Fig. 6. The solid composite curve is determined by the data from  $-5^\circ$  to  $35^\circ\text{C}.$  and extends over a sizable nine decades of reduced time. The influence attributed to the crystallinity at  $-24^\circ\text{C}.$  is indicated by the deviation of the line of long dashes from the composite curve. The same broadening of the dispersion as indicated by the dynamic data is very clear here. Contrary to the logical expectation that the presence of crystallites will more influence the properties of the material at long rather than short times, the behavior of this system appears influenced to a greater degree in the transition region. The line of short dashes at the right reflects the deviation of  $15^\circ$  and  $25^\circ\text{C}.$  measurements in the long-time region. This deviation is most certainly due to the onset of flow which is evident from visual observation at room temperature. Assuming that the stress which has been applied is sufficiently small so that no stress melting of the crystallites occurs at  $15.5^\circ\text{C}.$  and that the onset of flow denotes melting, it can be suggested that the melting point is between  $5.5^\circ$  and  $15.5^\circ\text{C}.$

At this point it should be mentioned that the other physical properties of this sample studied as functions of temperature did not give evidence of

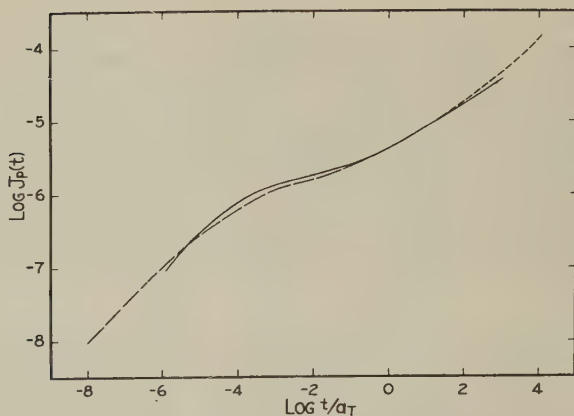


FIG. 6. Creep compliance reduced to 25°C. and plotted logarithmically against reduced time. Solid curve, reduced from temperatures between  $-4.9$  and  $35^\circ\text{C}$ . except for region where flow enters; short dashes, data from flow region at  $15^\circ$  and  $25^\circ\text{C}$ .; long dashes, reduced from  $-24^\circ\text{C}$ .

crystallinity. No spherulitic formation or spontaneous birefringence was found at  $-5^\circ\text{C}$ . with a polarizing microscope. The refractive index,  $n_D$ , was measured with an Abbé refractometer from  $-18^\circ$  to  $27^\circ\text{C}$ . and indicated a linear change with temperature [ $n_D(t) = 1.5039 - 3.68 \times 10^{-4}(t-25)$ ]. A Brice-Phoenix photometer, slightly modified for better temperature control, was used to observe the light scattered by the solution between  $3^\circ$  and  $29^\circ\text{C}$ . and no significant change was found. Dilatometric measurements from  $-2^\circ$  to  $25^\circ\text{C}$ . hint at a slight decrease in slope with increasing temperature at about  $9^\circ\text{C}$ ., but it was at best considered dubious. From these exploratory measurements it is obvious either that there is no crystallinity present at any of the temperatures measured or that the amount of crystallinity is so slight that no appreciable influence is seen in the above-mentioned physical properties. The latter possibility is not unreasonable, since, for example, spherulitic formation is not a necessary consequence of crystallinity and solutions of cellulose derivatives are known to exhibit small volume changes even when crystallization is appreciable (19-21). A few brief comments will be inserted to clarify further how the mechanical behavior in the transition region is in accord with the assumption that the system is a crystalline gel at the lower temperatures.

Of the known causes of reduction failure the presence of secondary relaxation phenomena possessing different temperature dependences from that of the primary chain-backbone motions can be immediately dismissed in the present case. Such a mechanism is known to exist in the cellulose nitrate-dibutyl phthalate system at higher concentrations (2); but if such were alone responsible for the failure of the lower temperature results

to superpose, the curves in their reduced positions on the time scale could not possibly cross one another as they do. This is the case simply because a secondary mechanism which complicates the behavior can only add varying additional amounts of compliance to the primary response. We are therefore at the present time left with a thermodynamic change in character of the material with respect to a change in temperature. Recently a change in the number of interchain entanglements of the polymer with temperature has been proposed as a possible mechanism which both from theoretical and experimental bases causes a shift along a line of slope  $-\frac{1}{2}$  in the double logarithmic plots of the real and imaginary components of the dynamic compliance versus the angular frequency (22). The changes in shape, most easily seen in Figs. 3 and 6, argue against this possible reason for lack of superposition. Furthermore identical shift factors would have to cause both the  $J_p'$  and  $J_p''$  curves to superpose satisfactorily, and this clearly cannot be done. Finally, as referred to earlier, the changes in shape of the dispersion with temperature are qualitatively the same as found in the system cellulose tributyrate-dimethyl phthalate (1), where the presence of crystallinity is indisputable. Thus, despite the lack of substantiating evidence it is felt that the only reasonable interpretation possible at the present time for the mechanical property results is one which includes the supposition of varying degrees of crystallinity at the lower temperatures of measurement.

During the extended period of time that these measurements were being carried out, the stress dependence of the creep behavior of cellulose nitrate was determined at the University of Wisconsin by Van Holde (7). It was shown that the creep behavior of the pure polymer could be represented by the expression

$$\epsilon = \epsilon_0 + \beta' t^{1/3}, \quad [4]$$

where  $\epsilon$  is the elongational strain at time  $t$ ;  $\epsilon_0$  is the "instantaneous" strain; and  $\beta'$  is a characterizing constant. In the limit of small strains this equation is equivalent to that of Andrade (5, 6)

$$\ell = \ell_0(1 + \beta t^{1/3})e^{\kappa t}, \quad [5]$$

when the "viscosity coefficient,"  $\kappa$ , is equal to zero. The length,  $\ell$ , is unity before the application of the stress and  $\ell_0$  is the zero time length. Kennedy (4) lists some of the materials known to behave in the manner described by Eq. [5] with values of  $\kappa$  both zero and non-zero.

Since the pure cellulose nitrate exhibits this Andrade creep, it was expected that the system reported here would behave similarly below the gel melting temperature. This expectation was realized and is illustrated in Figs. 7, 8, and 9, where most of the data from Fig. 5 have been replotted against the cube root of time. In Fig. 7 the results of six runs from  $-33.2^\circ$



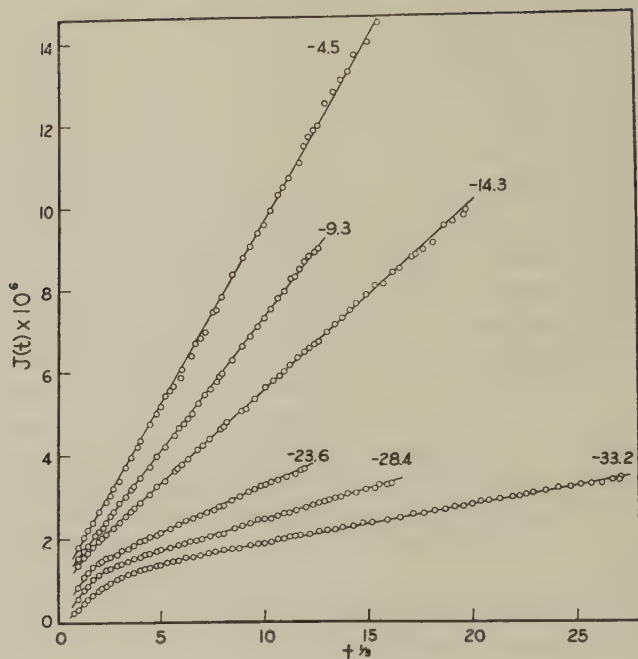


Fig. 7. Measured creep compliance,  $J(t) \times 10^6$ , plotted against  $t^{1/3}$  for 6 temperatures from  $-33.2^\circ$  to  $-4.5^\circ\text{C}$ . as indicated.

to  $-4.5^\circ\text{C}$ . are shown, the lowest temperatures exhibiting appreciable negative curvature which reflects the beginning of the transition region. At temperatures above  $-14.3^\circ\text{C}$ . the transition region has moved to shorter times and can no longer be detected by the direct creep measurements, the shortest possible time of measurement being about 1 sec. Therefore, the measurements from  $-9.3^\circ$  to  $5.5^\circ\text{C}$ . indicate deformations which are linear in  $t^{1/3}$  for the entire duration of the run. Presented along with the  $5.5^\circ\text{C}$ . data in Fig. 8 are the results from  $15.5^\circ$  and  $25.0^\circ\text{C}$ . which diverge from a similar behavior at long times. The transformed dynamic data in Fig. 9, reflecting the shorter time behavior, again show the beginning of the transition region and a limited portion of the linearity with  $t^{1/3}$  at temperatures from  $-5.3^\circ$  to  $34.6^\circ\text{C}$ . in a manner entirely consistent with the lower temperature creep measurements.

All these data with the exception of the mentioned divergence at  $15.5^\circ$  and  $25.0^\circ\text{C}$ . can be satisfactorily represented by the expression

$$J(t) = J_g + J_0\psi(t) + \beta t^{1/3} \quad [6]$$

with the slope (or limiting slope in the case of  $15.5^\circ$  and  $25.0^\circ\text{C}$ .) being designated<sup>6</sup> as  $\beta$ . For the sake of completeness the glassy compliance

<sup>6</sup> Here  $\beta$  is the shear equivalent of  $\beta'$  in Eq. [4] divided by the stress. Values of  $\beta$

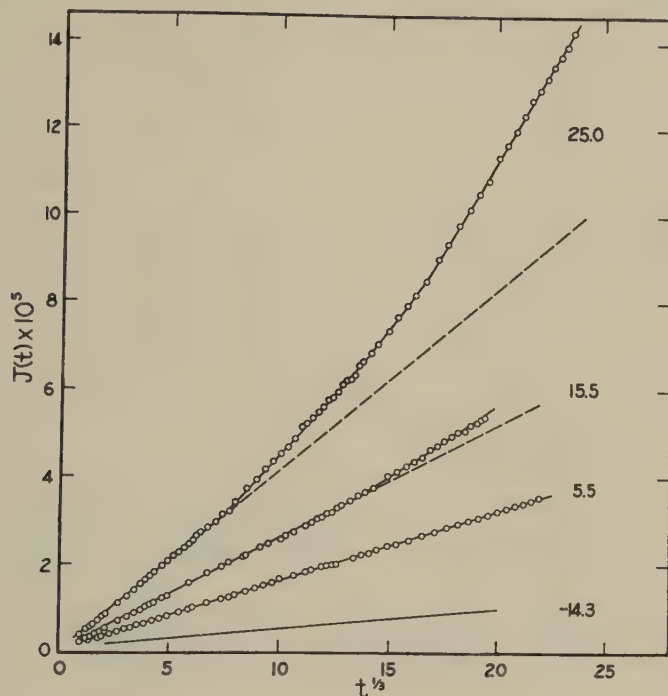


FIG. 8. Measured creep compliance,  $J(t) \times 10^5$ , plotted against  $t^{1/3}$  at 5.5°, 15.5°, and 25.0°C., together with curve at -14.3°C. from Fig. 7 for comparison.

$J_g$ , has been added though, as explained earlier, it is beyond these measurements. Proposed nomenclature (23) has been adhered to where possible, but since these experiments do not give any indication of an equilibrium compliance, the intercepts of the straight lines,  $J_0$ , in Figs. 7, 8, and 9 are given as the limiting value for only part of the retarded elasticity (in this case that associated with the transition region) with  $\psi(t)$  being the corresponding normalized time-dependent function. The measured values of the parameters  $J_0$  and  $\beta$  are given in Table II. The values of  $J_0$  are to be considered approximate since some of them were obtained from extrapolations to quite small experimental intercepts and a few from a limited  $t^{1/3}$  linearity. It may be concluded from the scattered values that to a first approximation  $J_0$  is temperature-independent and for this system is about  $1.05 \times 10^{-6}$  cm.<sup>2</sup>/dyne.

Mechanical parameters of polymeric systems are believed to undergo changes with temperature which depend primarily on the entropy of

reported here refer to those from Eq. [6] and should not be confused with values existing in the literature which were obtained in elongation using some form of the Andrade Eq. [5].

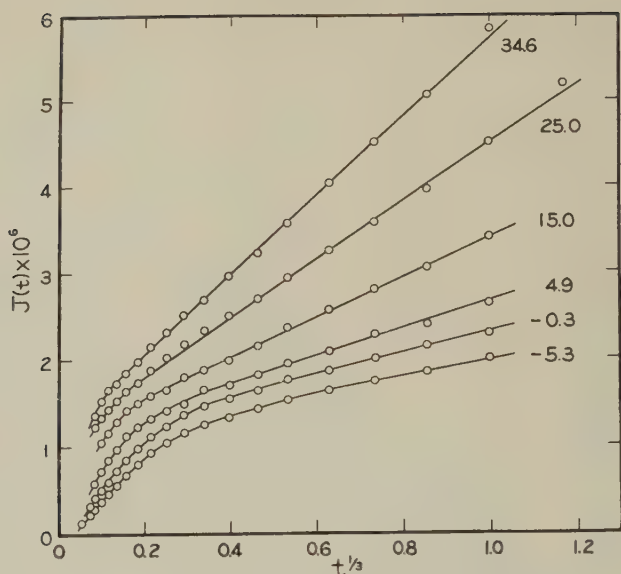


FIG. 9. Creep compliance,  $J(t) \times 10^6$ , calculated from dynamic data by Eq. [3] plotted against  $t^{1/3}$  at 6 temperatures as indicated.

TABLE II  
Temperature Dependence of Creep Parameters

Measurement <sup>a</sup>	$T(^{\circ}\text{C.})$	$J_0 \text{ cm.}^2/\text{dyne} \times 10^6$	$\beta \text{ cm.}^2/\text{dyne sec.}^{1/3} \times 10^7$	$\log \frac{\beta_0}{\beta} \left[ \frac{T_0 \rho_0}{T_p} \right]$
C	-33.2	1.0 <sub>0</sub>	0.89	1.66
C	-28.4	1.0 <sub>1</sub>	1.42	1.45
C	-25.0	1.0 <sub>4</sub>	2.04	1.29
C	-23.6	1.0 <sub>2</sub>	2.23	1.23
C	-14.3	1.0 <sub>6</sub>	4.5 <sub>1</sub>	0.93
C	-9.3	0.9 <sub>5</sub>	6.3 <sub>6</sub>	0.78
D	-5.3	1.1 <sub>2</sub>	8.5 <sub>4</sub>	0.64
C	-4.5	0.8 <sub>2</sub>	9.2 <sub>0</sub>	0.61
C	-4.5	0.9 <sub>0</sub>	8.7 <sub>5</sub>	0.63
D	-0.3	1.1 <sub>4</sub>	11.6	0.50
D	4.9	1.1 <sub>3</sub>	15.2	0.37
C	5.5	—	15.8	0.36
D	15.0	1.0 <sub>7</sub>	23.3	0.18
C	15.5	—	26.2	0.13
C	25.0	—	40.7	-0.07
D	25.0	1.1 <sub>0</sub>	34.3	0
D	34.6	1.1 <sub>2</sub>	46.1	-0.14

<sup>a</sup> C, creep; D, dynamic.

deformation and the rate of Brownian motion (14). Since  $\beta$  has the dimensions of  $\text{cm}^2/\text{dyne}^{-1} \text{sec.}^{-1/3}$ , it can be considered to be composed of two factors  $k$  and  $\lambda$  corresponding to the two respective processes; so that at a chosen standard temperature,

$$\beta_0 = k_0 \lambda_0^{1/3}, \quad [7]$$

where  $\lambda_0$  has the dimension of time. At another temperature  $k$  would be different from  $k_0$  by the usual entropy and density-controlled factor,  $T_0 \rho_0 / T \rho$ , and the time parameter,  $\lambda_0$ , would be changed by the factor  $a_T^{-1}$ . At the new temperature  $T$ ,

$$\beta = (T_0 \rho_0 / T \rho) k_0 (\lambda_0 / a_T)^{1/3}, \quad [8]$$

and

$$\frac{\beta_0}{\beta} \left[ \frac{T_0 \rho_0}{T \rho} \right] = a_T^{1/3}. \quad [9]$$

The temperature dependence of  $\beta$  specified by Eq. [9] is illustrated in Fig. 10, where the reduced values (also given in Table II) are plotted logarithmically against temperature;  $\beta_0$ , chosen from dynamic measurements, is the value at  $T_0$ , 298.2°K. The open circles are obtained from the transformed dynamic data, Fig. 9, and the filled-in circles from the creep runs, Figs. 7 and 8. The line is actually  $\frac{1}{3} \log a_T$  derived from Eq. [2]. In the range where Eq. [2] described the temperature dependence of the dynamic data, -10° to 35°C., the agreement is excellent, as it should be.

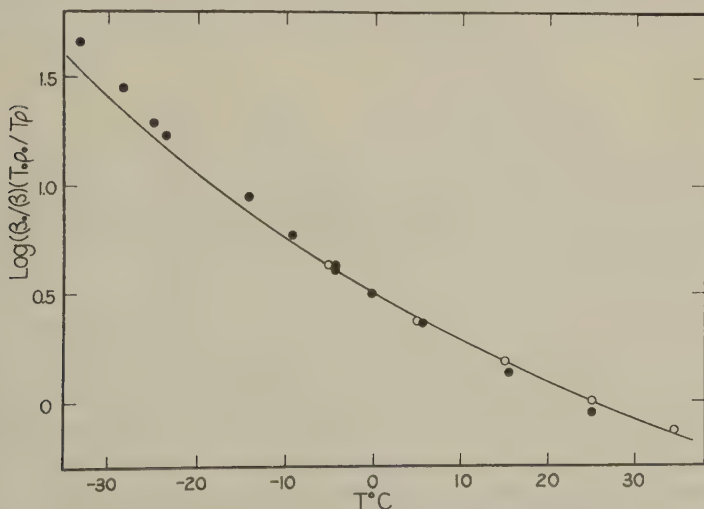


FIG. 10. Temperature dependence of  $\beta$  compared with shift factors for dynamic data. Points,  $\log (\beta_0 / \beta) (T_0 \rho_0 / T \rho)$ , closed circles from Figs. 7 and 8, open circles from Fig. 9; curve,  $(\log a_T) / 3$ .



The discrepancies for the 15.5° and 25.0°C. creep points reflect the uncertainty in the absolute magnitude of the sample coefficient. The lower temperature creep points could not be expected to fall on the line because of the influence of the crystallinity as seen also in the dynamic results.

Since there is no discontinuity in this temperature-dependence curve at or near the melting point (about 10°C.), it can be concluded that for this system the only change in character of the behavior, when it is melted, is the onset of flow. This unexpected result allows one to conclude further that the same processes are operative in the response of both the gel and the melt. Therefore the measured behavior of the system is completely described by

$$J(t) = J_0 + J_0\psi(t) + \beta t^{1/3} + t/\eta, \quad [10]$$

where the viscosity,  $\eta$ , becomes infinite below the melting point. If it is assumed that such an equation describes the behavior of an amorphous polymer solution for an indefinite length of time, so long as the final strain remains small, true steady-state flow is not possible; though in practice at long times the viscous process dominates and an apparent steady state is reached.

#### *Analysis of Recovery Measurements*

The recovery measurements were used to determine whether or not the behavior of the 23% CN-DEP system obeys the Boltzmann superposition principle. Since analytical expressions for the creep at long times, where  $J_0$  and  $J_0\psi(t)$  can be replaced by a single constant, are available, a direct test may be had by using the simple expression for the shear recovery strain (7),  $\gamma_r(t)$ :

$$\gamma_r(t) = \gamma_{\text{creep}}(t) - \gamma_{\text{creep}}(t - \theta), \quad [11]$$

where  $\theta$  is the time of the creep portion of the run, i.e., before the stress was removed, and  $t$  is the time elapsed since the application of the stress. Substitution of an equation in the form of Eq. [10] into Eq. [11] yields the following expression:

$$\gamma_r(t) = \mathfrak{C}\beta[t^{1/3} - (t - \theta)^{1/3}] + \mathfrak{C}\theta/\eta. \quad [12]$$

Two illustrative results from recovery measurements on the gel at -23.6° and -4.5°C. are shown in Fig. 11, where the percentages of recovered strain,  $100 [1 - \gamma_r/\gamma_{\text{max}}]$  are plotted as functions of time, and are compared with the lines calculated from the analytical expressions for the creep measurements. The agreement is satisfactory. This agreement and examination of the recoveries on the gel at other temperatures indicate that the system adheres to the Boltzmann superposition principle and that the deformation of the gel is entirely recoverable. Figure 12 presents the com-

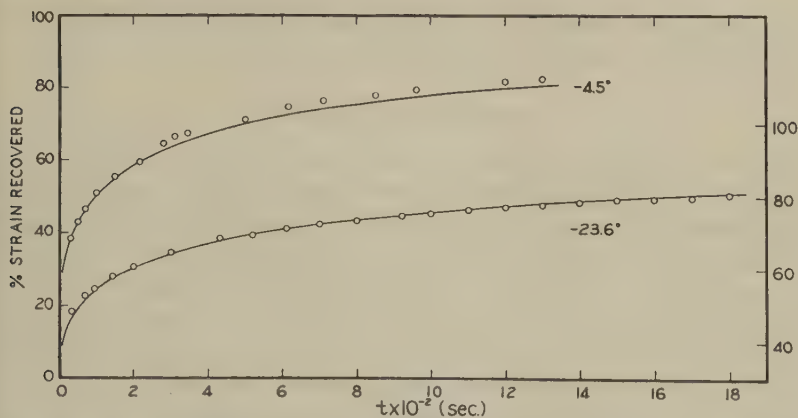


FIG. 11. Test of Boltzmann superposition illustrated at 2 temperatures below melting point: points, measured strain recovery; curves, calculated from Eq. [12]. Ordinate on left for  $-4.5^{\circ}\text{C}.$ ; on right for  $-23.6^{\circ}\text{C}.$

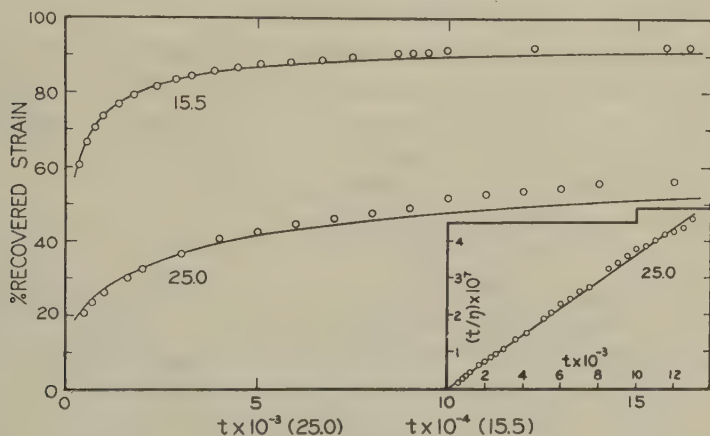


FIG. 12. Test of Boltzmann superposition illustrated at two temperatures above the melting point: presented as in Fig. 11. Viscous contribution to creep compliance at  $25.0^{\circ}\text{C}.$  plotted in right-hand corner vs. time. Time in each case is seconds.

parison for the recovery measurements made above the melting point,  $15.5^{\circ}$  and  $25.0^{\circ}\text{C}.$  The agreement is reasonably good, showing deviations from the predicted curve which are in the opposite direction from past observations (7). At  $25.0^{\circ}\text{C}.$  the enhanced recovery at long times is in accord with the possible presence of a 1% to 2% residual stress in the torsion wire. The presence of such a small residual stress in the later stages of recovery is disastrous when the system flows and yields an appreciable and continually changing erroneous deformation. The small stress error in the creep portion will lead only to a correspondingly small percentage error. It is therefore

obvious that the torsion wire method used here is not desirable for extended recovery studies on solutions or melt polymers.

### *Calculation of Viscosity*

The claim that the divergence of the creep measurements at 15.5° and 25.0°C. from the limiting slopes (dashed straight lines) in Fig. 8 is due to the presence of viscous flow demands that the divergence plotted against time should be a straight line through the origin and yield the viscosity. Because at 25°C. the flow gave rise to about 29% of the deformation a reasonably accurate viscosity was obtained. The plot shown in the right-hand corner of Fig. 12 gave a viscosity of  $2.8 \times 10^8$  poises. At 15.5°C. about 5% of the deformation was due to flow so that only an approximate viscosity,  $2 \times 10^9$  poises, was obtained. The time required for the above determination, when  $\beta$  is known, is orders of magnitude less than the usual procedure of waiting for apparent steady-state flow.

### *Retardation Spectrum*

If one assumes that Eq. [10] describes the behavior of the material correctly in the domain of small strains, the distribution function of retardation times,  $L(\ln \tau)$  (24), will diverge as  $\ln \tau$  approaches infinity. The exact expression for  $L$  in the long-time region after  $\psi(t)$  becomes unity has been calculated by Thor L. Smith (25) to be

$$L(\ln \tau) = [\beta/3\Gamma(\frac{2}{3})]\tau^{1/3} = 0.246\beta\tau^{1/3}. \quad [13]$$

It is worthy of note that the Williams and Ferry second approximation method (26), which has been developed for creep by Stern (27), gives the exact solution. This is so because the assumption involved in the method, that  $L$  can be described by  $k\tau^m$ , is true in this case.

The successfully reduced creep measurements were treated by Stern's expression and the results are represented in Fig. 13. The second approximation of  $L$  at 25°C. was also calculated directly from the reduced dynamic measurements where superposition was obtained, and the results are shown in Fig. 13. The recently developed Ninomiya and Ferry approximation method (18) was used here because it is believed to be superior to the Williams-Ferry method when the curvature in  $\log L$  is appreciable. At short times the peak associated with the glasslike to rubberlike transition is seen with a maximum at  $\log \tau$  equal to  $-3.8$ . To the right of the minimum in Fig. 13 the increase in  $\log L$  reaches times long enough for Eq. [13] to hold and the line drawn in this region has a slope of  $1/3$ .

An independent test of the validity of the separation procedure used to isolate the viscous component of deformation is obtained by the direct

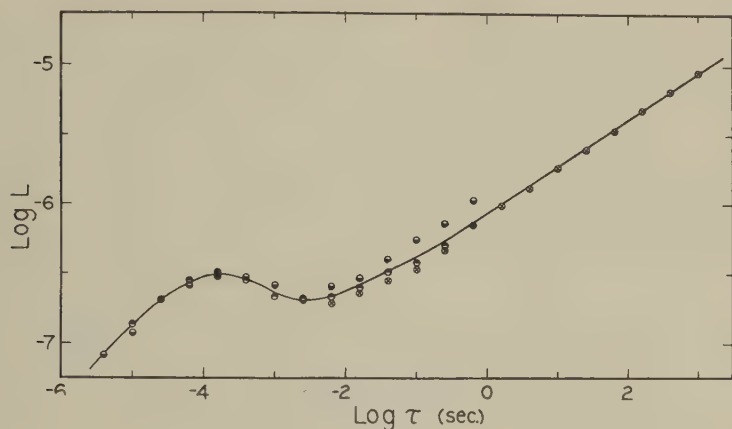


FIG. 13. Retardation spectrum,  $L(\text{cm}^2/\text{dyne})$ , calculated from composite curve reduced to  $25^\circ\text{C}$ . Points top black, from  $J'_p$ ; bottom black, from  $J''_p$ ; crossed, from creep.

calculation of  $L$  from the experimental  $J(t)$  curve. This calculation is possible using the expression

$$L(t/2) = \frac{d[J(t) - dJ(t)/d \ln t]}{d \ln t} \quad [14]$$

found by Leaderman (28) to be equivalent to the Schwarzl and Staverman second approximation (29). Equation [14] was used to calculate  $L$  from the  $25.0^\circ\text{C}$ . creep curve, viz., Fig. 5, and the results, shown in Fig. 14 as filled-in circles, are compared with the curve from Fig. 13, drawn in as a dotted line. The points are in fair agreement with the line and the determination of the viscosity appears to be substantiated.

Shown also in Fig. 14 are various calculations of  $L$  from the  $-24^\circ\text{C}$ . data reduced to  $25^\circ\text{C}$ . to illustrate the influence of crystallinity. It is reassuring that the Ninomiya-Ferry and Williams-Ferry approximations agree for both components of the complex compliance. The divergence of the values at  $-24^\circ$  confirms the conclusion that the apparent superposition of the low-temperature data in the  $\log J''_p$  curve, Fig. 4, is illusory.

### Derived Parameters

The temperature-dependence equation, Eq. [2], was transformed so that  $T_0$  would be the reference temperature (30). Quantities derived from the transformed expression,  $f_0$  and  $\alpha_f$ , which are interpreted as the fractional free volume and its thermal expansion coefficient, were found to be 0.016 and  $3.1 \times 10^{-4} \text{ deg.}^{-1}$ , respectively. Both of these values are lower than



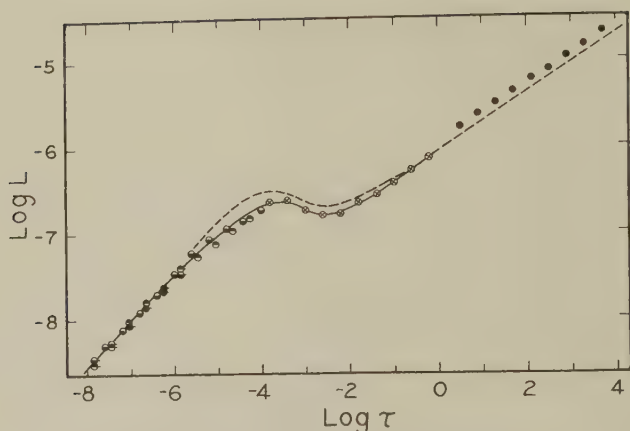


FIG. 14.  $\text{Log } \tau < 0$ : retardation spectrum, calculated from  $-24^{\circ}\text{C}$ . measurements reduced to  $25^{\circ}\text{C}$ . Points top black, from  $J'$ ; bottom black, from  $J''$ ; crossed, from creep; with pips, Williams, Ferry approximation used; no pips, Ninomiya, Ferry approximation used.  $\text{Log } \tau > 0$ : Filled-in points calculated from  $25^{\circ}\text{C}$ . creep run with Eq. [14]. Dashed line is curve from Fig. 13.

the "universal" values of  $0.025$  and  $4.8 \times 10^{-4} \text{ deg.}^{-1}$ . Sometimes  $\alpha_f$  is similar in magnitude to the difference,  $\Delta\alpha$ , of the expansion coefficients of the material below and above  $T_g$ . The experimental value for  $\Delta\alpha$  here is  $3.8 \times 10^{-4} \text{ deg.}^{-1}$  (10), representing about the kind of agreement found in the past (30). Not much, at present, can be said about the value for  $f_0$  except that it is, so far, the lowest observed value and that similar cellulose tributyrate-dimethyl phthalate gels (CTB-DMP) also have given low values (1, 10).

For comparative purposes the position of the transition region on the time scale is best specified by the monomeric friction coefficient,  $\zeta_0$ , at  $T_g$ . Its logarithm was calculated (30) from the relaxation spectrum,  $H$ , at  $T_0 = 298^{\circ}$  and  $T_g = 186^{\circ}\text{K}$ . and was found to be  $-7.1_5$  and  $10.2$ , respectively. The value at  $T_g$  is the same within experimental uncertainty as that of a 20.4% CTB-DMP gel:  $\log \zeta_0$  at  $T_g = 10.3$ . These cellulose derivative systems share the distinction of having values larger by four orders of magnitude than any other measured systems (30, 31). The low values of  $f_0$  and the relatively open configuration of the cellulose derivative molecules may give rise to this distinguishing feature.

## DISCUSSION

The number of polymeric systems exhibiting Andrade creep is sizable and is growing (4, 7), but all the systems heretofore reported have had a permanent or crystalline infinite network structure. The measurements on the 23% CN-DEP solution are the first to suggest that a linear amor-

phous polymer solution might behave in a similar manner. The rubberlike plateau in linear polymer melts and solutions is generally attributed to intermolecular coupling or entanglement. It is suggested that the transient network which is believed to exist, though it be transient, retains some aspects of the behavior of a permanent network in the presence of viscous flow. Since the mechanical behavior of high molecular weight polymers in the long-time region is known to be sensitive to molecular weight, it is further suggested that this dependence is a combination of the respective dependences of the viscosity and  $\beta$ .

Since  $J(t)$  can be described by the simple analytical expression  $J_0 + \beta t^{1/3} + t/\eta$  after  $\psi(t)$  becomes unity, the dynamic parameters  $J'(\omega)$  and  $J''(\omega)$  can be calculated with the equations of Gross (32). The results of such calculations are

$$J'(\omega) = J_0 + [\beta\Gamma(1/3)/2\sqrt{3}]\omega^{-1/3} = J_0 + 0.773 \beta\omega^{-1/3} \quad [15]$$

and

$$J''(\omega) = [\beta\Gamma(1/3)/6]\omega^{-1/3} + 1/\omega\eta = 0.447 \beta\omega^{-1/3} + 1/\omega\eta \quad [16]$$

For the 23% CN-DEP solution at 25°C. these become  $J'(\omega) = 1.1 \times 10^{-6} + 2.65 \times 10^{-6}\omega^{-1/3}$  and  $J''(\omega) = 1.53 \times 10^{-6}\omega^{-1/3} + 1/2.8 \times 10^8\omega$ . From the above expressions it can be seen that any system that behaves in the manner described by Eq. [6] will approach and maintain a constant loss tangent,  $J''/J'$ , as  $\omega$  approaches zero; surprisingly enough this value is independent of  $\beta$  and hence of the material itself. It is

$$J''/J' = 1/\sqrt{3} = \tan 30^\circ. \quad [17]$$

Log  $J''_p$  in Fig. 4 has reached the slope of  $1/3$  within experimental error, but the slope of  $\log J''_p$  in Fig. 3, though still increasing, has not quite reached the limiting slope. When the viscosity contribution becomes appreciable, of course, the slope of  $\log J''$  will surpass  $1/3$ . The measured loss tangent values of the gel, not shown here, are approaching but have not exceeded the limiting value of 0.577.

Since the creep behavior of the 23% CN-DEP solution above its melting point in the long-time region appears to depend in part on a transient process which obeys a specialized form of the more general Andrade equation [5], it is of interest to see if other polymeric materials of high molecular weight behave in a like manner. It would not be expected that the  $\beta$  deformation, if present, would dominate the behavior over an appreciable range of time scale if the molecular weight were not appreciably greater than the  $\bar{M}_c$  which characterizes the break in a  $\log \eta - \log \bar{M}_w$  plot (33) and the onset of a rubbery plateau in the relaxation spectrum (34).

Some of the measurements on the well-known National Bureau of Standards-polyisobutylene (NBS-PIB) sample (35) were chosen for re-examina-

tion because it is one of the few materials for which the necessary data are available. The most extensive and readily useful results are the stress relaxation measurements of Tobolsky and Catsiff (36) and the dynamic measurements of Ferry, Grandine, and Fitzgerald (37). The reduced dynamic results as tabulated in reference 36 were converted into creep with Eq. [3] in the appropriate region along with the predicted dynamic values of Tobolsky and Catsiff since the agreement in the overlap region was good and they extended to lower frequencies. The former are shown in Fig. 15 as right half-black circles and the latter as crossed circles where the creep compliance,  $J(t)$ , is plotted against  $t^{1/3}$ . In the region where the slope,  $m$ , of the double log plot of the stress relaxation modulus,  $G(t)$ , against  $t$  is low the approximation of Thor Smith (38) for converting  $G(t)$  into  $J(t)$ ,

$$J(t) = \sin m\pi / m\pi G(t), \quad [18]$$

is used on the tabulated reduced data, and the results are shown as left half-black circles. The stress relaxation data have previously been converted into creep by Hopkins and Hamming (39) by a more elaborate means and are presented as open circles. So in Fig. 15 we have represented two independent sets of measurements (one of which has been transformed by three methods) in a region where the viscous flow has not appreciably contributed to the deformation. The tabulated values are given in refer-

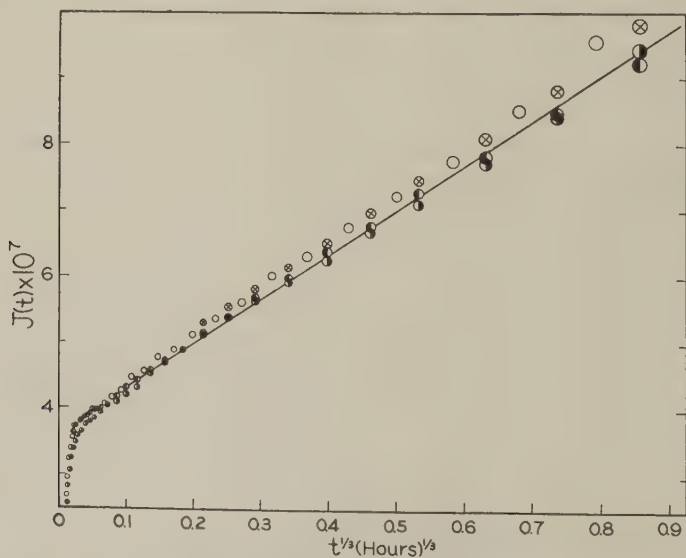


FIG. 15. Creep compliance of National Bureau of Standards polyisobutylene, calculated from stress relaxation, data of Tobolsky and Catsiff and from dynamic data of Fitzgerald, Grandine, and Ferry (see text for details), and plotted against  $t^{1/3}$ .

ence 36 to approximately plus or minus 1% and in reference 39 to plus or minus  $2\frac{1}{2}\%$ . The circles in Fig. 15 are plotted with a 1% radius and for over  $4\frac{1}{2}$  decades of time all the calculated values fall as close to the drawn straight line as can be expected. The negative curvature at short time indicating the beginning of the transition region is qualitatively the same as that in the CN-DEP solution measurements.

The long-time region where viscous flow has entered the picture is encompassed only by the stress relaxation measurements. Because the Smith approximation appears not to be applicable in this region, only two sets of calculations cover this region. In Fig. 16 the same qualitative behavior as shown by the CN-DEP solution is seen here. The dotted line is that established in Fig. 15 and the differences between this line and the calculated points ( $J_\eta = t/\eta$ ) are plotted in the right-hand corner, as before, versus time. This time the line is drawn as demanded by the directly measured viscosity at  $25^\circ\text{C}$ ., and all that can be said is that if the calculated points describe a straight line no other would be better.

It should be made clear that the analysis used here which makes no recourse to an equilibrium or steady-state compliance is a tentative proposal not in complete agreement with currently accepted analyses based on the structure of the phenomenological theory of viscoelasticity. It is admitted that the procedure has not been unequivocally established. However, the widespread occurrence of Andrade creep suggests that fortuitous curve fitting is not the reason for its existence; that a mechanism the response of which is at least well approximated by the  $\beta t^{1/3}$  term exists. Henderson (40), Kennedy (4), and Van Holde (7) have in the past pointed out that some organic materials as well as metals behave in a manner described by some form of the Andrade equation. Where such behavior has been found to be completely elastic in a manner following Boltzmann superposition it has not been necessary to place limits on this elastic com-

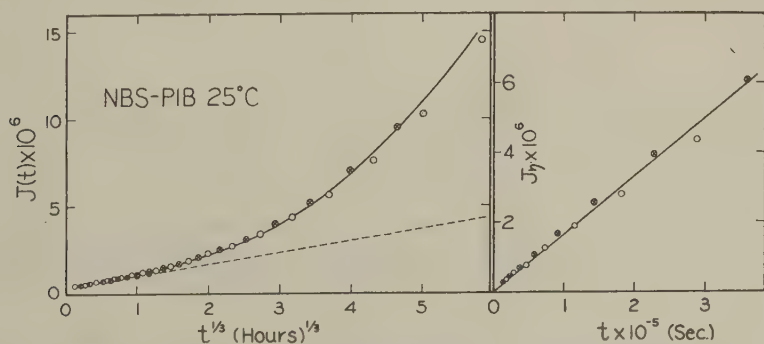


FIG. 16. Creep compliance of National Bureau of Standards polyisobutylene, calculated from stress relaxation data, plotted against  $t^{1/3}$ , covering larger time range than in Fig. 15. Dotted line extrapolated from Fig. 15 (see text for details).



ponent to describe the data. The existence of an equilibrium compliance in a permanently or crystalline cross-linked material or a steady-state compliance in a high molecular weight linear polymer is not precluded at times beyond the range of the experimental data; but considering the well-known difficulty of attaining equilibrium or steady-state conditions there remains the possibility that the Andrade type of response, when present, holds for all practicable lengths of time.

#### SUMMARY

The time-dependent mechanical properties of a 23 % solution of cellulose nitrate in diethyl phthalate have been extensively investigated. The nitrogen content of the polymer was 12.6 % and its number-average molecular weight was 94,000. Dynamic mechanical measurements were made at 14 temperatures from  $-47^{\circ}$  to  $35^{\circ}\text{C}$ . within a frequency range of 0.06 to 2800 cycles per second. Creep runs were made at 10 temperatures extending from  $-33^{\circ}$  to  $25^{\circ}\text{C}$ . Accompanying recovery measurements indicated that the system adhered to the Boltzmann superposition principle. The melting point of the solution was deduced to be in the neighborhood of  $10^{\circ}\text{C}$ ., but temperature reduction was successful to  $-10^{\circ}\text{C}$ . At  $-10^{\circ}\text{C}$ . and below, deviations from the master curves were attributed to the presence of crystallinity. It was found that the creep compliance,  $J(t)$ , could be described by a modified form of the Andrade expression

$$J(t) = J_0 + J_0\psi(t) + \beta t^{1/3} + t/\eta,$$

where  $J_0$ , the glassy compliance,  $J_0$ ,  $\beta$ , and  $\eta$ , the viscosity, serve as characterizing constants of the material;  $\psi(t)$  is a normalized retarded elasticity function. The limiting expressions required by this equation for the distribution function of retardation times and the components of the complex dynamic compliance are given. Measurements on the National Bureau of Standards polyisobutylene sample are re-examined in the light of the above equation.

#### ACKNOWLEDGMENTS

This work was supported principally by the Union Carbide Corporation and the National Science Foundation. It was also supported in part by a grant from the Research Corporation and by the Research Committee of the Graduate School of the University of Wisconsin from funds supplied by the Wisconsin Alumni Research Foundation. I wish to thank Miss Shirley Pomeroy, Miss Rowena M. Green, and Mrs. W. C. Frazier for help with calculations; and Dr. John W. Berge for assistance with some of the measurements. I wish especially to thank Professor John D. Ferry for his invaluable criticisms, suggestions, and help.

#### REFERENCES

1. LANDEL, R. F., AND FERRY, J. D., *J. Phys. Chem.* **60**, 294 (1956).
2. SCHMIEDER, K., AND WOLF, K., *Kolloid-Z.* **127**, 65 (1952).

3. FERRY, J. D., AND FITZGERALD, E. R., *J. Colloid Sci.* **8**, 224 (1953).
4. KENNEDY, A. J., *J. Mech. and Phys. Solids* **1**, 172 (1953).
5. ANDRADE, E. N. DA C., *Proc. Roy. Soc. (London)* **A84**, 1 (1910).
6. ANDRADE, E. N. DA C., *Proc. Roy. Soc. (London)* **A90**, 329 (1914).
7. VAN HOLDE, K., *J. Polymer Sci.* **24**, 417 (1957).
8. NEWMAN, S., LOEB, L., AND CONRAD, C. M., *J. Polymer Sci.* **10**, 463 (1953).
9. PLAZEK, D. J., AND FERRY, J. D., *J. Phys. Chem.* **60**, 289 (1956).
10. VRANCKEN, M. N., AND FERRY, J. D., *J. Polymer Sci.* **24**, 27 (1957).
11. FITZGERALD, E. R., AND FERRY, J. D., *J. Colloid Sci.* **8**, 1 (1953).
12. PLAZEK, D. J., VRANCKEN, M. N., AND BERGE, J. W., *Trans. Soc. Rheology* **2**, 39 (1958).
13. PLAZEK, D. J., Ph.D. Thesis, University of Wisconsin, Madison, 1956.
14. FERRY, J. D., *J. Am. Chem. Soc.* **72**, 3746 (1950).
15. WILLIAMS, M. L., LANDEL, R. F., AND FERRY, J. D., *J. Am. Chem. Soc.* **77**, 3701 (1955).
16. SCHWARZL, F., AND STAVERMAN, A. J., *J. Appl. Phys.* **23**, 838 (1952).
17. CHILD, W. C., JR., AND FERRY, J. D., *J. Colloid Sci.* **12**, 327 (1957).
18. NINOMIYA, K., AND FERRY, J. D., *J. Colloid Sci.* **14**, 36 (1959).
19. MANDELKERN, L., AND FLORY, P. J., *J. Am. Chem. Soc.* **73**, 3206 (1951).
20. FLORY, P. J., GARRETT, R. R., NEWMAN, S., AND MANDELKERN, L., *J. Polymer Sci.* **12**, 97 (1954).
21. RUSSELL, J., AND VAN KERPEL, R. G., *J. Polymer Sci.* **25**, 77 (1957).
22. BERGE, J. W., SAUNDERS, P. R., AND FERRY, J. D., *J. Colloid Sci.* **14**, 135 (1959).
23. LEADERMAN, H., *Trans. Soc. Rheology* **1**, 213 (1957).
24. STAVERMAN, A. J., AND SCHWARZL, F., in H. A. Stuart, ed., "Die Physik der Hochpolymeren," Vol. 4, p. 41. Springer, Berlin, 1956.
25. SMITH, T. L., private communication.
26. WILLIAMS, M. L., AND FERRY, J. D., *J. Polymer Sci.* **11**, 169 (1953).
27. STERN, D. M., Ph.D. Thesis, University of Wisconsin, Madison, 1957.
28. LEADERMAN, H., in F. R. Eirich, ed., "Rheology, Theory and Applications," Vol. 2, p. 49. Academic Press, New York, 1958.
29. SCHWARZL, F., AND STAVERMAN, A. J., *Appl. Sci. Research* **4**, 127 (1953).
30. FERRY, J. D., AND LANDEL, R. F., *Kolloid-Z.* **148**, 1 (1956).
31. DANNHAUSER, W., CHILD, W. C., JR., AND FERRY, J. D., *J. Colloid Sci.* **13**, 103 (1958).
32. GROSS, B., "Mathematical Structure of the Theories of Viscoelasticity," p. 36. Hermann & Cie., Paris, 1953.
33. FOX, T. G., AND LOSHAEK, S., *J. Appl. Phys.* **26**, 1080 (1958).
34. FERRY, J. D., LANDEL, R. F., AND WILLIAMS, M. L., *J. Appl. Phys.* **26**, 359 (1955).
35. MARVIN, R. S., in V. G. W. Harrison, "Proceedings of the Second International Congress on Rheology," p. 156. Butterworths, London, 1953.
36. TOBOLSKY, A. V., AND CATSIFF, E., *J. Polymer Sci.* **19**, 111 (1956).
37. FERRY, J. D., GRANDINE, L. D., AND FITZGERALD, E. R., *J. Appl. Phys.* **24**, 911 (1953).
38. SMITH, T. L., *Trans. Soc. Rheology* **2**, 131 (1958).
39. HOPKINS, I. L., AND HAMMING, R. W., *J. Appl. Phys.* **28**, 906 (1957).
40. HENDERSON, C., *Proc. Roy. Soc. (London)* **A206**, 72 (1951).

## EMULSION PARTICLE SIZE

### I. THE SOAP TITRATION OF ACRYLIC EMULSIONS<sup>1</sup>

J. G. Brodnyan and G. L. Brown

*Research Laboratories, Rohm & Haas Company, Philadelphia, Pennsylvania*

*Received June 29, 1959; revised September 15, 1959*

#### ABSTRACT

In soap titration experiments the soaps are usually calibrated by titrating emulsions characterized using an electron microscope. In this report an independent method was used to determine the effective surface areas of the soaps used. The interfacial tension between water solutions of the surface-active materials and *n*-hexane, an environment similar to the polymer phase, as a function of concentration is determined and used to calculate the effective surface area from the Gibbs adsorption isotherm. Then the soap titration method is used to determine the surface average radius of several acrylic emulsions using not only two anionic soaps, sodium lauryl sulfate and an alkyl aryl polyether sulfonate (Triton X-202), but also one nonionic surface-active agent, an octylphenoxy polyethoxy ethanol, OPE. The validity of this technique is shown by the agreement between the radii determined by the soap titration method and by the use of an ultracentrifuge.

#### INTRODUCTION

The soap titration method has been used extensively for the determination of surface area and particle size of synthetic latices. References to its use in the Government Synthetic Rubber Program (1-6) and for characterizing polystyrene latices (7) are found in the literature. The principles of the method have been described in detail by Maron *et al.* (7). They calibrated several fatty acids by characterizing several polystyrene emulsions using an electron microscope, titrating these emulsions with the fatty acids, and carrying out the calculations assuming coverage of the emulsion particles at the critical micelle concentration (c.m.c.). The average error reported was 5%. This method seems to be the one favored by most investigators.

In this report a simpler technique of determining the effective surface area of the soaps is described, and then the soap titration method is used to determine the surface-average radii of several acrylic emulsions using not only the usual anionic soaps but also one nonionic surface-active agent.

<sup>1</sup> Presented at the 135th American Chemical Society Meeting, Boston, April, 1959.

## MATERIALS USED

*Soaps.* The sodium lauryl sulfate (NaLS) was crystals of reported 99.5 % purity from American Alcolac Corporation. The Triton X-202 is the sodium salt of an alkyl aryl polyether sulfonate and the OPE is an octylphenoxy polyethoxy ethanol, a nonionic surface-active agent. Both these were commercial grade materials as supplied by the Rohm & Haas Company.

*Emulsions.* Three latices were emulsions of poly(*n*-butyl methacrylate) prepared with 2 % sodium lauryl sulfate based on the solids content. (I) was polymerized with potassium persulfate as initiator at 30°C. (II) also was prepared with potassium persulfate but the reaction was carried out at 50°–57°C. (III) was polymerized with a redox system of potassium persulfate, Lykapon, and a trace of  $\text{Fe}^{++}$ . (IV) was a copolymer of ethyl acrylate and methyl methacrylate prepared by a suspension polymerization technique, i.e., no soap was initially on the surface.

The *n*-hexane was reagent grade.

## EXPERIMENTAL METHODS

Any method that will indicate the c.m.c. can be used to follow the progress of a soap titration. However, in all the experiments described here a Du-Nouy ring tensiometer was used. It was found that reproducible measurements could be made almost immediately after the addition of the soap solution provided that there was sufficient agitation during the addition. All the experiments were carried out in a constant-temperature ( $23.2^\circ \pm 2^\circ\text{C}.$ ), constant-humidity ( $54 \pm 4\%$ ) room.

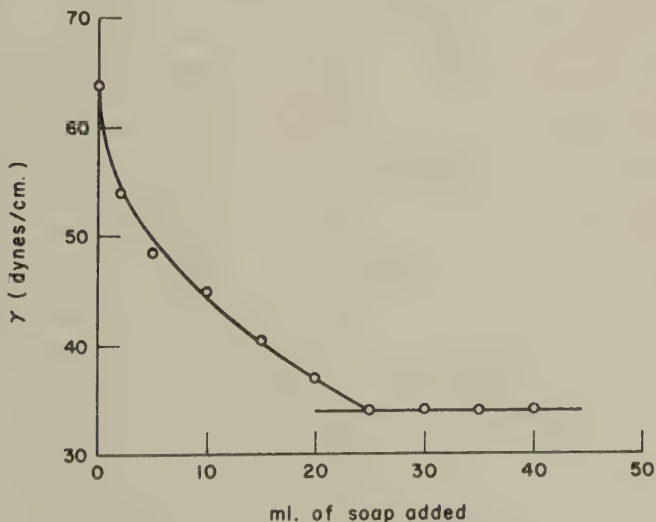
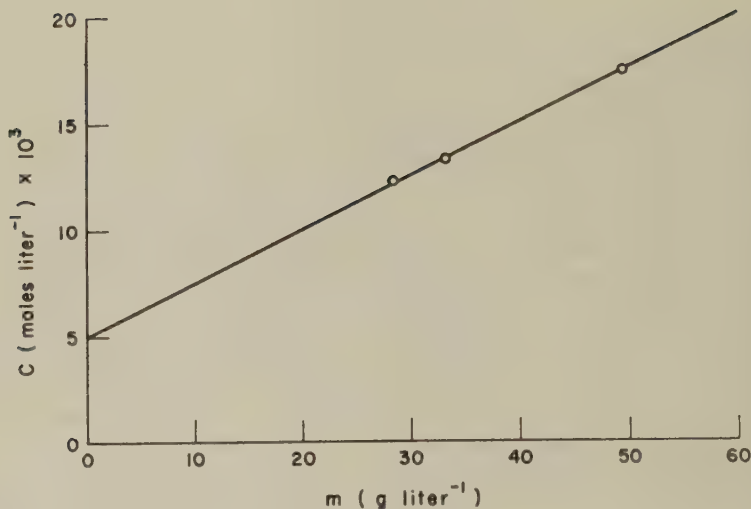


FIG. 1. Typical curve of surface tension ( $\gamma$ ) versus milliliters of soap.



FIG. 2. Typical curve of  $c$  versus  $m$ .

In Fig. 1 a typical curve of surface tension ( $\gamma$ ) versus milliliters of soap added is found. The usual soap concentrations were approximately 0.01  $M$ . The surface tension is uncorrected but this does not interfere with the results since only the milliliters of soap added at the c.m.c. is needed. Because of the curvature in the plot it is difficult to obtain the break in the curve which determines the c.m.c. accurately. However, the errors can be assumed to be random and will cancel out in the plot of concentration of soap at the c.m.c. ( $c$ ) versus the concentration of emulsion at that point ( $m$ ) if a sufficient number of concentrations of emulsions are titrated.

Figure 2 is a typical curve of  $c$  versus  $m$ . Only three concentrations of emulsions were needed because there is very little scatter. The slope of this line is equal to  $S_a$ , the grams of adsorbed soap per gram of emulsion solid, and the intercept equals the c.m.c. for the soap in the emulsion solution. If  $S_i$  is the grams of soap initially on the surface of a gram of emulsion solid and the emulsion is titrated with the original soap, then the surface area per gram of solid is  $a \cdot (S_a + S_i)$ , where  $a$  is the effective area of 1 gram of soap.

From this area and the weight of polymer the surface-average radius,  $r_s$ , is obtainable (7). This radius is defined by Eq. [1].

$$r_s = \frac{\sum_i n_i r_i^3}{\sum_i n_i r_i^2} \quad [1]$$

Here  $n_i$  is the number fraction of particles of radius  $r_i$ .

The particle size distributions obtained by the use of the Spinco Model L ultracentrifuge depend on the use of Stokes' law, etc. The applicability of

this technique has been shown by a number of investigators (8, 9). This technique has also been extensively investigated in our laboratories and found to give a possible error in determination of the radius of approximately 8%.

#### DETERMINATION OF THE EFFECTIVE SURFACE AREA OF EMULSIFIERS

The Gibbs adsorption isotherm was used to obtain the effective surface area of the soaps. The following equation defines the isotherm:

$$\frac{-d\gamma}{d \log C} = 2.303RT\Gamma \cdot n \quad [2]$$

where:  $\gamma$  = the interfacial tension at a concentration of soap  $C$ ;

$\Gamma$  = surface concentration;

$R$  = the gas constant,  $8.3 \times 10^7$ ;

$T$  = the absolute temperature;

$1 \leq n \leq 2$ ,  $n$  dependent on concentration of ions other than the surface-active agent being investigated.

The area ( $A$ ) is calculated from the relationship:

$$A = \frac{10^{16}}{\Gamma \times N}, \quad [3]$$

where  $N$  is Avogadro's number.

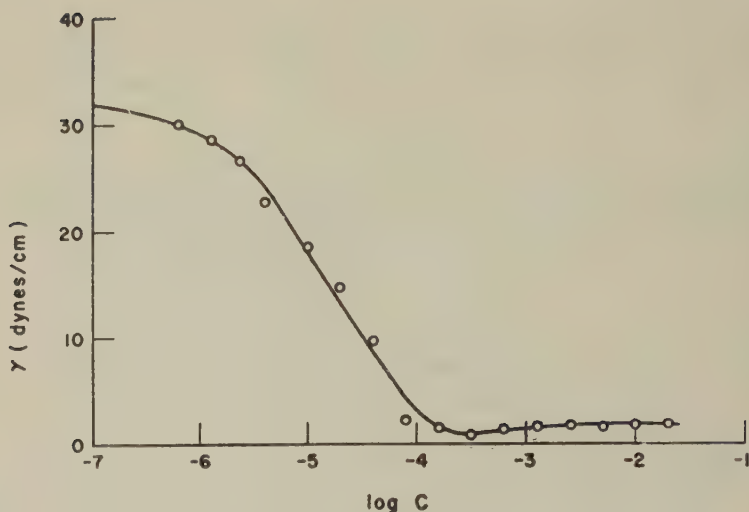
The interpretation of this type of data using the Gibbs adsorption isotherm has been described by Pethica (10) and Cockbain (11). To remove any ambiguity in interpreting the plot of  $\gamma$  versus the logarithm of the concentration, the soap solutions were made 0.2  $M$  with respect to NaCl. In this situation of an excess of salt  $n = 1$ . To have an environment for the soap similar to the polymer particles the interfacial tension between water and  $n$ -hexane (Fig. 3) was measured and not that between water and air. This gave an effective surface area of 61  $\text{A}^2$  for sodium lauryl sulfate, in good agreement with the value of 58  $\text{A}^2$  found by Tartar (12) from light scattering. The air environment gave an area of 38  $\text{A}^2$ , which was much too low.

The alkyl aryl polyether sulfonate, X-202, was treated in the same manner yielding an effective surface area of 62  $\text{A}^2$ .

In determining the effective surface area of the nonionic OPE it was not necessary to buffer the soap solution with salt. However, this experiment was tried and no difference was observed in the effective area obtained with or without the salt. This effective area was found to be 88.5  $\text{A}^2$ .

#### REPRODUCIBILITY OF THE TECHNIQUE

The reproducibility was checked by determining the surface-average radius of (IV) three times with sodium lauryl sulfate solutions, three concentrations of emulsion being titrated each time. The results (Table I) have

FIG. 3. Interfacial tension between *n*-hexane and soap solutions.TABLE I  
*Reproducibility of Soap Titration*

Experiment	$r_s(\mu)$	$r_s - \bar{r}_s$	$(r_s - \bar{r}_s)^2$
#1	0.26	0.00	$0.00 \times 10^{-4}$
#2	0.23	0.03	$9.0 \times 10^{-4}$
#3	0.29	0.03	$9.0 \times 10^{-4}$

$$\bar{r}_s(\mu) = 0.26 \pm 0.02 \mu, \quad \sigma = 0.03.$$

a probable error of approximately 7.7%, which is reasonable considering the small number of experimental points entering into each determination.

#### VALIDITY OF THE SOAP TITRATION RESULTS

The validity of the radii determined by soap titration can be shown by comparison with the surface-average radii determined from the particle size distributions obtained from the ultracentrifuge experiments. These radii are also defined by Eq. [1] as are those determined by soap titration. The comparisons are given in Table II.

The agreement found among the results is seen to be quite good. In the comparisons the question arises whether the sodium lauryl sulfate present initially on the surface of the emulsion particles of (I), (II), and (III) is displaced by either the OPE or the X-202 when they are used as titrants. The fact that the agreement between the three soaps and the ultracentrifuge is not different for (I) and (IV) indicates that displacement

TABLE II  
*Comparison of Radii Determined by Different Soaps and Methods*

	(I) $r_s$ ( $\mu$ )	(II) $r_s$ ( $\mu$ )	(III) $r_s$ ( $\mu$ )	(IV) $r_s$ ( $\mu$ )
Ultracentrifuge	0.070	0.045	0.022	0.28
NaLS	0.072	0.051	0.026	0.26
OPE	0.069	—	—	0.32
X-202	0.070	—	—	0.28

does not take place. Moreover, in one experiment emulsion (I) was mixed with a mixed-bed ion-exchange resin to remove the original sodium lauryl sulfate, and the remaining suspension was titrated with the OPE. The surface-average radius obtained in this manner was the same as that reported in Table II, which was obtained by assuming no displacement.

### CONCLUSIONS

The assumption of Maron *et al.* (7) that a monolayer was formed on the particles in the course of the soap titration seems self-evident. However, they essentially calibrated the soap and would get correct particle sizes even if multilayers were formed. The fact that the effective surface areas look reasonable for monolayers strongly indicates that the assumption is correct.

In the work reported here an independent method, i.e., the use of the Gibbs adsorption isotherm, was used to obtain the effective surface areas of the soaps. Since it has been shown (13) that a monolayer is present at such an interface, correct particle sizes would be calculated only if a monolayer is present on the particles at the completion of the soap titration. Therefore the good agreement shown in Table II leads to the conclusion that the latices must have been covered with a monolayer.

The soap titration technique is relatively fast and reasonably accurate and requires only inexpensive equipment provided the effective surface areas of the soaps used are known. In this report a method of obtaining this parameter which does not require an electron microscope or other elaborate equipment is demonstrated. Therefore it is possible to titrate any emulsion with the same soap that is initially on the surface, taking only a short time to determine its effective surface area. This use of the same soap will eliminate any problems of equilibrium between the two soaps on the surface, etc. However, there must be a reasonable differential between the surface tension of the original emulsions and that of the soap past its c.m.c. point for accurate determinations.

It has also been shown that acrylic emulsions can be soap titrated not only with the usual anionic soaps such as sodium lauryl sulfate but also with nonionics such as OPE.



## ACKNOWLEDGMENTS

The authors wish to thank Dr. B. E. Larsson for preparing the emulsion samples and Mr. J. E. Mark for making many of the measurements. The advice of Dr. H. Greenwald is also gratefully acknowledged.

## REFERENCES

1. KLEVENS, N. B., *J. Colloid Sci.* **2**, 365 (1947).
2. BORDERS, A. M., AND PIERSON, R. M., *Ind. Eng. Chem.* **40**, 1473 (1948).
3. WILLSON, E. A., MILLER, J. R., AND ROWE, E. H., *J. Phys. & Colloid Chem.* **53**, 357 (1949).
4. MARON, S. H., MADOW, B. P., AND KRIEGER, I. M., *J. Colloid Sci.* **6**, 584 (1951).
5. MORTON, M., SALATIELLO, P. P., AND LANDFIELD, H., *J. Polymer Sci.* **8**, 279 (1952).
6. MORTON, M., CALA, J. A., AND ALTIER, M. W., *J. Polymer Sci.* **19**, 547 (1956).
7. MARON, S. H., ELDER, M. E., AND ULEVITCH, I. N., *J. Colloid Sci.* **9**, 89 (1954).
8. NISONOFF, A., AND HOWLAND, L., *Anal. Chem.* **26**, 856 (1954).
9. BROWN, C., *J. Phys. Chem.* **48**, 246 (1944).
10. PETHICA, B. A., *Trans. Faraday Soc.* **50**, 413 (1954).
11. COCKBAIN, E. G., *Trans. Faraday Soc.* **50**, 874 (1954).
12. TARTAR, H. V., *J. Phys. Chem.* **59**, 1195 (1955).
13. ALEXANDER AND JOHNSON, "Colloid Science." Oxford University Press, London, 1950.

LETTER TO THE EDITOR

CRYSTALLINE POLYACRYLIC ACID

We have prepared stereoregular polyacrylic acid by acid (HCl) hydrolysis of crystalline poly(*t*-butyl acrylate) (1). The initial poly(*t*-butyl acrylate), which was prepared by polymerization with lithium dispersion, contained only 2 p.p.m. of residual lithium. Infrared examination of the polyacrylic

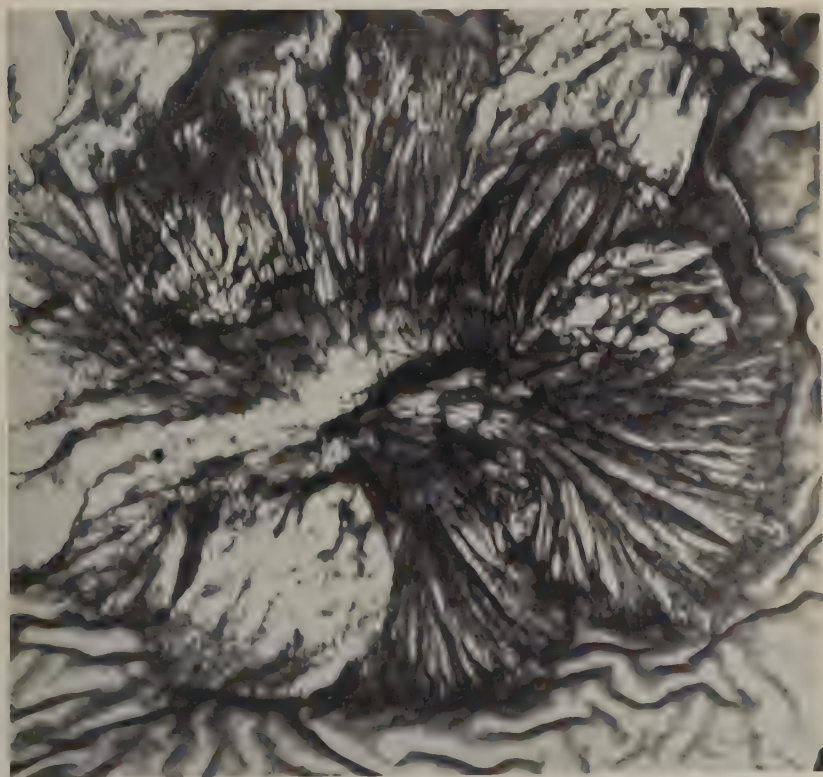


FIG. 1. Electron micrograph of crystalline polyacrylic acid, 4000 $\times$ .

acid showed no evidence of impurity or of ionized carboxyl. Films of stereoregular polyacrylic acid, which gave a crystalline X-ray pattern, were made by evaporating successive layers (10 or more) of a dilute aqueous solution (0.08% or less) at 7°C. When these films were examined with the polarizing



FIG. 2. Electron micrograph of crystalline polyacrylic acid, 4000 $\times$ .

microscope birefringent rodlike structures and birefringent spherulites were observed. These structures increased in size and in numbers when the films were kept at 7°C. for 4 to 6 weeks. Examination of the films with the electron microscope showed sheaf-like structures, Fig. 1, which are characteristic of crystalline polymers (2). The electron microscope also revealed a few regular rhomboidal structures, Fig. 2. These rhomboids are like the "single crystals" of linear polyethylene that were observed by Till (3) and by Keller (4). Keller also reported (4), but did not picture, similar structures in isotactic poly(4-methylpentene-1). The regularity of the rhomboids in Fig. 2 is evidence of a high degree of stereoregularity both in the polyacrylic acid and in the poly(*t*-butyl acrylate) from which it was made.

#### REFERENCES

1. MILLER, M. L., AND RAUHUT, C. E., *J. Am. Chem. Soc.* **80**, 4115 (1958).
2. KELLER, A., *Nature* **169**, 913 (1952).

3. TILL, P. H., JR., *J. Polymer Sci.* **24**, 301 (1957).
4. KELLER, A., AND O'CONNOR, A., *Discussions Faraday Soc.* **25**, 114 (1958).

M. L. MILLER

M. C. BOTTY

C. E. RAUHUT

*Polymer Chemistry Section,  
Research Division, Stamford Laboratories,  
American Cyanamid Company,  
Stamford, Connecticut.*

*Received August 13, 1959.*



## BOOK REVIEWS

**Estimation of Thermodynamic Properties of Organic Compounds.** By GEORGE J. JANZ, Department of Chemistry, Rensselaer Polytechnic Institute, Troy, New York. Academic Press, New York, 1958. x + 211 pp. Price \$7.00.

Many chemists and engineers fail to apply thermodynamic analysis to their research and development problems because the data they need often are not available in the literature and because they do not feel competent to make reliable estimates. Professor Janz's book is the first to make the task of estimating thermodynamic data easy for the nonexpert.

In Part I Janz summarizes the principles and methods of classical and statistical thermodynamics. Then he describes in adequate detail the most useful methods for estimating thermodynamic data for organic compounds. The liberal use of detailed numerical examples will help the reader learn to apply each method described. The last chapter of the descriptive text contains instructive examples of thermodynamic analysis of chemical processes.

Part II of the book is a convenient collection of all the numerical information needed in using the methods of calculation described in Part I. Thus, this book is a complete manual for practical application of thermodynamics to problems in organic chemistry. A detailed table of contents, good author and subject indexes, and adequate literature references should make the book easy to use in everyday work.

As Janz points out, some of the methods of correlation are based on obsolete thermodynamic data. However, he describes the construction of the correlations in enough detail so the user can revise the correlations on the basis of more recent results available in other literature. The book contains no more errors (perhaps chiefly typographical) than are expected in a first edition with so many equations and tables. However, use of erroneous symmetry number terms in several places (Examples 5.4, 5.5, and 5.9 and Equation 6.3) may confuse the reader who is learning to apply symmetry corrections for the first time.

Because the book collects information that is scattered through the literature of the past 30 years, it will prove useful to any practicing thermodynamicist. Likewise, it should be valuable for the nonexpert to use in learning how to apply the powerful tool of thermodynamics in his own research.

JOHN P. McCULLOUGH, Bartlesville, Oklahoma

**Sulfur in Proteins.** Proceedings of a Symposium Held in Falmouth, Massachusetts, in May, 1958. Edited by RHEINHOLD BENESCH and six others. Academic Press Inc., New York, 1959. 469 + vii pp. Price \$14.

This volume contains twenty-eight papers presented at the symposium, with edited accounts of the discussion following each paper (almost fifty active investigators participated). In addition, an excellent and critical summary by Professor John Edsall of Harvard does much to unify the proceedings and to place them in perspective.

The papers presented are almost wholly concerned with the sulfur of cysteine and cystine in proteins, but the scope of the topics covered in the collection is remarkably broad, not only with respect to the proteins considered (numerous enzymes, hemoglobin, muscle proteins, fibers, transport proteins, and viruses), but in the techniques

evaluated or used (mercaptide titrations with various metals, amperometry, suppression or modification of specific activity, isotopic labeling, light scattering, fluorescence analysis, ultracentrifugation, optical rotation, and "unmasking" with hydrogen bond breaking reagents such as urea). The aims of the various papers also differ very widely—from elucidation of the part played by disulfide bridges in the tertiary structure of each protein, or of the possible specific role of thiols and disulfides in their characteristic active sites, to broad considerations of the basic mechanisms of, for example, the dehydrogenases or of muscular contraction, in which the role of sulfur is only one aspect or in which its significance is still not firmly demonstrated. There are even a few papers that are concerned primarily with the analysis of biological structures such as the mitotic apparatus, and make use of sulfur chemistry primarily as a tool in aiding the isolation or recovery intact of these elusive structures after the destruction of the organization of cells. Nutrition, alone, seems to have been omitted—a circumstance which is undoubtedly related to the lack of attention to the essential amino acid, methionine.

It would be difficult to make specific comments on each of so many papers, and general comments would be inappropriate for a collection that represents such diverse primary interests. Although the papers are by no means uniformly excellent or persuasive, those which are of outstanding interest are sufficiently numerous to make one hesitate to single out a small number for special praise. The reviewer must therefore content himself with noting that the collection is eminently successful as a comprehensive statement of our present knowledge of cysteine and cystine sulfur in proteins, and as such, will be found stimulating and useful by all workers in the protein field.

JACINTO STEINHARDT, Cambridge, Massachusetts

**The Structure and Properties of Porous Materials.** Edited by D. H. EVERETT and F. S. STONE. Proceedings of the tenth symposium of the Colston Research Society, Bristol, England. March 24–March 27, 1958. Academic Press Inc., New York, 1958. xiv + 389 pp. Price \$12.00.

This book is made up of a series of lectures presented by some of the leading scientists in the world in the field of adsorption and capillary condensation. The context of the volume can perhaps be best judged by the titles of the papers and the names of the authors who contributed to the symposium. These are as follows: "Introductory Lecture," Sir Eric Rideal; "Aspects of sorption in porous crystals," R. M. Barrer; "The surface characteristics of carbons," W. F. K. Wynne-Jones; "Energetics of sorption," G. L. Kington; "The shapes of capillaries," J. H. de Boer; "Some problems in the investigation of porosity by adsorption methods," D. H. Everett; "The flow of low boiling gases through Saran charcoal," J. R. Dacey and J. A. Fendley; "Statistical descriptions, correlation factors, and physical properties of granular and porous solids," E. A. Flood; "The relation between gas permeability and pore structure of solids," P. K. C. Wiggs; "The structure of certain corpuscular adsorbents and its influence on their adsorptive properties," A. V. Kiselev; "The preparation and adsorptive properties of silica gels," A. G. Foster and J. M. Thorp; "Influence of surface charges on the properties of porous materials," R. K. Schofield; "The influence of the adsorption of cations on the texture and structure of silica gels," C. Mougey, J. Francois-Rossetti, and B. Imelik; "The structure of porous metal films and its influence on chemisorption properties," N. N. Kavtaradze; "The porous structure of paper," H. F. Rance; "The interaction of swelling agents with wool and nylon," G. King; "The structure of porous building stone and its relation to weathering behaviour," D. B. Honeyborne and P. B. Harris; "The ascent of sap and the movement of soluble carbohydrates in stems of higher plants," R. D. Preston. As is evident from the titles, most of the chapters are devoted to the discussion of basic scientific problems that

have been dealt with in the literature for many years but have never been completely solved. In a sense one might term most of these papers as up-to-date progress reports on the present status of our knowledge in regard to various aspects of the structure and properties of porous materials.

The articles are critical, authentic, and very valuable for those working in the field of porous solids. This reviewer gets the impression that they are not intended as historic and detailed reviews of all that has been published on the topics treated but rather are up-to-date summaries of the present status of our knowledge in regard to the topics treated. The last four sets of chapters are excellent illustrations of the importance of capillary phenomena in a variety of natural processes and industrial processes.

The book is beautifully written and carefully edited; the paper, the illustrations, and the reproductions in the book impress this referee as being of the very highest quality. In brief, this book will be very valuable to those who wish to maintain up-to-date information relative to theory of the structure and properties of porous materials, with regard both to the scientific aspects of the subject and to applications to problems involving adsorption and capillary condensation.

PAUL H. EMMETT, Baltimore, Maryland

## CAPILLARY VISCOMETER FOR NON-NEWTONIAN LIQUIDS

A. W. Sisko

*Research and Development Department, Standard Oil Company (Indiana),  
Whiting, Indiana*

*Received August 1, 1959*

### ABSTRACT

A capillary viscometer having a wide range of shear rates (0.02 to 40,000  $\text{sec}^{-1}$ ) has been developed, and factors contributing to the response of the instrument have been analyzed. The analysis showed that time and sample can be conserved by the proper selection of pressure gauges and by the exclusion of air. The instrument has been used to study the flow behavior of lubricating greases over a range of shear rates wide enough that both pipe and capillary viscometers are usually needed to cover it.

### INTRODUCTION

Capillary viscometers are widely used for measuring the flow characteristics of liquids. In these instruments, the viscosity of Newtonian liquids is determined from the measurement of a single pressure drop and a single flow rate. Non-Newtonian liquids, however, require observations that extend over a range of flow rates. Usually the flow rate is measured at various pressures, or the pressure at various flow rates. Viscometers of the latter type are particularly convenient to use and have found wide acceptance in grease research (1-4).

A desirable feature of viscometers for non-Newtonian liquids is that they allow the determination of viscosity over a wide range of shear rates. Data over such a range provide means for severely testing theories of flow. Suitable data have been obtained by the use of capillary viscometers in conjunction with pipe viscometers (5, 6). The inconvenience of operating two viscometers and the saving in time and material that would be realized prompted the development of a single instrument of wide shear-rate range.

### DESCRIPTION

Viscometers in which pressures are measured at fixed flow rates require nonpulsating volumetric pumps, a wide range of flow rates, and rapid pressure response. The new instrument features a piston pump with a 224-fold range of flow rates and strain-gauge pressure transducers. It also includes a sample cylinder with floating piston and stainless-steel capillaries. The shear-rate range is 0.02 to 40,000  $\text{sec}^{-1}$ .



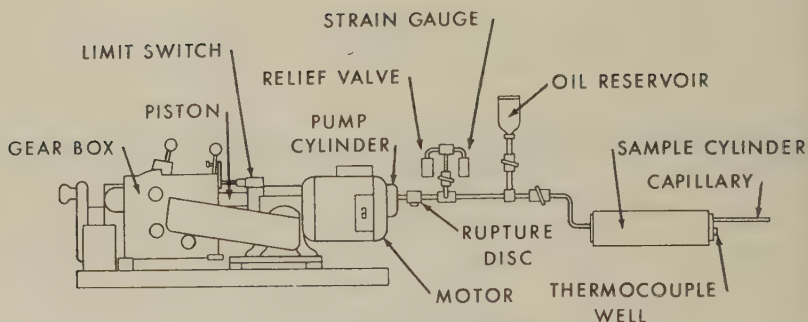


FIG. 1. Diagram of viscometer.

The arrangement of components is shown in Fig. 1. A 500-c.c. piston pump (Ruska Instrument Co., Houston, Texas), driven by a synchronous motor, forces a hydraulic fluid (SAE-40 oil) into the sample cylinder of the instrument. Delivery is controlled by a gear box that provides 28 piston speeds to give flow rates from  $1.56 \times 10^{-3}$  to  $350 \times 10^{-3}$  c.c. per second. Without leaking, the pump dispenses up to its maximum operating pressure of 4000 p.s.i. It is equipped with a travel-limit switch.

Pressure in the hydraulic fluid is measured by strain-gauge transducers. Three gauges with ranges of 30, 500, and 5000 p.s.i. are used. The 30- and 500-p.s.i. gauges are protected by relief valves and can be isolated from the system by manual valves; the 5000-p.s.i. gauge and the pump are protected by a 4000-p.s.i. rupture disk. (For simplicity, Fig. 1 shows only one of the strain gauges and relief valves.) The gauges are operated from a dry-cell power supply equipped for independent zeroing of each gauge. A low-resistance microammeter measures the gauge output.

The sample cylinder is a 660-c.c. pressure vessel with smooth internal walls. The threaded caps of the cylinder have O-ring seals that hold full pressure when tightened by hand. The selected capillary and a thermocouple well are threaded into the cap at the sample end.

Three pairs of stainless-steel capillaries are used. The members of each pair have the same radius but differ in length. The length difference permits correction for friction of the floating piston and for capillary-entrance effects.

#### OPERATION

The sample cylinder is filled by setting it upright, removing the cap at the sample end, and pouring or packing the sample into the cylinder. The end cap is replaced, the cylinder is inverted, and the other end is filled with hydraulic oil. The cylinder is then attached to the hydraulic-oil outlet, and the desired capillary is threaded into place. Care must be taken to avoid introducing air when filling and assembling the sample cylinder,

as air slows the response of the instrument. The valve below the oil reservoir is opened, and the pump cylinder is filled by retracting the piston. The power supply is turned on and adjusted to 12 volts. After a 15-minute warm-up period, the strain gauges are individually zeroed against a reference head of oil in the reservoir, the reservoir valve is closed, and the viscometer is ready to operate.

The pump is started and a gear setting is selected. As sample is discharged, pressure in the instrument rises and levels off at a value determined by the flow rate and the viscosity. Pressures are measured at the same flow rates in each member of a capillary pair.

### CALCULATIONS

In capillary viscometry, flow rate  $Q$  and pressure drop  $P$  are measured and used in Poiseuille's equation to obtain viscosity  $\eta$ , shearing stress at the wall  $F$ , and rate of shear  $\dot{\gamma}$ . These quantities are defined by

$$\eta = \frac{\pi R^4 P}{8 L Q}; \quad F = \frac{R P}{2 L}; \quad \dot{\gamma} = \frac{4 Q}{\pi R^3};$$

where  $R$  and  $L$  are the radius and length of the capillary in centimeters,  $P$  is measured in dynes/cm.<sup>2</sup>, and  $\eta$  is measured in poises. The rate of shear in a capillary varies from zero at the center to a maximum at the wall. For non-Newtonian fluids, viscosity varies with shear rate, and use of these relationships results in the calculation of an apparent viscosity and a nominal shear rate at the wall. When data from viscometers of different geometries are to be compared, these quantities must be converted to viscosity and shear rate. The standardized treatment of viscometric data (7) is convenient for doing so.

In this viscometer, flow rates in cubic centimeters per second are obtained directly from the gear-box setting by multiplying by a proportionality factor. The factor is calculated from the speed of the motor, the gear reduction, and the area of the piston.

Pressure in the hydraulic fluid is directly related to strain-gauge output in microamperes,  $\mu\text{a}$ . The constant for each gauge was determined by calibration at 12 volts against a dead-weight gauge. Constants for the three gauges used are:

30-p.s.i.	0.4454 p.s.i./ $\mu\text{a}$ .
500-p.s.i.	5.780 p.s.i./ $\mu\text{a}$ .
5000-p.s.i.	59.95 p.s.i./ $\mu\text{a}$ .

Capillary dimensions were determined with a traveling microscope and checked by the use of viscosity standards. The dimensions, in centimeters, of the three pairs of capillaries are:

<i>Radius</i>	<i>L</i>	<i>S</i>
0.4415	88.74	17.78
0.09299	19.05	3.91
0.02330	4.541	0.976

where  $L$  and  $S$  are the lengths of the long and short capillaries. Corrections for piston friction and capillary-entrance effects are made from pressure drops measured at the same flow rate in the long and short members of a capillary pair. The true pressure drop,  $P$ , is then given by

$$P = (P_L - P_S) \frac{L}{L - S},$$

where  $P_L$  and  $P_S$  are the pressure drops in the long and short capillaries.

#### RESPONSE

Time and material are saved if the pressure drop  $P$  rapidly comes to equilibrium at any pumping rate. Delay in reaching equilibrium is caused by extrusion of the sample, expansion of the sensing element of the pressure gauge, and compression of any entrapped air. The time required can be calculated from an over-all rate equation:

$$Q = Q_c + Q_g + Q_a$$

summing capillary flow, gauge filling, and air compression. The term  $Q_c$  is represented by Poiseuille's equation. An expression for  $Q_g$  is obtained by assuming a linear dependence of gauge volume on pressure,  $P - P_0 = b(V_g - V_0)$ , where  $P_0$  is atmospheric pressure,  $V_g$  is the gauge volume,  $V_0$  is the gauge volume at atmospheric pressure, and  $b$  is a compressibility constant. The flow rate into the gauge is:

$$Q_g = \frac{dV}{dt} = \frac{1}{b} \frac{dP}{dt}.$$

An expression for  $Q_a$  is derived from the ideal-gas law,  $(P + P_0)V_a = nk$ , where  $V_a$  and  $n$  are the volume and moles of air and  $k$  is a constant. The rate of compression of the air is:

$$Q_a = -\frac{dV}{dt} = \frac{nk}{(P + P_0)^2} \frac{dP}{dt}.$$

The over-all rate equation then becomes

$$Q = \frac{\pi R^4}{8L\eta} P + \frac{1}{b} \frac{dP}{dt} + \frac{nk}{(P + P_0)^2} \frac{dP}{dt}.$$

Integrating and applying the condition that the pressure drop is zero when  $t = 0$  gives the response equation:

$$t = \frac{1}{Ab} \ln \frac{Q}{Q - AP} + \frac{nk}{AP_0 + Q} \left[ \frac{P}{P_0(P + P_0)} + \frac{A}{AP_0 + Q} \ln \frac{Q(P + P_0)}{P_0(Q - AP)} \right],$$

where  $A = \pi R^4/8L\eta$ .

In the absence of entrapped air, the response equation simplifies to:

$$t = \frac{1}{Ab} \ln \frac{Q}{Q - AP}.$$

Substituting the expression for  $A$  and solving for  $P$  gives the change in pressure drop with time

$$P = \frac{8LQ\eta}{\pi R^4} \left[ 1 - e^{-\frac{\pi R^4 b}{8L\eta} t} \right].$$

When the final pressure drop for the particular flow rate has been reached, no more liquid flows into the gauge,  $Q_c = Q$ , and  $P = 8LQ\eta/\pi R^4$ . Sample and time are conserved if the factor  $R^4b/L\eta$  is large. With a fixed set of capillaries, response is speeded by increasing the value of the gauge constant  $b$ . This means that the volume of the sensing element must change little with pressure. For this reason, manometers are unsuitable. More desirable

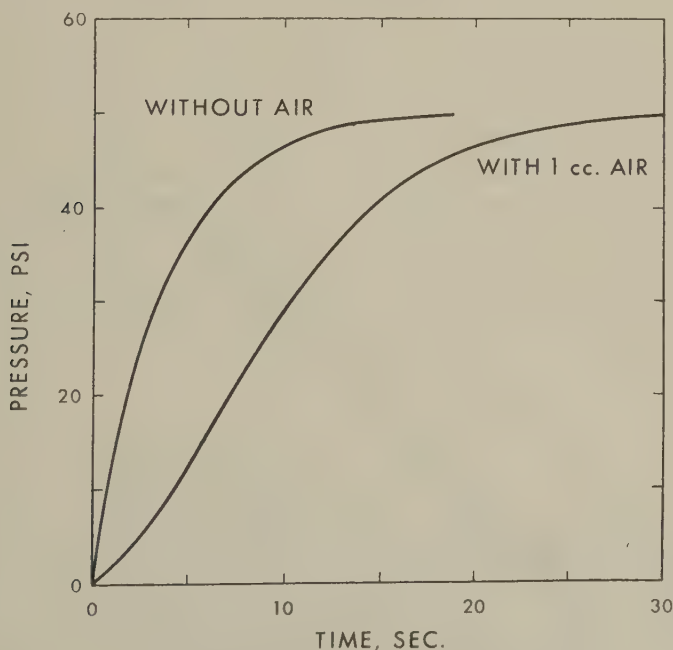


FIG. 2. Calculated effect of air on response.



is a gauge in which the deflection of the sensing element is mechanically or electrically amplified. Strain-gauge pressure transducers have high values of  $b$  and are thus particularly suitable.

The response equation permits calculation of the time required to reach 99% of the final pressure drop with or without entrapped air present. Figure 2 shows the calculated response curves for these conditions. The calculations are for the flow of a liquid of 100 poise viscosity in a capillary 10 cm. in length and 0.1 cm. in radius. At a pumping rate of 0.135 c.c. per second, the final pressure is 50.0 p.s.i. The gauge constant  $b$  was assumed equal to 100 p.s.i./c.c. In the absence of entrapped air, 17.2 sec. are required to reach 99% of full pressure. To determine the effect of 1 c.c. of entrapped air, a reasonable value for the gas constant was assumed,  $nk = 16.2$  p.s.i. c.c., and  $P_0$  was taken as 14.7 p.s.i. The time required for 99% of full pressure with 1 c.c. of air present is 30.8 sec.

### RESULTS

The viscosities of several Newtonian and non-Newtonian liquids were determined with the viscometer. For a Newtonian fluid,

$$F = \eta \dot{\gamma}.$$

A plot of  $\log \dot{\gamma}$  against  $\log F$  is a straight line of slope 1, and  $\log \eta = \log F$  when  $\log \dot{\gamma} = 0$ . Figure 3 shows such a plot for a commercial lubricating

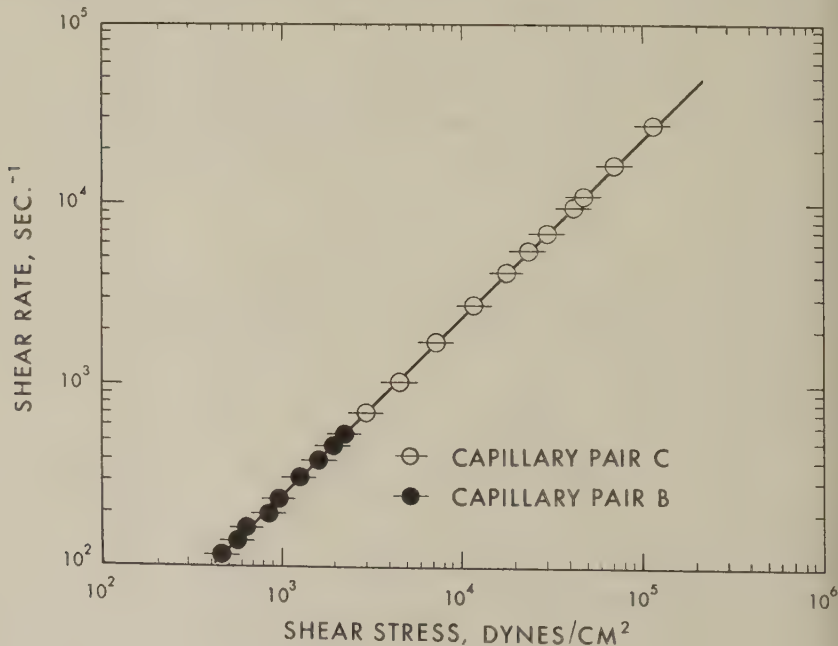


FIG. 3. Flow of SAE-40 oil at 25°C.

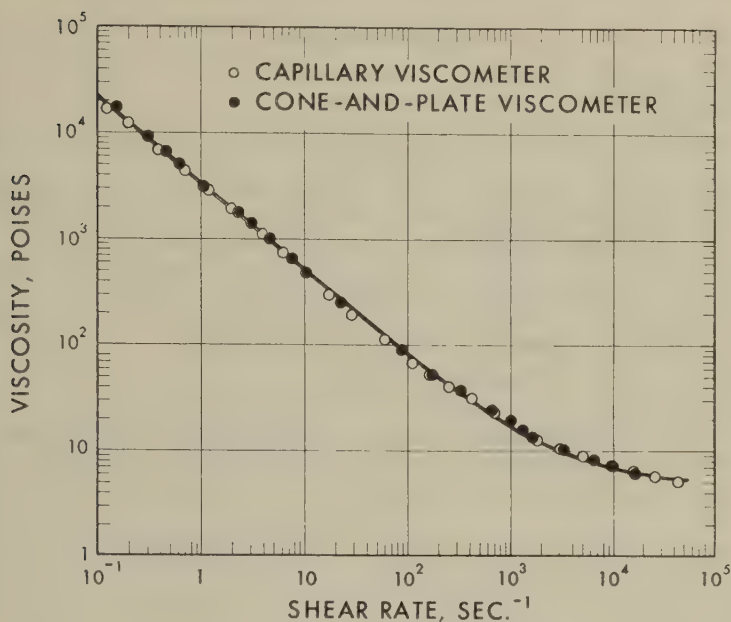


FIG. 4. Flow of lithium-soap grease.

oil that shows Newtonian behavior and has a viscosity of 4.08 poises at 25°C. The data were obtained with two of the capillary pairs.

The flow behavior of a non-Newtonian fluid, a lithium-soap grease, was determined in the viscometer and also in a cone-and-plate viscometer (8). Viscosity and shear rate can be calculated directly from data obtained with the cone-and-plate viscometer because the sample is uniformly sheared in this instrument. Apparent viscosities and nominal shear rates from the capillary viscometer were converted to viscosities and true shear rates. Figure 4 shows the effect of shear rate in these viscometers on the viscosity of the grease. The data from both instruments fall on a single smooth curve. An equation that has been proposed for the flow of lubricating greases (6):

$$\eta = 5.00 + 3,300 \dot{\gamma}^{-0.812}$$

fits the data well.

### CONCLUSION

The design of the new viscometer gives a response as rapid as is practically possible. With it the effect of the concentration and geometry of dispersed particles, as well as that of the viscosity of the continuous phase on the flow of non-Newtonian systems, can be studied. With suitable temperature control, the dependence of viscosity on temperature can be determined.

## ACKNOWLEDGMENTS

The author thanks Professors I. M. Krieger and S. H. Maron of Case Institute of Technology for their contributions to the project.

## REFERENCES

1. American Society for Testing Materials, "ASTM Standards on Petroleum Products and Lubricants," Philadelphia, 1955, D1092-55.
2. ARVESON, M. H., *Ind. Eng. Chem.* **24**, 71 (1932).
3. BRUNSTRUM, L. C., AND STEINBRUCH, R., *Institute Spokesman* **13**, No. 8, 10 (1949).
4. MARUSOV, N., *Institute Spokesman* **15**, No. 5, 8 (1951).
5. SUMMERS-SMITH, D., in "Proceedings of Conference on Lubrication and Wear," The Institution of Mechanical Engineers, London, 1957.
6. SISCO, A. W., *Ind. Eng. Chem.* **50**, 1789 (1958).
7. KRIEGER, I. M., AND MARON, S. H., *J. Appl. Phys.* **25**, 72 (1954).
8. MCKENNELL, R., in V. G. W. Harrison, ed., "Proceedings of the Second International Congress on Rheology," p. 350. Academic Press, London, 1953.

## THE SUCCESSIVE-EXTRACTION OF COLLAGEN FROM HIDE POWDER

Harry R. Elden and Robert J. Boucek

*Howard Hughes Medical Institute, Miami, Florida*

*Received May 25, 1959, revised August 13, 1959*

### INTRODUCTION

Numerous attempts have been made to purify collagen on the basis of its solubility. Salt- (1), acetic acid- (2), citric acid- (3), and alkali- (4) fractionations have been described. Mucopolysaccharides intimately associated with collagen add to the overall complexity.

Knowledge of the solubility properties of collagen-rich tissues would be a valuable asset to understanding their numerous physiological processes. The influence of aging—perhaps the direct process itself—might be ascertained by measuring the extractability of collagen from connective tissues.

Described in this report is a method of successive-extractions which was used to separate *hide powder* collagen into acetic acid-soluble and insoluble fractions. The dependence of concentration of dissolved collagen on extraction number followed a simple empirical relationship. The slope in this expression was shown to depend upon the pH of the solvent. The molecular characteristics of the solubilized collagen were determined by hydrodynamic methods and showed the presence of "native" collagen molecules.

### EXPERIMENTAL METHODS

American Standard Hide Powder<sup>1</sup> was used as the source of collagen for the following experiments.

*Equilibrium.* Solubilization equilibrium was studied by shaking 100, 150, 200, and 250 mg. of collagen at 6°-8°C. with 5.0 ml. of 0.5 *M* acetic acid for periods ranging from 0.25 to 24 hours. The samples were agitated on a mechanical shaker during the equilibration period. After 15 minutes centrifugation at 2500 r.p.m. the supernatant solution was analyzed for its collagen content by the biuret method.

*Successive Extractions.* Five milliliters of 0.5 *M* acetic acid were added to 100-mg. samples and shaken for 24 hours at 6°-8°C. The supernatant solution containing the acetic acid-soluble collagen was removed after

<sup>1</sup> Frank F. Marshall, Ridgeway, Pennsylvania.



centrifugation for 15 minutes at 2500 r.p.m. Fresh solvent was added and the process repeated until the collagen concentration of the solution decreased to a constant value of less than 0.01 mg./ml. Collagen concentration was determined by a Kjeldahl (Conway) analysis for nitrogen.

*pH and Temperature Dependence of Extraction.* Acetic acid-sodium acetate buffered solvents were made up with pH values ranging from 3.0 to 6.0 at 0.1 ionic strength (sodium acetate). The alkaline buffers ranging up to pH 8.0 were made up by using mono- and disodium acid phosphate salts with sufficient sodium chloride added to give 0.1 ionic strength. Solubilization was achieved by shaking 100-mg. samples for 24 hours with 5.0 ml. of buffered solvent and the supernate was removed after centrifugation as described previously. Five extractions were performed over the pH range of 3.0 to 8.0 at temperatures of 6.0° and 31.0°C. The collagen concentration ( $C$ ) was determined by nitrogen analysis and expressed as milligrams per milliliter.

*Molecular Characteristics of Soluble Phase.* The ultracentrifugal sedimentation of collagen soluble in 0.5  $M$  acetic acid was studied by using the Spinco analytical ultracentrifuge. Runs were made at  $250,000 \times g$  at 6°–8°C. and photographs were taken at 16-minute intervals. The sedimentation coefficient was calculated in the usual way from the slope of a plot of  $\log$  (distance from the center of the rotor to the peak) as a function of time. The concentration dependence of  $S$  was measured and plots of  $1/S$  vs.  $C$  and  $S$  vs.  $SC$  were made. The sedimentation coefficient at infinite dilution and the slope of the concentration dependence were evaluated from these graphs. Experimental  $S$  values were corrected for the viscosity of the solvent to that of water at 20°C.

The intrinsic viscosity and its concentration dependence were obtained at 6°–8°C. by using Ostwald-Fenske viscometers in which 5.0 ml. of 0.5  $M$  acetic acid had a flow time of 95 seconds. Five milliliters of a concentrated stock solution were added to the viscometer and flow times were measured at  $6.0^\circ \pm 0.1^\circ\text{C}$ . Measured volumes of 0.5  $M$  acetic acid were added in order to obtain flow times at lower concentrations of collagen. The reference flow times for the solvent were done in exactly the same manner. Collagen concentrations were determined by using a turbidimetric method which was standardized by Kjeldahl nitrogen analyses. The data were analyzed by plotting the concentration-reduced viscosity ( $\eta_{sp}/C$ ) as a function of the concentration ( $C$ ).

## RESULTS

*Rate of Solubilization.* Figure 1 shows that 100- and 200-mg. samples of collagen rapidly approached a solubilization equilibrium. No difference was detected in the concentration (absorption of the biuret complex) of collagen obtained between 15 minutes and 24 hours of extraction at 6°–8°C. by

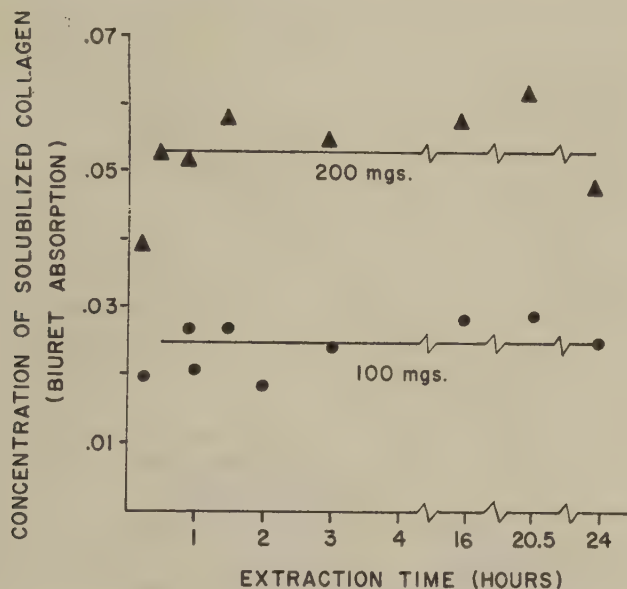


FIG. 1. Dependence of extractability on time in 0.50 *M* acetic acid at 6.0°C.

0.5 *M* acetic acid. However, it was observed that with insufficient agitation solubilization equilibrium either was not reached or was approached at a very slow rate.

The equilibrium concentration was found to be related linearly to the quantity of hide powder initially added to the 5.0 ml. of 0.5 *M* acetic acid. See Fig. 2.

*Dilute Acetic Acid-Soluble Component.* The successive extractions of hide powder collagen by 0.5 *M* acetic acid showed that there were at least two types of collagen present in the original structure; one component called acetic acid-soluble was removed by four successive extractions. The residue remaining after four extractions was considered insoluble. A plot of the logarithm of the concentration ( $\log C$ ) as a function of the number of extractions minus one ( $n - 1$ ) is shown in Fig. 3. The  $\log C_n$  terms obtained during the first four extractions decreased linearly to a constant concentration value of 0.01 mg./ml., a tenfold reduction in solubility. Thereafter, they remained constant for three succeeding extractions. This phenomenon was observed for extractions done with 0.1, 0.5, and 1.0 *M* acetic acid. The slope of these three lines was calculated to be  $-0.24$ ,  $-0.30$ , and  $-0.33$ , respectively. Equation [1] was arrived at empirically on the basis of these data.

$$\text{Log } C_n = \text{Log } C_1 - (n - 1)B. \quad [1]$$

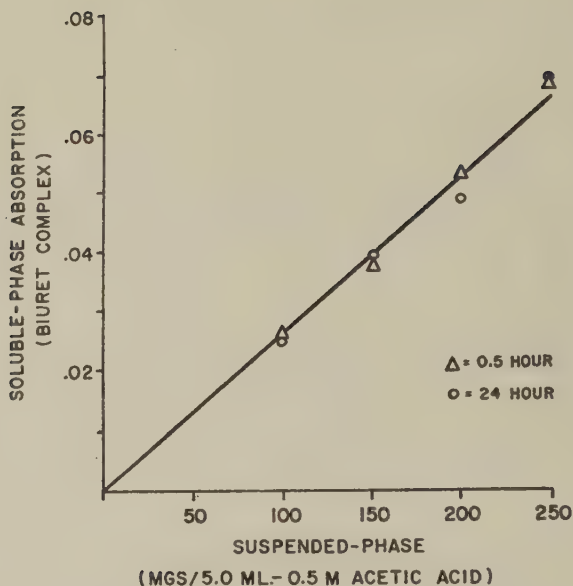


FIG. 2. Linear relationship between concentration of solubilized collagen and quantity of solid hide powder suspended in 0.5 M acetic acid.

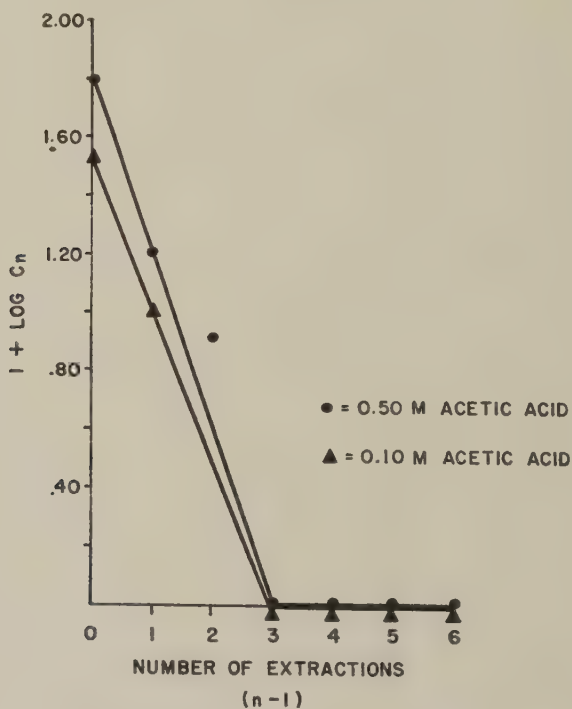


FIG. 3. Linear relationship between log (concentration of soluble phase) and extraction number minus one.

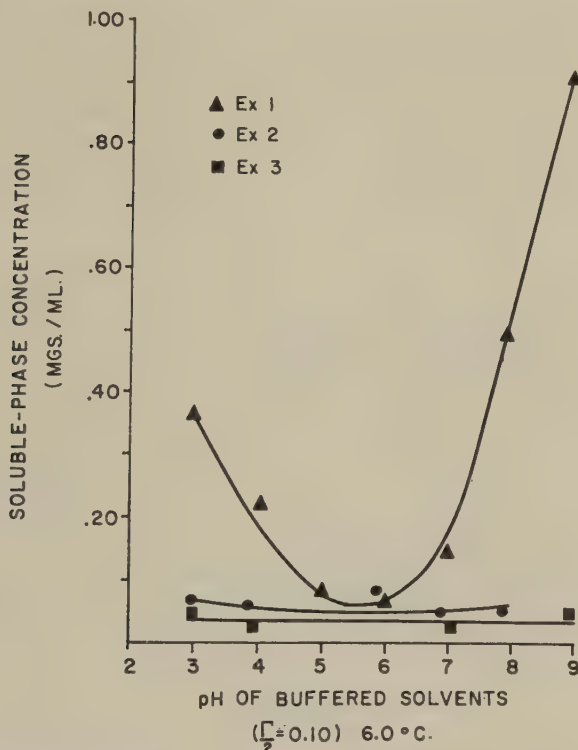


FIG. 4. Dependence of extractability on pH and extraction number.

The quantity ( $Q$ ) of collagen removed from the original 100 mgs. may be calculated by adding up the  $C_nv$  terms for the four extractions used to define this component; i.e.,  $Q = (C_1 + C_2 + C_3 + C_4)v$ , where  $v$  is the average of the four volumes of collagen solution. The quantity  $Q$  was found to be 3.3% of the original quantity of collagen.

*The Effect of pH and Temperature upon Extractability.* The concentration of soluble collagen was plotted as a function of pH. Figure 4 shows a minimum in the solubility at pH 5.5 for extract 1 at 6.0°C. The second and third extracts appear less dependent upon pH. A minimum at the same pH was observed for extract 1 made at 31.0°C. The second and third extracts also were dependent less upon pH at this temperature. Figure 5 shows that the slope ( $B$ ) was zero when the extractions were done at the isoelectric point of limed hide powder (pH 5-6). However, when the proteins were charged positively the solubilization showed a pronounced dependence upon number of extractions. Increased temperature raised the concentration ( $\log C_n$ ) of solubilized collagen but did not influence the slope ( $B$ ).

*Molecular Characteristics of Soluble Collagen.* The sedimentation coefficient



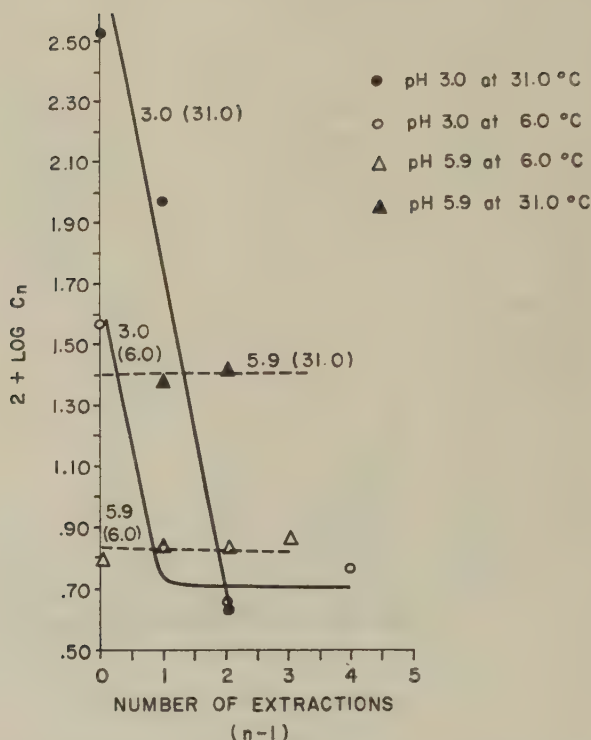


FIG. 5. The pH and temperature dependence of extractability of collagen.

at infinite dilution was found to be  $2.2 \times 10^{-13}$ . The slope of a linear regression line connecting 5 points for the equation  $1/S = 1/S_0 + K'C$  was  $K' = 4.3 \times 10^{13}$ . Thus, the slope of the function  $S_0/S = 1 + KC$  became  $S_0K' = 9.5$ . The experimentally determined intrinsic viscosity  $[\eta]$  was 13.5 dl./g., whereas the Huggins constant ( $k'$ ) in the viscosity equation  $\eta_{sp}/C = [\eta] + k'[\eta]^2C$  was 0.49.

#### DISCUSSION

The rate at which the concentration of soluble-phase collagen approaches its equilibrium value probably depends upon (a) the rate of diffusion of the solvent toward the surface of the insoluble phase, (b) the rate of diffusion of the soluble molecules away from the surface of the insoluble phase, or (c) the rate of interaction of the insoluble phase with the solvent on its surface. Sufficient mechanical agitation such as was used in these experiments removes the restrictions of (a) and (b) because an equilibrium was approached in about 15 minutes at 6°–8°C. When the samples were not agitated solubilization did not occur or did so at a very slow rate. This

finding agrees with those of Kritzing (5), who studied the influence of mechanical agitation on the saline-solubility of hide collagen.

The true solubility of collagen cannot be determined by this method. The data in Fig. 2 point out that the quantity solubilized depends upon the amount of solid added originally to the solvent. One explanation of this is that hide powder contains a number of "different" collagens. Whether these are different components or phases cannot be determined from these findings.

The more nearly "ideal" behavior occurs at pH 5-6, the isoelectric region for limed hide powder. At lower pH the system of collagens becomes heterogeneous and nonconstant solubility results. Temperature does not influence the heterogeneity, determined by comparing the slopes of Fig. 5, but merely changes the concentrations ( $\log C_n$ ). Further studies of the slope ( $B$ ) might yield an interpretation which would help in deciphering the complex heterogeneity of collagen.

The sedimentation coefficient of highly asymmetric macromolecules, such as collagen, depends upon their intrinsic viscosity. Golder (6) has shown that the sedimentation slope and the intrinsic viscosity can be related empirically so that an estimate of one can be obtained from the other. It was suggested that Eq. [2] be used to evaluate  $[\eta]$  from  $K$  when the latter was greater than 8.

$$K = 0.75 [\eta] + 5.5. \quad [2]$$

Using this an estimate of  $[\eta]$  was found to be 6.0. The data that were used by Golder as a basis of Eq. [2] show considerable spread and a better approximation can be made by Eq. [3], which was derived from thermodynamic considerations by Powell and Eyring (7).

$$A \approx [\eta] \quad [3]$$

Thus, the experimental values of  $A$  (9.5) and  $[\eta]$  (13.5) are closer. Further comment along these lines does not appear profitable except to say that the acetic acid extracts of hide powder contain large asymmetric molecules typical of native collagen (8, 9).

#### SUMMARY

Numerous attempts have been made to purify collagen on the basis of its solubility, and various fractionation schemes have been proposed to achieve this end. In this paper a method is presented for the successive extraction of American Standard Hide Powder using dilute acetic acid. It is shown that (1) an equilibrium concentration of solubilized collagen was reached in 15 minutes, (2) the amount dissolved was related linearly to the amount added to a given volume of solvent, (3) the concentration ( $C_n$ )

achieved obeyed the empirically observed equation,  $\log C_n = \log C_1 - (n - 1)B$ , where  $n$  is the extraction number and  $B$  is the slope of the log-plot, and (4) the slope ( $B$ ) was not influenced by temperature but it did depend upon pH.

Sedimentation and intrinsic viscosity measurements were done and showed the presence in acetic acid solutions of large asymmetric molecules typical of native collagen.

#### ACKNOWLEDGMENTS

We wish to express our appreciation to Drs. N. L. Noble, W. B. Dandliker, and J. F. Woessner, Jr., for their many stimulating thoughts and suggestions.

#### REFERENCES

1. GROSS, J., HIGHBERGER, J., AND SCHMITT, F., *Proc. Natl. Acad. Sci.* **41**, 1 (1955).
2. ZACCHARIADES, P. A., *Compt. rend. soc. biol.* **52**, 182, 1127 (1900).
3. OREKHOVITCH, V., AND SHPIKITER, V., *Science* **127**, 1371 (1958).
4. HARKNESS, R., MARKO, A., MUIR, H., AND NEUBERGER, A., in J. Randall, ed., *Nature and Structure of Collagen*, p. 208. Academic Press, New York, 1953.
5. KRITZINGER, C., *J. Am. Leather Chemists' Assoc.* **43**, 351 (1948).
6. GOLDER, R., *J. Am. Chem. Soc.* **75**, 1739 (1953).
7. POWELL, R. E., AND EYRING, H., *Advances in Colloid Sci.* **1**, 183 (1942).
8. BOEDTKER, H., AND DOTY, P., *J. Am. Chem. Soc.* **78**, 4267 (1957).
9. NODA, H., *Biochim. et Biophys. Acta* **17**, 92 (1955).

# THE MECHANISM OF PARTIAL COALESCENCE OF LIQUID DROPS AT LIQUID/LIQUID INTERFACES<sup>1</sup>

G. E. Charles and S. G. Mason

*Physical Chemistry Division, Pulp and Paper Research Institute of Canada,  
and Department of Chemistry, McGill University, Montreal, Canada*

*Received July 22, 1959*

## LIST OF SYMBOLS

- $a_i$  = diameter of  $i$ th stage drop.
- $L_i$  = height of  $i$ th stage liquid column.
- $p$  =  $\eta_1/\eta_2$  = viscosity ratio.
- $q$  = instability factor.
- $r_i$  =  $a_{i+1}/a_i$  = diameter ratio  $i$ th stage.
- $R, R_0$  = radius of liquid column; radius of column formed during partial coalescence.
- $t_b, t'_b$  = column break-up time; measured break-up time for partial coalescence.
- $Z$  =  $\lambda/2R$ .
- $\alpha, \alpha_0$  = amplitude of disturbance at time  $t$  and  $t = 0$ , respectively.
- $\eta_1, \eta_2$  = viscosity of Phases 1 (internal) and 2 (external), respectively.
- $\lambda_{\text{opt.}}$  = disturbance wavelength; optimum wavelength.
- $\rho_1, \rho_2$  = phase densities.
- $\sigma$  = interfacial tension.
- $\tau$  = rest time.

## INTRODUCTION

When a drop of liquid (Phase 1) immersed in an immiscible liquid of lower density  $\rho_2$  (Phase 2) falls gently on a flat interface separating Phases 1 and 2, it coalesces with the underlying phase after a rest-time  $\tau$  elapses (1-4). In many combinations of liquids, the coalescence is not complete, i.e., the primary drop is succeeded by a smaller secondary drop of Phase 1, and the cycle is repeated (1, 3, 4). As many as eight such stages of "partial coalescence" have been visually observed (4) with water drops at a benzene/water interface, and it is probable that there were additional stages which yielded submicron droplets (3, 4). This may be the reason for the

<sup>1</sup> Conducted with financial assistance from the Defence Research Board of Canada, RB Grant 9510-05.



reported accumulation of a fine mist after the coalescence of a large number of primary drops with the same interface in spite of elaborate measures to eliminate contamination (3). It may also be a cause of polydispersity in the coalescence of emulsions and mists.

In this paper we describe an investigation of the mechanism of partial coalescence and of the phase properties which determine its occurrence. The present investigation is limited to liquid drops falling on a flat liquid/liquid interface, i.e., where  $\rho_1 > \rho_2$ .

Since the phenomena described later have been analyzed with the aid of the theory of unstable liquid jets, it is appropriate to start with a brief discussion of the relevant parts of this theory.

### THEORETICAL PART

The stability of an infinitely long cylindrical column of radius  $R$  of an incompressible inviscid liquid initially in equilibrium with respect to the surface tension was treated theoretically by Rayleigh (5). He attributed the instability to a statistical distribution of capillary disturbances of amplitude  $\alpha$  and wavelength  $\lambda$  which are rotationally symmetrical about the axis of the column and which act to break it up (Fig. 1). According to Rayleigh, disturbances of  $\lambda > 2\pi R$  will grow in amplitude and cause the column to break up. This means that a column of finite length will tend to break up only if the length exceeds the circumference.

Neglecting inertial effects of the surrounding fluid as well as those from general translational motion of the liquid column and assuming  $\alpha$  of a disturbance of wavelength  $\lambda$  to increase with time according to

$$\alpha = \alpha_0 e^{qt}, \quad [1]$$

Rayleigh showed that  $q$ , the degree of instability ( $>0$  for a divergent disturbance), is given by

$$q = + \left( \frac{\sigma}{\rho_1 R^3} \right)^{1/2} F(Z). \quad [2]$$

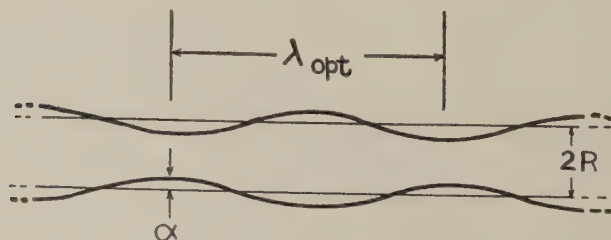


FIG. 1. Undulations in a liquid cylinder which lead to break-up as predicted by Rayleigh (5).

where  $\sigma$  is the interfacial tension,  $\rho_1$  is the liquid density, and  $F(Z)$  is a function of the dimensionless parameter  $Z = \lambda/2R$ .

Thus, according to Rayleigh, the disturbance for which  $F(Z)$  is a maximum will preponderate. It was shown (5-7) that the values of  $F(Z)$  calculated from Rayleigh's theory pass through a maximum of 0.343 near  $Z = 4.508$ , which gives directly the dominant (or optimum) wavelength of the disturbances leading to break-up as

$$\lambda_{\text{opt.}} = Z_0(2R) = 4.508 (2R). \quad [3]$$

A convenient parameter is  $\pi/Z_0$ , the ratio of circumference to optimum wavelength. Thus according to Eq. [3]  $\pi/Z_0 = 0.697$ . For the same case, Weber (8) calculated practically the same value, viz.,  $(\pi/Z_0) = (1/\sqrt{2}) = 0.707$ . Haenlein (9) obtained experimental values of  $(\pi/Z_0)$  ranging from 0.698 to 0.449 for water jets in air issuing from an orifice. Later, Tyler (10) reported an average value of about 0.68 for mercury, aniline, and water jets.

It follows from Eq. [1] that the time required for a rotationally symmetrical disturbance to attain an amplitude  $R$ , when the jet pinches off and breaks up, is

$$t_b = \frac{1}{q} \log_e \frac{R}{\alpha_0}. \quad [4]$$

Weber (8), neglecting external fluid effects, extended the Rayleigh analysis to the case of an infinite column of finite viscosity  $\eta_1$  and gave the following equations for the optimum conditions leading to break-up:

$$\frac{\pi}{Z_0} = \left[ 2 \left( 1 + \left( \frac{9\eta_1^2}{2\rho_1 \sigma R} \right)^{1/2} \right) \right]^{-1/2}; \quad [5]$$

$$t_b = \left[ \frac{1}{q} + \frac{6\eta_1 R}{\sigma} \right] \log_e \frac{R}{\alpha_0}, \quad [6]$$

where  $q$  is defined by Eq. [1].

Inspection of Eqs. [5] and [6] shows that  $t_b$  increases and  $(\pi/Z_0)$  decreases as  $\eta_1$  increases; this was confirmed experimentally by Haenlein (9).

The case in which the column of viscosity  $\eta_1$  is surrounded by a fluid of viscosity  $\eta_2$  was treated theoretically by Tomotika (11). Neglecting inertial effects, he predicted that  $(\pi/Z_0)$  corresponding to the maximum instability varies with the viscosity ratio  $p = \eta_1/\eta_2$ , passes through a maximum of 0.589 at  $p = 0.28$ , and tends to zero as  $p \rightarrow 0$  or  $\infty$ . For the limiting case when  $p \rightarrow \infty$ , the results are identical to those previously predicted by Rayleigh (12) for a column of a very viscous liquid. For simplicity, the complex equations deduced by Tomotika are not presented here; his final results are considered later.

In the experiments described below, the effects of varying  $p$  and  $\sigma$  upon partial coalescence were studied. Values of  $(\pi/Z_0)$ ,  $t_b$ , and  $\alpha_0$  were estimated from observations of drop break-up made by means of conventional and high-speed cine-photography.

## EXPERIMENTAL PART

### *Apparatus and Procedure*

The apparatus employed is illustrated schematically in Fig. 2 and consisted of a square optical-glass cell ( $A$ ) into which were placed the two immiscible liquids under study. The drop-forming assembly consisted of a tip ( $B$ ) immersed in the top phase (Phase 2), a manifold ( $C$ ) with reservoir ( $D$ ), and a microburet ( $E$ ). Drop volumes were read directly from the dial micrometer gauge of a Gilmont microburet (Emil Greiner Co.) to an accuracy of  $2 \times 10^{-4}$  ml. Volume measurements from the latter agreed to 0.1% with those calculated from weight determinations using water at a known temperature.

The tips employed were carefully prepared from stainless steel hypodermic needles of various sizes, cut to the desired lengths and ground to a  $45^\circ$  bevel. The radii of the two tips employed here were measured microscopically and were 0.0578 and 0.1162 cm.

Upon release, a Phase 1 drop fell gently onto the liquid/liquid interface

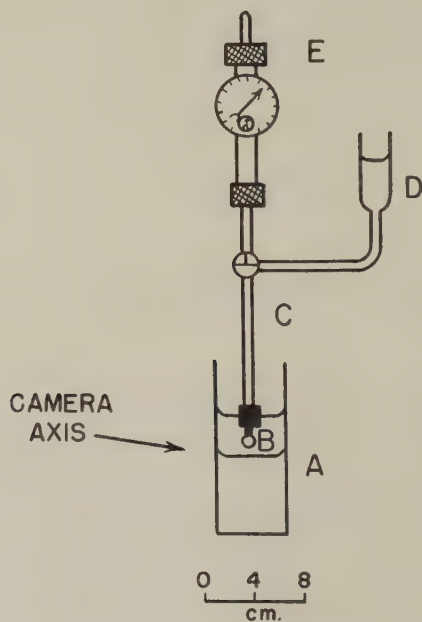


FIG. 2. Experimental arrangement for studying partial coalescence (schematic).

within the cell. To minimize impact effects, the level of the interface was maintained only 1 to 2 mm. below the drop at the time of release. All drops were aged for about 3 min. and released in accordance with the conventional drop-volume method for the determination of interfacial tension (13). Accurate knowledge of the drop volume and the tip radius permitted the interfacial tension to be calculated.

A Paillard-Bolex 16-mm. cine-camera adapted with a 25-mm. lens and a  $\frac{1}{2}$ -inch extension tube was used for the cine-photography study of the phenomena at speeds up to 64 pictures/sec. The diameters of the drops in successive stages were measured from the photographic film projected at known magnification.

The mechanism of partial coalescence was established with the aid of high-speed cine-photography using a Fastax Model WF-3 (Wollensak Optical Company, Rochester, New York) 16-mm. camera operated at film speeds ranging from 1000 to 3500 pictures/sec. The film speed was registered directly on the film by the built-in timing light operated at 1000 impulses/sec. from a crystal-controlled pulse generator. Two 1000-watt Wollensak Floodlites supplied the necessary illumination. All experiments, except those on drop stability, were conducted at a temperature of  $25^{\circ} \pm 2^{\circ}\text{C}$ .

### *Materials*

Distilled water was used as one of the liquid phases. Benzene, carbon tetrachloride, aniline, cyclohexanol, ethyl ether, toluene, heptane, mercury, cyclohexane, and Nujol (medicinal—heavy grade) were used as second phases. The organic liquids were of A.C.S. certified quality.

Mixtures of glycerol (96% by weight) and water of different proportions were substituted for water in some of the experiments.

Tergitol NPX was used in the system benzene/water to study the effect of a surface-active agent. This nonionic material is an alkyl phenyl polyethylene glycol ether made by Carbide and Carbon Chemicals Co.

## RESULTS

### *Mechanism of Partial Coalescence*

The events occurring during the partial coalescence of an aniline drop at a water/aniline interface are illustrated in the sequence of images in Fig. 3. These are typical of all the systems examined.

Prior to coalescence, the primary aniline drop resting at the interface (Fig. 3a) is separated from the bulk of the underlying similar liquid by a thin intervening layer of water (Phase 2). Following the rupture of this thin film (Fig. 3b), the hole expands very rapidly (at speeds up to 300 cm./sec. for various other systems (4)) and allows the liquid in the drop to drain into the bulk phase. The rapid retraction of the punctured film



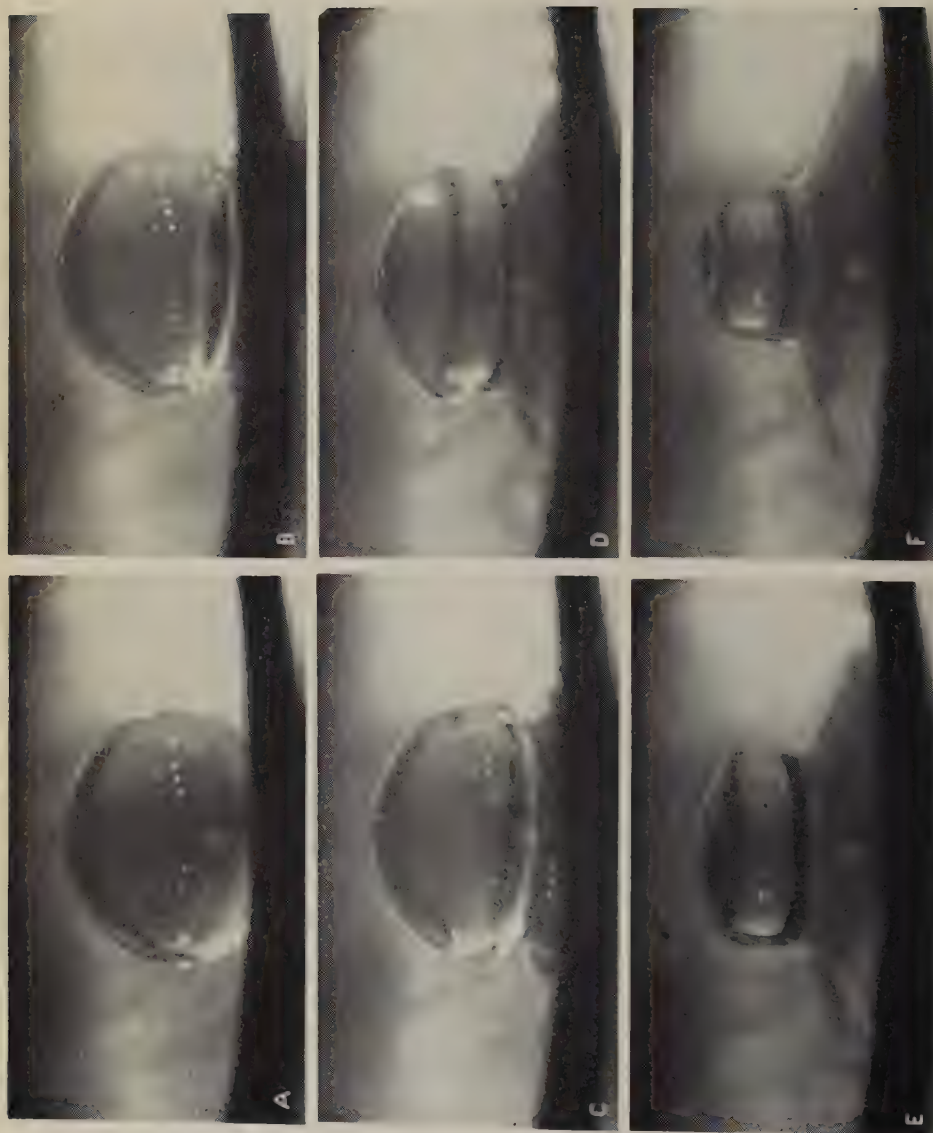


FIG. 3. Successive stages of partial coalescence of a parent drop (frame *a*) resulting in the formation of a single drop (frame *f*). The drops were formed by the injection of a small volume of aniline into a larger volume of water. The pictures were taken at 2160 pictures/sec. of an aniline drop (drop diameter 0.1 mm) and a water drop (drop diameter 0.1 mm) on a dark surface.



Fig. 3—G—L

generates a shock wave at the base of the domed interface (*c*). Eventually, this is transmitted symmetrically upwards along the domed interface (*c* and *d*) to create an unstable bulge on reaching the summit (*e*). As drainage from beneath the dome proceeds, the bulge contracts into the dome to form a cavity in the top (*f*). Another bulge appears shortly (*g*) to become the top portion of the column of residual liquid from the original drop (*h*). This column then contracts at the base and becomes spherical at the top (*i*). In time, the column detaches itself at the base (*k*) to form the secondary drop (*l*).

The contraction and the break-up of the column create at the interface a system of waves propagating radially outwards from the point of detachment.

The total time for partial coalescence, i.e., between the beginning of coalescence (frame *a*) and the separation of the secondary drop (frame *j*), was 156 milliseconds for the system shown in Fig. 3. The partial coalescence time of the secondary drop ( $a_2 = 0.214$  cm.) in this case was 42 milliseconds.

Similar determinations for a water drop at a heptane/water interface revealed first- and second-stage partial coalescence times of 27.5 and 7 milliseconds for drop diameters of 0.540 and 0.186 cm., respectively.

On several occasions, it was observed that large primary water drops ( $a_1 > 0.60$  cm.) yielded two secondary drops of unequal size when coalescing at a benzene/water interface. High-speed photographs showed that the smaller of the two secondary drops was formed from the contracting portion of the liquid column, as illustrated schematically in Fig. 4. The diameters of the drops were approximately one-third and one-sixth that of the primary drop.

When the drop was colored, it was observed that, after coalescence, a vortex ring, similar to a smoke ring, formed in the lower phase with a colored liquid trailing the ring, as illustrated in Fig. 5 and as reported recently (14). As  $a$  diminished, the colored column and the ring were formed

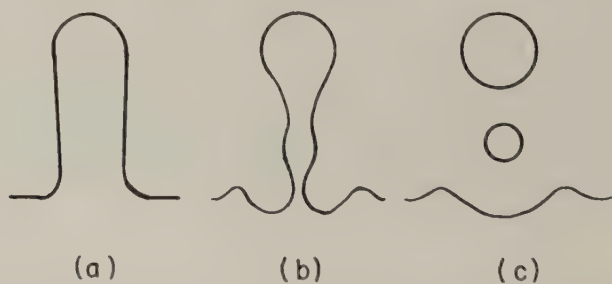


FIG. 4. Simultaneous formation of two secondary drops during partial coalescence (schematic).

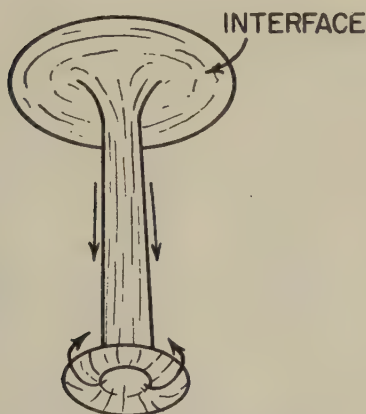


FIG. 5. Vortex ring formed during the partial coalescence of a colored drop viewed from below (schematic).

more rapidly and with sharper definition, presumably because of the increased internal (propulsive) pressure in the smaller drops. Similar rings are formed by the bursting of gas bubbles rising to the surface of a liquid (15, 16).

Partial coalescence was also observed in liquid/liquid systems where  $\rho_1 < \rho_2$ , e.g., when benzene drops rise to a water/benzene interface. The phenomena involved in these systems, however, were not examined in detail, but were presumably the same as described above.

It is worth mentioning here that partial coalescence of water droplets was observed when high-speed cine-film were taken of the bursting of an air bubble rising to the surface of water. The bursting bubble caused the ejection of a satellite water drop (17, 18) into the air which returned and then coalesced in five stages over a total period of 125 milliseconds, i.e., too rapidly to be seen by eye.

#### *Drop Diameter Ratio*

With the exception of the primary drop diameter which was calculated from the microburet volume readings, the successive drop sizes were measured from projections of the low-speed cine-films. The results were reproducible as illustrated by the data for four successive stages of coalescence of five different water drops in benzene given in Table I.

Drop diameter ratios  $r_i = a_{i+1}/a_i$  corresponding to the different stages  $i$  for the various systems investigated are given in Table II. When possible, the drops resulting from the partial coalescence were measured down to sizes of  $150\ \mu$ . In a few cases, the interface in contact with the glass cell (Fig. 2) obstructed the camera view and made it possible to observe only two or three stages.



TABLE I  
*Reproducibility of Successive Stages of Partial Coalescence Water Drops at  
 Drops at a Benzene/Water Interface*

Expt. no.	$a_1^*$	$a_2$	$a_3$	$a_4$	$a_5$
	(cm.)	(cm.)	(cm.)	(cm.)	(cm.)
1	0.416	0.1497	0.0680	0.0340	—
2	0.416	0.1542	0.0703	0.0363	—
3	0.416	0.1497	0.0703	0.0340	—
4	0.416	0.1519	0.0692	0.0318	0.0166
5	0.416	0.1497	0.0680	0.0329	0.0136
Mean	0.416	0.1510	0.0692	0.0338	0.0152

\* From measured primary drop volume.

The viscosity ratio  $p$  for each system is included in Table II. The liquid viscosities were obtained from the literature.

Table II shows that  $r_1$  was generally lower than that of the subsequent stages. The maximum value of  $r_1$  ( $= 0.41$ ) was obtained with the system water/toluene.

The distribution of rest-times  $\tau$  for three successive stages in the system benzene/water is shown in Fig. 6. The curves follow the same trends found previously (4) and indicate a decrease in drop stability with decreasing size.

#### *Effect of Viscosity Ratio*

Table II shows that  $r_i$  varies with  $p$ .

From the glycerol-water/carbon tetrachloride system, it is noted that  $r_i$  decreases as  $p$  decreases. In the systems water/cyclohexanol, water/Nujol, and mercury/glycerol for which  $p < 0.02$ , the primary drops coalesced in one step, i.e.,  $r_1 = 0$ .

It is also noted that, above  $p = 1$  approximately,  $r_1$  decreases as  $p$  increases and the coalescence again becomes single-staged above a limiting value of  $p$  between 7 and 11.

#### *Effect of Interfacial Tension*

The influence of  $\sigma$  on the ratio  $r_i$  was studied for the system benzene/water in which surfactant was added to the water. Tergitol NPX in concentrations of 0.005, 0.01, and 0.2 g/100 ml. was used. The diameter ratios for three successive stages of partial coalescence are given in Table III. Lowering the surface tension had little or no effect upon  $r_i$  in these experiments.

It was previously reported (1) that with a given system, partial coalescence ceased to occur when a high concentration of soap was used. In the

TABLE II  
Diameter Ratios Secondary/Primary Drops

System		$\sigma$ (dynes/ cm.)	$p$	Stage	Drop diam. $a_i$ (cm.)	$r_i$
Phase 1 (Drop)	Phase 2					
Carbon tetra- chloride	Water	41.9	1.014	1	0.414	0.24
				2	0.1006	0.41
				3	0.0408	0.46
				4	0.0186	
Carbon tetra- chloride	25% glycerol/ 75% water	37.0	0.443	1	0.414	0.19
				2	0.0836	0.41
				3	0.340	
Carbon tetra- chloride	50% glycerol/ 50% water	31.4	0.149	1	0.410	0.16
				2	0.0644	
Carbon tetra- chloride	75% glycerol/ 25% water	26.0	0.023	1	0.404	0.13
				2	0.0506	
Water	Ether	10.9	4.023	1	0.331	0.31
				2	0.1032	0.57
				3	0.0590	
25% glycerol/75% water	Ether	11.5	9.212	1	0.310	0.29
				2	0.0896	0.54
				3	0.0488	
50% glycerol/50% water	Ether	11.9	27.342	1	0.296	Single stage
Water	Cyclohexane	41.1	1.018	1	0.584	0.36
				2	0.2320	0.54
				3	0.1134	0.54
				4	0.0612	0.54
				5	0.0328	0.52
				6	0.0170	
25% glycerol/75% water	Cyclohexane	35.7	2.332	1	0.506	0.34
				2	0.1724	0.51
				3	0.0862	
50% glycerol/50% water	Cyclohexane	34.7	6.921	1	0.464	Single stage
Aniline	Water	6.1	4.155	1	0.698	0.31
				2	0.2132	0.39
				3	0.0838	0.32
				4	0.0272	
25% glycerol/75% water	Aniline	5.5	0.487	1	0.458	0.21
				2	0.0976	
Water	Benzene	30.5	1.483	1	0.416	0.36
				2	0.1510	0.46
				3	0.0692	0.49
				4	0.0338	0.45
				5	0.0152	
25% glycerol/75% water	Benzene	22.1	3.397	1	0.406	0.32
				2	0.1316	0.47
				3	0.0624	0.44
				4	0.0272	

TABLE II (Continued)

System		$\sigma$ (dynes/ cm.)	$p$	Stage	Drop diam. $a_i$ (cm.)	$r_i$
Phase 1 (Drop)	Phase 2					
50% glycerol/50% water	Benzene	20.7	10.083	1	0.442	Single stage
Water	Toluene	28.0	1.603	1	0.610	0.41
				2	0.2318	0.51
				3	0.1032	0.53
				4	0.0544	0.46
				5	0.0250	0.50
				6	0.0186	
25% glycerol/75% water	Toluene	24.9	3.671	1	0.508	0.32
				2	0.1622	0.48
				3	0.0772	0.47
				4	0.0262	0.50
				5	0.0182	
50% glycerol/50% water	Toluene	25.0	10.898	1	0.458	0.32
				2	0.1462	0.44
				3	0.0636	
75% glycerol/25% water	Toluene	23.3	70.323	1	0.410	Single stage
Water	Heptane	47.0	2.313	1	0.540	0.34
				2	0.1858	0.43
				3	0.0794	
25% glycerol/75% water	Heptane	42.0	5.298	1	0.480	0.35
				2	0.1666	0.42
				3	0.0704	0.48
				4	0.0340	
50% glycerol/50% water	Heptane	38.7	15.725	1	0.444	Single stage
Water	Nujol	50.8	0.006	1	0.776	Single stage
Water	Cyclohexanol	3.9	0.019	1	0.420	Single Stage
Mercury	Glycerol	370	0.004	1	0.300	Single stage

present experiments, single-stage coalescence occurred when the concentration of Tergitol NPX exceeded about 2.0 g./100 ml.

#### *Effect of Electrostatic Field*

The partial coalescence of electrically charged (positive) liquid drops at liquid/liquid interfaces (negatively charged) was studied briefly by applying a d.-c. potential to the drop-forming tip (Fig. 2) as described elsewhere (4). The effect was studied with water drops coalescing at heptane/water and at benzene/water interfaces.

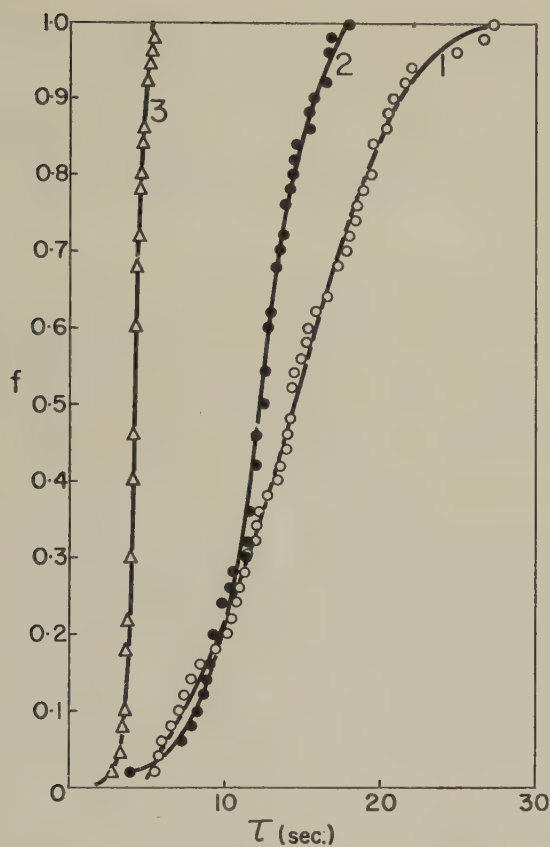


FIG. 6. Distributions of rest-times  $\tau$  for primary, secondary, and tertiary water drops coalescing at a benzene/water interface at 20°C.;  $a_1 = 0.566$ ,  $a_2 = 0.179$ , and  $a_3 = 0.082$  for the curves 1, 2, and 3, respectively. In this plot  $f$  is the fraction of the total number of drops investigated which had coalesced in time  $\tau$ .

TABLE III

*Effect of Interfacial Tension on Diameter Ratio Water Drops in Benzene*

Temp. = 25° ± 2°C.

Tergitol NPX (gm./100 ml. water)	$\sigma$ (dynes/cm.)	$a_1$ (cm.)	$r_i$		
			Stage 1	Stage 2	Stage 3
0	30.5	0.62	0.29	0.47	0.43
0.055	22.4	0.58	0.29	0.47	0.46
0.01	19.6	0.56	0.30	0.46	0.44
0.20	16.7	0.52	0.28	0.50	0.44



With no electrical field, the primary drops coalesced in stages as described above. On increasing the potential, the primary drops yielded progressively smaller secondary drops and eventually coalesced in one stage. This occurred between 450 and 1000 volts d.c. with the systems investigated.

It was also noticed that the mean rest-time  $\bar{\tau}$  of the primary drops decreased on increasing the potential and became zero (i.e.,  $\tau < 0.1$  sec.) when a critical voltage was attained (4).

### DISCUSSION

The formation of a secondary drop may be considered to occur in the following way. Following rupture of the Phase 2 film, the primary drop is deflated by the excess internal pressure resulting from the curved interface until a cylindrical column is formed as in Fig. 3b. The radius  $R$  of the column continues to decrease from the action of the excess pressure ( $= \sigma/R$ ) until the circumference becomes less than the height and a Rayleigh disturbance can grow. From here on there is a race between drainage and the necking-down process, the outcome of which determines the size of the secondary drop. One would expect that: (1) the rate of drainage is a function of:  $(\rho_1 - \rho_2)$ ,  $1/\eta_1$ ,  $1/\eta_2$ ,  $\sigma/R$  and (2) the necking-down process (rate  $= q$ ) is a function of:  $1/\rho_1$ ,  $1/\rho_2$ ,  $1/\eta_1$ ,  $1/\eta_2$ ,  $\sigma$ ,  $1/R$ . Clearly an exact analysis of the events will be complicated.

The Rayleigh theory can, however, be applied approximately by making the following simplifying assumptions:

1. At any stage  $i$  the coalescing drop drains to form a cylindrical column (as in Fig. 3h) of height  $L_i = a_i$ .
2. Drainage continues at constant  $L_i$  with a reduction in column radius to a value  $R_0$  at which

$$\lambda_{\text{opt.}} = L_i = Z_0(2R_0). \quad [7]$$

A capillary disturbance of wavelength  $\lambda_{\text{opt.}}$  then grows which, after an interval  $t_b$  when  $\alpha = R_0$ , causes separation at the nodal point formed at the base of the cylinder.

3. The volume of the secondary drop is equal to that of the column in the condition given by Eq. [7], i.e., further drainage during the break-up time  $t_b$  is neglected. This, obviously, is the weakest of the three assumptions.

It follows from the third assumption that

$$\frac{4}{3} \pi \left( \frac{a_{i+1}}{2} \right)^3 = \pi R_0^2 a_i,$$

which, on reduction and combination with Eq. [7], yields the following equations:

$$r_i = \left( \frac{a_{i+1}}{a_i} \right) = \left( \frac{3}{2Z_0^2} \right)^{1/3} \quad [8]$$

and

$$R_0 = \frac{a_{i+1}}{(12Z_0)^{1/3}}. \quad [9]$$

For the classical case of an inviscid liquid considered by Rayleigh (5), i.e., for  $Z_0 = 4.508$ , Eq. [8] yields  $r_i = 0.42$ , which falls within the range of the experimental values listed in Table II. Thus to a first approximation the Rayleigh theory applies.

In all cases  $r_i$  increased between the first and second stages and then remained approximately constant (Tables II and III). The low values of  $r_1$  can be attributed to the following two causes:

1. Deformation of the primary drops resting at the interface (Fig. 3a). The effect could be seen to be greatest with the large primary drops as was previously shown theoretically (4). Since  $a_1$  was calculated from the measured volume, it follows that  $L_1 < a_1$ , and hence  $r_1$  was less than given by Eq. [8].

2. Appreciable drainage from the column during the interval  $t_b$  while the disturbance leading to break-up was growing. Unfortunately  $t_b$  could not be determined without ambiguity; it was taken as the time  $t_b'$  between the formation of the liquid column (Fig. 3h) and its detachment to form the secondary drop (Fig. 3j). Since  $t_b'$  included the time for drainage between the condition in Fig. 3h and that corresponding to Eq. [7], it was somewhat greater than the true  $t_b$ . Values for several systems are included in Table IV and are seen to be appreciably greater in the first stage. This could also cause  $r_1$  to be less than predicted by Eq. [8].

The formation of double drops from large primary drops (Fig. 4) may also have resulted from drainage during the interval  $t_b$ . It is possible that rapid reduction in  $R$  during growth of the disturbance led to a condition in which  $\lambda_{opt.}$  became less than the height of the column thus allowing for

TABLE IV  
*Disturbance Parameters for Partial Coalescence*

System		Stage $i$	Observed $t_b'$ (msec.)	Calculated values			
Phase 1 (drop)	Phase 2			$Z_0$ Eq. [8]	$R_0$ (cm.) Eq. [9]	$F(Z)$ ref 7	$\alpha_0 10^3$ (cm.)
Aniline	Water	1	31	7.10	0.0485	0.278	6.7
		2	6	5.03	0.0213	0.337	4.3
Water	Heptane	1	5.2	6.17	0.0442	0.303	13.7
		2	1.6	4.31	0.0213	0.342	6.4
5% glycerol/ 75% water	Heptane	1	6	5.94	0.0400	0.308	9.4

Note: For other data on these systems see Table II.

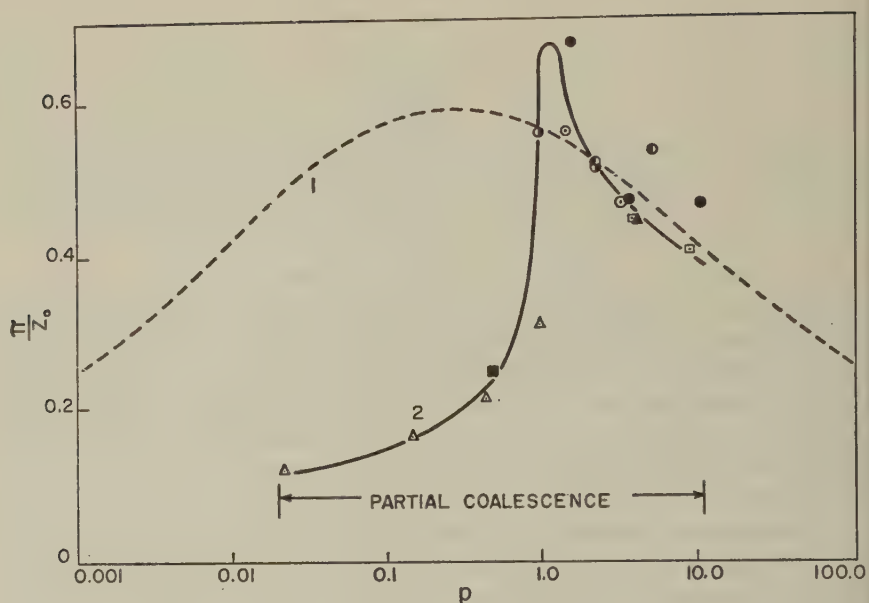


FIG. 7. The effect of  $p$  on  $(\pi/Z_0)$  for liquid column break-up. The value of  $Z_0$  was calculated from Eq. [8]. Curve 1 was obtained from Tomotika's theory of unstable jets (11). Curve 2 is for the stage 1 coalescence of the systems of Table II. Legend for Curve 2:

Phase 1	Phase 2
△ carbon tetrachloride	glycerol-water
○ glycerol-water	benzene
□ glycerol-water	ether
● glycerol-water	toluene
⊙ glycerol-water	cyclohexane
⊖ glycerol-water	heptane
▲ aniline	water
■ glycerol-water	aniline

the growth of two disturbances as indicated in Fig. 4(b) each yielding a drop.

The variation in  $(\pi/Z_0)$  taking into account the viscosity of both phases is plotted as a function of  $p$  from Tomotika's theory (11) in Fig. 7 (curve 1). The variation in  $(\pi/Z_0)$  with  $p$  for the stage 1 coalescence with the systems of Table II is given by curve 2. The values of  $Z_0$  here were calculated from  $r_1$  using Eq. [8]. It is noted from curve 2 that  $(\pi/Z_0)$ , and hence  $r_1$ , has a maximum value of about 0.67 at  $p = 1.2$ . The use of  $r_i$  ( $i > 1$ ) yields a similar but more scattered curve with a maximum of 1.2 at  $p = 1.5$ . These results are in reasonable agreement with Tomotika's predictions in view

of the difference in conditions involved, particularly since the liquid column has a high radial momentum at break-up which is neglected in the theory.

The decrease in  $(\pi/Z_0)$  with  $p$  for curve 2 above  $p = 1.2$  can be explained qualitatively by considering the influence of  $\eta_1$  on  $(\pi/Z_0)$  from Eq. [5] derived for the case where external fluid effects are negligible. By analogy, one would expect that for a small finite value of  $\eta_2$ , as for the systems investigated here, an increase in  $\eta_1$ , and hence in  $p$ , decreases  $(\pi/Z_0)$ . In addition, it follows from Eq. [6] that  $t_b$  will increase with increasing  $p$ , thus allowing further drainage from the column and hence a further decrease in the secondary drop size at break-up. When  $t_b$  becomes sufficiently large, the column will drain without the formation of a secondary drop as was observed above  $p = 11.0$ . It is believed that the same considerations apply as  $p$  decreases below  $p = 1.2$  until  $p = 0.02$ , below which coalescence again becomes single-staged.

An exception is the water/air system already mentioned in which  $p \gg 11$  and which is multi-staged. This may be due to the high  $\sigma$ , which as indicated earlier may also be a factor.

According to Eqs. [2] and [4],  $t_b$  is proportional to  $\sigma^{-1/2}$ ; at the same time the rate of drainage during growth of the disturbance may be expected to increase with increasing  $\sigma$ . It is evident that the two effects compensated one another when  $\sigma$  was depressed by adding small quantities of surfactant since  $r_s$  remained unchanged (Table III). With the addition of a sufficiently large amount, however,  $t_b$  was made sufficiently great that the column drained completely into the underlying phase before break-up occurred. A contributing factor may have been the reduction in dynamic  $\sigma$  resulting from the rapid reduction of interfacial area and the compression of the surfactant film (19).

The effect of interfacial electrical charges on partial coalescence is presumably due to the electrocapillary effect (20), i.e., a lowering of  $\sigma$  due to the repulsion between similar charges. Thus, with increasing voltage,  $t_b$  increased progressively and, for the same reasons mentioned above, resulted in a decrease in the secondary drop size at break-up. When  $\sigma$  was reduced sufficiently by increasing the potential, partial coalescence ceased to occur.

The instantaneous coalescence (i.e.,  $\tau < 0.1$  sec.) of the electrified primary drops above a critical potential is attributed to the electrostatic attractive force between the drop and the oppositely charged interface as discussed elsewhere (4).

Values of  $\alpha_0$  for the systems of Table IV were calculated from Eq. [4] using  $t_b'$ . The value of  $q$  in each case was obtained from Eq. [2]. Values of  $Z_0$  and  $R_0$  were calculated from Eqs. [8] and [9], respectively;  $F(Z)$  was obtained from the data of Castleman (7). The values of  $\alpha_0$  are considerably greater than values (*circa*  $10^{-5}$  cm.) found (7-9) for water atomized in air



probably because of the high radial momentum during column formation in coalescing drops.

In view of the complexity of the phenomena involved in partial coalescence, it is considered that the agreement with modified Rayleigh theory is good.

#### ACKNOWLEDGMENT

The authors are indebted to Dr. A. A. Robertson for valuable comments and suggestions.

#### SUMMARY

The mechanism of formation of a secondary drop from the coalescence of a liquid drop (Phase 1) at a liquid/liquid interface was investigated. It was shown by means of high-speed photographs that partial coalescence results from the formation of a liquid column of Phase 1 in Phase 2 which contracts at the base and detaches itself to form the secondary drop. The diameter ratio, secondary to primary, varied with the viscosity ratio  $p = \eta_1/\eta_2$ , and passed through a maximum near  $p = 1$ . When  $p$  was less than 0.02 or greater than 11, no secondary drops formed. Secondary drop formation could be suppressed by adding a high concentration of surfactant or by applying an electrostatic field.

The experimental results were analyzed with reasonable success with the aid of Rayleigh's theory of unstable liquid threads.

#### REFERENCES

1. COCKBAIN, E. G., AND McROBERTS, T. S., *J. Colloid Sci.* **8**, 440 (1953).
2. GILLESPIE, T., AND RIDEAL, E., *Trans. Faraday Soc.* **52**, 173 (1956).
3. PICKNETT, R. G., Ph.D. Thesis, University of London, 1957.
4. CHARLES, G. E., AND MASON, S. G., Forthcoming publication.
5. RAYLEIGH, LORD, *Proc. London Math. Soc.* **10**, 4 (1879).
6. CASTLEMAN, R. A., *Nature* **114**, 857 (1924).
7. CASTLEMAN, R. A., *Bur. Standards J. Research* **6**, 369 (1931).
8. WEBER, C., *Z. angew. Math. Mech.* **11**, 136 (1931).
9. HAENLEIN, A., *Forsch. Gebiete Ingenieurw.* **A2**, 139 (1931).
10. TYLER, E., *Phil. Mag.* **16**, 504 (1933).
11. TOMOTIKA, S., *Proc. Roy. Soc. (London)* **A150**, 322 (1935).
12. RAYLEIGH, LORD, *Phil. Mag.* **4**, 145 (1892).
13. HARKINS, W. D., AND BROWN, F. E., *J. Am. Chem. Soc.* **41**, 499 (1919).
14. WATANABE, T., AND KUSUI, M., *Bull. Chem. Soc. Japan* **31**, 237 (1958).
15. ROGERS, W. B., *Am. J. Sci.* **26**, 246 (1858).
16. CAMPBELL-SWINTON, A. A., AND BEALE, E., *Nature* **98**, 469 (1917).
17. NEWITT, D. M., DOMBROWSKI, N., AND KNELMAN, F. H., *Trans. Inst. Chem. Engrs. (London)* **32**, 244 (1954).
18. WOODCOCK, A. H., *Sewage and Ind. Wastes* **27**, 1189 (1955).
19. HELLER, S., *Kolloid-Z.* **136**, 120 (1954).
20. ADAM, N. K., "The Physics and Chemistry of Surfaces," 3rd ed., p. 336. Oxford Univ. Press, 1941.

## THE EFFECT OF THE SPREADING SOLVENT ON THE PROPERTIES OF MONOLAYERS\*

Max L. Robbins and Victor K. La Mer

*Department of Chemistry, Columbia University, New York, New York*

*Received May 8, 1959*

### ABSTRACT

The effects produced by benzene or hexane as spreading solvents upon the surface pressure-area isotherms of octadecanol and stearic acid were investigated. Diluting the spreading solution resulted in an increase in the area/molecule at  $\pi = 1$  dyne/cm. This expansion was greater with hexane than with benzene. Monolayers of stearic acid expanded more than those of octadecanol upon adding benzene liquid or vapor to the surface. Benzene vapor was irreversibly adsorbed on a monolayer of stearic acid. Octadecanol monolayers expanded when the concentration of benzene in the subphase was increased. An expansion of the monolayer with age was noted. This effect was greater for octadecanol than stearic acid monolayers. Aging could be attributed to changes in the structure of the monolayer as well as to contamination. Expansions resulting from both aging and solvent effects were greater at low surface pressures.

A model based on the relative rates of solvent evaporation and diffusion into the subphase during the spreading process is proposed. The surface concentrations of benzene evaluated from experimental data and the model are compared. The two values agree within a factor of three.

### INTRODUCTION

With few exceptions (1), the effect of the spreading solvent upon the properties of monolayers has been ignored in the literature. Possibly investigators have assumed that since the partial pressure of solvent vapor above the surface is effectively zero in an open system, the solvent must evaporate completely. But interactions between solvent and other components in the surface may so retard evaporation, that a small surface concentration of solvent remains during the time required to make a series of measurements.

The effect upon the surface pressure-area ( $\pi$ - $a$ ) isotherm produced by varying the concentration of stearic acid in a benzene spreading solution has already been considered (1). An eightfold dilution of the spreading solution resulted in increases as large as 25% in the reciprocal slope ( $-da/d\pi$ ) and 6% in the molecular area of stearic acid. This expansion

\* Presented at the 136th National Convention, A.S.C. Colloid Division, Atlantic City, New Jersey.

of a stearic acid monolayer with decreasing concentration of the spreading solution was attributed to the formation of a mixed monolayer with benzene.

The present paper treats the effect of varying the concentration of octadecanol in the spreading solution upon the  $\pi$ - $a$  isotherm; benzene and hexane are compared as solvents. The use of octadecanol permits concentration effects to be determined in the high-pressure "solid" region of the  $\pi$ - $a$  isotherm. This region could not be reproduced using stearic acid. Concentration effects were reported previously (1) only in the "liquid condensed" region of stearic acid monolayers.

The importance of the solvent in determining the shape and position of the  $\pi$ - $a$  isotherm is clarified by the addition of benzene liquid or vapor to monolayers of stearic acid and octadecanol. The changes in the  $\pi$ - $a$  isotherm produced are independent of such variables in the spreading process as incomplete spreading, systematic errors, or changes in molecular orientation. Variations in the  $\pi$ - $a$  curve depend only upon the amount of benzene introduced into the system.

#### EXPERIMENTAL

Monolayers of stearic acid (m.p. 68.8°–69.3°C.) and octadecanol (m.p. 58.2°–59.4°C.) were spread from benzene (b.p. 79.8°–80.3°C.) or hexane (b.p. 68°–69°C.). The analytical grade solvents were twice redistilled in pyrex apparatus. Fifty milliliters of each was evaporated to dryness at room temperature and the residue weighed. Less than 0.2 mg. of residue remained. Benzene was further tested for surface-active impurities. A sufficient amount was delivered to a clean water surface, so that after evaporation a detectable surface pressure was developed on compression. This required 6.16 ml. of benzene. The surface pressure,  $\pi$ , was measured as a function of the area,  $A$ , occupied by the film-forming residue. The results are given in Fig. 1.

The area per milliliter of benzene at  $\pi = 1$  dyne/cm. is 21.4 cm.<sup>2</sup>/ml. The area occupied by a monolayer consisting of 1 g. of octadecanol at a surface pressure of 1 dyne/cm. is  $4.60 \times 10^6$  cm.<sup>2</sup>/g. Therefore, the amount of nonvolatile impurity, reported as octadecanol, per milliliter of benzene is  $21.4/4.60 \times 10^6 = 4.65 \times 10^{-6}$  g./ml. ( $1.72 \times 10^{-5}$  m./l.). This represents the error in the concentration of the spreading solution due to impurities. Using a 0.001 g./ml. spreading solution results in an error in the area/molecule of octadecanol at  $\pi = 1$  dyne/cm. of +0.46% or approximately +0.1 Å.<sup>2</sup>. The actual error may be considerably smaller than this. When delivering a large volume of benzene, i.e., 6.16 ml., to the water surface, small amounts of paraffin from the edges of the tray are unavoidably dissolved and spread as a film. Since Fig. 1 represents the surface pressure exerted by all surface-active contaminants in the solvent and

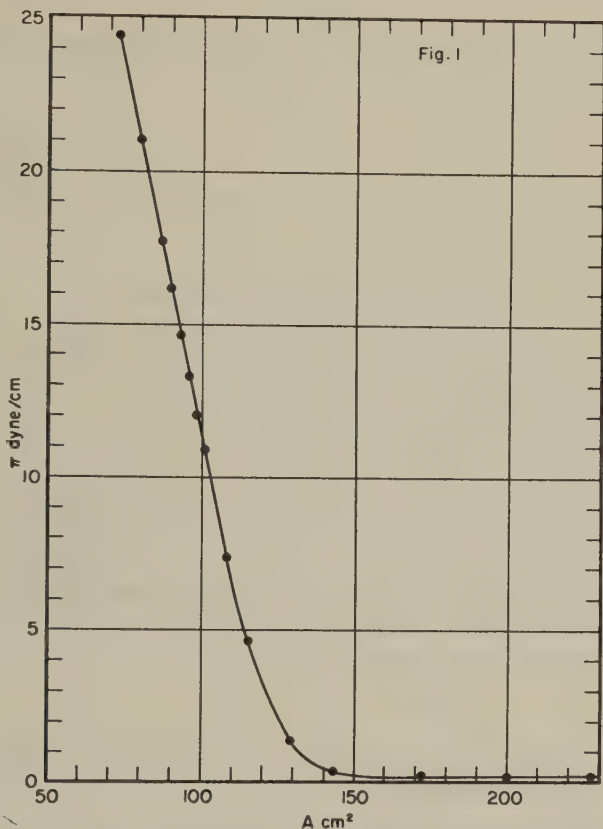


FIG. 1. The  $\pi$ - $A$  curve for nonvolatile impurities in benzene obtained by allowing .16 ml. of benzene to evaporate from a clean water surface.

subphase including dissolved paraffin, the error in the concentration of the spreading solution calculated above represents the maximum possible error due to impurities in benzene.

The spreading solution was delivered, precise to  $\pm 0.0002$  ml., from an  $\mu$ -l syringe. The  $0.01$   $M$   $HCl$  subphase used in all experiments was prepared from laboratory distilled water redistilled from acid-fermanganate solution in an all-pyrex apparatus. The subphase, contained in a pyrex tray, was thermostated at  $25^\circ \pm 0.05^\circ C$ . As described previously (1), surface pressures precise to  $0.05$  dyne/cm. were measured at maximum pull with a Wilhelmy plate of depolished platinum suspended from a torsion assembly. This method requires that the receding contact angle between the plate and subphase remain zero with a monolayer on the surface.

Contact angles were measured (2) between clean glass and  $0.01$   $M$   $HCl$



TABLE I

*The Contact Angle on Glass of 0.01 M HCl Covered with a Stearic Acid Monolayer*

	$a(\text{\AA}^2/\text{molec.})$	$\theta^\circ$
a.*	—	1.8
b.	28.2	1.5
c.	21.4	1.0

\* The contact angle on glass of a clean 0.01 M HCl surface.

covered with monolayers of stearic acid confined to various molecular areas. With the plate immersed, 0.0281 or 0.0370 ml. of a  $6.58 \times 10^{-5}$  g./ml. solution of stearic acid in benzene was spread on an area of 11.04 cm.<sup>2</sup>. The molecular areas for these monolayers were 28.2 and 21.4 Å<sup>2</sup>, respectively. The plate was lowered and raised 10 times in succession but not removed from the surface. The receding contact angle was measured 3–5 min. after the last withdrawal. The results of these measurements are given in Table I. The contact angle remains effectively zero, independent of the surface pressure exerted by a stearic acid monolayer.

Contact angles were measured on glass rather than platinum because the interferometric method requires a highly reflective solid surface. Contact angles measured on glass should be similar to those obtainable on platinum. Both glass and platinum present high-energy surfaces.

## EXPERIMENTAL RESULTS

*A. The  $\pi$ -a Isotherm of Octadecanol as the Concentration of the Benzene Spreading Solution is Varied*

Table II lists the experimental results obtained by varying the concentration of the spreading solution while holding constant the volume of solution spread, the initial area, and the time allowed for benzene to evaporate at 0.0700 ml., 780 cm.<sup>2</sup>, and 60 sec., respectively. Each experiment was performed on a freshly spread monolayer and represents about 25 successive readings of the surface pressure as the area is decreased. The results of each experiment were plotted as surface pressure vs. molecular area. The number of such plots at each concentration is indicated in column 2. The area/molecule at a given surface pressure was read from each plot and averaged over the experiments performed at each concentration. This average area,  $\bar{a}$ , at the respective surface pressure,  $\pi$ , is listed in columns 5–12. Included are the corresponding average deviations. The average molecular area at collapse of the monolayer appears in column 13. The initial mole ratio of benzene to octadecanol,  $n_b^0/n_a$ , is given in column 4;  $n_b^0/n_a$  was evaluated from the concentration of the spreading solution.

$$\frac{n_b^0}{n_a} = \frac{M_a}{M_b} \cdot \frac{\rho_s}{c_s} = \frac{3.043}{c_s},$$

TABLE II

*Experimental Areas/Molecule of Octadecanol Averaged over the Experiments within a Set*

Set or curve	No. expts. in set	10 <sup>3</sup> Conc. (g./ml.)	10 <sup>-3</sup> ( $n_b^0/n_a$ )	Area/molecule ( $A_s^2$ ) at the surface pressure (dynes/cm.)								collapse
				1	4	8	12	14	20	28	36	
a	2	2.94 <sub>0</sub>	1.03 <sub>5</sub>	20.83	20.52	20.12	19.70	19.50	19.41	19.31	19.22	19.14
				±.05	±.04	±.04	±.04	±.03	±.04	±.04	±.04	±.04
b	3	2.22 <sub>0</sub>	1.37 <sub>1</sub>	20.93	20.58	20.13	19.69	19.52	19.43	19.32	19.20	19.03
				0.14	0.12	0.10	0.10	0.09	0.09	0.08	0.08	0.07
c	3	1.11 <sub>0</sub>	2.74 <sub>2</sub>	21.26	20.87	20.38	19.90	19.71	19.58	19.40	19.22	19.08
				0.14	0.10	0.09	0.10	0.09	0.10	0.10	0.10	0.10
d	3	0.73 <sub>5</sub>	4.14	21.41	21.01	20.52	20.03	19.80	19.68	19.47	19.30	19.22
				0.21	0.18	0.18	0.16	0.15	0.12	0.14	0.14	0.08
e	3	0.55 <sub>5</sub>	5.48	21.82	21.31	20.73	20.16	19.99	19.79	19.54	19.28	19.19
				0.09	0.09	0.07	0.05	0.02	0.02	0.02	0.02	0.01
f	2	0.36 <sub>8</sub>	8.28	22.18	21.65	21.01	20.36	20.05	19.86	19.60	19.34	19.14
				0.14	0.10	0.04	0.04	0.05	0.09	0.10	0.12	0.10
g	2	0.27 <sub>8</sub>	10.97	23.48	22.58	21.77	20.99	20.67	20.27	19.77	19.26	19.20
				0.25	0.22	0.20	0.18	0.18	0.19	0.17	0.17	0.16
x	—	—	0	20.68	20.38	20.00	19.61	19.45	19.38	19.28	19.19	—
				0.05	0.03	0.02	0.02	0.04	0.03	0.02	0.01	—

where  $M_a$ ,  $M_b$  are the molecular weights of octadecanol and benzene, respectively;  $\rho_s$  is the density of the spreading solution; and  $c_s$  is the concentration of the spreading solution. The spreading solutions were sufficiently dilute that the density of the solution may be approximated by the density of benzene with a negligible error in  $n_b^0/n_a$  of  $+0.004 \times 10^3$ .

In 9 experiments (sets b, c, and e), two successive  $\pi$ - $a$  isotherms were measured on compression of the same monolayer. Prior to remeasuring the isotherm, the monolayer was compressed to collapse and then reexpanded. A small increase in molecular area of 0.05–0.1  $A_s^2$  was noted at pressures below 13 dynes/cm. This expansion is within experimental precision and has, therefore, been neglected.

The volume of solution spread was varied within sets b, c, and e at volumes equal to 0.06, 0.065, and 0.07 ml. The  $\pi$ - $a$  isotherms within each set were independent, within experimental precision, of the volume of solution.

The series of experiments was randomized, using a table of random numbers, with respect to the ordering of the various concentrations and the replications at each concentration.

Figure 2 shows the dependence of the molecular area upon the initial mole ratio of benzene to octadecanol, a quantity proportional to the

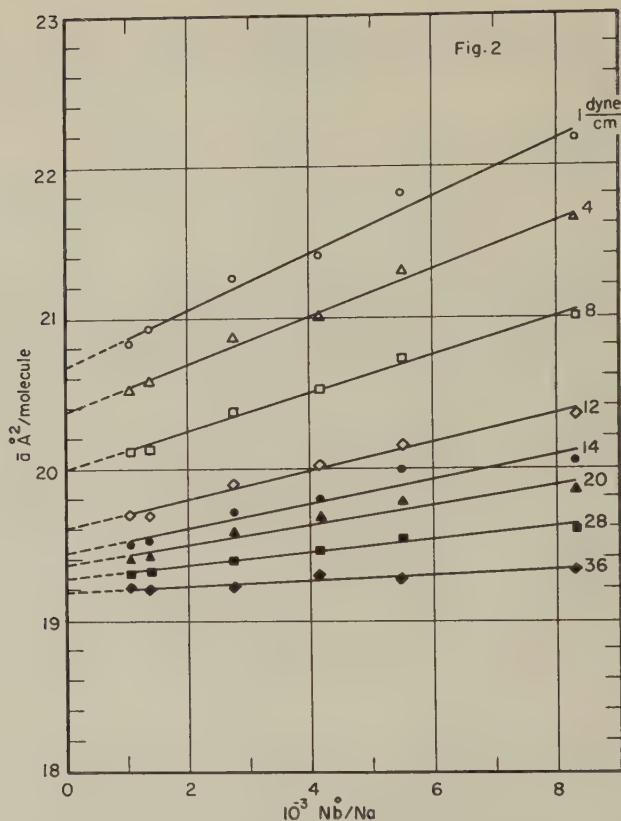


FIG. 2. The average molecular areas of octadecanol spread from benzene on 0.01 *M* HCl at 25° C. measured at the stated constant surface pressures as a function of the initial mole ratio of benzene to octadecanol. The volume of solution, initial area, and time for evaporation of solvent are held constant.

reciprocal of the spreading solution concentration. The average areas at fixed surface pressures plot linearly against  $n_b^0/n_a$  within experimental precision. The line drawn through the points at constant surface pressure represents a least squares fit to the data. The least squares intercepts, i.e. the molecular areas extrapolated to  $n_b^0/n_a = 0$ , are listed as set x in Table II.

Figure 3 demonstrates the effect of varying the spreading solution concentration upon the  $\pi$ - $a$  isotherm of octadecanol. Curves representing sets b, c, e, and g of Table II are reproduced.

Curve x is a plot of  $\pi$  vs. the molecular areas extrapolated to  $n_b^0/n_a = 0$ . Curve x is assumed to be the  $\pi$ - $a$  isotherm of a "pure" octadecanol monolayer.

Note the increase in area/molecule, compressibility, and curvature with

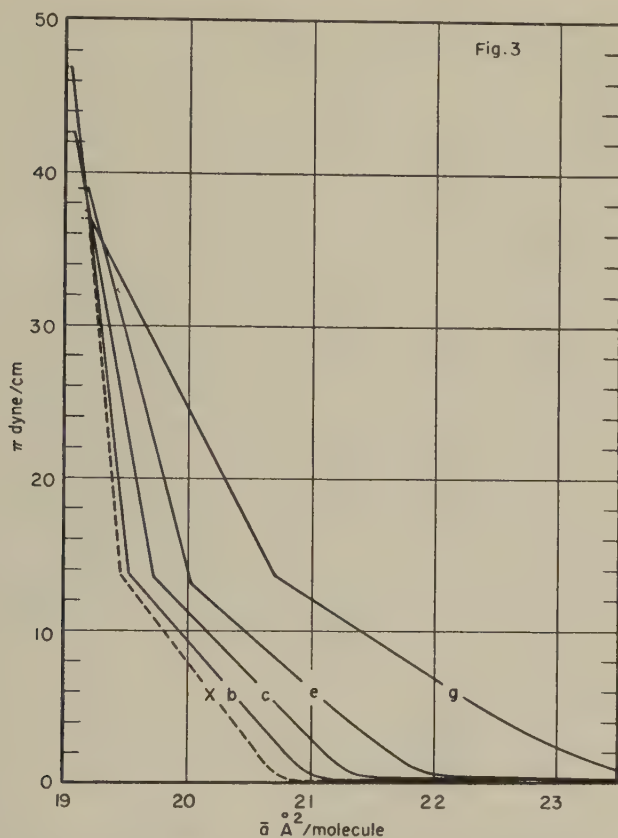


FIG. 3. The surface pressure as a function of the molecular area of octadecanol spread from benzene on 0.01 *M* HCl at 25° C. Curves *b*, *c*, *e*, and *g* refer, respectively, to the initial mole ratios of benzene to octadecanol  $10^3$  (1.37, 2.74, 5.48, and 10.97). Curve *x* is the  $\pi$ - $\bar{a}$  isotherm of octadecanol extrapolated to  $n_b^0/n_a = 0$ .

increasing initial mole ratios. These results are in accord with the observed expansion of stearic acid monolayers with decreasing concentration of the spreading solution. As with stearic acid, solvent effects on an octadecanol monolayer are minimized at the relatively low value of approximately  $10^3$  for  $n_b^0/n_a$ , which corresponds to a spreading solution concentration of approximately 0.003 g./ml. The high-pressure region, which is not reproducible for stearic acid owing to a slow collapse of the monolayer, is reproducible for octadecanol. This high-pressure region exhibits a concentration dependence similar to that of the liquid condensed region. Although collapse pressures are dependent upon concentration, the molecular areas at collapse of octadecanol monolayers are approximately constant 19.14 Å.<sup>2</sup>.



### B. The Addition of Benzene to the Monolayer

To determine whether the observed concentration effects might be due to some feature in the spreading process other than the solvent, e.g., systematic errors, incomplete spreading, or changes in molecular orientation, benzene may be added to the surface after spreading is complete. Since no known variables are involved except time and the amount of benzene in the system, any change in the  $\pi$ - $a$  isotherm not caused by aging of the monolayer must result from the added benzene. Benzene may be added to the system (1) directly to the surface as droplets, (2) as vapor above the monolayer, or (3) dissolved in the subphase.

1. *The Variation of the  $\pi$ - $a$  Isotherm of Octadecanol as a Function of the Volume of Benzene Added Directly to the Surface.* A volume of 0.300 ml. of a 0.00300 g./ml. benzene solution of octadecanol was delivered to an initial area of 780 cm.<sup>2</sup>. After allowing 100 sec. for benzene to evaporate from the surface, the  $\pi$ - $a$  isotherm was measured on compression for surface pressures between 0 and 3 dynes/cm. The monolayer was then re-expanded to 780 cm.<sup>2</sup>. A known volume of benzene was added to the surface and the  $\pi$ - $a$  curve was remeasured after allowing 50 sec. for evaporation. Seven successive increments of benzene were delivered to the monolayer. Each addition of benzene followed by measurement of  $\pi$  vs.  $a$

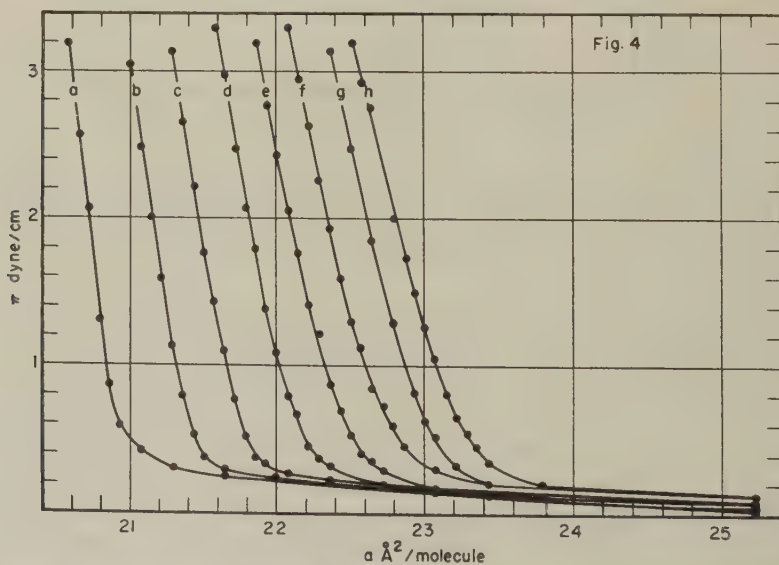


FIG. 4. The effect of successive additions of benzene upon the  $\pi$ - $a$  isotherm of octadecanol spread from benzene on 0.01 *M* HCl at 25° C. Curves *a-h* represent, respectively, total volumes of benzene of 0, 0.06, 0.15, 0.27, 0.39, 0.51, 0.63, and 0.75 ml. added successively to the same monolayer.

required approximately 450 sec. to complete. The dipping plate remained in contact with the surface during the entire sequence of measurements.

Figure 4 shows the variation in the low-pressure region of the  $\pi$ - $a$  isotherm of octadecanol as the total volume of benzene,  $v_b$ , added to the surface is increased. The set of measurements was taken on the same monolayer. Curves  $a$  through  $h$  represent benzene volumes of 0, 0.06, 0.15, 0.27, 0.39, 0.51, 0.63, and 0.75 ml., respectively.

The random scatter associated with the spreading process has been eliminated by using the same monolayer throughout the set of measurements. Therefore, the molecular areas for  $v_b > 0$  are in error relative to each other as determined by the errors involved in reading  $\pi$  and setting  $a$ . These errors result in a relative error in area of  $\pm 0.03 \text{ \AA}^2$ .

The data represented in Fig. 4 also include time as a variable. Therefore, a blank determination is required to separate effects caused by varying the volume of added benzene from those caused by aging of the monolayer. The blank is determined by measuring the dependence of the  $\pi$ - $a$  isotherm upon the age of the monolayer with  $v_b = 0$ . Curve  $b$ , Fig. 5, represents the results of this experiment. The area at  $\pi = 1 \text{ dyne/cm.}$  is plotted vs. the age of the monolayer in seconds. Curve  $a$ , Fig. 5, represents the total change in area at  $\pi = 1 \text{ dyne/cm.}$  caused by both added benzene and aging.

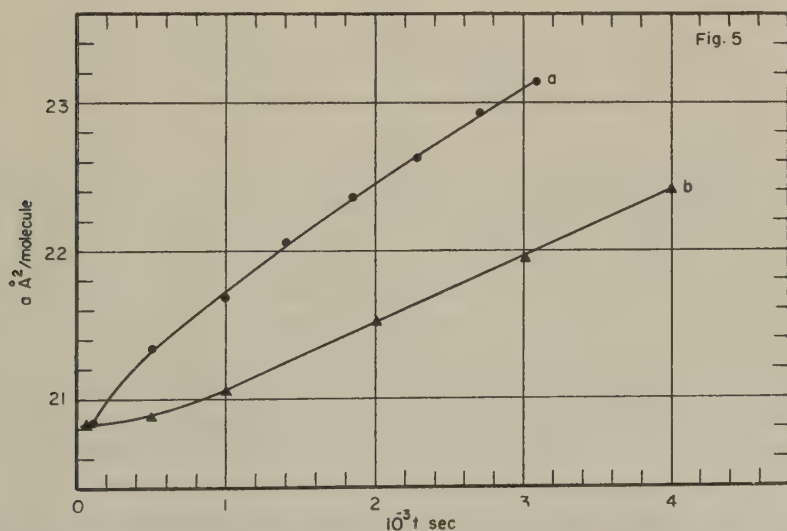


FIG. 5. The area/molecule of octadecanol at  $\pi = 1 \text{ dyne/cm.}$  as a function of the age of the monolayer both with (curve  $a$ ) and without added benzene (curve  $b$ ). The abscissas of the points in curve  $a$  represent the age of the monolayer at each successive addition of benzene. Curve  $b$  is a blank determination representing aging of the monolayer in the absence of added benzene.

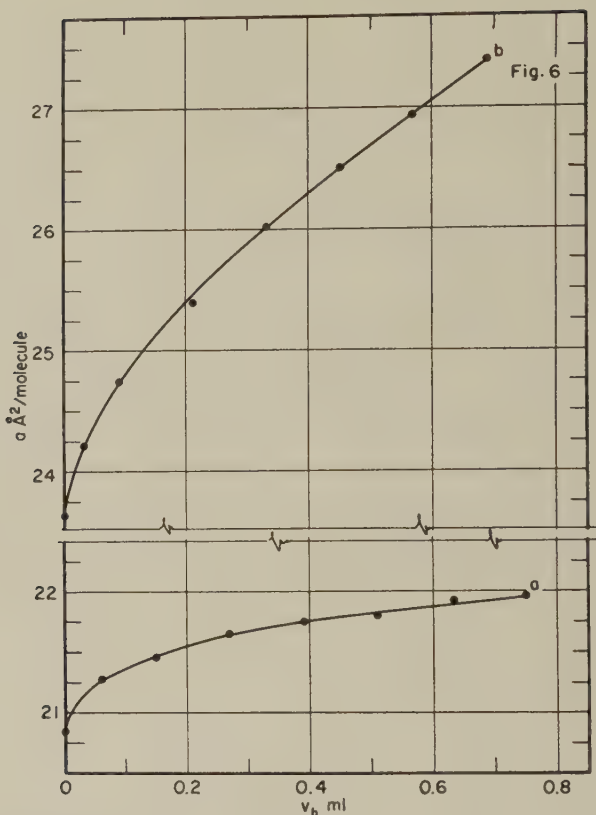


FIG. 6. The area/molecule at  $\pi = 1$  dyne/cm. as a function of the volume of benzene added to the monolayer. The increase in area with  $v_b$  is independent of the age of the monolayer. Curve *a* represents data for octadecanol; curve *b* for stearic acid.

This curve was obtained by measuring the time elapsed between spreading the monolayer and successive additions of benzene. The area at  $\pi = 1$  dyne/cm. measured after each addition of benzene was then plotted against the elapsed time. The difference between curves *a* and *b* at time  $t$  represents the increase in area above  $20.84 \text{ \AA}^2$  caused solely by the added benzene. Since  $v_b$  at time  $t$  is known, the variation of area with  $v_b$  independent of monolayer aging may be determined and is given in Fig. 6. Curve *a* shows the dependence of the area/molecule of octadecanol, corrected for aging effects, upon the volume of added benzene. Curve *b* represents the same experiment performed with stearic acid. The expansion of stearic acid monolayer upon adding 0.4 ml. of benzene to the surface is approximately 2.9 times greater than the expansion of an octadecanol monolayer under the same conditions.

## 2. The Variation in the $\pi$ -*a* Curve of Stearic Acid Resulting from

*Flushing the Surface with Benzene Vapor.* The tray containing the monolayer and subphase was enclosed in an open-bottom, wood-reinforced, corrugated cardboard carton. When in place, the enclosure fitted flush with the marble slab upon which the tray was mounted. The dimensions of the enclosure were: length 87 cm., depth 21 cm., and height 16 cm. A  $1.5 \times 70$  cm. slot, through which the barrier could be adjusted manually and areas read, extended the length of the tray. The nylon thread from which the platinum dipping plate was suspended passed through a 0.5 cm. hole in the removable lid. Two tubes at the end of the enclosure admitted separate streams of air and benzene vapor. The streams of air and benzene vapor were deflected upward from the surface by a vane. The compartment formed by the vane and the end of the enclosure also served as a mixing chamber for the air and benzene supplies. Benzene vapor was supplied by bubbling filtered air through liquid benzene thermostated at 25° C. The benzene-laden air then passed through a pyrex flowmeter (Emil Greiner, cat. no. G 9145) into the enclosure. Only pyrex glassware and copper tubing came in contact with benzene or its vapor. Filtered air, on a separate line, passed through a second flowmeter before entering the mixing chamber. A valve in each of the benzene and air lines permitted the relative flow rates of benzene vapor and air to be varied while keeping the total flow constant.

A volume of 0.077 ml. of a 0.0014 g./ml. benzene solution of stearic acid was delivered to an area of 780 cm.<sup>2</sup> and the  $\pi$ - $a$  curve measured between 0 and 20 dynes/cm. after allowing 60 sec. for solvent evaporation. The monolayer was then re-expanded to 780 cm.<sup>2</sup>. With the dipping plate still in contact with the surface, the enclosure lid was fastened. (The dipping plate never left the surface throughout the series of measurements.) Flow of benzene vapor and air into the enclosure was then begun at some fixed relative rate, e.g., benzene flow: 150 cm.<sup>3</sup>/sec., air flow: 0 cm.<sup>3</sup>/sec. The  $\pi$ - $a$  isotherm was remeasured at various times, the monolayer being re-expanded to 780 cm.<sup>2</sup> immediately following each measurement.

Figure 7 represents the expansion of a stearic acid monolayer upon flushing the surface with benzene vapor. The flow rates were, benzene: 150 cm.<sup>3</sup>/sec.; air: 0 cm.<sup>3</sup>/sec. Curves  $a$ - $f$  refer, respectively, to times 0, 300, 900, 1800, 3600, and 5400 sec. The surface pressure of the horizontal portion of the  $\pi$ - $a$  isotherm, i.e., the two-dimensional liquid-gas equilibrium, increases from 0.2 to 1.3 dynes/cm. when benzene vapor is introduced. Flushing a clean water surface with benzene vapor results in a similar rise in surface pressure to approximately 1.5 dynes/cm. within 50 sec., after which  $\pi$  remains constant. When measured against air, the surface pressure of a solution of benzene in water is less than 0.2 dyne/cm. The observed increase in  $\pi$  is caused by the change in composition of the vapor phase from air to benzene in air.



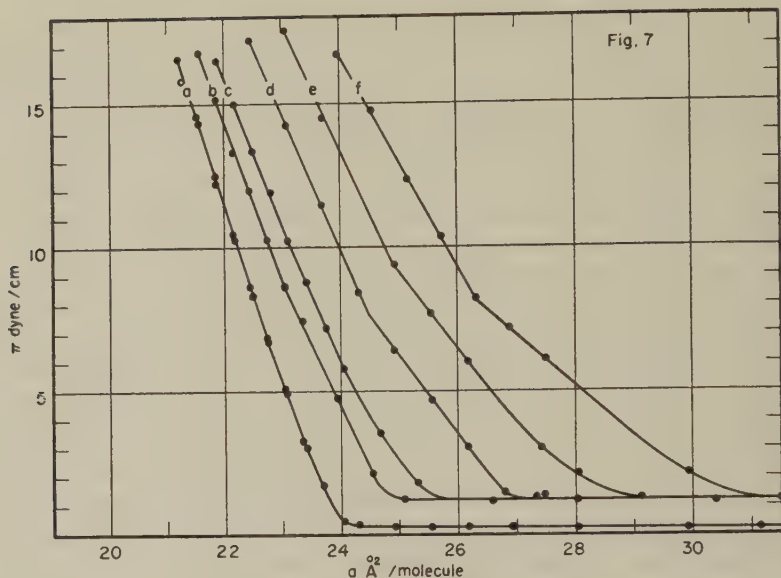


FIG. 7. The expansion in the  $\pi$ - $a$  isotherm of stearic acid upon flushing the surface with benzene vapor. The flow rates are: benzene, 150 cm.<sup>3</sup>/sec.; air, 0 cm.<sup>3</sup>/sec. Curves  $a$ - $f$  refer, respectively, to times 0, 300, 900, 1800, 3600, and 5400 sec. Curves  $a$ ,  $b$ , and  $f$  represent measurements on a single monolayer. Curves  $a$ ,  $d$ , and  $e$  were measured on a second monolayer. Curve  $c$  was measured separately.

The areas at  $\pi = 2$  dynes/cm. were read from the curves of Fig. 7 and plotted against the time during which the surface was flushed. See curve  $a$  in Fig. 8. The age of the monolayer is again included as a variable. Curve  $b$  in Fig. 8, shows the dependence of area at  $\pi = 2$  dynes/cm. upon the age of the monolayer in the absence of benzene vapor. Aging accounts for about 20% of the expansion shown in curve  $a$  for times greater than 2000 sec. The effect of aging is smaller for shorter times.

To determine whether the monolayer contracts if benzene vapor is removed from the system, the expanded monolayer was flushed with air at 150 cm.<sup>3</sup>/sec. Figure 9 shows the result. Curves  $a$  and  $c$  correspond to curves  $a$  and  $c$  of Fig. 7. Curve  $a$  is the  $\pi$ - $a$  isotherm of stearic acid before the introduction of benzene vapor into the system. Curve  $a$  is unchanged by initially flushing the monolayer with air. Curve  $c$  shows the expansion after 900 sec. flushing with benzene vapor. Curve  $g$  was measured after 900 sec. flushing with air to remove benzene vapor. Curve  $h$  was measured after 6000 sec. flushing with air. Monolayer aging accounts for approximately 70% of the 1.95 Å.<sup>2</sup> increase in area at  $\pi = 2$  dynes/cm. between curves  $c$  and  $h$ . Note that the surface pressure of the horizontal portion of the  $\pi$ - $a$  curve falls to its original value of 0.2 dyne/cm. when benzene vapor is removed from the system.

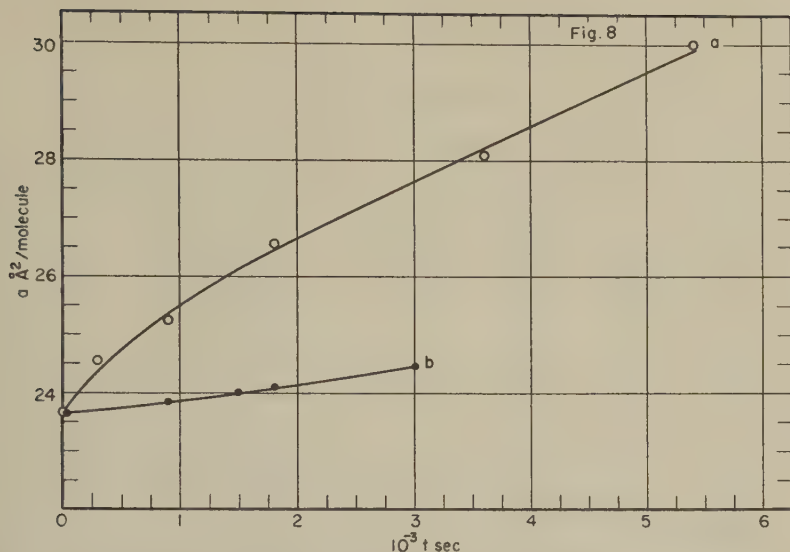


FIG. 8. The area/molecule of stearic acid at  $\pi = 2$  dynes/cm, as a function of the time the surface is flushed with benzene vapor. Curve *a* includes the expansion due to monolayer aging. Curve *b* represents aging of the monolayer in the absence of benzene vapor.

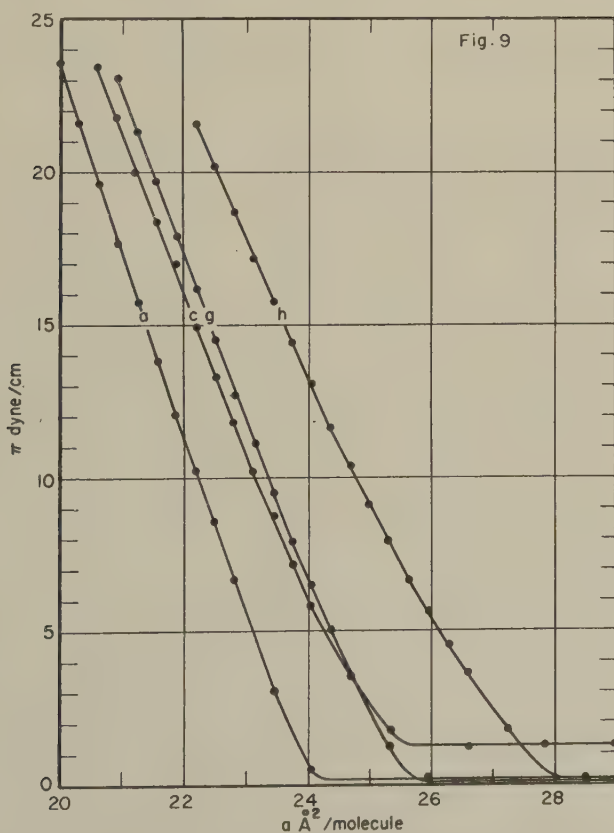


FIG. 9. The effect of removing benzene vapor above an expanded monolayer of stearic acid. Curve *a* is the  $\pi$ -*a* isotherm before introducing benzene vapor. Curve *c* measured after 900 sec. flushing with benzene vapor. Curves *g* and *h* represent, respectively, 900 and 6000 sec. flushing with air at 150 cm.<sup>3</sup>/sec.

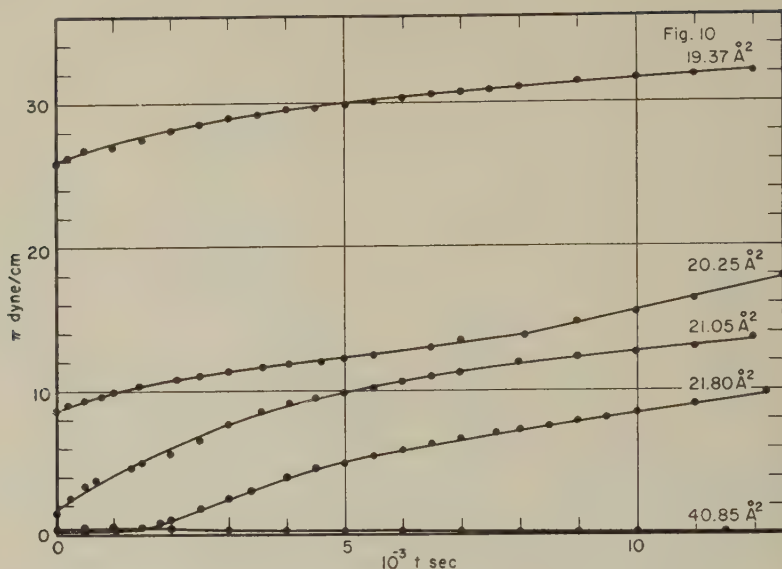


Fig. 10. The surface pressure at constant area/molecule of octadecanol as a function of the time during which benzene diffuses into the subphase.

3. *The Effect of Benzene Dissolved in the Subphase upon the  $\pi$ - $a$  Curve of Octadecanol.* An inverted crystallizing dish was immersed in the subphase to a depth of approximately 0.3 cm. and was positioned about 15 cm. from the dipping plate. The dish was  $71.7 \text{ cm.}^2$  in cross section and had a 1 cm. hole in the bottom. A volume of 0.0700 ml. of a 0.00111 g./ml. benzene solution of octadecanol was delivered to an area of  $708 \text{ cm.}^2$ , i.e., the total area of the subphase less that bounded by the dish. The water surface inside the dish remained free of monolayer. The  $\pi$ - $a$  isotherm was measured after allowing 60 sec. for solvent evaporation. The monolayer was then re-expanded to a known area/molecule, e.g.,  $21.05 \text{ \AA}^2$ . With the plate at maximum pull, 1 or 2 ml. of benzene was delivered to the water surface inside the dish, and the hole corked. The surface pressure at constant area was measured as a function of time. This measurement was interrupted at various times greater than 5000 sec. and the complete  $\pi$ - $a$  isotherm measured on compression.

Since no benzene, either vapor or liquid, can come in direct contact with the monolayer, any expansion not caused by aging of the monolayer must result from diffusion of benzene into the subphase with subsequent penetration of the monolayer. Figure 10 shows the increase in surface pressure at constant area as a function of the time during which benzene diffuses into the subphase. The rate of increase of  $\pi$  is greater at large areas for those areas at which the monolayer develops a surface pressure

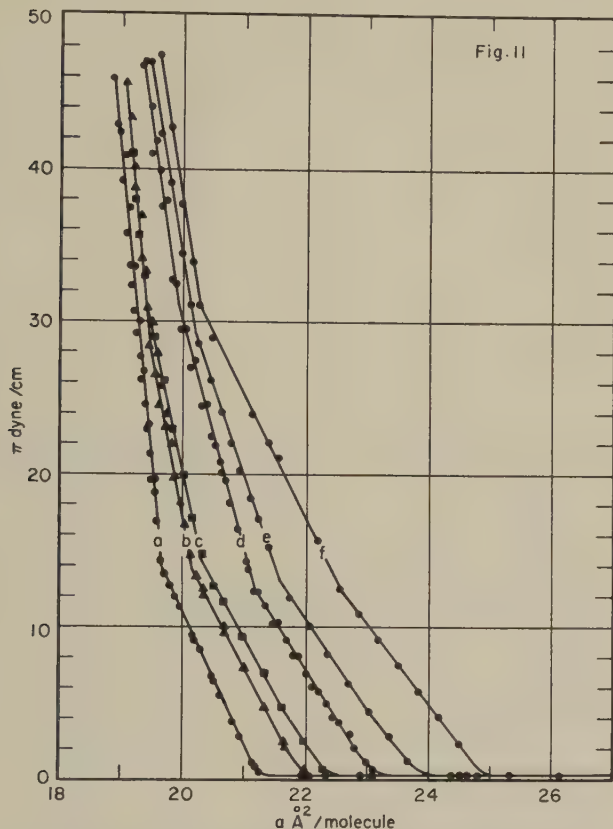


FIG. 11. The  $\pi$ - $a$  isotherm of octadecanol as benzene diffuses into the subphase. The conditions for each curve are listed in Table III.

At  $40.85 \text{ Å}^2$  no pressure is developed for times in excess of 20,000 sec. The increase in slope of the  $20.25 \text{ Å}^2$  curve at 8000 sec. is analogous to that occurring in the  $\pi$ - $a$  isotherm at  $\pi = 13.8$  dynes/cm.

Figure 11 shows the shift of the  $\pi$ - $a$  isotherm of octadecanol to larger molecular areas as benzene diffuses into the subphase. Table III gives the conditions under which each curve was measured. The column headings refer to the area/molecule to which the monolayer was confined. These areas are also referred to in Fig. 10. The body of Table III lists the times at which the  $\pi$ - $a$  isotherm was measured. Thus three different sets of conditions resulted in the same curve,  $d$ , within  $\pm 0.1 \text{ Å}^2$ , i.e., after 16,300 sec. diffusion at  $20.25 \text{ Å}^2$  or 12,000 sec. at  $21.05 \text{ Å}^2$  or 10,000 sec. at  $21.80 \text{ Å}^2$ . Curve  $f$  was measured after 22,000 sec. diffusion at  $21.80 \text{ Å}^2$ .

The set of curves of Fig. 11 establish the shape of the  $\pi$ - $a$  isotherm as benzene diffuses into the subphase. Since  $\pi$  at a given area is known as a

TABLE III  
Conditions for Fig. 11  
Area/molecule during diffusion

	19.37 Å. <sup>2</sup>	20.25 Å. <sup>2</sup>	21.05 Å. <sup>2</sup>	21.80 Å. <sup>2</sup>
a	0 sec.	0 sec.	0 sec.	0 sec.
b	15,000	5,500	—	—
c	—	10,000	—	—
d	—	16,300	12,000	10,000
e	—	—	—	16,000
f	—	—	—	22,000

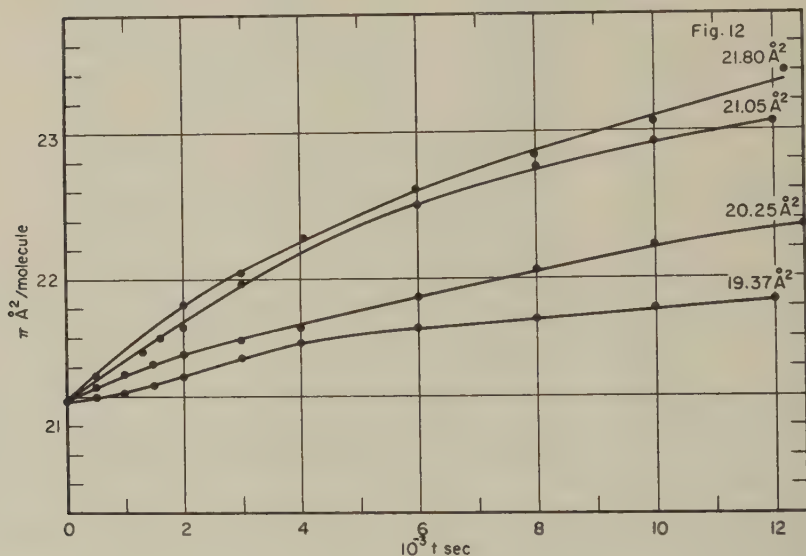


FIG. 12. Area/molecule of octadecanol at  $\pi = 1$  dyne/cm. vs. time during which benzene diffuses into the subphase. The area labeling each curve refers to the area/molecule to which the monolayer was confined during diffusion.

function of time (see Fig. 10), interpolation in the curves of Fig. 11 allows  $a$  at constant  $\pi$  as a function of time to be calculated to a precision of  $\pm 0.14$  Å.<sup>2</sup>. Figure 12 shows  $a$  at  $\pi = 1$  dyne/cm. plotted vs. time. The rate at which the monolayer expands under the influence of benzene in the subphase and aging increases as the area/molecule is increased.

Figure 13 shows the expansion of an octadecanol monolayer with age in the absence of added benzene in the subphase. The monolayer was confined to areas of 40.85 and 20.25 Å.<sup>2</sup>/molecule, respectively, and the area/molecule at  $\pi = 1$  dyne/cm. was measured with time. Aging at 40.85 Å.<sup>2</sup>/molecule resulted in an area increase approximately 3.6 times that obtained at 20.25 Å.<sup>2</sup>.

The area increase on aging without added benzene was applied as a



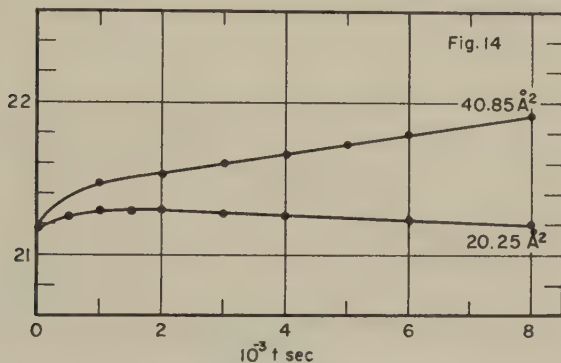
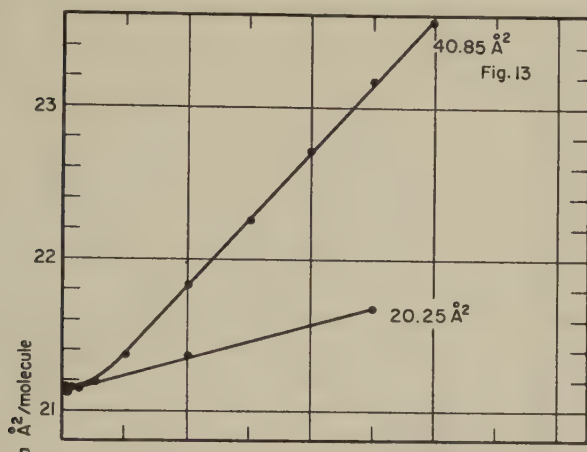


FIG. 13. The area/molecule of octadecanol at  $\pi = 1$  dyne/cm. vs. the age of the monolayer without added benzene in the subphase. The labels refer to the areas to which the monolayer was confined during aging.

FIG. 14. Area/molecule of octadecanol at  $\pi = 1$  dyne/cm., corrected for aging, vs. time during which benzene diffuses into the subphase.

correction to the  $20.25 \text{ Å}^2$  curve of Fig. 12. The result is given in Fig. 14. Aging accounts for essentially all the observed expansion at  $20.25 \text{ Å}^2$ . The data at  $40.25 \text{ Å}^2$  was obtained from  $\pi$ - $a$  curves taken at 0, 5,000, 10,000, 16,000, and 23,000 sec. The area at  $\pi = 1$  dyne/cm. plotted linearly against time. The region between 0 and 8000 sec., corrected for aging, is shown in Fig. 14. The precision of the data represented in Fig. 14 is approximately  $\pm 0.2 \text{ Å}^2$ . A significant expansion about 20% larger than accounted for by aging is obtained with the monolayer confined to  $40.85 \text{ Å}^2$  during benzene diffusion into the subphase.

### C. Stearic Acid and Octadecanol Spread from Various Solvents

Figure 15 shows the expansion of octadecanol or stearic acid monolayers, spread from various solvents, with increasing initial mole ratios. The

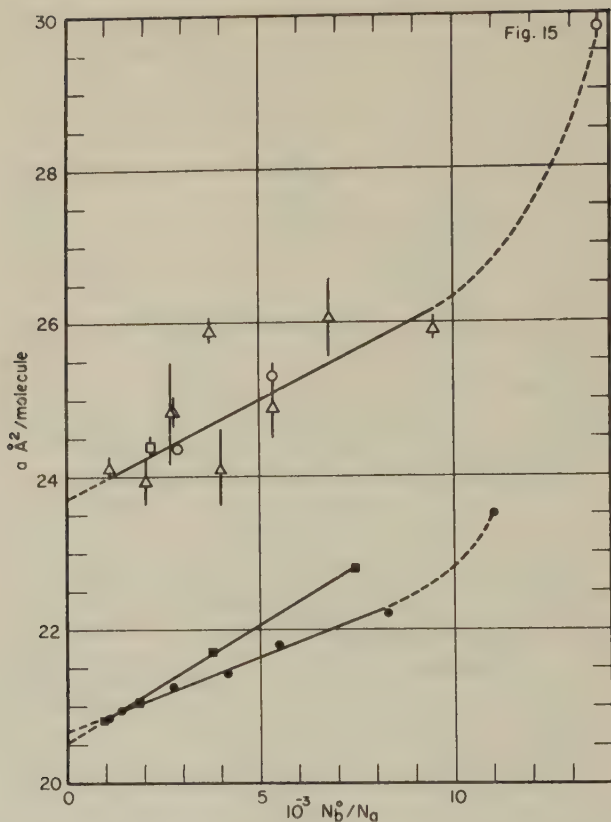


FIG. 15. The molecular area at  $\pi = 1$  dyne/cm. vs.  $n_b^0/n_a$ . The open points represent stearic acid spread from benzene (triangles), ethyl ether (circles), and petroleum ether (squares). The closed points are for octadecanol spread from benzene (circles) and hexane (squares).

molecular area at  $\pi = 1$  dyne/cm. is plotted vs.  $n_b^0/n_a$ . The open points represent measurements on stearic acid monolayers spread from benzene (triangles), ethyl ether (circles), and petroleum ether (squares). The closed points represent data for octadecanol monolayers spread from benzene (circles) and hexane (squares). Differences in the area/molecule of stearic acid spread from benzene and ethyl ether may be obscured by the relatively poor precision of these early experiments. Octadecanol spread from hexane has an area increase at  $\pi = 1$  dyne/cm. approximately 1.6 times greater than when spread from benzene at the same initial mole ratio. The area at  $\pi = 1$  dyne/cm. extrapolated to  $n_b^0/n_a = 0$  obtained from the hexane curve has a value of  $20.55 \text{ Å}^2/\text{molecule}$  and lies  $0.13 \text{ Å}^2/\text{molecule}$  below that given by the benzene curve. This difference may not be significant.

Figure 16 shows the expansion of an octadecanol monolayer with age.

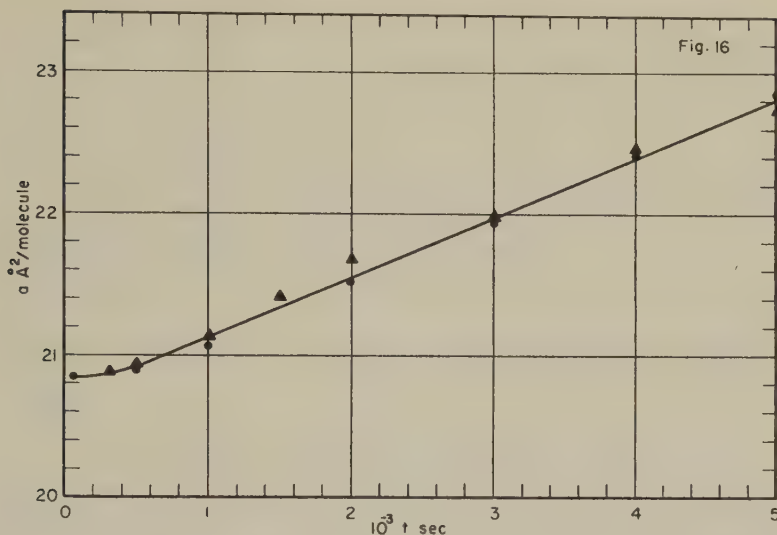


FIG. 16. The increase with age in the area/molecule at  $\pi = 1$  dyne/cm. of an octadecanol monolayer. The circles represent a monolayer spread from benzene and confined to 39.05 Å.<sup>2</sup>/molecule during aging. The triangles represent a monolayer spread from hexane and confined to 22.77 Å.<sup>2</sup>/molecule.

The circles represent a monolayer spread from benzene and confined to 39.05 Å.<sup>2</sup>/molecule during aging. The triangles represent one from hexane and confined to 22.77 Å.<sup>2</sup>/molecule. No surface pressure was developed at the respective confining areas during the sequence of measurements.

#### DISCUSSION

In all experiments where the mole ratio of benzene to stearic acid or octadecanol was increased, an expansion of the monolayer was observed. This was true for experiments where benzene was added after the monolayer had been spread, as well as those in which the concentration of the spreading solution was decreased. If this mole ratio was held constant, e.g., in experiments where the volume of solution or the initial area was varied, holding constant the concentration of the spreading solution, then no change in the  $\pi$ - $a$  isotherm was observed (1).

The mole ratio of benzene to monolayer was increased by (1) diluting the spreading solution; (2) adding droplets of benzene to the monolayer; (3) flushing the monolayer with benzene vapor; and (4) increasing the concentration of benzene in the subphase.

Experiments 2, 3, and 4 above were time dependent and showed an expansion of the monolayer with age. This expansion may be attributed to (1) diffusion into the surface of benzene or other impurities dissolved in the subphase; (2) adsorption of atmospheric impurities; (3) slow changes in the structure of the monolayer.

Experimental observations relating to the expansion with age of a monolayer of stearic acid or octadecanol are:

1. The expansion with age may be increased 20 % to 30 % by increasing the concentration of benzene in the subphase (Figs. 9 and 14). Since no benzene vapor was present in either of these experiments, the source of increased aging was, probably, benzene dissolved in the subphase.

2. Benzene in the subphase contributes significantly to the expansion of an octadecanol monolayer with age only when the monolayer is confined to molecular areas at which no surface pressure is developed. (See Fig. 14.)

3. Aging of monolayers of octadecanol spread from both benzene and hexane occurs to a similar degree. (See Fig. 16.)

4. The expansion with age of an octadecanol monolayer increases as the monolayer is confined to larger molecular areas (Fig. 13).

5. Aging is relatively small during the first 1000 sec.

6. The increase in area at  $\pi = 1$  dyne/cm. with the age of the monolayer is linear between 1000 and 5000 sec.

7. Octadecanol ages more rapidly than stearic acid.

Diffusion into the surface of benzene dissolved in the subphase accounts for only part of the expansion of a monolayer with age (experimental observations 1 and 2 above). The buildup of solvent in the subphase is small during the spreading process since most of the 0.1 ml. of solvent delivered to the surface evaporates. Even with the relatively large concentration of benzene in the subphase represented by Figs. 9 and 14, the expansion of the monolayer with age is increased by only 20 % to 30 %. Other evidence that solvent in the subphase cannot account for all the observed expansion with age is:

1. Aging is independent of the specific solvent employed (experimental observation 3).

2. Aging is dependent upon the substance forming the monolayer (observation 7).

The large expansion with time, obtained when a monolayer of stearic acid is flushed with benzene vapor, implies that the adsorption of other atmospheric impurities may make a significant contribution to aging of the monolayer. The concentration of surface-active contaminants in the atmosphere should be, on a average, constant with time. The amount of adsorbed impurity would, therefore, be expected to increase linearly with time (experimental observation 6).

The fact that octadecanol ages more rapidly than stearic acid indicates that aging may be inherent in the structure of the monolayer. Factors which might contribute to the expansion of the monolayer with age are (1) the gradual breakdown of internal hydrogen bonding among the end groups; (2) the formation of hydrogen bonds between the end groups and



water; (3) the hydration of the end groups; and (4) the two-dimensional evaporation from liquid to gaseous monolayer in the two-phase region, i.e., the horizontal portion of the  $\pi$ - $a$  curve. The possibilities enumerated above may contribute to either reduced cohesion within the monolayer or increased adhesion between the monolayer and subphase, both of which tend to expand the monolayer. In view of the possibility that the expansion with age may represent changes in the structure of the monolayer, further investigation of aging effects is warranted.

The possible causes of aging listed above are all consistent with experimental observation 4. The increased surface pressures at small molecular areas would resist (1) the adsorption of atmospheric or dissolved impurities including solvent, and (2) any changes in the structure of the monolayer.

Additional evidence that aging involves structural changes in the monolayer is provided by Fig. 11. The kink point in the  $\pi$ - $a$  curve of octadecanol at 13.8 dynes/cm. gradually disappears, and a second kink point at approximately 30 dynes/cm. develops as the monolayer ages and benzene diffuses into the subphase. The  $\pi$ - $a$  curve for octadecanol gradually assumes a shape analogous to that of stearic acid (1).

A similar situation is obtained with stearic acid under the influence of aging and flushing with benzene vapor (Fig. 7). Here a kink point develops at approximately 8 dynes/cm. The  $\pi$ - $a$  curve for stearic acid gradually assumes a shape analogous to that obtained with palmitic acid (3). Thus aging and adding benzene to the system cause structural changes in the monolayer similar to those resulting from decreasing chain length or changing the nature of the polar group.

Although the expansion with age is greater for octadecanol than stearic acid monolayers, the reverse holds true with regard to the expansion caused by benzene added to the surface (Fig. 6). The opposed directions taken by aging and solvent effects provides further evidence that aging is not simply a process involving the adsorption of solvent and atmospheric contaminants.

Why benzene should expand a stearic acid monolayer more readily than an octadecanol monolayer is not obvious. The two substances differ only in the nature of the end group. There is no apparent reason why benzene should interact more strongly with a carboxyl than an alcohol group.

Perhaps the answer lies in the relative cohesive properties of the two monolayers. Octadecanol monolayers are less compressible than stearic acid monolayers. This indicates that cohesion within octadecanol monolayers is stronger than within stearic acid monolayers. Further evidence that cohesion within fatty alcohol monolayers is greater than in fatty acids is provided by the "expansion temperature" (4). The "expansion temperature" is somewhat analogous to a two-dimensional boiling point



and is defined, on the basis of a plot of area/molecule at  $\pi = 1.5$  dynes/cm. vs. temperature, as that temperature at which a monolayer exists half in its condensed state and half in its expanded state (liquid or vapor expanded, or gaseous). The "expansion temperature" for cetyl alcohol is  $54^\circ\text{C}$ . whereas that for palmitic acid is  $37.5^\circ\text{C}$ . (5). Apparently, fatty acids are more easily expanded than fatty alcohols. It, therefore, seems probable that the stronger cohesion in octadecanol monolayers makes more difficult the penetration of solvent molecules into the monolayer.

A possible reason why aging effects are greater for octadecanol whereas solvent effects are greater for stearic acid may be that aging depends on both reduced cohesion within the monolayer and increased adhesion to the subphase, while solvent effects may depend only upon the penetrability, i.e., the cohesive properties of the monolayer. Octadecanol forms a more stable monolayer (exhibits higher collapse pressures), indicating that it interacts more strongly with the aqueous subphase than does stearic acid. Likewise, the rate of spreading of octadecanol is greater than that of stearic acid. This may be readily demonstrated by sprinkling some talc on two clean water surfaces and delivering a crystal of octadecanol to one surface and stearic acid to the other. The extent to which the talc is pushed aside at a given time is a measure of the spreading rate. It is, perhaps, the greater adhesion demonstrated by the above observations which causes octadecanol to age more rapidly than stearic acid.

The relative effects of benzene and hexane as spreading solvents for octadecanol monolayers are described in Fig. 15. There is apparently little difference in the expansions caused by either solvent for values of  $n_b^0/n_a$  less than  $2 \times 10^3$ . This value of  $n_b^0/n_a$  corresponds to a concentration of the spreading solution of about 1 mg./ml. In this range of concentrations, hexane may be preferable to benzene because it spreads more rapidly and more evenly. However, for more dilute spreading solutions, the monolayer expands more markedly with hexane than with benzene as the solvent. Hexane, being an elongated hydrocarbon, should pack better among the octadecanol chains than does benzene. This should result in a larger concentration of hexane than benzene retained in the surface.

The above results with hexane do not agree with Mme. Saraga's observations using petroleum ether as the spreading solvent (6). Mme. Saraga concluded that petroleum ether is not retained in a monolayer of myristic acid. She based this conclusion upon the following experiment. The  $\pi$ - $a$  isotherm of myristic acid was measured. Petroleum ether vapor was introduced above the monolayer and the  $\pi$ - $a$  curve remeasured. An expansion of the monolayer was observed. The surface was then flushed with air. The  $\pi$ - $a$  curve returned to its original value within a reported precision of  $\pm 0.2$  dyne/cm. The results of this experiment may not be directly applicable to the spreading process.

The observations reported in Fig. 15 comparing benzene and hexane as spreading solvents are in fair agreement with the results obtained by Archer and La Mer in their studies on the resistance exhibited by fatty acid monolayers to the evaporation of water (7). These investigators found that the resistance of nonadecanoic acid monolayers to the evaporation of water was more sensitive to variations in the concentration of the spreading solution when petroleum ether was employed as solvent than when benzene was used. (A similar sensitivity to hexane is shown by the  $\pi$ - $a$  isotherm and is represented in Fig. 15.) Using either solvent, the resistance decreased with decreasing concentration. This decreased resistance probably correlates with an expansion of the monolayer (1). At a concentration of 0.0035  $M$  and surface pressures above 8 dynes/cm., petroleum ether spreading solutions yielded higher values for the resistance to evaporation than did benzene solutions. On this basis, the surface concentration of petroleum ether was assumed to be less than that of benzene. A concentration of 0.0035  $M$  corresponds to a mole ratio of solvent to nonadecanoic acid of  $3.2 \times 10^3$ . Archer and La Mer did not examine more dilute solutions.

The results reported in Fig. 15 may be interpreted as representing a lower surface concentration of hexane than benzene for values of  $n_b^0/n_a$  less than  $1 \times 10^3$ . This agrees qualitatively with the conclusions of Archer and La Mer but only at high concentrations. The discrepancy between the two sets of results may result from the use of different monolayer-forming materials and/or the higher volatility of the petroleum ether fraction (b.p. 35°–40° C.) used by Archer and La Mer.

The experiments reported in this paper all show that the expansion of the monolayer depends directly upon the mole ratio of solvent to monolayer delivered to the system. The simplest assumption is that the expansion represents the surface concentration of retained solvent. This assumption is based upon the following evidence.

1. Expansions, similar to those obtained by diluting the spreading solution, result from the addition of benzene liquid or vapor to the surface.

2. In experiments where the monolayer was flushed with benzene vapor the law of mass action predicts that both the surface concentration and the concentration of benzene in the subphase should increase with an increase in the partial pressure of benzene vapor. The observed expansion is, therefore a function of the surface concentration of benzene as well as the partial pressure of benzene above the surface.

3. Once expanded, the monolayer cannot be induced to contract by lowering the partial pressure of benzene above the surface, i.e., the observed expansions are irreversible. Since benzene can be adsorbed but not desorbed, the initial presence of benzene in the surface from the spreading solution should result in some benzene being retained in the surface.

4. Fifty monolayers of stearic acid together with 60 ml. of subphase were collected by suction. Upon standing 48 hours in a stoppered bottle, the odor of benzene was detected.

5. Benzene when wiped on a clean ground glass surface evaporated within 5 to 10 sec. Benzene required 1 to 2 min. to evaporate from the same surface covered with paraffin.

6. Alternate hypotheses based on the assumption of incomplete spreading or changes in molecular orientation have been shown to be unsatisfactory (1).

Assuming that the expansion of the monolayer, i.e., the increase in area/molecule at  $\pi = 1$  dyne/cm. ( $\Delta a$ ), represents the area occupied by benzene, the surface concentration of benzene ( $n_b/A$ ) may be evaluated from the equation: (see Appendix B for development)

$$\frac{n_b}{A} = \frac{1}{a_b} \left( \frac{\Delta a}{a} \right),$$

where  $\Delta a$  is the increase in the area/molecule at  $\pi = 1$  dyne/cm. and is evaluated by subtracting the area extrapolated to  $n_b^0/n_a = 0$  from the area at a given value of  $n_b^0/n_a$ ;  $a$  is the molecular area at the given value of  $n_b^0/n_a$ ; and  $a_b$  is the area/mole of benzene in the monolayer. Assuming the area of the benzene ring in the monolayer as that given by monolayers of long-chain phenols, phenylamines, and phenyl ethers, i.e.,  $24.0 \text{ \AA}^2/\text{molecule}$  (8),  $a_b = 1.45 \times 10^9 \text{ cm}^2/\text{mole}$ . Table IV shows the increase in  $n_b/A$  (column 2) with increasing  $n_b^0/n_a$  (column 1). Since experimental precision does not allow measurement of molecular areas to better than  $0.1 \text{ \AA}^2$ , the smallest value of  $n_b/A$  which can be detected experimentally is

$$\frac{1}{a_b} \left( \frac{0.1}{20} \right) = 3.5 \times 10^{-12} \text{ moles/cm}^2.$$

The values of  $n_b/A$ , though precise to about 10%, may be accurate only within a factor of 2 owing to the uncertainty in the value of  $a_b$ . This uncertainty arises because the orientation of the benzene molecule in the monolayer is unknown.

The experimental observations pertaining to the spreading process are:

1. Spreading is completed within 1 to 2 sec. after delivering the solution to the aqueous surface (1).

2. Evaporation of solvent from the surface is complete within 30 to 50 sec. after spreading. The rate of evaporation after 50 sec. becomes immeasurably slow as measured by a decrease in surface pressure with time (1).

3. The expansion of the monolayer with age is negligible during the first 500 sec. after spreading. This, together with observation 2, implies that the surface concentration of solvent established during the spreading process remains constant from 50 to 500 sec.

TABLE IV

*The Surface Concentration of Benzene in a Monolayer of Octadecanol\**

$n_b^0/n_a$	$n_b/A$ (mole/cm. <sup>2</sup> )	$\Gamma_b$ (mole/cm. <sup>2</sup> )
$1.03 \times 10^3$	$0.5 \times 10^{-11}$	$1.9 \times 10^{-11}$
1.37	0.8	2.6
2.74	1.9	5.4
4.14	2.4	8.4
5.48	3.6	11.6
8.28	4.7	17.6

\* The surface concentration of a "pure" octadecanol monolayer at  $\pi = 1$  dyne/cm<sup>2</sup> is  $8 \times 10^{-10}$  mole/cm.<sup>2</sup>.

4. The expansion of the monolayer in excess of aging depends upon the concentration of solvent in the subphase. Consistent with the above observations, the following model is proposed for the spreading process.

air + benzene		vapor
<hr/>		
soln. of octadecanol + benzene	(d)	
concn. of benzene = $c_b^s$		
<hr/>		
soln. of benzene + water	(e)	surface
+ octadecanol		
concn. of benzene = $c_b^w$		
<hr/>		
water		subphase

FIG. A. Initial system immediately after adding the spreading solution to the surface.

A small volume of a solution of octadecanol in benzene, the concentration of benzene being  $c_b^s$ , is added to the aqueous surface. The solution spreads immediately (less than 2 sec.) to form a layer consisting of a solution of octadecanol and benzene (Fig. A, layer (d)) and a layer (e) containing a saturated solution of benzene in water of concentration  $c_b^w$ . Evaporation and diffusion into the subphase deplete the surface of benzene. The number of moles of benzene in the subphase,  $N_b$ , increases as governed by the rate of diffusion. The concentration of benzene in layer (d) decreases as controlled by the rate of evaporation. (The relatively small decrease in the concentration of benzene in the surface due to diffusion into the subphase may be neglected if the rate of evaporation is assumed to be much larger than the rate of diffusion.) Consider the time,  $t_1$ , required for the concentration of benzene in layer (d),  $c_b$ , to drop from the initial concentration of benzene in the spreading solution,  $c_b^s$ , to the concentration of benzene in a saturated solution of benzene in water,  $c_b^w$ . This is approximately the time required for the evaporation of benzene to become "complete," i.e., the time re-



quired for layer (d) to vanish. During time  $t_1$  the concentration of benzene in layer (e) remains constant at the concentration of benzene in a saturated water solution,  $c_b^w$ . During this time,  $N_b$  moles of benzene diffuse into the subphase under the influence of the constant concentration gradient  $c_b^w/h$ , where  $h$  is the thickness of the subphase. Therefore, if diffusion is assumed to be sufficiently slow that the concentration of benzene at the bottom of the tray remains 0 during time  $t_1$ , an integrated form of the diffusion equation can be written as (9)

$$N_b = DA(c_b^w/h)t_1$$

where  $N_b$  is the number of moles of benzene which diffuse into the subphase through cross section  $A$  in time  $t_1$  under the influence of a constant concentration difference  $c_b^w$  between two surfaces of a layer of water of thickness  $h$ . The time  $t_1$  may be evaluated from the equation representing the net rate of evaporation,  $r_e$ , from a system of changing volume,  $V$ .

$$-\left(\frac{dc_b}{dt} + \frac{c_b}{V} \frac{dV}{dt}\right) = r_e \quad [1]$$

(10) where  $c_b$  is the concentration of benzene in layer (d) at time  $t$ .

Equation [1] may be transformed to (see Appendix C for development)

$$r_e = -\left(\frac{dc_b}{dt} + \frac{c_b \bar{v}_b}{1 - c_b \bar{v}_b} \cdot \frac{dc_b}{dt}\right) \quad [2]$$

where  $\bar{v}_b$  is the partial molar volume of benzene in layer (d).

Assuming (1) that there are no interactions, which is equivalent to setting  $\bar{v}_b = \text{constant} = v_b^0$ , the molar volume of benzene, and (2) that the partial pressure of benzene above the surface is zero for an open system the rate equation becomes (see Appendix C)

$$\frac{dc_b}{c_b} + \frac{v_b^0 dc_b}{1 - c_b v_b^0} = -kA dt. \quad [3]$$

Integrating Eq. [3] over the limits

$c_b^s =$  concentration of benzene in the spreading solution

to  $c_b^w =$  concentration of benzene in a saturated water solution,

$$\ln \frac{1 - c_b^w v_b^0}{c_b^w} - \ln \frac{1 - c_b^s v_b^0}{c_b^s} = kA t_1. \quad [4]$$

Equation [4] may be transformed to (Appendix C)

$$\ln \frac{1 - c_b^w v_b^0}{c_b^w v_a^0} + \ln \frac{n_b^0}{n_a} = kA t_1, \quad [5]$$

where  $v_a^0 =$  molar volume of octadecanol; and  $n_b^0/n_a =$  initial mole ratio of benzene to octadecanol.



Solving for  $t_1$  and substituting into the diffusion equation,

$$N_b = \frac{Dc_b^w}{kh} \left( \ln \frac{1 - c_b^w v_b^0}{c_b^w v_a^0} + \ln \frac{n_b^0}{n_a} \right). \quad [6]$$

The Gibbs' adsorption isotherm expresses the relationship between the bulk concentration of a component and its surface concentration. For a dilute solution of benzene in water, neglecting interactions with either water or dissolved octadecanol (11),

$$\Gamma_b = - \frac{c_b}{RT} \frac{d\gamma}{dc_b}.$$

For a constant volume of solution and substituting  $d\pi$  for  $-d\gamma$ ,

$$\Gamma_b = \frac{N_b}{RT} \frac{d\pi}{dN_b}, \quad [7]$$

where  $N_b$  is the number of moles of benzene in the subphase. Solving Eqs. [6] and [7] simultaneously,

$$\Gamma_b = \frac{\frac{Dc_b^w}{kh} \left( \ln \frac{1 - c_b^w v_b^0}{c_b^w v_a^0} \cdot \frac{n_b^0}{n_a} \right)}{RT} \cdot \frac{d\pi}{dN_b}. \quad [8]$$

Defining the symbols again,

- $\Gamma_b$  = surface concentration of benzene.
- $D$  = diffusion coefficient of benzene into water.
- $k$  = specific rate of evaporation of benzene.
- $h$  = thickness of the subphase.
- $c_b^w$  = concentration of benzene in a saturated water solution.
- $v_b^0$  = molar volume of benzene.
- $v_a^0$  = molar volume of octadecanol.
- $n_b^0/n_a$  = initial mole ratio of benzene to octadecanol.
- $R$  = gas constant in ergs/degree.
- $T$  = absolute temperature.
- $\pi$  = surface pressure.
- $N_b$  = total no. of moles of benzene in the subphase.

For a given solute and solvent, i.e., octadecanol and benzene,  $D$ ,  $k$ ,  $h$ , and  $c_b^w$  are constant and occur in both numerator and denominator of Eq. [8]. Likewise,  $v_b^0$  and  $v_a^0$  are constant. Equation [8] therefore becomes

$$\begin{aligned} \Gamma_b &= \frac{\ln \frac{1 - c_b^w v_b^0}{c_b^w v_a^0} \cdot \frac{n_b^0}{n_a}}{RT} \cdot \frac{d\pi}{d(\ln n_b^0/n_a)} \\ &= \frac{\left[ \ln \left( \frac{1 - c_b^w v_b^0}{c_b^w v_a^0} \cdot \frac{n_b^0}{n_a} \right) \right] \frac{n_b^0}{n_a}}{RT} \frac{d\pi}{d(n_b^0/n_a)}. \end{aligned}$$

The terms  $v_b^0$  and  $v_a^0$  may be evaluated from the molecular weights and densities of benzene and octadecanol, respectively, as  $v_b^0 = 89$  ml./mole and  $v_a^0 = 333$  ml./mole, while  $c_b^w = 1.05 \times 10^{-5}$  mole/ml. The values are based on data obtained from the *Handbook of Chemistry and Physics* (12).

The value of  $d\pi/d(n_b^0/n_a)$  was derived from experimental data. The surface pressures in the horizontal portion of the  $\pi$ - $a$  curves represented in Fig. 3, i.e., at  $a = 23, 24, 26$ , and  $30$  A.<sup>2</sup>/molecule, were plotted vs.  $n_b^0/n_a$ . The values of  $\pi$  were precise to approximately 0.1 dyne/cm., i.e., about 40%. The plots of  $\pi$  vs.  $n_b^0/n_a$  at constant area/molecule were linear within this precision. The slopes,  $d\pi/d(n_b^0/n_a)$ , obtained from these plots were within approximately 20% of the value  $3.6 \times 10^{-5}$  dyne/cm. for areas/molecule between 23 and 30 A.<sup>2</sup>. The calculated values for  $\Gamma_b$  precise to roughly 50% are given in column 3 of Table IV.

A comparison between the theoretical values for the surface concentration,  $\Gamma_b$ , and those evaluated from experimental data,  $n_b/A$ , show good order-of-magnitude agreement. The values for  $\Gamma_b$  are high by a constant factor of approximately 3.5.

The error in  $\Gamma_b$  introduced by the assumption of no interactions is probably smaller than the estimated precision of 50%. Moreover, the inclusion of interactions between benzene and octadecanol in the model would serve to increase the theoretical surface concentration of benzene, thereby making the discrepancy between  $\Gamma_b$  and  $n_b/A$  even larger. Apparently, the neglect of interactions in deriving the model does not contribute to the discrepancy between  $\Gamma_b$  and  $n_b/A$ .

Not considered in developing the model was the possibility of the continued evaporation of solvent after time  $t_1$ . The resulting reduction in the surface concentration of benzene might partially account for the low values of  $n_b/A$  compared with  $\Gamma_b$ .

Qualitatively, the model appears to be satisfactory. An almost linear dependence of surface concentration upon the initial mole ratio of benzene to octadecanol is predicted. This prediction is borne out by the experimental results represented in Fig. 2. The model also takes into account the increase in the surface concentration of benzene with increasing concentration in the subphase as demonstrated in Fig. 14.

## CONCLUSIONS

Many investigators have assumed that organic liquids of high volatility and low solubility in water would serve as suitable solvents for spreading monolayers. It is now apparent, however, that volatile solvents differ in the degree they affect the properties of monolayers. Not only the specific solvent, but the amount of solvent per molecule of monolayer, contribute to the measured properties. Consistent with complete spreading, the smallest contributions are made by the smallest ratio of solvent to

monolayer. Apparently, these effects are caused by solvent retained in the surface.

#### ACKNOWLEDGMENTS

The authors wish to express their gratitude to Martin Friedlander and Dr. Geoffrey T. Barnes for many helpful suggestions they made during the course of discussion. Thanks are also extended to the Eastman Kodak Company and Columbia University for the award to M.L.R. of the Eastmen Kodak Fellowship for the year 1957-58.

#### APPENDIX A

##### *An Interferometric Method for the Measurement of the Contact Angles of Liquids on Solids<sup>1</sup>*

A pencil-line of monochromatic light ( $\lambda = 5461 \text{ \AA.}$ ) is passed through a vertical illuminator mounted on a microscope and is focused on the edge of the meniscus formed by water on a vertically suspended glass plate. The beam of light is perpendicular to the glass plate. Therefore, the angle of incidence is  $0^\circ$  as measured from the normal to the surface of the plate. The reflected image is viewed through the microscope as a series of interference fringes. This reflected image together with a superimposed image of a previously calibrated reticule in the eyepiece is photographed. The spacings on the photographic plate of both the fringes and the reticule are determined by means of a recording micro-densitometer. The absolute spacing between the 1st and 2nd dark fringes,  $h$ , may be evaluated by comparing the spacings of the fringes with the spacings on the reticule. The measurement of  $h$  is taken vertically along the glass surface. An upper limit to the contact angle may be obtained from the trigonometric relationship

$$\tan \theta = t/h,$$

where  $t$  is the thickness of the film at a distance  $h$  from the edge of the meniscus. The evaluation of  $t$  derives from the condition for interference minima (13)

$$N\lambda = 2nt \cos \varphi$$

where  $\varphi$  is the angle of refraction = the angle of incidence =  $0^\circ$ ;  $n$  is the refractive index of the liquid;  $\lambda$  is the wavelength of the incident light; and  $N = 0, 1, 2, \dots$  for the 1st, 2nd, 3rd,  $\dots$  dark fringes, respectively.

#### APPENDIX B

##### *The Evaluation of $n_b/A$ , the Experimentally Determined Surface Concentration of Benzene*

Assuming that the increase in the molecular area of octadecanol represents the area of benzene per molecule of octadecanol in the monolayer,

<sup>1</sup> Devised by Martin Friedlander, Columbia University.

the total area occupied by benzene is

$$\Delta A = \Delta a n_a N,$$

where  $\Delta a$  is the increase in area/molecule at  $\pi = 1$  dyne/cm. for a given value of  $n_b^0/n_a$ ,  $n_a$  is the no. of moles of octadecanol in the surface, and  $N$  is Avogadro's number. The number of moles of benzene in the surface is

$$n_b = \Delta A/a_b,$$

where  $a_b$  is the area/mole of benzene in the monolayer. The total area occupied by the monolayer is

$$A = a n_a N,$$

where  $a$  is the area/molecule of octadecanol at  $\pi = 1$  dyne/cm. for the given value of  $n_b^0/n_a$ . Therefore, the surface concentration of benzene is

$$\frac{n_b}{A} = \frac{1}{a_b} \cdot \frac{\Delta A}{A} = \frac{1}{a_b} \cdot \frac{\Delta a}{a}.$$

#### APPENDIX C

##### *Evaluation of $t_1$*

Definition of symbols:

$r_e$  = rate of evaporation of benzene.

$c_b$  = surface concentration of benzene at time,  $t$ .

$V$  = volume of layer  $d$  (see Fig. A) at time,  $t$ .

$n_b$  = no. moles of benzene in layer  $d$ , at time,  $t$ .

$n_a$  = no. moles of octadecanol in surface.

$\bar{v}_b$  = partial molar volume of benzene in layer  $d$ .

$\bar{v}_a$  = partial molar volume of octadecanol in layer  $d$ .

$v_b^0$  = molar volume of benzene.

$v_a^0$  = molar volume of octadecanol.

$k$  = specific rate constant for evaporation of benzene.

$A$  = area of surface before compression.

$c_b^w$  = concentration of benzene in a saturated water solution.

$c_b^s$  = concentration of benzene in the spreading solution.

$n_b^0$  = initial no. moles of benzene.

$V^0$  = initial volume of layer  $d$ .

The rate of evaporation of benzene from a system of changing volume is

$$r_e = -\left(\frac{dc_b}{dt} + \frac{c_b}{V} \frac{dV}{dt}\right); \quad [1]$$

$$V = n_b \bar{v}_b + n_a \bar{v}_a;$$

$$dV = n_b d\bar{v}_b + \bar{v}_b dn_b + n_a d\bar{v}_a + \bar{v}_a dn_a;$$

$$n_b d\bar{v}_b + n_a d\bar{v}_a = 0 \quad (\text{Gibbs-Duhem equation});$$

$$\frac{dV}{dt} = \bar{v}_b \frac{dn_b}{dt} + \bar{v}_a \frac{dn_a}{dt}.$$

Since  $n_a$  is constant for any set of initial conditions, i.e., any given concentration and volume of spreading solution,

$$\frac{dV}{dt} = \bar{v}_b \frac{dn_b}{dt}$$

$$n_b = c_b V$$

$$\frac{dn_b}{dt} = c_b \frac{dV}{dt} + V \frac{dc_b}{dt} = \frac{1}{\bar{v}_b} \frac{dV}{dt}$$

$$\frac{dV}{dt} = \frac{V}{(1/\bar{v}_b - c_b)} \frac{dc_b}{dt}$$

$$\frac{c_b}{V} \frac{dV}{dt} = \frac{c_b \bar{v}_b}{1 - c_b \bar{v}_b} \frac{dc_b}{dt}$$

$$r_e = - \left( \frac{dc_b}{dt} + \frac{c_b \bar{v}_b}{1 - c_b \bar{v}_b} \frac{dc_b}{dt} \right) = kA c_b \quad [2]$$

Setting  $\bar{v}_b = \text{constant} = v_b^0$

$$\int_{c_b^s}^{c_b^w} \left( \frac{dc_b}{c_b} + \frac{v_b^0}{1 - c_b v_b^0} dc_b \right) = -kA \int_0^{t_1} dt \quad [3]$$

$$\ln c_b \Big|_{c_b^s}^{c_b^w} - \ln (1 - c_b v_b^0) \Big|_{c_b^s}^{c_b^w} = -kA t_1$$

$$\ln \frac{1 - c_b^w v_b^0}{c_b^w} + \ln \frac{c_b^s}{1 - c_b^s v_b^0} = kA t_1 \quad [4]$$

Adding  $\ln v_b^0 - \ln v_b^0 = 0$

$$\ln \frac{1 - c_b^w v_b^0}{c_b^w v_b^0} + \ln \frac{c_b^s v_b^0}{1 - c_b^s v_b^0} = kA t_1, \quad [4a]$$

$$c_b^s = n_b^0 / V^0;$$

$$c_b^s v_b^0 = \frac{n_b^0 v_b^0}{V^0} = \frac{n_b^0 v_b^0}{n_b^0 v_b^0 + n_a v_a^0};$$

$$\begin{aligned} \frac{c_b^s v_b^0}{1 - c_b^s v_b^0} &= \frac{1}{1 + \frac{n_a v_a^0}{n_b^0 v_b^0}} \Bigg/ \left[ 1 - \frac{1}{1 + \frac{n_a v_a^0}{n_b^0 v_b^0}} \right] \\ &= \frac{1}{\frac{n_a v_a^0}{n_b^0 v_b^0}} = \frac{n_b^0}{n_a} \cdot \frac{v_b^0}{v_a^0}. \end{aligned}$$



Substituting into Eq. [4a]

$$\ln \frac{1 - c_b^w v_b^0}{c_b^w v_a^0} \cdot \frac{n_b^0}{n_a} = k A t_1. \quad [5]$$

#### REFERENCES

1. LA MER, V. K., AND ROBBINS, M. L., *J. Phys. Chem.* **62**, 1291 (1958).
2. Measurements of contact angles were performed by Martin Friedlander using a technique developed by him. A paper on this technique has been submitted for publication to the *J. Phys. Chem.* A brief description is included as Appendix A.
3. SCHULMAN, J., *Ann. Repts. Progr. Chem. (Chem. Soc. London)* **36**, 194 (1939).
4. ADAM, N. K., "The Physics and Chemistry of Surfaces," 3rd ed., p. 61. Oxford University Press, London, 1941.
5. ADAM, N. K., "The Physics and Chemistry of Surfaces," 3rd ed., p. 64. Oxford University Press, London, 1941.
6. TER MINASSIAN-SARAGA, LISBETH, *J. chim. phys.* **52**, 80 (1955).
7. ARCHER, R. J., AND LA MER, V. K., *J. Phys. Chem.* **59**, 200 (1955).
8. ADAM, N. K., "The Physics and Chemistry of Surfaces," 3rd ed., p. 50. Oxford University Press, London, 1941.
9. "Handbook of Chemistry and Physics," 37th ed., p. 2799. Chemical Rubber Publ. Co., Cleveland, Ohio, 1955-1956.
10. HAMMETT, L. P., "Introduction to the Study of Physical Chemistry," 1st ed., p. 166. McGraw-Hill, New York, 1952.
11. ADAM, N. K., "The Physics and Chemistry of Surfaces," 3rd ed., p. 112. Oxford University Press, London, 1941.
12. "Handbook of Chemistry and Physics," 37th ed. Chemical Rubber Publ. Co., Cleveland, Ohio, 1955-1956.
13. MARGENAU, H., WATSON, W. W., AND MONTGOMERY, G. G., "Physics—Principles and Applications," 2nd ed., p. 687. McGraw-Hill, New York, 1953.
14. COOK, H. D., AND RIES, H. E., JR., *J. Phys. Chem.* **60**, 1533 (1956).
15. HARKINS, W. D., "The Physical Chemistry of Surface Films." Reinhold, New York, 1952.
16. STENHAGEN, E., "Surface films," in E. A. Braude and F. C. Nachod, eds., "The Determination of Organic Structures by Physical Methods," p. 325 et seq. Academic Press, New York, 1955.
17. LANGMUIR, I., AND SCHAEFER, V. T., *J. Franklin Inst.* **235**, 119 (1943).
18. NUTTING, G. C., AND HARKINS, W. D., *J. Am. Chem. Soc.* **61**, 1180 (1939).
19. ROSANO, H. S., AND LA MER, V. K., *J. Phys. Chem.* **60**, 348 (1956).
20. ALLAN, A. J. G., *J. Colloid Sci.* **13**, 273 (1958).
21. DEAN, R. B., AND MCBAIN, J. W., *J. Colloid Sci.* **2**, 383 (1947).
22. DEAN, R. B., AND LI, FA SI, *J. Am. Chem. Soc.* **72**, 3979 (1950).
23. DEAN, R. B., AND HAYES, K. E., *J. Am. Chem. Soc.* **73**, 5583 (1951).
24. MICHELI, L. I. A., *Phil. Mag.* [7] **3**, 895 (1927).
25. JONES, D. C., OTTEWILL, R. H., AND CHATER, A. P. J., 2nd International Congress on Surface Activity, Vol. 1, p. 188. Academic Press, New York, 1957.

## THE SURFACE CHEMISTRY OF WHEAT GLUTEN

### I. SURFACE PRESSURE MEASUREMENTS

N. W. Tschoegl and A. E. Alexander

*Bread Research Institute of Australia, North Sydney, New South Wales;  
Department of Physical Chemistry, The University of Sydney,  
New South Wales*

*Received September 15, 1959, revised November 30, 1959*

#### INTRODUCTION

Wheat gluten is the elastic, coherent protein complex obtained by washing out the starch and the water-solubles from a dough of wheat flour. Since variations in gluten quality are thought to be chiefly responsible for variations in the handling properties and baking quality of different types of wheat flour doughs, an understanding of the physical chemistry of gluten is of great interest to the baking industry. However, despite considerable efforts, gluten structure has remained something of a mystery, owing in large measure to the insolubility of gluten, which makes examination by the usual physicochemical methods rather difficult. It was therefore thought that monolayer techniques might prove useful, particularly in view of their recent applications to high polymers, synthetic polypeptides, and proteins. Monolayer techniques combine the advantages of speed and versatility with low cost of equipment and the need for only small quantities of test material. Since the monolayer may be spread at a great variety of interfaces, insoluble proteins may be examined under a wide range of conditions.

As a recent example of monolayer studies on an insoluble protein the work of Ellis and Pankhurst (1, 2) on collagen should be mentioned. No surface chemical studies have hitherto been reported on whole wheat gluten, although gliadin and to some extent zein, the prolamines of wheat and maize, have been studied, mainly because they could be spread from aqueous alcohol. Gliadin, however, when doughed up with water, is inelastic, though extensible, and does not show the remarkable properties of gluten. Furthermore, as the ultimate aim of this work is the understanding of the nature of "baking quality," whole gluten was made its object of study.

This paper, which is the first of a series describing surface chemical studies on gluten, deals with surface pressure measurements carried out on gluten films spread from dispersion in a 0.1 *M* solution of hydrogen chloride in anhydrous chloroethanol. The reasons for the use of this dispersant are detailed elsewhere (3, 4).

## EXPERIMENTAL

*Dispersions*

The gluten used in these experiments was obtained from a medium strength New South Wales flour of 12.5% protein content (dry basis). The preparation of the vacuum-dried gluten, the anhydrous acid chloroethanol (0.1 *M* hydrogen chloride in 2-chloroethanol), and the preparation and analysis of the dispersions is described elsewhere (3). The dispersion of protein in this medium was virtually complete (99.2%). Two-milliliter aliquots of these stock dispersions containing about 5 mg. of protein ( $N \times 5.7$ ) (5) per milliliter of dispersion were diluted with the same anhydrous acid chloroethanol to a spreading concentration of about 0.4 mg./ml.

*Substrates*

The aqueous substrates were solutions of hydrochloric acid (at pH 1.0 and 2.1), sodium hydroxide (at pH 12.0 and 13.0), and various buffers (acetate, glycine, phosphate, and borate) of different pH and ionic strength. Veronal buffers were found to give anomalous results. The buffer used at pH 6.8 was the phosphate buffer of Dill and Alsberg (6). Wherever necessary, adjustment to the required ionic strength was carried out with sodium or potassium chloride. A few experiments were also carried out using 10% w/v sodium salicylate and 24% w/v urea.

Twice-redistilled carbon tetrachloride was used as the oil phase.

Sodium salicylate and urea were of B.P. quality; all other reagents were of A.R. grade. Water was first deionized and then distilled from an all-glass still containing a trace of sulfuric acid.

Surface-active impurities in the carbon tetrachloride and the aqueous substrates were allowed to collect on the surface in wide storage bottles, the solutions being syphoned out from below the surface.

*Surface Pressure Measurements*

These measurements were carried out with the aid of two hanging plate type surface balances. All  $\pi$ -*A* isotherms shown represent the average of at least two runs. At the A/W interface, the films were spread on a shallow rectangular Perspex trough between two waxed glass barriers. Compression and decompression was carried out in the usual way with the aid of a movable barrier operated through a worm gear either by hand or with the aid of a small reversible electric motor.

At the O/W interface, the films were spread in a glass crystallizing dish of 12 cm. diameter. Compression of the film at this interface was achieved by successive additions of dispersion (7). Check measurements at selected areas gave identical results within the expected experimental error.

Surface pressures ( $\pi$ ) were calculated from the deflection of the vertical movement of a 10-cm. mica plate (A/W) or a 6-cm. Teflon plate (O/W) suspended in each case from one of the arms of two torsion strip balances (8). Calibration with known weights in the usual way gave straight-line responses over the required range of 0–40 dynes/cm. The sensitivity of the A/W balance was 0.05 dyne/cm, that of the O/W balance 0.13 dyne/cm. Care was taken to keep the Teflon plate completely immersed even at maximum surface pressure. The Teflon plate was cleaned before each spreading by boiling it for 5–10 min. in a 1/2 mixture of concentrated nitric and sulfuric acid (9). The mica plate was rubbed with very fine silicon carbide paper and rinsed before each spreading.

Compressibility coefficients ( $c_s = (dA/d\pi)/A$ ) were obtained from the  $\pi$ - $A$  isotherms by graphical differentiation (10).

All measurements were carried out at  $25^\circ \pm 0.5^\circ\text{C}$ .

### *Spreading*

The dispersions were spread from an all-glass Burroughs-Wellcome "Agla" micrometer syringe mounted on a rack-and-pinion. The micrometer screw was turned by a small synchronous motor through a simple friction drive.

At the A/W interface, the tip of the syringe was carefully lowered until it touched the surface, slightly withdrawn to form a hill, and the motor was started. As soon as the required amount of dispersion was deposited, the motor was stopped and the tip completely withdrawn from the surface as the heavy dispersions would otherwise continue to flow out of the syringe.

For the same reason, successive additions could not be made at an interface between water and a light oil such as the customary benzene or petroleum ether. Furthermore, at such an interface the dispersion had a tendency to sink to the bottom of the dish when spread against an existing pressure. Satisfactory reproducibility could be achieved only when the interface was that between a heavy oil (such as chloroform or carbon tetrachloride) and water. In order to lower the syringe through the aqueous phase without loss of dispersion, an air-seal was applied by turning the micrometer screw back some ten divisions (0.10 mm.) immediately before spreading. The tip was then brought just underneath the interface and kept there throughout the run, additions being made with a minimum of disturbance simply by starting and stopping the electric motor.

No spreading agent was necessary with these dispersions, the chloroethanol apparently acting as such (4). A period of 5 min. was found sufficient for the film to reach equilibrium after deposition. The interfacial pressure of protein films generally rises sharply (11, 12) immediately after compression and then falls to a limiting value with time. The reverse hap-

pens on decompression. The effect is more pronounced the smaller the area and is believed to be due to molecular rearrangements. One minute was allowed after compression (or decompression) for this rearrangement to take place. Changes in the pressure after this period were found to be negligible.

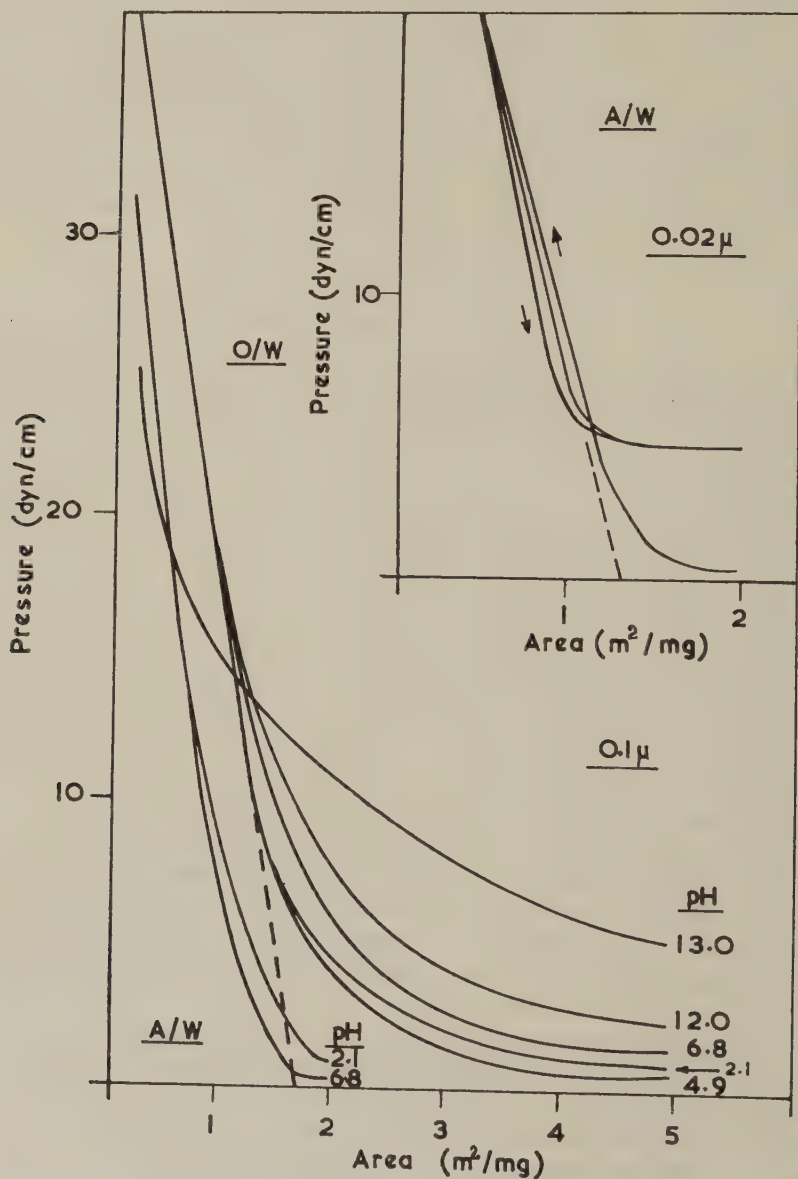


FIG. 1. Effect of interface and pH on the  $\pi$ -A isotherms of gluten films.



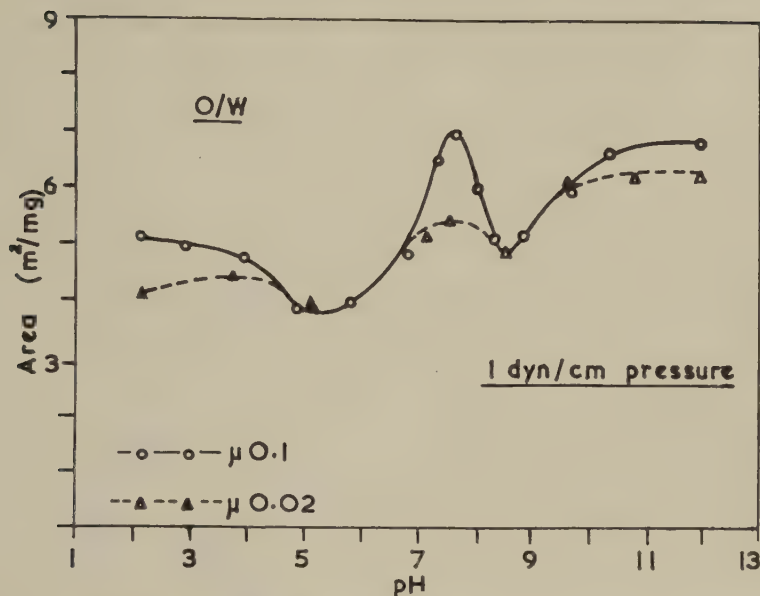


FIG. 2. Dependence of area at constant pressure of gluten films on pH and ionic strength at the O/W interface.

## RESULTS

Figure 1 shows a number of  $\pi$ -A isotherms obtained at the A/W and the O/W interfaces on substrates of  $\mu 0.1$  at different pH values. The behavior on  $\mu 0.02$  substrates was very similar. There was practically no indication of collapse at either interface. At areas below about  $1.1 \text{ m}^2/\text{mg}$ ., the isotherms were identical within the experimental error with the exception of the very expanded isotherm at pH 13. The isotherm at pH 1.0 (not shown) was found to be normal.

The unusually long straight portions of the curves allowed an extrapolation to be made to zero pressure. This gave an "area of close-packing" of  $1.33 \text{ m}^2/\text{mg}$ . at the A/W interface and of  $1.54 \text{ m}^2/\text{mg}$ . at the O/W interface (Fig. 1).

The influence of pH on the expansion of the film at areas above  $1.1 \text{ m}^2/\text{mg}$ . is shown in Fig. 2 where the area at 1 dyne/cm. pressure (at the O/W interface) is plotted against pH. Both the  $\mu 0.1$  and the  $\mu 0.02$  curves have minima at about pH 5.5 and 8.5 and a maximum at about pH 7.5. The W-shape is seen to be more pronounced at the higher ionic strength.

At the A/W interface, where the film could be decompressed by simply reversing the direction of travel of the movable barrier, gluten films showed interesting hysteresis phenomena. At pH 6.8 and  $\mu 0.02$  (inset, Fig. 1) the pressure on decompression rapidly fell to a minimum value roughly corre-

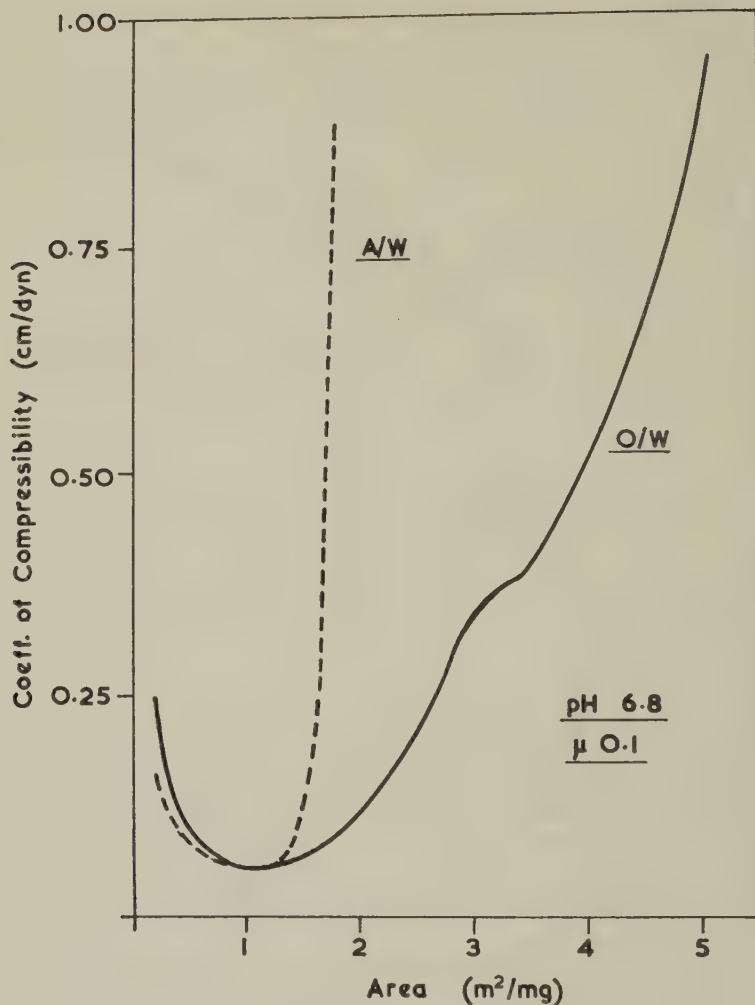


FIG. 3. Compressibility of gluten films.

sponding to that measured at about 1.1 m.<sup>2</sup>/mg. in the first compression. No further decrease occurred on continued decompression. On recompressing the initial pressures were gradually regained. At the same pH but  $\mu$  0.1 the hysteresis loops were the same but the minimum pressure was only very slightly higher than the initial pressure.

Figure 3 shows the coefficient of compressibility as a function of the area at pH 6.8 and  $\mu$  0.1. The minimum compressibility is about 0.05 cm./dyne at both interfaces and occurs at about 1.1 m.<sup>2</sup>/mg., i.e., at the area at which the  $\pi$ -A isotherms at different pH's coalesce. The pH had no influence on either the magnitude or the location of the minimum compressibility. The

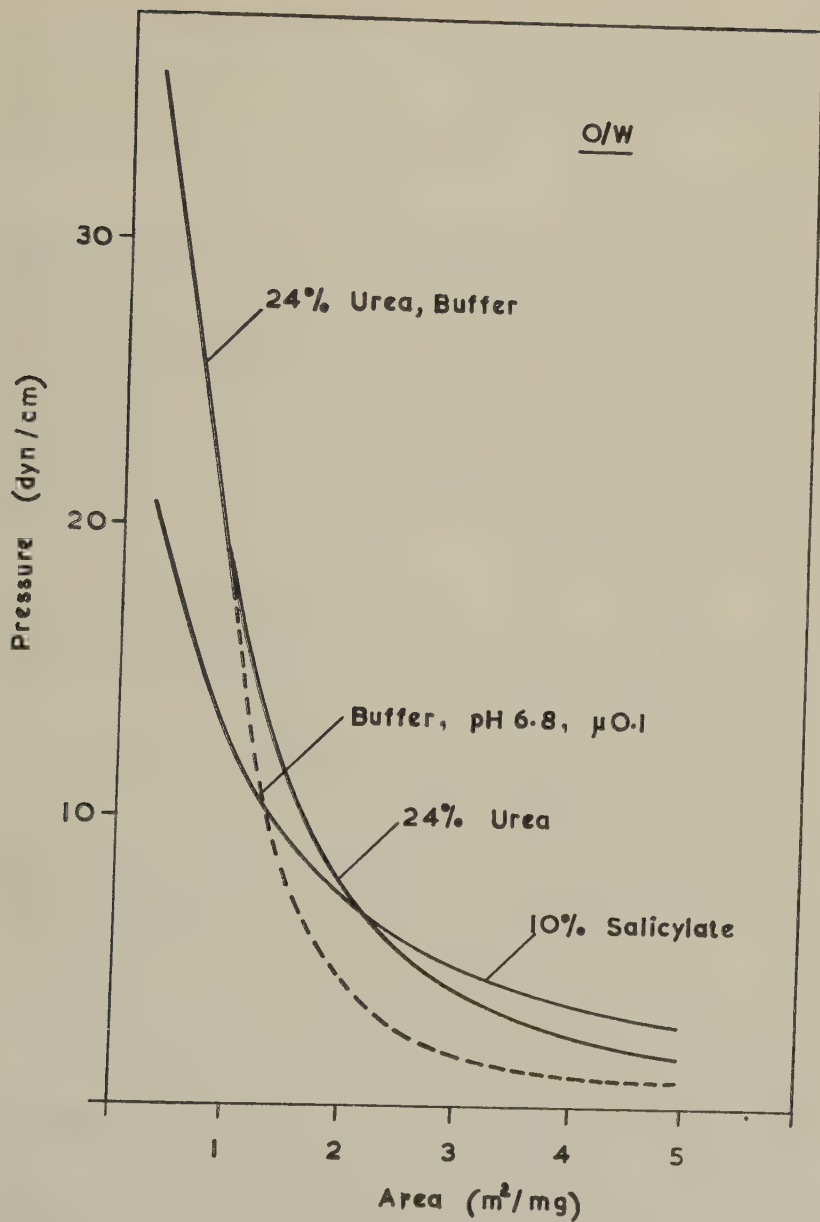


FIG. 4. Effect of urea and sodium salicylate on the  $\pi$ -A isotherms of gluten films.

kink in the O/W curve was present in all cases between 2.5 and 3.5 m.<sup>2</sup>/mg.

Figure 4 shows the results of spreading under 10% w/v sodium salicylate and 24% w/v urea, at the O/W interface. Under salicylate the  $\pi$ -A curve

is similar to that at pH 13 in Fig. 1. Under urea, however, although the film is considerably expanded at the higher areas, the isotherm joins the pH 6.8 curve at ca.  $1.1 \text{ m.}^2/\text{mg.}$

## DISCUSSION

### *Stability*

A characteristic feature of most protein monolayers appears to be their low stability. Around about 20 dynes/cm. pressure the film "collapses," i.e., the  $\pi$ - $A$  curve flattens out (11, 13-15). The collapse pressure of gliadin, in particular, is variously given as 16 to 22 dynes/cm. (7, 16-18).

Gluten films, on the contrary, were found to be remarkably stable. The cohesion in gluten films, which is independent of the type of interface and the pH and ionic strength of the substrate within considerable limits (Fig. 1), appears to be due to hydrogen bonding rather than salt bridges or nonpolar attraction of the van der Waals' type. This view seems to be supported by the completely different type of pressure-area curve obtained under 10% sodium salicylate (Fig. 4) which is known to break hydrogen bonds. The failure of 24% urea to produce a similar curve might be due to its less surface-active nature and its relatively smaller efficiency as a hydrogen bond breaker (19). As urea is not capable of disrupting salt-links, it is also possible that the effect of salicylate is due to its ability to break these as well as hydrogen bonds.

The marked reduction in the cohesion of the film at pH 13 might be due to similar reasons, although a partial solubility of the film or the effect of hydrolytic changes must also be considered.

About a third of the amino acids in gluten are glutamine residues (20). It is tempting to correlate this unusually high amount of potentially strong hydrogen bond forming amide groups (21) with the strong cohesion of these films. Evidence of interaction existing between materials containing large numbers of primary amide groups, interpreted as being due to intermolecular hydrogen bonding, was obtained by Holme (22). It should be noted, however, that the stability of gliadin films does not seem to be different from that of the globular proteins (7, 16), although gliadin contains an even larger proportion of amide groups (23).

The uncommon stability of gluten films, shown by their ability to withstand considerable pressures even at areas where the film must be several times thicker than a monolayer (the film thickness calculated at  $0.2 \text{ m.}^2/\text{mg.}$ , assuming a protein density of 1.33, is about 38 Å, i.e., about four times that of the usual thickness of 10 Å. (24) for a protein monolayer), is difficult to explain unless one assumes that on compression below about  $1.1 \text{ m.}^2/\text{mg.}$  the less surface-active anchoring points of the strongly bonded coherent gluten films are pushed out of the interface, segments of the film forming loose loops or folds. The polar groups remaining in the interface

would be the more hydrophilic ones, i.e., residues containing ionized side chains. Some support for this view may be found in the work on mixed films of gliadin and cholesterol (25, 26) and of gliadin and tannic acid (27). Such a folded film might be called *ptygmatic* (from the Greek *ptygma*, a fold) to distinguish it from the homalic (from the Greek *homalos*, even or level) (28) monolayer where the polypeptide chains are pictured lying flat in the surface.

### *Compressibility*

The considerable compressibility (Fig. 3) of gluten films might best be explained by the assumption that chain segments of gluten films are relatively free to form folds. The minimum compressibility of gluten films (ca. 0.05 cm./dyne) was found to be in excellent agreement with that of gliadin films as reported by Gorter and Blokker (29). This is, on the average, about twice as high as the minimum compressibilities reported for other proteins (11, 15). The kink in the O/W compressibility curve might indicate the area at which the side chains begin to be detached from the interface.

### *Hysteresis*

Little information is available on the hysteresis of  $\pi$ -A isotherms of other protein films. Dervichian (30) studied serum albumin, ovalbumin, and hemoglobin. With these proteins, as well as with several synthetic high polymers (31-33), the final film pressure was either equal to or lower than the initial pressure on complete decompression. These experiments were carried out using the horizontal float film balance.

The hysteresis phenomena observed in the present work appear to be interesting in relation to the network-forming ability of gluten. However, in view of some uncertainty regarding contact angle with the hanging plate method, further investigation (e.g., by surface potential measurements) is required.

### *Influence of Interface, pH and Ionic Strength*

The difference between the expansion of protein monolayers at the A/W and the O/W interface is usually ascribed to elimination of van der Waals' attraction between nonpolar side chains, due to penetration of oil molecules between these chains. An examination of its amino acid composition (20) shows that the nonpolar/polar side chain ratio of gluten is about 1/1, which would readily account for the observed expansion.

The influence of the pH and ionic strength of the substrate on the  $\pi$ -A curves is more difficult to explain. Whereas W-shaped curves similar to those shown in Fig. 2 were frequently reported in earlier studies on protein monolayers, it was soon realized that spreading factors had to be considered. The maximum around the isoelectric point decreased when sufficient time



was allowed for the film to reach equilibrium (15, 34), or when spreading was facilitated either by increasing the ionic strength of the substrate (2, 35), or by spreading at the O/W interface (7, 36), or by the use of a spreading agent (7, 37-39).

Later reports on proteins and synthetic polypeptides are rather conflicting. Thus Guastalla (38) found that the  $A_{(\pi)}$ -pH curve of hemoglobin had a minimum at the isoelectric point when the proper precautions were observed. On the other hand, Holt and Went (40) recently reported a W-shaped curve for insulin. Ellis and Pankhurst (2) found a clear maximum at pH 2.2 in films of collagen spread at the A/W interface from anhydrous formic acid dispersion. This maximum disappeared as the ionic strength of the substrate was increased. Similarly, the 1,2,1-(poly)lysine/leucine/glutamic acid copolypeptide of Isemura and his co-workers (41) exhibited a maximum at pH 7. Their 1,3,1-(poly)lysine/phenylalanine/glutamic acid copolypeptide showed no maximum. This compound, however, was spread on salt solutions because of its solubility in the substrate, due, apparently, to a low degree of polymerization.

As regards gliadin, Gorter and Blokker (29) found minima in the  $A_{(\pi)}$ -pH curve at the A/W interface within quite narrow pH limits around pH 3.4 and 9.2. The curve had no clear maximum but exhibited a flat plateau. The minima became shallower as the areas were taken at increasing surface pressures of 2, 8, and 16 dynes/cm. This is in accordance with the present measurements on gluten films (cf. Fig. 1). Alexander and Teorell (7), spreading gliadin at the O/W interface, found no appreciable effect of the pH over the range from pH 2 to pH 9 on the area of the film at 3.5 and 15 dynes/cm. pressures.

The conditions under which the present films were spread should have ensured satisfactory spreading; and in fact, no effect of time on the surface pressure was noticeable over periods of at least 30 min. It is felt, therefore, that the data in Fig. 2 represent a genuine phenomenon. An increase in  $A_{(\pi)}$  at both ends of the pH range is generally attributed to electrostatic repulsion between charged groups, and convincing evidence to support this view has been adduced (42). The appearance of a maximum around the isoelectric point, however, is more difficult to explain.

Isemura and co-workers (41) attempt this in terms of a competition between the expanding effect of a net charge on the molecule and the condensing effect of salt links. However, it is difficult to see why  $A_{(\pi)}$  should be at a maximum at the isoelectric point when the film is least expanded because of the absence of a net charge and most condensed because of maximum salt bridge formation. Miller (43) considers the effect of pH on the rigidity of the chain network. According to his view, the film would have the most rigid configuration at the isoelectric point. Increasing or decreasing pH causes rupture of the rigid structure and segments of the

chain tend to dissolve, causing a decrease in the area. At still higher or lower pH values, apart from the effect of electrostatic repulsion, the number of water-soluble ionized groups decreases and the area at constant pressure again rises.

Whatever the explanation, however, there seems to be no doubt that the maximum at pH 7.5 in Fig. 2 marks the surface isoelectric point of gluten spread from chloroethanol. This coincides with maxima observed in the surface viscosity and rigidity of gluten films as discussed in the following paper (44).

#### *Areas of Close-Packing and Minimum Compressibility*

Finally some comment seems to be indicated concerning the areas of close-packing and of minimum compressibility of gluten films. These are rather higher than those usually found with other proteins or synthetic polypeptides. At the A/W interface, an identical area of close-packing ( $1.3 \text{ m.}^2/\text{mg.}$ ) was found by Ellis and Pankhurst (2) for collagen and was attributed by them to the high content (25%) of proline, which is known to interfere with the usual regular arrangement of amino acids. Since gluten contains about 12% of proline (20) a similar explanation seems justified. This view has recently received convincing support from the work of Isemura, Ikeda, and Yamashita (45) on monolayers of (poly)-L-proline and (poly)-L-proline-L-leucylglycine.

#### SUMMARY

Wheat gluten dispersed in a 0.1 *M* solution of hydrogen chloride in anhydrous chloroethanol was spread at the A/W and the O/W interface and the surface pressure ( $\pi$ ) of the film measured as a function of the area (*A*) over a wide range of pH (1–13) at the ionic strengths of 0.02 and 0.1. Some measurements were carried out at the interface between oil and 10% sodium salicylate or 24% urea.

Gluten films were found to be more compressible and more stable than those of most other proteins. Pressures as high as 32 dynes/cm. (A/W) and 36 dynes/cm. (O/W) were obtained at an area of  $0.2 \text{ m.}^2/\text{mg.}$  while the minimum compressibility was 0.05 cm./dyne. The extrapolated area of close-packing was  $1.33 \text{ m.}^2/\text{mg.}$  at the A/W and  $1.54 \text{ m.}^2/\text{mg.}$  at the O/W interface. The area of minimum compressibility was  $1.1 \text{ m.}^2/\text{mg.}$  at both interfaces.

At the O/W interface variation in the pH of the substrate caused differences in the degree of expansion of the films at higher areas but all the  $\pi$ -*A* isotherms between pH 1 and 12 met at about the area of minimum compressibility. The area at constant pressure (1 dyne/cm.) as a function of pH gave a W-shaped curve showing minima at about pH 5.5 and 8.5 and a maximum at about pH 7.5. Variation in ionic strength from 0.02 to

0.1 had no effect on the minima; at the lower ionic strength the curve was flatter at the maximum and at the extreme ends. At pH 13 the  $\pi$ - $A$  isotherm was quite different, indicating reduced cohesion in the film. The isotherm at the oil/aqueous salicylate interface was very similar to the pH 13 curve. At the oil/aqueous urea interface the isotherm was much expanded at the higher areas but met the control curve at about the area of minimum compressibility.

It is concluded that spread gluten forms strongly bonded, coherent films, parts of which, when compressed below the area at which the films may be regarded as a close-packed monolayer, are displaced from the interface with relative ease and are folded up into loops. The unusually strong cohesion shown by these films may be due in part to hydrogen bonding between the numerous glutamine side chains, modified by electrostatic attraction. The rather high areas of close-packing and of minimum compressibility are probably due to the relatively high proline content of gluten.

#### ACKNOWLEDGMENTS

One of the authors (N.W.T.) is indebted to the Director and the Council of the Bread Research Institute of Australia for their encouragement and provision of facilities. The initial stages of the work were carried out at the University of New South Wales.

#### REFERENCES

1. ELLIS, S. C., AND PANKHURST, K. G. A., *Discussions Faraday Soc.* **No. 16**, 177-190 (1954).
2. ELLIS, S. C., AND PANKHURST, K. G. A., *Trans. Faraday Soc.* **50**, 82-89 (1954).
3. TCHOEGL, N. W., submitted to *Cereal Chem.*
4. TCHOEGL, N. W., in preparation.
5. BAILEY, C. H., "The Constituents of Wheat and Wheat Products," p. 106. Reinhold, New York, 1944.
6. DILL, D. B., AND ALSBERG, C. L., *Cereal Chem.* **1**, 222-246 (1924).
7. ALEXANDER, A. E., AND TEORELL, T., *Trans. Faraday Soc.* **35**, 727-737 (1939).
8. ALEXANDER, A. E., in "Surface Chemistry," pp. 123-126. Butterworths, London, 1949.
9. FOX, H. W., AND ZISMAN, W. A., *J. Colloid Sci.* **5**, 514-531 (1950).
10. ALEXANDER, A. E., AND JOHNSON, P., "Colloid Science," p. 496. Clarendon Press, Oxford, 1950.
11. BULL, H. B., *Advances in Protein Chem.* **3**, 95-121 (1947).
12. FOURT, L., AND SCHMITT, F. O., *J. Phys. Chem.* **40**, 989-996 (1936).
13. CUMPER, C. W. N., AND ALEXANDER, A. E., *Trans. Faraday Soc.* **46**, 235-253 (1950).
14. HAUROWITZ, F., BOUCHER, P., DICKS, M., AND THERRIAULT, D. *Arch. Biochem. Biophys.* **59**, 52-60 (1955).
15. NEURATH, H., AND BULL, H. B., *Chem. Revs.* **23**, 391-435 (1938).
16. BENHAMOU, N. J., *J. chim. phys.* **53**, 32-43 (1956).
17. HUGHES, A. H., AND RIDEAL, E. K., *Proc. Roy. Soc. (London)* **A137**, 62-77 (1932).
18. MITCHELL, J. S., *Trans. Faraday Soc.* **33**, 1129-1139 (1937).
19. COURTS, A., in "Recent Advances in Gelatin and Glue Research," pp. 145-148. Pergamon Press, London, 1958.

20. PENCE, J. W., MECHAM, D. K., ELDER, A. H., LEWIS, J. C., SNELL, N. S., AND OLCOTT, H. S., *Cereal Chem.* **27**, 335-341 (1950).
21. WAUGH, D. F., *Advances in Protein Chem.* **9**, 325-437 (1954).
22. HOLME, J., *Dissertation Abstr.* **15**, 2398 (1955).
23. BOURDET, A., *Ann. technol.* **2**, 181-318 (1956).
24. CUMPER, C. W. N., AND ALEXANDER, A. E., *Rev. Pure and Appl. Chem. (Australia)* **1**, 121-151 (1951).
25. LANGMUIR, I., AND SCHAEFER, V. J., *Chem. Revs.* **24**, 181-202 (1939).
26. SCHULMAN, J. H., AND RIDEAL, E. K., *Proc. Roy. Soc. (London)* **B122**, 46-57 (1937).
27. COCKBAIN, E. G., AND SCHULMAN, J. H., *Trans. Faraday Soc.* **35**, 1266-1276 (1939).
28. RIDEAL, E. K., *Proc. Roy. Soc. (London)* **A155**, 687 (1936).
29. GORTER, E., AND BLOKKER, P. C., *Proc. Koninkl. Ned. Akad. Wetenschap.* **45**, 228-232 (1942).
30. DERVICHIAN, D. G., *Kolloid-Z.* **126**, 15-20 (1952).
31. MÜLLER, F. H., *Z. Elektrochem.* **59**, 312-329 (1955).
32. MÜLLER, F. H., AND HUFF, K., *Kolloid-Z.* **129**, 49-51 (1952).
33. SCHULLER, H., *Kolloid-Z.* **136**, 134-136 (1954).
34. GORTER, E., AND PHILIPPI, G. T., *Proc. Acad. Sci. Amsterdam* **37**, 788-793 (1934).
35. LANGMUIR, I., *Cold Spring Harbor Symposia Quant. Biol.* **6**, 171-184 (1938).
36. ASKEW, F. A., AND DANIELLI, J. F., *Trans. Faraday Soc.* **36**, 785-794 (1940).
37. DERVICHIAN, D. G., *Nature* **144**, 629-630 (1939).
38. GUASTALLA, J., *Cahiers phys.* **13**, 5-17 (1943).
39. STÄLLBERG, S., AND TEORELL, T., *Trans. Faraday Soc.* **35**, 1413-1416 (1939).
40. HOLT, P. F., AND WENT, C. W., *Biochem. J. (London)* **65**, 13P-14P (1957).
41. ISEMURA, T., HAMAGUCHI K., AND IKEDA, S., *J. Polymer Sci.* **23**, 651-664 (1957).
42. DAVIES, J. T., AND LLOPIS, J., *Proc. Roy. Soc. (London)* **A227**, 537-552 (1955).
43. MILLER, I., *J. Polymer Sci.* **23**, 664 (1957).
44. TSCHOEGL, N. W., AND ALEXANDER, A. E., *J. Colloid Sci.* **15**, 168-182 (1960).
45. ISEMURA, T., IKEDA, S., AND YAMASHITA, T., *Mem. Inst. Sci. and Ind. Research, Osaka Univ.*, **15**, 167-172 (1958).



## THE SURFACE CHEMISTRY OF WHEAT GLUTEN

### II. MEASUREMENTS OF SURFACE VISCOELASTICITY

N. W. Tschoegl and A. E. Alexander

*Bread Research Institute of Australia, North Sydney, New South Wales;  
and Department of Physical Chemistry, The University of Sydney,  
New South Wales*

*Received September 15, 1959*

#### INTRODUCTION

A previous paper (1) dealt with surface pressure studies of gluten monolayers; the present one deals with their viscoelastic properties, in particular the dependence of these properties on the pH and the ionic strength of the substrate. Some measurements were also carried out on substrates known to break hydrogen bonds.

In general, films were spread at the O/W interface, at which the viscoelasticity of protein monolayers, being usually higher than at the A/W interface, is more easily observed. Determinations near the isoelectric point were carried out at pH 6.8 using the phosphate buffer of Dill and Alsberg (2). Gluten is claimed to be least soluble at this pH, which was therefore chosen as the most likely isoelectric point. The surface isoelectric point of gluten spread from acid chloroethanol was later found to be somewhat higher but, for reasons of comparability, measurements were continued at this pH, which may be regarded as the lower limit of the surface isoelectric range.

#### EXPERIMENTAL

##### *Dispersions and Substrates*

The present study was carried out on dispersions of wheat gluten in anhydrous acid chloroethanol, prepared as described previously. The films were spread at an interface between carbon tetrachloride and various aqueous substrates as detailed in the preceding paper.

##### *Measurements of Surface Viscoelasticity*

These were carried out at the O/W interface with the aid of an oscillating needle surface torsion pendulum (3) having a moment of inertia of 65 g. cm.<sup>2</sup> and a period in air of 14.29 sec. The platinum needle (4 cm. long) was



flamed with a microburner and quenched in distilled water before each spreading.

The torsion wire and the brass bob of the pendulum were surrounded by a glass tube as a protection against air drafts. The pendulum was suspended from the shaft of a Magslip telemotor the movement of which could be followed by the usual optical arrangement. The shaft could be turned by twisting the rotor of its twin, situated in the operating panel.

Another optical arrangement allowed observation of the oscillations of the bob. From the period and damping of the oscillations, the surface viscosity (in surface poises) was calculated (4) as

$$\eta_s = \frac{9.21I}{l^2} \left[ \frac{\lambda}{T} - \frac{\lambda_0}{T_0} \right], \quad [1]$$

and the surface rigidity (in dynes/cm.) was obtained (5) from

$$G_s = \frac{8\pi^2 I}{l^2} \left[ \frac{1}{T^2} - \frac{1}{T_0^2} \right]. \quad [2]$$

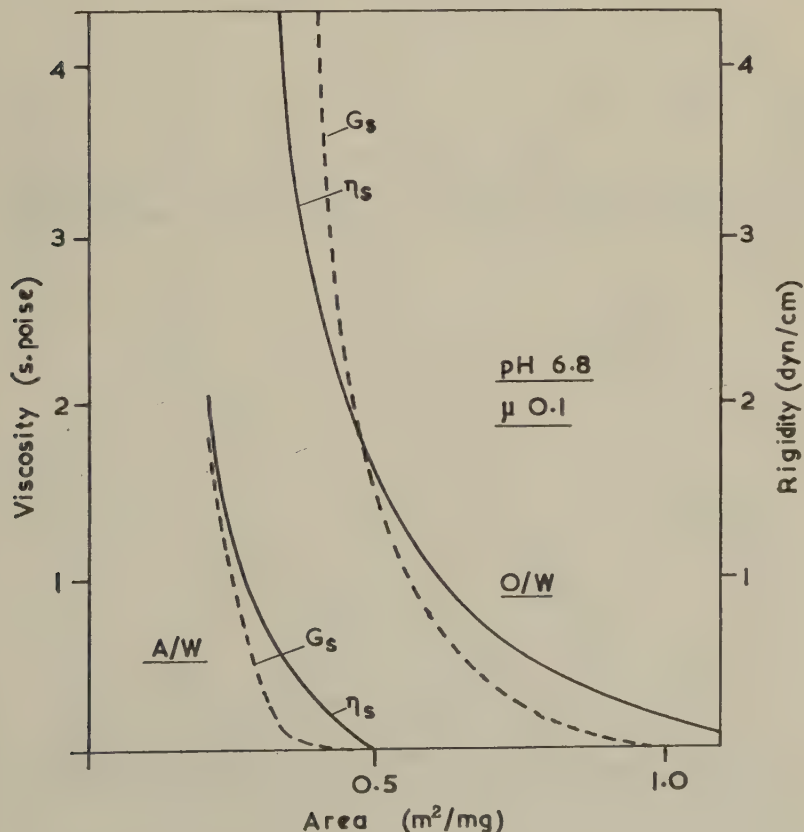


FIG. 1. Effect of interface on surface viscosity and rigidity of gluten films.

In these equations  $I$  is the moment of inertia,  $l$  the length of the needle,  $\lambda$  the (decadic) logarithmic decrement of the oscillations, and  $T$  their periodic time when the surface is covered by the film;  $\lambda_0$  and  $T_0$  are the respective values for the clean interface.

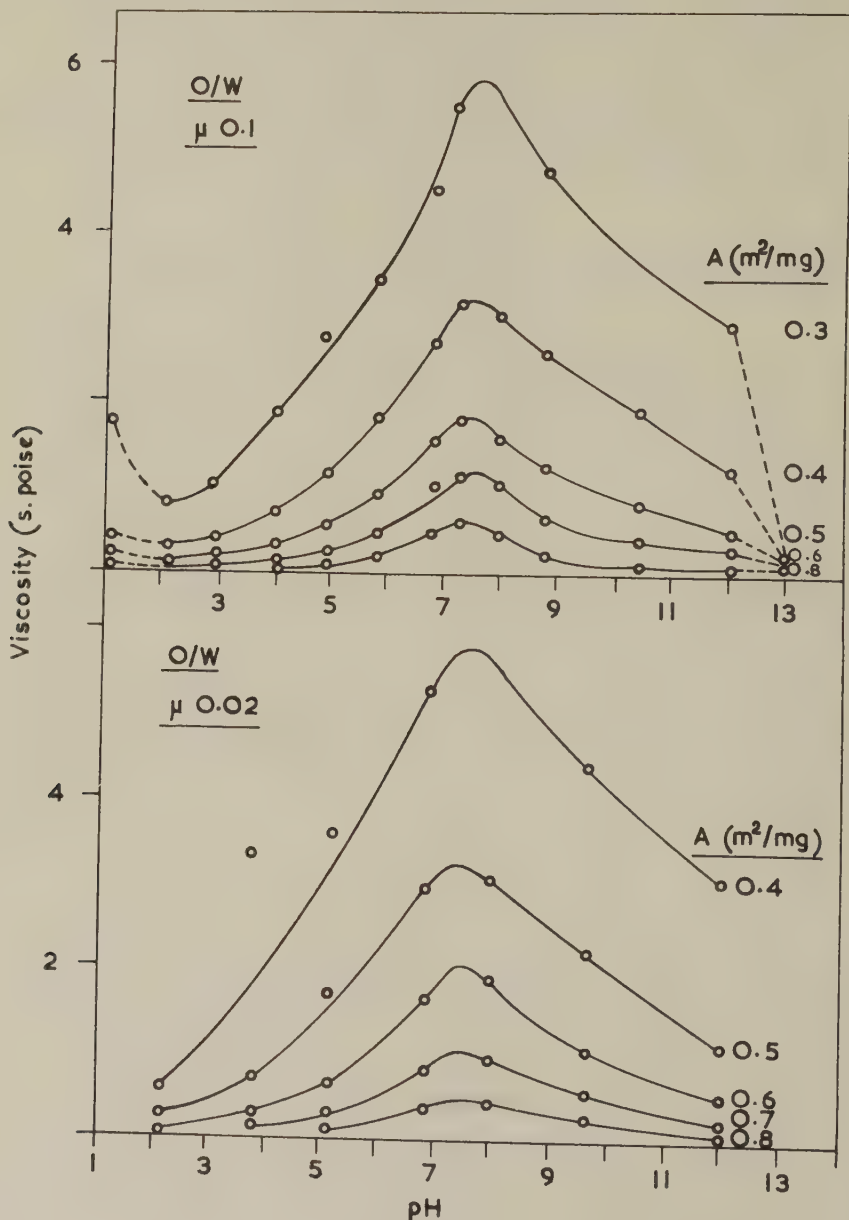


FIG. 2. Effect of pH and ionic strength on surface viscosity of gluten films.

The period of oscillation was determined by timing three full swings with a stop watch to 0.1 sec. and taking the average. When the films were highly elastic, the period decreased in successive swings.

The viscoelasticity of a film can be characterized not only by surface

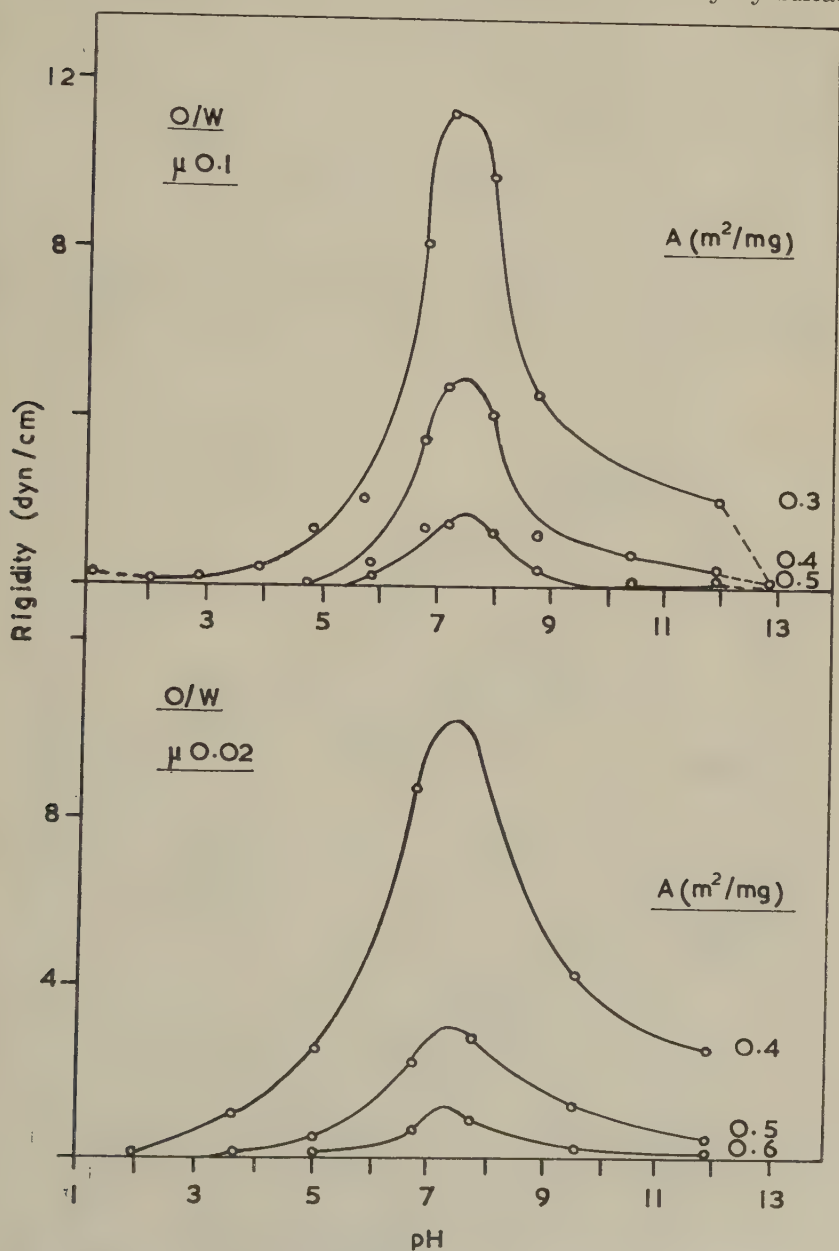


FIG. 3. Effect of pH and ionic strength on surface rigidity of gluten films.

viscosity ( $\eta_s$ ) and rigidity ( $G_s$ ) but also by the absolute surface modulus ( $\tilde{G}_s$ ) and the surface loss angle or dissipation factor ( $\phi_s$ ). These are the amplitude and argument, respectively, of the complex surface modulus

$$G^* = G_s + jw \eta_s, \quad [3]$$

where  $j = \sqrt{-1}$  and  $w$  is the radian frequency of the oscillations when the surface is covered with the film (6).

From this one obtains

$$\tilde{G}_s = \frac{G_s}{\cos \phi_s} = \frac{2\pi\eta_s}{T \sin \phi_s}; \quad [4]$$

$$\phi_s = \tan^{-1} (2\pi\eta_s/TG_s). \quad [5]$$

The absolute modulus  $\tilde{G}_s$  is the ratio of the peak stress to the peak strain while  $\phi_s$  is the phase angle between strain and stress. A purely viscous film

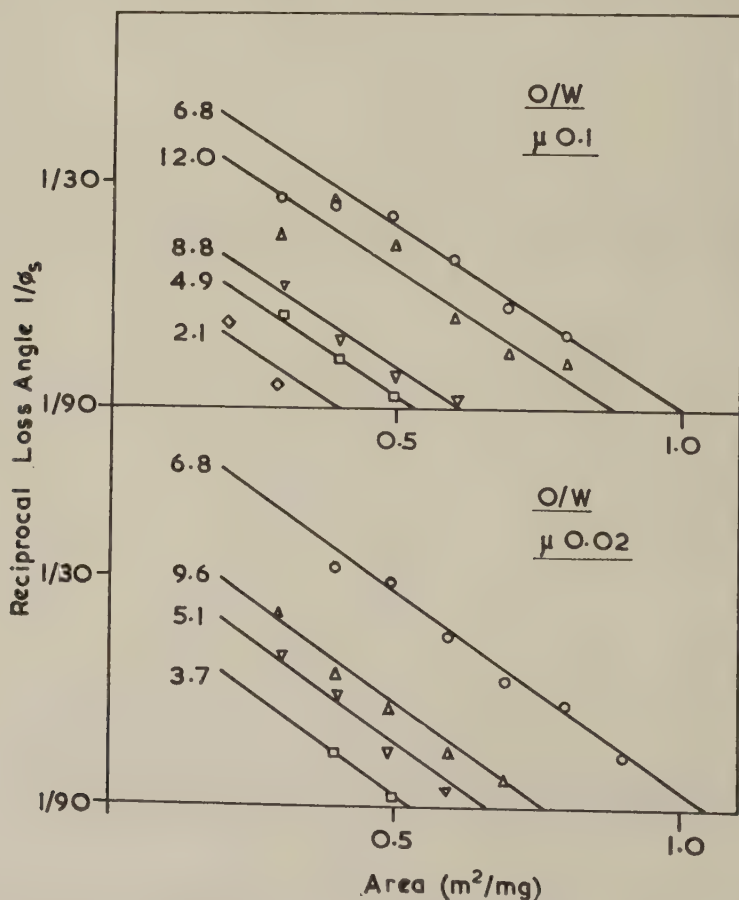


FIG. 4. Effect of pH and ionic strength on reciprocal loss angle of gluten films.

would have a loss angle of  $\pi/2$  or  $90^\circ$ , while a purely elastic film would have one of zero. This mode of representing dynamic behavior has certain advantages when the system is treated from a rheological point of view.

When determining the viscoelasticity of the films as a function of the area, measurements with the oscillating surface torsion pendulum were usually begun at an area of  $1.50 \text{ m}^2/\text{mg}$ . At higher areas changes in  $T$  or  $\lambda$  were too small to be measured except in a few cases. Contrary to  $\pi$ ,  $T$  and  $\lambda$  showed a marked increase with time. The measurements were therefore standardized by starting the oscillations 5 min. after addition of dispersion. Viscoelasticity measurements as a function of time were begun exactly 5 min. after the beginning of spreading and were repeated at 5-min. intervals for not less than 35 min. A few measurements were also carried out at the A/W interface on a Langmuir trough with a simple hand-operated pendulum.

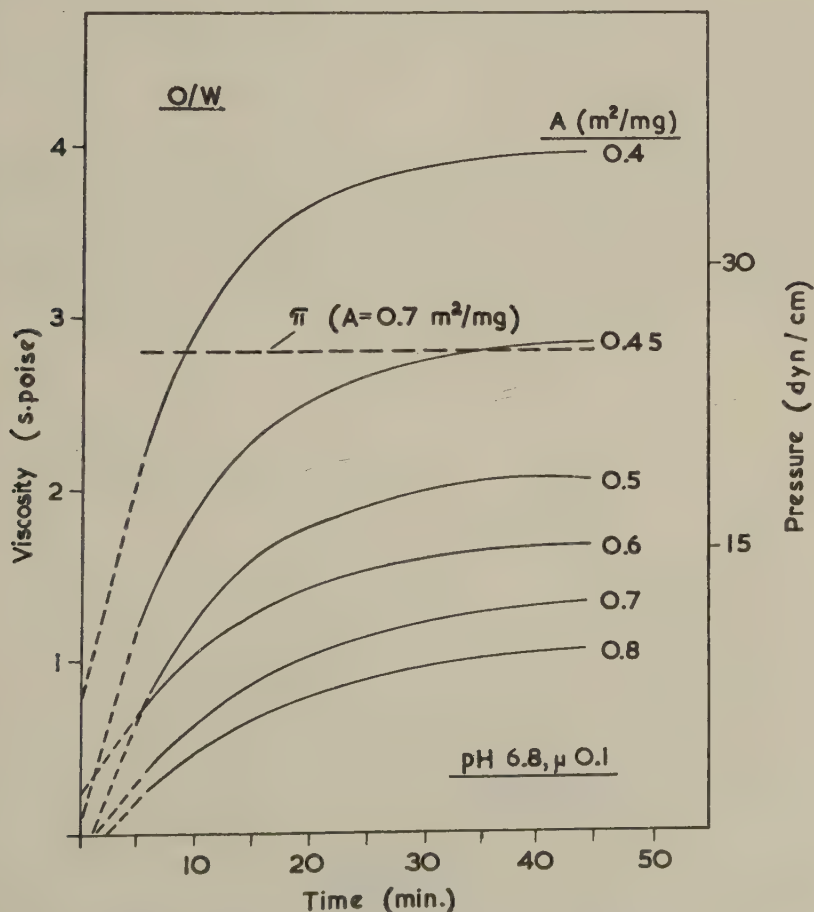


FIG. 5. Effect of time on surface viscosity and pressure of gluten films.



The curves shown represent the average of at least two runs. All measurements were carried out at  $25.0^\circ \pm 0.5^\circ\text{C}$ .

### RESULTS

Typical viscosity-area and rigidity-area curves are shown in Fig. 1 for pH 6.8,  $\mu$  0.1, at both interfaces. The viscoelasticity at the O/W is markedly greater than at the A/W interface. Measurable viscosity appears at about  $1.5 \text{ m}^2/\text{mg}$ . at the O/W interface, and at about  $0.5 \text{ m}^2/\text{mg}$ . at the A/W interface. Measurements carried out at the A/W interface showed that there was very little hysteresis, the viscosities obtained on decompression being only very slightly lower than those on compression.

Figures 2 and 3 show the interfacial viscosity and rigidity at different areas as functions of pH and ionic strengths. The dependence on pH is marked, a pronounced maximum occurring at about pH 7.5. The viscosity rises steeply on the acid side and falls more gradually on the alkaline side of the pH scale. At pH 1.0 a small rise is apparent. Between pH 12 and 13,  $\eta_s$  and  $G_s$  both show a sudden fall. The ionic strength also had a decided influence on  $\eta_s$  and  $G_s$  at the same pH. Both were always higher at the lower ionic strength.

Plots of the absolute modulus  $\bar{G}_s$  as a function of pH at various areas were very similar to the  $\eta_s$ -pH and the  $G_s$ -pH curves shown in Figs. 2 and 3. Essentially similar plots were also obtained by plotting the loss angles  $\phi_s$  as a function of pH. In these plots, however, minima appeared instead of maxima around pH 7.5, indicating that the proportion of the energy stored elastically is greatest at this pH. These curves are not reproduced here.

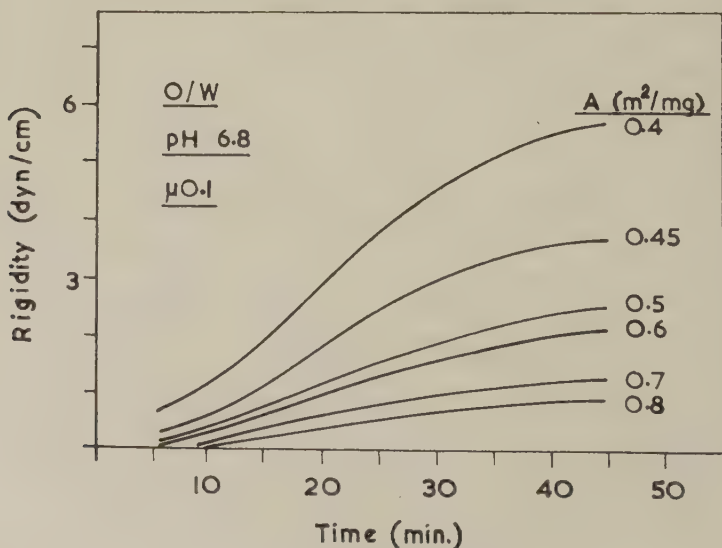


FIG. 6. Effect of time on surface rigidity of gluten films.

A more useful representation is obtained by plotting the reciprocal loss angles as a function of the area at various pH's. These plots seem to lie on parallel straight lines as shown in Fig. 4 for some pH values at  $\mu$  0.1 and 0.02.

The effect of time on the interfacial rigidity and viscosity was examined in detail at pH 6.8,  $\mu$  0.1. The plots of  $\eta_s$  as a function of time at different areas are shown in Fig. 5. The corresponding plots of  $G_s$  versus time are shown in Fig. 6.

The increase of  $\eta_s$  with time was found to obey the relation

$$\ln(\eta_\infty - \eta_t) = -K(t - t_0), \quad [6]$$

where  $\eta_\infty$  is the limiting viscosity at infinite time,  $\eta_t$  the instantaneous viscosity,  $K$  the rate constant,  $t$  the instantaneous time, and  $t_0$  the time at which the viscosity is zero. The curves in Fig. 5 were fitted to Eq. [6] by Hartley's (7) method of "Internal least squares." As may be seen from Fig. 7, the rate constants  $K$  calculated by this method lie on a straight line when plotted against the area. The regression line was found to intersect the area-axis at 1.54 m.<sup>2</sup>/mg.

The  $G_s$  curves (Fig. 6) differ in shape from the  $\eta_s$  curves. They are sigmoid rather than exponential. The shape of the  $\eta_s$ - $t$  and  $G_s$ - $t$  curves was the same at lower and higher pH (2.1 and 10.6) and also at the A/W interface.

It is important to note that during these rather considerable changes in  $\eta_s$  and  $G_s$  the interfacial pressure remained quite steady, as shown by one example in Fig. 5.

By spreading a film at 0.5 m.<sup>2</sup>/mg. and beginning the measurements 30 min. after deposition, it could be shown that the agitation of the film

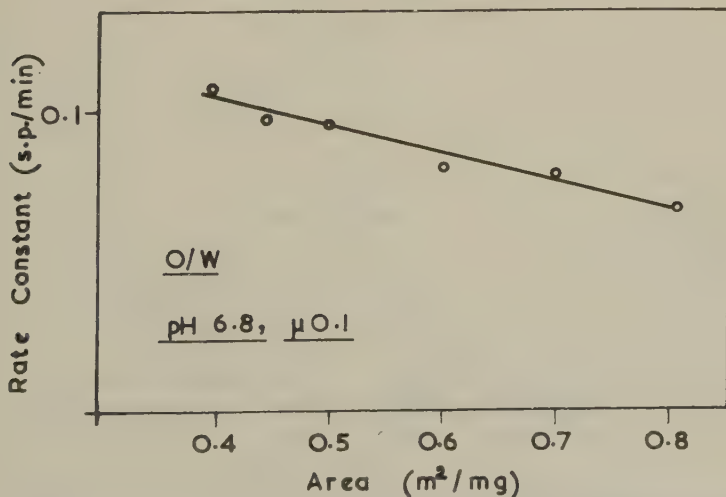


FIG. 7. The rate constant of the surface viscosity of gluten films as a function of the area.

by the oscillating needle had no effect on the rise of  $\eta_s$ . The viscosities obtained in this way agreed, within the experimental error, with those obtained by starting the measurements 5 min. after spreading.

In order to see whether the effect of pH on  $\eta_s$  and  $G_s$  was reversible, a film was spread at 0.5 m.<sup>2</sup>/mg. under a dilute buffer of pH 6.8 and measurements were taken every 5 min. At 27.5 min., the pH of the aqueous phase was changed by running in a calculated amount of acid. The resulting pH was determined on completion of the run. The experiment was also carried out in the reverse way, by starting under dilute acid of pH 2.1 and changing to near neutral. The results are shown in Fig. 8.

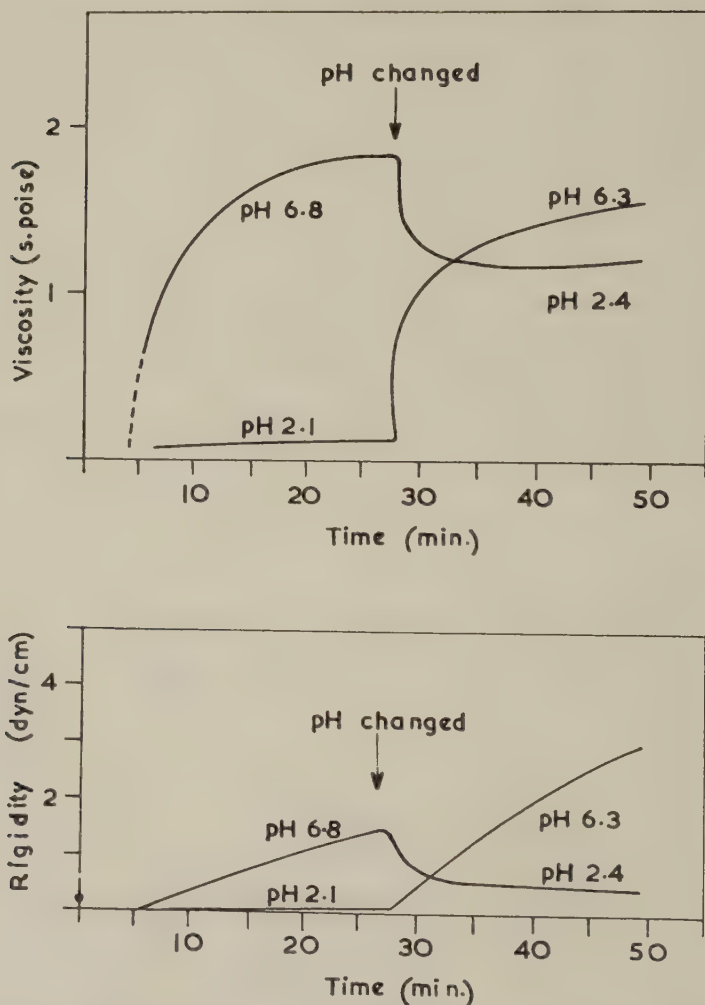


FIG. 8. Effect of change in pH on surface viscosity and rigidity of gluten films.

It appears that when the pH is changed from acid to neutral, the film rapidly attains the viscosity and rigidity it would have had, had it been spread initially under that pH. When, however, the change is from neutral to lower pH,  $\eta_s$  and  $G_s$  do not drop to the lower value they would have attained if spread initially at that pH.

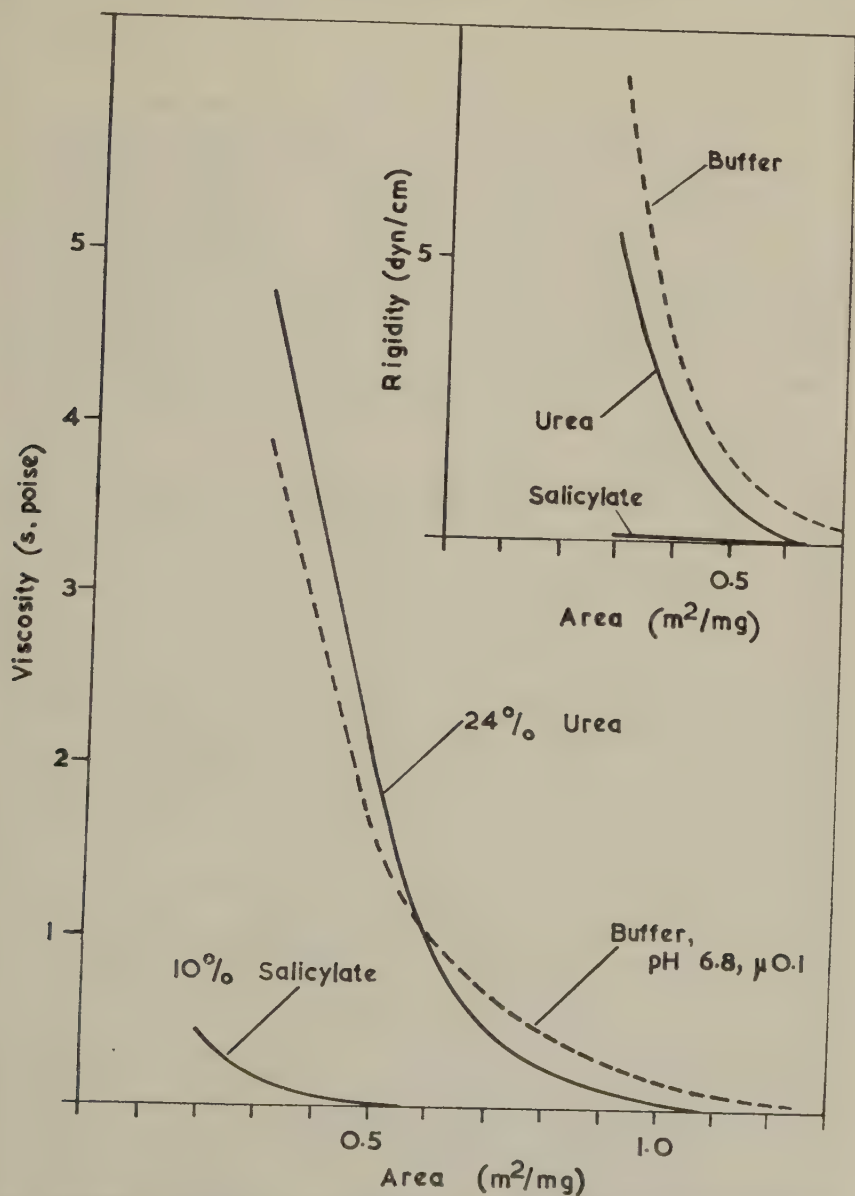


FIG. 9. Effect of urea and sodium salicylate on surface viscosity and rigidity of gluten films.

Some experiments were carried out by spreading under 10% w/v sodium salicylate and 24% w/v urea. Under salicylate (Fig. 9) the gluten film showed hardly any viscosity and no rigidity even at the lowest areas. Under urea, however, the viscoelasticity of the film was only slightly affected, as may be seen on comparing the curves with the control curve at pH 6.8,  $\mu$  0.1.

## DISCUSSION

### *Influence of the Interface, pH, and Ionic Strength*

Cumper and Alexander (3) found that protein films begin to show surface viscosity at the O/W interface at the area of close-packing. This agrees with the appearance of surface viscosity at an area of about 1.5 m.<sup>2</sup>/mg. (Fig. 1) in gluten films at the O/W interface. For these films, the area of close-packing was found to be 1.54 m.<sup>2</sup>/mg. from extrapolation of the  $\pi$ -A isotherm to zero pressure (1). The expansion of the  $\eta_s$ -A curves at the O/W interface is similar to the behavior of the  $\pi$ -A isotherms. It is believed that both have essentially the same origin, namely, the extension of the polypeptide chains arising from the reduced van der Waals' attraction between the nonpolar side chains (8, 9).

Surface rigidity appears only when the surface viscosity has reached about 0.3 surface poise. As will be discussed in more detail later, the formation of a rigid network is most favored in the vicinity of the isoelectric point. It is, therefore, interesting to note that at pH 6.8 the extrapolation of the regression of the reciprocal loss angles on the area to 1/90° (zero rigidity, Fig. 4) intersected the area-axis at about 1 m.<sup>2</sup>/mg. This is in good agreement with the area of minimum compressibility as obtained by graphical differentiation of the  $\pi$ -A isotherms in the previous paper. As described there, gluten films, when compressed below about 1 m.<sup>2</sup>/mg., probably form a ptygmatic, or folded, monolayer, and it seems possible that rigidity in the film is linked with the appearance of these folds, either in a purely mechanical sense or as a result of cross-link formation between folds.

The dependence of the viscoelasticity of gluten films at the O/W interface on the pH and ionic strength of the substrate is quite remarkable. There is relatively little information on this point in the literature, most surface viscosity measurements having been carried out at selected pH values rather than over a complete range.

Pouradier (10), without presenting any data, reported a slight maximum in the viscosity of gelatin films at the A/W interface. Joly (11) noted that the surface viscosity of the proteins investigated by him (at the A/W interface) was highest near the isoelectric point, low at pH 2, and intermediate at pH 12. His films, however, were spread from solid particles, and his results are therefore difficult to interpret. Tachibana, Inokuchi, and



Inokuchi (12) reported surface viscosity and elasticity curves of ovalbumin at the A/W interface. These showed a maximum at pH 0.2, a plateau between pH 2 and 7, and again lower values between pH 7 and 10. These results are at variance with the earlier findings of Joly (11), who also investigated ovalbumin. They are also very different from those reported here on gluten films.

Gorter and Blokker (13) examined gliadin films at the A/W interface, but found no evidence of a pH effect on the surface viscosity over the pH range 1-11. As they state, however, that their measurements were rather poorly reproducible, their results cannot be regarded with confidence.

Some light on the pH dependence is shed from the recent work of Isemura, Hamaguchi, and Ikeda (14) on the surface chemistry of the synthetic copolypeptides 1,2,1-(poly)lysine/leucine/glutamic acid and 1,3,1-(poly)lysine/phenylalanine/glutamic acid. These copolypeptides, particularly the former, may be regarded as simplified gluten models in two important respects, namely, having about an equal number of basic and acidic side chains and a similar polar-nonpolar side chain ratio.

At constant area, both copolypeptides were found to exhibit a maximum in surface viscosity at the isoelectric point of pH 7, and an increase in the ionic strength of the substrate resulted in a lowering of the surface viscosity. The authors attribute the former to maximum salt-link formation and the latter to the screening effect of the added electrolyte.

It seems reasonable to adopt the same explanation for gluten films although a certain difficulty arises from the fact that the overall number of acidic and basic side chains in gluten films must be considerably less than the number of such groups in the synthetic copolypeptides (15). It is, however, a well-known fact that even a small number of cross-links will have a profound influence on the physical properties of a polymeric material.

The asymmetrical shape of the curves in Figs. 2 and 3 seems to be explicable by a consideration of the ionogenic groups in the chain. On the acid side there are only  $\alpha$ -carboxyl, glutamyl, and aspartyl groups with nearly the same pK. On the alkaline side there are histidyl, lysyl, arginyl, and  $\alpha$ -amino groups dissociating at different pK's, with the amino group of arginine still ionized (16) even at pH 12. This would appear to account for the fact that the influence of pH on either interfacial viscosity or rigidity is greater on the acid side of the maximum than on the alkaline side. If all ionogenic groups would dissociate within narrow pK ranges one would expect a stepped curve showing discontinuities at the corresponding pH values. However, the pK's of the various groups are influenced by adjacent groups (17), and this accounts for the continuous curves observed.

The occurrence of maximum viscoelasticity at the pH of maximum salt-link formation (14) makes it most likely that the isoelectric point of gluten films when spread from chloroethanol is around pH 7.5. This value agrees

well with that found from the plot of the area at constant pressure against pH (1) but is higher than the values obtained by other methods.

Maximum precipitation of gluten dispersed in formic acid (18) occurs at pH 5.5–6.0. Bungenberg de Jong and Klaar (19) considered the isoelectric point of gluten to be 6.1. Dill and Alsberg (2) found that gluten was least soluble at pH 6.8, maximum yield of gluten being obtained when washing it from dough with a dilute buffer of this pH. Values ranging from 5.7 to 6.3 were obtained from microelectrophoresis measurements of quartz particles coated with gluten (20).

Work on simple compounds has shown that surface dissociation constants are not identical with bulk  $pK$ 's (21–23). However, these investigations have so far not been extended to charged high polymers, and no information seems to be available at present concerning the influence of the interface on the isoelectric point of such compounds. The possibility of chemical reaction between the chloroethanol and groups such as amide or free carboxyl, which would tend to shift the isoelectric point, also needs consideration and is being currently investigated.

#### *Time Dependence of Surface Viscoelasticity*

An increase in surface viscoelastic properties with time was observed by Joly (11) with a number of proteins. However, as mentioned above, his films were spread from solid particles and showed not only a rise in viscosity but also a simultaneous rise in surface pressure, indicating slow spreading or gradual unfolding of the molecules.

In contrast, the rise in viscosity and rigidity of gluten films when spread at the O/W interface from chloroethanol dispersions, was not accompanied by any rise in the interfacial tension (cf. Fig. 5). These rises must therefore correspond to a genuine change in the rheological properties of the films, and are thought to reflect intermolecular bonding. Pouradier (10) observed the same phenomenon with gelatin films at the A/W interface and also attributed it to a gradual, spontaneous linking of the molecules.

On this assumption the area at which a time increase becomes detectable in the surface viscosity (zero  $K$ , Fig. 7) should indicate the area at which bonding begins to occur. Support for the above assumption may therefore be found in the fact that this area ( $1.54 \text{ m.}^2/\text{mg.}$ ) is in complete agreement with the area at which surface viscosity becomes measurable, i.e., the area of close-packing (1).

Since the films were spread at the O/W interface, van der Waals' attraction between nonpolar side chains might be eliminated as a contributing factor. The immediate response to a pH change of the substrate (Fig. 8) suggests that electrostatic attraction must be involved. On the other hand, the fact that bonding occurs even at pH 2.1 where only a few salt bridges

would be likely to exist, points to some participation by hydrogen bonds. This is supported by the observation that such bonds, once established, are much less affected by a change in pH.

The results obtained on spreading under sodium salicylate and under urea (Fig. 9) also seem to support this view. Thus no viscoelasticity appeared under salicylate which would break hydrogen bonds as well as salt-links. The viscoelasticity was much less influenced by spreading under urea. A similar behavior was also apparent in the  $\pi$ - $A$  isotherms obtained on these substrates (1).

Some evidence that the stability of hydrogen-bonded structures in proteins is dependent on favorable side chain interaction has been obtained by Harrington and Schellmann (24) and by Kauzmann and Douglas (25).

### SUMMARY

The dependence of surface viscoelasticity of gluten films at the O/W interface on the pH and the ionic strength of the substrate was studied by means of an oscillating needle surface torsion pendulum. Some experiments were carried out at the interface between oil and 10% sodium salicylate or 24% urea.

Gluten was spread from dispersion in anhydrous chloroethanol containing 0.1 *M* hydrogen chloride. Film behavior showed a marked dependence on the pH and the ionic strength of the substrate. The highest viscoelasticity was observed around pH 7.5, which may be regarded as the surface isoelectric point of gluten when spread from chloroethanol. The decrease in viscoelasticity away from the isoelectric point was more pronounced on the acid side. The viscoelasticity, at the same area and pH, decreased with an increase in the ionic strength.

Extrapolation of the regression of the reciprocal loss angles on area gave the area at which elasticity begins to appear as about 1.0 m.<sup>2</sup>/mg. This agrees well with the area of minimum compressibility as obtained from the  $\pi$ - $A$  isotherms.

The viscoelasticity of gluten films spontaneously increased with time after spreading while the interfacial pressure remained constant. This increase is believed to reflect intermolecular bond formation. Extrapolation of the regression of the rate constants  $K$  of the time increase of the surface viscosity on the area to zero  $K$  indicated that bonding begins to occur at about 1.54 m.<sup>2</sup>/mg. This is identical with the area of close-packing found from an extrapolation of the  $\pi$ - $A$  curves to zero pressure.

Urea had little effect but films spread under sodium salicylate showed hardly any viscoelasticity. These findings, together with the effect produced by a change in the pH of the substrate, point to an interplay between hydrogen bonds and ionic linkages.

## ACKNOWLEDGMENTS

One of the authors (N.W.T.) wishes to thank the Director and the Council of the Bread Research Institute of Australia for their encouragement and provision of facilities. The initial stages of the work were carried out at the University of New South Wales.

## REFERENCES

1. TSCHOEGL, N. W., AND ALEXANDER, A. E., *J. Colloid Sci.* **15**, 155-167 (1960).
2. DILL, D. B., AND ALSBERG, C. L., *Cereal Chem.* **1**, 222-246 (1924).
3. CUMPER, C. W. N., AND ALEXANDER, A. E., *Trans. Faraday Soc.* **46**, 235-253 (1950).
4. FOURT, L., *J. Phys. Chem.* **43**, 887-899 (1939).
5. TSCHOEGL, N. W., *J. Colloid Sci.* **13**, 500-507 (1958).
6. TSCHOEGL, N. W., in preparation.
7. HARTLEY, H. O., *Biometrika* **35**, 32-45 (1948).
8. DAVIES, J. T., *Biochim. et Biophys. Acta* **11**, 165-177 (1953).
9. DAVIES, J. T., *J. Colloid Sci. Suppl.* **1**, 9-13 (1954).
10. POURADIER, J., *J. chim. phys.* **46**, 627-634 (1949).
12. TACHIBANA, T., INOKUCHI, K., AND INOKUCHI, T., *Biochim. et Biophys. Acta* **24**, 174-177 (1957).
13. GORTER, E., AND BLOKKER, P. C., *Proc. Koninkl. Ned. Akad. Wetenschap.* **45**, 335-340 (1942).
14. ISEMURA, T., HAMAGUCHI, K., AND IKEDA, S., *J. Polymer Sci.* **23**, 651-664 (1957).
15. UDY, D. C., *Cereal Chem.* **31**, 389-395 (1954).
16. COHN, E. J., AND EDSALL, J. T., "Proteins, Amino Acids and Peptides as Ions and Dipolar Ions," p. 445. Reinhold, New York, 1943.
17. ALBERTY, R. A., in Neurath, H., and Bailey, K., eds., "The Proteins," Vol. 1, Part A, pp. 461-548. Academic Press, New York, 1953.
18. CUNNINGHAM, D. K., GEDDES, W. F., AND ANDERSON, J. A., *Cereal Chem.* **32**, 91-106 (1955).
19. BUNGENBERG DE JONG, H. L., AND KLAAR, W. I., *Kolloid-Z.* **128**, 164-176 (1952).
20. KEMP, I., *Trans. Faraday Soc.* **32**, 837-843 (1936).
21. GLAZER, J., AND DOGAN, M. Z., *Trans. Faraday Soc.* **49**, 448-455 (1953).
22. HARTLEY, G. S., AND ROE, J. W., *Trans. Faraday Soc.* **36**, 101-109 (1940).
23. HAVINGA, E., AND DEN HERTOOG-POLAK, M., *Rec. trav. chim.* **71**, 64-71 (1952).
24. HARRINGTON, W. F., AND SCHELLMANN, J. A., *Compt. rend. trav. lab. Carlsberg, ser. chim.* **30**, 21-43 (1956).
25. KAUZMANN, W., AND DOUGLAS, R. G., *Arch. Biochem. Biophys.* **65**, 106-119 (1956).



## PREPARATION OF REPLICAS OF SILVER BROMIDE FOR ELECTRON MICROSCOPY<sup>1</sup>

E. J. Meehan and Willard H. Beattie<sup>2</sup>

*School of Chemistry, University of Minnesota, Minneapolis, Minnesota*

*Received October 13, 1959*

The decomposition of silver halides in the electron beam has been investigated by several workers. Trillat (1) observed decomposition of  $10\ \mu$  silver bromide crystals by 50 kv. electrons to silver crystals in a time varying from several seconds to several minutes. Fischer (2) observed decomposition of silver chloride to silver globules, leaving envelopes outlining the original particles. By electron diffraction he detected free silver as far as several microns from the nearest particle, and he concluded that decomposition was accompanied by effervescence. Hall and Schoen (3) electron-bombarded particles of silver chloride and silver bromide in photographic emulsions. They observed decomposition into irregular masses of silver, leaving an outline of the original crystal. The silver mass from silver chloride was observed to creep during a period of 10 min., then become stable. Krummenerl (4) found that large silver bromide crystals decompose faster than small ones. Similar Bowers (5) observed decomposition of silver bromide particles while taking electron micrographs. Obviously direct application of electron microscopy to silver halides cannot give a reliable value of size of the original particle.

It was desired to obtain accurate estimates of average particle size in silver bromide sols by electron microscopy to compare with results obtained by light scattering (6). It was therefore necessary to develop reliable methods for making replicas. For purposes of comparison, the results by direct electron microscopy are included.

A  $5 \times 10^{-3}\ M$  dialyzed silver bromide sol was sprayed onto formvar coated copper grids with an atomizer, and placed in the electron microscope. (The preparation and properties of this sol, denoted as C-2, are described in detail elsewhere (6). Decomposition in the electron beam was so rapid that no change could be detected after the time necessary to focus the beam at medium intensity (20 to 30 sec.). Under a low-intensity beam, particles broke into pieces, and extrusions grew from the particles. This is shown in

<sup>1</sup> Taken from the Ph.D. thesis of Willard H. Beattie, October, 1958.

<sup>2</sup> Present address, Shell Chemical Corporation, Box 211, Torrance, California.





FIG. 1. Electron micrograph of silver bromide particles exposed to low-intensity electron beam ( $\times 24,000$ ).

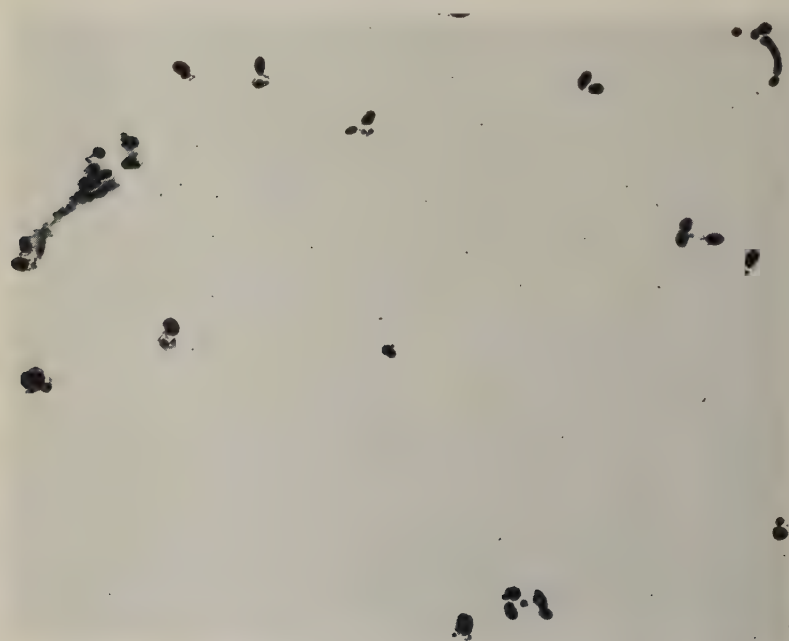


FIG. 2. Electron micrograph of same silver bromide particles shown in Fig. 1 after exposure to high-intensity electron beam ( $\times 24,000$ ).

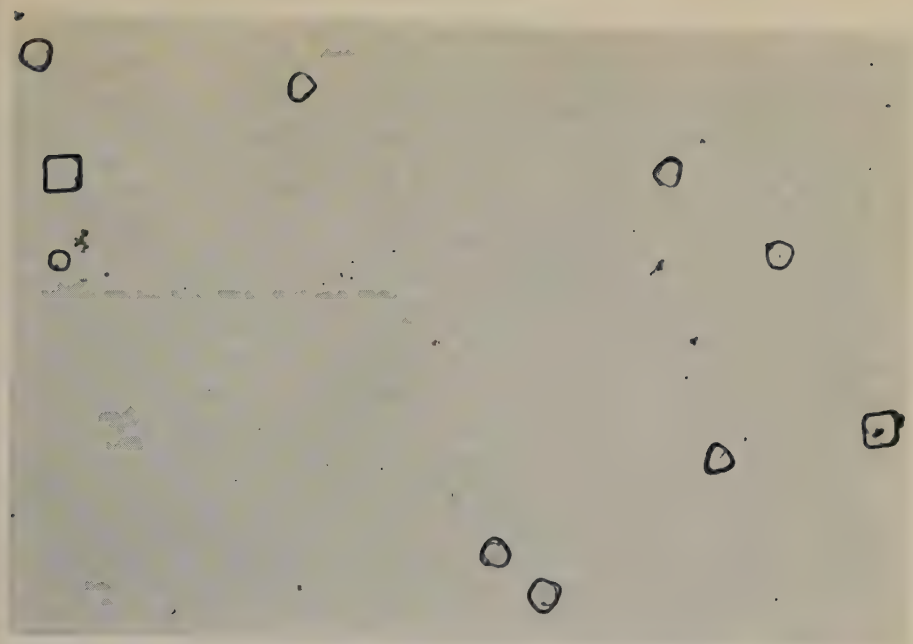


FIG. 3. Electron micrograph of carbon replicas of silver bromide particles ( $\times 24,000$ ).

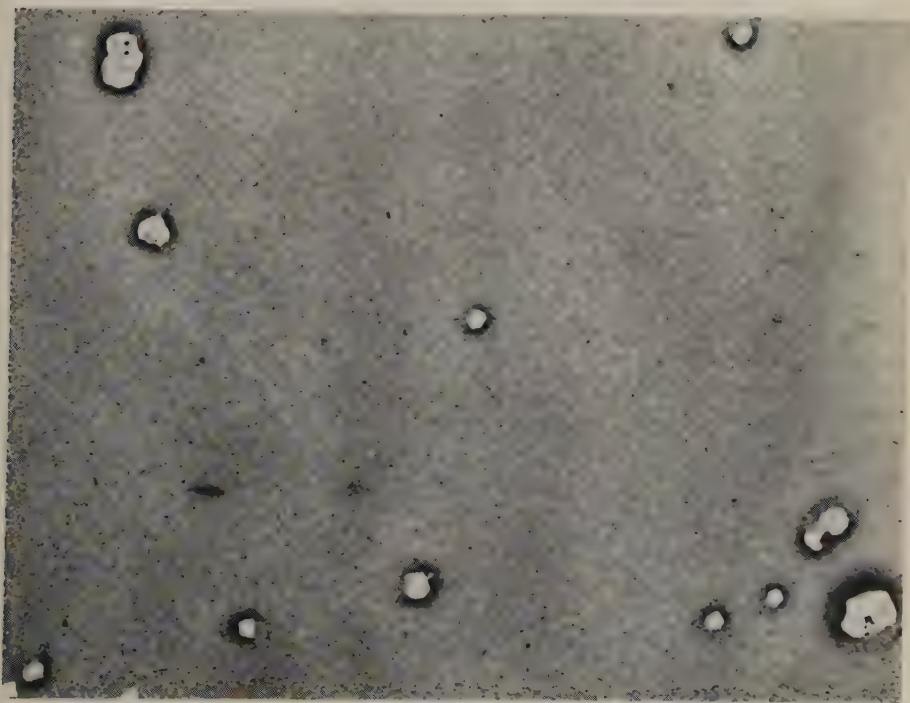


FIG. 4. Electron micrograph of collodion replicas of silver bromide particles, shadowed with chromium at an angle of  $60^\circ$  ( $\times 24,000$ ).

Fig. 1. Subsequent exposure to a high-intensity beam rounded the corners of the pieces and separated them into apparently individual particles, as shown in Fig. 2 for the same area shown in Fig. 1.

Unknown systematic errors may be introduced in the making of replicas. To check the reliability, two different kinds were made.

Carbon replicas were prepared as follows. Dialyzed sol was sprayed with an atomizer onto a formvar coated slide. Spraying was used in an effort to reduce coalescence of particles. The slide was placed in a shadow caster under high vacuum, and coated with carbon by exposure for 2 to 3 min. to a carbon arc about 6 inches above the slide and normal to it. The formvar-carbon layers were separated from the slide by dipping the slide in water, allowing the carbon and formvar to float. The formvar was dissolved by floating on 5% 2-chloroethanol. The carbon replicas were then floated on 1% sodium thiosulfate to dissolve the silver bromide, and washed twice by floating on water. The replicas were mounted on grids and placed in the electron microscope. A representative replica is reproduced in Fig. 3. The danger in this method obviously is the possible reduction of silver bromide during exposure to the carbon arc (v.i.).

Collodion replicas were prepared as follows. Dialyzed sol was sprayed onto a formvar coated slide. A film of collodion was spread over the slide and allowed to dry. The formvar and collodion were separated from the glass by dipping the slide in water, allowing the formvar and collodion to float. The formvar and silver bromide were dissolved as above and the collodion film was washed twice by floating on water. Impressions of the particles were left in the collodion film. The collodion replica was placed on a grid with the impressions exposed. The grids were placed in the shadow caster under high vacuum, and chromium was evaporated from a hot filament onto the replica at roughly  $60^\circ$  to the grid. A typical replica is shown in Fig. 4. In this procedure there is no danger of photochemical reduction or decomposition of the silver bromide.

The average diameter of the particles, determined from measurement of 415 carbon replicated particles, was  $0.119\ \mu$ , and determined from measurement of 341 collodion replicated particles, was  $0.115\ \mu$ . The excellent agreement indicates that any reduction of the silver bromide which may have occurred during exposure to the carbon arc had no effect upon the particle size. Also, the average value was in excellent agreement with that determined by scattering, after allowance was made for the effect of particle size distribution (6).

#### ACKNOWLEDGMENT

The authors are much indebted to Dr. Donald Hickman of the Department of Anatomy, University of Minnesota, for his cooperation in preparing the replicas and making the electron micrographs.

# REFERENCES

1. TRILLAT, J. J., *Acta Cryst.* **5**, 471 (1952).
2. FISCHER, R. B., *J. Appl. Phys.* **25**, 894 (1954).
3. HALL, C. E., AND SCHOEN, A. L., *J. Opt. Soc. Amer.* **31**, 281 (1941).
4. KRUMMENERL, T., in J. W. Mitchell, ed., "Fundamental Mechanisms of Photographic Sensitivity," p. 74. Butterworth, London, 1951.
5. BOWERS, R. C., Ph.D. Thesis, University of Minnesota, 1953.
6. MEEHAN, E. J., AND BEATTIE, W. H., *J. Phys. Chem.*, to be published.

## BOOK REVIEWS

**Fine Particle Measurement.** Size, Surface and Pore Volume. By CLYDE ORR, JR., AND J. M. DALLAVALLE (Georgia Institute of Technology, Atlanta, Georgia). The Macmillan Co., New York, 1959. L.C. 57-5973. 353 pp. Price \$10.50.

Finely divided matter is put to surprisingly many uses, and its importance is by no means limited to manufacturing processes and commercial products. It concerns the meteorologist and even the astronomer and cosmologist, "for on a cosmic scale something like one-half of the universe is believed to exist in the form of fine particles. The soil scientist finds agriculture vitally related to the microscopic properties of near-surface soils, whereas the sedimentary petrographer deals with the particle size and pore distribution of the deeper layers of the earth in his quest for oil. . . . Particles in the atmosphere affect the colors of sunsets, influence precipitation and cause some of our illnesses."

This book deals with the speciality measurement, in contrast to *Micromeritics*, written by Dallavalle in 1943 as a survey of the technology. The field has since grown tremendously. No attempt has been made to relate measures of particle size, surface adsorptivity, grindability, filterability, or catalytic activity, as they are regarded as outside the scope of this volume. Instead the authors present information that will permit the reader to understand basic principles, construction, and use of apparatus, methods of data appraisal, applications, and limitations. An idea of the scope comes from key words of chapter headings and table of content: Significance of Measurement Techniques; Microscopy and Sieving; Sedimentation; Inertial Techniques; Radiation Scattering and Transmission; Permeametry (Kozeny-Carmen); Gas Adsorption for Surface Areas; Pore Size Distribution.

The authors are to be congratulated on doing a good job which will be of paramount interest and value to readers of this Journal. The book is an improvement over *Micromeritics* in that light scattering is given adequate treatment, and a general, coordinated treatment of other new methods is presented. There are many well-chosen illustrative figures and numerous tables and appendices of very useful data, with a bibliography of 400 references as guide to the pertinent literature. There are a few minor errors which do not merit special attention until future editions are issued. Meanwhile all serious students of particle size measurement will find it the best book available in this field.

VICTOR K. LA MER, New York, New York

**Spray Literature Abstracts.** Compiled and edited by KALMAN J. DE JUHASZ. Published with the support of National Science Foundation by The American Society of Mechanical Engineers. New York, 1959. Price \$12.00.

Study of liquid aerosols is an important part of Colloid Science, particularly so because aerosols in many respects are less complicated than other colloidal systems and thus are well suited for investigating some of the fundamental problems of colloids, for instance, the effect of surface tension on stability. Hence, a bibliography of sprays is certain to arouse interest among the readers of this journal.

The book is 383 pages long and contains, it is said, over 1300 abstracts ranging from 1880 to 1958. In addition to papers which undoubtedly deal with sprays, many publications on only loosely related topics are listed. This is not very fortunate because a credulous user of the book may imagine that the coverage also of these



topics is complete and thus may miss valuable communications, while a reviewer naturally asks why just these publications and none other were included? For instance, in 1953 almost simultaneously two books on Foams appeared, one in the United States and the other in Germany; only the American book is mentioned in the bibliography. If this preference might be justified in a bibliography destined for American scholars, no justification of this kind is possible for the inclusion of "Praktische Mathematik fuer Ingenieure und Physiker" by R. Zurmühl; surely, there is no shortage of mathematical textbooks in the English language. Thus, we remain in doubt: did the Editor include the titles present in the bibliography because he recommends these books or papers in preference to those not included, or did he not know of the existence of the others?

The coverage of publications on sprays seems to be good; of the 14 references in the short chapter on sprays in the reviewer's volume on *Surface Chemistry* (1958), 10 can be found in Dr. Juhasz' bibliography. On the contrary, liquid aerosols are not well treated; of the 31 references in the reviewer's monograph, only 4 are included in *Spray Literature Abstracts*.

The abstracts range in length from title only to about half page and, whenever tested, are informative.

Unfortunately, this review cannot be concluded without mentioning the main defect of the book. All abstracts in it are arranged alphabetically according to the name of the author of the paper, and no subject index is provided. Thus, a person interested in a definite problem (e.g., how do I measure the size distribution of spray droplets?) has to look at every one of the 1300+ abstracts! As, presumably, nobody will tackle this job, the book will not be used as it was intended to be. This is a very sad conclusion because the compilation obviously was a work of love and it would have been easy to make it useful.

J. J. BIKERMAN, Cambridge, Massachusetts

**Light-Scattering in Physical Chemistry.** By K. A. STACEY, Ph.D. Academic Press Inc., New York, and Butterworths Scientific Publications, London, 1956. 230 pp. Price \$6.75.

In contrast to the monograph by H. C. van de Hulst, this author restricts his studies almost exclusively to that of macromolecules and has little or nothing to say about the fundamental work on the scattering by independent particles. In this respect the title is misleading; otherwise the two books are complementary. The author has made an extensive survey of the literature and reported the work that has appeared up to 1956 with emphasis on experimental methods and equipment as applied to high polymers, proteins, and polyelectrolytes. Unfortunately, when he discusses the basic Mie theory, as on page 6, he betrays some misunderstanding of the fundamental theory which is correctly expressed by van de Hulst. Stacey ought to have developed the Mie theory carefully and correctly, and then shown that the remainder of his text followed by a consideration of fluctuation theory as developed by Smoluchowski, Einstein, and Debye.

The statements on pages 6 and 10 are unfortunate in that they imply that the Rayleigh theory is sufficient when the index of refraction of particle and medium is small, whereas the Mie theory is needed only for large differences in refraction. The Rayleigh theory is really a zero-order form of the general Mie theory in which the range of application is set primarily by the size of particles rather than by the difference of index of refraction. The aspect is treated clearly and correctly by van de Hulst on page 132.

In spite of these shortcomings in theoretical presentation, this book will prove useful to students approaching the subject for the first time, particularly when their field of interest deals with concentrated solutions of dependent scatterers.

VICTOR K. LA MER, New York, New York

**Thermodynamics and Statistical Thermodynamics.** By JOHN C. ASTON, Professor Organic Chemistry, and JAMES J. FRITZ, Associate Professor Chemistry, The Pennsylvania State University. John Wiley & Sons, Inc. New York; Chapman and Hall, London, 1959. 556 pp. Price \$8.25.

This text is designed for a one-year graduate course. The first fifteen chapters are devoted to the macroscopic and the remaining eight to the statistical approach without overlapping of the two disciplines. Two hundred and ninety problems, of which 130 involve derivations of formulas, are interspersed after each appropriate subchapter. Nine appendixes (pp. 463-537) are attached as aids in the numerical solutions of the problems.

The objective (p. 3) "has been to cover those important parts of thermodynamics and statistical thermodynamics which allow exact calculation and are *now quite fully understood*" (p. VII). The order of presentation of subject matter has been governed "by our experience that lack of understanding of the First Law is often responsible for difficulty in using the Second Law. If the concept of thermodynamic temperature is properly understood, the full meaning of the Second Law is as easy to grasp intuitively as that of the first. . . ." Amen. However, after studying this text one wonders if the presentation has been made clearer and easier, or even logically self consistent.

After thirty years of teaching graduate students from different texts, this reviewer has reached the conclusion that there remain a number of topics, particularly in thermodynamics, which have been glossed over and sometimes misrepresented since the days of Kelvin, Clausius, and Planck; they are *not* "now quite fully understood." At least, recent texts are not in agreement in respect to fundamental interpretations—strange as this may seem to those who consider thermodynamics a closed chapter of science. The present text is not an exception.

The opening sentence under Temperature, (p. 11) reads: "In order to account for *heat disposal* in thermodynamical calculations it is necessary to specify the temperature." Although a correct statement, this approach is hardly in accord with historical development, nor is its restricted viewpoint helpful in orienting the attention of the graduate student—if his attention has not already been so directed—toward inquiry into the meaning and development of the fundamentals of the temperature concept. However, it is in accord with the primary objective of this book; namely, how to teach students to make calculations. Is facility in computing the real goal of a course in thermodynamics?

The authors' presentation of fundamental principles does not appear to have been influenced in any way by the pertinent writings of Brønsted (1935-46); P. S. Epstein's *Thermodynamics* (Wiley, 1937); Guggenheim (1933 to date); Caratheodory (1909); Max Born (1921); or of the Belgian School under the leadership of Prigogine and Defay (1935 on). These authors have made significant advances in the presentation, semantics, and fundamental understanding of thermodynamics over that of Lewis and Randall (1923), and every graduate student should have at least some acquaintance with their views.

Carnot's ideas (p. 23) and procedures are incorrectly presented. This is due to reliance upon a translation and interpretation, long since discredited, without consulting the original memoir for the facts. The points at issue were clarified by H. L. Callendar in his Presidential address to the London Physical Society (*Proc. Phys. Soc. (London)* 23, 153 (1911)) and in his writings on heat in *The Encyclopedia Britannica*, 1911 on. They have since been verified and elaborated upon by La Mer (*Am. J. Phys.* 22, 20 (1954); 23, 95 (1955)) and by others, notably E. T. Whittaker and Leon Brillouin (reference cited by La Mer).

This book merits criticism not so much for misuse of technical words and for in-

correct sentences—of which there are many—as for fundamentally illogical or incorrect presentations of the basic concepts of thermodynamics.

On page 46: "Consider an expansion process against a piston exerting a force which *exactly balances* the pressure of the gas, which does no work other than by the expansion." The thoughtful student will inquire how can the gas expand and work be produced if the forces are exactly balanced? Nowhere do we find mention of the quasi-statically conducted process, which produces work, as opposed to one of complete equilibrium (rest). Irreversible and reversible processes are not mentioned until pages 62 and 67, long after they are needed.

This incomplete presentation of a basic concept is followed on page 47 by the equally unintelligible, if not illogical, treatment of the Gay Lussac-Joule free expansion of a gas. "Two identical calorimeters, each separately insulated, are connected by a valve; one of the calorimeters (*A*) is filled with a gas at a pressure  $p'$ , while the other is evacuated. When the valve is opened, the gas in calorimeter *A*, as it *continues to expand, does work on the gas already expanded into calorimeter B*. As a result of the work done, when the gas expands the energy of *A* is decreased, so that its temperature falls by an amount  $\Delta T_A$ ; at the same time the temperature of *B* increases by an amount  $\Delta T_B$  because of the work done on the gas in it." (Footnote 5. Some readers will be gratified that they held out against apparently opposite statements)."

Nowhere is mention made that heating and not cooling results from the free expansion of hydrogen or helium at ordinary temperatures, and that a free expansion, by virtue of the great rapidity of the process, is always effectively conducted adiabatically; i.e.,  $q = 0$ , regardless of the insulating character of the containing walls. If the gas were hydrogen or helium one would reach the absurd conclusion from the authors' arguments that work was done by the vacuum upon the expanding gas!

The prescription of the process (no opposing force) makes it irreversible and hence no work can be obtained. The authors' primary definition "when a gas is expanded from one pressure to another without doing any work on the surroundings, the process is called a "free expansion," puts the cart before the horse. Nor does footnote 6 contribute to a clarification of the confused argument.

Most thermodynamicists today (cf. also Lewis and Randall, p. 53) would express the essential difference between work and heat as depending upon whether or not the loss of energy which a system experiences in a process requires description in macroscopic mechanical co-ordinates, or whether or not consideration of the thermal co-ordinate, temperature, is sufficient. Compare page 227, where we learn that "the product of the two variables ( $PV$ ) is work." This product represents volume energy. It may or may not be convertible into work depending upon whether or not a difference in potential (pressure  $p$ ) exists to drive the process and also upon whether the conduct of the process is reversible or irreversible. These generally accepted views seem to be foreign to this text.

Just how a freely expanding gas *A* can perform (thermodynamic) work on gas *B* without the aid of a piston to sense (and measure) the forces acting upon it, passes understanding. The modern interpretation is that, in general, free expansions (or dilutions) by virtue of their irreversible conduct always entail an increase (i.e., creation) of entropy equal to  $\Delta S'' = R \ln V_{\text{final}}/V_{\text{initial}}$ , which corresponds to a created heat  $Q'' = T\Delta S''$ . This created heat  $Q''$  is compensated energetically by the loss of

potential energy  $\int_i^f v dp$ . If the compensation is exact, as is the case with perfect gases, (or solutions), no cooling or heating is observed.  $\Delta T_A = \Delta T_B = 0$ .

In the case of a real gas,  $\int v dp$  does not equal  $Q''$  so that cooling usually occurs, but an elevation of the temperature can and does actually occur, as is well known for



hydrogen and helium above their inversion temperatures. Nowhere in this text is this aspect, so important for the liquefaction of gases, touched upon. The student who conscientiously works out the problems may gain a feeling for thermodynamic magnitudes but the operations will be painful, with only an incomplete understanding of their real meaning for his pains.

The Gibbs ( $TS$ ) temperature-entropy diagram is introduced late in the presentation (p. 144) and is illustrated by a complex of unintelligible curves which are neither defined nor explained in any way in the text, except that they have been compiled by students using the methods of problems 10.5 to 10.5-4.

Rather than mystifying the reader it would have been better to introduce the  $TS$  diagram (as Gibbs does) for a simple Carnot cycle and explain its meaning and use. The student would then see that Gibbs' diagram is an apt illustration of the modern Carnot-Brønsted approach.

Under dilute solutions (p. 160) we find the statement: "although, in a solution, concentration of the solute plays a role analogous to that of pressure in a gas, *it is not necessary that any actual solution approach perfect solution behavior as the concentration of the solute approaches zero, etc. . .*." Did not Van T'Hoff and Gibbs prove just the contrary?

The chapters on electrolytes and e.m.f. of cells are modernized by mentioning the Debye-Hueckel limiting law with references to Harned and Owen; otherwise the treatment remains that of Lewis and Randall (1923). The complicated calculation of activity coefficients by freezing points is developed at length but the much simpler isothermal solubility method is not even mentioned.

In developing statistical thermodynamics, the authors appear to be on sounder grounds. They claim that using "the distribution laws and energy levels to calculate the energy of a system *first* with many numerical examples has considerable advantage over a more general introduction."

There may be good pedagogic reasons for this order but it postpones a development of the general methods of Gibbs to the last chapter. The authors recognize that this order means that much of this part of the book can deal only with systems without interaction, so that systems with interactions require a repetitious development. This is akin to developing a thermodynamics applicable only to perfect gases, leaving real systems as an afterthought. There are many problems and helpful appendixes for dealing with the detailed calculations of chemical physics. The limitations and relationships to the more general presentations noted above are clearly stated, so that these sections can be commended to the reader.

VICTOR K. LAMER, New York

## VISCOELASTIC BEHAVIOR OF NYLON 6-6 MONOFILAMENTS BELOW ROOM TEMPERATURE

B. A. Dunell, Ann A. Joanes<sup>1</sup>, and R. T. B. Rye

*Chemistry Department, University of British Columbia, Vancouver 8, Canada*

*Received November 13, 1959*

### INTRODUCTION

Stress relaxation studies and the determination of dynamic modulus and energy loss have led to an understanding of the viscoelastic character of amorphous polymers over a wide range of conditions and to a quantitative evaluation of this character in terms of spectra of relaxation times. Tobolsky recently reviewed progress in stress relaxation studies (1), Ferry has done the same for vibrational studies and other mechanical experiments (2), and Woodward and Sauer have summarized the results of dynamic mechanical experiments at low temperatures (3). The reviews of Tobolsky and Ferry remind the reader of the applicability of a time-temperature superposition principle to stress relaxation and vibrational results obtained from amorphous polymers (4, 5). The principle allows the characterization of the mechanical behavior of a polymer over a very wide time or frequency range, and hence the spectrum of relaxation times can be derived for a correspondingly wide time range. From this spectrum one should be able to predict any type of mechanical behavior for the amorphous polymer.

The situation for polycrystalline polymers has been less well understood. Recently, however, evidence has been published for the applicability of the time-temperature superposition principle even to polycrystalline materials within certain restricted conditions. Nagamatsu, Yoshitomi, and their co-workers have applied it successfully to nylon 6 in torsional stress relaxation at low strains (6), and to polytetrafluoroethylene in longitudinal stress relaxation at strains below 0.7 % (7). For polyethylene, Tobolsky found that the time-temperature superposition principle was inapplicable to stress relaxation data (8), but the results of more recent experiments by Nagamatsu, made at lower strain, have been amenable to treatment by this principle (9).

This paper presents stress relaxation and vibrational results for nylon 6-6 at temperatures between 10° and -100°C. and examines the application of the time-temperature superposition principle to them.

<sup>1</sup> Née Ann A. Walter.



## EXPERIMENTAL

The material on which all experiments were done was a finished commercial 15-denier monofilament nylon 6-6 supplied through the kindness of Dr. R. D. Bennett of the du Pont Company of Canada (1956) Ltd. The monofilament had a nominal finish content of 0.55% and, being semi-dull, had a content of titanium dioxide delustrant.

In the stress relaxation apparatus, a length of monofilament was attached one end to each of two long, heavy sewing needles, one of which screwed onto the moving member of a Satham Instrument Co. strain gauge and the other of which was clamped by a pin vise to the mechanism which stretched the sample suddenly to preset elongation. This mechanism was such as to allow the elongation to be varied at will from experiment to experiment, and to facilitate setting the initial tension (before zero time of the relaxation experiment) just to zero. The output from the Satham strain gauge model G1-1.5-350 was fed to a rapid-balancing Speedomax recorder. The test filament was enclosed by a well-insulated chamber of internal dimensions  $3 \times 6 \times 1\frac{1}{2}$  inches into which vapor from liquid nitrogen was introduced in a reasonably uniform way through a manifold tube. Four thermocouples in this chamber served to monitor the temperature of the test space, which was uniform to within  $\pm 1^\circ\text{C}$ . Small holes top and bottom of the chamber allowed passage of the "lead in" needles, to which the test sample was attached, from the strain gauge and elongating mechanism, both of which were outside the insulated chamber.

A filament about 11 cm. long, mounted between needles, was suspended freely in the test chamber from the strain gauge, which was at the top end of the apparatus. Air that had been dried by passage through a calcium chloride column was passed through the test chamber overnight to bring the sample to minimum moisture content before testing it. Vapor from liquid nitrogen was then circulated through the chamber to bring the sample to a predetermined temperature. One half hour after this temperature had been established the lower needle was clamped by the pin vise to the stretching mechanism and the mechanism adjusted just to zero tension in the fiber. After a further half hour, allowed to ensure that the system was in equilibrium, the sample filament was stretched suddenly and the stress recorded as a function of time by the Speedomax recorder. The strain gauge was calibrated frequently with known weights and calibrating resistors.

The apparatus and technique used for measuring the dynamic tensile and loss moduli were a slight variation of those described elsewhere (10, 11). The test filaments were jacketed by a pair of metal tubes just less than 1 inch in diameter. Vapor from liquid nitrogen was circulated to the air space in these tubes through a small manifold running along the bottom

of each tube. It was found necessary selectively to block off certain holes in the manifold to obtain a reasonably uniform temperature along the whole length of the sample in the test space. The temperature in the sample space was measured by thermocouples placed near the middle and near each end of the enclosing tubes. The cooled spaces were jacketed by a substantial rock wool insulation. The variation in temperature along the filament and from one filament to the other, depended on the nominal temperature at which the experiment was performed. It varied from mean value  $\pm 1^\circ\text{C}$ . near  $-10^\circ$  and  $-20^\circ\text{C}$ . to mean value  $\pm 3^\circ\text{C}$ . near and below  $-60^\circ\text{C}$ .

Before the experiment was run at low temperature, the test filaments were allowed to creep overnight in the apparatus under a load of 8 g. on the 15-denier filament. During this time dried air from a calcium chloride column was passed over the filaments. The vibrational experiments were done at a strain amplitude of 0.0015.

### RESULTS

The stress relaxation curves shown in Fig. 1 represent the average behavior of 15-denier nylon monofilaments at each indicated temperature for

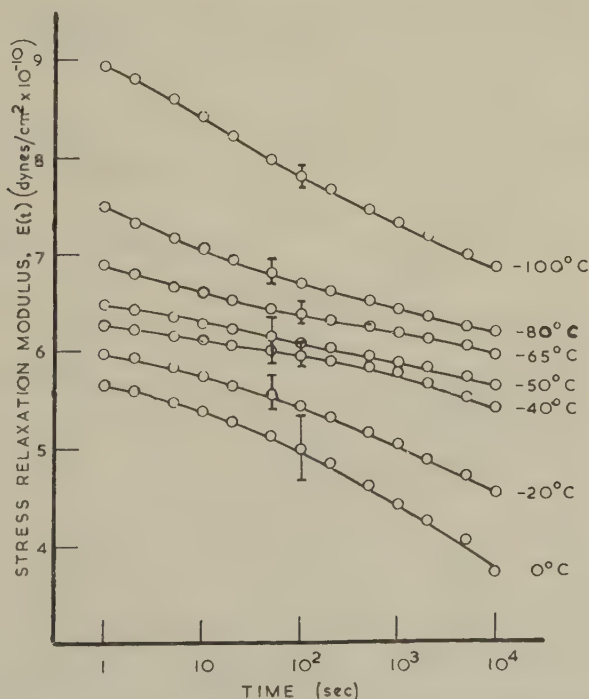


FIG. 1. Average stress relaxation curves for 15-denier nylon 6-6 monofilaments at various temperatures.

a strain of 0.015. Experimental scatter, which is troublesome in most single-filament work, was found to give special difficulty in the low-temperature work. Although the shapes of the individual curves for different samples at the same temperature were fairly uniform, the position of the curve on the vertical axis varied considerably, and an indication of this is given in Fig. 1 by showing the extreme limits of variation of the relaxation modulus at 100 sec. or 50 sec. The points plotted in Fig. 1 are the average of several runs made each on a separate filament. At  $-65^{\circ}\text{C}$ . only four samples were tested. At other temperatures six samples were tested, but at  $-80^{\circ}\text{C}$ . one run was arbitrarily rejected because the curve it yielded differed considerably in shape from the other curves at that temperature, and at  $-100^{\circ}\text{C}$ . two runs were rejected on the same basis.

The results of the vibrational experiments are displayed as dynamic tensile modulus,  $E'$ , against frequency at various temperatures in Fig. 2 and as loss modulus,  $E''$ , against frequency for each temperature in Fig. 3. The moduli at a radian frequency of  $150\text{ sec}^{-1}$  are then plotted as a function of temperature in Fig. 4. A single run was made for each of  $+10^{\circ}$ ,  $-10^{\circ}$ ,  $-70^{\circ}$ ,  $-75^{\circ}$ , and  $-80^{\circ}\text{C}$ ., and two or more runs, each on a fresh pair of filaments, were made at the other temperatures. The values of the tensile modulus were found to be satisfactorily consistent, but the results for the loss modulus were badly scattered, especially near  $-40^{\circ}\text{C}$ . One

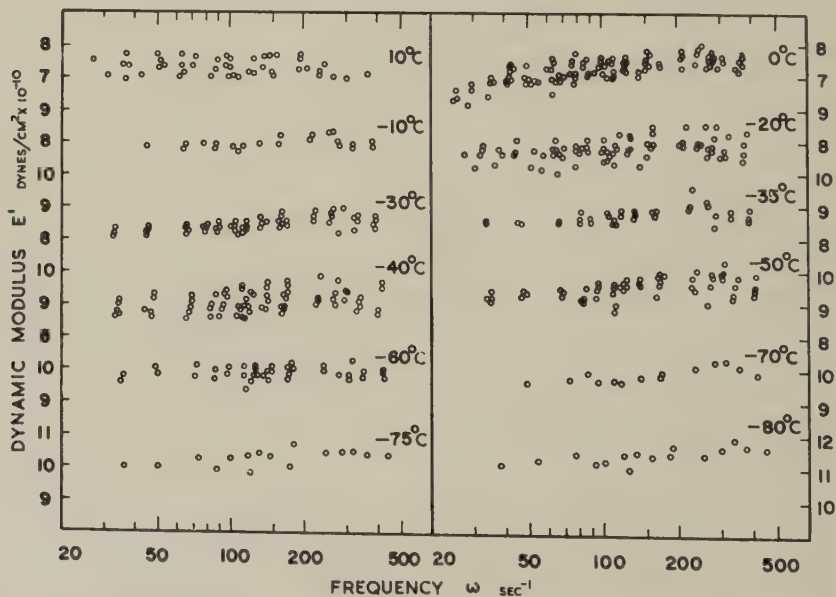


FIG. 2. Dynamic tensile modulus,  $E'$ , for 15-denier nylon 6-6 monofilaments as a function of frequency at various temperatures.

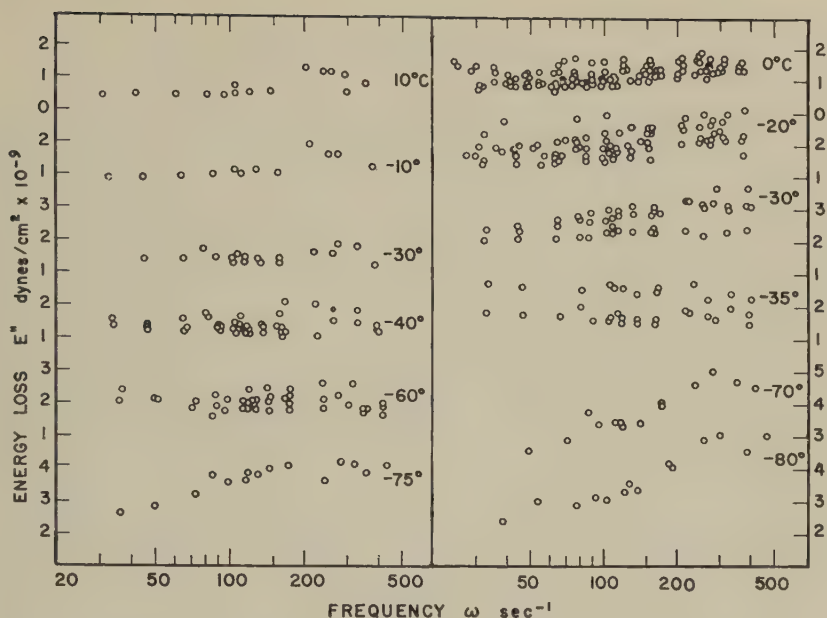


FIG. 3. Dynamic loss modulus,  $E''$ , for 15-denier nylon 6-6 monofilaments as a function of frequency at various temperatures.

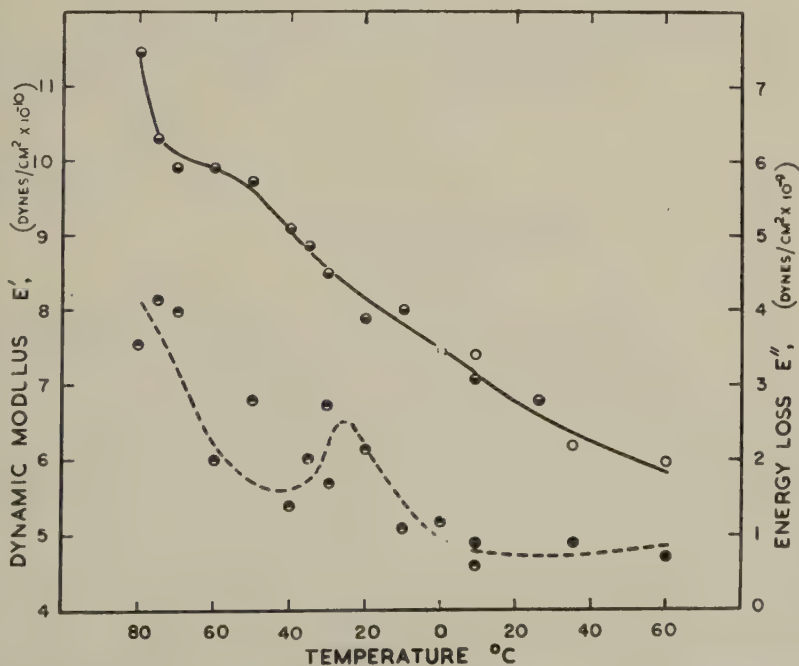


FIG. 4. Dynamic tensile and loss moduli for 15-denier nylon 6-6 monofilaments as a function of temperature at  $\omega = 150 \text{ sec}^{-1}$ . Filled bottom— $E'$ , filled top— $E''$ , open— $E'$  obtained by Quistwater (11, 14), completely filled— $E''$  obtained by Quistwater.

group of experiments at  $-40^{\circ}\text{C.}$  showed energy loss,  $E''$ , values ranging from  $4(10^9)$  to  $5(10^9)$  dynes/cm.<sup>2</sup> and a group at  $-50^{\circ}\text{C.}$  showed  $E''$  values of  $3.5(10^9)$  to  $2.5(10^9)$  dynes/cm.<sup>2</sup>, decreasing values being obtained with increasing frequency. Such behavior would be consistent with a rather rapid decrease in  $E''$  with decreasing temperature near  $-50^{\circ}\text{C.}$  These two groups of loss moduli are not shown in Figs. 3, 4, or 7 because they are quite inconsistent with the other results which are obtained and with the results of Woodward *et al.* (12). Ninomiya and Fujita (13) noted difficulty in obtaining consistent stress relaxation results for polyvinyl acetate films near the second-order transition, the result they obtained depending on the thermal and mechanical history of the sample. It is possible that we have a comparable situation here, for no special pretreatment was given the samples to anneal out previous history. Further, the fact noted above that the observed change of  $E''$  with frequency at  $-50^{\circ}\text{C.}$  agrees with a high maximum in  $E''$  somewhere near  $-40^{\circ}\text{C.}$  suggests that the rejected results are not entirely spurious but arise from some peculiarity of a portion of the sample, possibly its thermal or mechanical history.

Also shown in Fig. 4 are  $E'$  and  $E''$  values obtained at higher temperatures by Quistwater (11, 14). At  $35^{\circ}$  and  $60^{\circ}\text{C.}$  they have been obtained for zero relative humidity by extrapolation from 10 % humidity. His results agree satisfactorily with those reported in this paper. Comparison with the energy loss reported by Woodward *et al.* (12) shows that we are dealing chiefly with the  $\beta$  dispersion and energy absorption range with a short excursion into the  $\gamma$  region at the lowest temperature we have investigated. The fact that we have used a drawn monofilament nylon and Woodward used a "bulk" nylon rod may very well account for the absence of significant  $\alpha'$  dispersion at zero humidity even at  $60^{\circ}\text{C.}$ , though it is well developed in Woodward's results at that temperature.

#### DISCUSSION

Since it appeared that the stress relaxation curves might form a composite by appropriate displacement horizontally along the log time axis until they superimposed, this treatment was applied to the unmodified average curves of Fig. 1. The success may be judged from Fig. 5. The reduction factors,  $a_T$ , which govern the displacement of each curve required to give the composite plot on a log  $(t/a_T)$  base, give a satisfactory straight line if they are recorded as log  $a_T$  against  $T^{-1}$ .

It is generally assumed that the relaxation mechanisms manifested in the  $\alpha'$ ,  $\beta$ , and  $\gamma$  dispersion and energy loss regions have their origin in motions of molecular segments within the amorphous parts of the polymer (12, 15, 16). Acting on this assumption, and following Ferry and Fitzgerald (17), we have pictured the sample to have a rubbery compliance,  $D_k$ , and a glassy or crystalline (non-rubbery) compliance,  $D_g$ , contributing to the total meas-



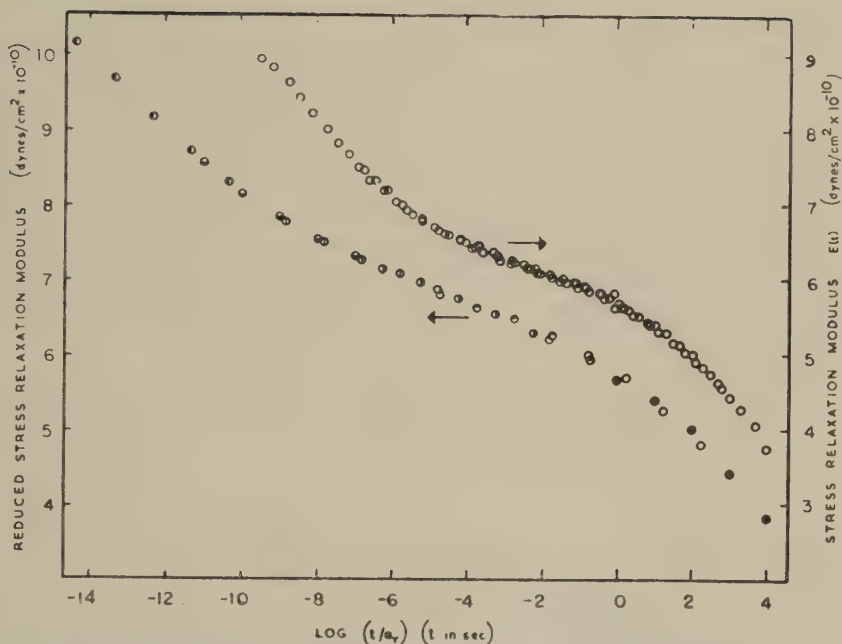


FIG. 5. Composite stress relaxation curves for nylon 6-6 monofilaments from unmodified stress relaxation curves and from "reduced" stress relaxation curves. In the reduced curve, the different kinds of points represent the several temperatures from 0° to -100°C.

ured compliance

$$1/E = D = D_k + D_g.$$

In terms of a mechanical model, this is equivalent to considering the system to be two springs in series. The rubbery compliance is corrected for temperature according to the kinetic theory of rubber elasticity

$$D_{k,T_0} = (T/T_0)D_{k,T},$$

but no correction has been made here for change in density. The potential energy compliance,  $D_g$ , is considered temperature independent. One obtains, then, an expression for the tensile modulus, reduced to a reference temperature by the correction made to the rubbery contribution,

$$E_{T_0} = E_T / \{ (T/T_0) + (E_T/E_g)(1 - T/T_0) \}. \quad [1]$$

The modulus  $E$  at temperature  $T$  and at reference temperature  $T_0$  may be the stress relaxation modulus  $E_T(t)$  and  $E_{T_0}(t)$  or the dynamic tensile modulus  $E_T'(\omega)$  and  $E_{T_0}'(\omega)$ .

The value of  $E_g$  has been taken as  $13(10^{10})$  dyne cm.<sup>-2</sup> for our nylon by the arbitrary expedient of multiplying the maximum value we have ob-

served for the dynamic tensile modulus, a value of  $11.5(10^{10})$  dyne cm.<sup>-2</sup> at 193°K., by the root of the ratio of resonant frequencies observed by Woodward at 80°K. and 193°K. (page 366 of reference 12), viz.,  $\sqrt{15/12}$ .

Equation [1] was applied to the average points for the stress relaxation curves in Fig. 1, using  $T_0 = 273^\circ\text{K.}$  as reference, and the time-temperature superposition principle applied to the resulting set of curves. The composite curve thus obtained is shown in Fig. 5, in which the reduced stress relaxation modulus,  $E_{T_0}(t)$  is plotted as a function of the logarithm of the reduced time,  $\log(t/a_T)$ . The reduction factors  $a_T$  are a smooth function of the temperature;  $\log a_T$  versus  $T^{-1}$  is shown in Fig. 8. From this composite stress relaxation curve, the spectrum of relaxation times

$$2.303H(\tau) = -\left(\frac{dE_{T_0}(t)}{d \log t}\right)_{t=\tau} / \Gamma(1+m)$$

where

$$m = -\frac{d}{d \log t} \log \left( -\frac{dE_{T_0}(t)}{d \log t} \right)$$

may be derived (18). This is plotted in Fig. 6. From the spectrum of relaxation times values for the dynamic tensile modulus  $E'_{T_0}(\omega)$  were calculated using Catsiff and Tobolsky's approximation (19) to Marvin's difference formula

$$E'_{T_0}(\omega) - E_{T_0}(t) \mid_{t=1/\omega} = \Upsilon(m) 2.303H(\tau) \mid_{\tau=1/\omega},$$

where the function  $\Upsilon(m)$  is defined and tabulated in the paper of Catsiff and Tobolsky. These predicted modulus values are shown in Fig. 6 along with values for the loss modulus determined by graphical integration of the relation

$$E''(\omega) = \int_{-\infty}^{\infty} 2.303H(\tau) \frac{\omega\tau}{1 + \omega^2\tau^2} d(\log \tau)$$

for each of a succession of values of  $\omega$ .

Since the dynamic tensile modulus,  $E'$ , shows a distinct increase with increasing frequency at each temperature, and since the time-temperature superposition principle seems to apply to the stress relaxation results, it was considered worth while to try to make a composite curve of dynamic modulus against reduced frequency  $a_T\omega$  and to compare this with the predicted dynamic parameters. Accordingly, the tensile modulus observed at temperature  $T$ ,  $E'_T(\omega)$ , was corrected to the reference temperature  $T_0 = 273^\circ\text{K.}$  by using Eq. [1], and a composite curve shown in Fig. 7 was constructed. The reduction factors  $a_T$  for these dynamic moduli are of very similar magnitude, at any particular temperature, to those which apply to stress relaxation, and are compared with them in Fig. 8.

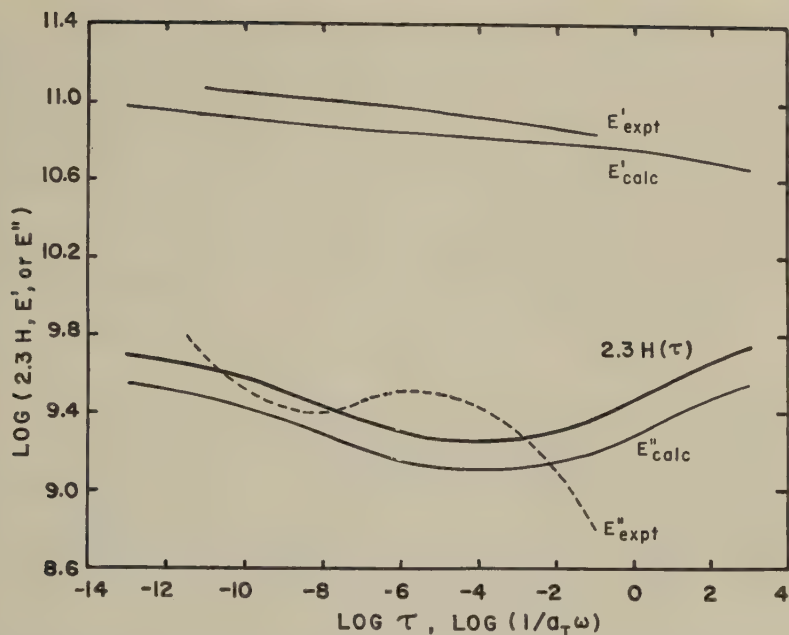


FIG. 6. Spectrum of relaxation times,  $2.303 H(\tau)$ , calculated from composite reduced stress relaxation curve. Predicted and observed spectra of dynamic moduli  $E'$  and  $E''$ .

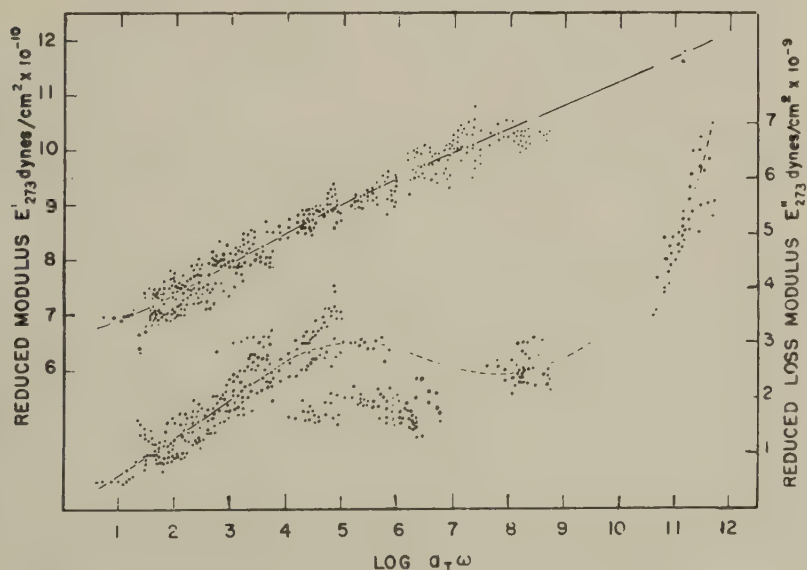


FIG. 7. Reduced dynamic moduli as functions of the reduced frequency,  $a_T \omega$ .

The loss moduli  $E''$  are not sufficiently consistent to be used to test the time-temperature superposition principle and derive values of  $a_T$ . However, applying the values of  $a_T$  already obtained for moduli  $E'$  to the energy loss results yields a composite curve which is not unreasonable, although the values of  $a_T$  previously obtained for  $-70^\circ$  and  $-75^\circ\text{C}$ . will not serve for loss modulus. This "composite" is shown in Fig. 7 in order that the observed fragments of the energy loss spectrum can be compared with the energy loss predicted from the relaxation time spectrum,  $H(\tau)$ . The loss moduli were corrected to the reference temperature  $T_0 = 273^\circ\text{K}$ . by the relation

$$E''_{T_0}(\omega) = E''(\omega)(T_0/T)$$

before they were plotted in Fig. 7.

The observed dynamic tensile modulus, obtained for a wide frequency range by the time-temperature superposition principle and shown in Fig. 7, has been replotted in Fig. 6, beside the calculated tensile modulus for comparison. It will be seen that these differ by about 20% to 40% over the available frequency range. This agreement is poor compared to that obtained for the N.B.S. polyisobutylene, for which Catsiff and Tobolsky show a maximum disagreement of some 25% between measured and predicted dynamic shear modulus and where the range of modulus values involved is very large (20). Nevertheless, the measure of agreement that is obtained here is taken as indicating that to a first approximation the rheological character of nylon is of the same nature as that of the amorphous polymers like polyisobutylene and polymethylmethacrylate and hence due to a relaxation time distribution within the amorphous part of the material. The lack of agreement between predicted and observed loss modulus is much more serious, as can be seen in Fig. 6. Whatever the exact value of the loss modulus in the range  $\log(a_T\omega) = 1$  to 11, it is clear that near  $a_T\omega = 10$  the observed value of  $E''$  lies below that predicted by as much as a factor of 3.5, that there must be a maximum in the observed  $E''$  which is not predicted, and that  $E''$  near  $a_T\omega = 10^{11}$  is larger than predicted. It is especially difficult to see how the observed loss might be smaller than the predicted value, and this discrepancy remains as a troublesome problem. Even in the case of the amorphous polymers, however, the agreement between the experimental loss modulus and the predicted value is less good at a number of frequencies than that between observed and predicted stiffness modulus (10).

The reduction factors,  $a_T$ , which were used to obtain superimposition of the stress relaxation curves and the dynamic tensile modulus vs.  $\log$  frequency curves have been plotted as  $\log a_T$  against  $T^{-1}$  in Fig. 8. The line which has been drawn through these points corresponds to an activation energy of 31 kcal./mole. This value corresponds reasonably with the value

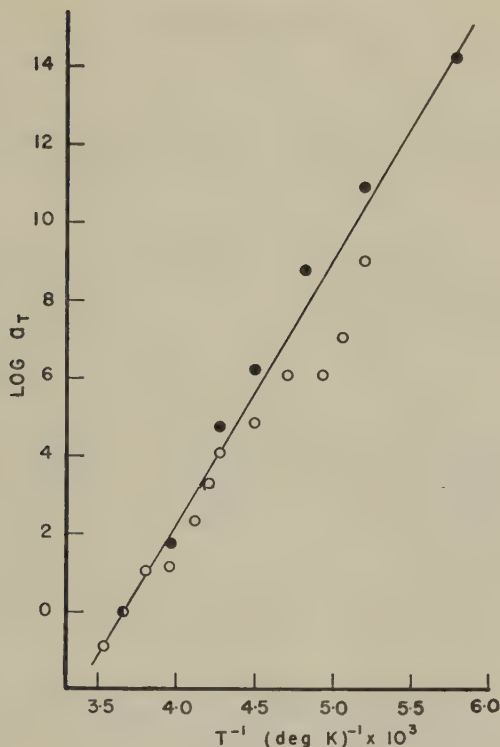


FIG. 8. Reduction factors  $a_T$  for both stress relaxation and dynamic tensile modulus as a function of  $1/T$ . Open circles refer to dynamic tensile modulus, closed circles to stress relaxation modulus.

of 21 kcal./mole given by Woodward *et al.* as an estimate of the activation energy for both the  $\beta$  and  $\gamma$  dispersion mechanisms of nylon 6-6 (12).

### SUMMARY

Results are reported for stress relaxation and forced longitudinal vibration studies on nylon 6-6 monofilaments at temperatures between  $+10^\circ$  and  $-100^\circ\text{C}$ . Although the scatter in the values obtained for the dynamic loss modulus is too large to allow satisfactory interpretation, the dynamic tensile modulus and stress relaxation modulus yield composite curves when the time-temperature superposition principle is applied. The reduction factors,  $a_T$ , for the dynamic and stress relaxation moduli are sufficiently similar that they can reasonably be represented by one function of temperature. The distribution of relaxation times has been calculated from the stress relaxation curves, and values of the dynamic moduli predicted and compared with experimental values.



## ACKNOWLEDGMENTS

The authors thank the Defence Research Board of Canada for their financial support by Grant No. 7570-07. We are also grateful to Dr. R. D. Bennett and the duPont Company of Canada (1956) Ltd. for their kindness in supplying the nylon monofilament, and to Mr. L. G. Wilson of the Defence Research Chemical Laboratories for arranging for the loan of a liquid nitrogen pump.

## REFERENCES

1. TOBOLSKY, A. V., *J. Appl. Phys.* **27**, 673 (1956).
2. FERRY, J. D., in Stuart, H. A., ed., "Die Physik der Hochpolymeren," Vol. 4, Chapt. 6. Springer, Berlin, 1956.
3. WOODWARD, A. E., AND SAUER, J. A., *Fortschr. Hochpolym. Forsch.* **1**, 114 (1958).
4. ANDREWS, R. D., HOFMAN-BANG, N., AND TOBOLSKY, A. V., *J. Polymer Sci.* **3**, 669 (1948).
5. FERRY, J. D., *J. Am. Chem. Soc.* **72**, 3746 (1950).
6. YOSHITOMI, T., NAGAMATSU, K., AND KOSIYAMA, K., *J. Polymer Sci.* **27**, 335 (1958).
7. NAGAMATSU, K., YOSHITOMI, T., AND TAKEMOTO, T., *J. Colloid Sci.* **13**, 257 (1958).
8. CATSIFF, E., OFFENBACH, J. A., AND TOBOLSKY, A. V., *J. Colloid Sci.* **11**, 48 (1956).
9. NAGAMATSU, K., TAKEMURA, T., YOSHITOMI, T., AND TAKEMOTO, T., *J. Polymer Sci.* **33**, 515 (1958).
10. DUNELL, B. A., AND DILLON, J. H., *Textile Research J.* **21**, 393 (1951).
11. QUISTWATER, J. M. R., AND DUNELL, B. A., *J. Polymer Sci.* **28**, 309 (1958).
12. WOODWARD, A. E., SAUER, J. A., DEELEY, C. W., AND KLINE, D. E., *J. Colloid Sci.* **12**, 363 (1957).
13. NINOMIYA, K., AND FUJITA, H., *J. Colloid Sci.* **12**, 208 (1957).
14. QUISTWATER, J. M. R., AND DUNELL, B. A., *J. Appl. Polymer Sci.* **1**, (1959).
15. SCHMIEDER, K., AND WOLF, K., *Kolloid-Z.* **134**, 149 (1953).
16. TOKITA, N., *J. Polymer Sci.* **20**, 515 (1956).
17. FERRY, J. D., AND FITZGERALD, E. R., *J. Colloid Sci.* **8**, 224 (1953).
18. FERRY, J. D., AND WILLIAMS, M. L., *J. Colloid Sci.* **7**, 347 (1952).
19. CATSIFF, E., AND TOBOLSKY, A. V., *J. Colloid Sci.* **10**, 375 (1955).
20. CATSIFF, E., AND TOBOLSKY, A. V., *J. Colloid Sci.* **10**, 375 (1955); see Fig. 4.

## A SPACING LAW FOR LIESEGANG RINGS MERCUROUS IODATE SYSTEM

Prem Behari Mathur and A. S. Lakshmanan

*Central Electrochemical Research Institute, Karaikudi, India*

*Received April 30, 1959, revised August 13, 1959*

A number of theories have been put forward to account for the phenomenon of Liesegang Rings (1). Morse and Pierce (2), Wagner (3), and others (4) made attempts to analyze the phenomenon of periodic precipitation quantitatively. They correlated the time required for the formation of rings with the distances of the rings from the diffusion level. Jablczynski (5), however, gave a relation independent of time for spacings between the rings. From Fick's diffusion equation a new spacing law for Liesegang rings has been derived (6):

$$(x_n - x_{n-1}) = a \left( \frac{S}{C_0 C_0'} \right) e^{\alpha x_n} \quad [1]$$

or

$$\log (x_n - x_{n-1}) = A + \alpha x_n. \quad [2]$$

Here  $x_n$  and  $x_{n-1}$  represent the distances of  $n$ th and  $(n - 1)$ th rings from any sharp level, and  $a$ ,  $\alpha$ , and  $A$  are constants;  $\alpha$  is the spacing coefficient. The symbol  $S$  is the solubility product of the sparingly soluble salt and  $C_0$  and  $C_0'$  are the initial concentrations of the reacting substances.

In Eq. [1]  $e^{\alpha x_n}$  can be expanded and the higher terms in the expression may be neglected in the case of the first few rings, as  $\alpha x_n$  is small in the case of the first few rings. So Eq. [1] reduces to

$$(x_n - x_{n-1}) = A' + \alpha x_n. \quad [3]$$

Now Jablczynski's equation is

$$x_n = ak^n. \quad [4]$$

or

$$\frac{x_{n-1}}{x_n} = \frac{1}{k};$$

or

$$1 - \frac{x_{n-1}}{x_n} = 1 - \frac{1}{k};$$

or

$$(x_n - x_{n-1}) = \alpha' x_n, \quad [5]$$

where  $\alpha'$  is a different constant. Equation [3] differs from [5] in the constant  $A$ . The plot of  $(x_n - x_{n-1})$  against  $x_n$  does not pass through the origin, showing that Eq. [3] is more appropriate than [5]. Equation [3] will give good results for lower order rings only, whereas Eq. [2] gives good results for all rings. It may also be noted that Jableczynski's relation is more sensitive and appropriate in the form represented by Eq. [5] than in that by Eq. [4].

Periodic differences in temperature during day and night affect the constants  $A$  and  $\alpha$  of Eq. [2] and so a slight periodic displacement is expected in the points in the graphs. This effect can be eliminated if the experiment is carried out at constant temperature. The temperature effect was found to be predominant in soft gels like gelatin gel, and therefore precipitate systems which could give rings in agar-agar have been chosen for the present studies. Though the influence of temperature differences during day and night may not be eliminated under ordinary conditions, it is minimized to a large extent if they are not large.

Owing to the fact that in most cases precipitation leads to blurred zones, the quantitative recording of rings attracted little attention by workers. In order to examine Eq. [2] a few new and quite sharp rings systems

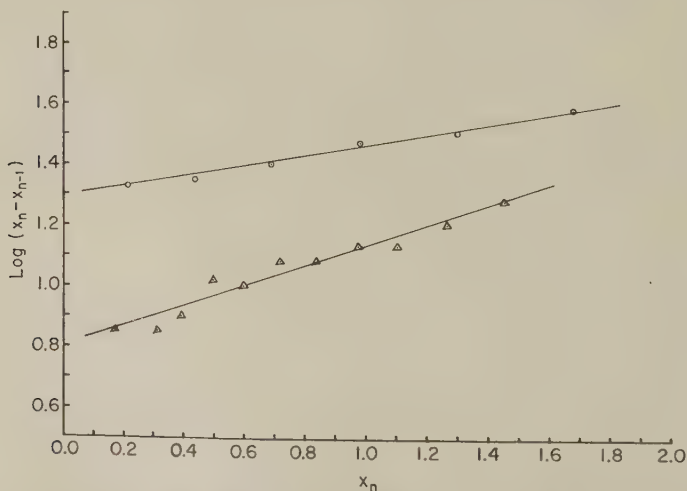


FIG. 1. Mercurous iodate system 1% agar agar gel. ○ 0.016 M KIO<sub>3</sub>; △ 0.0066 M KIO<sub>3</sub>.

as those of mercurous iodate and lead iodate in agar agar gel, and silver chromate in gelatin-agar mixture under acidic pH have been produced. Mercurous iodate system is reported here.

### EXPERIMENTAL

Gels containing 1 %, 0.75 %, and 0.5 % agar agar impregnated with 0.033, 0.016, 0.006, and 0.003 *M* potassium iodate are prepared as follows: 3 g.

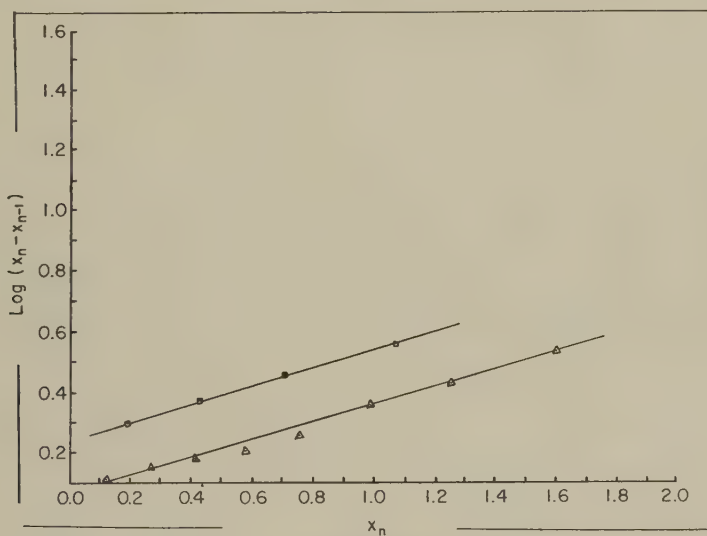


FIG. 2. Mercurous iodate system 0.75% agar agar gel.  $\Delta$  0.0066 *M*  $\text{KIO}_3$ ;  $\square$  0.0033 *M*  $\text{KIO}_3$ .

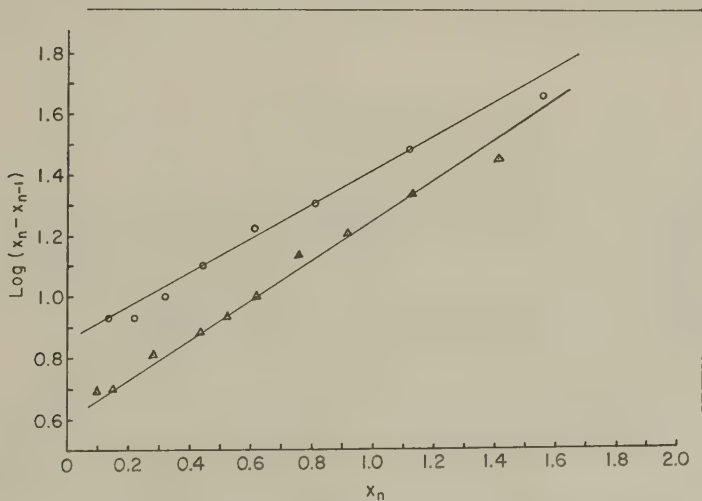


FIG. 3. Mercurous iodate system 0.5% agar agar gel.  $\odot$  0.016 *M*  $\text{KIO}_3$ ;  $\Delta$  0.0066 *M*  $\text{KIO}_3$ .

of agar agar fibers are accurately weighed and washed with distilled water. About 100 ml. of distilled water are added, and the mixture is heated for about 15 minutes in a water bath and then for half an hour over the flame. The mixture is kept continuously stirred during heating. It is seen that no undissolved particles remain in the solution and then the whole is made up to 150 ml. with hot water (at 80°C.) and shaken well to ensure uniform concentration. Now, to prepare 1 % agar agar gel containing 0.016 *M* potassium iodate, 25 ml. of the prepared solution is taken, 5 ml. of 0.16 *M*  $\text{KIO}_3$  solution added, and the resulting mixture made up to 50 ml. with hot water. This is mixed thoroughly and placed in different test tubes for setting. In the same way other concentrations are also prepared.

After 48 hours 5 ml. of the saturated mercurous nitrate solution (30°C.) are placed in each of the test tubes and the test tubes are corked and left undisturbed for 5 days in the diffused room light. Beautiful, sharp, white discs of precipitate, having wide spaces in between, are obtained. The system is of direct nature, viz., the distances between successive rings go on increasing when moving away from the diffusion level. The rings are not good in low concentrations of potassium iodate, for example, in 0.003 *M*. The best results are observed in systems containing 0.016 *M* potassium iodate.

The ring spacings are measured by cathetometer. One sharp ring has been chosen as the reference level for the subsequent measurements. The nature of Eq. [2] is not affected by using any reference level; only the values of the constants are altered slightly.

The data have been plotted in Figs. 1, 2, and 3. The curves are straight lines in agreement with the equation.

The authors wish to express their gratitude to Professor K. S. G. Doss, Director, Central Electrochemical Research Institute, Karaikudi, for his interest in the work.

#### REFERENCES

1. STERN, K. H., *Chem. Revs.*, **54**, 83 (1954).
2. MORSE, H. W., AND PIERCE, C. W., *Z. physik. Chem.* **45**, 589 (1903).
3. WAGNER, C., *J. Colloid Sci.* **5**, 85 (1950).
4. NIKOFOROV, V. K., AND KHARAMONENKO, S. S., *Acta Physicochim. U.R.S.S.* **8**, 25 (1938); RAMAN, C. V., AND RAMAIAH, K. S., *Proc. Indian Acad. Sci.* **9A**, 455 (1939); RAMAN, C. V., AND RAMAIAH, K. S., *Proc. Indian Acad. Sci.* **9A**, 467 (1939).
5. JABLONZYNSKI, K., *Bull. soc. chim. France* [4], **33**, 1952 (1923).
6. MATHUR, P. B., communicated to *Bull. Chem. Soc., Japan*.



## THE CHARACTERIZATION OF DENATURED PROTEINS BY ADSORPTION INDICATORS<sup>1</sup>

Ira Blei<sup>2</sup> and Benjamin Carroll

*Rutgers University, Newark, New Jersey*

*Received September 15, 1959, revised December 15, 1959*

### ABSTRACT

The interaction between crystal violet, a cationic dye, and native and denatured forms of bovine serum albumin has been investigated using spectrophotometry and equilibrium dialysis. Changes in the extent of binding as a function of pH indicate that the sites of binding of crystal violet by bovine serum albumin may be the carboxylate groups. The complex formation was used to characterize the proteins through thermodynamic quantities derived from an analysis of binding data, and by the unique spectral properties of the dye bound to the different substrates.

The interaction of dyestuffs with proteins appears to be closely related to the fine structure or detailed local configurations of the constituent polypeptide chains (1-4). In view of this, dye adsorption methods have been used in the study of protein denaturation, since changes in the secondary and tertiary structures of proteins would be expected to result in changes in the binding of dye by protein. Klotz (5) found that exposure of bovine serum albumin [BSA] to heat and alkali destroyed the protein's affinity for methyl orange. The exposure of BSA to high concentrations of urea was shown by Uzman (6) to increase its capacity for binding methyl orange. The differences in reactions between congo red and native and denatured ovalbumin and serum albumin have been used by Haurowitz and co-workers (7) in a study of thermal denaturation. In none of these cases was the change in binding properties of the protein used to characterize the denatured protein thoroughly. Previously, the use of metachromatic dyestuffs in adsorption studies of proteins in solution has not been exploited. The reason for this may be that in a study of the multiple equilibria between the dye and the protein, additional equilibria in the form of reversible aggregation of the dye would complicate the treatment of such systems. However, it can be shown (8) that the metachromatic dyes may adhere to

<sup>1</sup> This material is taken from the dissertation submitted by Ira Blei in partial fulfillment of the requirements for the Ph.D. degree of Rutgers University, New Brunswick, New Jersey.

<sup>2</sup> Present address: Lever Bros. Research Center, Edgewater, New Jersey.

Beer's law at sufficiently high dilutions and that these materials probably are in monomeric form at infinite dilution. In this investigation several classes of metachromatic dyes were scanned in an attempt to find a cationic substance which was bound by a native protein. As a result of this preliminary investigation, it was found that both native and variously denatured forms of bovine serum albumin interacted with the cationic dye, crystal violet [CV]. The adsorption of this metachromatic dye was shown to reflect properties of the colloidal substrate in a sensitive manner. This report concerns the characterization of native and variously denatured bovine serum albumin through interaction with the cationic dye, crystal violet.

### EXPERIMENTAL

Crystalline bovine serum albumin, Lot No. 29633, was purchased from Armour and Company. The triphenylmethane dyes employed were of histological grade and were purchased from the National Aniline Company. These were purified by precipitation of the carbinol with sodium hydroxide, followed by neutralization of the dye base with hydrochloric acid and crystallization as the cationic chloride. All other chemicals used were either C.P. or reagent grade.

A moisture determination of the crystalline native BSA was made by drying at 100°C. for 2 hours, and all protein stock solutions subsequently prepared were corrected for this moisture. Occasionally during the course of this investigation, the protein concentration of a solution was checked using the absorption at 279  $\mu$ . Sterile, distilled water was used to prepare all protein stock solutions. Millimolar stock solutions of the dyes were prepared and placed in amber, paraffined bottles for storage. Spectrophotometric checks of CV showed that the concentration of this dye remained constant over several months. Colorimetric determinations were made utilizing a Beckman Model DU spectrophotometer, which was provided with a cooling block. This device permitted temperature control to within  $\pm 0.2^\circ\text{C}$ . Calibrated cuvettes having a 1-cm. light path were used in all determinations.

The extent of binding of CV below  $1 \times 10^{-5} M$  dye concentration was determined by a spectrophotometric technique, using a molar extinction coefficient at 600  $\mu$  of  $8.5 \times 10^4$  for the free form of the dye, and  $9.3 \times 10^4$  for the bound dye at pH 7 and 23°C. This value for the extinction coefficient of the bound dye was obtained by measuring the extinction coefficients of a series of solutions of constant concentration of buffered dye as a function of increasing protein concentration. The extinction coefficient of the dye reached a maximum value of  $9.3 \times 10^4$ , which remained constant above 0.16% BSA. The details of the method to determine the extent of adsorption are given by Klotz (9).

The interaction between BSA and CV above  $1 \times 10^{-5} M$  dye was meas-

ured by the method of equilibrium dialysis. Ten milliliters of 0.2% native BSA, in 0.02 *M* phosphate buffer, pH  $7.0 \pm 0.05$ , was added to a bag of Visking sausage casing. This was placed in a rubber stoppered test tube, containing 10 ml. of CV of varying concentrations, buffered at pH  $7.0 \pm 0.05$  with 0.02 *M* phosphate buffer. The tube and its contents were rocked gently at constant temperature. The concentration of dye in the outer solution was determined spectrophotometrically. Control experiments were used to determine the extent of binding to the dialysis casing. These measurements also established that there was a uniform distribution of the dye on both sides of the membrane in the absence of protein. The value of " $\gamma$ ", defined as the moles of bound dye per mole of total protein, was determined as a function of time for a period of 4 days. In the case of the highest initial concentration, it was found that the extent of binding remained constant after the first 15 hours.

Crystalline bovine serum albumin was denatured in three ways: by exposure to dilute alkali, concentrated urea, and heat. The alkali denaturation was effected by preparing a 1.4% solution of native BSA in 0.06 *M* KOH. The mixture was kept at 5°C. for 50 hours. At the end of that time the solution was neutralized with HCl. Denaturation under these conditions was considered complete since the treated protein was completely insoluble at pH 4.7, and, in addition, did not bind methyl orange or orange I by spectral criteria. A 3% native BSA solution was prepared which was also 7 *M* with respect to urea. The solution was maintained at 30°C. for 72 hours. At the end of that time the solution was transferred to a dialysis sack and exhaustively dialyzed against distilled water until all the urea was removed. A gelatinous precipitate appeared in the dialysis sack, and at the end of the dialysis it was filtered off. The final solution contained approximately 40% of the original protein. The dialyzed solution was examined for urea by the Conway microdiffusion (10) method using urease, and it was found that none was present. Amounts of urea readily detected by the above technique were added to dye solutions and were found to have no effect on the spectrum of crystal violet. Native BSA was heat denatured by heating a solution of the protein buffered at pH 7 with 0.01 *M* phosphate buffer (at 80°C.) for 3 hours, until the previously mentioned criteria of solubility and anionic dye binding ability were satisfied.

## RESULTS AND DISCUSSION

Crystal violet belongs to a class of cationic dyes which is described as metachromatic (11). Such dyes stain mast cells and cartilage a color different from that of their dilute aqueous solutions. Metachromatic effects have been correlated with changes in the electronic states of dyes (12) and with their state of aggregation (11). We found Beer's law to hold for CV from  $1 \times 10^{-7}$  mole/l. up to  $1 \times 10^{-5}$  mole/l. in 0.01 *M*  $\text{PO}_4$  buffer. Beyond

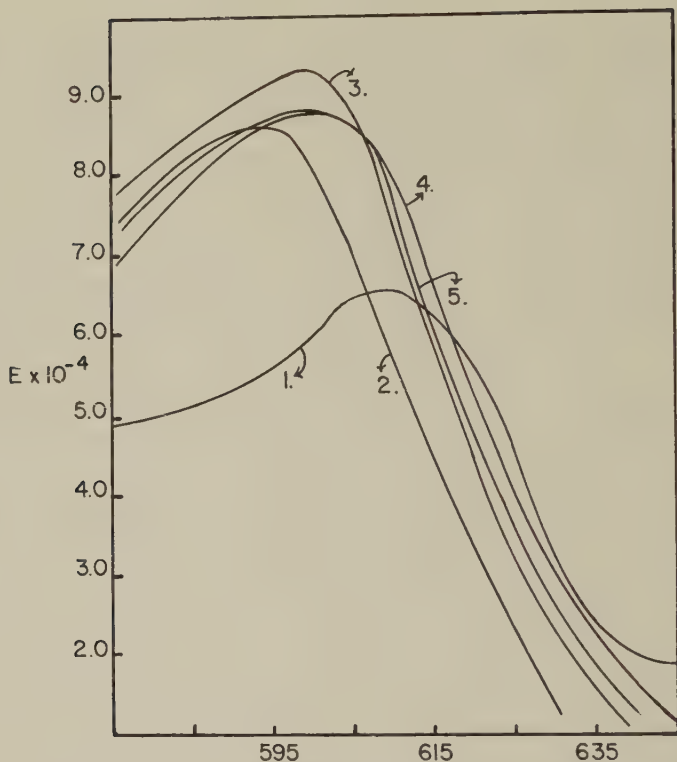


FIG. 1. Spectral curves of crystal violet bound to various forms of bovine serum albumin, at pH 7 and 23°C. Curve 1, alkali-denatured BSA; curve 2, dye alone; curve 3, native BSA; curve 4, heat-denatured BSA; curve 5, urea-denatured BSA.

that concentration, the extinction coefficient at the absorption maximum falls and the extinction coefficient of a shoulder in the curve at shorter wavelengths begins to increase, which is typical of metachromatic dyes. All spectrophotometric studies were therefore performed at concentrations less than  $1 \times 10^{-5}$  mole/l. of dye, and in 0.01 M  $\text{PO}_4$  buffer. Under these conditions, it was probable that the principal species of dye present was the monomeric form. The criterion adopted to demonstrate the binding of the triphenylmethane dyes by native BSA involved a change in the spectral characteristics of a buffered solution. This was verified by equilibrium dialysis measurements. It was found that spectral changes occurred which indicated that ethyl violet, victoria blue, brilliant green, and malachite green were bound. In addition, it was found that rosaniline and para rosaniline did not interact with the protein. The latter point verifies the observation of Cavalieri *et al.* (13). The spectral curves of CV bound to various denatured forms of BSA may be seen in Fig. 1. The dye in these



systems may be considered to be completely bound, since the extinction coefficients at the absorption maxima remain constant with varying concentration of protein. This also indicates that the bound form of the dye follows Beer's law. It is important to note that the spectra of the dyes bound to each form of the protein are different and apparently unique. In each case there is a shift in the absorption maximum to longer wavelengths; however, the extent of this shift varies for each bound form of the dye. In addition, the molar extinction coefficients at various wavelengths are different for each form of the bound dye and appear to be characteristic of the substrate to which it is bound. The values of the extinction coefficients vs. wavelength for each modified protein may be found in Table I.

It has been found in several cases that regardless of the type of substrate which binds anionic dyes, e.g., starch-congo red (14) and soluble protein-methyl orange (15), the extinction coefficient of the bound form of the dye is the same. It is apparent that the spectral properties of these materials cannot be used to distinguish between colloidal substrates. On the other hand, it has been established that in interactions between polyanions, e.g., nucleic acids (16), mucopolysaccharides (17), and cationic dyes, the changes in extinction coefficients and the wavelength maxima shifts are, in part, a function of the type of substrate binding the dyes. In addition, it was reported in these cases that the variation in extinction coefficient at some fixed wavelength did not stop with variation of concentration of colloidal substrate. This may have been because not all the dye had been bound or because the increase in concentration caused a continual variation in the configuration of the polyanion and consequently changes in the environment of the bound dye (18). In the case of the binding of CV by the various forms of BSA, continual variation in substrate concentration caused no change in spectral characteristics beyond a certain concentration of protein. We may infer from this that the configurations of these proteins are probably not significantly altered by the binding

TABLE I

*Spectral and Thermodynamic Characteristics of the Interaction between CV and Various Denatured Forms of BSA in 0.01 M Phosphate Buffer at pH 7*

Form of BSA	$Em \times 10^{-4}$			$k_a^0 \times 10^{-6}$	$n_a$
	595 $\mu$	620 $\mu$	630 $\mu$		
None	8.6	4.25	1.6	—	—
Native	9.3	4.3	2.25	0.93	1.3
Urea-treated	8.65	5.05	2.75	0.79	17.7
Heat-treated	8.65	5.9	3.1	9.05	20.8
Alkali-treated	5.6	5.35	3.6	2.29	4.8



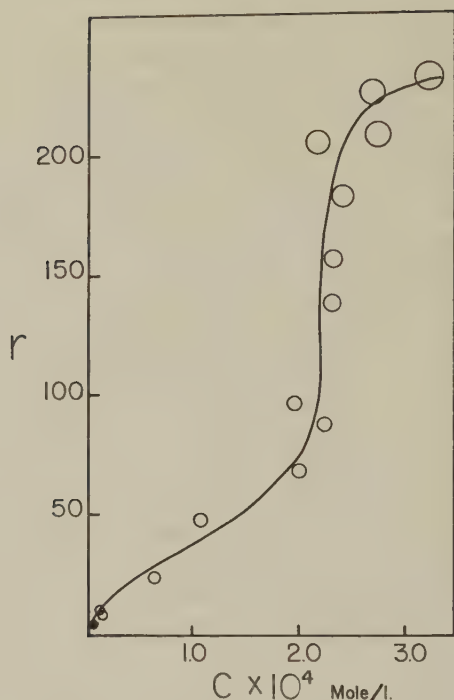


FIG. 2. Adsorption isotherm of crystal violet on native bovine serum albumin at pH 7 and 23°C.

reaction at these concentrations of dye, and probably do not exist in solution as Gaussian coils. The data presented here provide a useful tool for characterization of BSA which has been altered by the methods described above.

Quantitative analysis of the binding reaction between CV and modified BSA should provide an additional method, independent of the above technique, for the characterization of the proteins. We present first adsorption data for the binding of CV by native BSA to establish a basis for comparison with the modified proteins. The isotherm for CV bound to native BSA may be found in Fig. 2. Equilibrium dialysis measurements verified the spectrophotometric determination of adsorption data below  $1 \times 10^{-5}$  mole/l. The filled-in circle at low dye concentration in Fig. 2 represents the upper limit of the spectrophotometric method. The abscissa is  $C$ , the concentration of free dye, and the ordinate is  $r$ , the moles of bound dye per mole of protein. The binding increases rapidly beyond  $r$  values of 110 and appear to approach a limit of about 240. The first value of  $r \sim 110$  corresponds to the number of carboxyl groups per mole of protein. The rapid increase of  $r$  with increase in dye concentration at that point may

correspond to the filling of all binding sites, and the neutralization of the charge of the bound dye. Crystal violet does not follow Beer's law beyond  $2 \times 10^{-5}$  mole/l. in aqueous solution. It would seem likely, therefore, that if all binding sites were occupied, and the charge on the bound dye ions thus reduced, aggregation of the dye by dimerization with previously bound ions could occur. The leveling off of the binding occurs at a point where  $r$  is about twice the value of the number of carboxylate groups per mole of protein, indicating that the cessation of binding occurs after dimerization of the dye on the protein.

Cockbain (19) found that the limit of binding of the anionic detergent sodium dodecyl sulfate to BSA corresponded to twice the acid-binding capacity of that protein. Carroll (20) also found that in acid solutions BSA bound an amount of methyl orange equal to twice the acid-binding capacity of the protein. It is felt therefore that the maximum number of binding sites for CV on BSA corresponds to the number of carboxylate groups on the molecule, and further that the limiting value of  $r$  attained in this work reflects the tendency of the dye to aggregate with dye already bound to the protein.

To substantiate the hypothesis that CV may be bound to the carboxylate groups of BSA, the effects of variation in pH upon the extent of binding were investigated. The results of this study may be seen in Fig. 3 plotted as the molar extinction coefficient,  $E_m$ , vs. pH at 13°C. The distance be-

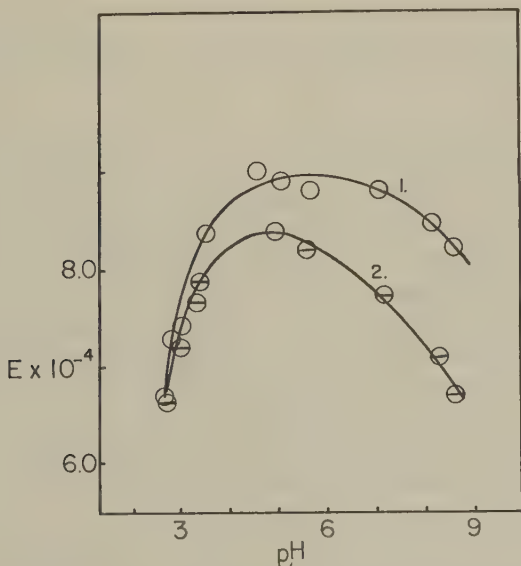


FIG. 3. Effect of pH on the extent of binding of crystal violet by bovine serum albumin at 13°C. Curve 1, values of the molar extinction coefficient of dye at  $600 \mu$  in the presence of protein; curve 2, the same systems in the absence of protein.

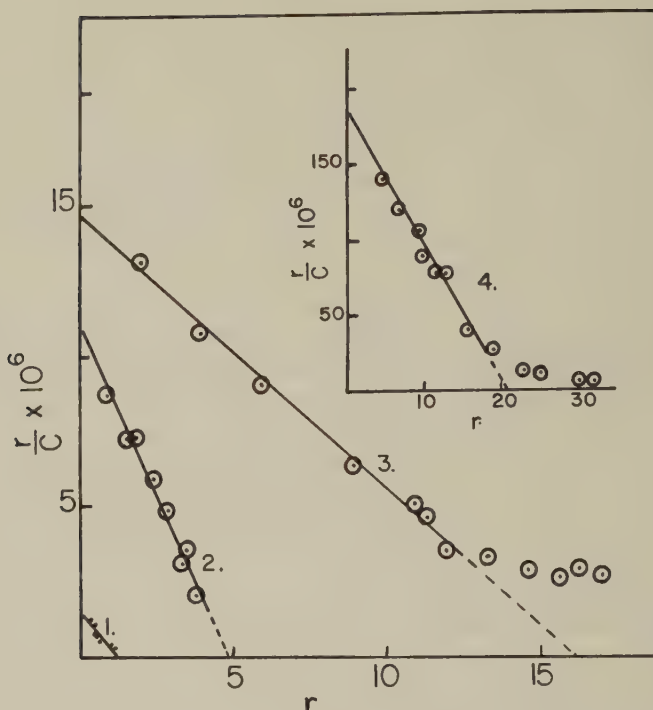


FIG. 4. Adsorption isotherms of crystal violet on various forms of bovine serum albumin, at pH 7 and 23°C. Curve 1, native protein; curve 2, alkali-denatured protein; curve 3, urea-denatured protein; curve 4, inset, heat-denatured protein.

tween the two curves is a measure of the extent of binding, and it can be seen that the difference approaches zero at about pH 2.5. The isoelectric point of BSA is at pH 4.7. Therefore, both the protein and dye are positively charged below pH 4; yet the binding apparently does not cease until the carboxyl groups approach complete neutralization (21). This evidence lends weight to the hypothesis that the sites of binding of CV by BSA may be the carboxylate groups.

The spectral properties of the CV-BSA systems described previously permitted the determination of adsorption data at low dye concentrations. These may be seen in Fig. 4. The data were obtained by a spectrophotometric technique and were verified by equilibrium dialysis. The results are plotted according to the equation (22):

$$r/C = kn - kr, \quad [1]$$

where  $r$  = moles of bound dye/mole protein;  $C$  = the free dye concentration;  $n$  = the maximum number of binding sites;  $k$  = the intrinsic affinity of each site for a dye ion. Equation [1] as written implies ideal binding, with all  $k$ 's equal and no interaction between bound ions. It has been

shown (23) that if measurements are made at low enough concentrations of ligand, every system of the type under discussion will yield data which conform to the above linear plot. According to one's choice of ligand concentration, one may find ideal binding in one case and not in another, where in fact both systems could be nonideal. In the case of CV bound to native and alkali-denatured BSA, over the concentration range probed, the data yielded linear plots according to Eq. [1].

Adsorption data with both heat- and urea-denatured BSA gave linear plots at low concentrations of dye but at higher concentrations showed curvature, similar to the isotherms reported by Carsten and Eisen (24) for neutral molecules, and by Goodman (25) for fatty acid anions bound by BSA. The fact that the adsorption isotherms of CV on native and alkali-denatured BSA were linear is fortuitous since we have shown that the value of  $n$  is in the neighborhood of 110 for native BSA, and the linear plot of Eq. [1] yields a value of  $n$  of 1.3 for the native protein. The problem then is to evaluate the quantity ( $kn$ ) in as meaningful a way as possible, since it is the only theoretically significant quantity which can be derived from the experimental data. Carsten and Eisen found that  $kn$  varied significantly with temperature for the binding of neutral molecules by BSA, and so reported the enthalpy of binding as a function of structure of ligand. In our case, we found that the variation of  $kn$  with temperature was about +3 kcal./mole, and was the same for the interaction of the dye with each of the forms of BSA studied. It has been shown (26) that in the case of heterogeneity of binding sites it is possible to represent the data, over limited concentration ranges, with an equation which assumes several kinds of binding sites, each having an intrinsic binding constant,  $k_a^0$ ,  $k_b^0$ , etc., and a number of binding sites  $n_a$ ,  $n_b$ , etc., associated with it. We have shown that the above dye concentrations which lead to low values of  $r$ , the interaction between dye and protein becomes increasingly influenced by the tendency of the dye to aggregate. It therefore seems appropriate to focus our attention on the binding at low concentrations of dye since we are interested in characterizing the protein-dye interaction. Because we are dealing with the binding of a dye by proteins which have been derived from a common precursor, we felt that, provisionally at least, we might be able to obtain the most useful data for characterizing the structural changes which have occurred if we used the values of  $kn$  and  $n$  for the interaction which corresponded to the initial linear portion of the isotherm. We could then represent the structural alterations which occurred upon denaturation by the changes in  $k_a^0$  and  $n_a$  using the native protein as our standard. The data obtained in this manner may be found in Table I.

It is interesting to note that for the monodisperse proteins, native and urea denatured (27), the values of  $k_a^0$  are close. However, the number of sites available on the urea-denatured sample has increased, corresponding to Uzman's findings with urea-denatured BSA and methyl orange. The

heat- and alkali-denatured BSA were polydisperse, with number-average molecular weights between 2 and  $4 \times 10^5$  (28), and their  $k_a^0$ 's were somewhat higher than for the monodisperse proteins. The fact that the  $k_a^0$ 's are different for the interaction of CV with each form of denatured BSA supports the finding that the spectrum of each bound form of the dye was different. One would expect differences in the microenvironment to lead to differences in the electronic states of the bound dye.

#### ACKNOWLEDGMENTS

We wish to thank the Research Council of Rutgers University for its encouragement and financial support during this work. The authors also wish to acknowledge the contributions of D. H. Rackowitz in the initial stages of this investigation.

#### REFERENCES

1. KARUSH, F., *J. Am. Chem. Soc.* **73**, 1246 (1951).
2. KARUSH, F., *J. Phys. Chem.* **56**, 70 (1952).
3. KLOTZ, I. M., BURKHARD, R. K., AND URQUHART, J. M., *J. Am. Chem. Soc.* **74**, 202 (1952).
4. KLOTZ, I. M., AND URQUHART, J. M., *J. Am. Chem. Soc.* **71**, 1597 (1949).
5. KLOTZ, I. M., TRIWUSH, H., AND WALKER, F. M., *J. Am. Chem. Soc.* **70**, 2935 (1948).
6. UZMAN, L. L., *Nature* **171**, 653 (1953).
7. HAUROWITZ, F., DiMOIA, F., AND TEKMAN, S., *J. Am. Chem. Soc.* **74**, 2265 (1952).
8. TURGEON, L., AND LAMER, V. K., *J. Am. Chem. Soc.* **74**, 5988 (1952).
9. KLOTZ, I. M., WALKER, F. M., AND PIVAN, R. B., *J. Am. Chem. Soc.* **68**, 1486 (1946).
10. CONWAY, E. J., "Microdiffusion Analysis and Volumetric Error." Crosby, Lockwood, & Son, London, 1939.
11. MICHAELIS, L., AND GRANICK, S., *J. Am. Chem. Soc.* **67**, 1212 (1945).
12. MATAGA, N., *J. Inst. Polytech., Osaka City Univ.* **4**, 189 (1953).
13. CAVALIERI, L., *et al.*, *J. Am. Chem. Soc.* **73**, 4902 (1951).
14. CARROLL, B., AND VAN DYK, J. W., *J. Am. Chem. Soc.* **76**, 2506 (1954).
15. CARROLL, B., Unpublished observations.
16. MORTLAND, F. W., DeBRUYN, P. P. H., AND SMITH, N. H., *Exptl. Cell Research* **7**, 201 (1954).
17. SCHUBERT, M., AND LEVINE, A., *J. Am. Chem. Soc.* **75**, 5842 (1953).
18. FUOSS, R. M., AND STRAUSS, U. P., *Ann. N. Y. Acad. Sci.* **51**, 836 (1949).
19. COCKBAIN, E. G., *Trans. Faraday Soc.* **49**, 104 (1953).
20. CARROLL, B., *Trans. N. Y. Acad. Sci.* **12**, 152 (1950).
21. TANFORD, C., *J. Am. Chem. Soc.* **72**, 441 (1950).
22. SCATCHARD, G., *Ann. N. Y. Acad. Sci.* **51**, 660 (1949).
23. SCHELLMAN, J. A., LUMRY, R., AND SAMUELS, L. T., *J. Am. Chem. Soc.* **76**, 2808 (1954).
24. CARSTEN, M. E., AND EISEN, H. N., *J. Am. Chem. Soc.* **75**, 4451 (1953).
25. GOODMAN, D., *J. Am. Chem. Soc.* **80**, 3887 (1958).
26. SCATCHARD, G., SCHEINBERG, J. H., AND ARMSTRONG, S. H., *J. Am. Chem. Soc.* **72**, 535 (1950).
27. NEURATH, H., COOPER, G. R., AND ERICKSON, J. O., *J. Biol. Chem.* **142**, 249 (1942). Confirmed in this laboratory.
28. Determined in this laboratory.



## AN EXTENSION OF GOODEVE'S IMPULSE THEORY OF VISCOSITY TO PSEUDOPLASTIC SYSTEMS

Thomas Gillespie

*Physical Research Laboratory, 2-280 Building, The Dow Chemical Company,  
Midland, Michigan*

*Received December 28, 1959*

### ABSTRACT

An attempt has been made to derive a theory of pseudoplasticity which may be used as a guide in combined studies of rheology and flocculation kinetics. Goodeve's impulse theory of viscosity was used as a starting point. The shear stress-shear rate relation obtained is a more general form of the well-known Williamson empirical equation for pseudoplasticity. The behavior of a given system may be traced in terms of link formation and link rupture rate constants which are related to flocculation and deflocculation rate constants which are susceptible to experimental investigation. Some preliminary data obtained with thickened pseudoplastic latex systems are used to illustrate the application of the theory.

### I. INTRODUCTION

It is generally recognized that the rheology of colloidal systems is connected with the state of flocculation and possible changes in it with changes in shear rate. The precise manner in which aggregation affects flow properties will not be known until much more pertinent experimental evidence is available, particularly data from combined studies of flocculation and rheology. At the moment there is a need for a working hypothesis which can be used to correlate data and help in the choice of the kinetic experiments which are needed to back up rheological studies.

This theory should introduce flocculation phenomena in such a way as to make these independent experimental checks possible. Goodeve's general impulse theory of viscosity (1) seems to be an appropriate basis for the development of such a theory.

Goodeve began by assuming that strictly hydrodynamic or Newtonian effects and particle interaction effects are simply additive. His basic equation is

$$S = \eta^*G + \theta, \quad [1]$$

where  $S$  is the shear force per unit area and  $G$  is the shear rate. Here  $\eta^*$  is a parameter which is descriptive of Newtonian effects;  $\theta$  refers to particle interaction effects. Goodeve called it the coefficient of thixotropy. This

quantity should describe all types of particle interaction and may be more aptly termed "the Goodeve stress." It may be time dependent as well as shear dependent.

To calculate  $\theta$  Goodeve proposed (1) that when shearing occurs links between particles would be stretched, broken, and reformed, and during this process an impulse would be transmitted from a fast-moving layer to a slower adjacent layer. Non-Newtonian behavior would be due to the effect of shear on the number of links, the average life of a link, and any change in the size of the interacting particles. The momentum transferred per unit area from one layer to the next per second by the interaction of particles is represented by  $\theta$ .

When the number of links, the link lifetime, and the particle size are independent of shear the momentum transfer is directly proportional to the shear rate and the system is Newtonian. Probably because Goodeve intended his paper (1) to be a preliminary introduction to his general ideas he considered only one other case in detail, namely, that in which particle size is constant and the number of links and link lifetime are not affected by thermal effects. His calculations predicted that in this case  $\theta$  would be constant and Eq. [1] would be descriptive of an ideal Bingham body. His theory offers the most complete explanation of such a system that has been put forward so far.

In studying industrial rheological problems we have found that Goodeve's theory helps one to trace qualitatively what occurs in various systems. This has prompted the attempt to extend his theory quantitatively to some of the simpler cases of rheological behavior commonly encountered. The important phenomenon of pseudoplasticity was chosen first because of the absence of time effects in the normal type of rheological experiment.

A shear stress-shear rate relation for pseudoplastic system was derived by taking into account thermal effects as well as shear effects. Using certain approximations it reduces to the well-known Williamson empirical relation (2, 3) which has been defended by Nieuwenburg (3, 4) in comprehensive experiments. The constants in the general equation and in the Williamson equation are expressed in terms of physical quantities which should be subject to independent experimental study. Some preliminary data have been obtained which indicate that the kinetic-impulse approach offers a promising working hypothesis for rheological studies.

## II. DERIVATION OF THE SHEAR STRESS-SHEAR RATE RELATION FOR PSEUDOPLASTIC SYSTEMS

To calculate  $\theta$  Goodeve (1) assumed that the force characteristic of a link obeyed Hooke's law and the link was broken when the link extension,

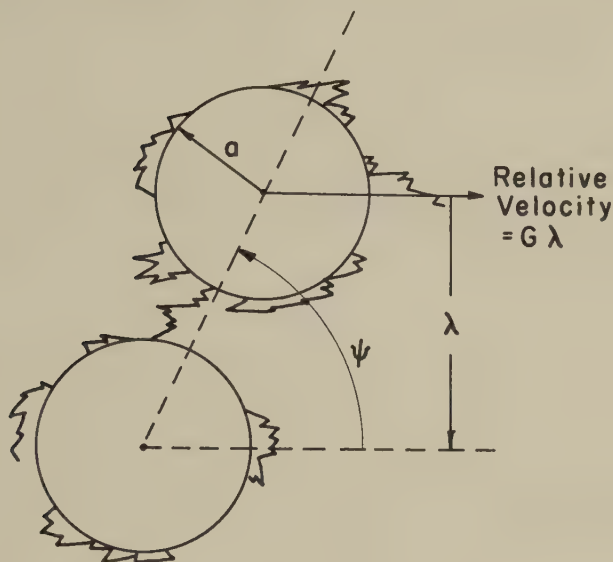


FIG. 1. Schematic illustration of the interaction of two latex particles coated with methylcellulose.

denoted by  $x$ , was equal to a critical value  $x_c$ . His expression for the impulse per collision, denoted by  $I$ , is

$$I = \int_0^{t_c} H \lambda G t \, dt, \quad [2]$$

where  $H$  is the modulus of elasticity,  $t_c$  is the duration of the impulse, and  $\lambda$  is as illustrated in Fig. 1. Taking  $\lambda$  to be constant during a collision he integrated Eq. [2] to get

$$I = \frac{H \lambda G t_c^2}{2}. \quad [3]$$

The assumption that  $\lambda$  is a constant implies that the angle through which contact is maintained is small or that there is rectilinear separation.

Using Eq. [3] Goodeve calculated the transfer of momentum from one layer to another per cm.<sup>2</sup>/sec., i.e.,  $\theta$ . His result is

$$\theta = \frac{H \lambda^2 G}{2} t_c n_c, \quad [4]$$

where  $n_c$  is the number of links per cubic centimeter.

To determine  $n_c$  it is convenient to consider the number of links formed

by each particle. Let  $\nu$  equal the average number of links involving a given particle

$$\frac{d\nu}{dt} = KN - \beta\nu, \quad [5]$$

where  $K$  is the rate constant descriptive of the rate at which links are formed and  $\beta$  is a rate constant descriptive of the rate of link rupture.

At equilibrium

$$\nu = \frac{KN}{\beta}; \quad [6]$$

taking into account the fact that each link is shared by two particles,

$$n_c = \frac{KN^2}{\beta}; \quad [7]$$

combining Eqs. [4] and [7] and taking  $t_c$  equal to  $1/\beta$

$$\theta = \frac{H\lambda^2 KN^2 G}{4\beta^2}. \quad [8]$$

As the variation of  $K$  and  $\beta$  with shear rate is known, Eq. [8] is the required expression for the Goodeve stress.

The particles may be brought into contact by Brownian movement or by their relative motion due to shear. Taking the probability of collision by each mechanism to be independent of the other

$$K = (K_0 + K_1 G)n_L, \quad [9]$$

where  $K_0$  is the rate constant for the flocculation of particles due to Brownian movement;  $K_1 G$  is the rate constant for flocculation due to shear; and  $n_L$  is the number of links formed when two particles come in contact.

For dilute, homogeneous systems, in which there is only one link when two particles come in contact, Schmoluchowski (5, 6) has shown

$$K_0 = 8\pi D a_{\text{eff}} W, \quad [10]$$

where  $D$  is the relative diffusion coefficient for two particles;  $a_{\text{eff}}$  is the effective radius for contact; and  $W$  is a factor determined by the forces of interaction (7). The term  $K_0$  is equal to twice the flocculation rate constant one would measure in an ultramicroscope cell (8).

It has also been shown for the same simple systems (7)

$$K_1 = 32a_{\text{eff}}^3/3. \quad [11]$$

Taking the probability of rupture of links by thermal processes and by shear to be independent

$$\beta = \beta_0 + \beta_1 G, \quad [12]$$

where  $\beta_0$  and  $\beta_1 G$  are descriptive of thermal rupture and shear-induced rupture, respectively. Following Goodeve's arguments (1) it can be shown

$$\beta_1 = \bar{\lambda}/X_c, \quad [13]$$

where  $X_c$  is the critical separation for rupture if there were no thermal effects on rupture;  $\bar{\lambda}$  is the mean value of  $\lambda$  in Fig. 1.

Combining Eqs. [1], [8], [9], [12], and [13],

$$S = G + \frac{E_A N^2 (K_0 + K_1 G) G}{2(\beta_0/\beta_1 + G)^2}, \quad [14]$$

where

$$E_A = \frac{1}{2} H X_c^2 \cdot n_L = \epsilon_A n_L. \quad [15]$$

Here  $\epsilon_A$  is the binding energy of each link, and  $E_A$  is the total binding energy between two particles.

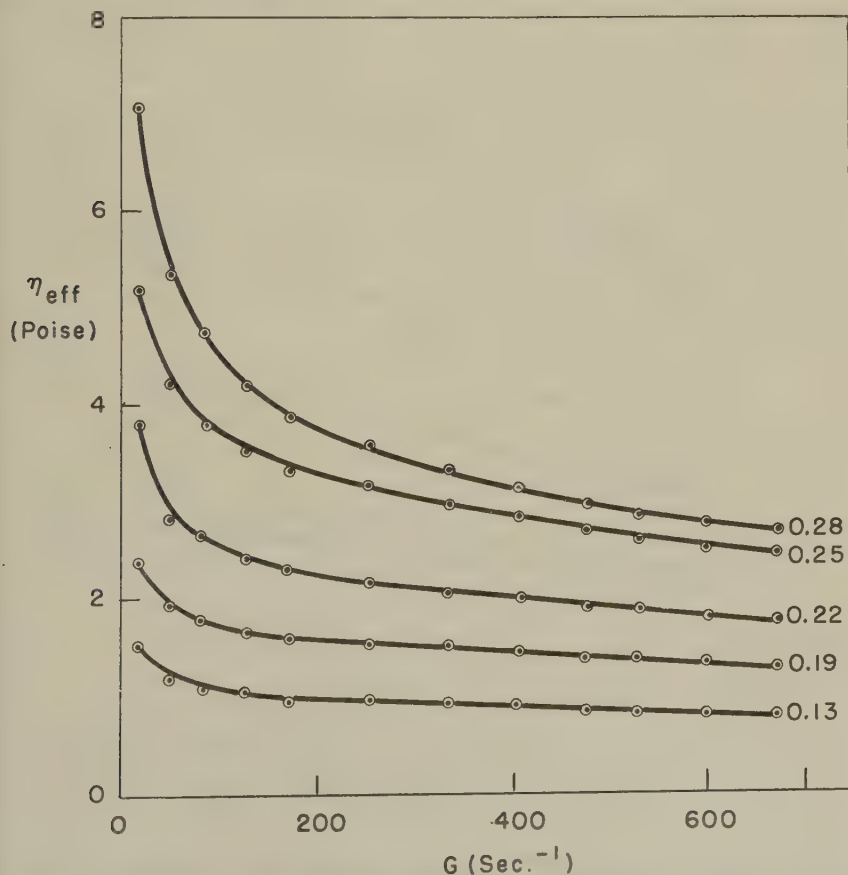


FIG. 2. Variation of the effective viscosity of pseudoplastic thickened latexes with changes in shear rate. The numbers refer to the fractional latex solids volume.



At high shear rate

$$S = \eta^*G + \frac{C_1G}{2C_2 + G}; \quad [16]$$

$$C_1 = \frac{1}{2}E_A K_1 N^2; \quad [17]$$

$$C_2 = \beta_0/\beta_1. \quad [18]$$

Equation [16] is equivalent to the Williamson empirical equation (2). Here  $\eta^*$  is the plastic viscosity and  $C_1$  is the dynamic yield value, both being measured at a shear rate such that  $G \gg 2C_2$ .

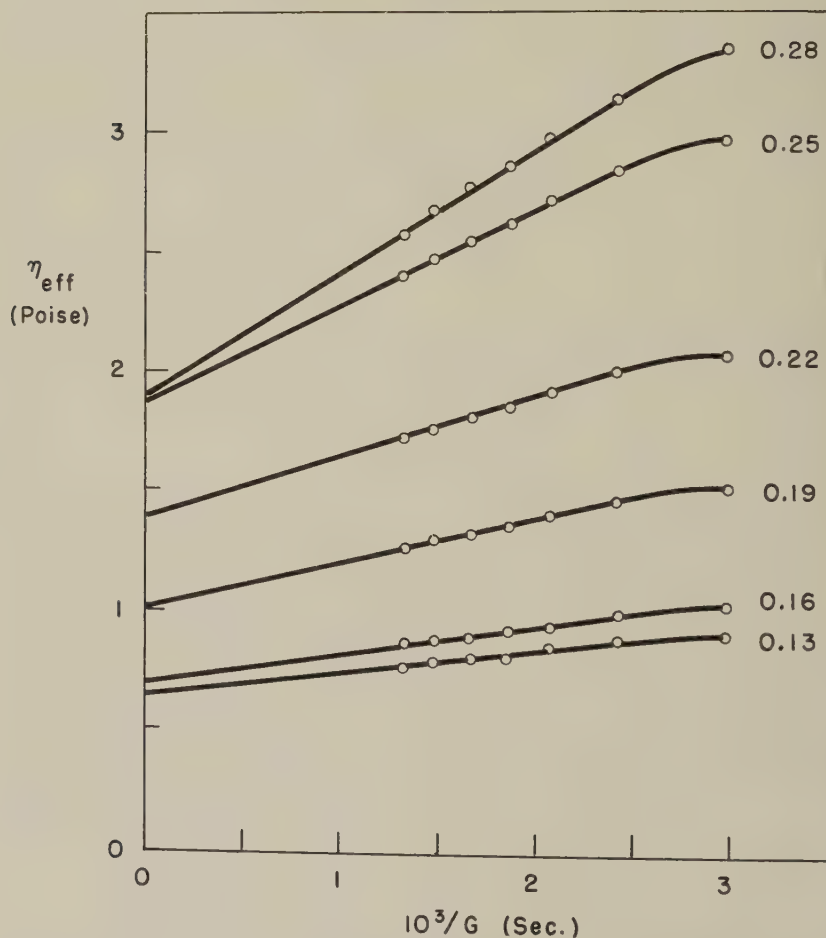


FIG. 3. Illustration of the method of determining  $\eta^*$ . The numbers refer to the fractional latex solids volume.

Testing Eq. [16] and Eq. [14] is not simply a matter of seeing whether experimental shear stress-shear rate data fit them or not. The wide application of Eq. [16] has already been pointed out by the work of Williamson (2) and Nieuwenburg (4). What is required is the determination of the various constants with well-defined systems over a range of conditions and the subsequent comparison of the values of the quantities in Eq. [14] and eq. [16] with what would be expected from established theory or independent experiments. The thickened latex experiments outlined below were carried out as a step in that direction.

### III. EXPERIMENTAL

A polystyrene latex was prepared using sodium lauryl sulfate as the emulsifier and using potassium persulfate as the initiator. The latex contained some rather large particles which settled and were subsequently removed by decantation. The final latex had a very narrow size distribution with a mean particle diameter of 2000 Å. The latex was post stabilized by adding 1.5 % of Triton X100 based on latex solids. To eliminate foam one part in 3000 of water of a colloid defoamer was added. (The defoamer was #581-B, obtained from Colloids Incorporated, Freylinghuysen Avenue, Newark, New Jersey.)

In a subsidiary set of experiments the adsorption of methylcellulose on the latex particles was assessed. The methylcellulose used was Dow Methocel 90 HG (4000 c.p.s.). The adsorption was determined by adding varying amounts of methylcellulose to samples of latex and dialyzing the mixtures in a large excess of a 1.5 % aqueous solution of Triton X100 containing one

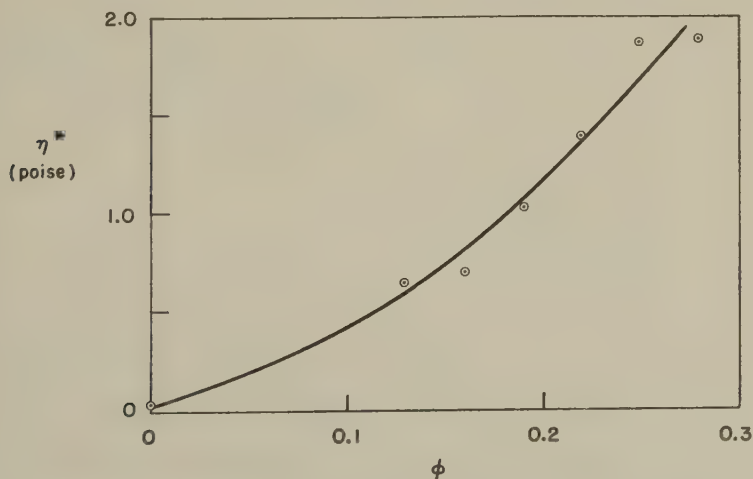


FIG. 4. Variation of  $\eta^*$  with fractional latex solids volume.

part in 3000 of the defoamer. The samples were then centrifuged and the serum was analyzed for methylcellulose by weighing.

The adsorption results were used as a guide in preparing a series of samples of latex thickened with methylcellulose containing various amounts of latex solids. The samples were dialyzed for three days in a solution similar to that used in the adsorption studies. The concentration of methyl-

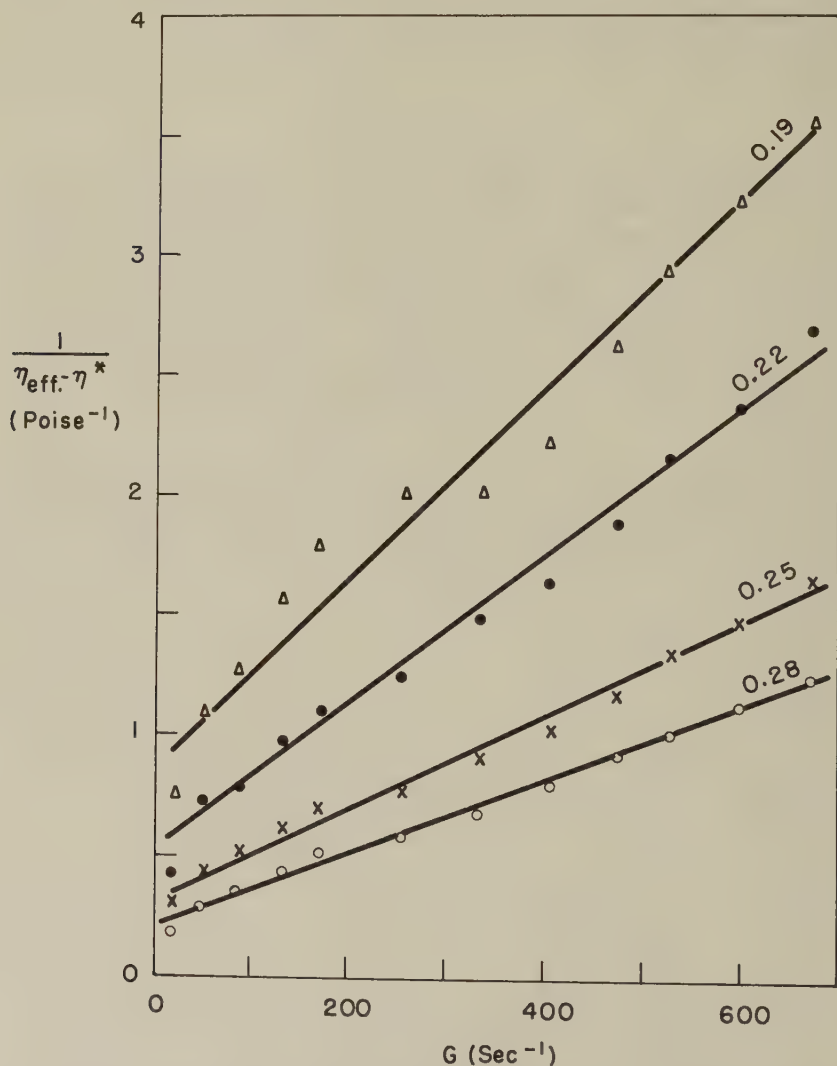


FIG. 5. Plots of typical experimental data as suggested by Eq. [20]. The numbers refer to the fractional latex solids volume.

cellulose in the aqueous phase was of the order of 0.15 % in each case. At this concentration a subsidiary study of methylcellulose solution rheology indicated that non-Newtonian effects due to methylcellulose molecular interactions would be very small compared to coated latex particle interactions. The viscosity of the serum in each sample was 3 centipoises at a shear rate of 400  $\text{sec.}^{-1}$ . It was only slightly greater at lower shear rates.

The shear stress-shear rate relations for the samples of thickened latex were determined using a modified Interchemical Precision concentric cylinder viscosimeter at 25°C. The modifications consisted of the installation of air bearings and finer torsion wires than those which were supplied with the instrument.

Typical data are illustrated in Fig. 2. In this figure  $\eta_{\text{eff}}$  is equal to  $S/G$ .

#### IV. ANALYSIS OF THE DATA

To analyze data such as those in Fig. 2, Eq. [16] may be put in the form

$$\eta_{\text{eff}} = \eta^* + \frac{C_1}{2C_2 + G} \quad [19]$$

At high values of  $G$  plots of  $\eta_{\text{eff}}$  against  $1/G$  should be linear. The intercept should be  $\eta^*$ . Typical plots are illustrated in Fig. 3. The variation of  $\eta^*$  with latex solids is illustrated in Fig. 4. (The volume fraction of each system which was made up of the polystyrene is denoted by the symbol  $\phi$ ).

Equation [16] may also be put in the form

$$\frac{1}{\eta_{\text{eff}} - \eta^*} = \frac{2C_2}{C_1} + \frac{G}{C_1} \quad [20]$$

In Fig. 5 experimental data are plotted as suggested by this equation. From the slope and intercept of the straight line drawn through the high shear rate points the corresponding values of  $C_1$  and  $C_2$  (i.e.,  $\beta_0/\beta_1$ ) were obtained and are given in Table I.

To check the validity of Eq. [14], which should apply over a wider

TABLE I  
*A Summary of the Constants Derived from the Experimental Data*

$\phi$	$\eta^*$ (poise)	$C_1$ (dynes/cm <sup>2</sup> )	$\beta_0/\beta_1$ (sec. <sup>-1</sup> )	$K_0/K_1$ (sec. <sup>-1</sup> )	$K_0 \times 10^{12}$ (c.c./sec.)	$W$	$E_A$ ( $kT$ units)
0.13	0.65	115	75	37	6.7	1.9	40
0.16	0.70	135	51	19	3.4	1.0	31
0.19	1.02	250	107	55	9.9	2.7	40
0.22	1.39	325	85	33	6.0	1.7	40
0.25	1.87	510	77	22	4.0	1.1	47
0.28	1.89	640	64	29	5.2	1.5	48

range of shear rate than the Williamson relation, it is convenient to express it in the form

$$Y = \frac{E_A K_0 N^2}{2} + \frac{E_A K_1 N^2 G}{2}, \quad [21]$$

where

$$Y = (\eta_{\text{eff}} - \eta^*)(\beta_0/\beta_1 + G)^2. \quad [22]$$

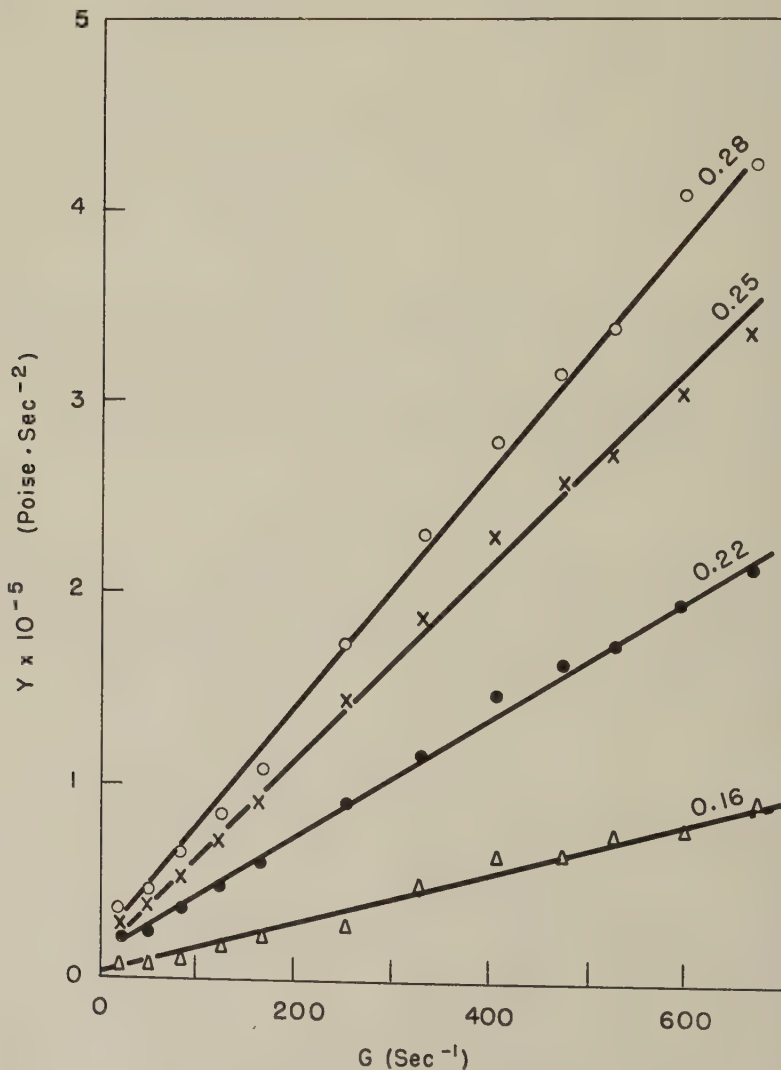


FIG. 6. Plots of typical experimental data as suggested by Eq. [21]. The numbers refer to the fractional latex solids volume.



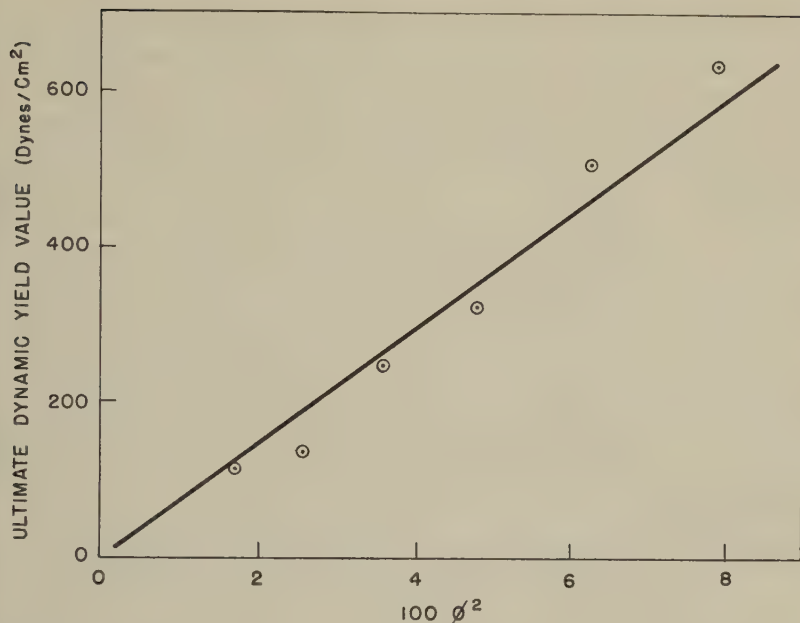


FIG. 7. Variation of the ultimate dynamic yield value with the square of the fractional latex solids volume.

Knowing the value of  $\eta^*$  and  $\beta_0/\beta_1$  in each sample  $Y$  may be calculated. According to Eq. [21] plots of  $Y$  versus  $G$  should be linear. Typical plots are illustrated in Fig. 6. The ratio of the intercept to the slope should in each case equal  $K_0/K_1$ . The determined values are given in Table I.

In Fig. 7 the ultimate dynamic yield value,  $C_1$ , is plotted against  $\phi^2$ . According to Eq. [17]

$$C_1 = b\phi^2, \quad [23]$$

where

$$b = \frac{E_A K_1 \rho^2}{2m^2}. \quad [24]$$

Here  $m$  is the mass of a latex particle of density  $\rho$ . It is reasonable to suppose from Fig. 7 that  $K_1$  is independent of particle concentration over a considerable range.

## V. DISCUSSION

The foregoing analysis shows that one cannot obtain the rate constants for link formation and rupture from shear stress-shear rate measurements. One can, however, obtain  $K_0/K_1$  and  $\beta_0/\beta_1$ . To determine the rate constants separately one must measure one part of each ratio in some independent experiment or if possible calculate them from first principles.

Of the four rate constants  $K_1$  is the easiest to calculate since it depends only on  $a_{\text{eff}}$ . Using the technique outlined by Badgley and Mark (9) the average effective length of the methylcellulose molecules in water at 25°C. was found to be 810 Å. as compared with the fully extended length of 4200 Å. Diffusion experiments (8) suggest that the adsorbed methylcellulose molecules would increase the radius by approximately 1500 Å., which is between 810 Å. and 4200 Å. This suggests that taking  $a_{\text{eff}}$  equal to 2500 Å. would not be unreasonable. The values of  $K_0$  in Table I were calculated from the ratio of  $K_0/K_1$  and the value of  $K_1$  was determined by taking  $a_{\text{eff}}$  equal to 2500 Å. in Eq. [11].

The values of  $W$  in Table I were calculated by assuming that  $a_{\text{eff}}$  for contact and  $a_{\text{eff}}$  for diffusion are the same and that the effective viscosity for diffusion is 3 centipoises (i.e., the value of  $\eta^*$  for  $\phi = 0$ ). The values of  $W$  are all less than 5 as expected from previous experience (7, 8). The fact that they are greater than 1 may indicate a weak long-range attractive force or it may be due to an error in the value assumed for  $a_{\text{eff}}$ .

The values of  $E_A$  were calculated from the measured values of  $C_1$  and the value of  $K_1$  was calculated for  $a_{\text{eff}}$  equal to 2500 Å. as above. The average value of  $E_A$  is 40  $kT$  units ( $k$  is Boltzmann's constant,  $T$  was taken as 298 Å.). There are reasons for believing that this represents the binding energy of several links formed when the coated particles come in contact. In Table I  $\beta_0/\beta_1$  is two to three times larger than  $K_0/K_1$ . This means that  $K_1/\beta_1$  is two to three times larger than  $K_0/\beta_0$  and hence the number of links per cubic centimeter at high shear rate is greater than the number at rest in the system studied. The measured decrease in viscosity is therefore due to the decrease in the lifetime of each link as the shear rate is increased. Had the number of links per cubic centimeter been independent of shear rate the absence of time effects would be expected. As it is, the rapid recovery indicates rapid link rupture due to Brownian movement. Taking the average value of  $\beta_0/\beta_1$  as 75  $\text{sec}^{-1}$  and  $\beta_1$  equal to  $\bar{\lambda}/X_c$  (see Eq. [13]) the average lifetime of a link at zero shear rate would be a fraction of a second.

Assuming that "transition state" theory can be applied, Kramers' analysis for the escape of a particle of mass  $m$  from a potential energy well of depth  $\epsilon_A$  (10) leads to

$$\frac{\beta_0}{\beta_1} = \frac{1}{2\pi\bar{\lambda}} (\epsilon_A/m)^{1/2} \exp [-\epsilon_A/kT]. \quad [25]$$

Taking  $a_{\text{eff}}$  equal to 2500 Å. and  $m$  equal to the mass of a latex particle,  $\epsilon_A$  is approximately 6.5  $kT$  units. Hence the average number of links per particle encounter would be at least 6 on this basis (see Eq. [15]). If the transition state cannot be applied  $n_L$  would be larger.

This preliminary study of thickened latexes illustrates the power of the Goodeve approach to rheology. It would seem to be worth while to use it in

combination with flocculation studies and other independent experiments in future attempts to understand non-Newtonian systems more fully.

#### ACKNOWLEDGMENT

During the course of this work I shared a laboratory with Ralph M. Wiley. I appreciate his interest and helpful comments.

#### REFERENCES

1. GOODEVE, C. F., *Trans. Faraday Soc.* **35**, 342 (1939).
2. WILLIAMSON, R. V., *Ind. Eng. Chem.* **21**, 1108 (1929).
3. HOUWINK, R., "Elasticity, Plasticity and Structure of Matter." Cambridge University Press, London, 1940.
4. NIEUWENBURG, C. J. VAN, "First Report on Viscosity and Plasticity." Academy of Science, Amsterdam, 1935.
5. SCHMOLUCHOWSKI, M. VON, *Physik. Chem.* **92**, 129 (1919).
6. SCHMOLUCHOWSKI, M. VON, *Physik. Z.* **17**, 557, 585 (1916).
7. KRUYT, J. R., "Colloid Science," Vol. 1, Chapter 7. Elsevier, New York, 1952.
8. GILLESPIE, T., *J. Colloid Sci.*, "The limited flocculation of colloidal systems." Submitted for publication, 1959.
9. BADGLEY, W. J., AND MARK, H., "High Molecular Weight Compounds," *Frontiers in Chemistry Series*. Dover Publications, New York, 1949.
10. KRAMERS, H. A., *Physica* **1**, 284 (1940).

## THE INTERACTION OF QUATERNARY AMMONIUM COMPOUNDS WITH STARCH<sup>1</sup>

Myer M. Fishman and Robert S. Miller

*Department of Chemistry, City College of New York, New York 31, New York*

*Received January 7, 1960*

Over the past two decades, many investigations have been made on the interaction between colloidal electrolytes and proteins (1, 2), but it is only within the past few years that similar studies have been carried out on the interaction between cationic detergents and polysaccharides. Scott (3) has investigated the formation of complexes between quaternary ammonium compounds and acid mucopolysaccharides, whereas others (4, 5) have described some qualitative observations on the interaction between quaternary ammonium compounds and neutral polysaccharides. It is the purpose of this note to present some preliminary results of a study on the interaction of cetyltrimethylammonium bromide (CTAB) with the corn starch fractions,<sup>2</sup> amylose and amylopectin, in weakly alkaline solutions.

Most of the experimental work on complex formation was carried out by following changes in turbidity, at 425 m $\mu$ . In the case of amylose, however, because of the apparent instability of the preparations, complex formation was indicated by almost immediate precipitation when the concentration of amylose was only 0.002 %, in 0.003 *N* NaOH. Consequently most of the results reported herein are based on our studies with amylopectin.

In these experiments, studies were made based on variations in the concentration of amylopectin, NaOH, and CTAB. In Fig. 1 are shown the results of the interaction of CTAB with amylopectin in 0.05 *N* NaOH. The turbidity increased with increasing concentrations of CTAB, but an excess of amylopectin produced a solubilization and a concomitant decrease in turbidity. However, when the concentration of amylopectin was kept constant, variations in the amount of NaOH were accompanied by increased turbidities and therefore increased binding of CTAB (Fig. 2). At any one concentration of CTAB, the turbidity rose to a maximum and then leveled off, but the results differed from those of similar studies with proteins, in that an excess of CTAB produced no apparent solubilization.

A comparison was also made between cetyltrimethylammonium bromide

<sup>1</sup> Aided in part by a grant from the Corn Industries Research Foundation.

<sup>2</sup> Supplied by the Northern Utilization Research Laboratories, Peoria, Illinois.

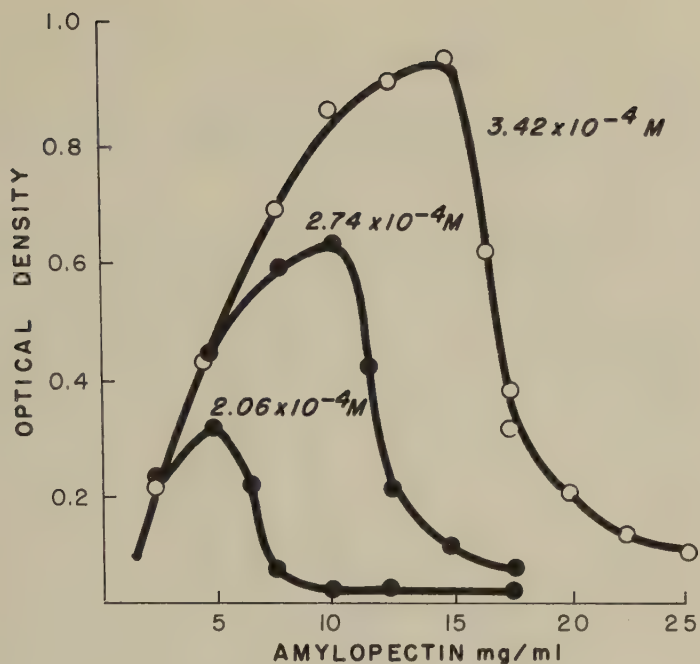


FIG. 1. The interaction of CTAB with amylopectin, in 0.05 N NaOH.

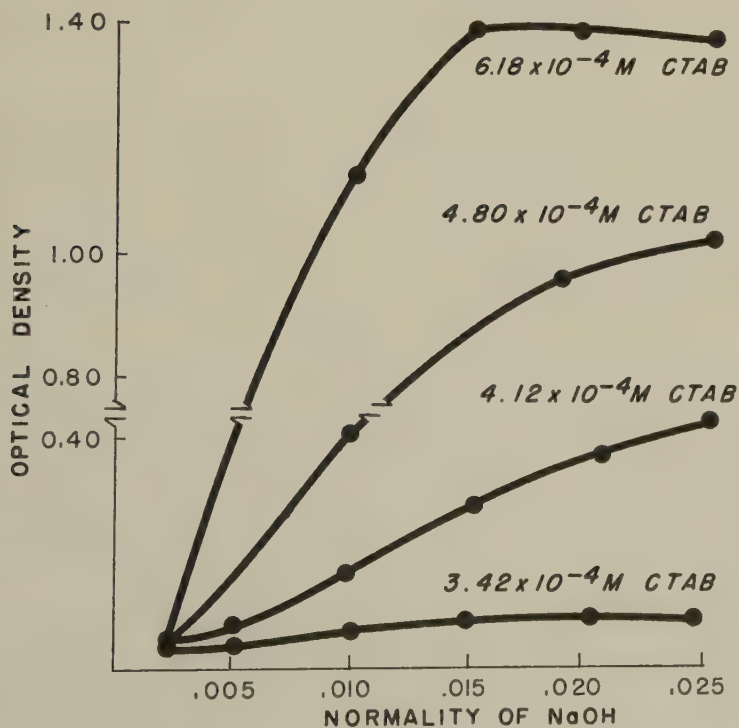


FIG. 2. The interaction of CTAB with amylopectin (0.025%) with variation in the concentration of NaOH.



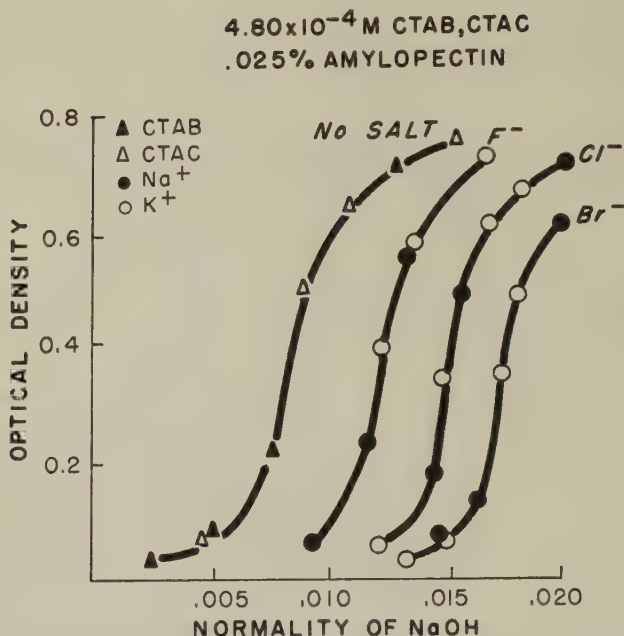


FIG. 3. The effect of neutral salts (0.05 *N*) on the interaction of both CTAB and CTAC ( $4.80 \times 10^{-4} M$ ) with amylopectin (0.025%).

and cetyltrimethylammonium chloride (CTAC) (Fig. 3). They were identical in their behavior with amylopectin, indicating that at this concentration of quaternary compound, the anion is without effect. When interactions between CTAB or CTAC and amylopectin were carried out in the presence of uni-univalent electrolytes, it was observed that there was a greater "salting-in" in going from  $F^-$  to  $Br^-$ , thus requiring higher concentrations of  $OH^-$  to reach the same point of turbidity. No apparent differences were found between  $Na^+$  and  $K^+$ .

These results appear to indicate that  $OH^-$  is bound to the amylopectin, presumably through hydrogen bonding and in turn is bound electrostatically to the quaternary ammonium ion. This is further supported by the observation that the complex is dispersed by warming to  $70^\circ C.$ , but reappears on cooling. Because of the electrostatic bond between the charged groups, the hydrophobic tail of the CTAB molecule should impart a lipophilic behavior to the whole complex. Again, this was indicated by the fact that the complexes were soluble in either alcohol or acetone.

In an earlier paper (6), it was reported that certain diquaternary ammonium compounds, e.g., curare, would complex with the acid mucopolysaccharide chondroitin sulfate. No such interaction was observed with amylopectin.

A more detailed study of the physiochemical properties of the complex is now in progress and will be reported at a later date.

## REFERENCES

1. PUTNAM, F., *Advances in Protein Chem.* **4**, 80 (1948).
2. YANG, J. T., AND FOSTER, J. F., *J. Am. Chem. Soc.* **75**, 5560 (1953).
3. SCOTT, J. E., *Biochim. et Biophys. Acta* **18**, 428 (1955).
4. BARKER, S. A., STACEY, M., AND ZWEIFEL, G., *Chemistry & Industry* **1957**, 330.
5. PALMSTIERNA, H., SCOTT, J. E., AND GARDELL, S., *Acta Chem. Scand.* **11**, 1792 (1957).
6. EHRENPREIS, S., AND FISHMAN, M. M., Abstracts 135 Meeting, Am. Chem. Soc., 7D (1959).

# THE COALESCENCE OF LIQUID DROPS WITH FLAT LIQUID/LIQUID INTERFACES<sup>1</sup>

G. E. Charles and S. G. Mason

*Physical Chemistry Division, Pulp and Paper Research Institute of Canada  
and Department of Chemistry, McGill University, Montreal, Canada*

*Received October 29, 1959; revised January 4, 1960*

## List of Symbols

$a, b$	= diameter and radius of drop.
$c$	= radius of circle of contact.
$c_D$	= radius of circle at minimum separation.
$d$	= distance between compressing planes.
$e$	= base of natural logarithms.
$f$	= fraction of drops which have coalesced before time $\tau$ , or before reaching a Phase 2 film thickness $h$ .
$F$	= force.
$g$	= acceleration due to gravity.
$h_{\min.}, h_{\max.}, h_{1/2}$	= film thickness at $\tau_{\min.}, \tau_{\max.}, \tau_{1/2}$ .
$h, \xi(r)$	= film thickness at $r = 0$ and $r = r$ , respectively, during hole expansion.
$k$	= slope of $1/v_r$ versus $r^2$ curve.
$n$	= total number of drops.
$\Delta p$	= excess drop pressure.
$Q$	= volume flux across a cylindrical surface at $r$ .
$r$	= radius of cylindrical coordinate; radius of hole.
$R$	= radius of curvature.
$t$	= time.
$u(z, r)$	= radial velocity in film at $z, r$ .
$v_r = dr/dt$	= rate of expansion of hole radius $r$ during rupture of Phase 2 film.
$V = -dh/dt$	= velocity of approaching surfaces.
$z$	= cylindrical coordinate.

<sup>1</sup> This work was conducted with financial assistance from the Defence Research Board of Canada (DRB Grant 9510-05).

$\Delta = [\Sigma (\tau_i - \bar{\tau})^2 / (n - 1)]^{1/2}$	= standard deviation from mean life $\bar{\tau}$ .
$\eta_1, \eta_2$	= viscosities of Phases 1 and 2, respectively.
$\xi(r)$	= distance between approaching surfaces at $r$ .
$\Delta\rho = \rho_1 - \rho_2$	= density difference of Phases 1 and 2.
$\sigma$	= interfacial tension.
$\tau$	= rest-time.
$\bar{\tau}, \tau_{\min.}, \tau_{\max.}, \tau_{1/2}$	= mean, minimum, maximum, and median rest-times.
$\psi(r)$	= velocity distribution function.

### INTRODUCTION

When a drop of liquid (Phase 1) falls gently through a lighter, immiscible liquid (Phase 2) onto a flat interface separating two phases, it "rests" on the latter for a time  $\tau$  before coalescing with the underlying phase. Early investigators (1-5) attributed this temporary stability to the presence of a residual film of Phase 2 liquid which is between the drop and the interface and which drains until coalescence suddenly occurs.

The rest-time  $\tau$  is defined (and can be measured without ambiguity) as the time interval between arrival of the drop at the interface and coalescence, and can be used as a measure of drop stability. It has been established (6-11) that, in a given system, there is a roughly Gaussian distribution of values of  $\tau$  between  $\tau_{\min.}$  and  $\tau_{\max.}$ .

The mean rest-time  $\bar{\tau}$ , the distribution of  $\tau$  about  $\bar{\tau}$ , and the median life  $\tau_{1/2}$ , i.e., at  $f = 0.5$ , have been found to be influenced by various factors. In oil/water systems, the addition of surfactants (6, 11), a decrease in the temperature, or an increase in the drop size (7-9) generally increased  $\bar{\tau}$  and  $\tau_{1/2}$ . It was also reported (9, 11) that a change in the curvature of the interface from convex to concave with respect to the drop increased the drop stability. Electrolytes added to the water phase markedly reduced  $\bar{\tau}$  (8, 9). In general the scatter in  $\tau$  about the mean value increased as  $\tau$  and  $\tau_{1/2}$  increased (7-9, 11).

Other factors have been reported to influence the rest-time. For example, temperature gradients and dirty interfaces decreased the drop stability (6, 7, 9, 10). Mechanical vibrations, on the other hand, appeared to increase the rest-time (5, 9).

Several theories have been proposed to explain the wide distribution of  $\tau$ . Cockbain and McRoberts (6), from a study of systems containing surfactants, proposed that a displacement of adsorbed surfactant molecules from the interface was necessary for coalescence to occur. This concept, although supported by other investigators (10, 11), fails to explain the scatter in  $\tau$  in pure systems (7-9, 11).

An alternative theory was proposed by Gillespie and Rideal (7) based on

irregular thinning of the film as a result of capillary waves generated by thermal and mechanical disturbances. By a formulation (which is difficult to follow) of the increased probability of rupture in unit time as the film thins beyond a critical film thickness corresponding to  $\tau_{\min.}$ , the following semi-empirical relationship was derived:

$$\log_e (1 - f) = -K(\tau - \tau_{\min.})^{3/2}, \quad [1]$$

where  $K$  is a rate constant.

Gillespie and Rideal obtained linear plots of  $\log (1 - f)$  versus  $(\tau - \tau_{\min.})^{3/2}$  from their experimental data as suggested by Eq. [1]. The results of later investigators (8, 11), however, did not agree with Eq. [1].

A modification of this theory based on statistical fluctuations in temperature, equally obscure in presentation, was recently proposed by Sheludko (12), who obtained the relation

$$f = Ae^{-Bh^2}, \quad [2]$$

where  $A$  and  $B$  are constants characteristic of the system and  $f$  is the fraction of coalescences occurring above a film thickness  $h$ .

Sheludko found agreement with Eq. [2] using films of aqueous solutions of isoamyl alcohol up to 0.1 mole/l. In all cases,  $\log f$  versus  $h^2$  was found to be linear. The film thickness  $h$  at rupture was measured by means of an electrical conductivity method (13). For a given system, a wide variation in  $h$  at rupture was observed.

As will be seen the coalescence of a drop begins with the formation of a hole in the intervening Phase 2 film which expands with a resulting decrease of interfacial area and interfacial free energy (14-16).

In this paper we describe an investigation of the coalescence of liquid drops falling on flat liquid/liquid interfaces which was undertaken to extend the earlier observations and to provide a better understanding of coalescence in emulsions and of other dispersions of fluid particles. The influence of temperature, drop size, diffusion, interfacial contamination, and of an electrostatic field on the drop stability was investigated. A method is described for the study of the rupture in the Phase 2 film. The experimental data have been analyzed using equations for drop deformation, film drainage, and film rupture which are discussed in the Theoretical Part which follows.

## THEORETICAL PART

### 1. Drop Deformation

The deformation of a drop under a compressive force may be estimated by considering it to be contained in a fluid between two parallel planes which are pushed together with a force  $F$  until equilibrium is reached (Fig. 1a). Let  $a$  be the diameter of the undistorted, spherical drop and  $2d$



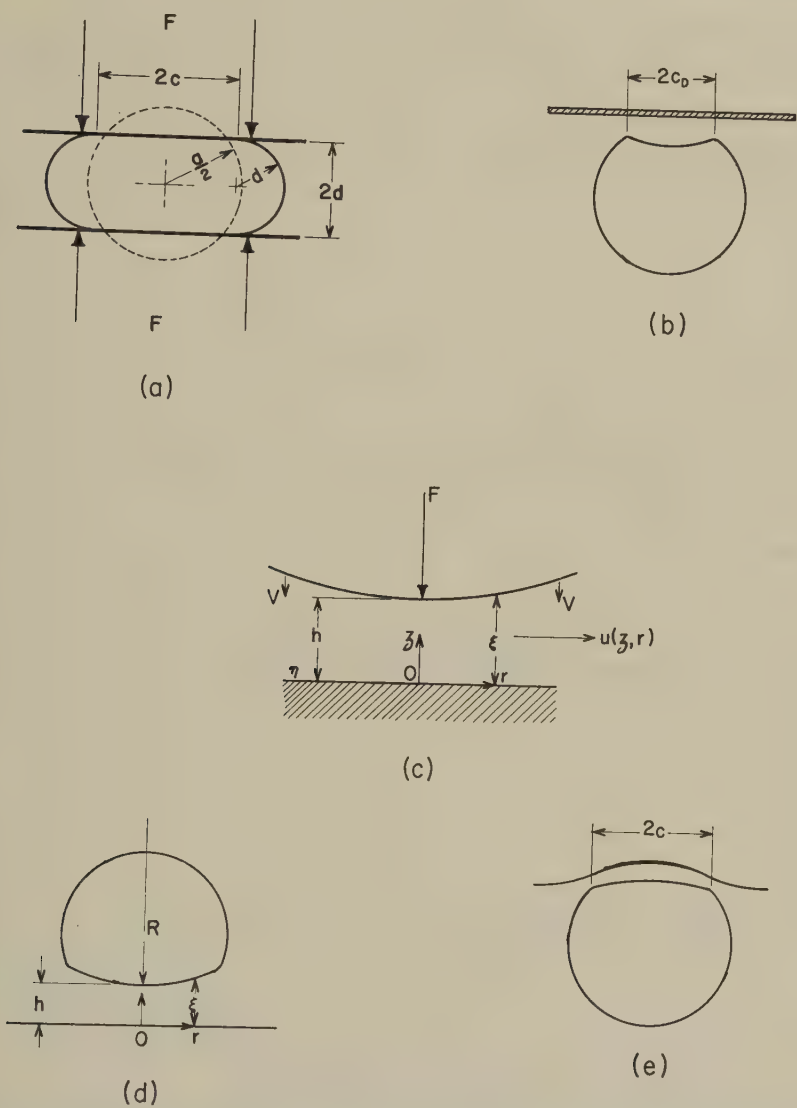


FIG. 1. (a) Deformation of a drop contained between two parallel planes. (b) Bubble profile at a rigid flat surface according to Derjaguin and Kussakov (17). (c) The close approach of surfaces immersed in a viscous fluid. (d) Idealized drop profile at rupture. (e) Proposed profile at the interface.

the equilibrium separation between the two planes. For simplicity, it is assumed that the bulging interface between the planes has a semicircular profile of radius  $d$  and that the drop interface adjacent to the planes is a flat disc of radius  $c$ .

At equilibrium,  $F$  is balanced by the excess pressure  $\Delta p$  inside the drop, i.e.,

$$F = \Delta p \pi c^2. \quad [3]$$

Substitution for  $\Delta p$  in accordance with Laplace's law in the form

$$\Delta p = \sigma \left[ \frac{1}{d} + \frac{1}{(d + c)} \right], \quad [4]$$

gives

$$F = \pi \sigma c^2 \left[ \frac{(2d + c)}{d(d + c)} \right], \quad [5]$$

where  $\sigma$  is the interfacial tension.

If it is assumed that the drop volume remains unchanged (i.e., the drop fluid is incompressible), the relation between  $c$  and  $d$  is readily found from a volume balance before and after compression:

$$\left( \frac{a}{2} \right)^3 = b^3 = d^3 + \frac{3}{4} \pi d^2 c + \frac{3}{2} d c^2. \quad [6]$$

For a small distortion, i.e., near  $d = b$ , it follows from differentiation of Eq. [6] with respect to  $d$  that, to a first approximation,

$$c = \frac{4}{\pi} (b - d), \quad [7]$$

and from Eq. [5] that

$$F = \frac{2\pi\sigma}{b} c^2. \quad [8]$$

Elimination of  $c$  from Eqs. [7] and [8] yields

$$F = \frac{32\sigma}{\pi b} (b - d)^2, \quad [9]$$

from which it follows that the force required to produce a given distortion  $(b - d)$  increases with  $\sigma$  and drop curvature  $(1/b)$ .

For the case of a drop resting on a plane surface and deformed by its own weight, Eq. [8] reduces to

$$c = b^2 \left[ \frac{2\Delta\rho g}{3\sigma} \right]^{1/2}, \quad [10]$$

where  $\Delta\rho$  is the difference in the density of the drop and the surrounding medium and  $g$  is the acceleration due to gravity.

Derjaguin and Kussakov (17) showed by an optical interference method that when a gas bubble under its buoyant force presses against a horizontal

glass plate immersed in a liquid, the bubble interface adjacent to the plate is not flat. Instead, the liquid film trapped between the interface is plano-convex in shape and is thinnest along the circumference of a circle of radius  $c_D$  as illustrated in Fig. 1*b*. Whereas there appears to be no satisfactory theoretical treatment leading to this profile, the experimental values of  $c_D$  for small air bubbles ( $a < 0.25$  cm.) in water were in good agreement with  $c$  from Eq. [10] (17).

2. Rate of Film Thinning

In previous investigations (7-9) the rate of thinning of the Phase 2 film was calculated from equations based on simple models. In this section a simple new equation is derived by use of a number of simplifying (and limiting) assumptions for a film of generalized profile. Particular solutions, which have been used before, are presented for two simple profiles.

Consider a rigid surface immersed in a viscous fluid and rotationally symmetrical about the  $z$ -axis, to approach a flat stationary plane from above in response to a constant force  $F$  as illustrated in Fig. 1*c*. Let the minimum separation at any time  $t$  be given by  $z = h$  at  $r = 0$ , where  $z$  and  $r$  are measured from the origin located in the stationary plane. Let  $V = -dh/dt$  be the velocity of the approaching surface at time  $t$ . During the approach, incompressible fluid of viscosity  $\eta_2$  is expelled radially from between the two surfaces at a velocity  $u(z, r)$ . It is assumed that the flow is laminar, radial (i.e., the  $z$ -component of fluid velocity is zero) and that inertial effects are negligible.

At a distance  $r$  from the origin, let the separation be  $\xi$  and assume the radial velocity  $u(z, r)$  to be given by

$$u(z, r) = z(\xi - z)\psi(r), \tag{11}$$

where  $\psi(r)$  is also a function of  $r$ . Equation [11] implies a parabolic profile without slip at the adjacent surfaces, i.e.,  $u(z, r) = 0$  at  $z = 0, \xi$ .

The flux  $Q$  in unit time across a cylindrical surface at  $r$  is

$$Q = \int_0^\xi 2\pi rz(\xi - z)\psi(r) dz. \tag{12}$$

By considering the flux at  $(r + dr)$  and equating the change in flux to the volume of liquid displaced by the approaching surface in unit time between  $r$  and  $(r + dr)$ , it follows that

$$\pi \frac{2}{3} d(\xi^3 r \psi(r)) = 2\pi V r dr, \tag{13}$$

which, on integration, yields

$$\psi(r) = \frac{3Vr}{\xi^3}. \tag{14}$$

The velocity distribution can now be obtained by substituting for  $\psi(r)$  in Eq. [11]:

$$u(z, r) = \frac{3z(\xi - z) Vr}{\xi^3}. \quad [15]$$

By equating the mechanical work done to the energy dissipated due to viscosity, we obtain from first principles

$$FV = \int \eta_2 \left( \frac{\partial u}{\partial z} \right)^2 d(\text{volume}) = \int_0^r \int_0^\xi \eta_2 \left( \frac{\partial u}{\partial z} \right)^2 2\pi r \, d\eta \, dr \quad [16]$$

Substituting for  $(\partial u / \partial z)$  from Eq. [15] and integrating Eq. [16] with respect to  $z$  yields the relation

$$V = -\frac{dh}{dt} = \frac{F}{6\pi\eta_2 \int_0^r \frac{r^3}{\xi^3} dr}. \quad [17]$$

The rate of approach can now be calculated from Eq. [17] if  $\xi(r)$  is known; two cases are considered.

*Case (i): Parallel disc approach.* When the approaching surface is a flat disc of radius  $c$ , i.e.,  $\xi = \text{constant} = h$ , Eq. [17] gives

$$\frac{dh}{dt} = -\frac{2F}{3\pi\eta_2 c^4} h^3. \quad [18]$$

It follows from integration of Eq. [18] that the time required for the disc to approach the plane surface from a distance  $h_1$  to  $h_2$  is

$$t_{1,2} = \frac{3\pi\eta_2 c^4}{4F} \left[ \frac{1}{h_2^2} - \frac{1}{h_1^2} \right]. \quad [19]$$

Equation [19] was first deduced by Stefan (18) to explain the force required to separate two circular discs in close proximity and immersed in a viscous fluid. Reynolds (19), in a classical treatment of the theory of hydrodynamic lubrication, also derived Eq. [19] for the approach of two parallel discs immersed in a viscous liquid. Other derivations of Eq. [19] are found in the literature (20-22).

Assuming that a liquid drop of radius  $b$  approaches a flat interface under its own weight and deforms according to Eq. [10], we obtain on substituting for  $F$  and  $c$  in Eq. [19]

$$t_{1,2} = \frac{\eta_2}{4} \left[ \frac{\Delta\rho g b^5}{\sigma^2} \right] \left[ \frac{1}{h_2^2} - \frac{1}{h_1^2} \right], \quad [20]$$

which reduces to

$$t_{1,2} = \frac{\eta_2}{4} \left[ \frac{\Delta\rho g b^5}{\sigma^2} \right] \frac{1}{h_2^2}, \quad [21]$$

when  $h_1 \gg h_2$ .

Gillespie and Rideal (7) used Eq. [20] to estimate the film thickness at

rupture from rest-time data. It should be emphasized that Eqs. [20] and [21] are subject to the limitation of Eq. [10], namely, that the deformation is small.

*Case (ii): Spherical-planar approach.* Here we consider a sphere of radius  $b$  approaching an unbounded plane. To render the equation tractable, we substitute for the approaching sphere a parabola of the same radius of curvature at the apex:

$$\xi = h + \frac{r^2}{2b}. \quad [22]$$

Substituting for  $\xi$  in Eq. [17] and integrating from  $r = 0$  to  $r = b$ , it is readily shown that, provided  $b \gg h$ ,

$$\frac{dh}{dt} = -\frac{Fh}{6\pi\eta_2 b^2}, \quad [23]$$

which, after integration, gives the analog of Eq. [20]:

$$t_{1,2} = \frac{6\pi\eta_2 b^2}{F} \log_e \frac{h_1}{h_2}. \quad [24]$$

Equation [24] was previously given without derivation by Hardy and Bircumshaw (23).

It must be emphasized that the application of Eqs. [19] and [24] to the approach of interfaces in close proximity is subject to several limitations, namely that the electrical double layer interaction (24), the electroviscous effects (25, 26), and the London-van der Waals (24, 27, 28) forces of attraction are negligible. Furthermore, the theory assumes that the interfaces are rigid and thus resist shear stresses due to the finite velocity gradient on each surface. This assumption may not apply for liquid/liquid and liquid/gas interfaces, particularly when pure systems are used. It has been predicted theoretically (29, 30) and confirmed experimentally (31–35) that liquid drops and air bubbles when subjected to tangential surface stresses will have internal circulation, thus indicating that surface motion occurs. Rigid behavior, however, was reported to occur with low velocity gradients, high interfacial tensions ( $>30$  dynes/cm.), small bubble diameters ( $a < 0.1$  cm.), and in presence of surfactants (31, 35).

### 3. Film Rupture and Collapse

Following the formation of a hole in the Phase 2 film, the interfacial tension will act to reduce the interfacial area. Assuming that the surface free energy released is completely converted into kinetic energy of the liquid displaced from the hole, Dupré (14) proposed that the velocity of hole expansion  $v$  for the rupture of a soap film is given by

$$v = \frac{dr}{dt} = \sqrt{\frac{4\sigma}{\rho h}}, \quad [25]$$

where  $r$  is the hole radius and  $\rho$  is the film density.



Obviously, Eq. [25] can give only an upper limit for  $v$  during the rupture of the Phase 2 film since energy will also be required for the incoming Phase 1 fluid, for overcoming the viscous drag on the receding edge, and for possible liquid motion within the Phase 2 film itself. Neglecting frictional effects and assuming that, as the hole expands, the Phase 1 liquid replaces it with a velocity  $v$ , a similar analysis as for Eq. [25] gives

$$v = \sqrt{\frac{4\sigma}{(\rho_1 + \rho_2)h}}, \quad [26]$$

when  $\rho_1$ ,  $\rho_2$  are the densities of Phases 1 and 2, respectively. It should be noted that Eq. [26] is, at best, only an approximation since the whole of the incoming phase does not move at velocity  $v$ .

According to Eqs. [25] and [26],  $v$  is independent of  $r$  and is constant for a film of uniform thickness.

In the experiments described below on film rupture,  $v$  decreased with increasing  $r$ . Here, the relation between  $v$  and  $r$  was established by assuming that the film configuration is that for spherical-planar approach given by Eq. [22] with a radius of curvature  $R$  instead of  $b$ . This is depicted in Fig. 1*d* for the case where  $R \gg b$ .

Substituting for  $\xi$  from Eq. [22] for the film thickness from [26] gives

$$\frac{1}{v_r^2} = \frac{1}{v_0^2} + kr^2, \quad [27]$$

where  $v_0$  is the initial velocity,  $v_r$  is the velocity when the hole radius is  $r$ , and  $k$  is given by

$$k = \left[ \frac{\rho_1 + \rho_2}{4\sigma} \right] \left[ \frac{1}{2R} \right]. \quad [28]$$

According to Eq. [27] the velocity of expansion of the hole decreases as the hole radius increases.

## EXPERIMENTAL PART

### 1. Drop Stability Measurements

Drop stability measurements are conducted in an all-glass pyrex cell (Fig. 2) consisting of three principal parts connected by ground-glass joints. The cell was similar to that employed by Gillespie and Rideal with modifications for renewal of the interface and for drop release.

The continuous phase (Phase 2) was contained in the central portion (A). Part B consisted of a Phase 1 reservoir (I), a flange-coupling for the attachment of a calibrated microburet (H), a glass reducing-connector (E), and a drop-forming tip (F). The bottom section (C) fitted B at the ball-and-socket joint (L) via the side-arm (J). Internally, a cupped-funnel

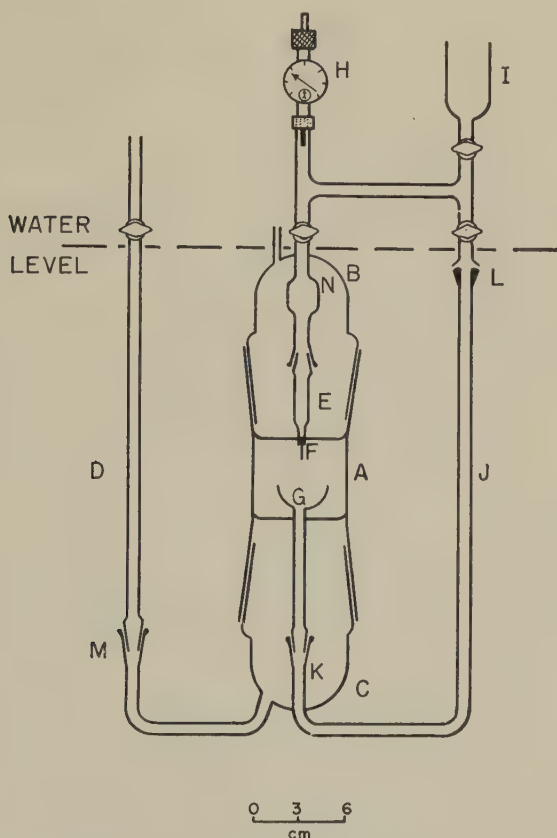


FIG. 2. Coalescence cell (schematic).

(*G*) was fitted to *C* at the ground-glass joint (*K*). The side-arm (*D*) permitted waste liquid (Phase 1) to be removed from section *C*.

The cell, supported rigidly by a special clamp, was immersed in a water reservoir to the level indicated in Fig. 2. The temperature in the latter was controlled to  $\pm 0.005^\circ\text{C}$ . by the gentle circulation of water from an external constant-temperature bath. The reservoir containing the cell was placed on an antivibration mount.

Before filling the cell, the two liquids were stored in the same vessel to allow for mutual saturation. After filling, all the joints to be immersed were sealed with latex rubber sleeves to prevent contamination from the surrounding water. Approximately 3 hours were allowed for temperature equilibrium after cell immersion. During operation, the reservoir *N* in section *B* provided sufficient residence to insure temperature equilibrium when fresh liquid was introduced from the microburet.

Before each experiment, the cell was thoroughly washed, degreased, and rinsed with ultrafiltered water.

Each drop was formed over a period of 5 minutes before release from the tip *F* in accordance with the conventional drop-volume method for surface and interfacial tension determination (36). The drop volume was read directly from the dial micrometer gauge of the microburet to an accuracy of  $2 \times 10^{-4}$  ml. The drop volume was used to calculate the drop diameter  $a$  and the interfacial tension  $\sigma$ .

Upon release, a drop fell gently onto the liquid/liquid interface within cup *G*. To avoid impact effects, the level of the interface was maintained 1 to 2 mm. below the drop at the time of release.

Elton and Picknett (8) found it necessary to prevent contaminants from accumulating at the interface, and for this reason they periodically renewed the interface. This was also done in the present experiments by means of the cup *G* by causing liquid (Phase 1) from the reservoir *I* to overflow into the lower part of *C*. The waste overflow was then sucked out through the side-arm *D*. The presence of even a trace of dirt at the interface promoted coalescence and gave erroneous low rest-times. Both drop and interface were observed through a stereomicroscope.

In the present experiments, the rest-time  $\tau$  of a drop at the interface was taken as the interval between leaving the tip *F* and coalescing with the bulk liquid in *G*. In actual fact, however, this measurement was in error by the time interval between the release of the drop and its arrival at the interface. With surrounding liquids of low viscosity, as generally employed in this investigation, the error introduced was found to be within the limits of error for the time measurements. This was revealed from a high-speed photographic study of a drop approaching the interface. Time measurements were made with a stopwatch to  $\pm 0.1$  sec. When the rest-time was less than 0.1 sec., the coalescence was considered to be instantaneous.

The rest-time distribution data were determined initially using a total of 100 drops. Subsequently, it was found that 50 drops were sufficient.

The drop-forming tips employed were prepared from various sizes of hypodermic needles, cut to the desired length, and carefully ground to a  $45^\circ$  bevel. Tip radii were measured microscopically and varied from 0.017 to 0.116 cm.

A few experiments were conducted on the effect of an electrostatic field in promoting coalescence. The field was applied across two parallel aluminum discs arranged as shown in Fig. 3. The discs (*D*) were positioned within the cell at equal distances below and above the interface in cup *G* and supported by means of a Teflon rod attached to connector *E* (Fig. 2). A small hole was made in the top disc to accommodate the drop-forming tip (*F*). The top disc and the tip were connected to the positive terminal of a 0–10 kilovolt d.c. power source (*S*). The lower disc was maintained at ground potential (*E*).

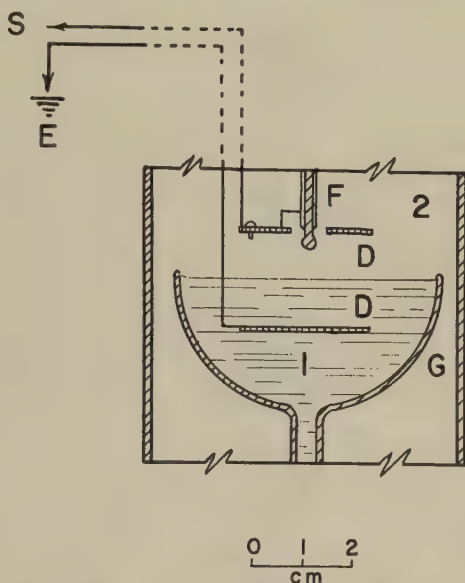


FIG. 3. Parallel disc arrangement for the study of the effect of an electrostatic field. Legend: *D*—discs; *E*—ground; *F*—drop-forming tip; *G*—cup; *S*—d.c. power source.

## 2. Film Rupture Measurements

The arrangement for photographing the rupture and collapse of the intervening liquid film consisted essentially of a square optical-glass cell (*A*) in the bottom of which was placed a front-surfaced mirror (*B*) at an angle of about  $45^\circ$  (Fig. 4). The latter permitted viewing vertically upwards from the front. The cell was filled with the two immiscible liquids to the levels indicated in Fig. 4. The drop-forming assembly consisted of a tip (*F*) immersed in Phase 2, a manifold (*C*) with reservoir (*D*), and a calibrated microburet (*H*).

A Fastax Model WF-3 high-speed 16-mm. cine-camera (Wollensak Optical Company, Rochester, N. Y.) was employed to photograph the rupture. The camera was operated at film speeds as high as 6500 pictures/sec. The film speed was registered directly on the film by the built-in timing light operated at 1000 impulses/sec. from a crystal-controlled pulse generator. The recorded impulses were easily visible on the photographic film.

The growth of the "hole" in the Phase 2 film was determined from a frame-by-frame analysis of the photographic film.

In general, the difference between the rest-times of two consecutive drops was greater than the total exposure time (1 sec. approximately) of

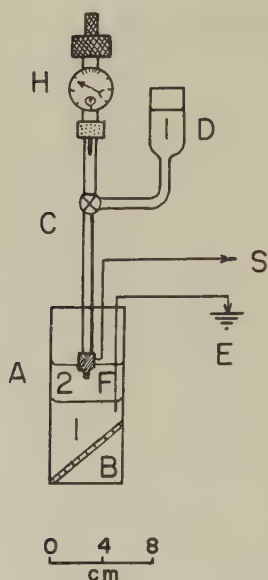


FIG. 4. Arrangement for film rupture study. Legend: *A*—optical-glass cell; *B*—front-surfaced mirror; *C*—manifold; *D*—Phase 1 reservoir; *E*—ground; *F*—drop-forming tip; *H*—microburet; *S*—d.c. power source.

the 100-foot roll of cine film. This made it impossible to photograph the rupture with any degree of certainty, particularly since it was desirable to start the camera about 0.5 sec. beforehand in order to photograph at maximum film speed. This difficulty was overcome by electrifying the drops and thus causing instantaneous coalescence ( $\tau < 0.1$  sec.). It was therefore possible to photograph the rupture with certainty by releasing the pendant drop about 0.5 sec. after starting the camera. The drop-forming tip was connected to the positive terminal of the high-tension supply (*S*) while the bottom phase was maintained at ground potential (*E*). Because of the appreciable electrostatic attraction between the drop and the interface which tended to elongate the drop, the minimum separation between the two was increased to 5 mm. in these experiments.

Two 1000-watt floodlights, focused on the area being photographed, supplied the necessary illumination.

In some of the experiments on film collapse in benzene/water systems, Tween 20 (polyoxyethylene sorbitan monolaurate, supplied by Atlas Powder Co.) a nonionic emulsifier was added to the water in amounts above and below the critical micelle concentration, which interfacial tension determinations indicated to occur between 0.01 and 0.02 g./ml. The interfacial tensions were determined as before, i.e., by the drop-volume method. Similar values of the critical micelle concentration were obtained from surface tension measurements in air.



The experiments on film rupture were conducted at  $25^\circ \pm 2^\circ\text{C}$ .

### 3. Materials

Distilled water was used as one of the liquid phases. Because of the possible influence of electrical double-layer effects (8, 9) on coalescence, the water was stabilized with KCl to a concentration of  $5 \times 10^{-5} \text{ N}$ . This procedure eliminated daily fluctuations in the specific resistivity of the water from the laboratory still.

Benzene, carbon tetrachloride, and heptane were employed as the other liquids. These were all of A.C.S. certified grade. All organic liquids were fractionally distilled and rendered dust-free by filtering through a fritted-glass ultrafilter before use.

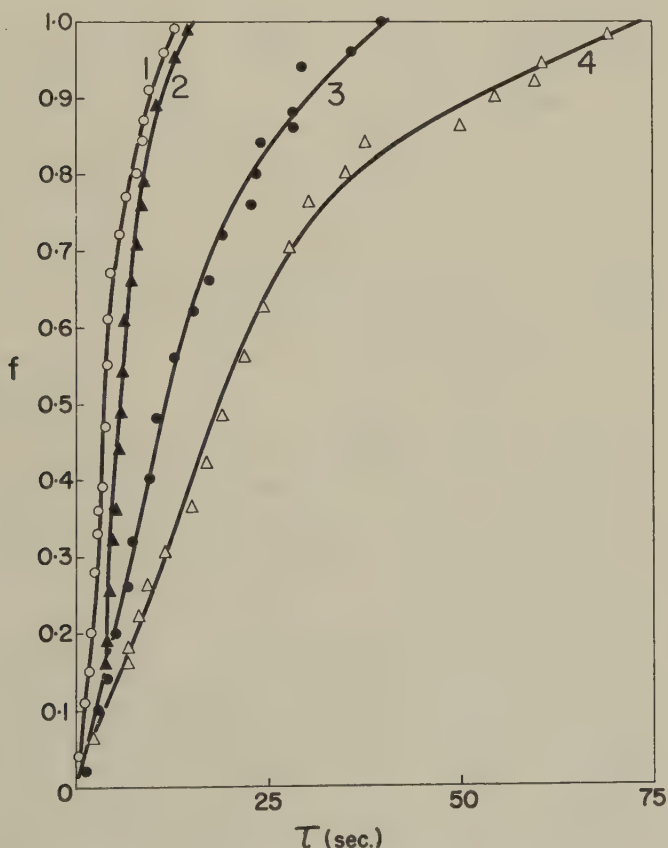


FIG. 5. Integral distribution function  $f$  of rest-times of water drops coalescing at a benzene/water interface at  $20^\circ\text{C}$ . Curves 1 to 4 represent drop diameters of 0.384, 0.416, 0.544, and 0.604 cm., respectively.

## RESULTS

## 1. Drop Stability

a). *Effect of Drop Diameter.* Figure 5 illustrates the distribution of  $\tau$  for water drops of various diameters at a benzene/water interface. The values of  $\tau_{\min.}$ ,  $\tau_{\max.}$ ,  $\bar{\tau}$ , and  $\tau_{1/2}$  characterizing each distribution are given in the top part of Table I. The standard deviation  $\Delta$  from  $\bar{\tau}$  is also given in Table I and was calculated in the usual way.

Table I shows that an increase in the drop size caused an increase in  $\tau_{\max.}$ ,  $\bar{\tau}$ ,  $\tau_{1/2}$ , and  $\Delta$ . These results are in general agreement with those of previous investigators on the same (7) and other systems (8, 9, 11).

The variation of  $\tau_{\min.}$  was erratic. This also appeared to be the case in the results given by Nielsen, Wall, and Adams (11), and was undoubtedly due to the large relative error involved in measuring the small values of  $\tau_{\min.}$  with a limited number of drops.

Gillespie and Rideal (7) obtained values for  $\tau_{\max.}$  ranging from 1.2 to 3.4 sec. with water drops of diameters 0.3 to 0.6 cm., respectively, coalescing at a benzene/water interface. It is interesting to note that their values are much smaller than those observed here (Table I).

b). *Effect of Temperature.* The effect of temperature on the stability of carbon tetrachloride and water drops coalescing at water/carbon tetrachloride and benzene/water interfaces, respectively, was investigated. The rest-times and  $\Delta$  (Table I) decreased as the temperature was raised. This trend agrees with the results of previous investigators (7, 9, 11) that drop stability decreases as the temperature is raised.

c). *Effect of a Diffusing Component.* In preliminary experiments with water/chloroform, the coalescence was found to be instantaneous ( $\tau < 0.1$  sec.). This effect was subsequently traced to ethanol which was present as a stabilizer in the chloroform used, which was A.C.S. grade. The usual distribution in  $\tau$  was observed when the ethanol was allowed to assume an equilibrium distribution between the two phases or was completely removed from the chloroform by distillation or washing. It was concluded that the instantaneous coalescence was due to the diffusion of ethanol across the phase interface.

A few controlled experiments were conducted to determine more precisely the effect of a diffusing component. Values of  $\tau$  were determined for water drops containing 0.01%, 0.03%, and 0.05% *p*-dioxane and coalescing at a benzene/water interface. In these experiments, the drops released were aged for only 1 min. to insure that diffusion continued to occur from the drop.

The stability data obtained are given in Table I. As before, the values of  $\sigma$  calculated from the measured drop volume are included in the table.

It is obvious that a progressive decrease in  $\tau$  and in  $\Delta$  occurred with

TABLE I  
Rest-time Distribution Data for Drops at Planar Liquid/Liquid Interfaces

Variable studied	System		$a$ (cm.)	Temp. (°C.)	$\sigma$ (dynes/cm.)	Rest-time (sec.)				$\Delta$ (sec.)	Film thickness ( $\mu$ )		
	Phase 1	Phase 2				$\tau_{\max.}$	$\tau_{\min.}$	$\bar{\tau}$	$\tau_{1/2}$		$h_{\max.}$	$h_{\min.}$	$h_{1/2}$
Drop diameter	Water	Benzene	0.384	20	35.6	14.0	0.2	4.8	4.1	3.3	0.5	4.4	1.0
			0.416			16.8	1.5	6.7	5.9	3.0	0.6	2.0	1.0
			0.544			39.8	1.1	14.5	11.7	10.2	0.7	4.5	1.3
			0.604			71.4	0.8	24.0	18.9	18.9	0.7	6.8	1.4
Temperature	Carbon tetrachloride	Water	0.336	15	41.1	5.7	1.6	3.3	3.1	1.2	1.4	8.7	2.0
			0.335	20	40.2	5.3	0.5	2.6	2.4	1.1	1.5	4.7	2.2
			0.328	25	37.5	3.2	0.8	1.7	1.5	0.6	1.8	3.7	2.7
			0.323	30	35.6	2.5	0.8	1.6	1.4	0.5	2.1	3.7	2.8
Temperature	Water	Benzene	0.578	15	36.2	33.6	6.5	16.3	16.1	5.7	1.0	2.2	1.4
			0.566	20	35.6	27.5	5.6	14.8	14.8	5.4	1.0	2.2	1.3
			0.550	30	34.7	23.3	2.2	14.0	13.8	4.3	1.0	3.2	1.3
			0.540	40	34.6	20.1	5.2	13.3	13.2	3.6	1.0	2.0	1.2
Diffusing component	Water + 0.01% p-dioxane 0.03% p-dioxane 0.05% p-dioxane	Benzene	0.550	20	32.8	14.9	1.0	7.1	6.3	3.5	1.4	5.3	2.1
					32.5	11.3	0.8	4.9	4.3	2.7	1.6	6.0	2.6
					31.8	5.4	0.4	1.9	1.3	1.5	2.3	8.6	4.8
Successive stages in stepwise coalescence	Water	Benzene	0.566	20	35.6	27.5	5.6	14.8	14.8	5.4	1.0	2.2	1.4
			0.179			18.0	4.2	12.3	12.5	2.9	0.1	0.2	0.1
			0.082			5.8	2.8	4.3	4.2	0.6	0.02	0.03	0.02
—	Water	Heptane	0.464	20	50.3	7.7	1.6	4.0	3.6	1.6	1.3	2.8	1.8

Note: Liquid densities and viscosities were obtained from the literature (37, 38).

increasing amounts of *p*-dioxane. At concentrations of 0.10 % and above, coalescence was instantaneous.

A similar observation was made in mutually unsaturated 2-component, 2-phase systems such as styrene/water, both with and without stabilizing surfactants.

d). *Stepwise Coalescence*. In all the systems investigated thus far the drop coalesced in a flash with the underlying phase and in a stepwise manner. Following the coalescence of the primary drop released from the tip, a smaller secondary drop of the same liquid was left behind. As many as eight such stages of coalescence could be visually observed with the benzene/water system after the coalescence of the primary drop. In each step, the diameter decreased by approximately one-half.

Rest-times at a benzene/water interface were recorded for a series of primary water drops and for each of the two successive drops. The diameters of the successive secondary drops were estimated using an eyepiece micrometer in the microscope.

As anticipated from the earlier experiments with the same system on the effect of drop size, the results (Table I) revealed a decrease in the stability in each successive stage. A detailed investigation of the mechanism of stepwise coalescence is reported elsewhere (39).

e). *Effect of an Electrostatic Field*. The application of an electrostatic field by the method illustrated in Fig. 3 caused a marked decrease in drop stability. The effect is illustrated by water drops coalescing at a heptane/water interface. At zero voltage, coalescence proceeded normally and showed a scatter in  $\tau$  (Table I).

With increasing potential, the rest-times of the primary and the successive drops decreased. In addition, the primary drop coalescing yielded a smaller secondary drop. Eventually, at approximately 450 volts d.c., single-stage coalescence occurred, i.e., there was no secondary drop. At 900 volts d.c., coalescence occurred instantaneously ( $\tau < 0.1$  sec.).

With benzene/water, instantaneous coalescence was obtained at voltages as low as 135 volts d.c. with the formation of a short-lived secondary drop. The size of the secondary drop formed decreased with increasing potential; above 1000 volts, the coalescence was single-staged (39).

## 2. Collapse of Intervening Liquid Film

a). *General Observations*. The high-speed cine-films revealed that rupture of the Phase 2 film could start at different positions in the film.

When the rupture occurred at the center, the expanding hole bounded by the receding edge of the film remained circular in shape as shown in the tracings of the photographic images in Fig. 6a.

When off-center rupture occurred, the initial shape of the hole invariably appeared elliptical (Fig. 6b). Occasionally a retarded film segment was

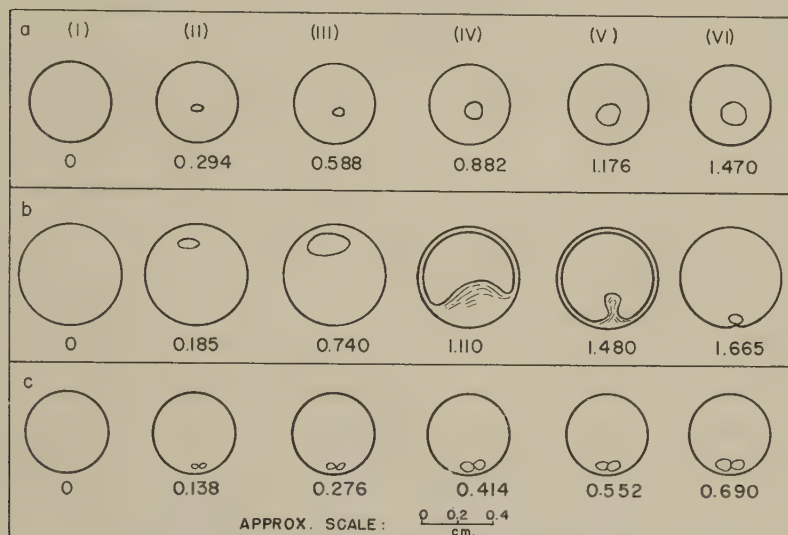


FIG. 6. Tracings of photographs showing central (Part a), off-center (Part b), and double rupture (Part c) of intervening Phase 2 film. (a) Water drop ( $a = 0.44$  cm.) coalescing at a benzene/water interface, the aqueous phase containing 0.01% Tween 20; (b) Water drop ( $a = 0.60$  cm.) coalescing at a benzene/water interface. At 500 volts; (c) Water drop ( $a = 0.40$  cm.) coalescing at a benzene/water interface, the aqueous phase containing 0.05% Tween 20. At 500 volts.

observed during the hole expansion, which frequently became detached from the film and formed a droplet of Phase 2 dispersed in Phase 1 (Fig. 6b (v)). In time, this droplet coalesced with the Phase 2 liquid.

Undoubtedly, the hole with off-center rupture appeared elliptical because the plane of the opening was not normal to the axis of view. In analyzing the data, the hole was assumed to be circular and of radius equal to the major axis of the elliptical image.

Occasionally the Phase 2 film ruptured at two places simultaneously (Fig. 6c). The liquid segment separating the two holes eventually collapsed when the holes had expanded sufficiently.

With pure benzene/water, the Phase 2 film generally ruptured at an off-center position. Only one of the six cases photographed showed central rupture (Table III). Central rupture, however, occurred frequently when a surfactant (Tween 20) was used in the system. Of the eleven cases photographed here, only two showed off-center rupture. A single case of double rupture was observed.

In some cases, the Phase 2 film appeared wrinkled near the receding edge. This was more noticeable with films showing low rates of hole expansion and gave the appearance of being thicker films.

Two experiments were performed in which the interface was deliberately



TABLE II  
Hole Expansion Rates  
Comparison of methods of calculation from experimental data

$r$ (cm.)	$v_r$ (cm./sec.)	
	From tangent	From numerical differentiation
0.03	88.5	90.0
0.04	80.7	80.0
0.05	75.0	72.0
0.06	65.4	64.0

contaminated by sprinkling with glass beads 50 to 150 $\mu$  in diameter. The photographs revealed that the beads remained stationary until reached by the receding edge of the ruptured Phase 2 film. This suggests progressive accumulation of liquid in the receding edge and the absence of liquid movement in the remainder of the film as implied in the Dupré analysis (14).

The Phase 1 drop generally coalesced instantaneously when the interface was contaminated with glass beads.

Since chloroform drops containing diffusing alcohol coalesced instantaneously at a water/chloroform interface, it was possible to photograph the rupture of the Phase 2 film without an electrostatic field. Here, central rupture was observed three times and double rupture once (Table III).

*b). Analysis of Film Rupture Data.* Unlike the results of De Vries (16) with soap films, the rate of hole expansion  $v_r$  was not constant but decreased progressively during the collapse of the Phase 2 film as indicated in Fig. 7.

The values of  $r$  were obtained from successive pictures on the cine-film, taking zero time as that of the frame preceding the rupture;  $v_r$  was obtained from the tangent of the  $r$ - $t$  curve and was in good agreement with that calculated by polynomial differentiation (40). Expansion rates determined by both methods for the curve of Fig. 7 are given in Table II.

According to Eq. [27] a plot of  $1/v_r^2$  versus  $r^2$  should be linear, with an intercept =  $v_0^{-2}$  and slope =  $k$ . The inset of Fig. 7 shows such a plot fitted by least squares. For all cases studied the linearity was good, particularly at small values of  $r$ .

The film thickness  $h$  at the point of rupture was calculated from  $v_0$  using Eq. [26]. The value  $R$  was obtained from  $k$  using Eq. [28].

*c). Film Rupture Measurements.* A total of 23 successful experiments was conducted in an attempt to evaluate various factors. By necessity, the data are somewhat fragmentary but a number of useful observations were made. The experimental data and the calculated values of  $h$  and  $R$  are given in Table III.

(i) *Reproducibility of  $v_0$  and  $k$ .* Values for 4 identical water drops in benzene show a scatter in  $v_0$  and  $k$  and hence in  $h$  and  $R$ . It is interesting

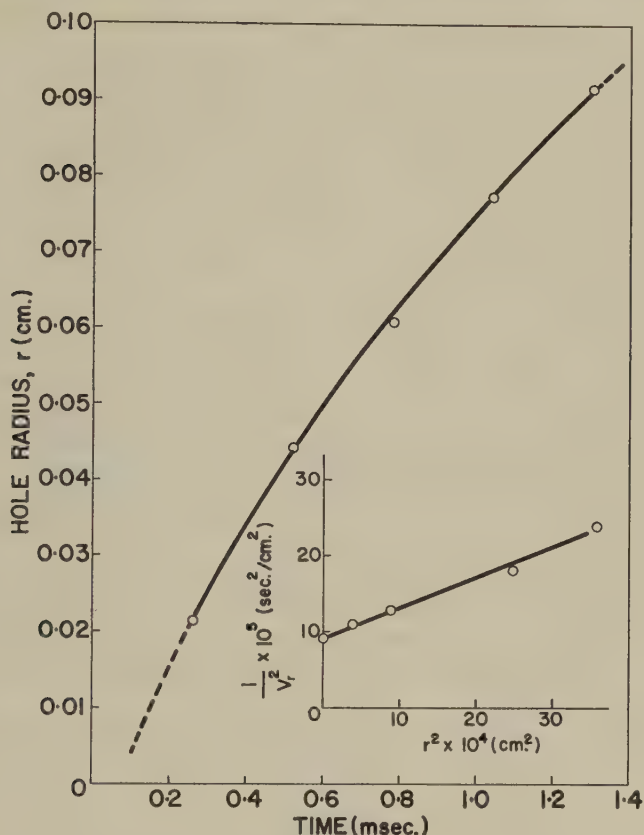


FIG. 7. Increase in hole radius with time during the coalescence of a water drop ( $a = 0.39$  cm.) at a benzene/water interface, the aqueous phase containing 0.05% Tween 20. Applied potential 500 volts. Photographic film speed at rupture was 3830 p.p.s. *Inset*: Plot of  $1/v_r^2$  versus  $r^2$  from the data of  $r$  versus  $t$ .

to note also that off-center rupture occurred in all cases, and that  $R \gg a/2$ .

(ii) *Electrostatic potential*. The effect of voltage up to 1000 volts was determined with water drops in benzene/water. The data at 500 volts represent the average from the 4 drops in the reproducibility experiments. A marked decrease occurred in  $v_0$  at 1000 volts, suggesting a higher  $h$ .

(iii) *Surfactant*. The effect of a surfactant (Tween 20) on  $v_0$  and  $k$  was investigated using benzene/water. The surfactant concentration in water was varied from 0.01 to 0.15 g./100 ml.

A total of 5 drops was studied at 0.05 g./100 ml. In one, illustrated in Fig. 6c, the rupture occurred at two points, in close proximity. Duplicate drops were investigated at the higher surfactant concentrations.

Considering the drops with central rupture, it would appear that  $v_0$  decreases and  $h$  increases with increasing surfactant concentration. The

results for  $k$  and  $R$  are somewhat erratic. In two cases  $R = \infty$ , indicating that the film was of uniform thickness, whereas in several cases  $R \ll a/2$ .

(iv) *Interfacial contamination.* These were the experiments previously mentioned which were conducted with glass beads at the interface and which showed no liquid movement in the collapsing Phase 2 film. In one case, a close-packed bead pattern was used; in the other, a few beads were scattered at random. With the former system, the density of the Phase 2 film was assumed equal to that of glass (2.5 g./c.c.), whereas in the latter the film was assumed to be all benzene.

It is interesting to note from Table III that both values of  $v_0$  were smaller than for the pure systems.

(v) *Diffusing component.* Film rupture measurements were made on four identical chloroform drops containing alcohol at the water/chloroform interface. Since coalescence was instantaneous, as discussed earlier, no electrostatic charge was applied. Double rupture was observed with one drop but, unlike the previous case (see Fig. 6c), the holes began from points approximately one drop radius apart.

Values of  $v_0$  and  $k$  of the two holes differed slightly (Table III).

As for benzene/water, the chloroform drops show a scatter in  $v_0$  and  $k$ , and hence in  $h$  and  $R$ . It is also interesting to note that the maximum values of  $v_0$  were obtained with the Phase 2 film which showed double rupture.

In all cases,  $R > a/2$  and is much smaller than for benzene/water.

## DISCUSSION

### 1. General

For purposes of discussion, the principal experimental observations may be summarized as follows:

a). The drop stability as measured by the distribution of  $\tau$  decreased with increasing temperature and increased with increasing drop diameter.

b). Stability was decreased by imposing an electrostatic field and also by adding small amounts of a third component which diffused from the drop.

c). The location of initial rupture of the Phase 2 film varied and occasionally occurred at two points simultaneously. The rate of hole expansion generally decreased as the hole grew in size.

All the experiments quoted were conducted with systems in which  $\rho_1 > \rho_2$ . It is believed, however, that the same behavior will be exhibited when  $\rho_1 < \rho_2$ .

### 2. Drop Stability Experiments

The approximately Gaussian distribution of  $\tau$  in a given system suggests that a given coalescence is governed by random statistics. In general, the

Effect studied	System		$\sigma$ (dynes/cm.)	D. C. potential volts	Experimental data		Calculated from Eqs. [26] and [28]		Position of rupture
	Phase 1	Phase 2			$v_0$ (cm./sec.)	$k$ (sec. <sup>2</sup> /cm. <sup>4</sup> )	$h$ ( $\mu$ )	$R$ (cm.)	
Reproducibility of $v_0$	Water	Benzene	0.65	500	340	$1.320 \times 10^{-3}$	6.0	5.45	Off-center
					289	$1.594 \times 10^{-3}$	8.3	4.51	Off-center
Electrostatic potential	Water	Benzene	0.66 0.65 0.61	135 500 1000	253	$3.261 \times 10^{-3}$	10.8	2.21	Off-center
					231	$1.946 \times 10^{-3}$	13.0	3.70	Off-center
Surfactant	0.01% aq. Tween 20	Benzene	0.42 0.40	500	324	$3.176 \times 10^{-3}$	6.6	2.27	Central
					278 <sup>a</sup>	$2.030 \times 10^{-3}$	9.0	3.54	Off-center
Interfacial con- tamination	Water	Benzene	0.66 0.66	0 0	141	$1.625 \times 10^{-3}$	34.7	4.43	Off-center
					91	0.505	30.8	0.039	Central
Diffusing com- ponent	Chloroform	Water	0.41	0	88	0	28.2	$\infty$	Central
					141	0.045	10.0	0.565	Off-center
	0.05% aq. Tween 20	Benzene	0.39	500	105	0.039	18.0	0.640	Off-center
					54	0.636	68.4	0.040	Central
	0.05% aq. Tween 20	Benzene	0.38 0.38	500	50	4.450	79.0	0.006	Central
					36	0	153.0	$\infty$	Double
	0.10% aq. Tween 20	Benzene	0.36 0.36	500	39	3.81	119.0	0.007	Central
					30	7.99	203.0	0.003	Central
	0.15% aq. Tween 20	Benzene	0.36 0.36	500	71	2.37	33.3	0.012	Central
					34	1.03	148.0	0.029	Central
	Water	Benzene	0.66 0.66	0 0	99	$7.71 \times 10^{-3}$	71	0.933	Off-center
					64 <sup>b</sup>	0	90	$\infty$	Off-center
	Chloroform	Water	0.41	0	284	$14.34 \times 10^{-3}$	6.7	0.642	Double
					241	$13.25 \times 10^{-3}$	9.3	0.695	
					199	$30.15 \times 10^{-3}$	13.8	0.306	Central
					136	$21.34 \times 10^{-3}$	29.3	0.432	Central
					106	$21.07 \times 10^{-3}$	48.0	0.437	Central

<sup>a</sup> Mean value from above. <sup>b</sup> Close-packed bead pattern.

Note: The densities of the liquids employed were 0.9971, 0.8735, and 1.4797 g./ml. at 25°C. for water, benzene, and chloroform, respectively (37).

distribution data of the present investigation showed agreement with Eq. [1] but, as discussed later, not with Eq. [2]. Plots of  $\log (1 - f)$  against  $(\tau - \tau_{\min.})^{3/2}$  in most cases yielded straight lines except at high values of  $f(>0.9)$ , where the points tended to become scattered, partly as a result of sampling errors.

Several generalizations can be made from the data summarized in Table I:

a. For all the systems studied, the ratio  $\bar{\tau}/\tau_{1/2} > 1$  with a mean value of 1.11.

b. For a given system, both  $\Delta$  and  $\tau_{\max.}$  increased as  $\tau_{1/2}$  increased,  $\tau_{\min.}$  showed a somewhat erratic variation but tended to increase with an increase in  $\tau_{1/2}$ .

c. The magnitude of  $(\tau_{1/2} - \tau_{\min.})$  is generally less than that of  $(\tau_{\max.} - \tau_{1/2})$ , indicating that the rate of drop disappearance was greater in the period before the median time.

Thus there are a number of criteria of stability based on rest-time measurements. As a matter of convenience we have selected  $\tau_{1/2}$  for most of the analyses presented below.

The influence of  $a$  on the rest-time may be discussed with the aid of the relations describing the rate of film thinning derived previously.

At constant temperature, Eq. [21] for the parallel-disc model reduces to

$$t_{1,2} = \frac{Ka^5}{h_2^2},$$

where  $K$  is constant.

Assuming the time scale of  $t$  to coincide with that of  $\tau$ , it follows that

$$\tau_{1/2} = \frac{Ka^5}{h_{1/2}^2}, \quad [29]$$

where  $h_{1/2}$  is the separation at rupture corresponding to the median rest-time  $\tau_{1/2}$ .

Assuming further that the rupture thickness  $h_{1/2}$  remains constant for all values of  $a$ , it follows from Eq. [29] that

$$\tau_{1/2} = K_1 a^5, \quad [30]$$

where  $K_1$  is a constant.

Equation [30] predicts that  $\tau_{1/2}$  increases with increasing  $a$  as was observed with the benzene/water and other systems (8, 9, 11). A log-log plot of  $\tau_{1/2}$  versus  $a$  for the benzene/water system (Fig. 8) yielded a straight line as predicted by Eq. [30] but had the following form

$$\tau_{1/2} = 86a^{3.15} \text{ sec.} \quad [31]$$

Equation [31] differs from Eq. [30], but the results nevertheless suggest



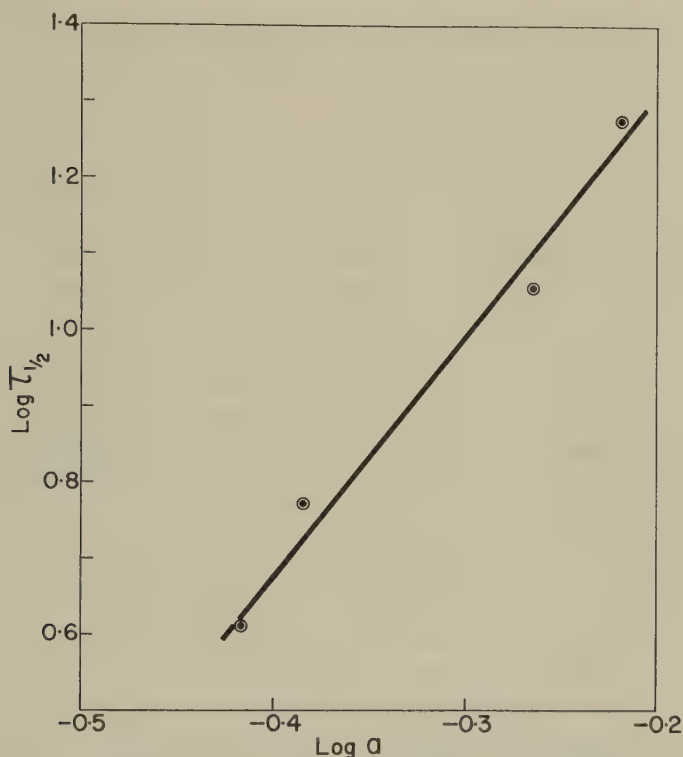


FIG. 8.  $\text{Log } \tau_{1/2}$  versus  $\text{log } a$  for water drops coalescing at a benzene/water interface at 20°C. ( $\tau_{1/2}$  in sec.;  $a$  in cm.).

that the adjacent surfaces of the Phase 2 film behave somewhat like parallel plates.

This becomes more obvious after considering the corresponding relationship predicted for the spherical-planar system. By substituting for  $F$  in Eq. [24] and adopting the same reasoning as in deriving Eq. [30], it is readily shown that

$$\tau_{1/2} = K_2 a^{-1}, \quad [32]$$

where, for a given system and a constant  $h_1/h_{1/2}$  ratio,  $K_2$  is constant. According to Eq. [32], therefore, stability decreases with increasing  $a$ , which is opposite to the prediction of Eq. [30] and to the finding with benzene/water.

Presumably a drop will behave like a rigid sphere when the deformation is small. From Eq. [10], the conditions for this are that either  $b$  ( $=a/2$ ) is small and/or  $\sigma$  is large. Cockbain and McRoberts (6), investigating oil/water systems containing surfactants, reported that  $\tau_{1/2}$  of benzene and paraffin drops showed no marked change between  $a = 0.1$  cm. and 0.47

cm. but increased rapidly with decreasing  $a$  below  $a = 0.1$  cm. Picknett (9) has described the accumulation at an oil/water interface of submicron droplets formed from stepwise coalescence which suggests these were more stable than the larger parent drops.

These observations, therefore, support qualitatively the predictions that the stability of easily deformable drops increases with increasing drop size and decreases with drops which resist deformation.

The decrease in stability with increasing temperature may be expected from the decrease in  $\eta_2$  and the resulting increase in the rate of film thinning indicated by both Eqs. [18] and [23]. However, temperature-dependent properties in addition to viscosity may be involved. Figure 9 shows a test of Eq. [21] in which the variation with temperature of  $\eta_2$  and  $\sigma$  are taken into account by plotting  $(4\sigma^2\tau_{1/2})/(\eta_2\Delta\rho gb^5)$  against temperature for the two systems studied. The results suggest that on increasing the temperature the median rupture thickness  $h_{1/2}$  decreased in benzene/water and increased in water/carbon tetrachloride.

The striking effect of a diffusing component in lowering the stability may be due to localized variations in  $\sigma$  resulting from variations in solute concentration at different positions in the drop interface.

One effect would be to cause surface movements, the so-called Marangoni effect (41), which could increase the rate of thinning. Also according to Eq. [4], a localized decrease in  $\sigma$  will produce outward impulses and interfacial turbulence (42, 43) which could accelerate the film rupture. There are other interesting possibilities but discussion of these appears unwarranted until further experiments are conducted.

The application of an electrostatic field produced an electrostatic attraction between the pendant drop and the flat interface which for small separations ( $h < 10\mu$ ) at the voltages employed was estimated from simple electrostatic theory to be several hundred times that due to gravity. This undoubtedly caused an increase in the rate of thinning, an increase in drop distortion, and hence a decrease in drop stability.

The effect of an electrification in suppressing stepwise coalescence is discussed in another paper (39).

The effect of electrostatic field in promoting coalescence of water droplets in air was reported as early as 1879 by Rayleigh (44). The coalescence of colliding droplets in a weak electrostatic field was attributed to small protuberances in the surfaces of the colliding drops which grow rapidly owing to electrostatic attraction and, eventually, bridge the intervening film (45, 46). Sartor (47) has recently demonstrated a similar effect with liquid droplets sedimenting in another liquid and concluded that this mechanism is important in the growth of raindrops.

The phenomena reported here are undoubtedly similar to those occurring in the technical processes of breaking water-in-oil and other emulsions by

imposing direct and alternating electrical fields (48). Little appears to have been reported on the theory of these processes.

The thicknesses at rupture  $h_{min.}$ ,  $h_{max.}$ , and  $h_{1/2}$  corresponding to  $\tau_{min.}$ ,  $\tau_{max.}$ , and  $\tau_{1/2}$ , respectively, were estimated from Eq. [21] and are given in Table I. The calculated values of  $h$  must be treated with some caution, however, in view of the previously discussed limitations of Eq. [21] and the established deviation from Eq. [30].

It will be noted from Table I that for benzene/water,  $h_{1/2}$  and the other rupture thicknesses increased with increasing  $a$  and with increasing concentration of diffusing component, although the latter calculations may be in error because of surface transport and other effects already mentioned. As suggested earlier, the values of  $h$  decreased with benzene/water and increased with water/carbon tetrachloride as the temperature was raised.

Equation [2] was tested by using the values of  $h$  corresponding to the rupture film thickness at various values of  $\tau$  calculated from Eq. [21] and the corresponding measured values of  $f$ . The relationship between  $\log f$  and  $h^2$  was not linear. In view of the uncertainties of Eq. [21], however, this disagreement does not necessarily invalidate Eq. [2].

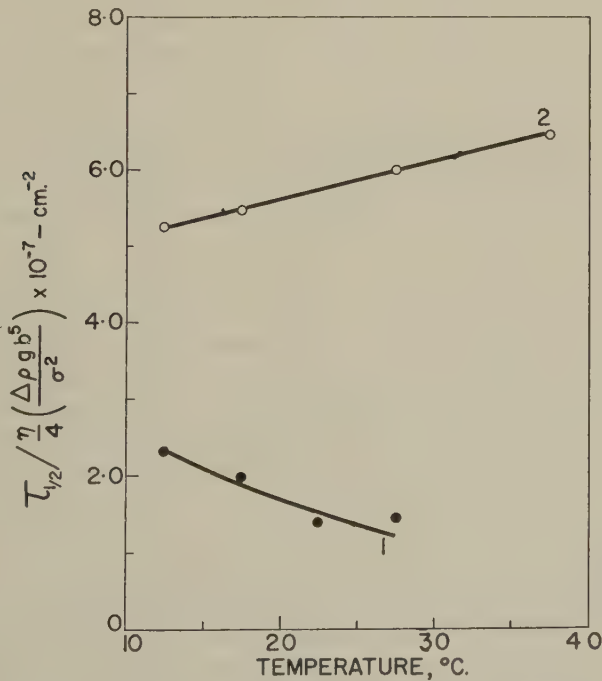


FIG. 9. A plot of  $\tau_{1/2}/(\eta/4)(\Delta\rho gb^5/\sigma^2)$  versus temperature. Curves 1 and 2 are for carbon tetrachloride drops ( $a \cong 0.33$  cm.) and for water drops ( $a \cong 0.56$  cm.) coalescing at water/carbon tetrachloride and benzene/water interfaces, respectively.

For the reasons previously mentioned, the use of the simple equations of approach is open to criticism, particularly when  $h$  is small and forces other than gravity influence the approach. It is evident that at close proximity repulsive interaction forces will arise owing to electrical surface charges (24, 49). In addition to these forces which are responsible for what Derjaguin *et al.* (24) term "disjoining pressures" and which act to stabilize the film, an attraction due to long-range London-van der Waals forces acts to decrease the film thickness (24, 27, 49, 50). It is believed that at separations below approximately  $0.1\mu$  the contribution of the latter to film thinning becomes appreciable (50).

### 3. Film Rupture Experiments

It is interesting to note from Table III the high frequency of off-center ruptures in the pure benzene/water system. These results appear to support the idea (7) that the probability of rupture is greatest where the film thickness is least, i.e., along the circumference of a circle of radius  $c$  from the center. This profile (Fig. 1b), first suggested by Derjaguin and Kussakov (17), was confirmed by others (25, 51) for the approach of a bubble to a solid surface. Such a profile was also recently observed (52) with elongated gas bubbles and liquid drops contained in a glass tube of diameter  $< a$ .

Recent observations made on gas bubbles rising to a liquid/gas interface also revealed that the draining film was thinnest along a ring at a distance from the center (53). Since during the approach the flat interface also deforms, the results suggested profiles for the approaching surfaces as shown in Fig. 1e. Presumably this profile also applies in the liquid/liquid systems under consideration, although no attempt has been made to determine to what extent Eqs. [21] and [26] must be modified to allow for this complication.

Table III shows that  $v_0$  and, hence,  $h$  of the pure benzene/water and water/chloroform systems vary widely even with constant experimental conditions. These results support the conclusions based on the distribution data of Table I and the predictions of others (7, 12) that the liquid film can rupture at different thicknesses. Furthermore, we note that in water/chloroform, the lowest value of  $h$  was obtained with the film showing double rupture, suggesting an increasing chance of rupture with decreasing film thickness.

The following will also be noted from the data in Table III:

a. The average value of  $h$  at low voltages for the benzene/water system, the only one for which comparison can be made, is about  $10\mu$  and is in disagreement with the median thickness  $h_{1/2}$  ( $= 1.4\mu$ ) from rest-time data for approximately the same drop size. These results suggest the possible influence of the electrostatic effects on the rupture of the Phase 2 film which, in view of the limitations of both methods, cannot be given quantitatively until a more direct method of measuring  $h$  is developed.



b. The drop size  $a$  decreased slightly with increasing potential for the system benzene/water. This is attributed to the electrocapillary effect (54), i.e., a decrease in  $\sigma$  due to mutual repulsion of like charges at the interface. This is illustrated by the progressive drop in  $\sigma$  from the drop-volume measurements to 32.3, 31.0, and 26.0 dynes/cm. at 135, 500, and 1000 volts. Since the  $\sigma$  at the other interface was not known but was presumed greater than of the drop, the data were analyzed using  $\sigma = 32.5$  dynes/cm. corresponding to an uncharged system. Thus the values of  $h$  reported in Table I may be slightly high; for example at 1000 volts,  $28 < h < 34.7\mu$  since  $26.0 < \sigma < 32.5$  dynes/cm.

c. Values of  $h$  from Eq. [26] increased markedly when the voltage was increased to 1000 volts. This may have been due to uneven drainage and enhanced thinning at the point of rupture where the film was possibly thinnest. Electrocapillarity, resulting in a lower  $\sigma$ , may have also contributed to the lowering of  $v_0$  and hence to an apparent increase in  $h$ .

d. The effect of dirt was as expected, i.e., bridging of the Phase 2 film and, hence, rupture at a higher  $h$ . With the exception of the systems containing surfactant, the highest values of  $h$  were obtained when glass beads were used.

e. In all the cases discussed above,  $R$  was invariably greater than the actual drop radius  $b(=a/2)$  from volume measurement. This suggests that flattening of the drop had occurred at the point of rupture as indicated also by the drop stability data previously discussed. The value of  $R$  was consistently much higher for pure benzene/water than for the water/chloroform system. This also is to be expected from the flattening effect of the electrostatic field employed with the first system but not the second.

f. The value of  $R$  varied erratically when surfactant was present in the benzene/water system. Although the individual values are scattered, there appears to be a decrease in  $v_0$  and hence an increase in  $h$  with increasing amount of surfactant. It would be expected, on the other hand, that a stabilizing surfactant would lead to a decrease in the film thickness at rupture. These anomalies may arise from the sudden compression (55) of the interfacial film causing a momentary increase in surface pressure, and hence decreases in  $\sigma$  before the surface concentration of surfactant can drop to the equilibrium value by diffusing into the bulk liquid in which it is soluble (56).

The last observation indicates one complication of the Dupré equation. It is, perhaps, appropriate to consider another complication already mentioned, namely, the surface energy required to overcome the viscous drag of the receding edge of the Phase 2 film.

An approximate analysis of this effect can be made with the aid of several simplifying assumptions. If, as before, we consider the film to rupture at one point and assume that: (a). the film thickness  $h$  is constant; (b). motion is limited to the periphery of the hole where the film rolls up



under the action of  $\sigma$ ; (c). the viscous force per unit length of periphery is given by  $(k_1 v_r)$ , where  $k_1$  is a constant to be considered later; then the energy balance at time  $t$  when the hole radius is  $r$  is given by

$$\frac{1}{2}\pi r^2 h(\rho_1 + \rho_2)v_r^2 + \int_0^r 2\pi r k_1 v_r dr = 2\pi r^2 \sigma. \quad [33]$$

The first term on the left-hand side is the kinetic energy and the second the viscous energy dissipation. On differentiating with respect to  $r$ , this equation reduces to

$$h(\rho_1 + \rho_2) \left[ v_r^2 + r v_r \frac{dv_r}{dr} \right] + 2k_1 v_r = 4\sigma, \quad [34]$$

from which it is readily shown that  $v_r$  decreases with increasing  $r$  as was found experimentally.

It follows from Eq. [34] that when  $r = 0$ , the film thickness is given by

$$h = \frac{(4\sigma - 2k_1 v_0)}{(\rho_1 + \rho_2)v_0^2}, \quad [35]$$

where  $v_0$  is the initial velocity. When  $k_1 = 0$ , Eq. [35] reduces to Eq. [26].

Unfortunately, the prediction of  $k_1$  for the present system is difficult. As an approximation we may consider the resistance of the peripheral ring equal to that of a solid cylinder moving at right angles to its axis through the fluid of viscosity  $\eta_1$ . According to Burgers (57), for this model at low Reynolds' numbers

$$k_1 = \frac{4\pi\eta_1}{\log_e \left( \frac{4L}{D} \right) + 0.5}, \quad [36]$$

where  $L$  and  $D$  are the length and the diameter, respectively of the cylinder.

For practical purposes, we will consider the value of  $k_1$  when  $r = D$  and assume that  $D = h$ . Then, from Eq. [36],  $k_1 = 3.4\eta_1$ . Substituting for  $k_1$  in Eq. [35] gives

$$h = \frac{4\sigma - 6.8\eta_1 v_0}{(\rho_1 + \rho_2)v_0^2}. \quad [37]$$

The observed decrease of  $v_r$  with increasing  $r$  may thus be due to viscous effects instead of the varying film thickness assumed in Eq. [27], which, under these circumstances, may be regarded as a convenient empirical equation for determining  $v_0$  from the experimental data.

It is evident from Eq. [37] that the effect of viscous drag upon  $h$  predicted by Eq. [26] may become appreciable when  $\eta_1$  and  $v_0$  are high. For example,  $h$  from Eq. [37] for benzene Phase 2 film ruptured at 135 volts is  $5.5\mu$ , whereas the value obtained from Eq. [26] is  $6.6\mu$ .

#### 4. *Concluding Remarks*

Whereas in general outline the coalescence phenomena described above can be explained, the details are complicated and warrant further study—particularly of the effects of electrostatic fields and of diffusing components. It is reasonably certain that the rupture process is random and in a given system occurs with increasing frequency as the film thickness decreases (7). However, the absolute values of film thickness are difficult to establish by measurements of drop stability or rupture velocity. Whereas rest-time measurements provide a useful experimental method of assessing drop stability, the data are difficult to analyze and do not afford a detailed insight into the mechanism of coalescence.

It is our belief that a theoretical analysis of 2-dimensional capillary waves in films similar to the 1-dimensional analysis put forward by Rayleigh (58) and others for the break-up of liquid jets and which we have applied to the study of stepwise coalescence (29) should prove valuable in analyzing film rupture data.

The foregoing remarks apply to 2-component systems. It is evident that the phenomena are even more complicated in systems containing surfactants such as emulsifiers, detergents, and foam-inhibitors which greatly complicate the properties of the interface.

#### ACKNOWLEDGMENT

The authors are indebted to Professor R. T. Sharpe, Department of Mathematics, McGill University, for valuable suggestions in connection with the theoretical treatment.

#### SUMMARY

A liquid drop (Phase 1) falling through a lighter liquid (Phase 2) onto a Phase 1/Phase 2 interface rests at the interface for a time  $\tau$  before coalescing with the underlying phase. In a given system  $\tau$  follows a roughly Gaussian distribution between  $\tau_{\min.}$  and  $\tau_{\max.}$ .

Results obtained with oil/water systems corroborate a number of earlier findings, e.g., stability increases with decreasing temperature and with increasing drop size. With oil/water systems,  $\tau$  was markedly reduced when the drop contained small amounts of a diffusing component, when an electrostatic field was applied, or when the interface was contaminated with solid particles.

High-speed cine-photographs of the Phase 2 film between the drop and interface showed that rupture does not always occur at the same position in the film and can occasionally occur at two places simultaneously. The expansion of the radius of the "hole" was rapid and generally decreased with time. The results from film rupture studies suggest that rupture of the Phase 2 film occurs over a range of thicknesses.

The experimental data were analyzed using equations derived for drop deformation, film thinning, and film rupture. The limitations of these equations are discussed in detail.

## REFERENCES

1. REYNOLDS, O., *Chem. News* **44**, 211 (1881).
2. GOSSART, E., *Ann. chim. et phys.* (5) **4**, 391 (1895).
3. REHBINDER, P. A., AND WENSTROM, E. K., *Kolloid-Z.* **53**, 145 (1930).
4. MAHAJAN, L. D., *Kolloid-Z.* **65**, 20 (1933).
5. MAHAJAN, L. D., *Kolloid-Z.* **69**, 16 (1934).
6. COCKBAIN, E. G., AND MCROBERTS, T. S., *J. Colloid Sci.* **8**, 440 (1953).
7. GILLESPIE, T., AND RIDEAL, E. K., *Trans. Faraday Soc.* **52**, 173 (1956).
8. ELTON, G. A. H., AND PICKNETT, R. G., "Proceedings of the 2nd International Congress of Surface Activity," Vol. 1, p. 287. Butterworths, London, 1957.
9. PICKNETT, R. G., Ph.D. Thesis, University of London, 1957.
10. WATANABE, T., AND KUSUI, M., *Bull. Chem. Soc. Japan* **31**, 236 (1958).
11. NIELSEN, L. E., WALL, R., AND ADAMS, G., *J. Colloid Sci.* **13**, 441 (1958).
12. SHELUDKO, A., *Z. Elektrochem.* **61**, 220 (1957).
13. SHELUDKO, A., *Kolloid-Z.* **155**, 39 (1957).
14. DUPRÉ, A., "Théorie Mécanique de la Chaleur," p. 350. Gauthier-Villars, Paris, 1869.
15. RAYLEIGH, LORD, *Proc. Roy. Inst. G. Brit.* **13**, 261 (1891); *Nature* **44**, 249 (1891).
16. DE VRIES, A. J., *Rec. trav. chim.* **77**, 383 (1958).
17. DERJAGUIN, B. V., AND KUSSAKOV, M., *Acta Physicochim. U.R.S.S.* **10**, 25 (1939).
18. STEFAN, J., *Sitzber. Akad. Wiss. Wien, Math.-naturw. Kl.* **69**, 713 (1874).
19. REYNOLDS, O., *Phil. Trans. Roy. Soc. (London)* **A177**, 157 (1886).
20. GREEN, H., *Ind. Eng. Chem., Anal. Ed.* **13**, 632 (1941).
21. BIKERMAN, J. J., *J. Colloid Sci.* **2**, 163 (1947).
22. BOWDEN, F. P., AND TABOR, D., "The Friction and Lubrication of Solids," p. 272. Oxford University Press, London, 1950.
23. HARDY, W. B., AND BIRCUMSHAW, I., *Proc. Roy. Soc. (London)* **A108**, 12 (1925).
24. DERJAGUIN, B. V., TITILEVSKAIA, A. S., ABRICOSSOVA, I. I., AND MALKINA, A. D., *Discussions Faraday Soc.* **No. 18**, 24 (1954).
25. ELTON, G. A. H., *Proc. Roy. Soc. (London)* **A194**, 259, 275 (1948).
26. ELTON, G. A. H., *Proc. Roy. Soc. (London)* **A197**, 568 (1949).
27. OVERBEEK, J. TH. G., AND SPARNAAY, J., *Discussions Faraday Soc.* **No. 18**, 12 (1954).
28. KITCHENER, J. A., AND PROSSER, A. P., *Proc. Roy. Soc. (London)* **A242**, 403 (1957).
29. HADAMARD, J., *Compt. rend.* **152**, 1735 (1911).
30. RUBCZYNSKI, W., *Bull. acad. polon. sci.* **1**, 40 (1911).
31. GARNER, F. H., *Trans. Inst. Chem. Engrs. (London)* **28**, 88 (1950).
32. GARNER, F. H., AND SKELLAND, A. P. H., *Trans. Inst. Chem. Engrs. (London)* **29**, 14 (1951).
33. GARNER, F. H., AND HALE, A. R., *Chem. Eng. Sci.* **2**, 157 (1953).
34. GARNER, F. H., AND HAMMERTON, D., *Chem. Eng. Sci.* **3**, 1 (1954).
35. LINTON, M., AND SUTHERLAND, K. L., "Proceedings of the 2nd International Congress of Surface Activity," Vol. 1, p. 494. Butterworths, London, 1957.
36. HARKINS, W. D., AND BROWN, F. E., *J. Am. Chem. Soc.* **41**, 499 (1919).
37. International Critical Tables, Vol. III, p. 27.
38. Handbook of Chemistry and Physics, 38th ed., p. 2031, Chemical Rubber Publishing Co., Cleveland, 1956.

39. CHARLES, G. E., AND MASON, S. G., *J. Colloid Sci.*, **15**, 105 (1960).
40. SHERWOOD, T. K., AND REED, C. E., "Applied Mathematics in Chemical Engineering," p. 288. McGraw-Hill, New York, 1939.
41. BIKERMAN, J. J., "Surface Chemistry," 2nd ed., p. 89. Academic Press, New York, 1958.
42. HAYDON, D. A., *Nature* **176**, 839 (1955).
43. DAVIES, J. T., AND HAYDON, D. A., "Proceedings of the 2nd International Congress of Surface Activity," Vol. 1, p. 400. Butterworths, London, 1957.
44. RAYLEIGH, LORD, *Proc. Roy. Soc. (London)* **A28**, 406 (1879).
45. RAYLEIGH, LORD, *Proc. Roy. Soc. (London)* **A34**, 130 (1882).
46. RAYLEIGH, LORD, *Phil. Mag.* **48**, 328 (1899).
47. SARTOR, D., *J. Meteorol.* **11**, 91 (1954).
48. CLAYTON, W., "The Theory or Emulsions and Their Technical Treatment," 5th ed., p. 582. Churchill, London, 1954.
49. VERWEY, E. J. W., AND OVERBEEK, J. TH. G., "Theory of the Stability of Lyophobic Colloids." Elsevier, New York, 1948.
50. VAN DEN TEMPEL, M., *J. Colloid Sci.* **13**, 125 (1958).
51. EVANS, L. F., *Ind. Eng. Chem.* **46**, 2420 (1954).
52. GOLDSMITH, H., AND MASON, S. G., forthcoming publication.
53. CHARLES, G. E., ALLAN, R. S., AND MASON, S. G., forthcoming publication.
54. ADAM, N. K., "The Physics and Chemistry of Surfaces," 3rd ed., p. 336. Oxford University Press, London, 1941.
55. HELLER, S., *Kolloid-Z.* **136**, 120 (1954).
56. RABINOVITCH, W., ROBERTSON, R. F., AND MASON, S. G., forthcoming publication.
57. BURGERS, J. M., "Second Report on Viscosity and Plasticity," p. 125. Academy of Sciences, Amsterdam, 1938.
58. RAYLEIGH, LORD, *Proc. Lond. Math. Soc.* **10**, 4 (1879).

## MICELLAR WEIGHTS OF NONIONIC SURFACTANTS IN THE PRESENCE OF *n*-DECANE OR *n*-DECANOL

T. Nakagawa, K. Kuriyama, and H. Inoue

*Research Laboratory of Shionogi & Co., Ltd., Amagasaki, Japan*

*Received November 24, 1959*

### ABSTRACT

The light scattering of methoxy polyoxyethylene decyl ethers solubilizing *n*-decane or *n*-decanol has been studied at the various solubilize/surfactant ratios. Reduced intensities obtained were analyzed according to Debye's treatment. The micellar weights increase with the addition of solubilizates within the saturation limit, and it is shown that the solubilization process is accompanied by the reconstitution of micelles.

### INTRODUCTION

Many reports concerning solubilization phenomena have appeared (1), and it is well known that soap micelles swell as a result of the solubilization of a hydrocarbon (2, 3, 4). In these latter papers the analysis of the X-ray scattering was done on the supposition of a periodic structure which could be characterized by spacings calculated from the Bragg equation. The validity of this procedure is questionable, because it assumes a quasi-crystalline arrangement of the micelles in the solution. Accordingly, it appears worth while to apply the light-scattering method to resolve the problem.

It is known that the nonionic surfactants in aqueous solution form micelles above the critical micelle concentration (5-14). In this work, using two samples of methoxy polyoxyethylene decyl ether the hydrophilic chain lengths of which differ from one another, the micellar weights have been determined by the light-scattering method, after the addition of various amounts of *n*-decane or *n*-decanol.

### EXPERIMENTAL

#### *Surfactants*

Two samples of methoxy polyoxyethylene decyl ether  $C_{10}H_{21}(O-CH_2-CH_2)_pOCH_3$  ( $p = 8$  and  $11$ ) were synthesized. They are abbreviated as MPd-8 and -11, respectively.

Methoxy polyethylene glycol (MPEG), which had been fractionated by



molecular distillation,<sup>1</sup> was converted to the sodium alcoholate by adding it to sodium dispersion in toluene. Decyl chloride was then added dropwise to the reaction mixture, which was subsequently heated to 100°C. for 5 hours.

After removing sodium chloride and toluene, the residue was dissolved in water and heated to 100°C. Two hours later, the originally clear solution separated into two layers; the lower water-rich phase was discarded and the upper phase was redissolved in water. This heat-separation procedure was repeated three times, and the product was dried *in vacuo*.

The product was fractionated in a molecular-distillation apparatus to remove the contaminating decyl chloride, dissolved in acetone, and decolorized by passing through a charcoal column. The purified samples contained no detectable free MPEG and decyl chloride; this was verified by paper chromatography (15) and chlorine analysis; the analytical values and molecular weights determined by the freezing point depression of benzene solution also coincided with those expected.

### *Light Scattering*

All measurements of reduced intensity were carried out with a commercial apparatus (Shimadzu Instrument Co., Kyoto, Japan) similar to the one described by Brice *et al.* (16). Minor modifications were made in the slit system to stabilize the light intensity.

The apparatus was calibrated against an opal glass diffusor the transmittance value of which had been determined precisely by the manufacturer.

The measurements were carried out at 30°C.  $\pm$  1°C. and 546 m $\mu$ .

### *Refractive Index Increments*

These were determined with a differential refractometer (Shimadzu Instrument Co.) similar to the one described by Debye (17), at the same temperature and wave length as above.

### *Preparation of Solutions*

Throughout this work, the light intensities scattered at 90° angle in the same semioctagonal cell were measured and used as calculation bases, although 45° and 135° scatterings were also determined. The reduced intensity  $R_{90}$  of water used was about  $1.5 \times 10^{-6}$  cm.<sup>-1</sup>. As the surfactant concentration was increased over 0.3 g./dl., the dissymmetry was about 1.03. Micellar weight, therefore, was obtained from the reduced intensity at 90° without the correction for the dissymmetry.

<sup>1</sup> The molecular weight was evaluated by OH value test; cf. *Drug Standards* 21, 116 (1953).

TABLE I  
*The Molecular Weight and the Analytical Value*

Surfactant	Molecular weight		Analytical value			
	Expected from synthesis	Detd. by freezing pt. depress.	C%		H%	
			Obs.	Calc.	Obs.	Calc.
MPd-8	522	520	62.02	61.83	10.77	10.69
MPd-11	663	660	60.33	60.34	10.57	10.43

TABLE II  
*Effect of Added Solubilizates on Micellar Constitution*

Surfactant (S)	Solubilizate (H)	H/S (wt. per cent)	dn/dc	Monomer conc. $C_0 \times 10^2$ (g./100 ml.)	Micellar weight ( $M \times 10^{-4}$ )	No. soap molecules per micelle	No. oil molecules per micelle
MPd-8	n-decane	0	0.126	6.0	4.31	83	0
		1.32	0.126	5.7	4.56	87	4
		2.33	0.126	5.4	4.78	90	8
		3.16	0.126	5.2	5.05	94	11
		3.78	0.126	5.1	5.20	96	13
		4.93	0.126	4.8	5.75	105	19
		(12.0)	0.126	4.0	8.85	158	46
		(150)	0.126	4.0	9.07	162	47
	n-decanol	3.40	0.126	5.2	4.78	89	10
		6.19	0.126	4.5	5.13	93	19
		8.50	0.126	4.0	6.13	109	30
		11.42	0.126	3.3	9.09	157	59
		16.61	0.125	2.0	21.3	351	192
MPd-11	n-decane	0	0.127	9.5	4.29	65	0
		1.40	0.127	9.2	4.48	67	4
		2.58	0.127	9.0	5.15	76	9
		3.31	0.127	8.8	5.43	80	12
	n-decanol	5.67	0.127	8.4	5.26	75	18
		10.18	0.127	7.5	6.29	86	37
		17.12	0.126	6.3	12.2	158	113

When the amount of solubilizate was within the solubilizing power of the surfactant, each test solution was made from the starting test solution, which had been prepared by diluting a mixture of solubilizate and surfactant (about 2 g.) to 100 ml. with water. Then, all the test solutions were made from the respective starting solution, by diluting it successively with water, and they were filtered into the cell through an "Ultra Cellafilter" (Membranfilter Gesellschaft, Göttingen, Germany) immediately before scattering measurements. That the filtration process causes no concentration change

was ascertained by weighing the residue, after evaporating off the solvent by freeze-drying.

The curves in Fig. 1 and analogous systems, and the refractive index increments  $dn/dc$  listed in Table II, were obtained by plotting the reduced intensities and the refractive indexes of a series of test solutions made from the same starting test solution, namely, a series having the same solubilize/surfactant ratio, against the total solute concentration  $c$  (surfactant + solubilize  $w/v$ ).

To prepare the solution saturated with respect to the solubilize, an excess of solubilize was added to the aqueous solution of MPd-8 (about 2 wt. %), and the mixture was shaken vigorously for 2 days at  $30^\circ \pm 1^\circ\text{C}$ . In the case of  $n$ -decane, an emulsion layer of the hydrocarbon floated on the transparent aqueous solution, which was saturated with the solubilize: in the case of  $n$ -decanol, there appeared three transparent layers, in which the predominant component is  $n$ -decanol, MPd-8, or water, respectively. In both cases, the lowest aqueous phase served as the starting test solution, the concentration of which was determined by weighing the solute after freeze-drying. The other test solutions were prepared as described above.

### RESULT AND DISCUSSION

Figure 1 shows the curves of reduced intensity  $R_{90}$  against total solute concentration  $c$  at various  $n$ -decane (g.)/MPd-11(g.) ratios. For other systems, analogous curves were obtained, but they are not reproduced here.

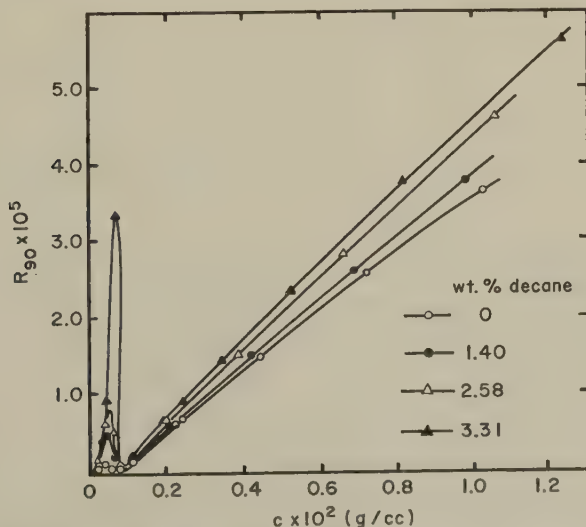


FIG. 1. Variation of  $R_{90}$  with total solute concentration at various  $n$ -decane/MPd-11 ratios.

We see in Fig. 1 that the solution containing no solubilize maintained almost zero value of scattering to a certain concentration, and this concentration may be interpreted (18) as the critical micelle concentration (CMC). But when additional solubilize was present, a peak appeared at a lower concentration and its height became greater, the more solubilize was present. Moreover, its height was also governed by time lapse after preparation of the solution. The peak illustrated in Fig. 1 represents that observed when the previously diluted solution was filtered into the cell, but when the concentrated solution was filtered into the cell and there diluted to the same concentration as above, the peak became much more distinct.

These phenomena may be interpreted as follows. When the solution is diluted, some of the micelles break up and the solubilize molecules, so far included in them, are ejected. These molecules, now insoluble, aggregate to form particles larger than micelles and cause the appearance of the peak. These particles may be finely divided emulsion particles of solubilize alone or of a molecular compound of solubilize and surfactant. Their real character or constitution can not be defined at present. Phillips and Mysels (19) reported the same phenomenon in the case of sodium dodecyl sulfate (SDS) solubilizing dodecanol, and they supposed that the composition of the particles is not the pure alcohol, but a molecular compound having the constitution  $C_{12}H_{25}OH \cdot 2SDS$ , characterized by Epstein *et al.* (20).

In order to evaluate the micellar weight from the light-scattering data, the Debye (18) equation below is generally used.

$$\frac{K(c - c_0)}{R_{90}} = \frac{1}{M} + 2B(c - c_0);$$

$$K = \frac{2\pi^2 n_0^2}{N\lambda_0^4} \left( \frac{dn}{dc} \right)^2,$$

where  $R_{90}$  = the reduced intensity of the solution at  $90^\circ$  minus that of the solvent;

$n_0$  = the refractive index of the solvent;

$n$  = the refractive index of the solution;

$c$  = the concentration (g./ml.);

$\lambda_0$  = the wavelength of incident light in vacuum;

$N$  = Avogadro's number;

$M$  = the micellar weight;

$B$  = the interaction constant; and

$c_0$  = the monomer concentration.

Here also, the above equation is applied, supposing that  $c_0$  is obtained by extrapolating each  $R_{90}$ - $c$  curve to  $R_{90} = 0$ . The monomer concentrations of surfactants ( $c_0$ ), the values of which are listed in Table II, decrease

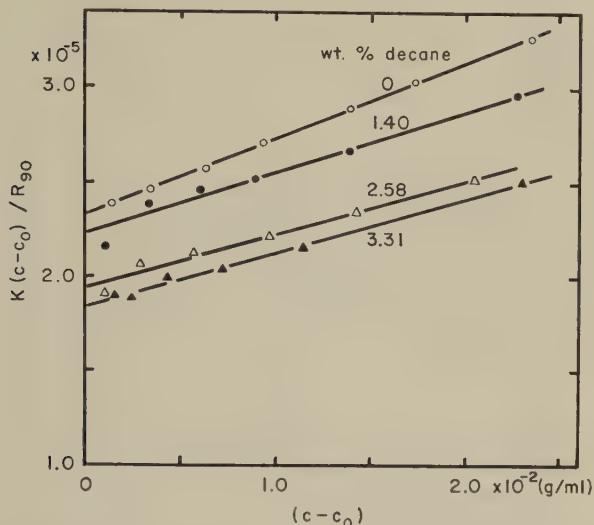


FIG. 2. The quantity  $K(c - c_0)/R_{90}$  as a function of micellar concentration  $(c - c_0)$  at various *n*-decane/MPd-11 ratios.

gradually with the addition of solubilizates, as shown in the case of ionic detergents (21-23). Debye's formula is derived assuming that the micellar constitution is not altered by concentration change, but its applicability may be suspect in the present case where some solubilize is included, especially in the lower concentration range of the solutions.

In Figs. 2-5 the data are plotted according to Debye's treatment. The derived curves form straight lines except at lower concentration. Extrapolating them, micellar weights are estimated from the intercepts with the ordinate. The numbers of surfactant and solubilize molecules constituting one micelle were calculated from the micellar weight and mixing ratio. They are listed in Table II.

Figure 6 shows how the micellar weight varies with the amount of solubilize.

As shown in Table II and Fig. 6, in any system in which the micellar weight becomes larger, the proportion of solubilize included in the micelle also increases (up to the solubilization limit). This increase of micellar weight does not originate from the simple incorporation of solubilize molecules into the existing micelle of definite composition but also from the number of surfactant molecules which are in the micelle, which increases with the added solubilize. Thus the solubilization process is accompanied by the reconstitution of the micelles. This result coincides with that obtained by Mattoon *et al.* (3), who estimated the micellar weights assuming that the Bragg spacing  $d_l$  was the distance between the center of a micelle and that of any one of its nearest neighbors. Brady and Huff (24) also



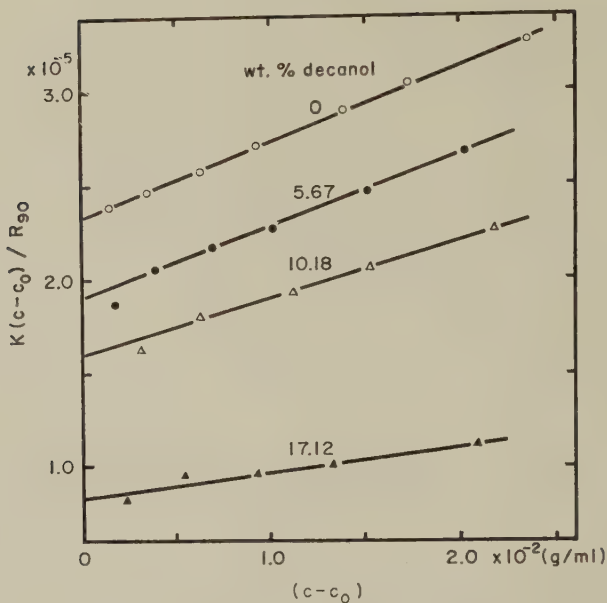


FIG. 3. The quantity  $K(c - c_0)/R_{90}$  as a function of micellar concentration  $(c - c_0)$  at various  $n$ -decanol/MPd-11 ratios.

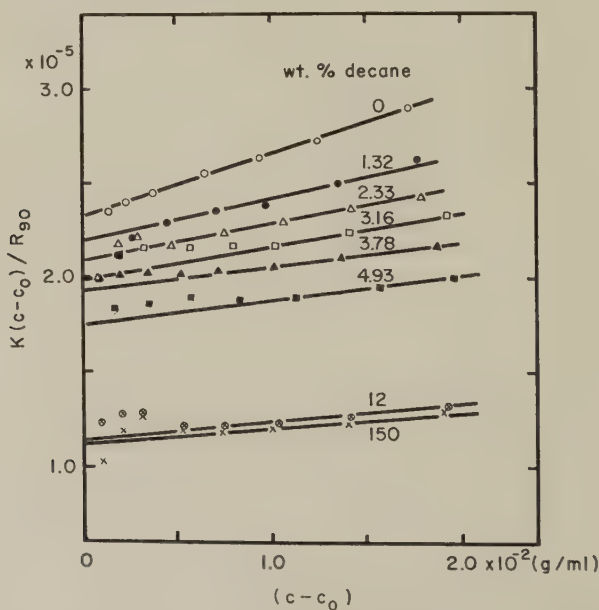


FIG. 4. The quantity  $K(c - c_0)/R_{90}$  as a function of micellar concentration  $(c - c_0)$  at various  $n$ -decane/MPd-8 ratios.  $\otimes$ ,  $\times$  Excess of  $n$ -decane ( $n$ -decane/MPd-8 ratios are 0.12 and 1.50, respectively) over solubilization limit was added, and the lower was measured after shaking and settling.

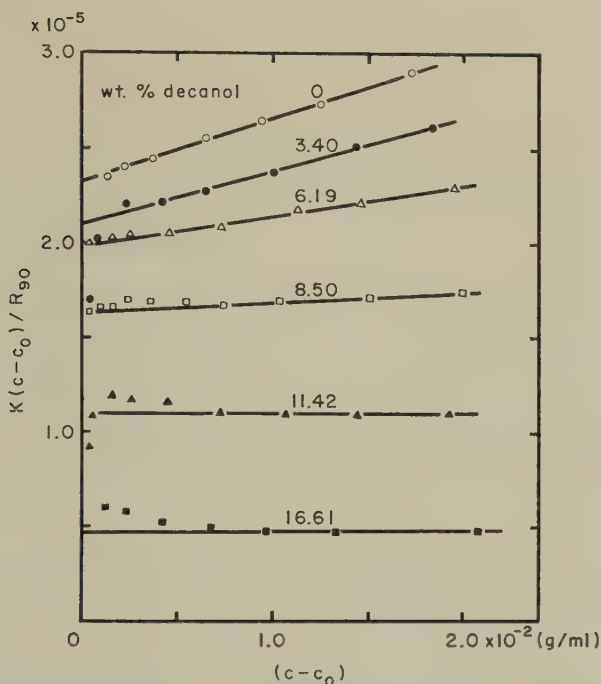


FIG. 5. The quantity  $K(c - c_0)/R_{90}$  as a function of micellar concentration  $(c - c_0)$  at various  $n$ -decanol/MPd-8 ratios.

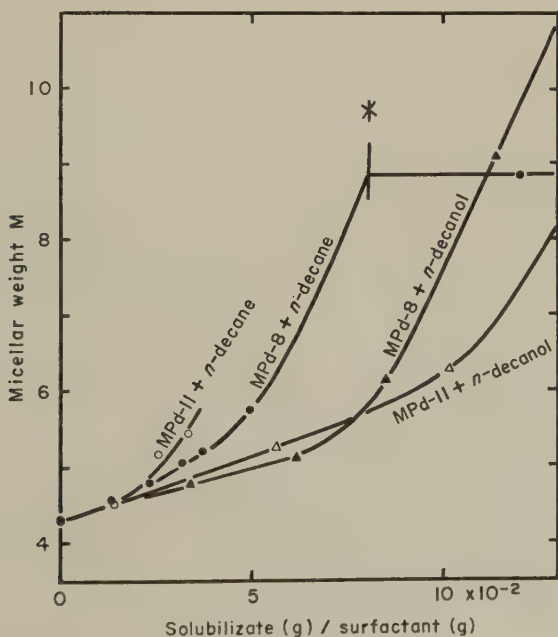


FIG. 6. Variation of the micellar weight  $M$  with solubilize/surfactant ratio. \* The solubilization limit was determined by transmission measurement.

arrived at an analogous conclusion from a quite different technique (the measurement of the vapor pressure of solubilized benzene).

When *n*-decane is added to the MPd-8 solution above its solubilization limit, little or no change of micellar weight is observed, whereas the addition of a large excess of *n*-decanol causes phase separation and gives three layers. In the latter case, the lowest layer is an aqueous solution of MPd-8 the concentration of which is almost equal to the CMC. The middle layer is rich in MPd-8 and the top is mainly composed of *n*-decanol. The above behavior seems to be interpretable as follows: in the system MPd-8-*n*-decanol, the inclusion of more and more decanol progressively lowers the clouding point of the solution and finally phase separation occurs, even at room temperature.

In order to analyze the light-scattering data obtained, we have previously assumed the following two conditions, i.e., (1) as in the solvent, with regard to micelles, there exists a solution having a definite concentration  $c_0$ , at each solubilize/surfactant ratio, and (2) the composition of the micelle is not affected by the concentration of solution.

However, in the present case where some solubilize coexists in the system, the adequacy of the above assumption is doubtful. In lower concentration range where monomolecularly dispersed surfactant is a large portion of the total surfactant present, it seems especially irrational to imagine a micelle of fixed composition. Indeed, this follows from the data, as shown in Figs. 2-5, where the  $K(c - c_0)/R_{90} - (c - c_0)$  curves deviate from straight lines in the lower concentration ranges. At higher concentrations, however, they form straight lines, thus supporting the assumption of micelles of nearly fixed composition in this range, although it should be borne in mind that the linearity of the curve does not necessarily warrant the adequacy of the assumption. The micellar weight, which is obtained by extrapolating the  $K(c - c_0)/R_{90} - (c - c_0)$  curve in the range of sufficiently high concentration to the ordinate, is scarcely affected by a small change of  $c_0$ ; thus the obscurity of  $c_0$  values introduces no significant difference in the final results.

Other treatments of the data may be devised, but perhaps they will also have weak points analogous to the above, and the correct method of analysis will probably not be found until more precise information about the structure of solutions become available.

In the present work, therefore, it is necessary to recognize that the results described here include some inevitable errors as to absolute values, but the results afford at least qualitatively a clearer picture of the behavior of micelles in the solubilization phenomena.

#### ACKNOWLEDGMENT

The authors wish to thank the Director of Shionogi Research Laboratory for encouragement to accomplish and permission to publish this work.

## REFERENCES

1. MCBAIN, M. E. L., AND HUTCHINSON, E., "Solubilization and Related Phenomena." Academic Press, New York, 1955; KLEVEN, H. B., *Chem. Revs.* **47**, 1 (1950).
2. HARKINS, W. D., MATTOON, R. W., AND CORRIN, M. L., *J. Colloid Sci.* **1**, 104 (1946).
3. MATTOON, R. W., STEARNS, R. S., AND HARKINS, W. D., *J. Chem. Phys.* **16**, 644 (1948).
4. MCBAIN, J. W., AND HOFFMAN, O. A., *J. Phys. & Colloid Chem.* **53**, 39 (1949).
5. MCBAIN, J. W., AND MARSDEN, S. S., JR., *J. Chem. Phys.* **15**, 211 (1947); *J. Phys. Chem.* **52**, 110 (1948).
6. GONICK, E., AND MCBAIN, J. W., *J. Am. Chem. Soc.* **69**, 334 (1947).
7. KUSHNER, L. M., AND HUBBARD, W. D., *J. Phys. Chem.* **58**, 1163 (1954).
8. KUSHNER, L. M., HUBBARD, W. D., AND DOAN, A. S., *J. Phys. Chem.* **61**, 371 (1957).
9. STAUFF, J., AND RASPER, J., *Kolloid-Z.* **151**, 148 (1957).
10. HSIAO, L., DUNNING, H. N., AND LORENTZ, P. B., *J. Phys. Chem.* **60**, 657 (1956).
11. NAKAGAWA, T., KURIYAMA, K., INABA, M., AND TORI, K., *Nippon Kagaku Zasshi* **77**, 1563 (1956); *cf. Chem. Abstr.* **51**, 10187 (1957).
12. NAKAGAWA, T., TORI, K., AND KURIYAMA, K., *Nippon Kagaku Zasshi* **77**, 1684 (1956); *cf. Chem. Abstr.* **51**, 10187 (1957).
13. NAKAGAWA, T., KURIYAMA, K., AND TORI, K., *Nippon Kagaku Zasshi* **78**, 1568, 1573 (1957); *cf. Chem. Abstr.* **52**, 12514 (1958).
14. NAKAGAWA, T., KURIYAMA, K., INOUE, H., AND OYAMA, T., *Nippon Kagaku Zasshi* **79**, 348 (1958); *cf. Chem. Abstr.* **52**, 21172 (1958).
15. NAKAGAWA, T., AND NAKATA, I., *Kogyo Kagaku Zasshi* **59**, 710, 1154 (1956); *cf. Chem. Abstr.* **52**, 4418, 14199 (1958).
16. BRICE, B. A., HALWER, M., AND SPEISER, R., *J. Opt. Soc. Amer.* **40**, 768 (1950).
17. DEBYE, P. P., *J. Appl. Phys.* **17**, 392 (1946).
18. DEBYE, P., *Ann. N. Y. Acad. Sci.* **51**, 575 (1949).
19. PHILLIPS, J. N., AND MYSELS, K. J., *J. Phys. Chem.* **59**, 325 (1955).
20. EPSTEIN, M. B., WILSON, A., JAKOB, C. W., CONROY, L. E., AND ROSS, J., *J. Phys. Chem.* **58**, 860 (1954).
21. HERZFELD, S. H., CORRIN, M. L., AND HARKINS, W. D., *J. Phys. & Colloid Chem.* **54**, 271 (1950).
22. RALSTON, A. W., AND EGGENBERGER, D. N., *J. Am. Chem. Soc.* **70**, 983 (1948).
23. GRIEGER, P. F., *Ann. N. Y. Acad. Sci.* **51**, 827 (1949).
24. BRADY, A. P., AND HUFF, H., *J. Phys. Chem.* **62**, 644 (1958).

## LETTERS TO THE EDITOR

THE EXISTENCE OF A MAXIMUM IN THE CURVE OF WASHING  
POWER vs. CONCENTRATION OF DETERGENT

It is generally known that the washing efficiency of a detergent increases up to a certain concentration of detergent, a critical washing concentration (c.w.c.), beyond which further addition of detergent has little effect. Preston (1) has pointed out that the c.w.c. of a detergent is about the same as its critical concentration for micelle formation (c.m.c.). In fact it has often been observed that the detergency curve falls slowly after passing through a maximum. However, the existence of a maximum washing concentration seems still not to be established, since most of the observation of detergency has been based on the difference in reflectance of washed and soiled cloths as a measure of the amount of soil content remaining on the cloths and this procedure has been subjected to serious question as to the validity (2).

Ashcraft (3) has obtained a detergency curve with a maximum, not only by the reflectance method but also by the radiotracer method. However, interpretation of his result is difficult since the soil used in his experiment consisted of a complicated system of three components: carbon black, glyceryl tristearate, and algal protein. Hence, in order to establish the existence of a maximum washing concentration, the following experiments were undertaken with a more simplified system.

Cloths of scoured and bleached cotton were soiled with fat alone. They were soiled with highly hydrogenated beef tallow (m.p., 57.6°C., iodine value, 3.1) which was dissolved in carbon tetrachloride. Test pieces 10 cm.  $\times$  10 cm. in size were cut from a roll of soiled cloth after the removal of the solvent by evaporation. The detergent was sodium dodecyl sulfate (SDS), prepared according to the usual method (4), and purified by ether extraction and repeated crystallizations from ethyl alcohol. Washing was carried out by the Launder-Ometer of the Atlas Electric Devices Co. One test sample was placed in each jar with 100 ml. of detergent solution and twenty rubber balls to provide agitation and was washed for 30 minutes at 40°C. Thereafter each of the cloth samples was rinsed with 600 ml. of distilled water and dried in a vacuum desiccator.

Fat adhering to cloths was extracted by benzene in a Soxhlet apparatus. The concentration of fat in the benzene solution was measured by employing the equilibrium lens method (5). The benzene solution of the extract was added dropwise on a known area of a substrate of tap water in a tray



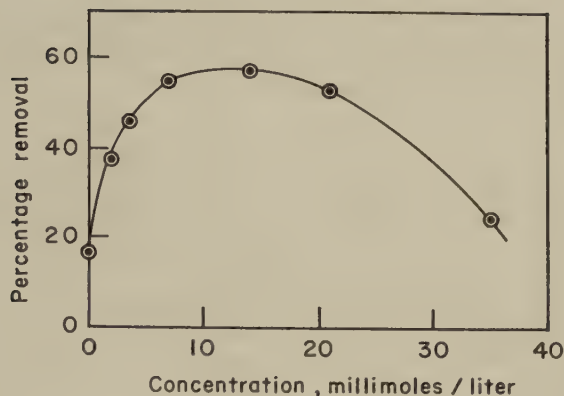


FIG. 1. Effect of SDS concentration on soil removal.

until the first stable lens was formed. At this point the surface of the substrate is covered with a monolayer at a definite surface pressure and, therefore, the value,  $V$ , of volume of the solution added to the end point is in inverse proportion to the concentration. The amount of fat on the originally soiled cloth was estimated as 0.003 g. per 100 cm.<sup>2</sup> of cloth from a calibration curve. Washing efficiency,  $W$ , was expressed by

$$W(\text{per cent}) = 100 \times \frac{V_w - V_s}{V_w},$$

where  $V_w$  and  $V_s$  is  $V$  obtained from washed cloths and from soiled cloths, respectively. Appropriate correction was made against the spreading impurity from the original cloth. Preliminary experiments showed that the washing efficiency reached a constant reproducible value at each concentration of detergent under the above-mentioned conditions of washing.

The effect of detergent concentration is shown in Fig. 1, from which it is seen that the detergency curve passes through a maximum at a concentration of about 12 millimoles per liter, a somewhat higher concentration than the c.m.c. of SDS as determined by the surface tension method, which is 8 millimoles per liter.

On the other hand, it has been found by several investigators (6) that the adsorption of a detergent on various textile fibers passes through a maximum, as the concentration of detergent in an aqueous solution is increased. The concentration of maximum adsorption of the SDS-cotton system was obtained as about 12 millimoles per liter from the curve of Vold and Phansalkar (7), and 10 millimoles per liter from our experiment using SDS labeled with S<sup>35</sup> and the same cotton as used in the present detergency study.

It was thus shown that the concentration of maximum adsorption agrees

approximately with the maximum washing concentration. This result may be regarded as an evidence that in the mechanism of detergent action, adsorption plays an important role.

## REFERENCES

1. PRESTON, W. C., *J. Phys. & Colloid Chem.* **52**, 84 (1948).
2. PHANSALKAR, A. K., AND VOLD, R. D., *J. Phys. Chem.* **59**, 885 (1955).
3. ASHCRAFT, E. B., *Am. Soc. Testing Materials, Spec. Tech. Publ. No. 215*, 30 (1958).
4. DREGER, E. E., *et al.*, *Ind. Eng. Chem.* **36**, 610 (1944).
5. MILLER, N. F., *J. Phys. Chem.* **45**, 289 (1941).
6. See, for example, VOLD, R. D., AND SIVARAMAKRISHNAN, N. H., *J. Phys. Chem.* **62**, 984 (1958); EVANS, H. C., *J. Colloid Sci.* **13**, 537 (1958).
7. VOLD, R. D., AND PHANSALKAR, A. K., *Rec. trav. chim.* **T74**, 41 (1955).

Chemical Laboratory,  
Ochanomizu University,  
Tokyo, Japan.

TARO TACHIBANA  
AKIHIKO YABE  
MICHİ TSUBOMURA

Received January 25, 1960.

## PURIFICATION OF SODIUM DODECYL SULFATE

The preparation of a pure sample of sodium dodecyl sulfate (SDS) with no minimum in its surface tension/log concentration curve is difficult. Miles and Shedlovsky (1) were able to remove the minimum associated with the presence of lauryl alcohol by a 36-hour extraction with ether, but as Ruyssen (2) showed, the presence of a trace of water will lead to hydrolysis and so give a minimum. Brady (3) foam fractionated SDS and was able to remove the impurity producing the minimum. The SDS was recovered by freezing the residual solution and subliming off the ice *in vacuo*. Mlle. Raison (4) was unable to remove the minimum, save by the addition of salt, and suggested that the minimum is a function of the structure of the solution.

In this laboratory we have attempted to remove the minimum in samples of SDS by the method of Brady (3) and Shedlovsky (1) with no more success than Mlle. Raison. The SDS was prepared by condensation of lauryl alcohol (better than 99.9% pure on gas chromatography) with chlorosulfonic acid in ether. The difficulties in purification have been overcome by using a liquid/liquid extraction technique in which a 10% solution of SDS in 50% aqueous alcohol is extracted with 60/80 petroleum ether. After ca. 18 hours the extracted liquor is cooled in dry-ice/alcohol and the SDS filtered off and air-dried. It is important to freeze and filter soon after the extraction is finished as a slight minimum develops if the solution is left to stand. This method has the advantage over foam fractionation that

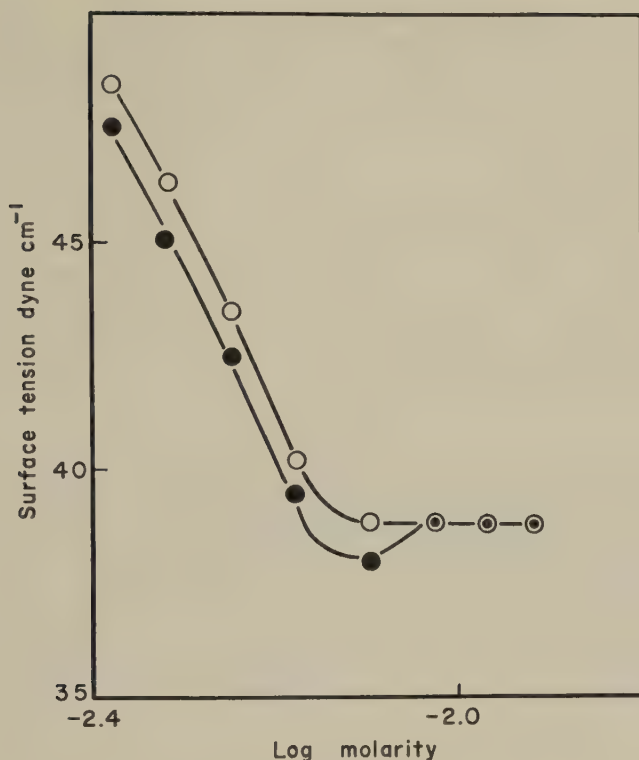


FIG. 1. Slow hydrolysis of sodium dodecyl sulfate shown by the appearance of a minimum in its surface tension/log concentration curve. ○—○ original solution; ●—● same solution four days later.

it can take place at a very much higher concentration than in water because no micelles which could solubilize the impurity are formed in 50% alcohol (5).

The difficulty of procuring pure SDS is further complicated by the fact that some hydrolysis to lauryl alcohol takes place in solution on standing. The lauryl alcohol is then adsorbed at the air/water interface. This is shown in Fig. 1, where the same solution of SDS in ion-free distilled water has been diluted on two occasions, four days apart. The first sign of a minimum is evident after only 24 hours. A solution in the region of the critical micelle concentration was also kept in a saturated atmosphere and its surface tension measured periodically by a du Noüy tensiometer, with as little disturbance of the surface as possible. It was noticed that the surface tension fell (Table I) to a greater extent than did that of the stirred solution in Fig. 1.

It is concluded that SDS may be purified as indicated so that there is

TABLE I

*Change in Surface Tension of  $7.9 \times 10^{-3}$  M Sodium Dodecyl Sulfate. Undisturbed Surface in Saturated Atmosphere: Measurements by du Noüy Tensiometer*

Time	Surface tension
(days)	(dyne cm. <sup>-1</sup> )
0	38.6
1	36.9
4	36.6

no minimum in its  $\gamma/\log C$  curve in the absence of salt. For surface tension studies fresh solutions should be used.

## REFERENCES

1. MILES, J. D., AND SHEDLOVSKY, L., *J. Phys. Chem.* **48**, 57 (1944).
2. RUYSSSEN, R., *Bull. soc. chim. Belges* **62**, 97 (1953).
3. BRADY, A. P., *J. Phys. & Colloid Chem.* **53**, 56 (1949).
4. RAISON, M., *Rev. franç. corps gras* **6**, 207 (1959).
5. WARD, A. F. H., *Proc. Roy. Soc. (London)* **A176**, 412 (1940).

Thos. Hedley & Co. Ltd.,  
Basic Research Department  
Newcastle upon Tyne,  
England

S. P. HARROLD

Received December 3, 1959.

## RELATION BETWEEN MAXIMUM RELAXATION TIME AND CHAIN LENGTH

In a recent publication (1) we have shown how a maximum relaxation time for linear amorphous polymers can be obtained from the limiting slope of  $\log E_r(t)$  versus  $t$ , where  $E_r(t)$  is the stress relaxation master curve and  $t$  is time.

We have obtained values of  $\tau_m$  for 15 samples of polystyrene of differing values of molecular weight but the heterogeneity index of which was 1.5 in all cases. We have also calculated  $\tau_m$  values for polyvinyl acetate and for polyisobutylene using published stress relaxation data (2, 3). The following relation among  $\log \tau_m$ ,  $\bar{n}_w$ ,  $T$ , and  $T_g$  was found for these polymers:

$$\log \tau_m (\text{seconds}) = \log A - 17.44 \frac{T - T_g}{51.6 + T - T_g} + 3.4 \log \bar{n}_w. \quad [1]$$

In Eq. [1]  $T$  is the temperature at which  $\tau_m$  is measured,  $T_g$  is the glass transition temperature, and  $\bar{n}_w$  is the weight-average number of links in the

polymer chain. The second term on the right corresponds to the WLF equation (4).

The values of  $\log A$  did not differ very much for these three polymers. The values are  $-0.52$  for polyisobutylene,  $-0.70$  for polystyrene, and  $0.86$  for polyvinyl acetate.

If this result is borne out for other polymers, Eq. [1] will provide a very simple way for obtaining an approximate weight-average molecular weight of a polymer by a single determination of  $\tau_m$  and a measurement of  $T_g$ , provided that  $\log A$  is known for the polymer.

The following relation has been obtained among  $\tau_m$ ,  $\bar{r}_\theta^2$ ,  $T$ , and  $T_g$ :

$$\log \tau_m (\text{seconds}) = \log B - 17.44 \frac{T - T_g}{51.6 + T - T_g} + 3.4 \log \frac{\bar{r}_\theta^2}{l_0^2}. \quad [2]$$

In Eq. [2]  $\bar{r}_\theta^2$  is the mean square end-to-end distance obtained on the polymer in a theta solvent (a solvent in which the polymer is just on the point of precipitation) and  $l_0$  is the length of the carbon-carbon bond, equal to 1.54 Å. In this case  $\log B$  is the same for all three polymers, namely,  $\log B = -2.21$ . If Eq. [2] is borne out for other polymers it will provide a method for obtaining  $\bar{r}_\theta^2$  directly from stress relaxation studies.

The values of  $\bar{r}_\theta^2$  were obtained from the equations of Krigbaum (5).

The support of the Quartermaster Corps, U. S. Army, is gratefully acknowledged.

#### REFERENCES

1. TOBOLSKY, A. V., AND MURAKAMI, K., *J. Polymer Sci.* **40**, 443 (1959).
2. NINOMIYA, K., *J. Colloid Sci.* **14**, 49 (1959).
3. TOBOLSKY, A. V., AND ANDREWS, R. D., *J. Polymer Sci.* **7**, 221 (1951).
4. WILLIAMS, M. L., LANDEL, R. F., AND FERRY, J. D., *J. Am. Chem. Soc.* **77**, 3701 (1955).
5. KRIGBAUM, W. R., *J. Polymer Sci.* **28**, 213 (1958).

Department of Chemistry,  
Frick Chemical Laboratory,  
Princeton University,  
Princeton, New Jersey.

A. V. TOBOLSKY  
K. MURAKAMI

Received March 17, 1960.

#### BINDING OF SURFACTANTS BY POLYMERS

Some ionic surfactants are bound in water by various nonionic polymers forming water-soluble adsorption complexes (1, 2). Thus the mixed solution



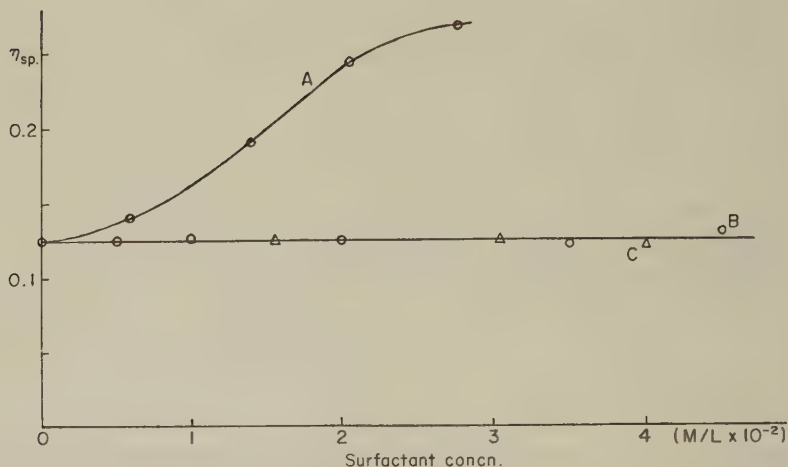


FIG. 1. Specific viscosity of 0.51% PVP solutions versus concentration of added anionic surfactants at 30°C.: A SDS, B Dodecyl-(oxyethylene)<sub>4</sub>-sulfate, C Dodecyl-(oxyethylene)<sub>10</sub>-sulfate.

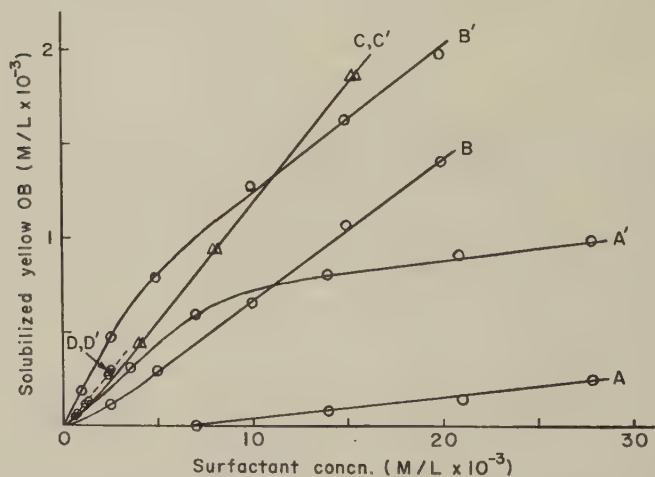


FIG. 2. Effect of PVP addition on the solubilization of an oil-soluble dye, Yellow OB, in surfactant solutions at 30°C.: A SDS, B Dodecyl-(oxyethylene)<sub>4</sub>-sulfate, C Dodecyl-(oxyethylene)<sub>10</sub>-sulfate, D Dodecyl-(oxyethylene)<sub>4</sub>-ether. The primes refer to the addition of 0.1% PVP to the corresponding surfactant solutions.

of surfactant and polymer shows sometimes interesting properties. For example, the specific viscosity of polyvinylpyrrolidone (PVP) and/or the solubilization power of sodium dodecyl sulfate (SDS) in their single solutions increase strongly by mixing both (Fig. 1, *A*, Fig. 2, *A*, *A'*). In previous papers (1, 2) a mechanism of the binding was tentatively advanced, but on the role of ionic substituent of surfactants in the binding some questions remain. In the present work further supplementary experiments were performed under the same procedures as before.

According to the solubilization experiment, it was observed that the sodium dodecyl polyoxyethylene sulfates,  $C_{12}H_{25}-(OC_2H_4)_n-SO_4Na$ , form complexes with PVP only when  $n$  is small (Fig. 2, *B*, *B'*, *C*, *C'*). However, in the latter case when  $n$  is equal to 4, the specific viscosity of PVP in the mixed solutions varies hardly (Fig. 1, *B*). Thus it is considered that the binding of the last-mentioned surfactant by PVP may be too small to change the chain configuration of PVP in solution. Therefore, it may be concluded that a hydrophilic polyoxyethylene chain situated between paraffin and sulfate in the said surfactants interferes in the binding of the latter to polymers.

On the other hand, dodecyl polyoxyethylene ether,  $C_{12}H_{25}-(OC_2H_4)_4-OH$ , nonionic surfactant having no sulfate but a chain of 4 oxyethylenes, shows, according to the solubilization experiment, no sign of complex formation with PVP (Fig. 2, *D*, *D'*). Since the above surfactant is scarcely soluble in water, the experiment was carried out in slightly turbid dilute solutions. It should be noted that, as previously pointed out (1), the surfactants once bound with polymers might be released sometimes in the process of solubilization. Anyhow, it is evident that the sulfate contributes to the binding in question. Hence, in the adsorptive binding of anionic surfactants by nonionic polymers, besides the long-chain nonpolar part of surfactant, the ionic substituent adjacent to it may play a significant role.

#### MATERIALS

SDS was a product (Texapon L100) of Deutsche Hydrierwerke GmbH (Düsseldorf), which was twice recrystallized from ethanol. Sodium dodecyl polyoxyethylene sulfates were specially prepared by the Research Laboratory of Nippon Oils & Fats Co. (Amagasaki). Dodecyl polyoxyethylene ether was a product of Nikko Shokai Co. (Tokyo). PVP was a product (K25) of General Aniline & Film Corp. (U.S.A.).

## ACKNOWLEDGMENTS

The thanks of the author are due to Professor N. Sata of Osaka University for his encouragement, to Mr. Y. Senoh of Nippon Oils & Fats Co. for the supply of some of the materials, and to Momotani-Juntanken Ltd. for the permission to publish.

## REFERENCES

1. SAITO, S., *Kolloid-Z.* **158**, 120 (1958).
2. SAITO, S., AND HIRATA, H., *Kolloid-Z.* **165**, 162 (1959); SAITO, S., *ibid.* **168**, 128 (1960).

*Research Laboratory of Momotani-Juntanken Ltd.*  
*Ichioka 5, Minatoku, Osaka (Japan).*

SHUJI SAITO

*Received March 25, 1960.*

# AUTOMATIC TITRATORS

By J. P. PHILLIPS, *University of Louisville*

*November 1959, 225 pp., illus., \$6.00*

*Automatic Titrators* surveys the rapidly advancing field of volumetric analysis by the most modern methods available. In addition to a complete account of the principles and theory of automatic titration, a guide to the selection of the best commercially available models is included. Both European and American instruments are given appropriate coverage.

This book is the sole complete source of information on automatic titrations by both continuous and semi-automatic techniques.

## CONTENTS

Introduction

General Considerations of Titrator Design

Automatic Potentiometric Titrators

Other Electrometric Automatic Titrators

Automatic Photometric Titrators

Automatic Coulometric Titrators

Fully Automatic and Continuous Titrators

Commercially Available Titrators

Applications of Automatic Titration Methods

Appendix: Terminology of Electronics

AUTHOR INDEX—SUBJECT INDEX.



ACADEMIC PRESS, New York and London

# INFRARED METHODS

By G. K. T. CONN, *The University, Exeter*  
and D. G. Avery, *Atomic Energy Authority, Copenhurst Works*

May 1960, about 210 pp., illus., approx. \$7.00

This book is a critical guide for the choice and evaluation of infrared methods. It is intended for the scientist in any field to whom a concise, reliable manual is important. The longer of the two parts, Principles, discusses the chief components used in exploring the infrared region: Sources of Radiation, Optical Materials, Detectors, Amplifiers, and Dispersive Systems. The second part, Practical Applications, is an introduction to specific techniques and the types of experiments for which they are suited. The chapters in this section are: Calibration of Detectors, A Simple Monochromator, Instruments for Gas Analysis and Plant Control, and Radiation Pyrometry.

# INFRARED ABSORPTION SPECTRA Index for 1945-1957

By HERBERT M. HERSHENSON, *Baird-Atomic, Inc.*

1959, III pp.,  $8\frac{1}{2} \times 11$ ", \$7.00

This index gives the location of infrared absorption spectra published in thirty-two representative American and European journals during the thirteen-year period from 1945 through 1957. It will greatly simplify the problems of locating infrared spectra and will in many instances eliminate the necessity of obtaining a pure specimen of a compound in order to determine its absorption characteristics.



**Academic Press, New York and London**

111 Fifth Avenue, New York 3, New York  
17 Old Queen Street, London, S.W. 1



# MEASUREMENT OF PARTICLE SIZES BY HIGHER ORDER TYNDALL SPECTRA ( $\theta_1$ METHOD)

Susumu Kitani

*Department of Chemical Technology, Japan Atomic Energy Research  
Institute, Tokai-mura, Ibaraki-ken, Japan*

*Received July 22, 1959; revised October 13, 1959*

## ABSTRACT

Particle size measurements by higher order Tyndall spectra have been developed. In a previous experiment it was found that the first angle,  $\theta_1$ , which is measured from the direction of propagation of the incident beam, of red spectra of higher order Tyndall spectra is related to the average particle size,  $\bar{r}$  (1). These relations have been discussed from the theoretical standpoint. The average radius of a monodisperse aerosol consisting of spherical particles can be evaluated by measuring  $\theta_1$  from the following equation independent of refractive index except for the value of 2.0:  $\log (\theta_1/10) + 1.43 \log (10 \bar{r}) = 1.43$ , where  $\theta_1$  is in degrees of angle and  $\bar{r}$  in microns.

## INTRODUCTION

Optical methods for measuring the size and concentration of aerosols have been investigated by many workers (2, 3). Light scattering by monodisperse spherical particles resulting in higher order Tyndall spectra was investigated by LaMer and his co-workers (2, 4, 5). It was found that the first angle,  $\theta_1$ , which is measured from the direction of propagation of the incident beam, in the red portion of high-order Tyndall spectra was simply related to the average radius,  $\bar{r}$ , of particles. That is

$$\log (\theta_1/10) + n \log (10 \bar{r}) = c, \quad [1]$$

where  $\theta_1$  is expressed in degrees of angle,  $\bar{r}$  in microns, and  $n$  and  $c$  are experimental constants (1). In the present paper the above result is discussed from a theoretical standpoint.

## THEORY

It is widely known that the light passing through a colloidal system is scattered. The intensity of polarized light scattered by a particle of radius,  $r$ , much smaller than the wavelength of the light employed, was given by Lord Raleigh (1881) as:

$$\left. \begin{aligned} J_1 &= \frac{\lambda^2 x^6}{8\pi^2 R^2} \left( \frac{m^2 - 1}{m^2 + 2} \right) \\ J_2 &= \frac{\lambda^2 x^6}{8\pi^2 R^2} \left( \frac{m^2 - 1}{m^2 + 2} \right) \cos^2 \theta \end{aligned} \right\}, \quad [2]$$

where  $J_1$  and  $J_2$  are the components of the scattered light, the electric vectors of which are perpendicular and parallel to the plane of observation,  $R$  is the distance from the particle to the point of observation,  $\lambda$  is the wavelength of the incident light,  $x$  is  $2\pi r/\lambda$ ,  $m$  is the refractive index of the particle, and  $\theta$  is the angle from the direction of propagation of the incident beam. A characteristic of the scattering is that the intensity of light scattered forwards and backwards by the particle is symmetrical with regard to the direction of the incident beam.

When the size of the particle approaches the wavelength, the phenomena become very complex. Light scattering by such particles was investigated by G. Mie in order to explain the scattering by colloidal gold systems (6). The angular distribution of light scattered by a spherical particle is shown as follows, using the same definitions:

$$\left. \begin{aligned} J_1 &= \frac{\lambda^2}{8\pi^2 R^2} \left| \sum_{l=1}^{\infty} \frac{2l+1}{l(l+1)} (a_l \pi_l + b_l \tau_l) \right|^2 \\ J_2 &= \frac{\lambda^2}{8\pi^2 R^2} \left| \sum_{l=1}^{\infty} \frac{2l+1}{l(l+1)} (a_l \tau_l + b_l \pi_l) \right|^2 \end{aligned} \right\} \quad [3]$$

where

$$a_l = \frac{y\phi_l'(x)\phi_l(y) - x\phi_l(x)\phi_l'(y)}{y\zeta_l'(x)\phi_l(y) - x\zeta_l(x)\phi_l'(y)}$$

$$b_l = \frac{y\phi_l(x)\phi_l'(y) - x\phi_l'(x)\phi_l(y)}{y\zeta_l(x)\phi_l'(y) - x\zeta_l'(x)\phi_l(y)}$$

$$y = mx$$

$m$  = refractive index

$$\phi_l(x) = \sqrt{\frac{\pi x}{2}} J_{l+1/2}(x)$$

$J_l$  = Bessell function

$$\zeta_l(x) = \sqrt{\frac{\pi x}{2}} H_{l+1/2}^2$$

$H_l^2$  = second kind of Hankel's cylindrical function

$$\pi_l = P_l'(\cos \theta) \frac{1}{\sin \theta}$$

$P_l'$  = associated Legendre function

$$\tau_l = \frac{\partial}{\partial \theta} P_l'(\cos \theta)$$

In the above equations  $a_l$  and  $b_l$  are functions of the particle size and the refractive index, but  $\pi_l$  and  $\tau_l$  are functions of the angle only. These functions have been calculated and published;  $A_l$  and  $B_l$  (corresponding to  $[(2l+1)/l(l+1)]a_l$  and  $[(2l+1)/l(l+1)]b_l$  in the notations of this paper) were computed for  $m = 1.05, 1.10, 1.15, 1.20, 1.25$ , and

1.30 and  $x = 0.2$ –15.0 and larger by Pangonis, Heller, and Jacobson (7). Values of  $\pi_i$  and  $\tau_i$  were calculated by Gucker and Cohn (8). Also values of  $J_1$  and  $J_2$  were calculated for  $m = 1.33, 1.44, 1.55$ , and  $2.0$  in a range of  $x$  from  $0.5$  to  $6.0$  over  $0^\circ$ – $180^\circ$  (every  $10^\circ$ ) by Lowan (9). For  $m = 1.33$ , Mori calculated  $J_1$  and  $J_2$  for a range of  $x$  from  $5.5$  to  $18.5$  over  $0^\circ$ – $180^\circ$  (10).

The particle size can be measured by observing the red spectra of the higher order Tyndall spectra. The angular positions of these red spectra are calculated by drawing  $J_1(628)/J_1(523)$  vs. scattering angle curves as a function of refractive index and radius, where  $J_1(628)$  and  $J_1(523)$  are  $J_1$  of the wavelengths of  $628 \text{ m}\mu$  and  $523 \text{ m}\mu$ , respectively. When  $J_1(628)/J_1(523)$  is greater than  $1$ , the scattering light is reddish and its maxima are the angles of the red spectra. In Fig. 1 and Fig. 2  $J_1(628)/J_1$

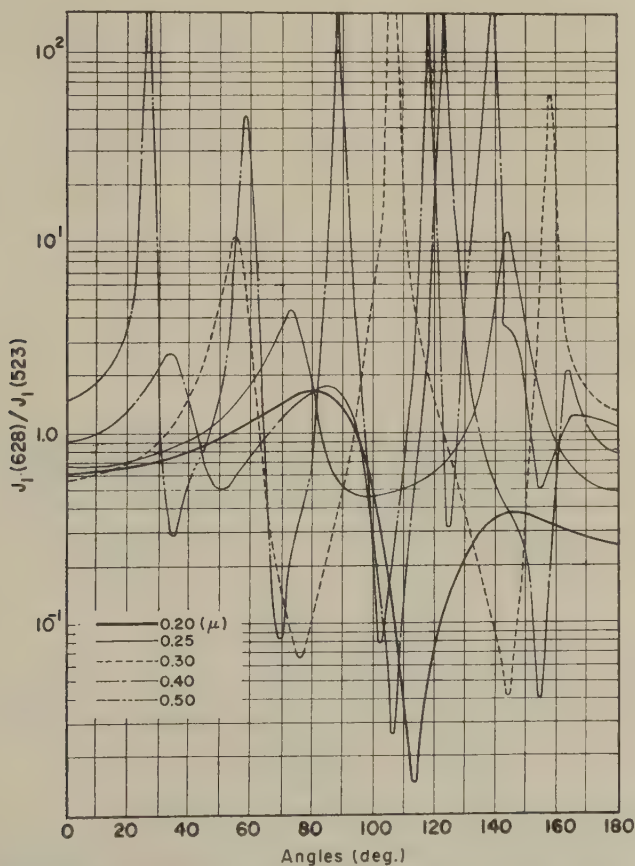


FIG. 1. The ratio  $J_1(628)/J_1(523)$  versus angle of scatter as a function of particle size in micron, where the refractive index  $m = 1.44$ .

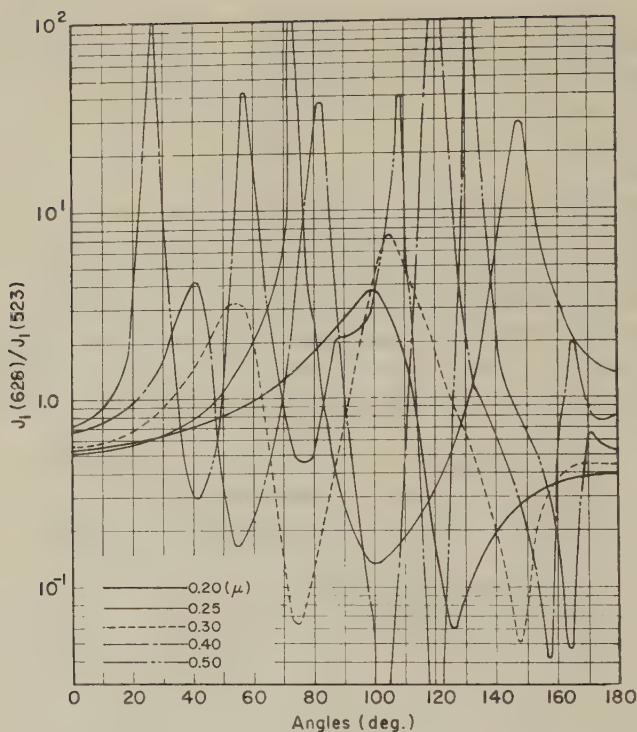


FIG. 2. The ratio  $J_1(628)/J_1(523)$  versus angle of scatter as a function of particle size in micron, where the refractive index  $m = 1.55$ .

(523) are given as functions of particle size and scattered angle calculated from the data by LaMer (11) for  $m = 1.44$  and  $1.55$ . The angle distributions of red spectra as functions of refractive index and particle radius calculated by the method described above are summarized in Table I (the data of  $1.33$  are those of Mori).

#### RESULTS AND DISCUSSION

The simple relation between  $\log \theta_1$  and  $\log \bar{r}$  can be deduced from Fig. 3 for refractive indexes of  $1.33$ ,  $1.44$ , and  $1.55$  except for  $2.0$ , as follows:

$$\log (\theta_1/10) + 1.43 \log (10r) = 1.43. \quad [4]$$

Such a relation has been confirmed experimentally. Aerosols of stearic acid, glycerin, dioctyl phthalate, dibutyl phthalate, and tributyl phthalate were produced by the LaMer-Sinclair aerosol generator (2) and the relation of  $\log \theta_1$  to  $\log \bar{r}$  was investigated (1). Particle sizes were mostly in the range

TABLE I

*Angular Distributions of Red Spectra of Higher Order Tyndall Spectra as a Function of Refractive Index and Particle Size*

Refractive index	Particle radius ( $\mu$ )	Angular distribution (deg)					
1.33	0.20	105					
	0.25	75,	156				
	0.30	61,	125				
	0.40	42,	82,	123			
	0.50	32,	66,	98,	132,	169	
	0.55	28,	57,	85,	112,	134,	169
	0.65	23,	48,	73,	98,	122,	144, 173
	0.75	17,	38,	61,	85,	108,	128, 150
1.44	0.20	100					
	0.25	73,	147				
	0.30	55,	106				
	0.40	41,	83,	122,	165		
	0.50	28,	58,	109,	132		
1.55	0.20	81,	145				
	0.25	73,	143				
	0.30	54,	104,	157			
	0.40	33,	85,	122,	162		
	0.50	26,	57,	87,	117,	136,	165
2.0	0.20	79					
	0.25	52.5,	115				
	0.30	33,	87,	130			
	0.40	52.5,	102,	160			
	0.50	33,	67.5,	103,	136,	158	

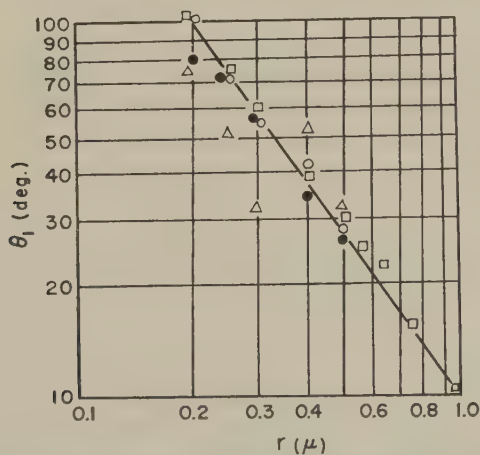


FIG. 3. The theoretical relations of particle radius  $r(\mu)$  and the first angle  $\theta$  of red spectra of higher order Tyndall spectra.:  $\square$   $m = 1.33$ .  $\circ$ :  $m = 1.44$ .  $\bullet$ :  $m = 1.55$ .  $\triangle$ :  $m = 2.0$ .



TABLE II

*Experimental Relations between Particle Radius  $r(\mu)$  and the First Angle,  $\theta_1$ , of Red Spectra of Higher Order Tyndall Spectra*

Substance	Refractive index	Equation
Theoretical	1.33-1.55	$\log (\theta_1/10) + 1.43 \log (10 r) = 1.43$
Stearic acid	1.43	$\log (\theta_1/10) + 1.20 \log (10 r) = 1.30$
Glycerin	1.47	$\log (\theta_1/10) + 1.50 \log (10 r) = 1.50$
Diocetyl phthalate	1.49	$\log (\theta_1/10) + 2.00 \log (10 r) = 1.80$
Dibutyl phthalate	1.50	$\log (\theta_1/10) + 1.40 \log (10 r) = 1.20$
Tricresyl phthalate	1.56	$\log (\theta_1/10) + 1.50 \log (10 r) = 1.20$

of 0.2-0.7  $\mu$ . The experimental and theoretical results are indicated in Table II.

There are some differences between the experimental and the theoretical results. These may arise because of (a) the width of the red spectrum, (b) slight errors in reading Fig. 1 and Fig. 2, and (c) measurement errors in the settling method.

Generally, the measurement for an aerosol is very difficult because of its instability. Therefore, it is necessary to measure the size as quickly as possible. LaMer and his co-worker reported the simple law previously, which was described as  $\bar{r} = n'/10$ , where the average particle radius  $\bar{r}$  is in microns, and  $n'$  is the number of red spectra in the range of 0°-180° (2). However, the sharpness of the spectra decreases with an increase of dispersion of the particle size distribution. When the standard deviation of the particle distribution exceeds 0.12  $\mu$ , the red spectra are not perfectly visible and it is impossible to estimate the size of the aerosol (12).

It is concluded that the  $\theta_1$  method is not completely rigorous, but is very useful for particle-size measurements of monodisperse aerosols (with a standard deviation of particle distribution of 0.12  $\mu$  or less). The method is especially useful when the vapor pressure of the aerosol is sufficiently high at room temperature, as with *n*-octyl alcohol.

#### ACKNOWLEDGMENT

The author is indebted to Mr. Nobuo Mori, Electrotechnical Laboratory, Tokyo, for valuable discussions and for calculations of higher order Tyndall spectra.

#### REFERENCES

1. KITANI, S., *J. Chem. Soc., Japan* **77**, 1621 (1956).
2. SINCLAIR, D., AND LAMER, V. K., *Chem. Revs.* **44**, 245 (1949).
3. *Brit. J. Appl. Phys. Suppl.* **3**, 1-210 (1954).
4. LAMER, V. K., INN, E. C. Y., AND WILSON, I. B., *J. Colloid Sci.* **5**, 471 (1950).
5. JOHNSON, I., AND LAMER, V. K., *J. Am. Chem. Soc.* **69**, 1184 (1947).
6. MIE, G., *Ann. Physik* **25**, 377 (1908).

7. PANGONIS, W. J., HELLER, W., AND JACOBSON, A. W., "Tables of Light Scattering Functions for Spherical Particles." Wayne State University Press (1957).
8. GUCKER, T., AND COHN, S. H., *J. Colloid Sci.* **8**, 555 (1953).
9. LOWAN, A., N. B. S., Applied Mathematics Series 4, "Tables of Scattering Functions for Spherical Particles." (1948).
10. MORI, N., AND KIKUCHI, H., *Bull. Electrotech. Lab. (Tokyo)* **21**, 561 (1957); *ibid.* **22**, 209 (1958).
11. LAMER, V. K., AND OTHERS, Atomic Energy Commission Report, OSRD-1857. (1943). U.S.A.
12. KITANI, S., *J. Chem. Soc., Japan* **77**, 1181 (1956).

## VISCOSITIES OF CONCENTRATED POLYMER SOLUTIONS. V. TWO POLYELECTROLYTES

George E. Heckler, Thomas E. Newlin, Donald M. Stern, Robert A. Stratton, Jerry R. Witt, and John D. Ferry

*Department of Chemistry, University of Wisconsin, Madison, Wisconsin*

*Received April 6, 1960*

### INTRODUCTION

In previous papers in this series (1-4), the dependence of viscosity on temperature, concentration, molecular weight, and solvent has been described for concentrated solutions of several different polymers. One of these, a 1:1 copolymer of styrene and maleic acid (3), was studied in 50% aqueous dioxane where the acid groups were unionized. The present paper describes measurements on this polymer (SYMA) converted to a polyelectrolyte by partial neutralization with strong alkali. The rather spectacular behavior is contrasted with that of another polyelectrolyte, polyacrylic acid (PAA), which has a simpler structure devoid of large nonpolar groups.

The viscosities of polyelectrolytes in dilute aqueous solution have been extensively studied and are qualitatively well understood (5-7). In concentrated solution, where the polymer coils interpenetrate and counterions are comparatively evenly distributed, the effects of electrostatic repulsion at high degrees of neutralization would be expected to be less striking. There appears to have been very little experimental work on such systems, however. The copolymer of styrene and maleic acid is an unusual type because the hydrophobic association between the phenyl groups in an aqueous medium (8) causes hypercoiling in dilute solution (9) unless counteracted by electrostatic repulsion from a few charged carboxyls. When the carboxyls are all combined with protons, phase separation occurs (8, 9). The present experiments show that in concentrated solution certain conditions lead to enormous viscosities, which may also be attributed to association of the phenyl groups.

### MATERIALS AND METHODS

The source and rough fractionation of the styrene-maleic acid copolymer were described in an earlier paper (8). The fraction B2 cited there was approximately duplicated in subsequent fractionations, though the later

TABLE I  
*Characterization of Polyelectrolyte Samples*

Sample	$\overline{M}_n$	$[\eta]$	Solvent for $[\eta]$	$\overline{M}_\eta$
Styrene-maleic acid copolymer (SYMA):				
Unfractionated (U)	—	0.68	Butanone-2 <sup>a</sup>	158,000
B2	207,000	0.81	Butanone-2 <sup>a</sup>	
	—	1.10	90% aq. dioxane <sup>b</sup>	
B2-DMS	—	1.18	90% aq. dioxane <sup>b</sup>	192,000
B2-RHB	200,000	1.21	90% aq. dioxane <sup>b</sup>	
Polyacrylic acid (PAA):				
Unfractionated (U)	—	0.48	Dioxane <sup>c</sup>	315,000
2-JRW	—	0.62	Dioxane <sup>c</sup>	540,000

<sup>a</sup> Copolymer in anhydride form, measured at 25°. The value of  $\overline{M}_\eta$  for sample U (calculated as acid form) estimated from relative  $[\eta]$  values assuming  $[\eta]$  proportional to  $\overline{M}^{0.67}$ .

<sup>b</sup> Copolymer in acid form, unionized, measured at 25°C.

<sup>c</sup> Measured at 30°C., the Flory temperature.

products (B2-DMS, B2-RHB) differed slightly in molecular weight as shown in Table I.

The polyacrylic acid was a special sample generously prepared by Dr. F. J. Glavis of Rohm and Haas Company with precautions to minimize branching, numbered Gm1122. Some experiments were made with a rough fraction (2JRW) obtained by precipitating with heptane from a dioxane solution; this represented a second cut of about 40% of the total material after an initial precipitation of about 11% of the material of highest molecular weights. The polyacrylic acid, like the copolymer, was dried from the frozen state, but from dioxane rather than aqueous solution. A few per cent of solvent was tenaciously held, as found by Newman and collaborators (10); the proportion was determined by titration of aliquots with sodium hydroxide (10), and the concentrations tabulated here have been correspondingly corrected.

The molecular weights of fractions SYMA-B2 and B2-RHB were determined by osmometry; those of the other copolymer samples were calculated from comparative intrinsic viscosity data, on the assumption that  $[\eta]$  in 90% aqueous dioxane is proportional to  $M^{0.67}$ . The details are given in Table I. Since they are all similar in magnitude, no great uncertainty arises from the assumption of the exponent, though the nature of the average is uncertain. The molecular weights of the PAA samples were calculated from intrinsic viscosities in dioxane at 30°C. using the formula of Newman (10),  $[\eta] = 0.85 \times 10^{-3} M^{1/2}$ . These are also given in Table I.

The aqueous solutions were made up by weight with different proportions of sodium hydroxide. Concentrations are expressed as grams polymer

(calculated as the acid) per gram or per cubic centimeter of solution. The densities of a few solutions were measured pycnometrically and the others were estimated adequately by interpolation. (For example, a 50% neutralized SYMA solution with weight fraction of polymer 0.134 had a density of 1.056.)

Most of the viscosities were measured by the falling sphere method, and calculated from steady-state velocities of fall by the equation of Faxén (11). Spheres of stainless steel, of glass (12), and of synthetic ruby<sup>1</sup> were employed in different experiments. Two sizes of ruby spheres were used, of 0.025 in. and 1.00 mm. diameter; their density was 3.98 g./cc.

In most cases, measurements were made promptly after the solutions were prepared. In two series on sample PAA-U, however, successive additions of sodium hydroxide were made to the same solution because of scarcity of material, and about a month was required for the sequence. A test of relative intrinsic viscosity before and after (the dilute solution viscosities run at 15% neutralization in 0.6*M* sodium chloride) showed a drop of 13%. Thus some degradation had occurred though the solution had been kept at 5°C. between measurements. This is not sufficient to affect the conclusions drawn from these data, however.

One solution of sample SYMA-U with 0.165 g. polymer per cc., 31% neutralized, was studied in a coaxial cylinder apparatus (13). The viscosity was measured in a steady-state rotation at an angular velocity of about  $3 \times 10^{-4}$  rad./sec., and measurements were also made of stress relaxation following a small instantaneous shear strain and following cessation of steady-state flow (13). In addition, this solution was subjected to measurements of transverse wave propagation at frequencies between 400 and 2000 cycles/sec. The time-dependent mechanical data are reported elsewhere (14).

## RESULTS

Viscosity measurements in the temperature range between 15°C. and 40°C. were made on three systems: SYMA-B2-DMS, 50% neutralized, at concentrations ranging from 0.09 to 0.25 weight fraction polymer; SYMA-B2-RHB, concentration 0.142 g. polymer per cc., at degrees of neutralization from 30% to 60%; and PAA-U, concentration 0.160 g. polymer per g. water, at degrees of neutralization from 0 to 97% (concentrations in g. polymer per cubic centimeter ranged from 0.179 to 0.173 depending on degree of neutralization). The data are summarized in Tables II–IV, and  $\log \eta$  is plotted against reciprocal absolute temperature in Figs. 1–3. Values of the apparent heat of activation of viscous flow calculated at 25° also appear in the tables. Measurements were made on aqueous solutions of unneutralized PAA-2-JRW at 25°C. only; these data are given in Table V.

<sup>1</sup> Crystal Products, Linde Company.



TABLE II  
*Viscosities of Sample SYHM-B2-DMS, 50% Neutralized*

$w_2$	log $\eta$ in poises at			$Q_{\eta}, 25^{\circ}\text{C.}$ (kcal.)
	14.9°	24.9°	40.0°	
0.091	1.486 <sup>a</sup>	1.345	1.143	5.5
0.121	1.976 <sup>a</sup>	1.840	1.648 <sup>b</sup>	5.3
0.155	2.567	2.391 <sup>c</sup>	2.226 <sup>d</sup>	5.7
0.180	3.057	2.898	2.684	6.2
0.207	3.526	3.326 <sup>e</sup>	3.107	6.6
0.250	4.514 <sup>e</sup>	4.199 <sup>f</sup>	3.850 <sup>d</sup>	10.5

<sup>a</sup> At 15.1°C.<sup>b</sup> At 39.8°C.<sup>c</sup> At 25.1°C.<sup>d</sup> At 40.2°C.<sup>e</sup> At 13.6°C.<sup>f</sup> At 24.3°C.

TABLE III  
*Viscosities of Sample SYHM-RHB, Concentration 0.142 g. Polymer per cc.*

Degree of neutralization	log $\eta$ in poises at					$Q_{\eta}, 25^{\circ}\text{C.}$ (kcal.)
	20.0°	25.0°	30.0°	35.0°	40.0°	
0.30					6.00	
0.35			5.30	4.61		
0.40	4.72	3.61	3.26	2.68		60
0.43	3.59	3.00		2.40		34
0.50	1.94	1.86	1.80			6.2
0.60	1.09	1.02				8.1

TABLE IV  
*Viscosities of Sample PAA-U*  
*Concentration 0.160 g. polymer per g. water*

Degree of neutralization	log $\eta$ in poises at			$Q_{\eta}, 25^{\circ}\text{C.}$ (kcal.)
	15.0°	25.0°	35.0°	
0	0.64	0.45	0.27	7.8
0.050	1.04	0.82	0.64	8.7
0.098	1.11	0.89	0.70	8.7
0.150	1.18	1.05 <sup>a</sup>	0.74	8.9
0.278	1.30	1.18 <sup>b</sup>	0.88	8.7
0.409	1.36	1.13	0.95	8.4
0.536	1.37 <sup>c</sup>	1.19	1.04	7.3
0.971	1.94	1.74	1.58	7.3

<sup>a</sup> At 20.0°C.<sup>b</sup> At 20.3°C.<sup>c</sup> At 16.0°C.

TABLE V  
Viscosities of Sample PAA-2-JRW, Unneutralized at 25.0°C.

Conc., g. polymer/c.c.	0.194	0.216	0.224	0.242	0.260	0.298
Log $\eta$	1.41	1.69	1.76	1.99	2.23	2.41

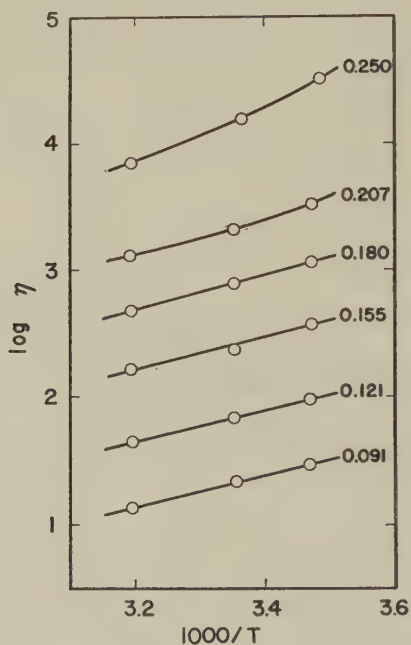


FIG. 1. Logarithm of viscosity (in poises) plotted against reciprocal absolute temperature, for solutions of SYMA sample B2-DMS 50% neutralized with sodium hydroxide. Numbers denote weight fraction of polymer.

In Fig. 1, the dependence of viscosity on temperature (as well as concentration) resembles that seen in concentrated solutions of many ordinary uncharged polymers. However, the magnitude of the viscosity is high. For example, the concentration dependence of this half-neutralized aqueous SYMA is compared in Fig. 4 with that of a closely similar sample, uncharged, in 50% aqueous dioxane, as reported previously (3). The relative viscosities of the former are higher by about a factor of 100. By contrast, the apparent heats of activation for viscous flow ( $Q_a$ ) are of comparable magnitude, as seen in Fig. 5, although that for the charged polyelectrolyte increases suddenly above a concentration of 0.25 g./cc.

In Fig. 2, a striking dependence of the viscosity of SYMA on degree of neutralization is revealed. With decreasing neutralization (average charge per carboxyl group) the viscosity increases by many orders of magnitude.

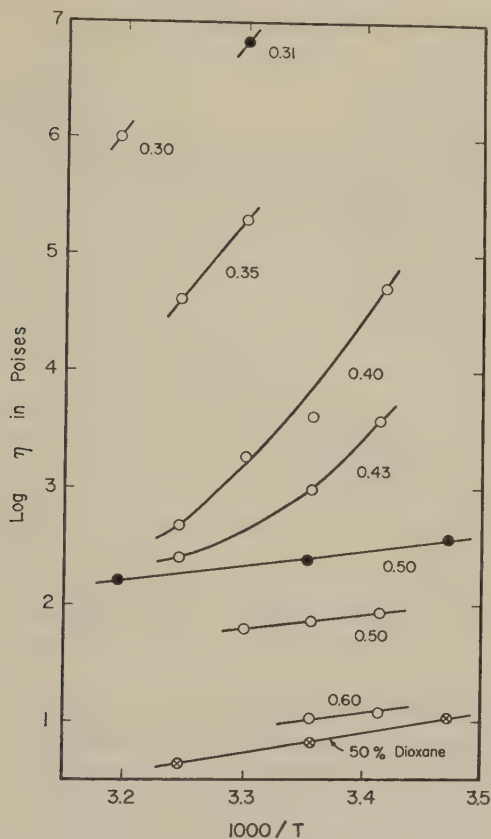


FIG. 2. Logarithm of viscosity (in poises) plotted against reciprocal absolute temperature, for solutions of SYMA sample B2-RHB with concentration 0.142 g. polymer per cubic centimeter of solution (open circles). Figures denote degree of neutralization with sodium hydroxide. The closed circle for 0.31 neutralization refers to sample U at  $c_2 = 0.165$  g./cc. solution; the closed circles at 0.50 neutralization to sample B2-DMS at  $c_2 = 0.165$  g./cc. solution; and the crossed circles to sample B2, unneutralized, in 50% dioxane at  $c_2 = 0.175$  g./cc. solution.

The plot includes one line reproduced from Fig. 1 and also the value of  $\eta = 7 \times 10^6$  poises measured on sample SYMA-U with the coaxial cylinder apparatus, representing data which are not strictly comparable with those on SYMA-B2-RHB but whose consistency supports the reality of the large effects observed. At 30% neutralization, the solutions might be superficially described as gelatinous, and indeed they exhibit viscoelasticity with very long relaxation times. However, steady-state flow occurs and the viscosity, though enormous, is finite; moreover, in stress relaxation experiments the stress decays to zero (14). Hence, strictly, these systems should not be referred to as gels. At 60% neutralization, the viscosity

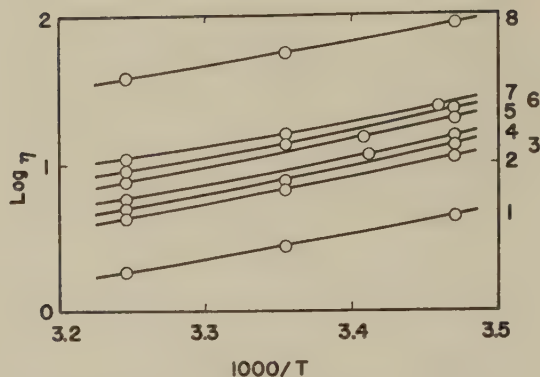


FIG. 3. Logarithm of viscosity (in poises) plotted against reciprocal absolute temperature, for aqueous solutions of PAA sample U with concentration 0.160 g. polymer per grams water. Figures correspond to the following degrees of neutralization with sodium hydroxide: (1) 0; (2) 0.050; (3) 0.098; (4) 0.150; (5) 0.278; (6) 0.409; (7) 0.536; (8) 0.971. The concentration in grams polymer per cubic centimeter solution ranges from 0.173 to 0.179.

approaches the much lower magnitude observed for the uncharged molecule in 50 % aqueous dioxane, comparable with that found in ordinary polymers.

In Fig. 3, the behavior of PAA is seen to be in marked contrast. Over a range of degree of neutralization from 0 to 97 %, the viscosity changes by only a factor of 20, and it increases instead of decreasing.

The dependence of the apparent heat of activation for viscous flow on degree of neutralization is also very different for the two polyelectrolytes, as shown in Fig. 6 ( $Q_\eta$  estimated at 25°C.). For PAA, it is almost independent of the charge per carboxyl group and is only a few kilocalories per mole higher than that for the pure solvent, in harmony with the behavior of most uncharged polymers (1-3). For SYMA,  $Q_\eta$  changes suddenly between 40 % and 50 % neutralization; at lower degrees of charge, it has a very high value of the order of 60 kcal./mole.

## DISCUSSION

### *Polyacrylic Acid*

The essentially normal dependence of viscosity on temperature and concentration for uncharged aqueous polyacrylic acid, shown in Curve 2 of Fig. 4 and Curve PAA of Fig. 6, indicates that its concentrated solutions are similar in structure to those of nonpolar polymers in nonpolar solvents. The molecules are intertwined with Gaussian configurations presumably resembling those occurring in a  $\Theta$ -solvent. The magnitude of the viscosity may be considered to be determined by the monomeric friction coefficient which governs the rates of local chain motions and the average number of

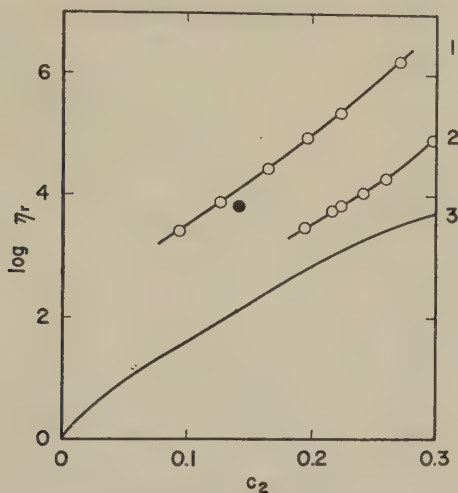


FIG. 4. Logarithm of relative viscosity at 25°C. plotted against polymer concentration in grams per cubic centimeter of solution. (1) SYMA-B2-DMS 50% neutralized with sodium hydroxide, from Fig. 1 (solid circle, SYMA-B2-RHB, with slightly lower molecular weight); (2) PAA-2-JRW unneutralized, in water; (3) SYMA-B2, unneutralized, in 50% aqueous dioxane (from reference 3).

entanglement coupling points per molecule (4). As the average charge per carboxyl group is increased from zero to 0.97, the apparent activation energy changes very little, so the mechanism of flow is evidently unaltered. The tremendous configurational expansion which occurs with increasing charge in dilute polyelectrolytes would not be expected in concentrated solution. The intertwined neighbors and their counterions prevent long-range electrostatic repulsion effects; stated differently, the amounts of alkali required for neutralization in concentrated solution provide a high ionic strength. Otherwise, very high viscosities would be expected as in sodium deoxyribonucleate (12), where an extended configuration arises from internal stiffness. The 20-fold increase in viscosity with neutralization may be attributed to an increase either in the monomeric friction coefficient or in the number of entanglements per molecule,  $\xi$ . If  $\eta$  is proportional to  $\xi^{3.4}$  (4, 15) a 2.4-fold increase in  $\xi$  would suffice; this might follow from a moderate configurational expansion, similar to that caused by steric hindrance in many polymers, and occasioned by *short-range* electrostatic repulsion between neighboring carboxyl groups.

#### *Styrene-Maleic Acid Copolymer*

At 60% neutralization, the magnitudes of  $\eta$  and  $Q_\eta$  are normal. This behavior corresponds to the situation in dilute solution where the clustering tendency of the phenyl groups in the aqueous medium is overcome by



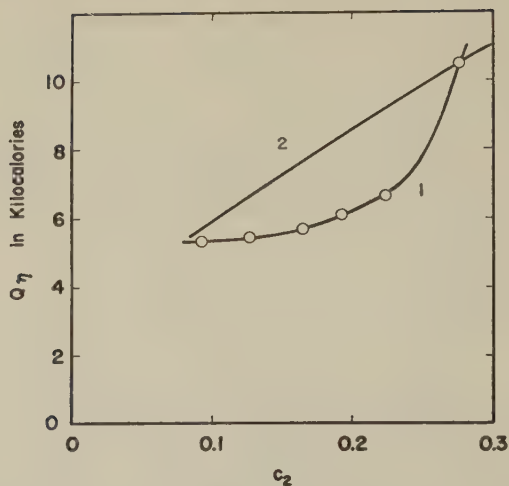


FIG. 5. Apparent heat of activation for viscous flow at 25°C., plotted against polymer concentration in grams per cubic centimeter of solution. (1) SYMA-B2-DMS 50% neutralized with sodium hydroxide; (2) SYMA-B2 unneutralized, in 50% aqueous dioxane.

electrostatic repulsion of the charged carboxyls (8). Again, the high ionic strength in concentrated solution prevents any long-range repulsive effects.

Below 50% neutralization, both  $\eta$  and  $Q_\eta$  increase very rapidly at a concentration of 0.142 g. polymer per cubic centimeter. The shapes of the curves in Fig. 2 and curve 1 of Fig. 5, as well as unpublished qualitative observations (14, 16), indicate that the transition shifts to higher degrees of neutralization with increasing concentration and decreasing temperature. This behavior corresponds to the situation in very dilute solution (8, 9), occurring at much lower neutralization (around 3%), where the association among phenyl groups in an aqueous medium causes hypercoiling of isolated molecules and eventual phase separation. The association can be suppressed either by ionization or by reducing the dielectric constant of the medium, as with dioxane, to a level which is compatible with the nonpolar portions of the molecule. In concentrated solution, such association (sometimes called "hydrophobic bonding") must lead to intermolecular adherence of the intertwined coils. The sharp increase in  $Q_\eta$  indicates a change in the mechanism of flow with the onset of association. When the latter is present (at low average charge, high concentration, and/or low temperature) the flow probably depends on the rate of dissociation of linkage points between chains.

Some qualitative evidence of the structure can be obtained by comparing the viscoelastic properties of the 31% solution of SYMA-U with those of ordinary concentrated polymer solutions. The relaxation spectrum  $H$  of

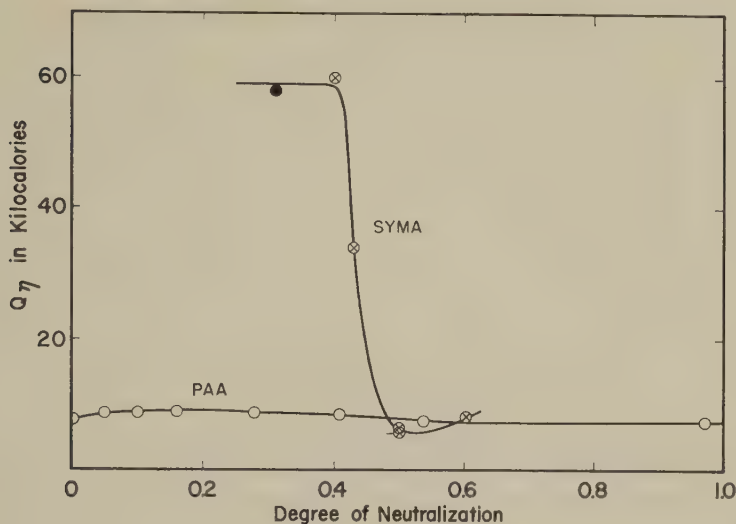


FIG. 6. Apparent heat of activation for viscous flow at 25°C., plotted against degree of neutralization with sodium hydroxide. Open circles, PAA at a concentration of 0.160 g. polymer per grams of water; crossed circles, SYMA-B2-RHB at  $c_2 = 0.142$  g. per cubic centimeter solution; crossed with tag, SYMA-B2-DMS at  $c_2 = 0.165$ ; solid circle, SYMA-U at  $c_2 = 0.165$  (calculated from temperature shift factors  $a_T$  observed in stress relaxation).

this excessively viscous system, determined from wave propagation and stress relaxation experiments, is plotted in Fig. 7. The terminal zone at the right has a normal shape for a polymer with molecular weight heterogeneity, and the terminal relaxation time calculated from the Rouse theory (17),  $\tau_1 = 6\eta M / \pi^2 c RT = 1.60 \times 10^2$  sec., falls in the customary position (17, 18) near the observed terminal drop in  $H$ . Thus the viscoelastic properties at long times reflect configurational changes in groups of molecules coupled by linkage points, and the latter prolong the viscoelastic time scale to the same degree that they prolong viscous flow. But the linkage points are not the ordinary long-range entanglements present in concentrated polymer solutions, because the plateau region in Fig. 7 is much too wide to be explained on this basis. The average molecular weight between ordinary entanglements,  $M_e$ , can be estimated (18) from the plateau width  $\Delta$  in logarithmic decades by the equation  $\Delta = 2.4 \log (M/2M_e)$ . Since  $\Delta \geq 8$ , we obtain  $M_e \leq 36$ , a meaninglessly small value. By contrast, estimation by the theory of rubberlike elasticity from the magnitude of the shear modulus at audiofrequencies (14), which is  $2 \times 10^5$  dynes/cm.<sup>2</sup>, gives a realistic figure of  $M_e = 20,000$ . For ordinary concentrated solutions in which the entanglements presumably arise from long-range geometrical relations, such alternative estimates of  $M_e$  agree in order of magnitude.

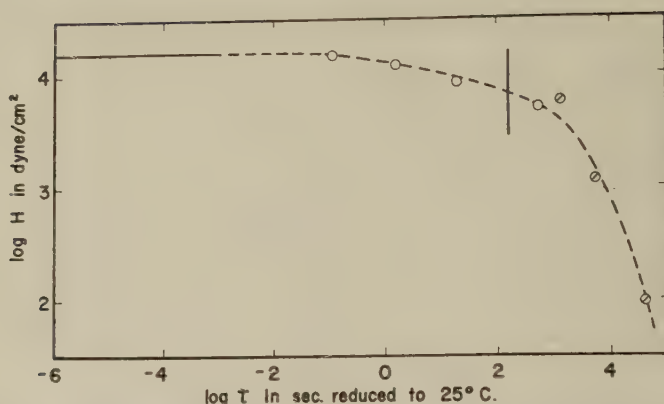


Fig. 7. Relaxation spectrum reduced to  $25^\circ\text{C.}$  for solution of SYMA-U at  $c_2 = 0.165$ , 31% neutralized with sodium hydroxide. Solid line at left, from wave propagation measurements; open circles, from stress relaxation following instantaneous strain; slotted circles, from stress relaxation following cessation of steady-state rate of strain. Vertical bar denotes terminal relaxation time calculated from Rouse theory.

The discrepancy in the present case provides further evidence that the linkage points are associations of a much tighter character.

The precise nature of the linkage points, and the reason why they are spaced so widely, remain to be clarified. High viscosities or gelation in concentrated aqueous solutions of polymethacrylic acid (7) have been attributed to hydrogen bonding. However, this molecule is quite different from SYMA in its structure and compatibility with an aqueous medium. Enormous viscosities have also been observed in the undiluted state for copolymers of styrene and methacrylic acid (19), in which there is good evidence that transient linkages are formed by dimerization of carboxyl groups. There, of course, such associations are favored by an environment of very low dielectric constant.

It should be emphasized that the anomalous behavior of SYMA pictured in Figs. 2 and 6 arises not primarily from its being a polyelectrolyte but from the combination of ionic and hydrophobic groups in an aqueous medium. Without the ionic groups, there would be no solubility in water. Some biological macromolecules have similar features (20).

#### SUMMARY

The effect of partial neutralization on the viscosities of concentrated solutions of polyacrylic acid and 1:1 styrene-maleic acid copolymer has been studied, together with some measurements of the dependence of viscosity on temperature and concentration. In unneutralized polyacrylic

acid the concentration dependence, and at all degrees of neutralization the temperature dependence, are normal in that they resemble the behavior of nonpolar polymers in nonpolar solvents. The magnitude of the viscosity increases by about a factor of 20 as the degree of neutralization is increased from zero to 0.97. In styrene-maleic anhydride copolymer with a degree of neutralization of 0.60 and concentration 0.14 g./cc. the viscosity and apparent activation energy for flow are of normal magnitude, but both quantities increase enormously with decreasing neutralization. This change is shifted to higher degrees of neutralization by raising the concentration or lowering the temperature. At 0.31 neutralization, concentration 0.165 g./cc., the viscosity is  $7 \times 10^6$  poises at 25°C. and the heat of activation is 58 kcal./mole; the viscoelastic relaxation spectrum exhibits a plateau zone extending over at least 8 logarithmic decades and a terminal zone located near the position predicted from the viscosity by the Rouse theory. These results are interpreted in relation to the behavior of the two poly-electrolytes in very dilute solution as known from earlier investigations.

#### ACKNOWLEDGMENTS

This work was supported in part by the Research Committee of the Graduate School of the University of Wisconsin from funds supplied by the Wisconsin Alumni Research Foundation, and in part by the Office of Naval Research under Contract N7onr-28509. We are indebted to Mr. Ronald H. Baney for fractionation and characterization of Sample SYMA-B2-RHB, and to Mr. Stephen D. Morton for characterization of Sample PAA-U.

#### REFERENCES

1. FERRY, J. D., FOSTER, E. L., BROWNING, G. V., AND SAWYER, W. M., *J. Colloid Sci.* **6**, 377 (1951).
2. JOHNSON, M. F., EVANS, W. W., JORDAN, I., AND FERRY, J. D., *J. Colloid Sci.* **7**, 498 (1952).
3. FERRY, J. D., GRANDINE, L. D., JR., AND UDY, D. C., *J. Colloid Sci.* **8**, 529 (1953).
4. LANDEL, R. F., BERGE, J. W., AND FERRY, J. D., *J. Colloid Sci.* **12**, 400 (1957).
5. EISENBERG, H., AND FUOSS, R. M., in Bockris, J. O'M., "Modern Aspects of Electrochemistry," Chapter 1. Academic Press, New York, 1954.
6. RICE, S. A., *Rev. Mod. Phys.* **31**, 69 (1959).
7. SILVERBERG, A., ELIASSAF, J., AND KATCHALSKY, A., *J. Polymer Sci.* **23**, 259 (1957).
8. FERRY, J. D., UDY, D. C., WU, F. C., HECKLER, G. E., AND FORDYCE, D. B., *J. Colloid Sci.* **6**, 429 (1951).
9. DANNHAUSER, W., GLAZE, W. H., DUELGTEN, R. L., AND NINOMIYA, K., *J. Phys. Chem.*, in press.
10. NEWMAN, S., KRIGBAUM, W. R., LAUGIER, C., AND FLORY, P. J., *J. Polymer Sci.* **14**, 451 (1954).
11. BACON, L. R., *J. Franklin Inst.* **222**, 251 (1936).
12. HELDERS, F. E., AND FERRY, J. D., *J. Phys. Chem.* **60**, 1536 (1956).
13. SCHREMP, F. W., FERRY, J. D., AND EVANS, W. W., *J. Appl. Phys.* **22**, 711 (1951).

14. HECKLER, G. E., Ph.D. Thesis, University of Wisconsin, Madison, 1952.
15. BUECHE, F., *J. Chem. Phys.* **20**, 1959 (1952).
16. UDY, D. C., Ph.D. Thesis, University of Wisconsin, Madison, 1950.
17. FERRY, J. D., WILLIAMS, M. L., AND STERN, D. M., *J. Phys. Chem.* **58**, 987 (1954).
18. FERRY, J. D., "Viscoelastic Properties of Polymers," Ch. 10, Wiley, New York, 1960.
19. LONGWORTH, R., AND MORAWETZ, H., *J. Polymer Sci.* **29**, 307 (1958).
20. WAUGH, D. F., WILHELMSON, D. F., COMMERFORD, S. L., AND SACKLER, M. L., *J. Am. Chem. Soc.* **75**, 2592 (1953).



## THERMAL FORCE ON PARTICULATE MATERIAL AT HIGH KNUDSEN NUMBERS IN THE ABSENCE OF A THERMAL GRADIENT

William H. Hughes

*Western Precipitation Corporation, Los Angeles, California*

*Received July 22, 1959; revised February 15, 1960*

### ABSTRACT

A mechanism for a force arising from thermal effects is considered for small particles surrounded by gas under conditions of high Knudsen number in the absence of a thermal gradient. A simplified model is assumed. The force is found to be proportional to the pressure and the cross-sectional area of the particle. The resulting velocity is found to be independent of these parameters.

### INTRODUCTION

Thermal forces, such as radiation pressure and the so-called radiometric forces were studied by Tyndall (1), Frankland (2), Rayleigh (3, 4), Lodge (5), Crookes (6, 7), and Reynolds (8) before the currently acceptable explanation was advanced by Aitken (9) in 1884: "... the principal part of the energy producing the motion being transferred from the hot surface to the repelled surface by the kinetic energy of the molecules, and not by radiation." Maxwell (10) recognized the validity of this explanation as did the others and used it as the basis for his treatment of the radiometric force. This was elaborated on by Knudsen (11), Einstein (12), Epstein (13), Caywood (14), Rosenblatt and La Mer (15), and Saxton and Ranz (16), and, more recently, Schadt and Cadle (17) have investigated and discussed the various thermal forces on a particle within a gaseous medium for the case in which a thermal gradient exists. Most of these works have been concerned with effects which exist at low Knudsen numbers, which is to say that the size of the particle suspended in the gas is large with respect to the mean-free path of the molecules of the gas.

Crookes (6, 7) showed that radiometric forces are a function of the gas pressure, and Reynolds (8) demonstrated the existence of an optimum pressure at which the forces are maximized. Einstein (12), using a simplified model, suggested that rather large terminal velocities might be expected at high Knudsen numbers for the case wherein a thermal gradient exists. Rosenblatt's (15) experiments tended to confirm Einstein's model. All this work was concerned with models which demanded the existence of a

thermal gradient, and, in fact, the work of Rosenblatt and La Mer (15), Saxton and Ranz (16), and Schadt and Cadle (17) all demonstrated the direct proportionality of the thermal force to the thermal gradient.

Waldmann (18) has shown that forces may be expected in the absence of a thermal gradient if there is a gradient of molecular weight in the gas such as would be found in the classical model of a static stratosphere. This paper advances an argument predicting the existence of a thermal force which does not depend on the existence of either a thermal or a molecular weight gradient. A simplified model, which can be readily modified in obvious ways, is chosen in order to keep the mathematical discussion within bounds.

Ehrenhaft (19, 21) demonstrated the existence of a force on particulate material in gases which resulted from intense illumination. His experiments were verified by Whytlaw-Grey and Patterson (20) and discussed qualitatively by Tauzin (22-24). They have referred to this force as "photophoresis," and it has been shown to be occasionally in the negative direction for certain very special particles. It is suggested that this "photophoretic force" may be a combination of several effects, one of these being the thermal force predicted herein.

#### DISCUSSION

In the model adopted for discussion we choose a region between two infinite, black, parallel planes whose temperatures are  $T_1$  and  $T_2$ . Let us, for convenience, make the assumption that

$$T_1 \geq T \geq T_2, \quad [1]$$

where  $T$  is the mean temperature of the gas between the plates. We make the assumption that the gas is monatomic and has a negligible temperature gradient over dimensions of the order of the diameter of the particle,  $2a$ . We neglect gravitational and other fields so that spatial orientation is of no consequence. Within our region we place a black, spherical particle which is composed of a substance with a thermal conductivity that provides an internal heat transfer that is low with respect to the heat transfer resulting from the gas. It is seen that this is a very simplified model and, as such, is unlikely to be found in nature; but such simplification is useful in isolating effects and allows us to comprehend one thing at a time.

If we let  $N_1$  be the number of molecules per unit time colliding with that hemisphere of our particle which is nearest the plane with temperature  $T_1$  in a direction that is perpendicular to that plane, then if  $\bar{c}$  be the mean molecular speed of the gas, and  $n$  be the number of molecules per unit volume of the gas, the following relation is true

$$N_1 = \frac{1}{6} n \pi a^2 \bar{c}, \quad [2]$$

where  $a$  is the radius of the particle. It is clear that the number of molecules colliding with the opposite hemisphere in the direction perpendicular to the planes is the same, and in the absence of thermal effects—as, for instance, the case where  $T_1 = T_2$ —the particle will experience no force at all.

If as many molecules leave a given incremental surface of the particle as are absorbed onto it in any unit time, and if they leave with the mean kinetic temperature equal to the local temperature of the surface, then it is clear that a net force is exerted upon the particle. Let us designate that net force  $F$  and take it as the difference in the unequal forces on the two hemispheres which we designate by means of subscripts in a like manner as before as  $F_1$  and  $F_2$ . Then

$$F = F_1 - F_2, \quad [3]$$

providing that the direction from the hot toward the cool plane be taken as positive. If the corresponding mean molecular speeds be taken as  $\bar{c}_1$  and  $\bar{c}_2$ , then

$$F_1 = N_1(m\bar{c}_1 - m\bar{c}); \quad [4]$$

$$F_2 = N_2(m\bar{c} - m\bar{c}_2), \quad [5]$$

where  $m$  is the molecular weight of the gas and  $N_1$  and  $N_2$  are given by

$$N_1 = N_2 = N \quad [6]$$

from Eq. [2].

Hence the net force  $F$  of Eq. [3] may be written as

$$F = Nm(\bar{c}_1 - \bar{c}_2). \quad [7]$$

Let us take  $\bar{c}_j$  as the mean molecular speed corresponding to the temperature  $T_j$  of any surface element of the particle. We designate the surface element as  $ds_j$ . The relation between  $\bar{c}_j$  and  $\bar{T}_j$  is given by the kinetic theory as

$$\bar{c}_j = (3RT_j/M)^{1/2}, \quad [8]$$

where  $R$  is the gas constant and  $M$  is the molecular weight of the gas.

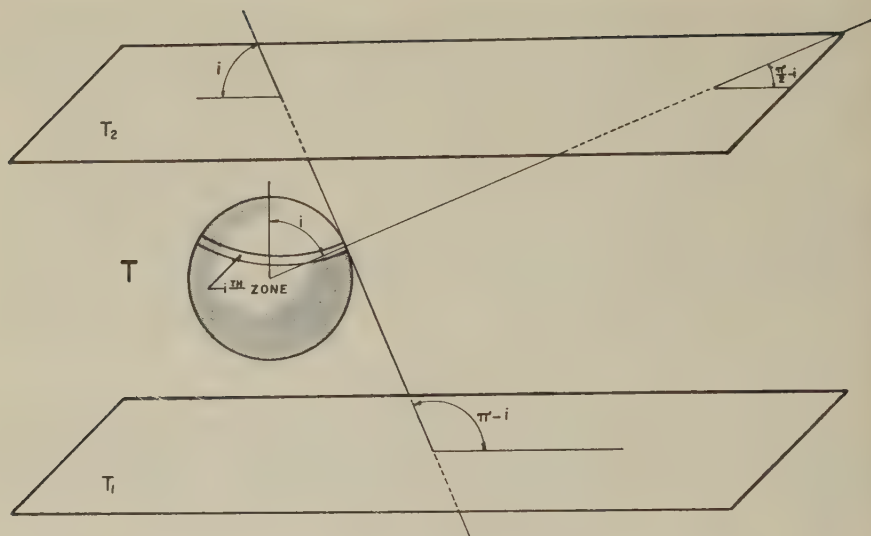
The values of  $\bar{c}_1$  and  $\bar{c}_2$  may be found by integrating over the respective hemisphere

$$\bar{c}_1 = \frac{1}{s} \int_{s_1} \bar{c} ds \quad [9]$$

and

$$\bar{c}_2 = \frac{1}{s} \int_{s_2} \bar{c} ds \quad [10]$$

where  $s$  is the area of a hemisphere.



PARTICLE IN GAS AT TEMPERATURE "T" BETWEEN TWO  
PARALLEL PLANES AT TEMPERATURES "T<sub>1</sub>" & "T<sub>2</sub>" RESP.

FIG. 1. Particle in gas at temperature "T" between two parallel planes at temperatures  $T_1$  and  $T_2$  respectively.

We substitute Eq. [8] into these two equations and define a mean temperature by the mean value theorem. Thus

$$\bar{c}_1 = (3R\bar{T}_1/M)^{1/2}; \quad [11]$$

$$\bar{c}_2 = (3R\bar{T}_2/M)^{1/2}. \quad [12]$$

These we substitute into Eq. [7] and, utilizing the gas law,

$$F = \frac{1}{2}\pi a^2 P T^{-1/2} (\bar{T}_1^{1/2} - \bar{T}_2^{1/2}) \quad [13]$$

where  $P$  is the pressure of the gas.

In order to evaluate  $\bar{T}_1$  and  $\bar{T}_2$  we apply the Stefan-Boltzmann law. The sphere is divided into zones of width  $a \, di$ , where  $i$  is the colatitude as shown on the illustration. From considerations of symmetry it is seen that the temperature of any zone is the same for every element in the zone. This temperature we call  $T_i$ . Radiative equilibrium is expressed by the Stefan-Boltzmann law

$$A_1 F_{1i} (T_1^4 - T_i^4) = A_2 F_{i2} (T_i^4 - T_2^4), \quad [14]$$

where  $A$  is the integrated area associated with the view-factor  $F$ .<sup>1</sup> The

<sup>1</sup> For a discussion of these topics in thermodynamics the reader is directed to any standard undergraduate text on thermodynamics such as McAdams: "Heat Transmission," 3rd ed, pp. 63 ff. McGraw-Hill, New York (1954).

indeterminate ratio is solved by application of L'Hospital's rule to get

$$\frac{A_1 F_{1i}}{A_2 F_{i2}} = \frac{1 - i/\pi}{i/\pi}, \quad [15]$$

and we may solve for  $T_i$

$$T_i = \left[ T_1^4 + \frac{i}{\pi} (T_2^4 - T_1^4) \right]^{\frac{1}{4}}. \quad [16]$$

To arrive at  $\bar{T}_1$  it is necessary to find the mean by integrating over the hemisphere nearest the plane at temperature  $T_1$

$$\bar{T}_1 = \frac{1}{\frac{1}{2}\pi - 0} \int_0^{1/2\pi} T_i \, di \quad [17]$$

$$= \frac{8}{5(T_2^4 - T_1^4)} \left[ \left( \frac{T_1^4 + T_2^4}{2} \right)^{5/4} - T_1^5 \right]. \quad [18]$$

Similarly we may find  $\bar{T}_2$  by integrating over the other hemisphere

$$\bar{T}_2 = \frac{1}{\pi - \frac{1}{2}\pi} \int_{1/2\pi}^{\pi} T_i \, di \quad [19]$$

$$= \frac{8}{5(T_2^4 - T_1^4)} \left[ T_2^5 - \left( \frac{T_1^4 + T_2^4}{2} \right)^{5/4} \right]. \quad [20]$$

From these equations one sees immediately that the equatorial temperature  $T_{1/2}$  of the particle is given by

$$T_{1/2}^4 = \frac{1}{2}(T_1^4 - T_2^4), \quad [21]$$

just as may be expected intuitively.

The drag force  $F_D$  experienced by the sphere is given (21) by

$$F_D = \frac{4}{3} \pi \phi n m \bar{c} a^2 w, \quad [22]$$

where  $w$  is the velocity of the sphere with respect to the gas and  $\phi$  is a coefficient depending on the material.

In order to find the steady-state velocity  $w$ , we may equate the thermal force to the drag force

$$w = (3R/M)^{1/2} (\bar{T}_1^{1/2} - \bar{T}_2^{1/2}) / 8\phi, \quad [23]$$

where the values of  $\bar{T}_1$  and  $\bar{T}_2$  are found from Eqs. [16] and [18], and the value of  $\phi$  does not differ greatly from 1.4.

It will be noted that the final result is independent of the density or the size of the sphere. This implies considerable independence of shape and so our model may be generalized from a spherical particle to a fairly general particle. We note also that the result is not dependent on the pressure, temperature, or density of the gas; but only on the composition of the gas



(which does not show in the equation but is implicit in our assumptions), the temperatures of the planes, and the validity of the assumptions for an application to a real system. One notes that the validity of the result is not affected by setting the temperature of the cool infinite plane equal to zero.

## REFERENCES

1. TYNDALL, A. M., *Proc. Roy. Inst.* **6**, 3 (1870).
2. FRANKLAND, *Proc. Roy. Soc. (London)* **25**, 542 (1877).
3. RAYLEIGH, LORD, *Proc. Roy. Soc. (London)* **34**, 414 (1882).
4. RAYLEIGH, LORD, *Nature* **XXVIII**, 139 (1883).
5. LODGE, O. J., *Nature* **28**, 297 (1883).
6. CROOKES, W., *Nature* **15**, 224 (1877).
7. CROOKES, W., *Nature* **15**, 229 (1877).
8. REYNOLDS, O., *Phil. Trans.* **166**, 727 (1880).
9. AITKEN, *J. Roy. Soc. Edinburgh* **32**, 293 (1884).
10. MAXWELL, J. C. "Collected Works." Dover, New York, 1951.
11. KNUDSEN, *Ann. Physik* **32**, 809 (1910).
12. EINSTEIN, A., *Z. Physik* **27**, 1 (1924).
13. EPSTEIN, *Z. Physik* **54**, 537 (1929).
14. CAYWOOD, W., *Trans. Faraday Soc.* **32**, 1068 (1936).
15. ROSENBLATT, P., AND LA MER, V. K., *Phys. Rev.* **70**, 385 (1946).
16. SAXTON, R. L., AND RANZ, W. E., *J. Appl. Phys.* **23**, 917 (1952).
17. SCHADT, C. F., AND CADLE, R. D., *J. Colloid Sci.* **12**, 362 (1957).
18. WALDMANN, L., *Z. Naturforsch.* **14a**, Heft 7, 589 (1959).
19. EHRENHAFT, F., *Ann. Physik* **56**, 81 (1918).
20. WHYTLAW-GREY, R., AND PATTERSON, H. S., "Smoke: A Study of Aerial Disperse Systems," p. 120. E. Arnold & Co., London, 1932.
21. EHRENHAFT, F., *Phys. Rev.* **68**, 102 (1945).
22. TAUZIN, P., *Compt. rend.* **225**, 350 (1947).
23. TAUZIN, P., *Compt. rend.* **232**, 493 (1951).
24. TAUZIN, P., *Compt. rend.* **235**, 1119, 1718 (1952).

# THE LIMITED FLOCCULATION OF COLLOIDAL SYSTEMS

Thomas Gillespie

*Physical Research Laboratory, The Dow Chemical Company,  
Midland, Michigan*

*Received December 17, 1959; revised February 15, 1960*

## ABSTRACT

The flocculation of a styrene-butadiene latex by methylcellulose has been examined in detail by direct measurement of the particle concentration as a function of time. The apparent particle concentration decreased in all cases to a steady value corresponding to limited or partial flocculation. The present data and similar literature data on the flocculation of gold sols by salt are in agreement with an equation due to Goodeve which assumes a competition between flocculation and deflocculation processes. The experimental rate constants were compatible with those calculated from established colloid theory using particle diffusion coefficients and the coated particle radius determined from Brownian movement measurements. The present results indicate that the well-known sensitization-stabilization effect of hydrophilic colloid on a hydrophobic colloid is, in the system examined, due to changes in the balance of the flocculation and deflocculation processes.

## INTRODUCTION

Although colloid systems which exhibit limited flocculation are common, they have not been studied extensively. Most of the colloid literature on flocculation deals with either rapid or slow coagulation (1). They are essentially the same except that in the latter case the presence of electric forces slows down the rate of coagulation. Following Smoluchowski (1-3), if  $n$  is the apparent number of particles per cubic centimeter at time  $t$ , we may write for homogeneous systems,

$$-\frac{dn}{dt} = Kn^2; \quad [1]$$

$$\frac{1}{n} = \frac{1}{n_0} + Kt; \quad [2]$$

$$K = 4\pi Da_{\text{eff.}} W, \quad [3]$$

where  $K$  is called the coagulation constant. Here  $n_0$  is the apparent number of particles per cubic centimeter at time  $t = 0$ ;  $D$  is the relative diffusion coefficient of the particles (1); and  $a_{\text{eff.}}$  is the effective radius of the particles for "contact." The factor  $W$  is dependent upon the repulsive and

attractive forces between the particles. For rapid coagulation  $W$  and  $K$  are large; for slow coagulation they are small. The coagulation constant is determined by plotting the particulate volume (i.e.,  $1/n$ ) against time and measuring the slope of the resulting straight line. In some cases these plots are not linear. Westgren (1, 4) has reported data from a gold sol study which seemed to indicate that the rate of coagulation slowed down continuously until apparently stable systems were obtained which did not seem to coarsen any further. These data are an example of what may be called limited flocculation.

The classical explanation for this behavior (1) is that the rate of coagulation decreases because the repulsive forces between doublets is expected to be greater than those between single particles. In some experiments with latex we have observed limited flocculation in this laboratory and have noticed that there were many single particles left when flocculation had apparently ceased. An analysis of Westgren's data suggested that this was also the case in his experiments. If  $N$  is the initial number of elementary particles per cubic centimeter in a colloid and  $n$  is the apparent number of particles per cubic centimeter at some time  $t$ , then the number of doublets per cubic centimeter should be  $N - n$ . Assessment of Westgren's results for the flocculation of a gold sol ( $0.012 \mu$  radius) coagulated by sodium chloride (1, 4) indicated that approximately 65 % of the particles in the final stable system were elementary particles. These results, and the latex data referred to above, indicate the necessity for a better explanation than the classical arguments given above.

An obvious possible explanation is that when two particles come in contact they are not held together permanently but may deflocculate at some later time as a result of relative Brownian movement. The observed equilibrium would be due to the competition between flocculation and deflocculation. The available data seem to agree with this hypothesis.

Of special interest is the fact that the introduction of the idea of flocculation-deflocculation competition leads to a more revealing picture of the action of protective colloids. The well-known sensitization-stabilization effect of a hydrophilic colloid on a hydrophobic colloid (1) appears to be complex and to be dependent upon both the rate of flocculation and deflocculation.

#### EXPERIMENTAL

The experimental results of Westgren (1, 4) which illustrate limited flocculation were obtained by counting the apparent number of particles in a known volume with an ultramicroscope. In the present work, the same technique was used to assess the behavior of styrene-butadiene latex and mixtures of methylcellulose and latex.

The latex was supplied by Dr. J. W. Vanderhoff of this laboratory. It was

a uniform particle size latex of diameter 5800 Å. It was a 60 % styrene-40 % butadiene latex. The emulsifier was Dupanol M.E. and the initiator was potassium persulfate. This latex was chosen for two reasons. First, the density was close to that of water and this prevented complications due to gravitational settling. Secondly, the large particle size made it possible to distinguish clearly between elementary particles and doublets.

The methylcellulose was Dow Methocel 65HG (4000 c.p.s.), which has a molecular weight of approximately  $1.4 \times 10^5$ .

The latexes were diluted with deionized water so that they contained  $10^{-3}$  % latex solids. Fifty cubic centimeters of this was added to 50 c.c. of deionized water containing various amounts of methylcellulose. Each of these samples contained  $2.8 \times 10^{-5}$  % Dupanol M.E.,  $3.7 \times 10^{-6}$  % potassium persulfate, and  $3.7 \times 10^{-6}$  % sodium bicarbonate.

The latex-methylcellulose mixtures were shaken vigorously before a sample was put in a small glass ultramicroscope cell maintained at 25°C. Preliminary experiments indicated that samples which had reached equilibrium could be deflocculated by shaking so that the same mixture could be used in repeat experiments. A microscope with a 40× objective and a 12× eyepiece was used for counting. Counts were made by three observers, the author, Mr. L. Holysko, and Mr. V. Coomer, and there was reasonable agreement.

In order to analyze the results effectively it was necessary to measure the relative diffusion coefficients of the particles in various methylcellulose solutions. This was done by assessing the Brownian movement. Two single particles were selected and the distance between them along a chosen direction was noted. One minute later the distance was measured again. The difference was taken as the relative displacement. From the individual readings obtained in this way the mean-square displacement was calculated. From this the relative diffusion coefficient was calculated (see reference 1, page 280).

#### ANALYSIS OF THE EXPERIMENTAL RESULTS

In Fig. 1 typical  $1/n$  against  $t$  plots are illustrated. The data obtained when no methylcellulose was used indicated that very little, if any, coagulation was occurring. The slope of the straight line drawn through the  $1/n$  versus  $t$  plot which is equal to  $K$  in Eqs. [1], [2], and [3] was very small. When methylcellulose was used,  $1/n$  reached an equilibrium value and remained constant for many hours. The equilibrium values indicated by the dotted lines in Fig. 1 were determined from a number of counts 24 hours after the experiments began. This equilibrium behavior is similar to that observed by Westgren with gold sols (1, 4).

To analyze the data, the approach suggested by Goodeve (5) was adopted. Introducing the possibility of deflocculation into Eq. [1],

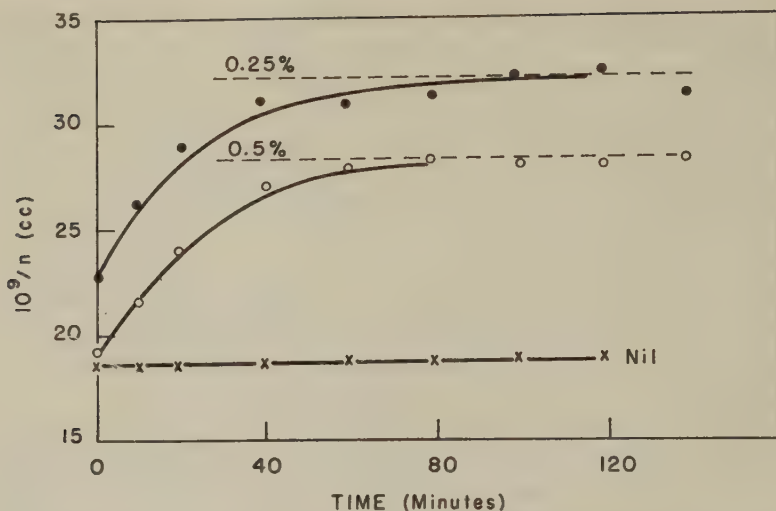


FIG. 1. Typical particulate volume versus time plots for the styrene-butadiene latex and methylcellulose system. The percentages refer to the concentration of methylcellulose. The dotted lines indicate the equilibrium particulate volume values at 24 hours.

$$-\frac{dn}{dt} = Kn^2 - \beta(N - n) \quad [4]$$

if the degree of flocculation is slight. Here  $\beta$  is a constant descriptive of the rate of deflocculation, and  $N$  is the number of elementary particles per cubic centimeter.

Integrating Eq. [4],

$$\frac{n - n_f}{n + B} = \frac{n_0 - n_f}{n_0 + B} e^{-\alpha t}, \quad [5]$$

where  $n_f$  is the apparent equilibrium number of particles per cubic centimeter, and  $n_0$  is the apparent number of particles per cubic centimeter at  $t = 0$ . The values  $n$ ,  $n_f$ , and  $n_0$  were all determined by counting doublets as single particles. In the experiments in which methylcellulose was used some flocculation had occurred at the time origin so that  $n_0$  was less than  $N$ .

$$B = \frac{Nn_f}{N - n_f}. \quad [6]$$

$$\alpha = \beta(1 + 4KN/\beta)^{1/2}. \quad [7]$$

$$\frac{K}{\beta} = (N - n_f)/n_f^2. \quad [8]$$

According to Eq. [5], plots of  $\ln(n - n_f)/(n + B)$  against  $t$  should be



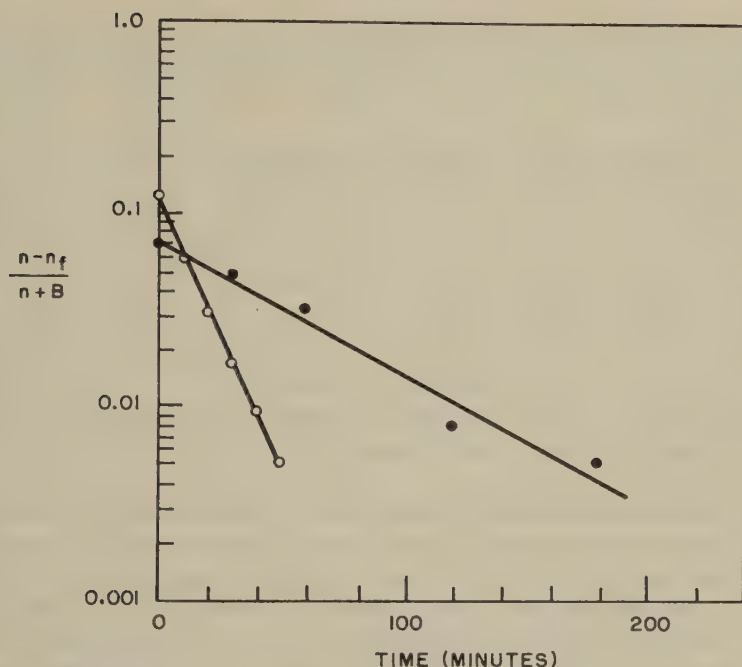


FIG. 2. Illustration of the linear relation between  $\ln (n - n_f)/(n + B)$  and time for systems which exhibit limited flocculation. The full circles and the open circles refer to Westgren's data (1, 4) for gold sols and to a typical result for the latex-methylcellulose systems, respectively.

straight lines of slope  $\alpha$ . Typical results are illustrated in Fig. 2. The rate constants  $K$  and  $\beta$  may be determined using the experimental  $n_f$  and  $\alpha$  and Eqs. [7] and [8].

In Fig. 2 the independent variable is determined to a large extent by the quantity  $n - n_f$ . When  $n$  approaches  $n_f$  in the later stages of each experiment the scatter in the experimental points was large and the points could not be used in plots such as Fig. 2. In order to assess the validity of Eq. [5] for all experimental points, the value of  $n$  at various times was calculated using the constants determined from the data obtained in the early stages of each experiment. The calculated values were in rough agreement with the experimental values over the whole range.

In Table I the data derived from the experiments on a latex-methylcellulose system are summarized. The gold sol results of Westgren (1, 4) yielded  $K$  equal to  $0.11 \times 10^{-12}$  c.c./sec. and  $\beta = 1.77 \times 10^{-4}$  sec.<sup>-1</sup>. For such a system,  $K$  should equal  $5 \times 10^{-12}$  c.c./sec. if there are no strong repulsive or attractive forces between the particles. The experimental result is reasonable, and it indicates that repulsive forces hinder the flocculation of the gold sol. The relatively small value of the deflocculation rate constant

TABLE I  
Summary of the Data Derived from the Experimental Results

Methylcellulose concentration (% by weight)	$\alpha \times 10^4$ (sec. <sup>-1</sup> )	$n_f \times 10^{-7}$ (c.c. <sup>-1</sup> )	$\beta \times 10^4$ (sec. <sup>-1</sup> )	$K \times 10^{12}$ (c.c./sec.)	$D \times 10^{10}$ (cm. <sup>2</sup> /sec.)	$\frac{W a_{\text{eff.}}}{a}$	$W$
0	—	—	—	0.05	166	0.008	0.005
0.063	7.8	3.64	4.5	4.5	66	1.84	1.2
0.125	10.3	3.72	6.4	5.4	53	2.78	1.8
0.25	10.5	3.15	4.9	8.7	36	6.6	4.3
0.5	9.3	3.53	5.2	5.7	23	6.8	4.4

indicates that the forces binding the gold sol particles when they come in contact, are larger than those which operate in the case of the latex particles covered with methylcellulose.

The fact the experimental latex results are in agreement with Eq. [5] does not prove that deflocculation is responsible for the observed equilibrium. The rate constant  $K$  which can be predicted approximately from theory should be of the right order if the analysis outlined above is correct. In Table I the relative diffusion coefficients for two particles which were measured experimentally for each system are tabulated. Using these values and the appropriate value of  $K$  from Table I, one may calculate from Eq. [3] the quantity  $W a_{\text{eff.}}/a$ . Values of this quantity are included in Table I.

One would expect

$$\frac{a_{\text{eff.}}}{a} = 1 + \frac{\delta}{a}, \quad [9]$$

where  $\delta$  is the effective thickness of the absorbed methylcellulose layer for particle contact. Here  $a$  was equal to 2900 Å. The fully extended length of the average methylcellulose molecule was approximately 4200 Å. One would expect that  $0 < \delta < 4200$  Å. A closer but still rough estimate of  $\delta$  may be obtained from the diffusion coefficient of the particles in dilute methylcellulose solutions. The relative diffusion coefficients in Table I are twice the diffusion coefficients for single particles. Taking  $33 \times 10^{-10}$  cm.<sup>2</sup>/sec. as the diffusion coefficient for a single particle in the 0.063% solution and taking the viscosity as 1.43 centipoises, the effective radius in diffusion is 4500 Å. This would mean that  $\delta$  is of the order of 1600 Å. or  $a_{\text{eff.}}/a$  is of the order of 1.55. Consequently  $W$  would range from  $5 \times 10^{-3}$  to 4.4 in the latex experiments (see Table I). This result is compatible with our present knowledge of colloid behavior (reference 1, page 294), and it supports the foregoing analysis.

In Table I the flocculation rate constant,  $K$ , increases with increase in the amount of methylcellulose, reaches a maximum, and then decreases.

From Eq. [3] and Table I we would infer that the two competing mechanisms responsible for this maximum are depression of the electric double layer and a decrease in the Brownian movement due to an increase in the effective viscosity.

Owing to our relative ignorance of deflocculation processes, the values of  $\beta$  cannot be checked at this time. A study of Table I, however, suggests that this rate constant may, in the future, be as useful as  $K$  has been in the past, in giving us an insight into the mechanisms of interaction of colloidal particles. In Table I,  $W$  is a measure of the presence of a repulsive barrier or the second minimum in the potential energy vs. interparticle distance function predicted by the currently accepted theory of colloid stability (6). The condition  $W < 1$  indicates a potential barrier to flocculation;  $W > 1$  indicates a secondary minimum. Here  $\beta$  is in part a measure of the depth of the primary minimum, although it may also depend upon the local viscosity (7).

Separate determination of the two rate constants is useful in elucidating the mechanisms of particle interaction, but the net effect of the competition between flocculation and deflocculation is more easily assessed by some measure of the degree of aggregation. The fractional number of particles which are aggregates should be equal to  $(N - n_f)/N$ . In Fig. 3 this quantity is plotted as a function of methylcellulose concentration. This curve is reminiscent of the well-known sensitization-stabilization effect of a hydro-

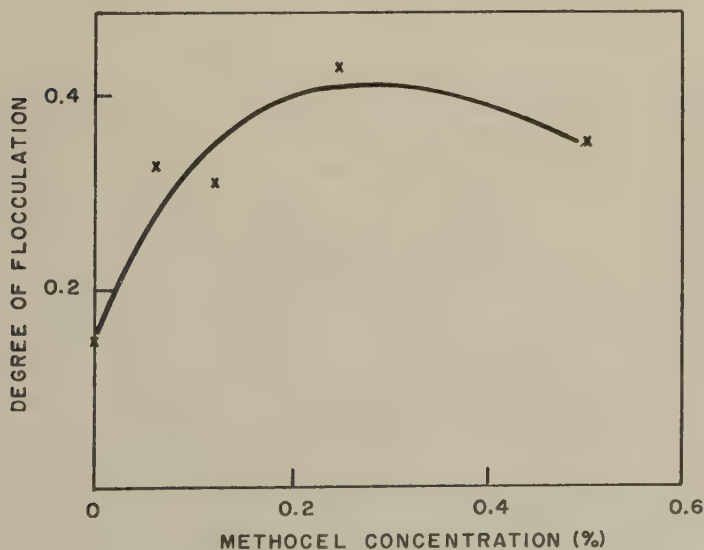


FIG. 3. Variation of the degree of flocculation of a styrene-butadiene latex (i.e.,  $(N - n_f)/N$ ) with methylcellulose concentration.

philic colloid on hydrophobic colloids. The present work indicates that it is a function of the rate of deflocculation as well as of the rate of flocculation.

## REFERENCES

1. KRUYT, H. R., "Colloid Science," Vol. 1. Elsevier, New York, 1952.
2. SMOLUCHOWSKI, M. VON, *Physik. Chem.* **92**, 129 (1917).
3. SMOLUCHOWSKI, M. VON, *Physik. Z.* **17**, 557, 585 (1916).
4. WESTGREN, A., *Arkiv Kemi, Mineral. Geol.* **No. 6, 7** (1918).
5. GOODEVE, C. F., *Trans. Faraday Soc.* **35**, 342 (1939).
6. VERWEY, E. J. W., AND OVERBEEK, J. TH. G., "Theory of the Stability of Lyophobic Colloids". Elsevier, New York, 1948.
7. KRAMERS, H. A., *Physica* **7**, 284 (1940).

## SOME OBSERVATIONS ON MONOLAYERS OF CARBON-14 LABELED STEARIC ACID<sup>1</sup>

George L. Gaines, Jr.

*General Electric Research Laboratory, Schenectady, New York*

*Received March 21, 1960*

### ABSTRACT

Films of radiostearic acid have been deposited on a variety of solids (Cu, Al, Pt, Cr, mica, glass), both by transfer from water surfaces and by adsorption from cetane and nitromethane solutions. The concentration of stearic acid in these films has been assessed radiometrically, and some observations on removal of the film by benzene rinsing have been made. At high surface pressures ( $>17$  dynes/cm.), stearic acid monolayers on water are transferred to solids at the same concentration which exists on the water. At lower pressure (10 dynes/cm.), lower concentrations are found after transfer. This may be related to the discontinuous structure of the film at this pressure. Adsorption of more than a single monolayer (based on the geometrical area of the surface) occurs with Cu and Al, probably because of soap formation. With inert substrates (Pt, Cr, mica), adsorption leads to only a fraction of a close-packed monolayer in times up to several hours. These results are discussed in terms of mechanisms of film deposition. Their importance in the Wilhelmy method for surface pressure measurement is emphasized.

In fundamental surface studies it is frequently desirable to apply monolayers of fatty substances to solid substrates in a controlled fashion. The techniques which have been used for this purpose fall into two groups: deposition of the monolayer, already formed on some other substrate, onto the solid surface, and adsorption of a monolayer onto the solid from a vapor, melt, or solution containing the molecules of interest. The first class includes, of course, the Langmuir-Blodgett technique (1, 2) and the "touching" technique recently used by Schulman *et al.* (3). Adsorption will produce monomolecular films under certain conditions (1, 4). Zisman *et al.* have recently studied methods of forming adsorbed monolayers and have suggested the use of the "retraction" method (5-10). They have shown that, in certain cases, the films remaining on the solid are monomolecular and fairly close-packed (5).

Recent work by Bartell and Ruch (11, 12), Levine and Zisman (10), and Cook and Ries (13) has indicated that, under some conditions, such

<sup>1</sup> Presented at the 136th National Meeting of the American Chemical Society, Division of Colloid Chemistry, Atlantic City, New Jersey September 14, 1959.



adsorption may lead to mixed solvent-solute film formation or to adsorption (probably associated with chemical attack on the solid) of much more than a single monolayer. In the present investigation, we have compared the concentration of radiostearic acid present on various solid surfaces after deposition of monolayers from water surfaces or exposure to solutions of the acid in hexadecane or nitromethane.

### EXPERIMENTAL

Stearic acid, labeled with  $C^{14}$  in the carboxyl group, of specific activity 1–2.5 mc./mmole, was obtained from Tracerlab, Inc., Waltham, Massachusetts, and Nuclear-Chicago Corp., Chicago, Illinois. The material was purified by dissolving it in reagent grade *n*-hexane and extracting first with 1 *N* HCl, then with several portions of water. After this, the solvent was evaporated and the stearic acid was dried over "Drierite." After purification, it melted at 68°–68.5°C. In Fig. 1, the  $\pi$ - $A$  curve obtained for this

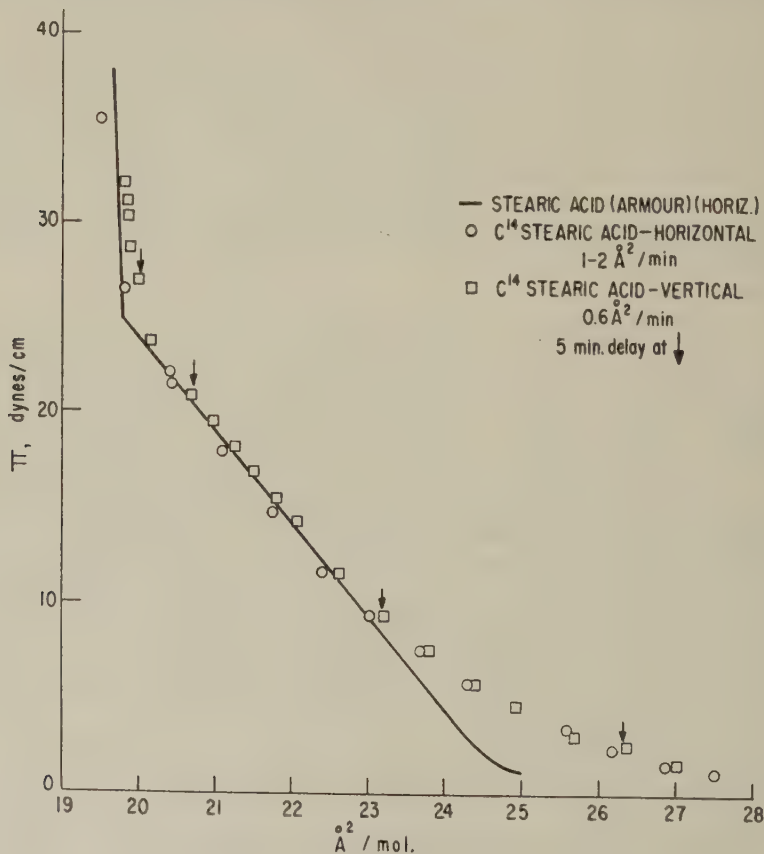


FIG. 1. Pressure-area curves for radiostearic acid monolayers on water.

material is compared with that obtained for highly purified nonradioactive stearic acid (Armour certified pure, m.p.  $> 69.4^{\circ}\text{C}.$ ) under similar conditions. For these experiments, the stearic acid,  $0.005M$  in *n*-hexane, was delivered with a micrometer syringe. The  $\pi$ - $A$  curves agree well in the range  $> 9$  dynes/cm. At lower pressures, there is some divergence, probably owing to impurities in the radioactive acid.

Solvents used were *n*-hexane (Phillips 99+ mole %), *n*-hexadecane (cetane) (Humphrey-Wilkinson, 95% minimum), and nitromethane (Matheson, Coleman, and Bell reagent grade). All were freed of polar impurities by percolation through columns of silica and alumina. After this purification, the cetane melted at  $16.8^{\circ}$ – $17.0^{\circ}\text{C}.$  and did not spread on  $0.1 N$  HCl or NaOH solution. The purity of the nitromethane was indicated by its surface tension, 35.2 dynes/cm. at  $27^{\circ}\text{C}.$  (determined by ring method,  $\pm 0.3$  dynes/cm.; International Critical Tables value 35.8 dynes/cm. at  $27^{\circ}\text{C}.$ ).

The solid substrates used, together with the methods of preparing them, are detailed in Table I. All were used as  $2 \times 3$ -inch rectangles. After cleaning and drying as noted, they were all found to be completely wettable by water. In all experiments, the plates were freshly prepared immediately before use. When monolayer deposition from water surfaces was carried out, the plates were not dried but were used wet after a final thorough rinse in running distilled water.

Films spread on water were deposited from a brass tray heavily coated with paraffin. For all withdrawal experiments, plates were placed in the tray before spreading of the film. The tray was arranged to permit withdrawal or touching of plates and simultaneous measurement of film pressure with a vertical-pull film balance. This balance allowed continuous monitoring of increasing film pressure; the plate, a freshly cleaved sheet of mica wet with water and inserted in the tray before the spreading of the stearic acid, was suspended on a quartz spiral the extension of which could easily be measured by observation of the reference cross-hair with a traveling microscope (see also under Discussion). Force-area curves were also measured with a commercial balance of the Langmuir-Adam type (Cenco Hydrophil balance) with a torsion wire giving 0.35 dyne/cm. per degree of rotation. The trays were thoroughly cleaned and rewaxed before each use. In all cases, water redistilled in quartz was used (14). Films were compressed with the aid of waxed silk thread barriers and piston oils as described by Blodgett (2). Piston oils used included tricresyl phosphate (9.0–10.5 dynes/cm.), castor oil (17.5–17.8 dynes/cm.), and oleic acid ( $30.1 \pm 0.1$  dynes/cm.). Stearic acid was spread from  $0.005 M$  solution in *n*-hexane, the appropriate piston oil was applied within 1 or 2 min., and the film was allowed to stand 5 min. to allow for evaporation of the solvent. Plates were then withdrawn or wetted with water and touched to the

TABLE I  
*Solid Substrates*

Substance	Type	Thick- ness	Cleaning procedure
		(mm.)	
Mica	Bengal Ruby Muscovite <sup>a</sup>	0.5	Freshly cleaved
Glass	"Pittsburgh Non-Corrosive" microscope slides	1.0	Rinsed with 10% HF, distilled H <sub>2</sub> O; dried over soft H <sub>2</sub> flame
Chrome	Commercial ferrotype plate <sup>b</sup>	0.5	Polished with Precisionite (<1 $\mu$ Al <sub>2</sub> O <sub>3</sub> ) in H <sub>2</sub> O with soft grease-free cloth, rinsed under distilled H <sub>2</sub> O with cloth buffing, dried with reagent-grade acetone and air jet.
Platinum	Commercial rolled sheet average roughness 0.1 $\mu$ , peak-to-valley <sup>c</sup>	0.5	Boiled in 1:1 conc. HNO <sub>3</sub> :H <sub>2</sub> SO <sub>4</sub> , rinsed in H <sub>2</sub> O, flamed.
Copper	OFHC (99.99 + %)	1.5	Polished with Precisionite (cf. chrome above), electropolished in H <sub>3</sub> PO <sub>4</sub> , washed in 0.05% H <sub>3</sub> PO <sub>4</sub> , <sup>d</sup> then H <sub>2</sub> O. Dried with acetone and air jet.
Aluminum	2S-O (99.0 + %)	1.5	Chemically polished in H <sub>3</sub> PO <sub>4</sub> , HNO <sub>3</sub> , H <sub>2</sub> SO <sub>4</sub> . <sup>e</sup> Rinsed in H <sub>2</sub> O, dried with acetone and air jet.

<sup>a</sup> Cf. G. L. Gaines, Jr., *J. Phys. Chem.* **61**, 1408 (1957) for analytical data.

<sup>b</sup> 0.2  $\mu$  Cr on Ni flash on Cu flash, on steel; cf. E. A. Ollard and E. B. Smith, "Handbook of Industrial Electroplating." London, Iliffe & Sons Ltd., 1954.

<sup>c</sup> As measured by interference microscope.

<sup>d</sup> Cf. Schulman, Waterhouse, and Spink (3), for details of the polishing and rinsing technique.

<sup>e</sup> Alcoa "Bright-Dip" process, U. S. Patent 2,650,157. Procedure used involved the following steps: 1 min. in boiling 5% HNO<sub>3</sub>; 10 min. in solution of 6 parts 70% HNO<sub>3</sub> and 94 parts 85% H<sub>3</sub>PO<sub>4</sub> at 80°-90°C.; 1 min. in conc. HNO<sub>3</sub> (room temperature); and 1 min. in boiling 10% H<sub>2</sub>SO<sub>4</sub>; with H<sub>2</sub>O rinses after each step.

film to accomplish the deposition. When the deposition was of the "reactive" type, with rapid expulsion of the water film (cf. Schulman, Waterhouse, and Spink (3)), the plates appeared dry immediately after withdrawal or "touching"; when less interaction between monolayer and substrate occurred, so that a water film remained on the plate after the deposition of the monolayer, it was necessary to stand the plate vertically in air until the water was removed by drainage and evaporation. (This type of deposition will be referred to below as "nonreactive.")

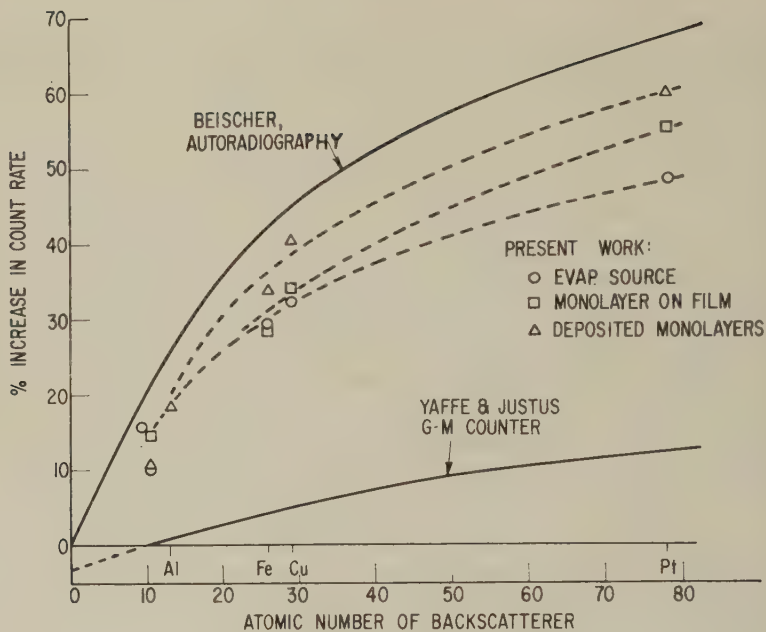
Adsorption from cetane and nitromethane solutions was carried out by

placing the appropriate solution in a freshly cleaned and flamed dip-cell made of platinum sheet. Details of the observations are given in the description of "Results."

All counting measurements were performed with an end-window Geiger-Müller tube, with a mica window of thickness 1.3 mg./cm.<sup>2</sup>. A conventional commercial sealing circuit was used. The counter tube was clamped to a vertical screw device so that it could be accurately positioned either over a rack to hold the sample plates within a conventional counting chamber (iron) or over the surface of the film balance tray at a central position near the well end. To restrict the area subtending the counter window a Dural cylinder could be fitted over the end of the tube, holding 1.6 mm. thick Dural masks of various shapes at a distance of 1.08 cm. from the window. Dead-time and background corrections were applied. (It should be noted that with mica substrates, background due to the natural K<sup>40</sup> content was significant and experimentally determined corrections were applied. All other substrates gave similar background counts, which always were in the range 30–35 counts/min.). Corrections for backscattering of the C<sup>14</sup> radiation were avoided in most cases by comparing all the films to monolayers of radiostearic acid deposited on the corresponding substrate by the Blodgett technique at high surface pressure (oleic acid piston oil). All substrates except the ferrotype plates were sufficiently thick to constitute uniform saturation backscatterers; in the case of chrome-plate, the steel backing was thick enough to lead to saturation, and this substrate was therefore considered as Fe. Mica and glass were assigned "effective atomic numbers" on the basis of approximate atomic percentage compositions. These deposited films exhibited backscattering effects of the expected magnitude; in Fig. 2, data obtained for them are compared with those for evaporated drops of radiostearic acid or radiostearic acid monolayers deposited on effectively weightless vinylite films (15), as well as other workers' measurements. Beischer's data (16) were obtained by autoradiography, where air- and window-absorption effects are not present. Yaffe and Justus (17) obtained their results by Geiger-Müller counters with evaporated point sources on thin films. The anisotropy and reduction of energy of the scattered radiation is of considerable importance with radiation of low energy, and the observed backscattering is therefore strongly dependent on sample nature and geometry, as appears in this comparison. These backscattering results together with further observations made at the same time will be treated in detail elsewhere (18). For the present it will suffice to point out that with C<sup>14</sup>  $\beta$ -radiation, it is essential to make backscattering corrections based on strictly analogous counting conditions.

Contact angles of various liquids on the film-covered solids were measured with a simple device of the type described by Langmuir and Schaefer (19). Several drops of the test liquid were carefully placed on the plates



FIG. 2. Backscattering of  $C^{14}$   $\beta$ -rays.

with a drawn-out medicine dropper so that an advancing angle was obtained. Precision and accuracy for a given drop was about  $\pm 1^\circ$ ; different drops of the same liquid on a given plate usually exhibited angles agreeing within  $\pm 2^\circ$ . Liquids used were distilled water and methylene iodide (Eastman White Label), as recommended by Levine and Zisman (10).

Monolayer removal experiments were carried out by immersing the plates completely in 150 ml. of fresh reagent-grade benzene and agitating them in the solvent for 1 min. At the end of this time the plates were removed and quickly dried by a jet of dry  $N_2$ .

All experiments were carried out at room temperature, which varied from  $24^\circ$  to  $28^\circ C$ .

## RESULTS AND DISCUSSION

### *The Vertical-Pull (Wilhelmy) Film Balance*

Harkins and Anderson (20) compared the experimental results obtainable with a vertical (Wilhelmy) plate and a horizontal (Langmuir) film balance on the same monolayer, and concluded that the agreement was good. They emphasized that the contact angle between the liquid surface and the plate must be zero—a condition that is difficult to ensure unless the plate is being raised through the liquid surface, i.e., unless the film is being compressed. LaMer and Robbins (21) have recently measured film pressures with a Wilhelmy plate in a maximum-pull method. They suggest



that in this way a zero contact angle is assured. They also found that a depolished platinum plate could be repeatedly immersed and withdrawn without altering the observed pull, from which they concluded that "no monolayer of stearic acid was deposited on the plate during a series of measurements." It is, of course, also possible that stearic acid molecules deposited on the slide during a withdrawal would be returned to the water surface on reimmersion. Such behavior was noted long ago by Langmuir (22), although observations by Mlle. Denard (23) and Trurnit (24) suggest that this process may be quite complicated and strongly dependent on the nature of both the film and the solid.

In our measurements, only increasing surface pressures were measured with a vertical pull balance. It was found that a pressure-area isotherm could not be traced as the film was expanded, because the contact angle between water and the plate was not zero when the plate was reimmersed in the tray. It is clearly apparent that some stearic acid is transferred to the mica plate as it passes upward through the water surface, and not all of this is removed if the mica is again lowered into the water. Radiometric observations on mica Wilhelmy plates used with radiostearic acid films confirm this observation. In one experiment a mica plate was used to determine a  $\pi$ - $A$  curve for radiostearic acid. Counts were taken over the film on the water surface with the masked Geiger-Müller counter. After the surface pressure had been raised to  $\sim 30$  dynes/cm. (under which condition the mica plate had risen through the water surface by  $\sim 4$  cm.), the plate was removed from the balance and allowed to dry. It was then placed under the Geiger-Müller counter equipped with a rectangular mask, so that successive bands across the mica plate could be observed, and the concentration of radiostearic acid was measured as a function of vertical distance along the plate. In Fig. 3, these data are compared. The pressure-concentration data, calculated from the displacement of the plate, the amount of stearic acid spread, and the area available to it (see below), are shown by the solid line. The observed count rate on the water surface is plotted against the observed pressure values, using the top "counts per minute" scale, which has been fitted to the molecular concentration at the highest observed count rate; it should be noted that this fitting leads to reasonable values of geometric, efficiency, and specific activity factors for which we have no precise values. The solid squares represent the observed count rate on the mica plate as a function of height, and are plotted on the lower "counts per minute" scale, which is fitted to the top (water surface) scale by the experimentally determined backscattering and geometry differences. It is apparent that, under the conditions of this experiment, radiostearic acid is transferred to the plate in nearly the same concentration that is present on the water and that little migration of the stearic acid occurs on the solid.

On the basis of these observations, it is necessary to allow for the amount

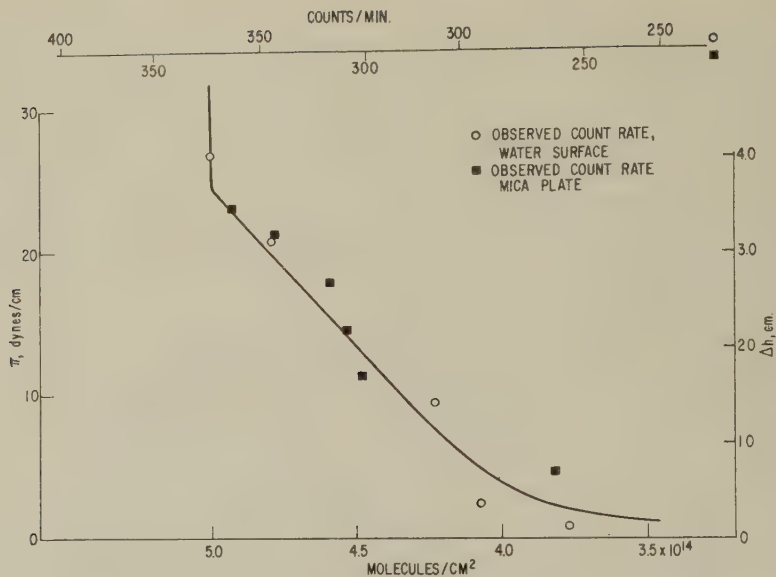


FIG. 3. Observed count rates and surface pressures for radiostearic acid monolayer on water and after transfer to mica plate.

of stearic acid on the mica plate in calculating the area per molecule in a  $\pi$ - $A$  curve determination. To a good approximation, this may be done by simply adding to the available area on the tray surface that area of the slide which has been withdrawn, and calculating the molecular area on the assumption that all the molecules applied to the surface are distributed over this area. The error in the correction introduced by the failure to allow for the concentration difference over the plate is small in our experiments, in which the area of the mica plate never exceeded 10% of the available tray area. Furthermore, with stearic acid the relative incompressibility of the monolayer at higher pressures (where the plate area correction is largest) minimizes this error. The agreement which is attainable between separate measurements on a horizontal and a vertical film balance is shown in Fig. 1. Neglect of any plate area correction in the vertical film balance run shown would lead to a molecular area at maximum compression of  $\sim 18 \text{ \AA}^2$ . Many investigators have failed to apply such corrections; it is quite possible, for example, that this can account for the low area reported by Harkins and Anderson (20) for calcium stearate.

#### *Deposited Stearic Acid Films*

It is generally assumed that when monolayers spread on liquid surfaces are transferred to solids, the film concentration is unchanged. Bikerman's work (25), for example, showed that a fairly closely packed monolayer,

in which the film molecules exert considerable influence on one another, will be deposited over the apparent surface of the solid just as it existed on the liquid surface. After the transfer, the water layer accompanying the monolayer may be removed and the film may collapse or reaction may occur between the film and substrate. Many studies have demonstrated that the attachment of the film to the substrate after deposition depends on the chemical and physical nature of the solid surface. Several studies (16, 26-28) have shown that reaction of stearic acid films with metal substrates proceeds after deposition. Trurnit's results (24), however, suggest that under some conditions reaction may occur almost simultaneously with transfer and that its extent may depend on film pressure.

We have examined films deposited at three surface pressures. Whether deposition is carried out by the conventional Blodgett technique (substrate withdrawn through the water surface) or by touching the wetted plate to the spread monolayer, the observed count rate is constant within experimental error over the surface of the plate.

At the two higher surface pressures (oleic acid,  $30.1 \pm 0.1$  dynes/cm. (measured) and castor oil,  $17.6 \pm 0.2$  dynes/cm. (measured)), observed count rates were reproducible within  $\pm 5\%$  on duplicate samples, which is about the error to be associated with our counting techniques. Absolute counting precision was always better than this, but minor geometry variations were impossible to control. Values obtained with "touched" and "withdrawn" monolayers on the same solid were also in agreement whenever they were compared. The ratio of concentrations deposited at the two surface pressures, which can be calculated to be 0.93 from the pressure-area curve on water, was found to be  $0.92 \pm 0.07$  for sixteen samples representing all six substrate materials. There seemed to be no difference whether "reactive" deposition occurred (all the metals when "touched," Pt and chrome when withdrawn; *cf.* the comments of Schulman *et al.* (3) on oxidation of metal surfaces in monolayer deposition) or not. In the case of mica at these higher film pressures, the plates exhibited both types of deposition on different areas, the water film being expelled rapidly from parts of the surface while other parts remained wet.

At the lower film pressure (trieresyl phosphate piston oil, measured film pressures 9.0-10.5 dynes/cm.), the concentration estimated from the pressure-area curve is  $4.30-4.37 \times 10^{14}$  molecules/cm.<sup>2</sup>, corresponding to 86% of a close-packed monolayer. In the deposition experiments, however, this value was never attained. Table II illustrates the results obtained on our various substrates, as compared with the observed activities of monolayers deposited at 30 dynes/cm. It is apparent that the values are scattered, with poor reproducibility even on a single substrate. The behavior of platinum in particular was striking; reactive deposition was observed on bright platinum which had been flamed and wetted with water before use, whereas

TABLE II  
*Observed Radiostearic Acid Concentration in Monolayers Deposited at  
 10 dynes/cm.*

Substrate	"Withdrawn" Conc. <sup>a</sup>	Depos. <sup>b</sup>	"Touched" Conc. <sup>a</sup>	Depos. <sup>b</sup>
Glass	0.53	<i>n</i>	0.45-0.69 (4 samples)	<i>n</i>
Mica	0.78, 0.80	<i>n</i>	0.67, 0.75	<i>n</i>
Pt	0.68	<i>n</i>	0.53	<i>n</i>
	0.84	<i>r</i>	0.73	<i>r</i>
Cr	—		0.67	<i>r</i>
Cu	—		0.62	<i>r</i>
Al	—		0.74	<i>r</i>

<sup>a</sup> Concentrations as fraction of close-packed (30 dynes/cm.) monolayer

<sup>b</sup> Nature of deposition; *r* = reactive, *n* = nonreactive.

nonreactive deposition occurred on plates washed in hot concentrated  $\text{HNO}_3\text{-H}_2\text{SO}_4$  mixtures and rinsed in water. Somewhat higher concentrations of stearic acid were found in the case of reactive deposition. On the average, this was also true for all the results taken without regard to the substrate, although several nonreactive depositions gave concentrations higher than some of the reactive ones. This was especially noticeable with mica, which, while it exhibited nonreactive deposition at this film pressure, picked up quite high concentrations of stearic acid (75%  $\pm$  8% of a close-packed monolayer for four samples). The particularly scattered results with glass may be a result of lack of reproducibility in the cleaning procedure. The extent of etching of the surface, removal of  $\text{Na}^+$ , or exchange adsorption of  $\text{F}^-$  might all vary considerably in our hydrofluoric acid rinse. It is likely that such uncontrolled variations would appreciably alter the sorptive properties of the glass and make deposition erratic.

Ries and Kimball (29) have presented evidence that even at 10 dynes/cm., stearic acid monolayers are composed of islands of stearic acid molecules. As pressure on films of this type is increased, these islands seem to join to form a continuous film in which there are holes or vacant patches. The progressive reduction in size of these vacant areas leads finally to the formation of the close-packed monolayer at high pressures. In the light of these observations, a possible explanation for our results suggests itself. The transfer of a monolayer from a liquid surface to a solid depends primarily on the interaction between the liquid and solid. (This may be inferred, of course, from differences in the deposition behavior of monolayers on hydrophilic and hydrophobic substrates (22, 25).) As the wetted solid is withdrawn or touched to the liquid surface, the surface film of liquid is spread over the solid. At high surface pressures, where the monolayer is



continuous and intermolecular forces (e.g., hydrocarbon chain adhesion) are sufficiently high, the monolayer is transferred as a carpet to the solid. However, if the monolayer is discontinuous or if its mechanical properties are such that it is disrupted in the transfer process (Langmuir and Schaefer (19) pointed out this difficulty), the deposited film may be more tenuous than on the liquid surface. The extent of reduction in concentration in the transfer process will obviously depend markedly on such factors as the rate of transfer, geometry, and the effects of gravity on the water film, as well as on the nature of the monolayer and the solid substrate. Our results with transferred monolayers are understandable on this basis; the difference between observed concentrations on mica plates which were touched or withdrawn relatively quickly from a monolayer (Table II) and those used in a film balance at slowly increasing film pressure (Fig. 3) in particular are not surprising.

#### *Adsorption of Stearic Acid from Cetane and Nitromethane*

In most of our experiments with cetane solutions of radiostearic acid, "oleophobic" films were not formed, and the plates remained wet with the solution when withdrawn even after several hours exposure to solutions with acid concentrations as high as  $5 \times 10^{-3} M$ . In one case, with copper plates and a  $5 \times 10^{-3} M$  stearic acid solution, retraction of the solution was obtained after both 1-min. and 30-min. immersion. The count rates observed on these samples corresponded to 1.05 and 1.69 times those for a close-packed deposited (Blodgett) monolayer, respectively. When the plates which emerged wet were wiped thoroughly with tissues to remove as much of the solution as possible, we found the amounts of radiostearic acid retained to fall into two groups. With chrome, platinum, and mica, activities corresponding to 0.2–0.6 monolayer were obtained after times ranging from 1 to 135 min., and stearic acid concentrations from  $1 \times 10^{-3} M$  to  $5 \times 10^{-3} M$ . Copper, aluminum, and glass plates, however, under similar conditions retained amounts of stearic acid ranging from 0.86 to 5.9 equivalent monolayers. In the case of two glass slides (out of four experiments with glass), counting indicated the presence of 1.0 monolayer of stearic acid within experimental error; this result was not obtained in any of six experiments with copper and aluminum.

Failure to observe oleophobicity in these systems may be due to a variety of effects. The presence of shorter chains or branched-chain molecules as impurities in either the cetane or the radiostearic acid might increase the wettability of the films formed. More likely, in most of the cases examined, the solid surfaces were not sufficiently smooth to permit the formation of oleophobic films. Brockway and Karle (30) pointed out that only very carefully polished copper, iron, and aluminum surfaces were able to form oleophobic films, and apparently even the roughening resulting from



surface oxidation in a water rinse inhibited this behavior. Young (28) reported similar observations.

With nitromethane solutions, on the other hand, "oleophobic" behavior was regularly obtained with all our substrates. In fact, on most of these materials pure nitromethane exhibits a small but finite contact angle. Radiometric observations were made on films adsorbed by all the substrates from saturated solutions of  $C^{14}$ -stearic acid in nitromethane. When these were compared with the count rates obtained from deposited close-packed monolayers, it was found that with reactive substrates, count rates increased with time of immersion, reaching values equivalent to several deposited monolayers, whereas inert solids did not adsorb more than about 0.5 monolayer in several hours. Figure 4 illustrates these results. In addition to the data shown, observations were made on glass slides after immersion in nitromethane solutions. These were erratic; in most cases, count rates were in excess of those for a single monolayer (up to 3 equivalent monolayers in some cases), but some samples exhibited very slight adsorption, giving count rates corresponding to only 0.1 monolayer. Undoubtedly this is another reflection of the uncontrolled variation in the sorptive properties of our HF-washed glass noted above.

These results are strikingly similar to those obtained by Cook and Ries (13) for the adsorption of radiostearic acid from cetane solutions on gold, mica, and iron. They too observed adsorption of the acid on the reactive metal to much more than a single monolayer, and only 0.1–0.3 monolayer adsorbed on inert substrates even after several days. The electron micrographs of Mathieson (31) also showed similar effects with oleophobic stearic acid films adsorbed on mica from cetane solutions. Our observation that almost five equivalent monolayers of stearic acid are associated with a copper surface after  $2\frac{1}{2}$  hours immersion in nitromethane solution, even though the copper still retains its original mirror polish, suggests that these large adsorptions are not due to surface roughening. The probability that chemical reaction of stearic acid with copper and association of the resulting soap with the surface may occur is supported by the observations of Greenhill (32), Young (28), and others.

The low adsorption of stearic acid on the more inert materials does not seem to be readily correlatable with the nature of the surface. For mica, the surface about which we have the most detailed knowledge (33), simple consideration of the lattice does not lead to numbers of sites corresponding to coverages found by Cook and Ries (0.26 monolayer) or in this study with short-time immersions in nitromethane (1 minute–45 minutes, 0.13–0.15 monolayer) or cetane (wiped plates, 0.33–0.35 monolayer). On the other hand, the solvent-solute interaction mechanism for the adsorption of solvent molecules associated with the polar molecules proposed by Cook and Ries to account for their results is independent of the nature of the solid.

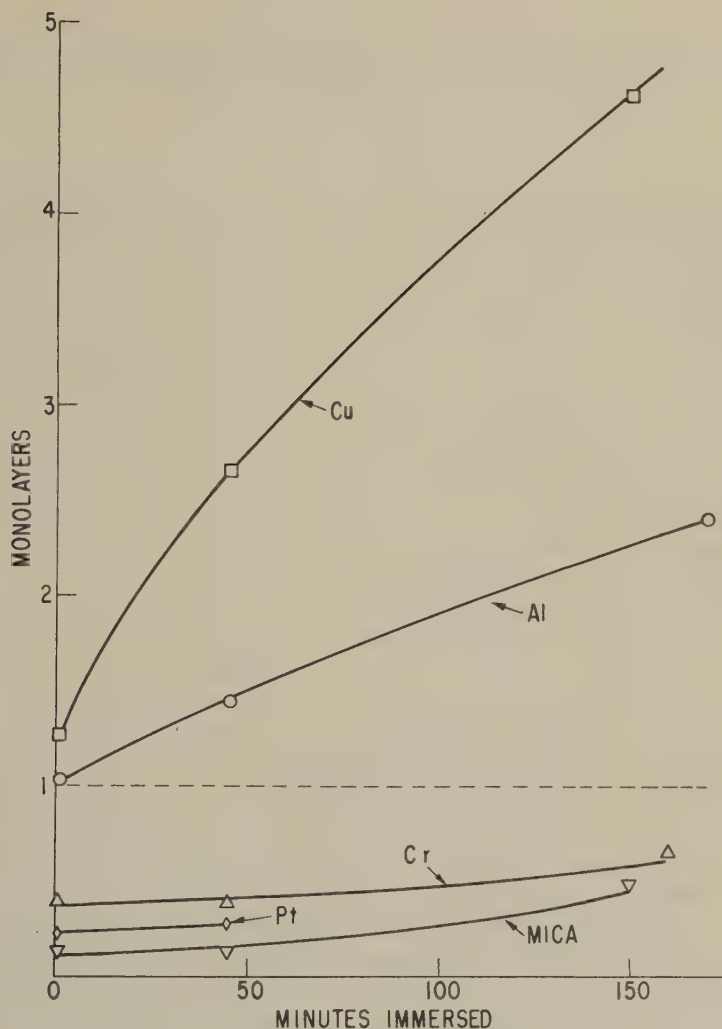


FIG. 4. Adsorption of radiostearic acid from nitromethane solution.

The marked association in liquid  $\text{CH}_3\text{NO}_2$  (b.p.  $101^\circ\text{C}$ .) suggests that an oriented structure in the liquid surrounding the stearic acid molecules is quite possible. Solvation of the carboxyl groups by hydrogen-bonded  $\text{CH}_3\text{NO}_2$  molecules is also likely. The volatility and water-miscibility of  $\text{CH}_3\text{NO}_2$  prevent the measurement of mixed-film force-area curves for comparison with Cook and Ries' data on the cetane-stearic acid system. We also have no direct measurement of solvent retention in the adsorbed film. These types of interactions might well lead to adsorption of stearic acid molecules surrounded by sheaths of nitromethane molecules, producing

the similarity between the present results and those for cetane solutions. It should be noted that these solvent-sorbate associations may be metastable; cf. the comments of Levine and Zisman (10).

### *Contact Angles*

The use of contact angles exhibited by various test liquids as a tool in studying monolayers is well known. Cottington, Shafrin, and Zisman have reported values of  $70^\circ$  for the contact angle of methylene iodide against stearic acid films adsorbed on glass and stainless steel (34). Zisman and co-workers (10, 34) and Bartell and Ruch (11, 12) have pointed out that the molecular size and shape of the test liquid will influence the degree of wetting observed. On the other hand, Langmuir (22) pointed out that water when used as a test liquid exhibited very different contact angles on monolayers of the same substance deposited on different substrates. This he attributed to the possibility of overturning of the molecules in the film in the presence of liquid water. Shafrin and Zisman (35) have suggested that even where such difficulties are absent, the diffusion of water molecules between the film molecules may lead to appreciable differences between advancing and receding angles.

We have made some measurements of the contact angles of water and methylene iodide on the films which have been described above. For radiostearic acid on aluminum, copper, and chrome-plated substrates, water exhibited a contact angle of greater than  $85^\circ$  (with our apparatus, it is not possible to measure contact angles greater than  $\sim 87^\circ$ ; it can be determined only that they are greater than this value). This was true whether deposited or adsorbed (from either cetane or nitromethane) films were examined, and whether their stearic acid content was high (e.g., adsorbed films on copper to 4.6 equivalent monolayers) or low (e.g., adsorbed films on Cr, 0.4 monolayer). For films on glass and mica, however, water contact angles were always low; observed range  $10^\circ$ – $44^\circ$ . In these cases, the receding contact angle was generally nearly zero. With platinum, the contact angles with water were sometimes  $>90^\circ$  (films deposited at high surface pressures and nonoleophobic adsorbed films from cetane solution), and sometimes as low as  $30^\circ$  (adsorbed oleophobic film from nitromethane solution; concentration of radiostearic acid in film =  $1 \times 10^{14}$  molecules/cm.<sup>2</sup>). This probably reflects the differences of ease of diffusion of H<sub>2</sub>O through these films, but the observations made were too few to be explicit on this point.

Methylene iodide contact angles, on the other hand, seemed to correlate fairly well with concentration of stearic acid on the inert substrates. Figure 5 illustrates this behavior for a variety of deposited and adsorbed films. It is apparent, however, that our method is not sufficiently sensitive to detect the change in the contact angle at concentrations above about 75%

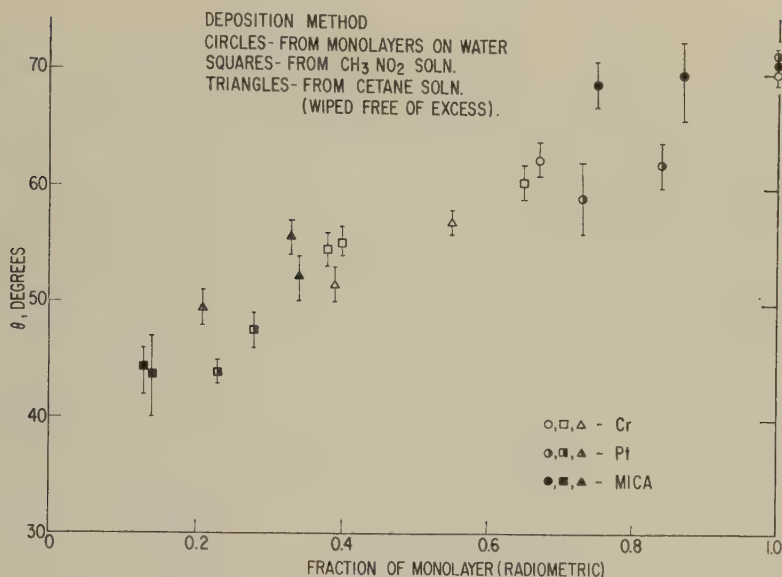


FIG. 5. Methylene iodide contact angles on stearic acid monolayers.

of the close-packed monolayer. With films adsorbed from nitromethane solution on copper, aluminum, and glass to give radiostearic acid concentrations of more than a single monolayer, the methylene iodide contact angles were always above 60°; generally values appropriate to fairly close-packed monolayers (68°–72°) were found. On these substrates, high-concentration films isolated by adsorption from cetane, with wiping to remove excess solution (1.0–1.6 equivalent monolayers), exhibited methylene iodide contact angles of 52°–68°. These lower values may reflect disorientation effects in the adsorbed film produced by wiping (*cf.* the electron diffraction results of Sutula and Bartell (36)).

It is apparent that several factors are important in the wetting of these films. For films containing only oriented polar molecules, firmly enough attached to the substrate so that the test liquid cannot cause reorientation, it seems that the conclusions reached by Bartell and Ruch (12) about penetration and orientation of liquid molecules in holes in the film are valid. For more "active" test liquids (such as water) and less tightly bonded monolayers, reorientation may occur and the contact angle is primarily a measure of the monolayer-substrate interactions. When mixed films of polar molecules and solvent are adsorbed, the properties of the solvent (if it does not evaporate before the measurement or dissolve in the test liquid) may have to be considered in interpreting subsequent wetting measurements on these films.



*Desorption Experiments*

Young (28) showed that desorption measurements with radiostearic acid provide a sensitive indication of the magnitude of substrate-sorbate interactions. In the present work a few measurements of the removal of stearic acid by rinsing with benzene were made. In most of the cases which we examined, this method removed stearic acid molecules only slowly, as has been found by other workers (11, 13). With radiostearic acid monolayers deposited on chromium plated slides, rinsing with benzene, hexane, acetone, methanol or washing with alkaline detergents in warm ( $\sim 50^{\circ}\text{C}.$ ) water never led to removal of more than a few per cent of the film at a time. Glass and platinum substrates showed somewhat different effects: Fig. 6 illustrates the fraction of the initially present stearic acid removed by successive rinses of these plates. It appears that with deposited films the *fraction* removed does not depend markedly on the radiostearic acid concentration initially present on either substrate; whether a close-packed monolayer (oleic acid piston oil) or only 69%–73% of that amount (tricresyl phosphate piston oil) was originally on the plate, about half of it is removed by the first rinse. Further rinses remove smaller amounts, with the acid being removed from the glass surfaces more readily than from platinum. With adsorbed films, similar behavior is found, but here both substrates show similar behavior, and each rinse is less effective than in the case of the deposited layers.

This behavior is consistent with a mechanism involving attachment of the deposited monolayers at isolated points (perhaps asperities on the solids or active sites of some sort) after deposition. The concentration of these points, and hence *fraction* of more tightly bound stearic acid molecules, is dependent on the nature of the solid, but, of course, independent of the concentration in the deposited monolayer (as the concentration changes the number of molecules in position to interact with the active sites changes in the same way). This mechanism is also consistent with Trurnit's results (24). With adsorbed films, however, stearic acid molecules will adsorb most readily at these active sites, without respect to what is happening over the rest of the surface. Adsorption may then proceed both by further interaction of other individual molecules with the surface or by lateral interactions in the interfacial film. For a given solute-solvent system (and, as noted above, it appears that in this sense, cetane and nitromethane behave rather similarly as solvents for stearic acid), it appears that the *total* amount adsorbed will depend primarily on the nature of the solid, up to some limit which will depend on the relative magnitudes of the interactions between solute, solvent, and solid surface. If a mixed solvent-solute film is formed as a result of lateral interactions, the *ratio* of tightly held molecules to the total adsorbed will depend on this association and



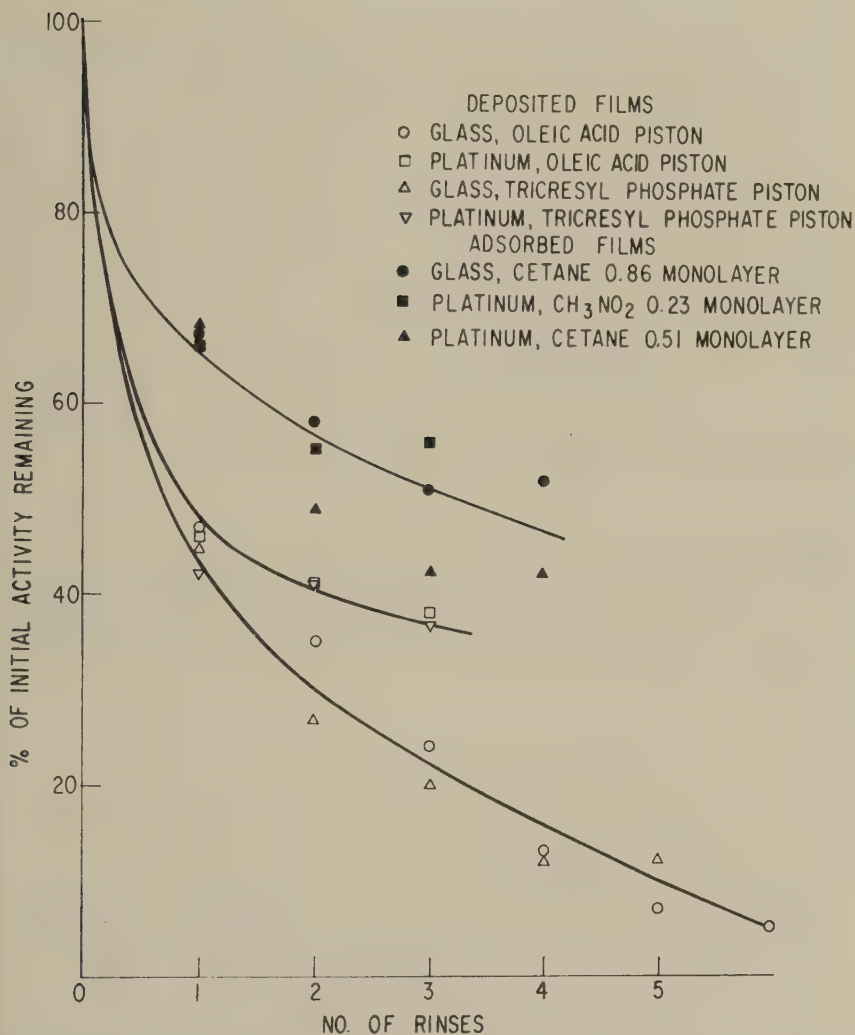


FIG. 6. Removal of radiostearic acid from deposited and adsorbed films by benzene rinses.

be largely independent of the nature of the solid. Should an activation process be involved in the adsorption, as suggested by Cook and Ries (13), it might shift the distribution after longer times; such a possibility cannot be assessed in our studies.

Our results on copper plates, the only other substrate material on which rinse tests were carried out, were odd. In some cases, the first benzene rinse was found to wet the film-covered plates completely. Whenever this happened, the plates quickly lost their mirror finish after removal from the

benzene and began to change color, apparently as relatively thick oxide layers formed. In every such case, radiometric measurement showed that nearly all the stearic acid had been removed, not more than 1%–3% of that initially present remaining after this single rinse. On the other hand, some of the plates were not wetted by the benzene, which retracted smoothly from the solid as it was removed from the rinse. These plates could be subjected to numerous successive rinses with no change in appearance, and each such rinse removed only a small amount (generally only 3%–6%) of the radiostearic acid. Similar behavior was found both with plates initially bearing much more than a single equivalent monolayer (adsorbed films) and with those on which lower concentrations (films deposited at low surface pressure) were present. This behavior may be associated with differences in the reactivity of the copper surfaces due to some uncontrolled variable in their preparation, but we do not have sufficient information to permit an explanation.

#### ACKNOWLEDGMENTS

I am greatly indebted to Miss C. P. Rutkowski for extensive experimental assistance. Several of my colleagues in this Laboratory provided helpful discussion of various points. The opportunity to discuss the results with Dr. H. W. Fox, Mrs. E. G. Shafirin, and Dr. W. A. Zisman is also acknowledged. I am grateful to Dr. H. J. Turnit for pointing out his previous work in this area.

#### REFERENCES

1. LANGMUIR, I., *Trans. Faraday Soc.* **15**, 62 (1920).
2. BLODGETT, K. B., *J. Am. Chem. Soc.* **56**, 495 (1934); *ibid.* **57**, 1007 (1935).
3. SCHULMAN, J. H., WATERHOUSE, R. B., AND SPINK, J. A., *Kolloid-Z.* **146**, 77 (1956).  
Cf. also K. B. BLODGETT, reference 2.
4. LANGMUIR, I., *J. Franklin Inst.* **218**, 143 (1934).
5. BIGELOW, W. C., PICKETT, D. L., AND ZISMAN, W. A., *J. Colloid Sci.* **1**, 513 (1946).
6. BIGELOW, W. C., GLASS, E., AND ZISMAN, W. A., *J. Colloid Sci.* **2**, 563 (1947).
7. FOX, H. W., HARE, E. F., AND ZISMAN, W. A., *J. Colloid Sci.* **8**, 194 (1953).
8. HARE, E. F., AND ZISMAN, W. A., *J. Phys. Chem.* **59**, 335 (1955).
9. ZISMAN, W. A., "The Relation of Chemical Constitution to the Wetting and Spreading of Liquids on Solids" in "A Decade of Basic and Applied Science in the Navy," p. 30. The proceedings of the ONR Decennial Symposium, March, 1957, Washington, Navy Department.
10. LEVINE, O., AND ZISMAN, W. A., *J. Phys. Chem.* **61**, 1068, 1188 (1957).
11. BARTELL, L. S., AND RUCH, R. J., *J. Phys. Chem.* **60**, 1231 (1956).
12. BARTELL, L. S., AND RUCH, R. J., *J. Phys. Chem.* **63**, 1045 (1959).
13. COOK, H. D., AND RIES, H. E., JR., *J. Phys. Chem.* **63**, 226 (1959).
14. GAINES, G. L., JR., *J. Phys. Chem.* **63**, 1322 (1959).
15. PATE, B., AND YAFFE, L., *Can. J. Chem.* **33**, 15 (1955).
16. BEISCHER, D. E., *J. Phys. Chem.* **57**, 134 (1953); U.S.N. School of Aviation Medicine, Naval Air Station, Pensacola, Florida, Project NM 001 059.16, Report No. 6, 1951.
17. YAFFE, L., AND JUSTUS, K. M., *J. Chem. Soc.* S341 (1949).
18. GAINES, G. L., JR., *J. Appl. Phys.* **31**, 741 (1960).

19. LANGMUIR, I., AND SCHAEFER, V. J., *J. Am. Chem. Soc.* **59**, 2400 (1937). See p. 2405.
20. HARKINS, W. D., AND ANDERSON, T. F., *J. Am. Chem. Soc.* **59**, 2189 (1937).
21. LAMER, V. K., AND ROBBINS, M. L., *J. Phys. Chem.* **62**, 1291 (1958).
22. LANGMUIR, I., *Science* **87**, 493 (1938).
23. DENARD, L., *J. chim. phys.* **36**, 210 (1939).
24. TRURNIT, H. J., *Angew. Chem.* **A59**, 273 (1947).
25. BIKERMAN, J. J., *Proc. Roy. Soc. (London)* **A170**, 130 (1939).
26. BOWDEN, F. P., AND MOORE, A. C., *Trans. Faraday Soc.* **47**, 900 (1951).
27. DOBRY, A., AND MAHNCKE, H. E., *Nature* **174**, 507 (1954).
28. YOUNG, J. E., *Australian J. Chem.* **8**, 173 (1955).
29. RIES, H. E., JR., AND KIMBALL, W. A., *Proc. 2nd Intern. Congr. Surface Activity* **1**, 75 (1957); *Nature* **181**, 901 (1958).
30. BROCKWAY, L. O., AND KARLE, J., *J. Colloid Sci.* **2**, 277 (1947).
31. MATHIESON, R. T., *Nature* **183**, 1803 (1959).
32. GREENHILL, E. B., *Trans. Faraday Soc.* **45**, 625 (1949).
33. GAINES, G. L., JR., *J. Phys. Chem.* **61**, 1408 (1957); *ibid.* **62**, 1526 (1958).
34. COTTINGTON, R. L., SHAFRIN, E. G., AND ZISMAN, W. A., *J. Phys. Chem.* **62**, 513 (1958).
35. SHAFRIN, E. G., AND ZISMAN, W. A., in H. Sobotka, ed., "Monomolecular Layers," p. 129. American Association for the Advancement of Science. Washington, 1954.
36. SUTULA C. L. AND BARTELL, L. S., Paper No. 8, Division of Colloid Chemistry, 135th National A.C.S. Meeting, Boston, April 5, 1959.

## MEASUREMENT OF THE PARTICLE SIZE DISTRIBUTION AND CONCENTRATION OF CIGARETTE SMOKE BY THE "CONIFUGE"<sup>1</sup>

C. H. Keith and J. C. Derrick

*Liggett and Myers Tobacco Company, Research Department,  
Durham, North Carolina*

*Received April 18, 1960*

### ABSTRACT

The particle size distribution and concentration of cigarette smoke has been measured with a centrifugal aerosol collector of the type developed by Sawyer and Walton. A conifuge designed to collect particles in the 0.05 to 10 micron diameter size range was constructed and used to study diluted tobacco smoke. From these measurements it was found that tobacco smoke as it comes from a cigarette is an extremely concentrated aerosol with a relatively stable distribution of sizes ranging from 0.1 to 1.0 micron, peaked between 0.2 and 0.25 micron. The coagulation rate was found to agree reasonably well with theoretical predictions, and the initial concentration of normally obtained smoke was found to be  $3 \times 10^9$  particles per cubic centimeter. The usefulness of this equipment in the analysis of this difficult aerosol suggests a wider application in other aerosol problems.

### I. INTRODUCTION

The smoke produced by a burning cigarette is a commonly encountered aerosol of considerable physiological significance. It also is an uncommonly concentrated aerosol which presents many of the various complications that make measurement of the particulate concentration and size distribution of aerosols quite difficult. These considerations have led a number of workers, particularly Sano *et al.* (1), Langer and Fisher (2), and Holmes *et al.* (3), to use it as a test aerosol with varying degrees of success. In this paper, a centrifugal sedimentation technique of general applicability to aerosols within a 0.05 to 10 micron size range is applied to tobacco smoke.

A centrifugal sedimentation technique is particularly suited to an aerosol such as tobacco smoke which combines a very high particulate concentration, a small and somewhat nonuniform particle size, and volatile and chemically unstable components (4, 5). The chief advantage arises from the indirect size estimation possible with such a technique, thereby avoiding

<sup>1</sup> Presented in part at the Southeastern Regional Meeting of the American Chemical Society, Durham, North Carolina, November 14, 1957.

the difficulties encountered with the use of microscopic, light-scattering, or electrostatic weighing techniques for size measurement.

Of the centrifugal techniques, impactors have been most commonly utilized for tobacco smoke (2-4). Some difficulty has been encountered, particularly with multiple-stage impactors, in a considerable loss of material through re-entrainment of previously deposited smoke particles. A centrifugal instrument which avoids this problem and provides a continuously graded spectrum of particle sizes is the "Conifuge" developed by Sawyer and Walton (6). Their demonstration of the ability of this machine to collect and size grade a variety of liquid and solid aerosols made it apparent that this approach had distinct possibilities for the analysis of tobacco smoke.

The instrument developed by Sawyer and Walton collected particles larger than 0.5 micron in diameter. To accommodate tobacco smoke, a new instrument based on the same principles was constructed. The design was such that particles with diameters ranging from 0.05 to 10 microns could be sampled.

This paper describes this instrument and its application to the particle size analysis of cigarette smoke. The limited data included serve to demonstrate the usefulness of the equipment for this and other aerosol problems, and allow the estimation of some of the factors of importance in altering the concentration of smoke issuing from a cigarette.

## II. EQUIPMENT

### A. The "Conifuge"

A cross-sectional view of the centrifuge head and the surrounding air chamber is given in Fig. 1. When rotating at high speeds, the head acts as a centrifugal air pump. The centrifugal force imparted to the air in the inner chamber between cones (*E*) and (*O*) causes it to flow from the axially located entrance tube (*P*) to and out of the off-axis outlet jets (*G*). Since the rotating head is enclosed in an airtight chamber (*Q* and *S*), this flow is recirculated through the outer chamber back to the entrance tube, as indicated by the arrows of Fig. 1. If a small portion of this circulating air is removed through the outlet tube (*T*), an equivalent volume of smoke is drawn in at (*A*). This incoming smoke is directed at the apex of the spinning head and spreads out in a thin film on the surface of the inner cone. As this film and the overlaying clean, circulating air are carried downward and outward through the conical chamber an increasing centrifugal force is applied to the individual particles owing to their excursion away from the axis of rotation. In conjunction with the increasing centrifugal force, the forward velocity of the air stream in which the particles are embedded is decreasing as the annular area of the conical chamber increases. This



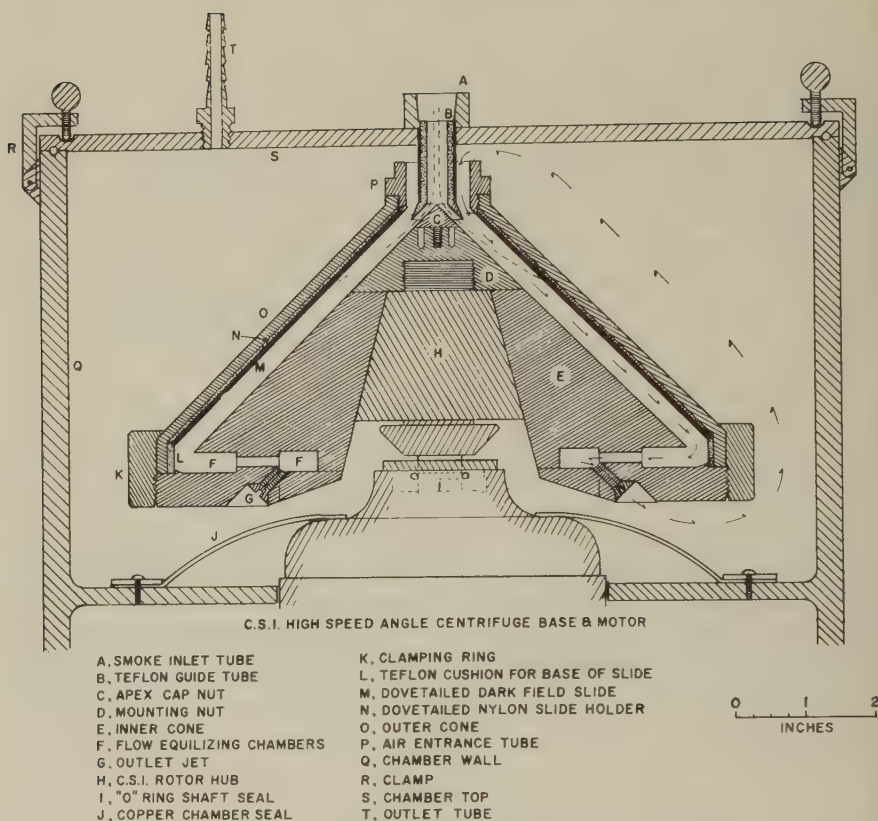


FIG. 1. Cross sectional diagram of the Conifuge.

combination of centrifugal force and stream velocity determines the trajectory of the individual particles. With a given set of dimensions and rotational velocity and assuming no significant slippage between the rotating head and incoming air stream, the trajectory of each particle is uniquely determined by its Stokes-Cunningham settling velocity. Since the trajectory of each particle determines its point of deposition on the outer wall of the chamber, a deposit is formed there which is continuously graded according to particle settling velocity. For spherical droplets of uniform density, such as cigarette smoke, the gradation may be expressed as a function of particle diameter. A representative sample of this graded size distribution suitable for counting numbers of particles is obtained from two dark-field microscope slides (*M*) embedded in the outer wall.

The conical shape of the chamber and the changing balance between stream velocity and centrifugal force are such that an extensive range of sizes are adequately represented on a relatively short collecting slide. The easily centrifuged and relatively less numerous large particles are deposited

near the apex of the cone or the head of the slide. The high stream velocity in this region fully sorts these particles, so that their distribution is opened out along the slide. However, an area deposit sufficient for counting purposes is maintained since the ring area in this region is relatively small. The more numerous smaller particles pass further down the conical chamber into a region of slower stream velocity and higher centrifugal force. This results in a compression of the range of sizes collected on a given length of slide, but the larger ring area in this region counterbalances this effect, so that the area deposit is not excessive.

By equating the centrifugal driving force and Stokes' law resistive forces acting on a particle, Sawyer and Walton (6) formulated an equation for the trajectory of individual particles. This equation is given in their paper and is not reproduced here. The derivation contains a number of assumptions, so that their equation is at best only approximate, particularly for large particles. Because the integrated equation is not analytical, the deposition points for particles of given settling velocities are best obtained by superimposing these trajectories on an outline of the chamber dimensions. Such plots were utilized to design a chamber of sufficient dimensions to capture the range of sizes thought to be present in cigarette smoke.

One of the chief requirements for the satisfactory operation of the confuge is a steady, nonturbulent air flow in the space between the cones. The design was made with this in mind, and sufficient flexibility was incorporated in the equipment so that turbulence might be avoided by an experimental choice of operating conditions. Extensive precautions were also taken in the machining of the head to eliminate any places which might cause turbulent mixing of the smoke and clean air streams. A set of operating conditions were experimentally chosen on the basis of excellence of size gradation, this being taken as an indication of lack of turbulence. These were a flow through the conical chamber of 54 c.c./sec. and a rotational velocity of 8000 r.p.m. Other chosen or fixed parameters were a horizontal cone separation of 1 cm., a semivertical angle of  $45^\circ$ , a 12.5-cm. slide length, and a smoke sampling velocity of 5 c.c./sec.

The design and construction of the equipment was considerably simplified and the cost reduced by adapting a commercial centrifuge to provide the driving mechanism. The machine used was a C.S.I. angle centrifuge (Custom Scientific Instruments, Arlington, New Jersey). The modifications chiefly consisted of replacing the manufacturer's safety shield with the airtight chamber and constructing the special centrifuge head, both of which are shown in Fig. 1.

### *B. Auxiliary Equipment*

Several pieces of equipment were necessary for reproducibly obtaining and immediately diluting cigarette smoke for use in the confuge. The latter was necessary because coagulation of the extremely concentrated

raw smoke stream would significantly change its particle size distribution very rapidly. A several hundred fold dilution was made by surrounding the smoke stream as it issued from the cigarette with a high-velocity, clean air stream. Both streams were directly introduced into a 12-l. flask from which smoke samples could be drawn through a small sampling chamber into the confuge. The sampling chamber was fitted at either end with plunger valves so designed that a small volume of smoke could first be drawn into the chamber and subsequently into the confuge without interrupting the normal flow of clean air into the instrument.

Since immediate dilution of the smoke stream was necessary, it was not possible to smoke the cigarettes in the orthodox manner by applying a controlled vacuum pulse to the end of the cigarette. It was, instead, necessary to puff on the cigarette by forcing air through the burning cone. This was accomplished by placing a bell over the previously lighted cigarette just before a pulse of slightly compressed air was delivered from a 4-l. storage tank.<sup>2</sup> The duration and intensity of the puff were controlled by a clock-operated solenoid valve and an adjustable pressure drop in the supply line to the bell. The larger diluting air stream was supplied from the same tank and was similarly controlled so that the ratio of diluting air to smoke remained constant during the puff. The timing was such that the diluting air was flowing slightly before and after the puffing air stream. Save for the use of compressed air in place of vacuum, the mechanism employs the sample principles as the smoking machine described by Keith and Newsome (7), and was adjusted to take a similar, reproducible 44-c.c., 2-sec. puff, every half minute.

A Bausch and Lomb research microscope equipped with a cardioid dark-field condenser, 20-power apochromatic objective, and a 25-power compensated eyepiece fitted with a standard Whipple disk was used for counting the number of particles collected on the dark-field slides. The light source was a B and L Model 48 carbon arc microprojector. The slides require an excellent flame-polished optical surface for they must be examined with a dry upper surface to avoid possible shifting of the position of the captured smoke particles. Suitable slides were obtained from the Baltimore Instrument Company of Baltimore, Maryland. The slides were prepared for use by cleaning in nitric acid and rinsing with water and redistilled alcohol. Any residual dust was then removed by coating the slide with collodion and subsequently removing the collodion film. The final step consisted of rubbing on a thin film of silicone oil, which prevented the captured smoke particles from spreading.

<sup>2</sup> In some early work, a puffing mechanism was used which utilized the suction induced by the high velocity diluting air stream to draw on the cigarette. This was discarded because of the extreme difficulty in controlling the volume and other characteristics of the puff.



### III. EXPERIMENTAL METHODS

#### *A. Calibration of the Conifuge*

In order to establish the relationship between particle size and place of deposition (as measured by distance from the head of the collecting slide), the conifuge was calibrated with several test aerosols, which were physically similar to tobacco smoke. These were atomized molten paraffin wax, homogeneous dioctyl phthalate aerosols obtained from a LaMer-Sinclair generator (8), and the homogeneous aerosols formed by atomizing greatly diluted samples of Dow monodisperse polystyrene latex by the method described by O'Konski and Doyle (9).

For the paraffin aerosol, the place of deposition of 0.5-micron or larger particles was correlated with particle size, as measured by ordinary microscopic techniques. For the homogeneous test aerosols the position of maximum deposition was correlated with the previously determined particle size. These sizes were determined by the red band structure of the D.O.P. aerosol and from the given particle size of the polystyrene dispersion, the measurement of which has been described by Bradford and Vanderhoff (10).

Figure 2 illustrates the distribution of particle counts obtained from 0.814-micron polystyrene particles. The ordinate of this curve is the calculated number of particles present in a conical segment of the outer cone of 1 mm. slant height, the calculation being based on the average slide count in that region. The abscissa is the distance from the top of the sampling slide in millimeters. The extreme sharpness of the maximum deposition peak is an indication of the quality of the size gradation obtained in this machine. The slight inflection on the left side of the curve and the somewhat slower rise on this side are thought to be caused by the presence of double and larger aggregate polystyrene particles which were formed either during the atomization process or by subsequent coagulation. The rapid fall of the curve on the right side, where the choice is between one or no polystyrene particles per atomizer droplet, is more representative of the deposition of a truly monodisperse aerosol.

The calibration curve for the instrument is given in Fig. 3. The separate calibrations form a continuous curve for particles between 5 and 0.08 microns, indicating an acceptable size grading action for liquid and solid aerosols over this range of particle size. The deposition curve predicted by Sawyer and Walton's equation (6) is given by the dashed curve of Fig. 3. The departure of the two curves in the region of large particles is not unexpected in light of the assumptions made in their development. In the small particle region the two curves again depart. This occurs because the equation predicts the maximum distance at which deposition of a particle of a certain size would occur. The experimental points are, however, based

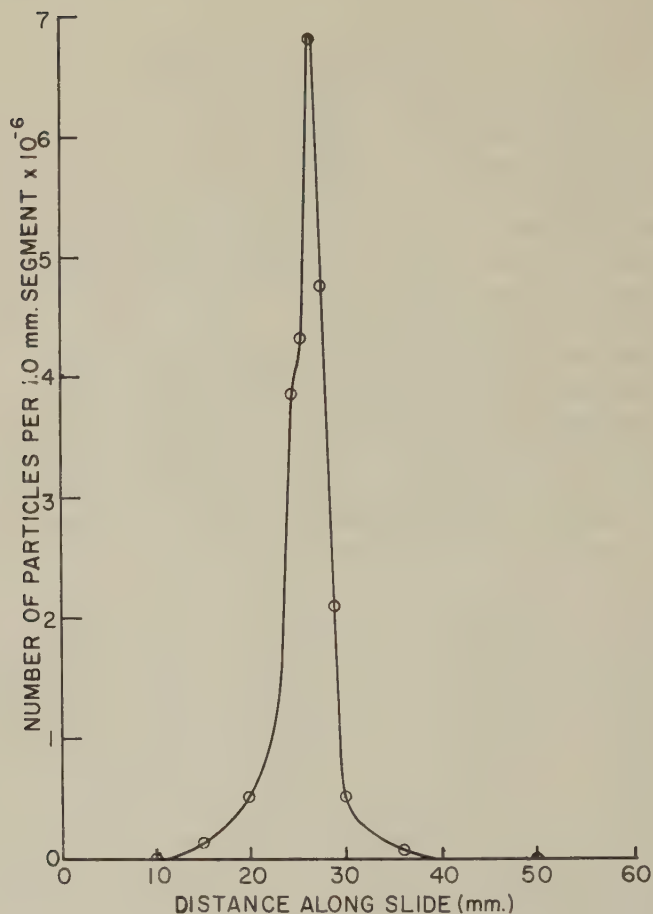


FIG. 2. Deposition pattern of 0.814 micron polystyrene aerosol in the Conifuge.

on the position of maximum deposition of a given particle size. From the distribution of deposition distances of the homogeneous aerosols, such as that illustrated in Fig. 2, it is found that the points of furthest deposition agree well with the theoretical curve.

#### *B. Size Distribution of Cigarette Smoke*

Uniformly blended cigarettes of known weight and resistance to draw were conditioned to an equilibrium moisture content by storage in an atmosphere of constant humidity and temperature. In the smoking operation, the cigarette was lighted by the operator, and the routine was continued in the previously described equipment. After sampling and collection of the smoke, the slides were removed and the numbers of particles



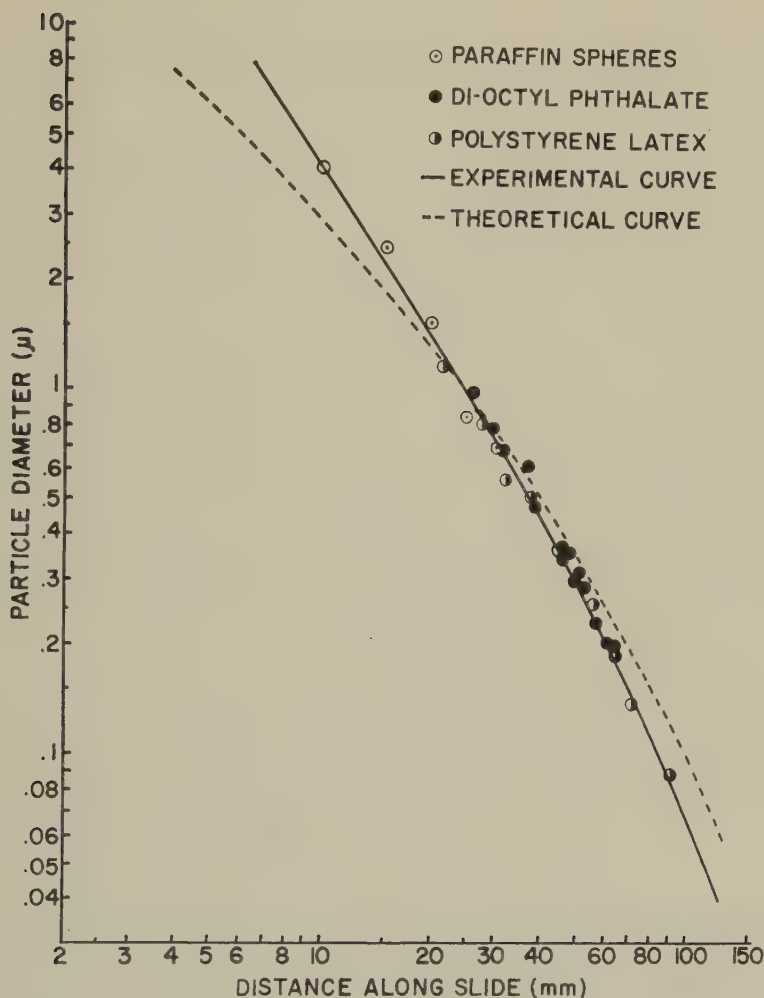


FIG. 3. Theoretical and experimental calibration curves for the Conifuge.

counted<sup>3</sup> at 5-mm. intervals along the slides. In general for each slide, 5 Whipple disk squares, each representing a field 0.033 by 0.033 mm. and containing from 1 to 30 particles, were counted. The average of these counts from both slides was multiplied by the appropriate factor to obtain a count of the number of particles in the frustrum of a cone of 0.033 mm. slant height and with a radius equivalent to that of the outer cone of the

<sup>3</sup> Although there was a generally low and somewhat variable background count for clean slides, no correction was applied to the observed counts. During the counting operation particles and slide imperfections which obviously appeared to be foreign to the sample were not included in the count.

conifuge at the counting position. Plotting these counts against a particle diameter as obtained from the calibration curve<sup>4</sup> formed a size distribution curve. A logarithmic scale was used for the diameter axis to open out the smaller particle end of the scale.

Graphical integration of the size distribution curves was used to compute the total number of particles collected in the conifuge. This figure divided by the known volume of the sample gave the concentration of diluted smoke, which in turn was converted to a concentration of raw smoke by multiplication with the dilution ratio. This ratio was generally 295 volumes of diluted smoke to 1 volume of raw smoke.

As was pointed out by Sawyer and Walton (6), the size distribution curves can be readily transformed into mass distribution curves, and from these the total mass of the sample may be obtained by integration. Computations of these quantities were not extensively used in this work, since the results are generally imprecise. This arises from the relatively few counts for large particles, which contribute heavily to the mass distribution and total mass of the smoke deposit. Calculations of the total mass of smoke were, however, found to be in reasonable agreement with estimates of this quantity obtained by direct weighing of the total particulate matter collected in a suitable trap.

Measurements of the size distribution of side stream smoke were obtained by allowing a cigarette, selected as above, to freely burn without puffing in the 12-l. collection flask for 1 min. The resulting sample was collected and counted in the same manner as main stream smoke samples.

#### IV. RESULTS AND DISCUSSION

##### *A. Reproducibility of Collection of Cigarette Smoke*

In order to test the reproducibility of the particle size distribution obtained from selected cigarettes, four separate cigarettes were smoked and the smoke from the fourth puff was diluted, aged for 30 sec., and collected in the conifuge. The results of these measurements are illustrated in Fig. 4, where the circles represent the measured counts and the smooth curve represents the average size distribution. Although there is considerable scatter of the points, the figure shows that it is possible to reproduce the particle size distribution from one cigarette to the next. A subsequent

<sup>4</sup> The diameters, as read from the calibration curve, are those for unit density particles, and may be called a "settling diameter" for particles of other densities. The "settling diameter" is defined as the product of the actual particle diameter and the square root of the density of the particle. These diameters were used throughout this work for lack of exact data on the density of cigarette smoke particles. Sam (4) measured a value of 0.98 g./c.c. and Sano (1) obtained values ranging from 0.62 to 1.00 g./c.c. Using Sam's value or Sano's highest values causes no sensible change in converting from settling to actual diameters. Using Sano's lower value would increase the listed diameter values by a factor of 1.27.

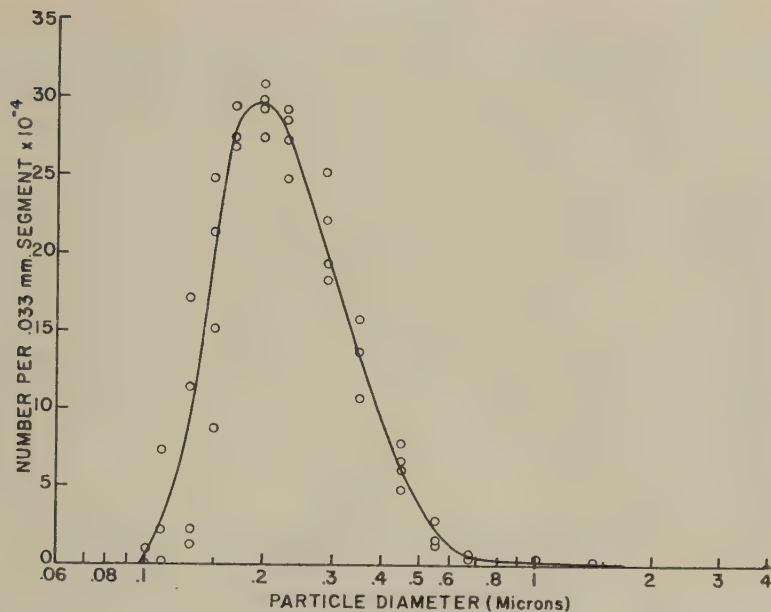


FIG. 4. Reproducibility of the particle size distribution of cigarette smoke.

series of ten measurements, each on a separate cigarette, gave essentially the same results for diluted smoke aged 60 sec., the most frequently occurring diameter being 0.21 micron, the geometrical mean diameter being 0.23 micron, and the standard deviation being 0.14 micron, the latter being obtained in the manner outlined in Table I.

#### *B. Aging Studies on Cigarette Smoke*

Although the previously described puffing mechanism provides a large sample of diluted tobacco smoke, this smoke is still relatively concentrated in comparison to other aerosols and therefore would be expected to coagulate at an appreciable rate. In order to study this process, the particle size distribution of cigarette smoke was determined at varying times after the puff. These distributions are presented in Fig. 5, and as expected for coagulation of small particles into larger aggregates there is a progressive decrease in the numbers of particles and an increase in mean particle size with aging. In Fig. 6 it is apparent that the particulate volume or reciprocal of the particulate concentration is a linear function of aging time, as has been observed for many coagulating aerosols (11). From this plot, the initial number of particles in the sample,  $N_0$ , was estimated to be  $1.8 \times 10^7$  particles per cubic centimeter of the diluted smoke sample, or 5.3 billion particles per cubic centimeter in the original smoke. The slope of the curve, or coagulation constant,  $K$ , was found to be  $2.4 \times 10^{-10}$  c.c./sec.

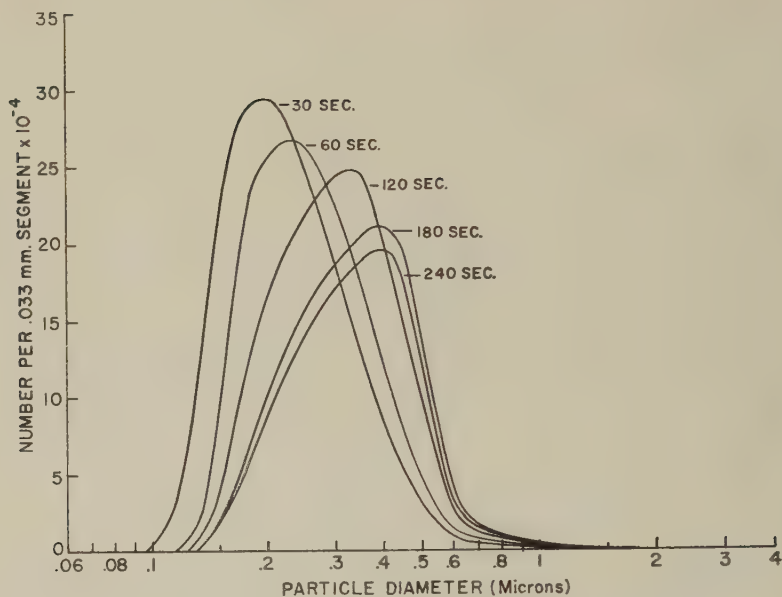


FIG. 5. The effect of aging on diluted cigarette smoke.

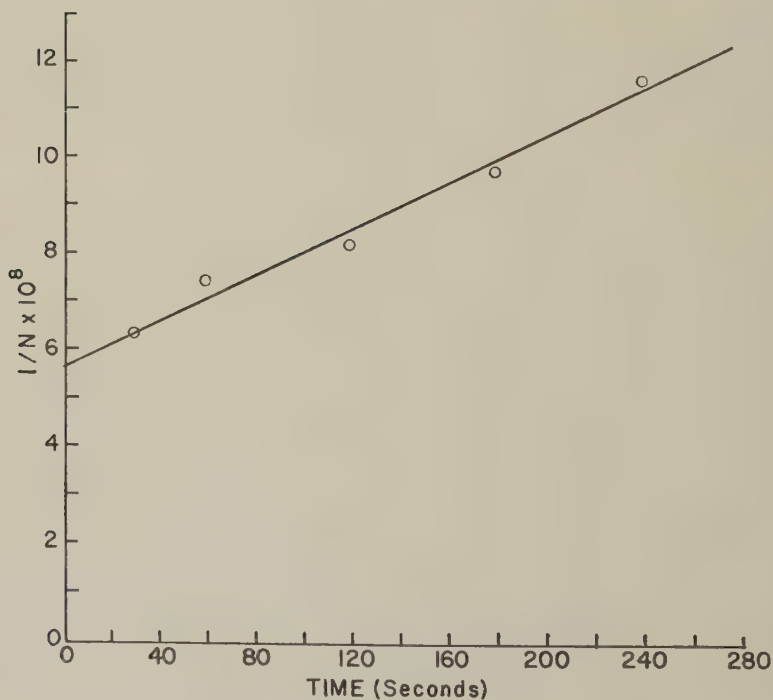


FIG. 6. Relation between particulate volume and aging time.

Further measurements of these quantities yielded an average coagulation constant of  $3.4 \times 10^{-10}$  c.c./sec. and 3 billion particles per cubic centimeter for the fourth puff on a regular length, blended cigarette of average weight and moisture content. This coagulation constant is somewhat less than the values obtained by others for a variety of considerably more dilute aerosols. Using Whytlaw-Gray's (12) modification of the Smoluchowski coagulation equation, a slightly curved relation between particulate volume and time was calculated with slopes ranging from 4.2 to  $4.5 \times 10^{-10}$  c.c./sec., which are in reasonable agreement with the experimentally determined slope of  $3.4 \times 10^{-10}$  c.c./sec., especially since the theoretical slope is for an ideal monodispersed aerosol, whereas the experimental value was obtained with a concentrated heterogeneous smoke.

### *C. Effect of Various Smoking and Cigarette Variables*

The data reported in earlier sections were obtained from the fourth, 44-c.c. puff on an unfiltered blended cigarette of normal weight and moisture content. Some data obtained from cigarettes in which one or more of these variables were altered are presented in Table I.

TABLE I  
*Effect of Smoking and Cigarette Variables*

Cigarette conditions	Smoking conditions <sup>a</sup>	Most freq. occurring diameter <sup>b</sup> ( $\mu$ )	Mean <sup>b, c</sup> diameter ( $\mu$ )	Standard deviation <sup>c</sup> ( $\mu$ )	No. of particles <sup>b</sup> per c.c. $\times 10^{-3}$
Blended, 1.08 g., 11% H <sub>2</sub> O	4th, 44-c.c. puff	0.21	0.23	0.14	3.01
Blended, 1.08 g., 11% H <sub>2</sub> O	4th, 35-c.c. puff	0.23	0.23	0.14	2.97
Blended, 1.08 g., 11% H <sub>2</sub> O	4th, 55-c.c. puff	0.21	0.21	0.14	2.89
Blended, 1.08 g., 11% H <sub>2</sub> O	2nd, 44-c.c. puff	0.22	0.21	0.14	2.24
Blended, 1.08 g., 11% H <sub>2</sub> O	5th, 44-c.c. puff	0.23	0.23	0.14	4.13
Blended, 1.08 g., 11% H <sub>2</sub> O	7th, 44-c.c. puff	0.23	0.21	0.14	4.66
Blended, 1.08 g., 11% H <sub>2</sub> O	10th, 44-c.c. puff	0.22	0.21	0.14	4.31
Blended, 1.00 g., 11% H <sub>2</sub> O	4th, 44-c.c. puff	0.23	0.22	0.14	3.57
Blended, 1.18 g., 11% H <sub>2</sub> O	4th, 44-c.c. puff	0.20	0.21	0.13	2.86
Blended, 1.08 g., <sup>d</sup> 3.6% H <sub>2</sub> O	4th, 44-c.c. puff	0.22	0.22	0.14	4.66
Blended, 1.08 g., <sup>d</sup> 6.2% H <sub>2</sub> O	4th, 44-c.c. puff	0.23	0.21	0.14	4.54
Blended, 1.08 g., <sup>d</sup> 20.4% H <sub>2</sub> O	4th, 44-c.c. puff	0.20	0.22	0.14	1.65
Bright, 1.09 g.	4th, 44-c.c. puff	0.20	0.21	0.14	3.25
Burley, 0.90 g.	4th, 44-c.c. puff	0.20	0.20	0.14	3.01
Turkish, 1.15 g.	4th, 44-c.c. puff	0.20	0.20	0.14	3.07

<sup>a</sup> All puffs of 2 seconds duration taken at  $\frac{1}{2}$  minute intervals.

<sup>b</sup> Extrapolated values at zero aging time.

<sup>c</sup> Estimated from a logarithmic-probability plot of particle size against cumulative frequency, the geometric mean being the size at which 50% of the particles are greater and less than that size. The standard deviation is taken as the ratio of the 84% size to the 50% size adjusted to the size range under consideration (13).

<sup>d</sup> Weight of the cigarettes at 11% moisture.



In Table I it is apparent that the particle size distribution is a relatively stable property of cigarette smoke over a considerable range of variations of cigarette and smoking conditions. It is also apparent in Table I and the previous distributions that cigarette smoke is a relatively homogeneous aerosol with regard to particle size. This stable and narrow distribution of sizes suggests that the distribution is formed by a combination of removal processes common to all cigarettes. At the small particle end of the spectrum, it is probable that processes such as coagulation, diffusional capture by the tobacco strands, and growth by condensation of vaporized materials would tend to eliminate particles less than 0.1 micron diameter. With regard to the coagulation process, in Fig. 5 it was shown that the peak diameter of diluted smoke would double within approximately 180 sec. In raw smoke, with its three hundred fold greater particulate concentration, this should occur in 0.6 sec., which is of the same order of magnitude as the 0.1 sec. residence time of the smoke within the cigarette. Thus it is apparent that this process would significantly contribute to the removal of small particles.

Another process which probably controls the particle size distribution of the exit smoke stream is removal of the larger particles through filtration by the tobacco strands in the cigarette butt. It is known from other work (14) that appreciable amounts of smoke are collected by this portion of the cigarette. In a later section this process will be considered in more detail.

Although the particle size distributions in Table I are relatively stable, there is a considerable variation in the total number of particles per cubic centimeter of smoke gasses for these cigarettes. In general these variations are in line with the effect of these parameters on the weight of smoke (14). Increments in puff volume have a nearly linear effect on the weight of smoke, which is consistent with a constant particulate density, the increment coming from the increased total volume. Later puffs on a cigarette have been found to produce more smoke, chiefly because less is filtered out by the stub, and such an increment is detected in Table I. With the smoking method employed herein the cigarette tends to become extremely moist after the seventh or eighth puff. This is thought to cause the observed decrease in numbers of particles between the 7th and 10th puff. The variables of cigarette weight and moisture content show the expected increase in numbers of particles with decreasing weight and moisture content. Bright, burley, and Turkish tobaccos appear to give slightly anomalous results as they produce nearly the same number of particles, although these tobaccos give somewhat different weights of smoke.

#### *D. Side Stream Measurements*

The smoke rising from the burning cone of a cigarette during the interval between puffs should have a different size distribution than the smoke drawn from the cigarette during a puff since it is not subjected to the same

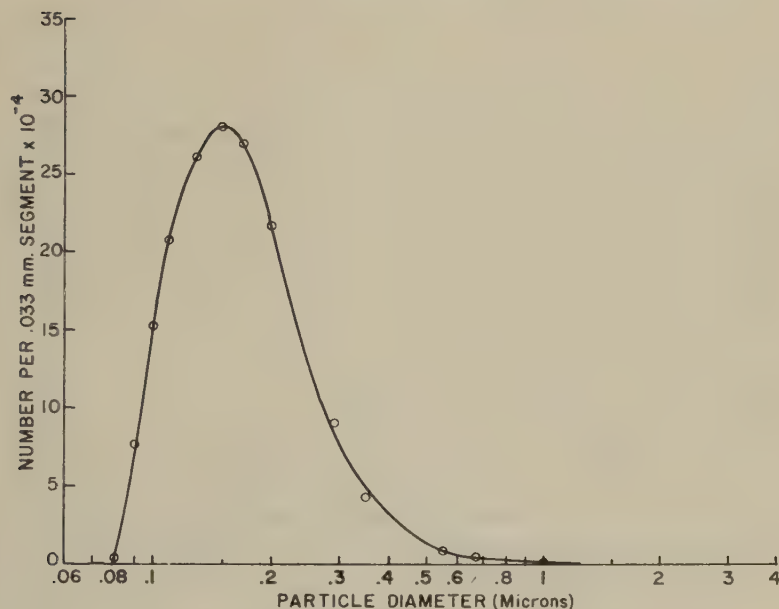


FIG. 7. Particle size distribution of side stream cigarette smoke.

size-determining processes as the latter. Figure 7 shows the distribution obtained for this smoke, which was collected by the previously described method. Larger numbers of small particles, down to 0.08 micron, were observed and the most frequently occurring size was 0.15 micron as compared to 0.20–0.23 micron for main stream smoke. It was estimated from this curve that free burning produces particles at the rate of 6.3 billion per second. Since the sample was obtained over a period of 60 sec., it is likely that the original smoke contains greater numbers of still smaller particles.

#### *E. Filtration of Tobacco Smoke*

To investigate the role of coagulation and filtration in the removal of larger tobacco smoke particles, the effect of drawing the smoke stream through additional cigarettes, open tubes, and efficient cigarette filters was studied. To isolate the effects of coagulation and filtration two assemblies were prepared by taping together three 70-mm. cigarettes and by attaching a 140 mm. long, 8-mm. glass tube to a single cigarette. The assemblies are thus equivalent cigarettes with an open 140-mm. mouthpiece and with a 140 mm. tobacco filter. The distributions obtained from the fourth puff on these cigarettes are illustrated in Fig. 8.

In Fig. 8, it is readily apparent that the tobacco filter removed considerably greater numbers of particles than the equivalent mouthpiece and also that this removal was selective for larger particles since the distributions are slightly displaced. The raw smoke coming from the mouthpiece was found to contain 2.1 billion particles per cubic centimeter, whereas the

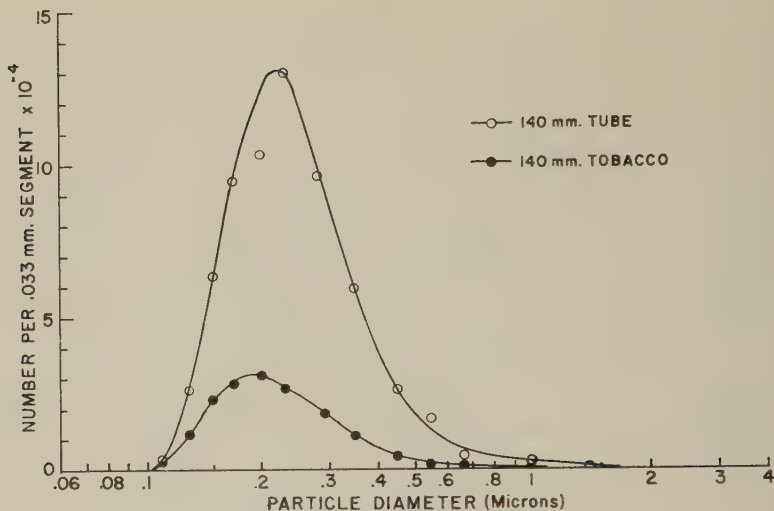


FIG. 8. Particle size distributions of tobacco smoke after coagulation and filtration in a 140-mm. tube and tobacco column.

tobacco filter delivered only 0.5 billion. From previous data it was estimated that 3 billion particles entered both assemblies, so that 0.9 billion particles were removed by the mouthpiece and 2.5 billion by the filter. From the residence time of the smoke in the mouthpiece and the coagulation curve, it was calculated that 0.5 billion particles were removed by coagulation, and that 0.4 billion remained in the tube at the end of the puff or were lost at the entrance or walls of the tube.

For the tobacco filter equivalent losses would be expected from coagulation and smoke remaining in the filter, so that the net removal of particles through filtration is 1.6 billion per cubic centimeter, amounting to a better than 50% removal by this mechanism.

From the distributions of Fig. 8, a figure for the weight filtration efficiency of the 140-mm. tobacco filter may be obtained and compared with an independent estimate of this quantity. Converting the number distributions of Figs. 4 and 8 to mass distributions and integrating in the region 0.1–1.0 micron gave a mass of raw smoke coming from the cigarette of 32  $\mu\text{g.}$  per cubic centimeter, while that issuing from the tube and tobacco filter was 30 and 5  $\mu\text{g.}$  per cubic centimeter, respectively. These yield an overall filtration efficiency for the tobacco filter of 84%. From measurements on shorter tobacco filters, an efficiency of 82% is calculated for a 140-mm. tobacco column; this agrees well with the efficiency calculated from the particle size distributions.

Figure 9 illustrates the effect of a relatively efficient 17-mm. cellulose acetate cigarette filter on the particle size distribution of cigarette smoke. The distributions illustrated were the average for diluted smoke aged for

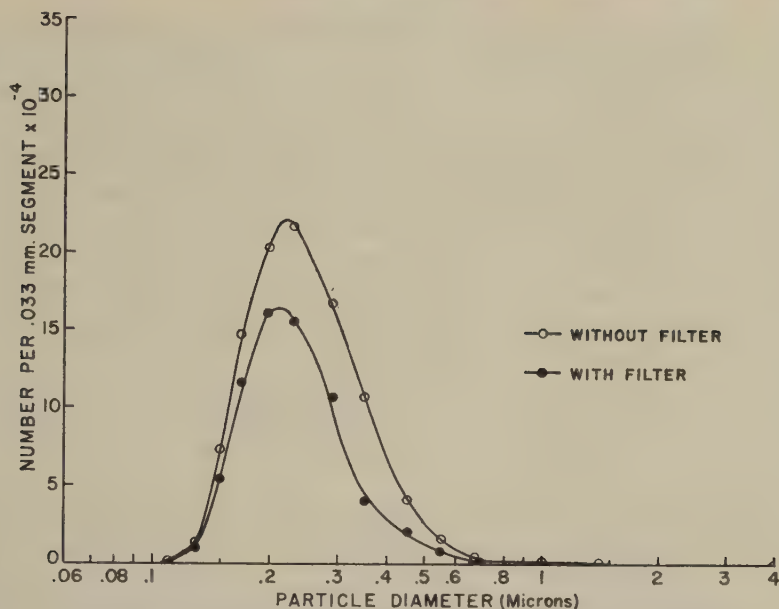


FIG. 9. Particle size distributions of the smoke from filtered and unfiltered cigarettes.

60 sec. from 4 cigarettes with, and 4 cigarettes without, filters. As in the case of the tobacco filter, a preferential reduction in the numbers of large particles is apparent in the shift of the filter distribution towards smaller sizes in addition to an overall lowering of the curve.

The total number of particles was found to be 2.3 and 3.6 billion per cubic centimeter of raw smoke for the filtered and unfiltered smoke, respectively. From these figures it is calculated that the filter removes 36% of the numbers of particles from the smoke stream. Converting the curves to mass distributions for particles less than 1.0 micron in diameter and again computing the filtration efficiency yields a figure of 39%, the increase stemming from the greater contribution of the larger particles to the total mass. Considering the fact that separate samplings of cigarettes were necessary for each determination, these figures agree well with the measured filtration efficiency of 37%.

These experiments with tobacco filters and relatively efficient cigarette filters indicate that the filtration mechanism is effective in removing larger particles. This in conjunction with the coagulation and other growth processes produce an essentially stable and narrow distribution of particle sizes in cigarette smoke as it comes from the cigarette.

## V. SUMMARY

The particle size distribution and particulate concentration of cigarette smoke has been measured using a centrifugal collection instrument called



the "Conifuge." The instrument avoids the difficulty of direct size measurement by continuously grading the particles according to settling velocity or size. It is capable of collecting particles ranging in diameter between 0.05 and 10 microns. For these reasons the instrument is well suited for measurement of the size distribution of cigarette smoke and other aerosols.

The size distribution and particulate concentration of smoke were found to be reproducible quantities for similar cigarettes, but were found to vary according to the age of the smoke sample, even after considerable dilution. The rate of decrease of the number concentration of smoke particles was found to agree reasonably well with the rate predicted by the modified Smoluchowski coagulation equation.

Alteration of a number of smoking and cigarette variables was found to have no detectable effect on the particle size distribution, but changed the concentration of particles in a manner similar to the effect of these variables on the weight of smoke.

A preferential removal of larger particles was observed for high-efficiency tobacco and cigarette filters, in addition to a considerable decrease in particulate concentration.

The essentially constant size distribution appears to arise through the removal of small particles through coagulation and larger particles through filtration by the tobacco strands.

#### ACKNOWLEDGMENT

The authors are indebted to Mr. Henry Pierce for his considerable assistance in the design and construction of the conifuge and accessory equipment.

#### REFERENCES

1. SANO, K., FUJIYA, Y., AND SAKATA, S., *J. Chem. Soc. Japan* **74**, 664 (1954).
2. LANGER, G., AND FISHER, M. A., *Am. Med. Assoc. Arch. Ind. Health* **13**, 373 (1956).
3. HOLMES, J. C., HARDCASTLE, J. E., AND MITCHELL, R. I., *Tobacco Sci.* **3**, 148 (1959).
4. SAM, A., "A Study of Particle Size Distribution and Dilution of Cigarette Smoke." Thesis, Duke University, Durham, North Carolina, 1956.
5. KAHLER, H., AND LLOYD, B. J., JR., *J. Natl. Cancer Inst.* **18**, 217 (1957).
6. SAWYER, K. F., AND WALTON, W. H., *J. Sci. Instr.* **27**, 272 (1950).
7. KEITH, C. H., AND NEWSOME, J. R., *Tobacco Sci.* **1**, 51 (1957).
8. SINCLAIR, D., AND LA MER, V. K., *Chem. Revs.* **44**, 245 (1949).
9. O'KONSKI, C. T., AND DOYLE, G. J., *Anal. Chem.* **27**, 694 (1955).
10. BRADFORD, E. B., AND VANDERHOFF, J. W., *J. Appl. Phys.* **26**, 863 (1955).
11. WHYTLOW-GRAY, R., AND PATTERSON, H. S., "Smoke: A Study of Aerial Disperse Systems," Chapter 5. E. Arnold & Co., London, 1932.
12. WHYTLOW-GRAY, R., AND PATTERSON, H. S., "Smoke: A Study of Aerial Disperse Systems," Chapter 6. E. Arnold & Co., London, 1932.
13. DRINKER, P., AND HATCH, T., "Industrial Dust," pp. 144-149. McGraw-Hill, New York, 1936.
14. NEWSOME, J. R., AND KEITH, C. H., *Tobacco Sci.* **1**, 58 (1957).



## ANOMALOUS BEHAVIOR OF AEROSOL PRODUCED BY ATOMIZATION OF MONODISPERSE POLYSTYRENE LATEX<sup>1</sup>

G. Langer and A. Lieberman

*Armour Research Foundation of Illinois Institute of Technology,  
Chicago, Illinois*

*Received April 18, 1960*

### ABSTRACT

A study was made of the uniformity of aerosol particles generated by the atomization of monodispersed polystyrene latices. It was found that the stabilizer associated with the latices formed extraneous particles as well as increased the size of the polystyrene particles. This was due to the fact that the stabilizer binds water strongly even in the presence of dry air. Heat drove the bound water off but adversely affected the polystyrene particles.

During development of an electrostatic classifier for submicron aerosol particles, it was decided that the monodisperse polystyrene latices produced by the Dow Chemical Company would produce ideal standardizing aerosols. These materials are available in a wide range of particle diameters from 0.09 to 1.1 microns; they are spherical; the diameter of a specific batch is accurately known. In addition, aerosols made from these latices have been used by other organizations as standard test aerosols for filter evaluation (1).

Therefore several batches of polystyrene latices were obtained for use as test materials. Aerosol was prepared by diluting the latex to a convenient concentration and dispersing it as an aerosol by means of a simplified Lauterbach generator (2). The aerosol was diluted with dry air to evaporate the water from the latex spheres. The aerosol was then passed to the classifier and precipitated. It was noted that the precipitation pattern was that of a polydisperse aerosol. Analysis of the classifier operation indicated that it was operating satisfactorily and that a closer examination of the aerosol was in order.

The Armour Research Foundation Electronic Particle Counter (3) was used for rapid analysis of the aerosol with the equipment shown in Fig. 1. Data are obtained within seconds of sampling the aerosol and the aerosol

<sup>1</sup> This work was performed as part of Contract No AF 19(604)2411 under the sponsorship of the Air Force Cambridge Research Center.

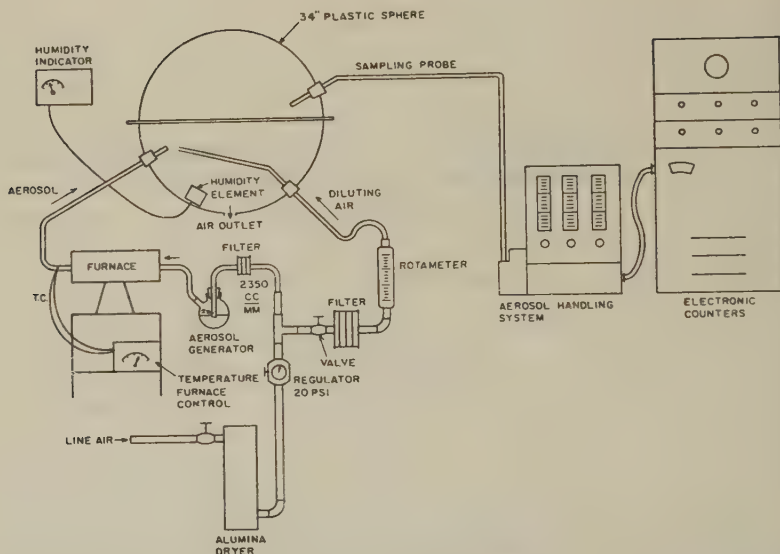


FIG. 1. Test equipment for studying aerosols produced by atomization of mono-dispersed polystyrene latex particles.

TABLE I  
*Particle Size Distribution of Polystyrene Latex Aerosols Made by Atomization*

Diam. of latex particle	Dilution of suspension	Rel. hum. in sphere (%)	Size distribution (%)						Conc. (particles/c.c.)	
			0.5-0.7	0.7-1.0	1.0-1.4	1.4-2.0	2.0-2.8	2.8-4.0	Meas.	Calcd.
0.138	1:500	4	72	19	5	3	1	0	15	0
0.814	1:100	4	12	24	52	12	0	0	109	2
0.814	1:10	4	3	13	36	33	13	2	500	20

Calculated concentrations refer to the stated size range for the particle counter for the latex particles only. The particle counter was set to obtain correct size data for water aerosol with refractive index 1.33. Although the polystyrene has a refractive index of 1.60, the error in the stated sizes is less than 25%.

is examined *in situ* by scattered light measurement. Examination with the particle counter verified the wide size distribution of the aerosol. The aerosol was sampled from a 34 in. diameter Lucite sphere where it was mixed with dry diluting air. Table I shows the data which were obtained with two latices that were dispersed and diluted with dry air at room temperature. The only possible conclusion is that, even at 4% relative humidity, all the water drops were not evaporated.

Information from Dow Chemical Company is that the original solids content of the latices is 7% polystyrene and 2% unidentified stabilizer of a

TABLE II

*Size Distribution of Polystyrene Latex Aerosols Diluted with Heated Air*

Diameter of latex particles	Dilution of suspension	Rel. hum. in sphere (%)	Air temp. (°F.) in heater	Size distribution (%)						Conc. (particles/c.c.)	
				0.5-0.7	0.7-1.0	1.0-1.4	1.4-2.0	2.0-2.8	2.8-4.0	Meas.	Calcd.
0.138	1:500	4	75	90	8	1	1	0	0	4.2	0
0.138	1:500	4	330	75	25	0	0	0	0	0.2	0
0.814	1:100	4	75	12	24	52	12	0	0	109	2
0.814	1:100	4	330	58	42	0	0	0	0	0.2	2
0.814	1:10	4	75	3	13	36	33	13	2	500	20
			250	14	31	36	16	1	0	147	20
			330	57	30	12	1	0	0	3.2	20
			340	55	34	11	0	0	0	2.4	20
			360	0	0	0	0	0	0	0	20

TABLE III

*Effect of Humidity on Size Distribution and Concentration of Heated 0.814  $\mu$  Polystyrene Latex Aerosol<sup>a</sup>*

Rel. hum. in sphere (%)	Air temp. (°F.) in heater	Size distribution (%)						Conc. (particles/c.c.)	
		0.5-0.7	0.7-1.0	1.0-1.4	1.4-2.0	2.0-2.8	2.0-4.0	Meas.	Calcd
4	340	55	34	11	0	0	0	2.4	20
19	350	33	24	29	4	0	0	52	20
100	340	30	37	22	5	0	0	100	20

<sup>a</sup> Aerosol from atomizer was diluted with dry air, passed through heater, and then entered the sphere which was at different humidities.

soap nature. Therefore, some experiments were performed in which the diluting airstream was heated in an attempt to evaporate water and/or decompose the stabilizer only. Table II shows the data obtained in this series of experiments.

The first two lines in Table II show that measurable particles were present in the sphere even after being heated to 350°F. The particle counter which does not count below 0.5 micron should not have detected any particles if only polystyrene was present. Lines 3 and 4 show that most of the water was evaporated from the numerically more dilute 0.814 micron suspension at 350°F. The remainder of the table shows the effect of increasing air temperature on both the resultant size distribution and concentration of particles. It appears that a temperature of approximately 340°F. is necessary to effectively evaporate the water droplets. Observation of the entire table indicates that the required temperature is dependent

on the amount of stabilizer present in the diluted latex suspension. It was surmised that the stabilizer holds water very tenaciously. If so, the polystyrene particles will retain a water film even in very dry air. In the case of the 0.814 micron suspension diluted 1:100 and under the condition of atomization used, only 1 in 50 drops should contain a polystyrene particle. The remainder of the droplets apparently do not evaporate completely because of the residual stabilizer until a temperature of 340° to 350°F. is reached.

The stability of the water drops alone indicates that at least some of the stabilizer is distributed throughout the liquid rather than attached only to the particles. Some further experiments were performed and are shown in Table III. These data show that aerosol can be regrown by exposing it to sufficient water vapor. In other words the heat just dried out the stabilizer but decomposed the polystyrene at 340°F. and above.

It was concluded from these experiments that atomization of monodisperse polystyrene latices does not necessarily produce a monodispersed test aerosol. These preliminary experiments did not solve the problem of proper treatment to obtain monodisperse aerosols. One difficulty was that neither the stabilizer nor the water appeared in ordinary sampling procedures with microscope slides, because these materials spread out in a thin film.

However, some electron microscope photographs by Dautrebande (4) show the presence of extraneous material from a latex aerosol collected on an electron microscope screen. Presumably, the extraneous particles are due to the stabilizer, which is also shown between closely spaced particles from a drop of evaporated latex. Further work is planned to show the presence of the stabilizer with the light microscope and to develop a procedure for effective removal of the stabilizer in order to obtain a true, monodisperse aerosol.

#### REFERENCES

1. STERN, S., "Simple technique for generation of homogeneous millimicron aerosols," *J. Appl. Phys.* **30**, 952 (1959).
2. LAUTERBACH, K. E., *Arch. Ind. Health* **13**, 156 (1956).
3. FISHER, M. A., *Proc. 3rd Natl. Air Pollution Symp.*, pp. 112-119 (April, 1955).
4. DAUTREBANDE, L., "Studies in Aerosols," p. 55, VR-530, University of Rochester AEC Project, 1958.

## IMMERSION CALORIMETRY STUDIES OF THE INTERACTION OF WATER WITH SILICA SURFACES

G. J. Young and T. P. Bursh

*Catalysis Laboratory Alfred University, Alfred, New York*

*Received April 18, 1960*

### ABSTRACT

The objectives of this investigation were (1) to correlate heats of immersion, in water, for several silicas with other of their surface properties and (2) to investigate differences in the character of surface bonds of various silicas.

Changes in the heat of immersion with activation temperatures of the silica samples followed known variations in the character of the silanol surface sites that occur on heating. The heat of hydration of siloxane sites on the quasi-amorphous silicas used in this investigation was 16.1 kcal./mole of water. The heat of hydration apparently varies considerably for different silicas, ranging from low values for silica gels to higher values for low-area quartz. Also, the polarity of the surface Si-OH groups appears to change for different silicas, increasing in the order: silica gels < flame process silicas < finely ground quartz < very low-area quartz.

### INTRODUCTION

The surface chemistry of silicas has been studied by numerous investigators with the result that our general understanding of this subject is becoming reasonably comprehensive. Nevertheless, there are certain aspects of the nature of silica surfaces, particularly their interaction with water, that require further detailed experimental studies. Recently several investigators (e.g., references 1, 2, and 3) have employed precision immersion calorimetry as a tool to index the interaction of water and other polar molecules with silica surfaces. However, generally no attempt was made to quantitatively relate the results of such studies with the extensive additional information obtained from adsorption techniques, infrared data, etc.

The objectives of the present investigation were (1) to extend previous studies by one of us (4) to enable a correlation to be made between the surface properties of silicas as indexed by other techniques and data obtained on the interaction of silicas with water from immersion calorimetry and (2) to obtain evidence concerning possible differences in the character of surface bonds in various silica samples.



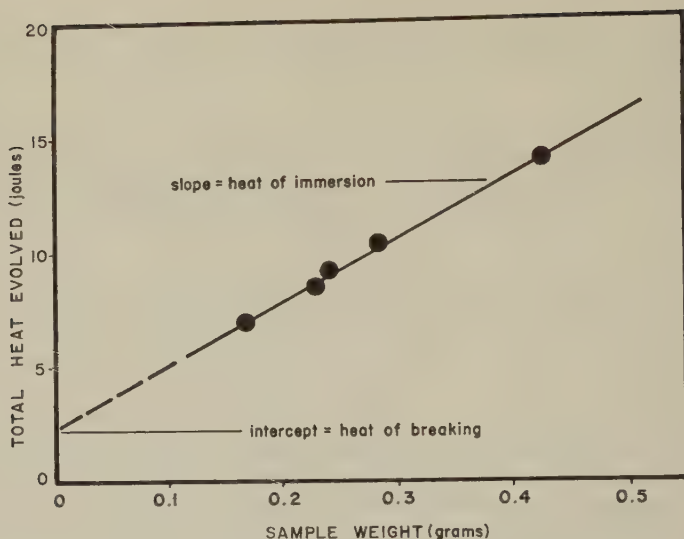


FIG. 1. Typical heat of immersion determination.

#### EXPERIMENTAL

Heats of immersion, in water, were determined by established calorimetric techniques. The calorimeter consisted of a Dewar flask suspended in an air bath and was, except for several minor modifications, essentially the same type as that described by Zettlemyer *et al.* (5). The temperature sensing system consisted of a paraffin-wax coated thermistor and a Mueller-bridge in conjunction with a highly sensitive ballistic galvanometer. With this, a resistance change of  $1 \times 10^{-4}$  ohm could be measured which corresponded to a temperature change of  $3 \times 10^{-5}$  degree Centigrade. A constant rate of stirring was accomplished through the use of a magnetic stirrer. A spring-loaded breaking-rod coupled with a solenoid was used to break the sample bulbs. This device eliminated some of the uncertainties encountered in the use of manually manipulated breaking-rods.

Sample bulbs were blown from thin-walled Pyrex tubing, and only those of approximately the same wall thickness and size were used. The heat evolved due to breaking of the bulbs was determined by plotting total heat, for several runs, versus sample-weight and extrapolating to zero sample-weight. A typical plot is shown in Fig. 1. The slope of the line is a measure of the heat of immersion while the intercept gives the heat of breaking. This procedure was repeated for each of the heat of immersion values reported.

The amorphous silica samples employed in this investigation were the same as those used in previous work (4) where their surface properties were determined from a variety of techniques. These silicas were prepared

TABLE I

Silica	$\Delta H_i$ ( <i>ergs/cm.<sup>2</sup></i> )	Surface area ( <i>m.<sup>2</sup>/g.</i> )		Per cent Hydroxyl surface	Hydroxyl sites/cm <sup>2</sup> ( $\times 10^{-13}$ )
		Total	Hydroxyl		
A	144 $\pm$ 3	420	105	25	23.6
B	143 $\pm$ 6	220	30	13	12.9
C	128 $\pm$ 3	76	12	16	14.9
Quartz	285 $\pm$ 3	9.1	6.8	75	70.5

by the flame hydrolysis of silicon tetrachloride and were not exposed to water prior to the heat of immersion experiment; hence, their surfaces exhibited only partial coverage with silanol groups. The quartz sample was prepared by dry grinding (under atmospheric conditions) of selected quartz crystals. The activated silica samples were evacuated (*ca.*  $10^{-6}$  mm. Hg) for 4 hours at activation temperatures ranging from 150° to 850°C. Those prepared at room temperature were evacuated for 8 hours or more.

### RESULTS

Heats of immersion for the silicas and quartz along with their respective total surface areas and the amount of hydroxyl surface are shown in Table I. These values refer to samples evacuated at room temperature, except for the quartz which was evacuated at 110°C. Recent Russian work (1) and Iler's analysis of Patrick's data (6) indicate that a linear relationship might be expected between the number of surface-hydroxyl groups per unit area and the heat of immersion. Whereas those silicas with the larger percentage of hydroxyl surface often exhibit the higher heats of immersion, there are many exceptions. Such a correlation between hydroxyl surface and heat of immersion may be valid for very similar silicas (such as a series of silica gels); however, it cannot be used for a general comparison of silica samples of different types. This is illustrated by the data of Tables I and II, in which the heats of immersion bear no direct relation to the amount of hydroxyl surface. In a qualitative manner, consideration may be given to the two extremes of distribution of hydroxyl sites on the surface: (1) the sites are concentrated in patches and (2) there is an even distribution of isolated single sites. Although the total number of hydroxyl sites might be the same in each case, the heat of immersion would probably be greatest when distribution (2) predominates.

Figures 2 and 3 show how the heat of immersion varies with heat treatment for a particular silica sample. In Fig. 2 the heat of immersion is given as a function of activation temperature. These determinations were made for silica A after evacuation at  $10^{-6}$  mm. Hg for 4 hours at temperatures

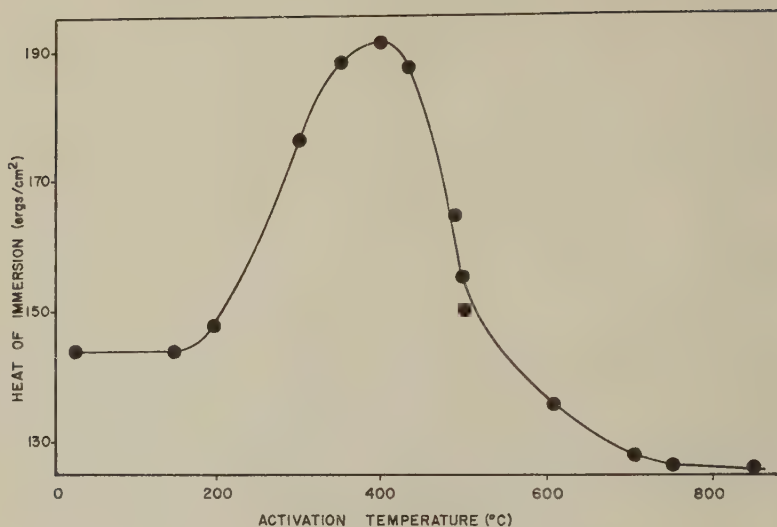


FIG. 2. Heat of immersion as a function of activation temperature.

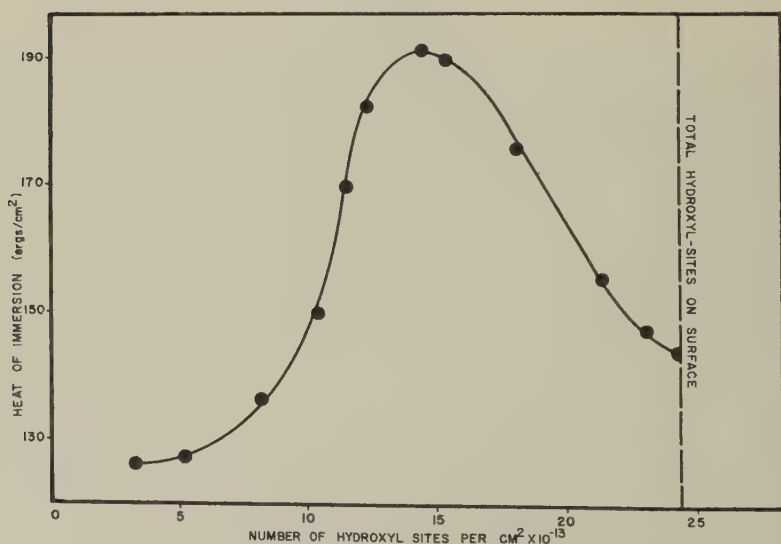


FIG. 3. Heat of immersion as a function of the number of hydroxyl sites (total hydroxyl sites on surfaces from reference 4).

ranging from 150° to 850°C. The heat of immersion is seen to remain constant up to 180°C. Above this temperature it increases, reaches a maximum at approximately 400°C., and decreases to an essentially constant value above 800°C. Other investigators (1, 2) have obtained results similar

to those given in Fig. 2. However, the temperature at which the maximum in the immersion curve occurs as well as the absolute heat of immersion values will vary depending on the nature of the silica samples.

In Fig. 3 the heat of immersion is plotted as a function of the number of hydroxyl sites on the surface after activation at various temperatures. The data for the number of hydroxyl sites had been obtained in previous work (4).

## DISCUSSION

### *Nature of the Immersion Curve*

It has been (4) shown that only physically absorbed water is removed, on heating to approximately  $180^{\circ}\text{C}.$ , from the amorphous silicas used in this work. The physically absorbed water can also be removed on evacuation for 8 hours at room temperature. Thus, the heat of immersion remains constant up to  $180^{\circ}\text{C}.$ , as illustrated in Fig. 2, since heating in this temperature range does not alter the surface. Above  $180^{\circ}\text{C}.$  dehydration of the surface silanol (hydroxyl) sites occurs. Those sites which are dehydrated in the temperature range of  $180^{\circ}$  to  $400^{\circ}\text{C}.$  may be readily rehydrated with bulk water or at a slower rate with water vapor (4). Thus, as rehydration of these condensed sites is rapid, the heat of immersion will increase with increasing activation temperatures between 180 and  $400^{\circ}\text{C}.$ , since an additional contribution to the heat of immersion will result from the rehydration of dehydrated sites. The heat of immersion is seen to decrease (Fig. 2) with activation temperatures above  $400^{\circ}\text{C}.$  Rehydration is not complete within the length of time of the immersion experiment (7) after heating above this temperature. Therefore, there is a lesser degree of hydration and hence fewer silanol sites for physical interaction with water, accounting for the decrease in the heat of immersion. Indeed, only a portion of the dehydrated sites formed by heating above  $400^{\circ}\text{C}.$  are rehydrated upon exposure to water vapor (4). This is not meant to imply that these sites may not be eventually rehydrated upon immersion in bulk water. However, the rehydration is presumably a slow rate process. Above  $800^{\circ}\text{C}.$  the heat of immersion remains practically constant. The remaining surface silanol sites are not easily condensed when this temperature is reached, and those which are condensed become more difficult to rehydrate. This is substantiated by water vapor adsorption studies presented previously (4), where it was shown that after the sample was heated to approximately  $800^{\circ}\text{C}.$  reversible rehydration did not occur upon exposing the sample to water vapor for several days.

These observations indicate a difference in rehydration between the surfaces formed upon activation of silicas at low temperatures ( $180^{\circ}$ – $400^{\circ}\text{C}.$ ) and those formed at higher temperature ( $400^{\circ}$ – $850^{\circ}\text{C}.$ ). Other investigators (8, 9) have noted that the surfaces of oxide catalysts are left in a

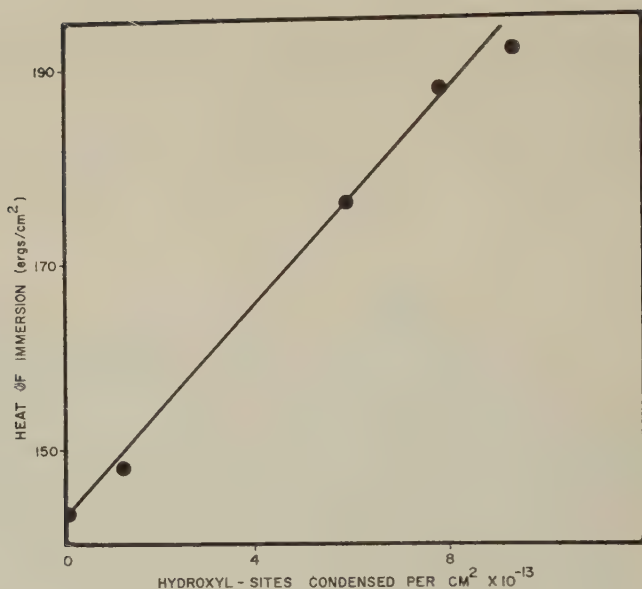


FIG. 4. Heat of immersion for the number of hydroxyl sites condensed below 400°C.

strained condition upon dehydration. This strained state would probably render the surface readily susceptible to hydration. However, at higher temperatures (400°–850°C.) the surface atoms may become sufficiently mobile to rearrange to a more stable structure. With the strain removed the surface would presumably chemisorb water only at a slow rate.

#### *Thermochemistry of Hydration*

Hydroxyl sites condensed from the surface upon activation below 400°C. are rapidly rehydrated upon exposure to liquid water. Differences between the heats of immersion (up to 400°C.) are due only to rehydration of the condensed sites. Thus, if the heat of hydration was nearly the same for all sites, a linear relationship between the heat of immersion and the number of hydroxyl sites condensed from the surface might be expected in this temperature range. Figure 4, which is a plot of the heat of immersion vs. the number of hydroxyl sites condensed, indicates that a linear relationship does indeed exist which allows a value for the heat of rehydration of the silica surface to be obtained. The slope of the line in Fig. 4 gives a value of 8.05 kcal. for each mole of hydroxyl sites replaced on the silica surface or, since one molecule of water is required for the regeneration of two hydroxyl sites, 16.1 kcal. per mole of water chemisorbed. This is more than three times the value ( $4660 \pm 230$  cal./mole of water) found by Brunauer (10). Brunauer's data, obtained from heat of solution measurements, appear consistent with surface energies he has determined for silica gel (10) and



TABLE II

Sample type and reference	Per cent hydroxyl surface	Total surface area ( $m^2/g.$ )	Heat of immersion ( $ergs/cm.^2$ )
Quartz (12)	—	0.07	810
Quartz (2)	—	0.91	450
Microsil (2)	—	5.5	290
Quartz (present work)	75	9.1	285
Flame silica (present work)	16	76	128
Santocel (13)	46	170	340
Cabosil (13) (flame silica)	25	187	180
Cabosil (2) (flame silica)	—	190	160
Flame silica (present work)	13	220	143
Silica gel (1)	Ca. 37	Ca. 275	190
Flame silica (present work)	25	420	144
Silica gel (1)	Ca. 27	Ca. 695	120

Tobermorite (11). Our flame process silicas, although possessing an initial heat of immersion similar<sup>1</sup> to the silica gels (as opposed to low-area crystalline silicas), nevertheless exhibit a rehydration behavior more like that of quartz. For example, our curves for the change in heat of immersion as hydroxyl groups are removed from the surface (these sites are then rehydrated in the immersion determination) are similar to that found by Makrides and Hackerman for quartz (2) and much more pronounced than those for silica gels (1). Thus, it appears that the heat of hydration of surface sites can vary considerably for the different types of silicas. Indeed, the data in Table II suggest that there is also a large variation in the surface energies.

#### *Nature of Silica Surfaces*

Data published by Makrides and Hackerman (2) for a number of silica samples appear to indicate that the heat of immersion (per unit area) in water varies inversely with the specific surface area. That is, those silicas with low surface areas generally have higher heats of immersion per unit area than samples with larger surface areas. This point is illustrated by the data in Table II, where heats of immersion in water are given for a variety of silicas with surface areas ranging from 0.07 to 695  $m^2/g.$  These samples were not heated above 115°C. during evacuation, and hence no appreciable removal of initial surface silanol sites has occurred. The variation in the heats of immersion for these samples cannot be explained entirely either on the basis of different amounts of hydroxyl surface available for physical interaction or by differences in hydration on immersion.

<sup>1</sup> Compared on the basis of equivalent amounts of hydroxyl surface, the heats of immersion for the flame process silicas are intermediate between those for silica gels and those for quartz.

Those samples with the larger surface areas (silica gels and flame process silicas) are usually considered amorphous, although there is evidence that the flame process silicas may possess some crystalline character (4). The low surface area samples (quartz) are crystalline, but presumably those that have been subjected to extensive grinding possess an amorphous surface layer (14, 15).

Holt and King have pointed out that when silicas are equilibrated in water or dilute acids a partial monolayer of silicic acid is adsorbed on the surface (16). Since quartz samples employed by other investigators (Table II) presumably were washed with water, it was of interest to compare these data with a quartz sample that had not been exposed to bulk water. The close agreement between the heat of immersion value for the quartz sample prepared by us by dry grinding of optical quartz crystals and those reported by Hackerman (2) for samples of similar surface area indicate that if an adsorbed silicic acid surface layer is formed during washing it does not significantly influence the heat of immersion.

The heats of immersion of the silica samples listed in Table II (which in general have either been washed with water or equilibrated with water vapor before evacuation) appear to result primarily from physical interactions between water molecules and the surface and not from hydration of the surface during the immersion process.

A part of the difference in immersion values between quartz and the amorphous silicas can be explained by the different amounts of hydroxyl surface of the various samples, but the divergence is too great to be explained entirely on this basis. Physical attractions between water molecules and a silica surface result either from dispersion (London) forces, induced polarization effects, or dipole interactions. For a polar molecule interacting with a polar surface, the contribution of the dispersion term<sup>2</sup> is usually much less than that for the polar van der Waals forces (17). Thus, the rather large differences in heats of immersion could<sup>3</sup> result from changes in the electrostatic force field associated with the surface. It is unlikely that any large variation in immersion values could arise from differences in the siloxane<sup>4</sup> portions of the surface on quartz or the amorphous silicas. The siloxane surface on both quartz and the more amorphous silicas gives rise to only weak interactions with water, insufficient to cause monolayer adsorption at the usual relative pressures. Indeed, the siloxane surface has a negligible electrostatic force field (4, 18). Therefore, the variation in

<sup>2</sup> The dispersion interaction between argon and a silica surface is not greatly different over the siloxane or silanol portions of the surface (4). It would appear that a similar situation exists for the dispersion interaction of water molecules at equivalent distances of approach to the two types of surface.

<sup>3</sup> Alternatively the greater heats of immersion of some of the quartz samples could be due to interactions arising from a porous silicic acid layer, several atoms thick. An indication that such a layer exists on some samples has been given by Hackerman (12).

<sup>4</sup> Surface Si-O-Si bridge structure.

heats of immersion shown in Table II quite probably results from differences in the electrostatic force field associated with the silanol portion of the surface of the various silica samples. This would imply that the polarity of the surface Si-OH groups changes as the silica assumes more crystalline character, perhaps owing to differences in the distribution of the silanol sites or to changes in the Si-O bond. From the limited data in Table II, it would appear that the polarity of the Si-OH bonds increased in the order:

silica gels < flame process silicas

< finely ground quartz < very low-area quartz.

#### REFERENCES

1. EGOROV, M. M., KISELEV, V. F., KRASIL'NIKOV, K. G., AND MURINA, V. V., *Akad. Nauk S.S.S.R., J. Phys. Chem.* **33**, No. 1, 1959 g.
2. MAKRIDES, A. C., AND HACKERMAN, N., *J. Phys. Chem.* **63**, 594 (1959).
3. EGOROV, M. M., KRASIL'NIKOV, K. G., AND SYSOEV, E. A., *Doklady Akad. Nauk S.S.S.R.* **108**, 103 (1956).
4. YOUNG, G. J., *J. Colloid Sci.* **13**, 67 (1958).
5. ZETTMLOYER, A. C., YOUNG, G. J., CHESSICK, J. J., AND HEALEY, F. H., *J. Phys. Chem.* **57**, 649 (1953).
6. ILER, R. K., "The Colloid Chemistry of Silica and Silicates," p. 241. Cornell Univ. Press, Ithaca, New York, 1955.
7. GUDERJAHN, C. A., PAYNTER, D. A., BERGHAUSEN, P. E., AND GOOD, R. J., *J. Phys. Chem.* **63**, 2066 (1959).
8. WEYL, W. A., *Trans. N. Y. Acad. Sci.* **12**, 245 (1950).
9. MILLS, G. A., AND HINDEN, S. G., *J. Am. Chem. Soc.* **72**, 5549 (1950).
10. BRUNAUER, S., KANTRO, D. L., AND WEISE, C. H., *Can. J. Chem.* **34**, 1483 (1956).
11. BRUNAUER, S., KANTRO, D. L., AND WEISE, C. H., Research Department Bulletin 105, Portland Cement Association, Portland, Oregon, April, 1959.
12. WADE, W. H., EVERY, R. L., AND HACKERMAN, N., *J. Phys. Chem.* **64**, 355 (1960).
13. YOUNG, G. J., AND CHESSICK, J. J., *J. Colloid Sci.* **13**, 358 (1959).
14. DEMPSTER, P. B., AND RITCHIE, P. D., *J. Appl. Chem.* **3**, 182 (1953).
15. GIBBS, J. G., RITCHIE, P. D., AND SHARP, J. W., *J. Appl. Chem.* **3**, 213 (1953).
16. HOLT, P. F., AND KING, D. T., *J. Chem. Soc.* **1955**, 773.
17. CHESSICK, J. J., ZETTMLOYER, A. C., HEALEY, F. H., AND YOUNG, G. J., *Can. J. Chem.* **33**, 251 (1955).
18. ZETTMLOYER, A. C., CHESSICK, J. J., AND HOLLABAUGH, C. M., *J. Phys. Chem.* **62**, 489 (1958).

## THE SOLUBILIZING PROPERTIES OF THE PROTEIN-DETERGENT COMPLEX

Ira Blei

*Lever Brothers Company, Research & Development Division,  
Edgewater, New Jersey*

*Received April 22, 1960*

### ABSTRACT

Solubilization of oil-soluble substances, not observed in sodium alkyl sulfate solutions below the critical micelle concentration, does occur if protein is present in the detergent solutions. The extent of solubilization was studied as a function of detergent concentration, pH, salt concentration, carbon chain length of detergent, and the structure of the dyes used. The protein detergent complex, and not an altered protein, was responsible for the solubilization of oil-soluble dyes in alkyl sulfate solutions below the critical micelle concentrations of these detergents. These experiments suggested that the form of the detergent on the protein was that of a small aggregate which had properties similar to micelles that exist above the critical micelle concentrations of pure detergent solutions.

### INTRODUCTION

The ability of polymer-surfactant complexes to solubilize oil-soluble substances in aqueous solution has been reported by Saito (1-3). He has shown that this property is common to complexes between all types of surfactants and polymers. Ekwall has also demonstrated that protein-detergent complexes can solubilize carcinogenic hydrocarbons (4). Solubilization of oil-soluble dyes by the bovine serum albumin-sodium dodecyl sulfate complex was recently reported by this laboratory (5). It is the purpose of this report to characterize the protein-detergent complex in terms of its dye solubilizing properties, and to propose a mechanism for the solubilization process.

### EXPERIMENTAL

#### *Materials*

Crystalline bovine serum albumin, purchased from Armour & Co., was used without further purification. Dyes were purchased from Eastman Organic Chemicals and were recrystallized three times from acetone-water mixtures. The dye used in the quantitative studies was *p*-aminoazobenzene (PAB). Sodium decyl and dodecyl sulfates were synthesized from pure



materials, and sodium tetradecyl and hexadecyl sulfates were purchased from the Dupont Co. and purified by repeated recrystallization from ethanol and extraction with ether. These alkyl sulfates exhibited no surface tension minima at their critical micelle concentrations. All salts used were of reagent grade and were used without purification. Dye concentrations were determined spectrophotometrically.

### *Method*

The method used to determine the amount of dye solubilized is essentially the same as that described by Kolthoff and Stricks (6). Appropriate volumes of the various reagents required were pipetted into graduated test tubes, and a charge of coarse crystals of dye was then added. The tubes were sealed, and fastened to a revolving drum in a constant-temperature water bath. After equilibrium had been attained, the tubes were arranged in an upright position in the bath and remained that way for 24 hours. The supernatant was then removed and centrifuged at 10,000 r.p.m. for about  $\frac{1}{2}$  hour. At that time, an aliquot was removed and diluted with ethanol to a final concentration of 1:1, alcohol:water. The molar extinction coefficient of para-aminoazobenzene in this solvent was  $2.25 \times 10^4$  l./mole cm. at 385  $\mu$ .

### RESULTS AND DISCUSSION

The ability of the protein-detergent complex to solubilize oil-soluble dyes was established by comparing the amount of dye solubilized by a solution containing protein plus detergent at a concentration below the critical micelle concentration of the detergent, with solutions containing protein alone and detergent alone at the same concentrations as in the protein-detergent mixture. It was found that although the protein alone solubilized some dye, the sum of the amounts solubilized by protein alone and detergent alone was less than that solubilized by the protein-detergent solution.

The solubilization of oil-soluble dyes in sodium alkyl sulfate solutions below their critical micelle concentrations, upon the addition of bovine serum albumin (BSA), may have been caused by several things. Solubilization might have been effected by the protein-detergent complex, by a protein which has been altered by detergent, or by a detergent solution altered by protein (e.g., micelles salted out by the protein). In order to explore these possibilities, the effect of pH on the solubilization was investigated. It has been shown by Klotz (7) that organic anions which are bound by BSA are dissociated from the protein above pH 11. It was believed that this is the result of the neutralization of free amino groups with consequent loss of charge of binding sites. Figure 1 is a plot of the moles of dye solubilized per mole of detergent in the system: 0.05% BSA,



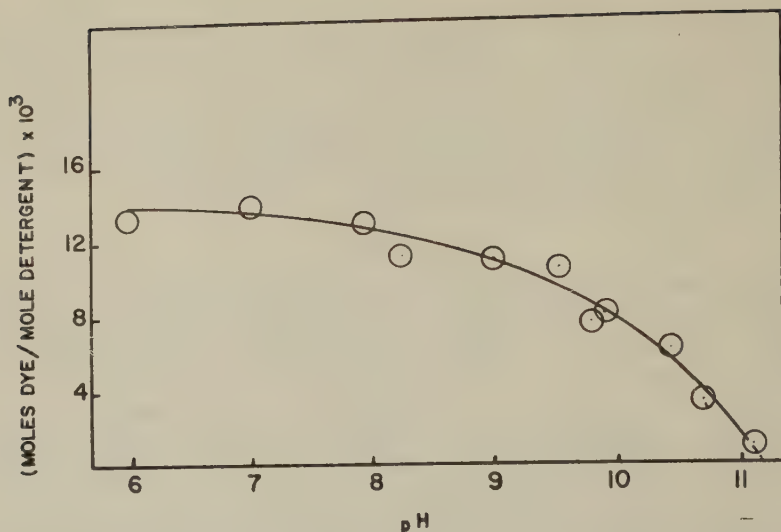


FIG. 1. The effect of pH on the solubilizing power of the bovine serum albumin-sodium dodecyl sulfate complex. All solutions contained 0.05% protein and 0.05% detergent.

0.05% sodium dodecyl sulfate, and buffer. Each solution was maintained at a constant ionic strength of 0.015. The solubilization of the dye tends towards zero at a pH slightly greater than pH 11. The data show that when the protein-detergent complex is dissociated, the solubilization ceases, indicating that it is the complex which is the solubilizing agent.

The presence of salt increased the amount of dye solubilized by the complex. This can be seen by comparing the value of moles of dye solubilized per mole of sodium dodecyl sulfate between pH 6 and pH 7 in Fig. 1, with the same quantity in the salt-free sodium dodecyl sulfate-protein system represented in Fig. 6.

This observation suggested that the effect of salt concentration and type on the binding of the sodium alkyl sulfates by BSA be studied, on the assumption that the increase in solubilizing power is, in part, a consequence of an increase in the amount of detergent bound to the protein.

The results of this study may be seen in Fig. 2. The systems studied consisted of fixed concentrations of BSA, 0.05%, and of sodium dodecyl sulfate, 0.05%. The open circles represent systems to which had been added varying concentrations of  $\text{CaCl}_2$ , the circles with line represent systems to which had been added varying concentrations of  $\text{KCl}$ . Dye was not solubilized in control solutions containing the same amounts of electrolyte alone. The increase in dye solubilized with increase in salt concentration does not follow any simple law, and it is represented as moles of dye per

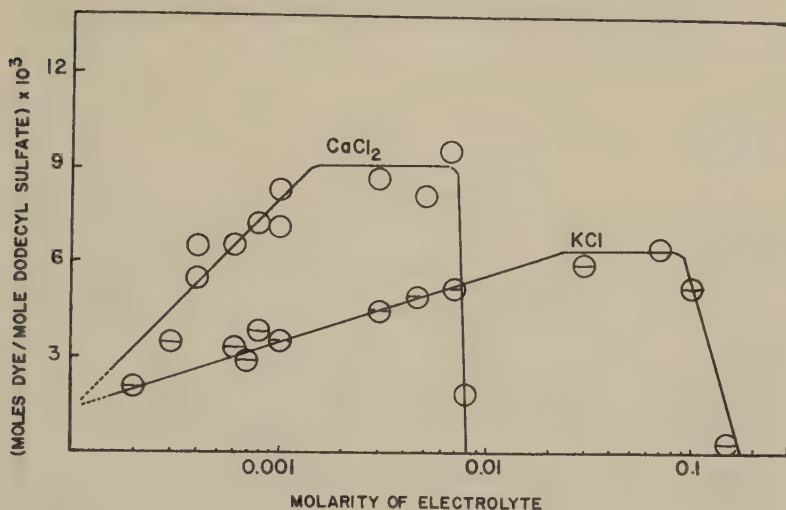


Fig. 2. The effect of electrolyte on the solubilizing power of the bovine serum albumin-sodium dodecyl sulfate complex.

mole detergent vs. log of salt concentration for graphical representation only. The amount of dye solubilized as salt concentration increased reached a maximum and then remained constant. There is a difference in the maximum amount of dye solubilized in the calcium and potassium salt systems, and in the rate at which the solubility increased as a function of salt concentration. It is probable that this is the result of several effects. The first is the salting out of the detergent due to the increase in ionic strength in solution and one would expect a divalent cation to have a greater effect than a univalent one at equal molar concentrations. Further, the charge on the complex becomes more negative as additional detergent is bound by the complex. In this event, it is probable that  $\text{Ca}^{++}$  would be more effective in reducing the net charge of the complex and would permit more detergent to be bound than the  $\text{K}^+$  salt. In addition, it has been shown (8) that the addition of salt to the protein-detergent complex causes it to assume a more compact configuration. Strauss (9) has reported that the configuration of polysoaps becomes more compact when they solubilize certain hydrocarbons. In view of this, one might attribute the increase in solubilizing efficiency to the more compact configuration of the complex in the presence of electrolyte. Beyond a critical salt concentration, dye solubilization ceases in both cases. These salt concentrations (0.0018 mole/l. and 0.13 mole/l.) may correspond to the limits of solubility of both the calcium and potassium salts of dodecyl sulfate, respectively.

The great advantage of probing colloidal systems with dyes is that their absorption spectra yield valuable information concerning the nature of

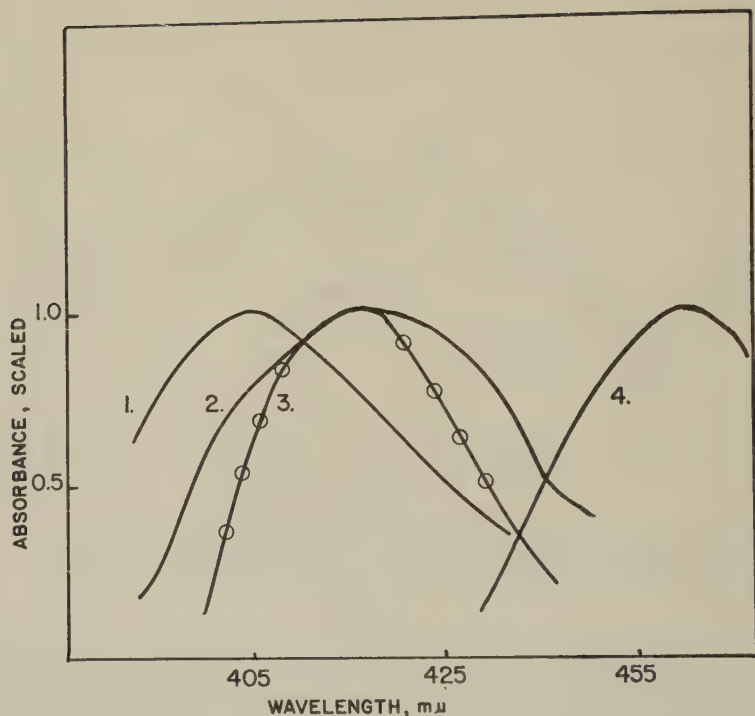


FIG. 3. Spectra of *p*-aminoazobenzene in various solvents. Curve 1, dye in water or sodium dodecyl sulfate below the CMC, 0.05%; Curve 2, dye in sodium dodecyl sulfate above the CMC, 0.5%; Curve 3, dye in 0.05% bovine serum albumin, plus sodium dodecyl sulfate below the CMC, 0.05%; Curve 4, dye in 0.5% bovine serum albumin.

their molecular environment. With this in mind, the spectra of *p*-aminoazobenzene (PAB) under various conditions were examined (Fig. 3). The maximum absorbance of the dye in each system was scaled so that each had a value of 1.0. The curve on the far left is the spectrum of PAB in water and in water containing dodecyl sulfate below the CMC. The absorption maximum is at 404  $\mu$ . The spectrum at the far right is that of PAB in 0.5% BSA. The absorption maximum here is at 460  $\mu$ . The two curves at the center have identical absorption maxima at 416  $\mu$ . The smooth curve is the spectrum of PAB in dodecyl sulfate above the CMC, and the curve with open circles is of PAB in 0.05% BSA and 0.05% dodecyl sulfate, well below the CMC. These curves indicate that the environment of dye solubilized in protein-detergent solutions below the CMC of the detergent closely corresponds with that of dye solubilized in detergent micelles above the CMC in the absence of protein.

If the dye were dissolved in micelles on the protein, the formation of

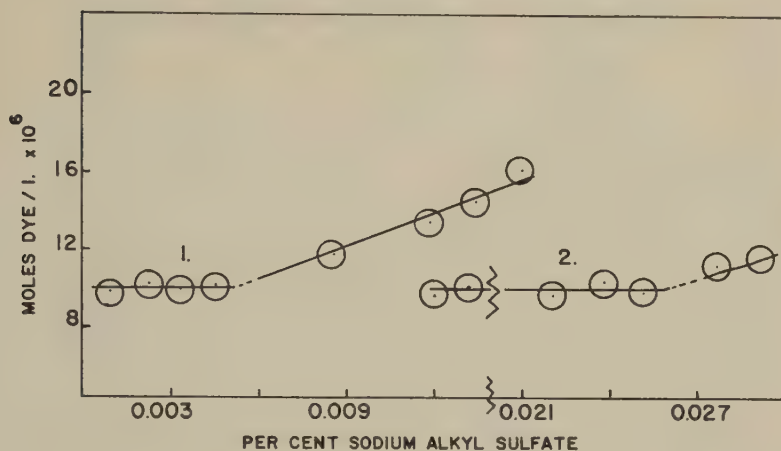


FIG. 4. Determination of the critical concentration for the formation of solubilizing complexes between bovine serum albumin, 0.05%, and sodium tetradecyl, 1, and dodecyl, 2, sulfate.

these micelles might occur at some critical concentration analogous to the CMC of detergent solutions in the absence of proteins. Experiments at low concentrations of detergent revealed that solubilization by the protein-detergent complex did not occur until a critical concentration was reached. These data may be found in Fig. 4. The intersections of the straight lines correspond to the critical concentrations for the formation of solubilizing complexes on BSA. These critical concentrations for solubilizing complex formation on the protein, were determined for decyl, dodecyl, and tetradecyl sulfates (Fig. 5). The half-filled circles represent the logarithms of the molar critical micelle concentrations of decyl, dodecyl, and tetradecyl sulfate in the absence of protein. The open circles represent the same detergent systems plus BSA. The slopes of the lines for formation of micelles in solution and for formation of solubilizing complexes are almost identical and correspond to within 4 % of the theoretical value predicted by the work of J. N. Phillips (10). This indicates that the free energy change per methylene group for both processes is comparable. On the basis of the data of Strauss and Strauss (11), for the binding of sodium dodecyl sulfate by bovine serum albumin in salt-free systems, the critical concentrations indicated in Fig. 4 for formation of dodecyl sulfate-BSA solubilizing complexes corresponded to approximately 35 moles of detergent adsorbed per mole of protein. Harrap and Schulman (8) have shown by viscosity measurements that BSA undergoes an extensive uncoiling presumably leading to denaturation at about 40 moles of sodium dodecyl sulfate bound per mole of protein. To substantiate this correlation, BSA was exposed to varying concentrations of dodecyl sulfate. The detergent was removed by dialysis

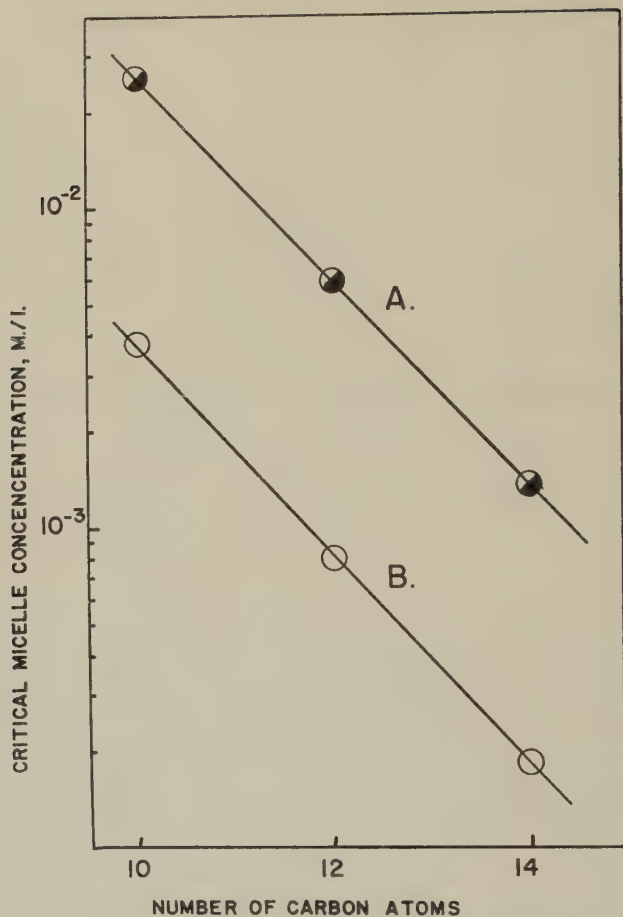


FIG. 5. Effect of carbon chain length on the critical concentration for *A*, the formation of micelles in aqueous solution, and *B*, the formation of solubilizing complexes with bovine serum albumin.

or precipitation with  $\text{BaCl}_2$ , and finally the solubility and dye adsorption characteristics of the remaining protein were measured. It was found that in those cases where the amount of dodecyl sulfate bound per mole of protein did not exceed 40, the reaction was reversible. At binding ratios greater than 40, an irreversible structural alteration, or denaturation, occurred. This was demonstrated by the fact that these recovered proteins did not bind methyl orange, and were completely precipitated from solution when the pH was adjusted to 4.7. In view of these results, the significance of the critical value of 40 moles of detergent bound per mole of protein may lie in the fact that at that point in the binding curve, an



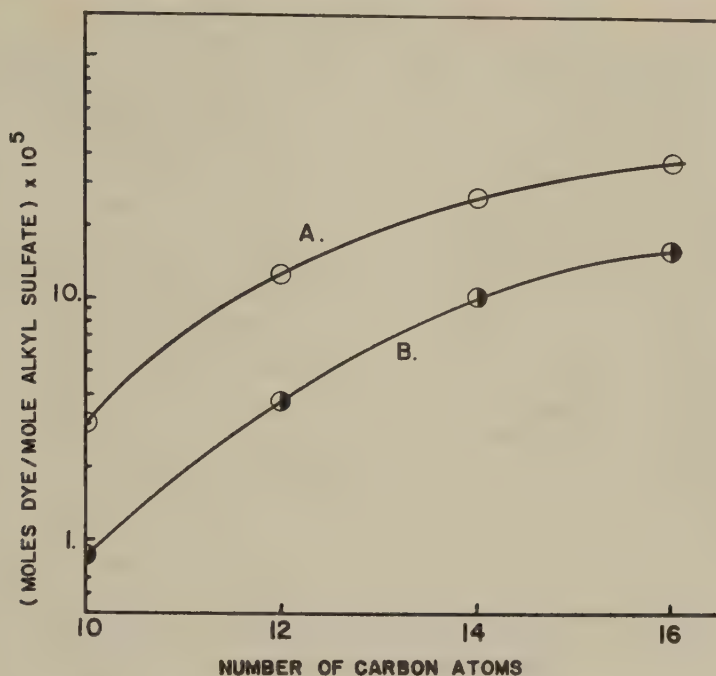


FIG. 6. The effect of carbon chain length on the solubilizing power of the sodium alkyl sulfates alone, A, and in combination with 0.05% bovine serum albumin, B, on the dye, *p*-aminoazobenzene.

irreversible uncoiling of the molecule occurs. This uncoiling may be a necessary preliminary step to the formation of solubilizing complexes. The data presented in Figs. 4 and 5 lend considerable weight to the view that above a certain critical concentration, the alkyl sulfates appear to form some sort of micelle on the protein.

In order to establish the nature of the detergent aggregates on the protein, the solubilizing capacity of the detergent on the protein was determined, as well as the solubilizing capacity of the detergent above the CMC in the absence of protein. These data are plotted in Fig. 6 as moles of dye solubilized per mole of detergent vs. the number of carbon atoms in the chain. The upper curve is that for detergent above the CMC in the absence of protein, and the lower curve is that for detergent below the CMC in the presence of 0.05% protein. The solubilizing power of the detergent below the CMC, in the presence of protein, is dependent upon the concentration of protein, reaching a maximum value which is about 75%–80% of the value for detergent solutions above the CMC in the absence of protein. The shape of the lower curve in Fig. 6 was the same for other protein concentrations and similar to that reported for the solubilization of fatty alcohols by soap solutions (12).

TABLE I

*The Effect of Variation of Structure on the Solubilization of Oil Soluble Dyes by the Bovine Serum Albumin-Sodium Dodecyl Sulfate Complex*

<u>Solubilized</u>	<u>Not Solubilized</u>

It is evident from the preceding data that the requirements for solubilization of polar hydrocarbons depend on the nature of the solubilizer and should also depend on the structure of the solubilize. Upon varying the structure of the dye which was added to the system, protein plus detergent, it was found that their solubilization was an all or none affair. Two groups of dyes are listed in Table I, those which were solubilized by the complex, and those which were not. The first of two notable features of the group which was solubilized, Group A, is that they are all, without exception, asymmetric with regard to polar groups. The group which was not solubilized, B, contains dyes which are both symmetric and asymmetric with regard to polarity. The next feature of importance is that in Group A, the parts of the molecules to the left of the polar group are colinear and are devoid of groups attached to the azobenzene nucleus. The structures of the last three dyes in Group B are in accord with the first of the two apparent requirements for solubilization, asymmetry of polar groups, but fall short of the second of the two conditions noted, that of having no groups attached to the azobenzene nucleus.

It is possible to propose a mechanism for the formation of the protein-detergent complex on the basis of the data presented above. As detergent is added to a protein solution, monomeric detergent ions are bound one at a time at cationic sites. In some critical concentration range of detergent,

below that for detergent micelle formation, two events occur. One is the loss in structural specificity of the protein or irreversible denaturation, and the other is the onset of solubilizing power of the complex because of aggregate formation around previously bound ions. These two events may or may not be related, but that question cannot be answered with the data presented here. The aggregates on the protein are similar to true detergent micelles in solution insofar as the free energy of aggregate formation per methylene group is the same, the spectra of dyes solubilized in the aggregates are similar to those of dyes in true detergent micelles, and the solubilizing power of the aggregates toward the dyes used varies with hydrocarbon chain length in the same manner as the solubilizing power of detergent micelles. There is, however, an important difference in the nature of the aggregates on the protein compared to detergent micelles. All the dyes in Table I can be solubilized by alkyl sulfate micelles. However, in order that the aggregate on the protein solubilize any of the dyes listed, the dye must be asymmetric in polarity. This indicates that the aggregate itself is probably asymmetric in the same sense, and may consist of a single palisade layer of a few molecules clustered about a binding site on the protein. Correlation of dye structure with solubilization indicates that in those cases where the azobenzene nucleus has a functional group attached, the number of chain-dye contacts is apparently insufficient to permit mixed micelle formation. Therefore, the hydrocarbon "phase" resulting from the aggregation of the alkyl chains of the detergent ions is probably not extensive. It is probable that the hydrocarbon tails of the detergent, bound in monomeric or polymeric form, are stabilized through interaction with the hydrophobic residues of amino acids along the polypeptide chain. The "loosening" of the polypeptide chains through denaturation, previously noted, probably permits a close approach of these hydrophobic residues to the bound aggregates. The interaction between the hydrophobic domain of the protein and the bound aggregates may well be the principal driving force for the denaturation of this protein by the alkyl sulfates.

#### SUMMARY

The adsorption of the sodium alkyl sulfates by bovine serum albumin was investigated by a dye solubilization technique. As a result of this study the following points were established.

1. The sodium alkyl sulfates combine with bovine serum albumin to form complexes which can solubilize oil-soluble dyes at concentrations of surfactant considerably below their normal critical micelle concentrations.
2. The spectra of dyes solubilized by the complex is very nearly the same as those of the same dyes solubilized in a conventional detergent micelle.
3. Solubilization of the dyes by the complexes does not occur until a

critical concentration of detergent is reached. In the case of sodium dodecyl sulfate, this concentration corresponds to the adsorption of 35–40 moles of detergent bound per mole of protein, at which point an irreversible structural alteration or denaturation of the protein occurs.

4. The variation of the critical concentration for the onset of solubilizing power of the protein-detergent complex with carbon chain length of the alkyl sulfate, is the same as the relationship between the critical micelle concentrations of the sodium alkyl sulfates and carbon chain length. The slopes of the plot of log CMC vs. carbon chain length for both processes agree with the theoretical value predicted by Phillips (10) to within 4%.

5. The variation of solubilizing power of the protein-detergent complex vs. carbon chain length shows the same behavior as conventional detergent micelles.

6. There appear to be two principal structural conditions required by the dyes used for solubilization by the protein-detergent complex. These are: (1) asymmetry in polarity, and (2) no functional groups attached to the linear azobenzene nucleus.

#### ACKNOWLEDGMENTS

The author wishes to express his appreciation to Drs. J. D. Justice, I. Reich, and L. J. Vinson for their advice and encouragement during the course of this work.

#### REFERENCES

1. SAITO, S., *Kolloid-Z.* **154**, 19 (1957).
2. SAITO, S., *Kolloid-Z.* **158**, 120 (1958).
3. SAITO, S., *Kolloid-Z.* **165**, 162 (1959).
4. EKWALL, P., *Biochemical Problems of Lipids*. Interscience, N. Y. 1956.
5. BLEI, I., *J. Colloid Sci.* **14**, 358 (1959).
6. KOLTHOFF, I. M., AND STRICKS, W., *J. Phys. & Colloid Chem.* **52**, 915 (1948).
7. KLOTZ, I. M., AND WALKER, F. M., *J. Am. Chem. Soc.* **69**, 1609 (1947).
8. HARRAP, B. S., AND SCHULMAN, J. H., *Discussions Faraday Soc.* **13**, 197 (1953).
9. JACKSON, E. G., AND STRAUSS, U. P., *J. Polymer Sci.* **7**, 473 (1951).
10. PHILLIPS, J. N., *Trans. Faraday Soc.* **51**, 561 (1955).
11. STRAUSS, G., AND STRAUSS, U. P., *J. Phys. Chem.* **62**, 1321 (1958).
12. MCBAIN, M. E. L., AND HUTCHINSON, E., "Solubilization and Related Phenomena." Academic Press, New York, 1955.

## LETTERS TO THE EDITOR

## A BAR VISCOMETER WITH CONICAL ANNULUS

## INTRODUCTION

The bar viscometer consisting of a cylindrical rod falling through a slightly wider cylindrical annulus in which the liquid is contained, has been described by several authors (1-3).

The increasing use of this viscometer in industrial laboratories no doubt has to be attributed to its simplicity and to the fact that high shearing stresses are obtained easily without risk of an appreciable rise in temperature.

Recently a new variant of the bar viscometer has been constructed by R. Laignou (4), who suggested the publication of the present calculation. In the new apparatus the ring has a conical bore which ensures a better centering of the bar.

The formula for the rate of fall in this instrument is somewhat different from the formula for the cylindrical annulus. Although the stress field is no longer homogeneous, the instrument can be used to measure approximate flow curves if the cone angle is not too large.

## RATE OF SHEAR AND SHEARING STRESS

Let the apparatus have the following dimensions (Fig. 1):

$r$ —radius of the falling bar;

$r_1$ —upper radius of the conical annulus;

$r_2$ —lower radius of the conical annulus;

$h$ —height of the annulus;

$$\operatorname{tg} \alpha = \frac{r_1 - r_2}{h}.$$

If the clearance between bar and ring is small enough to allow the assumption of a constant rate of shear  $D_z$  throughout one horizontal cross section at a distance  $z$  from the top we may write:

$$D_z = \frac{v}{r_1 - r - z \operatorname{tg} \alpha}. \quad [1]$$

In Eq. [1]  $v$  represents the downward speed of the bar. The shearing stress  $\tau_z$  at  $z$  is  $\eta D_z$  if  $\eta$  is the viscosity of the liquid.

Thus:

$$\tau_z = \frac{v \eta}{r_1 - r - z \operatorname{tg} \alpha}. \quad [2]$$





## REFERENCES

1. SEGEL, M., *Physik. Z.* **4**, 493 (1903).
2. POCHETTINO, A., *Nuovo cimento* **8**, 77 (1914).
3. TOLLENAAR, D., AND BISSCHOP, M. C., *J. Colloid Sci.* **10**, 151 (1955).
4. LARAIGNOU, R., Private communication.

D. TOLLENAAR

Research Institute TNO  
for Printing and Allied Industries,  
Amsterdam, Holland

Received October 28, 1959

## THE DAMPING OF VIBRATORY MOTION BY SOAP FILMS

A new technique has been developed to study liquid films which should be useful in future work on foams. Essentially the method consists of forming a soap film between the coils of a cylindrical helical spring and observing the damping effect of this film on the vibration of the spring.

The springs used for this purpose were about 1 cm. in diameter and about  $1\frac{1}{2}$  cm. in length. The first and second coils and the last and next to last coils were tied together with thread so that a continuous cylindrical film could be formed between the coils of the spring. The film was formed by dipping the entire spring into a solution of a surface-active agent. A small weight was quickly hung from the lower end of the spring and the system set into vibration by pulling the weight down a short distance and then releasing it. The vibrating spring was photographed with a motion picture camera operating at 60 frames a second. The amplitude of vibration was measured in arbitrary units, and the damping ratio was computed by taking the average ratio of the amplitude of one vibration to that of the succeeding vibration. In this manner the damping of the oscillations due to the presence of the attached soap film could be measured.

Films which were surface plastic (i.e., films the surfaces of which have a yield value and the viscosity of which is a function of the rate of shear) had a very marked dampening effect on the vibrations of the spring. For example, when a surface plastic sodium myristate film was attached to the spring the motion was nearly aperiodic so that the vibrations were damped out very rapidly after only a few cycles. Nonplastic films, on the other hand, after the same initial displacement, vibrated for as many as 20 to 30 cycles before the vibrations were damped out. However, of greater interest and importance was the fact that the damping caused by *nonplastic films* was a function of the concentration of the surface-active agent contained in the solution used to form the film. For example, solutions of pure sodium laurate

TABLE I  
*Damping of Vibrating Spring at 28° C.*

Normality of sodium laurate	0.010 <i>N</i>	0.014 <i>N</i>	0.020 <i>N</i>	0.025 <i>N</i>	0.028 <i>N</i>	0.035 <i>N</i>
Damping ratio	1.14	1.16	1.21	1.21	1.12	1.09
Frequency (cycles/second)	7.72	7.32	6.77	6.48	6.45	6.43

were prepared having concentrations in the range of 0.010 *N* to 0.035 *N*. The solutions were all found to be nonplastic and nonsurface viscous when tested by the oscillating disk (1) method at 28° C. However, when these same solutions were used to form films on the vibrating spring, differences in the rate of damping were observed. Table I shows some typical results obtained with nonplastic films. These results were obtained with a spring constructed from the hair spring of a pocket watch and gave frequencies in the range of 6.43 to 7.72 cycles per second. The observed increase in frequency with decreasing concentration is probably due to differences in the dynamic, nonequilibrium surface tensions exhibited by the vibrating films. The lowest concentration of sodium laurate which could be used was 0.010 *N* since at lower concentrations the films were so unstable that they broke almost immediately after being attached to the spring. The results reported in Table I show that as the concentration of sodium laurate was increased from 0.010 *N* to 0.035 *N* the damping ratio increased from 1.14 to a maximum of 1.21 and then decreased again to a value of 1.09. For a surface plastic film which causes essentially aperiodic motion of the spring the damping ratio would be a much higher value. In essence then, plastic films give damping ratios an order of magnitude higher than those for nonplastic films of sodium laurate, but for the latter, the rate of damping passes through a distinct maximum as the concentration is increased.

Since none of the sodium laurate solutions was surface viscous or surface plastic the change of the damping ratio with concentration must be explained on some other basis. The following explanation is suggested and is based on the increase in rate of surface tension lowering of sodium laurate solutions as the concentration increases (2). Consider a film of sodium laurate solution which is thick enough to contain an appreciable quantity of bulk liquid. If such a film is rapidly expanded the surface excess is diluted and the surface tension will increase. However, the surface-active agent dissolved in the bulk liquid of the film diffuses to the surface and reduces the surface tension. The increase in surface tension which occurs in the expanding film will be determined by the rate at which the film is extended and by the rate of surface tension lowering. The rate of surface tension lowering is in turn a function of the concentration of the surface active agent and will in general increase as the concentration increases.

Consider now the vibrating spring with its attached soap film. If the film contains a low concentration of surface-active agent the rate of surface tension lowering is relatively slow. There will be an increase in surface tension as the film is extended and after the spring reaches its maximum extension and contracts, the value of the surface tension will go back through essentially the *same* series of values that the film exhibited on expansion because of the low rate of surface tension lowering manifested under these conditions. Such a system would be truly elastic and the damping of the spring would be low since it is due only to the natural damping of the spring and to viscous effects in the film.

Consider next the case where the film contains a high concentration of surface-active agent and has a relatively high rate of surface tension lowering. As the film is extended the surface tension will remain essentially constant at its initial value because of the high rate of surface tension lowering exhibited by the film. Similarly on contraction the surface tension will remain essentially constant. Since there is no difference in the surface tension on expansion and contraction of the film the damping will be low in this case also.

Finally, consider the case where the film contains an intermediate concentration of surface-active agent so that the rate of surface tension lowering is moderate. On extension of the film the surface tension will go through a series of increasing values. When the film contracts, however, the surface tension will *not* go back through the same series of values since the surface-active agent has been continuously diffusing to the interface. Consequently the work done in expanding the film against surface tension forces will not be regained when the film contracts. This dissipation of energy results in a marked damping of a spring and its attached film when the concentration of the surface-active agent is moderate. It is suggested that the experimentally observed maximum damping which occurs with films containing intermediate concentrations of the surface-active agent can be accounted for by the mechanism described above. Furthermore, these experiments are evidence showing the existence of dynamic surface tensions in films whose surface area is rapidly being altered. Consequently these experiments tend to substantiate the idea that films possess a time-dependent elasticity which is an important factor in determining their stability.

#### REFERENCES

1. BURCIK, E. J., AND NEWMAN, R. C., *J. Colloid Sci.* **12**, 10 (1957).
2. BURCIK, E. J., *J. Colloid Sci.* **5**, 421 (1950).  
*College of Mineral Industries,  
The Pennsylvania State University,  
University Park, Pennsylvania*

EMIL J. BURCIK  
ROBERT C. NEWMAN

*Received November 20, 1959*





# ADVANCES IN CATALYSIS AND RELATED SUBJECTS

*Edited by* D. D. ELEY, P. W. SELWOOD, *and* PAUL B. WEISZ  
**Volume 12**

*July 1960, about 380 pp., illus.*

**Molecular Specificity in Physical Adsorption**

By D. J. C. Yates

**The Use of X-Ray K-Absorption Edges in the Study of Catalytically Active Solids**

By Robert A. Van Nordstrand

**The Electron Theory of Catalysis on Semiconductors**

By Th. Wolkenstein

**The Wave Mechanics of the Surface Bond in Chemisorption**

By T. B. Grimley

**Magnetic Resonance Techniques in Catalytic Research**

By D. E. O'Reilly

**Base-Catalyzed Reactions of Hydrocarbons**

By Herman Pines and Luke A. Schaap

AUTHOR INDEX—SUBJECT INDEX.

*Previously published:*

**Vols. 1-8, 1948-1956, each \$10.00**

**Vol. 9, 1957, 847 pp., \$16.00**

**Vol. 10, 1958, 326 pp., \$11.00**

**Vol. 11, 1959, 384 pp., \$12.50**



**ACADEMIC PRESS, NEW YORK AND LONDON**

111 Fifth Avenue, New York 3, New York

17 Old Queen Street, London, S.W. 1

# Journal of

*Editor-in-chief:* J. C. Kendrew,  
Peterhouse, Cambridge, England

VOLUME 1 1959, \$14.00

- Geoffrey Zubay and Paul Doty. The Isolation and Properties of Deoxyribonucleoprotein Particles Containing Single Nucleic Acid Molecules
- V. Moses, O. Holm-Hansen, J. A. Bassham and M. Calvin. The Relationship between the Metabolic Pools of Photosynthetic and Respiratory Intermediates
- I. M. Dawson and D. H. Watson. An Electron Microscope Study of the Structure of Crystalline Ribonuclease
- Robert L. Sinsheimer. Purification and Properties of Bacteriophage  $\phi$ X174
- Robert L. Sinsheimer. A Single-Stranded Deoxyribonucleic Acid from Bacteriophage  $\phi$ X174
- D. W. Green and R. Aschaffenburg. Twofold symmetry of the  $\beta$ -lactoglobulin Molecule in Crystals
- M. S. Santanam. Calcification of Collagen
- Pauline M. Harrison. The Structures of Ferritin and Apoferritin: Some Preliminary X-Ray Data
- C. O. Doudney and F. L. Haas. Gene Replication and Mutation Induction in Bacteria
- R. W. Horne, S. Brenner, A. P. Waterson, P. Wildy. The Icosahedral Form of an Adenovirus
- Ernest Freese. The Specific Mutagenic Effect of Base Analogues on Phage T4
- Jacques R. Fresco. Polynucleotides II: The X-Ray Diffraction Patterns of Solutions of the Randomly Coiled and Helical Forms of Polyriboadenylic Acid
- Benjamin D. Hall and Paul Doty. The Preparation and Physical Chemical Properties of Ribonucleic Acid from Microsomal Particles
- V. Luzzati and A. Nicolaieff. Etude par Diffusion des Rayons X aux Petits Angles des Gels d'Acide Désoxyribonucléique et de Nucléoprotéines: (Note Préliminaire)
- Gunter S. Stent, Gordon H. Sato and Niels K. Jerne. Dispersal of the Parental Nucleic Acid of Bacteriophage T4 among its Progeny
- Endre A. Balazs, Aksel A. Bothner-By and John Gergely. Proton Magnetic Resonance Studies on Water in the Presence of Various Macromolecular Substances
- R. E. Burge and R. D. Hynes. The Thermal Denaturation of Collagen in Solution and its Structural Implications
- Arthur B. Pardee, François Jacob and Jacques Monod. The Genetic Control and Cytoplasmic Expression of "Inducibility" in the Synthesis of  $\beta$ -galactosidase by *Escherichia coli*
- M. H. F. Wilkins, G. Zubay and H. R. Wilson. X-Ray Diffraction Studies of the Molecular Structure of Nucleohistone and Chromosomes
- Geoffrey Zubay. The Transition between Straight and Coiled-Coil Configurations of the  $\alpha$ -Helix
- Richard S. Morgan and Raymond Byrne. "Alkaline" Polyadenylic Acid
- Hideo Kon and Norman Davidson. Nuclear Magnetic Relaxation of Water Protons by Ferrihemoglobin and Ferrimyoglobin
- Cecil E. Hall, Elizabeth C. Maclean and Irwin Tessman. Structure and Dimensions of Bacteriophage  $\phi$ X174 from Electron Microscopy
- Ellen Borenfreund, Herbert S. Rosenkranz and Aaron Bendich. Studies on Deoxyribonucleic Acid after Exposure to Tritium Gas
- Masayasu Nomura and J. D. Watson. Ribonucleoprotein Particles within Chloromycetin-Inhibited *Escherichia coli*
- Robert L. Sinsheimer. Is the Nucleic Acid Message in a Two-Symbol Code?

# Molecular Biology

*Editorial Board:* P. Doty, A. F. Huxley, R. L. Sinsheimer,  
J. D. Watson, M. H. F. Wilkins

- A. Tissières, J. D. Watson, D. Schlesinger and B. R. Hollingworth. Ribonucleoprotein Particles from *Escherichia coli*
- R. W. Horne, G. E. Russell and A. R. Trim. High Resolution Electron Microscopy of Beet Yellows Virus Filaments
- P. F. Spahr and A. Tissières. Nucleotide Composition of Ribonucleoprotein Particles from *Escherichia coli*
- Marianne Grunberg-Manago. Phosphorolyse et Configuration Macromoléculaire des Polyribonucleotides biosynthétiques et des Acides Ribonucléiques
- Gebhard Koch and A. D. Hershey. Synthesis of Phage-Precursor Protein in Bacteria Infected with T2
- Kenneth M. Smith and G. J. Hills. Further Studies on the Electron Microscopy of the *Tipula* Iridescent Virus
- S. Brenner, G. Streisinger, R. W. Horne, S. P. Champe, L. Barnett, S. Benzer and M. W. Rees. Structural Components of Bacteriophage
- John W. Donovan, Michael Laskowski, Jr. and Harold A. Scheraga. Carboxyl Group Interactions in Lysozyme
- Thomas L. Hayes, Jack C. Murchio, Frank T. Lindgren and Alex. V. Nichols. A Determination of Lipoprotein Molecular Weight by use of the Electron Microscope
- Sandford Lacks and François Gros. A Metabolic Study of the RNA-Amino Acid Complexes in *Escherichia coli*
- Benjamin S. Friesen and Robert L. Sinsheimer. Partition Cell Analysis of Infective Tobacco Mosaic Virus Nucleic Acid
- C. E. Hall and H. S. Slayter. Electron Microscopy of Ribonucleoprotein Particles from *Escherichia coli*
- R. W. Horne and J. Nagington. Electron Microscope Studies of the Development and Structure of Poliomyelitis Virus
- E. A. Barnard and W. D. Stein. Histidine Residue in the Active Center of Ribonuclease. I: A Specific Reaction with Bromoacetic Acid
- W. D. Stein and E. A. Barnard. Histidine Residue in the Active Center of Ribonuclease. II: The Position of this Residue in the Primary Protein Chain
- Kazutomo Imahori and Jiro Tanaka. Ultraviolet Absorption Spectra of Poly-L-Glutamic Acid
- A. Tissières. Some Properties of Soluble Ribonucleic Acid from *Escherichia coli*
- Murray Vernon King. The Unit Cell and Space Group of Cubic Glucagon
- J. Weigle, Matthew Meselson and Kenneth Paigen. Density alterations Associated with Transducing Ability in the Bacteriophage Lambda
- R. D. B. Fraser and T. P. MacRae. Molecular Organisation in Feather Keratin
- C. R. Worthington. Large Axial Spacings in Striated Muscle
- M. F. Perutz, L. K. Steinrauf, Anne Stockell and A. D. Bangham. Chemical and Crystallographic Study of the two Fractions of Adult Horse Haemoglobin
- Index.



ACADEMIC PRESS, London and New York

*A New Journal*

*... serving biochemistry, biophysics, and  
related areas of experimental biology*

# Analytical Biochemistry

*Volume 1, Number 1, June 1960*

AN INTERNATIONAL JOURNAL

*Edited by* ALVIN NASON

ADVISORY BOARD

SAMUEL P. BESSMAN  
HARRY P. BROQUIST  
MELVIN CALVIN  
OSAMU HAYAISHI  
ROLLIN D. HOTCHKISS  
WALTER L. HUGHES  
VERNON M. INGRAM  
OLOV LINDBERG  
HUGH J. McDONALD  
EDWARD F. MacNICHOL, Jr.  
MANFRED M. MAYER  
HOWARD K. SCHACHMAN  
DONALD D. VAN SLYKE  
SIDNEY UDENFRIEND  
THEODOR WIELAND  
LEMUEL D. WRIGHT

ANALYTICAL BIOCHEMISTRY is intended to serve as a central, international source of information on new and improved methods in the various fields of biochemistry, biophysics, and related areas of experimental biology. It is designed to meet the need for a publication devoted solely to papers describing methods in these areas.

The new journal will publish detailed accounts of fundamental contributions on analytical and preparative procedures. It will include papers on qualitative and quantitative techniques based on chemical, physical, and biological principles; methods of preparation, purification, characterization, isolation and separation of biological substances and related materials; and instrumentation.

Short communications will also be considered.

Manuscripts and queries concerning editorial policy should be sent to the Editor,

DR. ALVIN NASON  
McCollum-Pratt Institute  
The Johns Hopkins University  
Baltimore 18, Maryland

Subscription orders should be sent to the publishers.

*Volume 1, 1960, \$15.00*



ACADEMIC PRESS, *New York and London*

111 Fifth Avenue, New York 3

17 Old Queen Street, London, S.W. 1



## THE TURBIDIMETRIC PRECIPITATION TITRATION OF POLYSTYRENE

A. R. Mathieson

*Department of Textile Industries, The University, Leeds 2, England*

*Received March 1, 1959; revised June 24, 1959*

### ABSTRACT

The turbidimetric precipitation titration of 7 fractions of polystyrene in the molecular weight range 39000 to 740000 has been studied, and the experimental requirements for reproducibility established. Calibration equations relating (a) the concentration of precipitated polymer to the optical density, (b) the initial precipitation point and the point of half precipitation to the polymer concentration and molecular weight, (c) the concentration of polymer remaining in solution to the volume fraction of precipitant added, have been established for toluene solutions with methanol precipitant. These equations allow the molecular weight distribution of polydisperse polystyrenes to be calculated from their turbidimetric precipitation curves. Good agreement is shown between molecular weight distributions obtained by this procedure and those obtained gravimetrically. The relation between optical density and precipitate concentration is not linear, and cannot be linearized by use of the Rayleigh refractive index correction. The precipitate consists of coacervate drops of size from  $1\mu$  downwards. The precipitation curves of mixtures of fractions are almost additive in precipitate concentration, indicating very little interaction between polymer molecules of different sizes. The point of half precipitation is a constant multiple (1.23 in mole fraction) of the initial precipitation point for all molecular weights and concentrations.

### INTRODUCTION

Turbidimetric precipitation titration is a very useful rapid method for determining the molecular weight distribution of polydisperse polymers. Bronsted (1) devised the method, and Morey and Tamblyn (2), who made the first detailed application, studied solutions of cellulose acetate-butyrate in acetone precipitated by ethanol-water mixtures, and they established the general conditions under which the suspended polymer-rich phase is stable enough for its optical transmission to remain constant. Using well-fractionated polymers they obtained a calibration relationship between the concentration of precipitant which just causes precipitation and the concentration and molecular weight of the polymer fraction. From this relationship they worked out a method for calculating the molecular weight distribution of a polydisperse polymer from its turbidimetric precipitation curve which gave good agreement with the molecular weight distribution determined gravimetrically. They assumed (a) the optical density of the



suspensions is proportional to the concentration of precipitated polymer; (b) a small amount of precipitate from a polydisperse polymer is of uniform molecular weight; (c) the fractions used for calibration are monodisperse; (d) the precipitation of one molecular species is uninfluenced by the presence of others. Although these assumptions are not strictly justified, the method was successfully applied also to nitrocellulose (3), polymethylmethacrylate (4), and polyvinylpyrrolidone (5), although for the latter it was experimentally shown that the optical density is not directly proportional to the concentration of precipitated polymer and a calibration curve was used.

A new method of calculating the molecular weight distribution from turbidity curves without assuming the sharpness of successive fractions or the monodispersity of the calibrating fractions was described by Claesson (6), and Scholtan (7) compared the Morey and Tamblyn and the Claesson evaluation methods with a new empirical method based on nomograms for polyvinylpyrrolidone. Fair agreement was obtained for this polymer (8) between the molecular weight distribution determined by turbidimetric precipitation and that calculated using Schulz's theory of fractionation (9), although distribution curves steeper on the high molecular weight side than those determined gravimetrically have been obtained (10). Turbidimetric precipitation titration has also been used in a more empirical way to study block (11) and graft (12) copolymers, to compare the properties of nucleic acids isolated from different sources (13), and to estimate the efficiency of fractionation by a zone-melting process (14).

The advantages of the method are its rapidity and the use of very small amounts of polymer in very dilute solution, but it can be used only for systems which have been calibrated. Extension of the method to polystyrene seemed desirable and the opportunity was taken to study the precipitation behavior from the standpoint of the assumptions required to calculate molecular weight distributions from the turbidity data.

## EXPERIMENTAL

### *Materials*

A sample of polystyrene which had already been fractionated into seven fractions was obtained through the kindness of Dr. A. Dijkstra. The properties of this polymer and of fractions obtained from it in the same way are well understood (15, 16). Toluene (B.D.H. sulfur-free) and methanol (Analar) were not further purified for the precipitation titrations, but for light scattering the toluene was dried over sodium and fractionated.

### *Molecular Weights*

Weight-average molecular weights of the polystyrene fractions dissolved in toluene were measured using a Brice-Phoenix 1000 series light-scattering photometer in conjunction with a differential refractometer and

light of wavelength 436 m $\mu$ . The dissymmetry method was used. Solvent was clarified by distillation and filtration through a sintered glass, and solutions by centrifugation at 25000 *g*. Cells and dust-free pipets were freed from dust using apparatus built to the design of Thurmond (17).

### *Turbidimetric Precipitation Titrations*

Polymer solutions in toluene in the concentration range 0.012 to 0.0003 grams per 100 ml. were used, since more concentrated solutions gave unstable suspensions and weaker solutions gave optical densities which were too small. Optical densities were measured using a Hilger Spekker with blue filters and 4 cm. glass cells of 25 ml. capacity. Twenty-five milliliters of polymer solution was used, and methanol precipitant was added rapidly from an automatic microburet with gentle hand stirring. Precipitant was added in 1 ml. aliquots until within 1 ml. of the commencement of precipitation, when 0.1 ml. aliquots were added until 50% precipitation, and 0.5 and 1.0 aliquots were then used until precipitation was complete. All the precipitation experiments were performed in a room kept at 21°C. but were not otherwise thermostated. With this procedure the optical densities were stable, remaining constant to 1% over at least 30 minutes, much longer than the time taken for titration, and the turbidimetric precipitation curves were reproducible to  $\pm 0.002$  in the optical density, representing  $\pm 0.2\%$  for optical densities of 1.0 and  $\pm 2\%$  for 0.10. The solutions had a very small optical density, about 0.01, before precipitation, and this value was determined and subtracted from the optical densities obtained during precipitation.

This standard procedure was evolved from a consideration of previous experimental methods and from a series of trial experiments in which the method was varied. In these experiments it was shown that (a) mechanical stirring renders the suspension unstable with progressive lowering of the optical density, previously observed (2, 4); (b) addition of 0.1 ml. aliquots of precipitant gives higher optical densities than addition of 0.5 or 1.0 ml. up to 50% precipitation, but thereafter addition of 0.1, 0.5, or 1.0 ml. gives the same optical density; (c) the use of aliquots of precipitant less than 0.1 ml. gives the same optical density as 0.1 ml.; (d) 0.5 ml. aliquots give the same result as 1.0 ml.; (e) the same result is obtained whether the buret tip is below the liquid surface or not; (f) the initial precipitation point is unaffected by all these variations of procedure. Exact definition of the experimental conditions is necessary to obtain reproducibility, and the calibration equations can strictly be applied only to experiments carried out as described here.

### *Separation and Analysis of the Turbid Suspensions*

Precipitation experiments beginning with 250 ml. of polymer solution were made, and at suitable intervals 100 ml. samples were withdrawn and

centrifuged at 9000 *g*. Eighty milliliters of the clear supernate were evaporated and heated at 120°C. to constant weight over 6 to 7 days. Appropriate blanks were performed on solvent-precipitant mixtures, and checks were made using solutions of known concentration containing no precipitate. The weight of polymer precipitated corresponding to the optical density was calculated.

## PRECIPITATION OF POLYSTYRENE FRACTIONS

### *Molecular Weights of the Fractions*

The weight-average molecular weights of the 7 fractions determined by light scattering were: fraction 1, 39000; fraction 2, 99000; fraction 3, 203000; fraction 4, 225000; fraction 5, 475000; fraction 6, 530000; fraction 7, 740000.

### *Turbidimetric Precipitation Titration of the Fractions*

The turbidimetric precipitation curve of each polymer fraction was determined at 5 or 6 initial polymer concentrations covering the whole possible range. Figure 1 shows typical results obtained for fraction 7 up to maximum optical density. The precipitate always forms a liquid coacervate, and the total volume of this precipitated phase is always less than

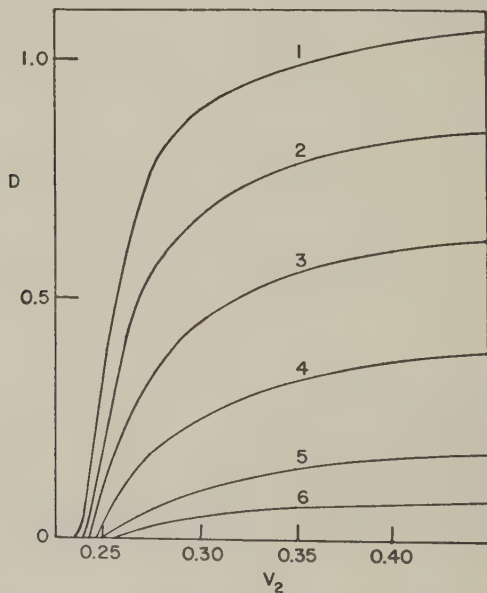


FIG. 1. Turbidimetric precipitation titration curves of fraction 7. (1)  $C_0 = 0.01184$ ; (2)  $C_0 = 0.00600$ ; (3)  $C_0 = 0.00296$ ; (4)  $C_0 = 0.00148$ ; (5)  $C_0 = 0.00074$ ; (6)  $C_0 = 0.00037$ .

0.2% of the total volume of the mixture even for complete precipitation of the most concentrated solutions examined. Allowing for the dilution of the polymer solution by precipitant, precipitation was complete for fraction 1 when the volume fraction of methanol reached 0.55. Higher molecular weight fractions required less methanol, and for a given polymer fraction solutions of lower concentration needed more methanol. For the most concentrated solution of fraction 7 examined precipitation began when the volume fraction of methanol was 0.235, and for the most dilute solution of fraction 1, at 0.344.

### *Notation and Symbols*

To describe the results the following symbols are required:

$v_1, v_2$ , volume fractions of toluene and methanol, respectively.

$(v_1)_0, (v_2)_0$ , volume fractions of toluene and methanol when precipitation just begins (initial precipitation point).

$C_0$ , concentration of polymer in the original toluene solution (grams per 100 ml.).

$C$ , concentration of polymer remaining unprecipitated at any point during the titration.

$C_{(v_2)_0}$ , concentration of polymer at the initial precipitation point.

$C_p$ , concentration of precipitated polymer, reckoned per total volume of solution.

$\bar{v}_2$ , volume fraction of methanol when half the polymer is precipitated.

$(v_2)_{1/2}$ , volume fraction of methanol when the concentration of polymer remaining unprecipitated is half its value at the initial precipitation point, i.e., when  $C = \frac{1}{2}C_0(v_1)_0 = \frac{1}{2}C_{(v_2)_0}$ .

$D$ , optical density of the turbid suspensions (minus that of the original toluene solution).

It is assumed in calculating  $v_1$  and  $v_2$  that the excess volume of mixing of toluene and methanol, and the volume fraction of the polymer are negligible. All polymer concentrations are expressed in grams per 100 ml. of the whole solution unless otherwise stated. Superscript  $i$  denotes the  $i$ 'th polymer fraction.

### *Relation of Optical Density to Amount of Precipitation*

Using fractions 2, 3, 5, 7, the amounts of polymer precipitated were determined by centrifugation and analysis for various optical densities during the course of precipitation. Values of the optical density at complete precipitation when the concentration of precipitated polymer is known, were obtained for these fractions at several initial concentrations. A given optical density always corresponds to the same concentration of precipitated polymer  $C_p$  irrespective of the initial polymer concentration and independently of the molecular weight of the polymer fraction. The optical



density gives therefore a true measure of the concentration of precipitated polymer valid for all polystyrenes under the experimental conditions, but the relationship is not one of simple proportionality.  $\log D$  plotted against  $\log C_p$  gives a smooth curve (Fig. 2) over the whole concentration range which approximates to  $C_p \propto D^2$  at high concentrations and to  $C_p \propto D$  at low concentrations. The whole curve can, however, be described by the single relation valid for all concentrations, optical densities, and molecular weights:

$$\log C_p = \frac{\log D}{0.35 - 0.45 \log D} - 2.31; \quad [1]$$

and results show a linear plot of  $1/\log D$  against  $1/(\log C_p + 2.31)$  from this equation. Equation [1] will be used throughout to obtain concentrations of precipitated polymer from measurements of optical density. It holds also for mixtures of fractions (q.v.).

The cause of this departure from linearity of the relation of  $C_p$  and  $D$  is not clear. For particles small compared to the wavelength ( $\lambda$ ) of incident light, the Rayleigh scattering equations hold and if  $I$ ,  $I_0$  are the intensities of incident and transmitted light, respectively, may be written

$$D = -\log I/I_0 = -\frac{24\pi^3 NV^2 L}{\lambda^4} \left( \frac{n^2 - n_0^2}{n^2 + 2n_0^2} \right)^2,$$

where  $V$  is the volume of a particle,  $N$  is the number of particles per milliliter,  $L$  is the path length through the medium, and  $n$  and  $n_0$  are the refractive indices of the particles (considered transparent) and the medium, respectively. Since  $n_0$  changes throughout the titration (at 20°C.,  $n(\text{toluene}) = 1.4968$  and  $n(\text{methanol}) = 1.3291$ ), it might be profitable to correct the observed  $D$  values back to a standard refractive index as has been suggested (2). However, for these polystyrene suspensions the particle

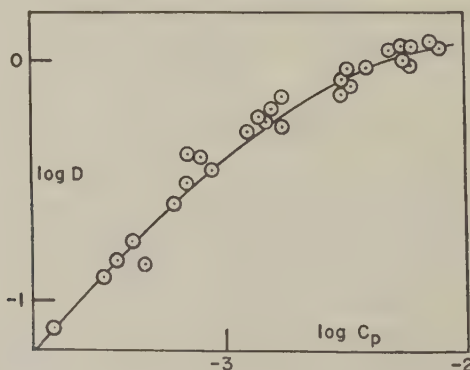


FIG. 2. Relation of optical density to concentration of precipitated polymer.



size is not small compared with the wavelength. Microscopical examination showed that the particles are coacervate droplets covering a wide range of size from about  $1\mu$  downwards (see also reference 13), so the Rayleigh equations are not likely to apply. Further, the coacervate suspension particles presumably consist of a concentrated solution of polystyrene in toluene with a small amount of methanol, of unknown refractive index and possibly with a composition which varies during the titration. Nevertheless the applicability of the refractive index correction was tested for two (presumably) limiting values of  $n$  as 1.585 (polystyrene) and 1.4968 (toluene), and the  $D$  values corrected to  $v_2 = 0.235$  were plotted against  $C_p$ . The plots were still nonlinear and the scatter was worse than for the uncorrected  $D$  values, being almost random for  $n = 1.4968$ .

The treatment of Mie (18) may be applicable but the computational difficulties, involving a continuously varying value of  $n/n_0$ , make it unprofitable. This treatment predicts a complex dependence of the scattered intensity on particle size which has been confirmed experimentally (19), and it may be that in this system the size of the particles formed depends on the composition of the mixture. The best alternative seems to be to employ the empirical relation of Eq. [1] to obtain concentrations of precipitated polymer from the experimental  $D$  values.

#### *The Initial Precipitation Point*

The initial precipitation point  $(v_2)_0$  was determined for each polymer fraction at several concentrations from the turbidimetric precipitation curves. It represents the value of  $v_2$  when the largest molecules present in the polymer fraction just become insoluble at the concentration of polymer prevailing at that stage of the addition of precipitant. For each polymer fraction

$$(v_2)_0^i = 0.210 - k \log C^i; \quad [2]$$

and Fig. 3 shows  $(v_2)_0^i$  plotted against  $\log C^i$ . The value of  $k$  depends on the molecular weight of the polymer fraction (Fig. 4) such that

$$(v_2)_0^i = 0.210 - (0.147 + 0.0230 \log 1/M^i) \log C^i. \quad [3]$$

Equation [3] for polystyrene may be compared with corresponding equations for other polymers. For cellulose acetate-butyrate (2), polymethylmethacrylate (4), and polyvinylpyrrolidone (5), in the same notation,

$$(v_2)_0^i = k \log C^i + f(M),$$

and for polymethylmethacrylate  $\log f(M)$  is linear in  $\log M$  but this is not so for polyvinylpyrrolidone (4), for which  $(v_2)_0^i$  is linear in  $\log M$  for small values of  $M$  but more nearly proportional to  $1/M$  over a large range of molecular weight (10). Elsewhere  $(v_2)_0^i$  for polyvinylpyrrolidone is given

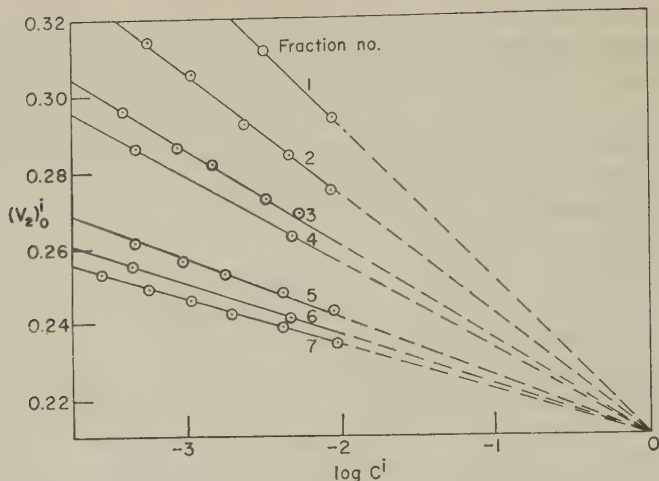


FIG. 3. Effect of concentration on the initial precipitation point.

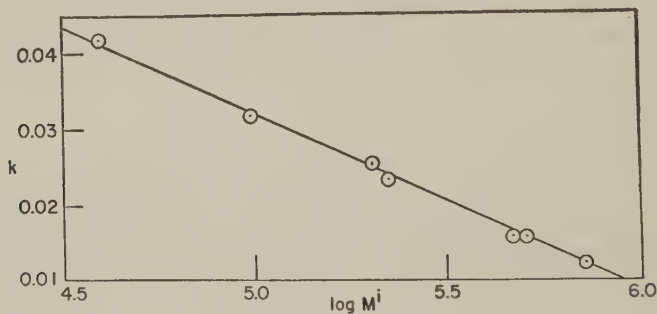


FIG. 4. Effect of molecular weight on the initial precipitation point ( $k$  from Eq. [2]).

as proportional to  $1/M^{0.8}$  and including a constant term like that in Eq. [3] (7). Schulz's theory of fractionation (9) leads to

$$(v_2)_0^i = K_0 + K_1 \log C^i/M^i + K_2/M^i,$$

which resembles Eq. [3] more than the other empirical expressions.

Plots of  $D$  against  $C$  made by diluting a suspension with solvent of the same composition cannot be expected to be linear, not only because of the nonlinear relation of  $D$  and  $C_p$ , but also because  $D$  becomes zero at finite concentrations owing to the effect of  $C$  on  $(v_2)_0$ . Figure 5 shows such plots for fraction 5 at various values of  $v_2$ . The curves extrapolate to the value of  $C$  corresponding to  $v_2$  as  $(v_2)_0$  according to Eq. [2] and [3] and form an additional check. For sufficiently high values of  $v_2$  the extrapolation is very close to zero on the particular scale of the abscissa of Fig. 5.

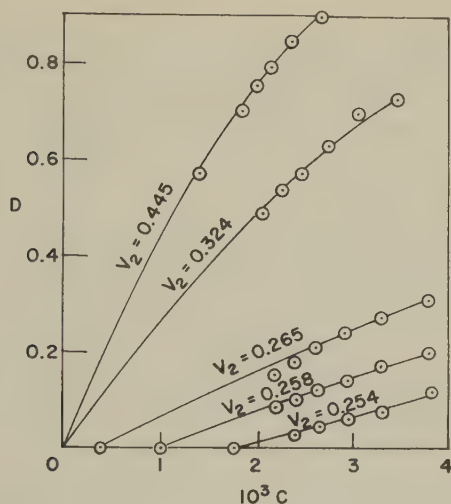


Fig. 5. Effect of dilution on optical density.

#### *Equation of the Precipitation Curves*

The turbidimetric precipitation curves of  $D$  versus  $v_2$  (e.g., Fig. 1) for fractions 2, 3, 5, 7 were converted into curves of  $C$  against  $v_2$  using Eq. [1] and  $C = C_0 v_1 - C_p$ . Figure 6 shows  $\log C^i$  against  $\log v_2$ , and the relation

$$\log C^i / C_{(v_2)_0}^i = -3.3 \log [v_2 / (v_2)_0] \quad (v_2 > (v_2)_0) \quad [4]$$

holds for all concentrations of all 4 polymer fractions. Equation [4] is considered to describe the precipitation curves of all polystyrene fractions at the accessible concentrations. It depends on molecular weight insofar as  $(v_2)_0$  is a function of molecular weight according to Eq. [3]. If  $(v_2)_0$  only is determined the whole precipitation curve may still be constructed using Eq. [4].

#### *The Point of Half Precipitation*

More truly representative of the polymer fraction than its initial precipitation point is the volume fraction of precipitant when half the polymer is precipitated,  $\bar{v}_2$ , or the volume fraction of precipitant when the concentration of polymer remaining unprecipitated is reduced to half its value at the initial precipitation point,  $(v_2)_{1/2}$ . From Eq. [4],

$$(v_2)_{1/2} = 1.23 (v_2)_0, \quad [5]$$

and since  $C_0 = C_{(v_2)_0} / (v_1)_0$ ,

$$\bar{v}_2 = (v_2)_{1/2} ((v_1)_0 / \bar{v}_1)^{0.303}. \quad [6]$$

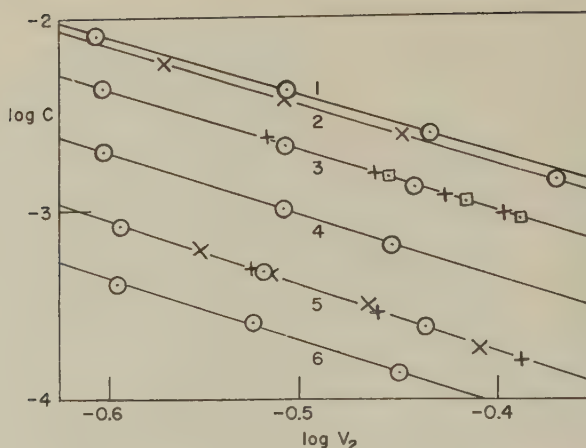


FIG. 6. Relation of concentration of polymer remaining unprecipitated to volume fraction of precipitant. ○, fraction 7; ×, fraction 5; +, fraction 3; ◻, fraction 2. (1)  $C_0 = 0.01184$ ; (2)  $C_0 = 0.0103$ ; (3)  $C_0 = 0.00600$ ; (4)  $C_0 = 0.00296$ ; (5)  $C_0 = 0.00130$ ; (6)  $C_0 = 0.00074$ .

This can be solved only by successive approximations beginning with  $\bar{v}_1 = (v_1)_{1/2}$ . Now  $\bar{v}_2$  is somewhat greater than  $(v_2)_{1/2}$  and some comparative values are, for  $(v_2)_0$ ,  $(v_2)_{1/2}$ , and  $\bar{v}_2$ , respectively, 0.210, 0.258, 0.263; 0.250, 0.308, 0.317; 0.300, 0.369, 0.383; 0.350, 0.430, 0.452; 0.400, 0.492, 0.530. Probably  $(v_2)_{1/2}$ , which is easily calculated from the experimental  $(v_2)_0$ , is sufficiently representative of a polymer fraction, particularly when used in conjunction with values of  $C$ .

Calibration equations for the determination of molecular weight distribution are obtained by combination of Eq. [3], [4], and [5], as

$$(v_2)_{1/2}^i = 0.258 - (0.181 + 0.0283 \log 1/M^i) \log C_{(v_2)_0}^i; \quad [7]$$

$$\log C^i / C_{(v_2)_0}^i = -3.3 \log (1.23 v_2 / (v_2)_{1/2}). \quad [8]$$

The weight-average molecular weight is probably to be preferred to the number-average for the description of precipitation processes.

#### PRECIPITATION OF MIXTURES OF POLYSTYRENE FRACTIONS

In order that the calibration equations [1], [7], and [8] determined from the polymer fractions may be applied to polydisperse polymers, it is necessary that (a) the same relation between  $D$  and  $C_p$  holds for a mixture as for the separate fractions; and (b) the precipitation curves of a mixture of fractions are additive in  $C$  and  $C_p$  (though not of course in  $D$ ). These conditions have been assumed by previous workers. To establish the validity of these conditions, precipitation experiments were made on nine mixtures of fractions 2 and 5 (Fig. 7), on three mixtures of fractions 2 and 7, on one mixture of fractions 2 and 3, and on a mixture containing all the fractions.

*Relation of Optical Density to Amount of Precipitation*

Corresponding values of  $D$  and  $C_p$  were obtained for complete precipitation of the nine mixtures of fractions 2 and 5. Equation [1] applies to the mixtures as well as to the separate fractions (Fig. 8).

*Additivity of the Precipitation Curves of the Mixtures*

The turbidimetric precipitation curves of mixtures of fractions 2 and 7 show clearly that fraction 2 begins to precipitate at its normal initial precipitation point in spite of the presence of fraction 7 already largely precipitated (Fig. 9). To investigate the additivity in detail, the experimental  $D$  values for the nine mixtures of fractions 2 and 5 were compared with the  $D$  values calculated by summing the  $C_p$  values for the appropriate concentrations of the separate fractions using Eq. [1]. Different concentrations of fractions 2 and 5 were chosen so that any variation in additivity

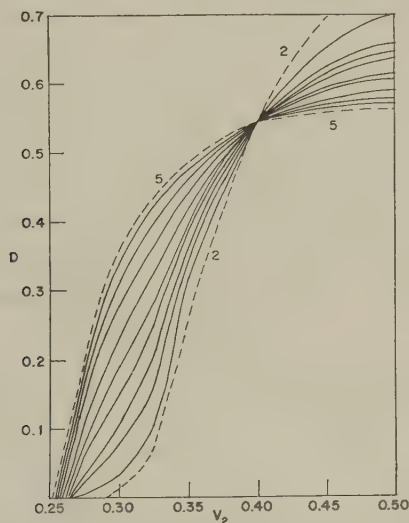


FIG. 7. Turbidimetric precipitation curves of mixtures of fractions 2 and 5 (relative concentrations given in text).

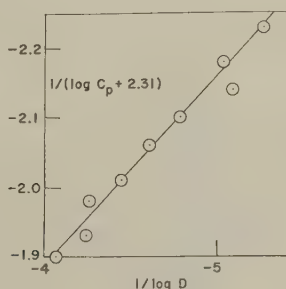


FIG. 8. Plot of Eq. [1] for the mixtures of fractions 2 and 5.



with total concentration would be revealed (Table I). Before the initial precipitation point of fraction 2 is reached the mixture curves follow those of fraction 5; thereafter the mixture curves are almost additive in the  $C_p$  values. Table I shows average values of the ratio of the experimental  $D$  value for the mixture to the calculated  $D$  value assuming additivity of the  $C_p$  values of the separate fractions ( $D_{\text{expt.}}/D_{\text{calc.}}$ ), beyond the initial precipitation point of fraction 2. There is evidence of a small trend in this ratio with the product of the concentrations of the fractions which may indicate some interaction of the polymer molecules, but the effect has no influence on  $(v_2)_0$  and is too small significantly to influence calculations of molecular weight distributions.

#### THE CALCULATION OF MOLECULAR WEIGHT DISTRIBUTION

The evaluation method of Morey and Tamblyn (2) may be applied to this system.

$$C_{v_2}^i = C_0^i(1 - v_2)$$

and

$$C_{v_2+\Delta v_2}^i = C_0^i(1 - \Delta Z)(1 - v_2 - \Delta v_2),$$

where  $\Delta Z$  is the fraction of total polymer precipitated in the small interval between  $v_2$  and  $v_2 + \Delta v_2$ . Taking logarithms of these equations and sub-

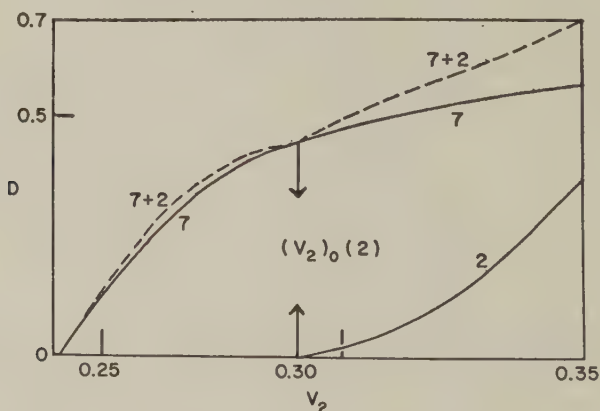


FIG. 9. Precipitation of mixture of fractions 2 and 7 ( $C_0(7) = 0.00336$ ;  $C_0(2) = 0.00414$ ).

TABLE I

*Additivity of the Mixture Curves for Fractions 2 and 5*

Mixtures of solutions of fraction 5 ( $C_0 = 0.00257$ ) and fraction 2 ( $C_0 = 0.00321$ ):

$D_{\text{expt.}}/D_{\text{calc.}}$	0.97	1.00	1.03	1.05	1.06	1.05	1.03	1.00	1.00
$10^6 \cdot C_0(5) \cdot C_0(2)$	0.743	1.32	1.73	1.97	2.06	1.97	1.73	1.32	0.743
Proportion of 5:2 solutions	9:1	8:2	7:3	6:4	5:5	4:6	3:7	2:8	1:9

stituting for  $\log C_{v_2}^i$  and  $\log C_{v_2+\Delta v_2}^i$  as  $\log C_{(v_2)_0}^i$  from the appropriate form of Eq. [3] in each yields two equations from which  $0.147 + 0.0230 \log M^i$  can be eliminated, giving

$$\log (C_0^i(1 - \Delta Z)) = \frac{0.210 - v_2 - \Delta v_2}{0.210 - v_2} (\log C_0^i + \log (1 - v_2)) - \log (1 - v_2 - \Delta v_2). \quad [9]$$

This can be solved for  $C_0^i$  by plotting on the same graph  $\log(C_0^i(1 - \Delta Z))$  against  $C_0^i$  for a set of  $\Delta Z$  values, and the right-hand side of Eq. [9] against  $C_0^i$  for a set of  $v_2$  values. The value of  $C_0^i$  can be found at the intersection of the appropriate  $v_2$  and  $\Delta Z$  lines and the corresponding value of  $M^i$  is found from Eq. [3]. Unfortunately the plots are not linear, and the two sets of lines intersect at acute angles, making the accurate location of the intersections difficult.

However, Claesson's method (6) can be adapted as follows, by using  $(v_2)_{1/2}^i$  to represent the precipitation of a polymer fraction  $M^i$ . It leads to linear plots more convenient for computation and to an easy and accurate location of intersections. From Eq. [7],

$$1/\log C_{(v_2)_0}^i = \frac{0.181}{0.258 - (v_2)_{1/2}^i} + \frac{0.0283 \log 1/M^i}{0.258 - (v_2)_{1/2}^i}. \quad [10]$$

By choosing values of  $(v_2)_{1/2}^i$  and plotting  $1/\log C_{(v_2)_0}^i$  against  $\log 1/M^i$  for these values, a set of straight lines is obtained. Values of  $1/\log \frac{1}{2}C_{(v_2)_0}^i$  corresponding to  $C^i$  at the half precipitation point  $(v_2)_{1/2}^i$  are used for  $1/\log C_{(v_2)_0}^i$  at fixed values of  $v_2$  to obtain the corresponding values of  $M^i$ . Table II

TABLE II  
*Data Required for the Claesson Evaluation Method*

$(v_2)_0$	$(v_2)_{1/2}$	$1/\log C_{(v_2)_0}^i$	
		$M = 10^6$	$M = 10^4$
0.21	0.257	-11.200	-67.8
0.22	0.270	-0.9330	-5.650
0.23	0.283	-0.4480	-2.7120
0.24	0.295	-0.3027	-1.8324
0.25	0.308	-0.2240	-1.3560
0.26	0.320	-0.1807	-1.0936
0.27	0.332	-0.1513	-0.9162
0.28	0.344	-0.1303	-0.7884
0.29	0.357	-0.1131	-0.6849
0.30	0.369	-0.1009	-0.6108
0.31	0.381	-0.0910	-0.5512
0.32	0.394	-0.0824	-0.4985
0.33	0.406	-0.0757	-0.4581
0.34	0.418	-0.0700	-0.4238
0.35	0.431	-0.0647	-0.3919

shows the data required for constructing a Claesson evaluation plot for this system.

Figure 10 shows the differential molecular weight distributions calculated in this way from the turbidimetric precipitation curves for (a) a mixture of all the fractions, (b), (c), and (d), mixtures of fractions 7 + 2, 5 + 2, and 3 + 2, respectively. For (a) there is good agreement with the gravimetric distribution curve for the height and position of the maximum with a somewhat steeper slope at the higher molecular weights as found for polyvinylpyrrolidone (10). In (d) it is shown that the separation of fractions as close as 3 and 2 is just possible by this method, and (b) suggests that fraction 7 (and possibly also fraction 5) contains a high molecular weight tail which could be the small amount of cross-linked material this polymer is known to contain (15, 16). For (b), (c), and (d) the fractions present are identified by the maxima of the curves. The positions of the maxima occur at lower values of the chain length than the weight averages determined for the fractions by light scattering and used for calibration. It seems likely that, for a given fraction, the distribution maximum occurs at lower molecular weights than the weight-average molecular weight, with distribution curves steeper on the low molecular weight side, as can be seen in the curves in Fig. 10. Nevertheless, Fig. 10 (a) shows that this turbidimetric precipitation titration method used in conjunction with Eqs. [1], [7], [8], and [10] will give the molecular weight distribution of a polydisperse polymer with sufficient accuracy.

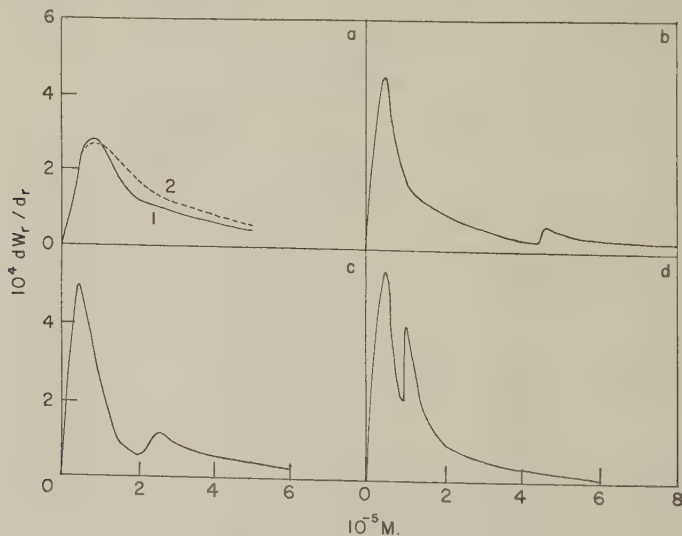


Fig. 10. Molecular weight distributions. (a) mixture of all the fractions (1, turbidimetric, 2, gravimetric); (b) mixture of fractions 2 and 7 (weight fraction of fraction 2 in polymer = 0.500); (c) mixture of fractions 2 and 5 (weight fraction of fraction 2 = 0.555); (d) mixture of fractions 2 and 3 (weight fraction of fraction 2 = 0.453).

The studies on the separate fractions and on the mixtures of fractions have shown that the optical density is not proportional to the precipitate concentration (even when refractive index corrections are made) but is related to it for this system by Eq. [1]. The spread of precipitation over a range of  $v_2$  even for the fractions, together with the relation of  $(v_2)_0$  to  $(v_2)_{1/2}$ , shows that a small amount of precipitate from a polydisperse polymer is not of uniform molecular weight, but the way in which this assumption is introduced in the Morey-Tamblyn method is unlikely to lead to significant error. The form of the  $D$  versus  $v_2$  curves depends not only on the molecular weight —  $v_2$  relation but also on the general solubility relations holding with respect to the equilibrium of the two phases and expressed in Eq. [4] as the relation between  $(v_2)_0$  and  $(v_2)_{1/2}$ . The results for the mixtures of fractions show that the precipitation of one molecular weight group is largely uninfluenced by others, as far as the shape of the precipitation curve is concerned.

#### REFERENCES

1. BRONSTED, J. N., *Compt. rend. trav. lab. Carlsberg, Sér. chim.* **22**, 99 (1938).
2. MOREY, D. R., AND TAMBLYN, J. W., *J. Appl. Phys.* **16**, 419 (1945).
3. OTH, A., *Bull. soc. chim. Belges* **58**, 285 (1949).
4. HARRIS, I., AND MILLER, R. G. J., *J. Polymer Sci.* **7**, 377 (1951).
5. CAMPBELL, H., KANE, P. O., AND OTTEWILL, I. G., *J. Polymer Sci.* **12**, 611 (1954).
6. CLAESSON, S., *J. Polymer Sci.* **16**, 193 (1955).
7. SCHOLTAN, W., *Makromol. Chem.* **24**, 104 (1957).
8. SCHOLTAN, W., *Makromol. Chem.* **24**, 83 (1957).
9. SCHULZ, G. V., *Z. physik. Chem.* **A179**, 321 (1937); **A184**, 1 (1939); **B46**, 105, 137 (1940); *J. prakt. Chem.* **155**, 115 (1940).
10. HENGSTENBERG, J., *Z. Elektrochem.* **60**, 236 (1956).
11. DUNN, A. S., STEAD, B. D., AND MELVILLE, H. W., *Trans. Faraday Soc.* **56**, 279 (1954).
12. MELVILLE, H. W., AND STEAD, B. D., *J. Polymer Sci.* **16**, 505 (1955).
13. MATHIESON, A. R., AND PORTER, M. R., *Nature* **173**, 1190 (1954); *J. Chem. Soc.* **1958**, 1301.
14. PEAKER, F. W., AND ROBB, J. C., *Nature* **182**, 1591 (1958).
15. BENNINGA, H., Thesis, Leyden, 1954.
16. DIJKSTRA, A., Thesis, Leyden, 1955.
17. THURMOND, C. D., *J. Polymer Sci.* **8**, 607 (1952).
18. MIE, G., *Ann. Physik* **25**, (4), 377 (1908).
19. BARNES, M. D., AND LA MER, V. K., *J. Colloid Sci.* **1**, 79 (1946).

## STUDY OF WETTABILITY OF POLYMERS BY SLIDING OF WATER DROP

Koji Kawasaki

*Electrotechnical Laboratory, Nagata-cho, Chiyoda-ku, Tokyo, Japan*

*Received June 30, 1959; revised October 13, 1959*

In order to obtain information on the wettability of some polymers, the sliding of water drops down tilted polymer slides has been examined. The angle of sliding is defined as the limiting angle between the slide and the horizontal plane at which the drop moves at a uniform rate, and can be taken as a measure of the wettability of the surface.

Bikerman (1) found as the first approximation

$$M \cdot \tan \alpha = \text{constant},$$

where  $\alpha$  is the angle of sliding and  $M$  is the mass of the moving water drop. An excellent confirmation of this relationship was obtained with octadecyl acetate multilayers on a chromium-plated brass slide by his measurements. But in our measurements (2) with sliding of water drops on some polymer surfaces, the above relationship does not hold, as shown in Fig. 1. A modified relationship is expressed as

$$M^n \cdot \tan \alpha = \text{constant}, \quad [1]$$

where  $n$  is a constant and its values are shown in Fig. 1.

In a further investigation, Bikerman (3) showed that the relation between  $M$  and  $\alpha$  is better represented by

$$Mg \cdot \sin \alpha = K \cdot L \cdot \sigma_l \quad [2]$$

where  $g$  is acceleration due to gravity,  $L$  is the width of the drop,  $\sigma_l$  is the surface tension of water, and  $K$  is a constant which depends on the wettability and roughness of the solid. Unfortunately Eq. [2] cannot be tested on our above-mentioned results, because the change of  $L$  has not been measured with the increase of drop mass.

On the other hand, Uriu and his co-workers (4) find that  $M \cdot \sin \alpha$  increases linearly with the mass of water drop so that  $M \cdot \sin \alpha / (1 + \gamma M)$  appears to be a constant, which can be taken as a measure of the water-proofness of polymers. The results of Fig. 1 are replotted in Fig. 2 according to Uriu's expression, and it is found that the relation between  $M \cdot \sin \alpha$  and  $M$  holds when  $M$  exceeds some critical value  $M_0$ , which is the value



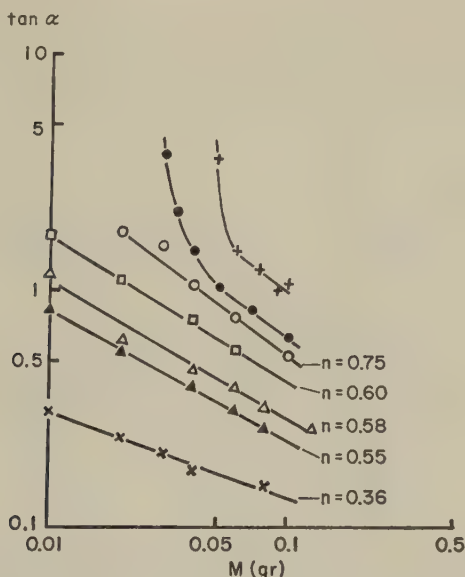


FIG. 1. Experimental data of  $\tan \alpha$  as a function of  $M$ . + Polyvinyl acetate; ● phenol resin; ○ urea resin; □ polyvinyl chloride; △ polyethylene; ▲ polytetrafluoroethylene; × paraffin.

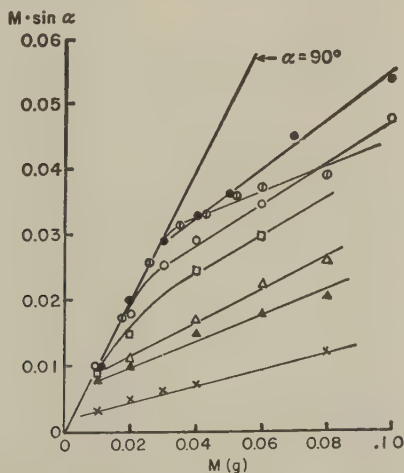
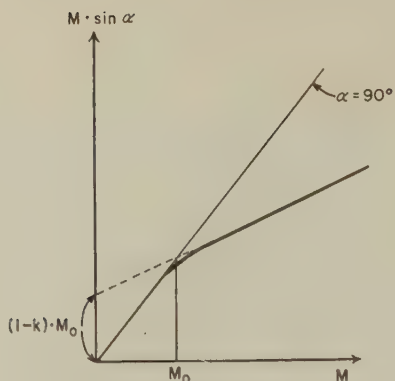
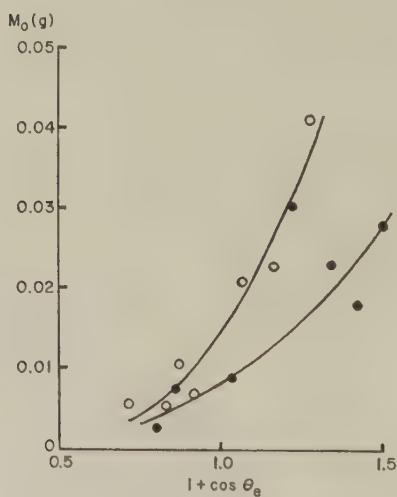
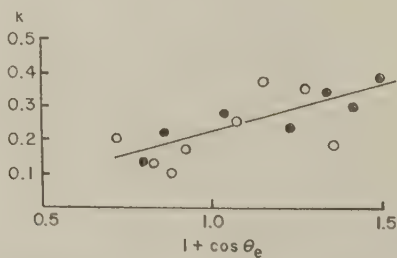


FIG. 2. Experimental data of  $M \cdot \sin \alpha$  as a function of  $M$ . ● Phenol resin; ⊕ polymethyl methacrylate; □ polyvinyl chloride; ○ urea resin; △ polyethylene; ▲ polytetrafluoroethylene; × paraffin.

of  $M$  for  $\alpha = 90^\circ$  and characteristic of the solid. The empirical relationship suggested by Uriu and co-workers is represented in Fig. 3 and can be expressed as

$$M \cdot \sin \alpha = M_0 + k(M - M_0) \quad \text{for } M \geq M_0, \quad [3]$$

FIG. 3. A general figure of  $M \cdot \sin \alpha \sim M$ .FIG. 4.  $M_0 \sim (1 + \cos \theta_e)$  relation. ● from the author's data; ○ from the data of Uriu *et al.*FIG. 5.  $k \sim (1 + \cos \theta_e)$  relation ● from the author's data; ○ from the data of Uriu *et al.*

where  $k$  is a constant. Thus,

$$\frac{M \cdot \sin \alpha}{1 + \gamma \cdot M} = (1 - k)M_0; \quad \gamma \equiv \frac{k}{1 - k} \cdot \frac{1}{M_0}. \quad [4]$$

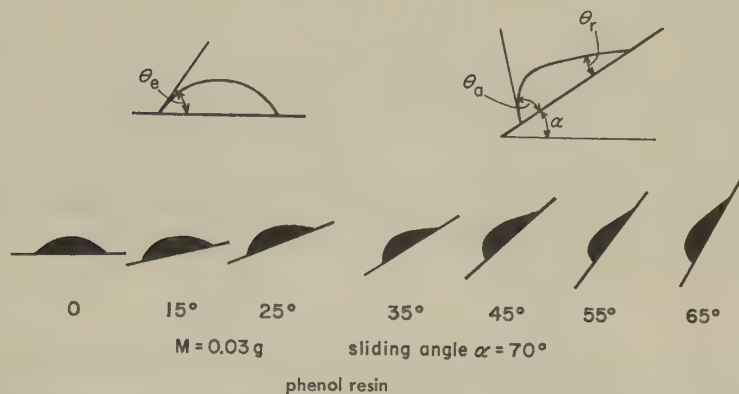


FIG. 6. Variation of drop form on tilted plate versus the angle of inclination ( $M = 0.03$  g.; sliding angle  $\alpha = 70^\circ$ ; phenol resin).

TABLE I

Substances	Author	$M_0(g)$	$\theta_a^\circ$	$\theta_r^\circ$	$\cos \theta_r - \cos \theta_a$
Polyvinyl acetate	Kawasaki	$46.5 \times 10^{-3}$	90	25	0.906
	Matsumoto				
Phenol resin A	Kawasaki	28.2	75	30	0.607
Phenol resin B*	Kawasaki	35.0	80	42	0.570
	Matsumoto				
	Kawasaki	18.0			
Polyvinyl chloride	Uriu <i>et al.</i>	21.0	81	26	0.742
	Matsumoto				
	Kawasaki	30.2			
Polymethyl methacrylate	Uriu <i>et al.</i>	23.0	75	35	0.560
	Matsumoto				
	Kawasaki	8.8			
Polyethylene	Matsumoto		97	70	0.464
	Uriu <i>et al.</i>	7.0	89	73	0.275
Polystyrene	Matsumoto				
	Kawasaki	2.3	112	100	0.201
	Uriu <i>et al.</i>	6.0	109	97	0.204
Paraffin	Matsumoto				
	Kawasaki	7.7, 15.0	118	91	0.452
	Matsumoto				
Polytetrafluoroethylene*	Kawasaki	22.0	83	60	0.370
Trifluoromonoethoxyethylene*	Matsumoto				

\* Measured values for the same sample.

The measure of the waterproofness given by Uriu *et al.* is equal to  $(1 - k)M_0$ , but the physical meaning of the measure is rather complicated and not clear, as shown in Figs. 4 and 5, in which the relation between the equilibrium contact angle  $\theta_e$  and the constants  $M_0$  and  $k$  is shown.

In order to make the phenomena clear, we have observed the sliding motion of water drops on tilted polymer slides. The variations of drop form on a tilted plate versus the angle of inclination are shown in Fig. 6 for a phenolic resin. If the angle of inclination reaches the value of the sliding angle  $\alpha$ , the equilibrium contact angle  $\theta_e$  changes to the advancing angle  $\theta_a$  at the head of the drop and to the receding angle  $\theta_r$  at the tail of drop, and then the water drop having mass  $M$  just begins to slide.

As the critical condition for the sliding of water drops we have, as the first approximation,

$$Mg \cdot \sin \alpha = L \cdot \sigma_l (\cos \theta_r - \cos \theta_a), \quad [5]$$

where  $L$  is the width of a water drop (having mass  $M$ ) perpendicular to the direction of motion.

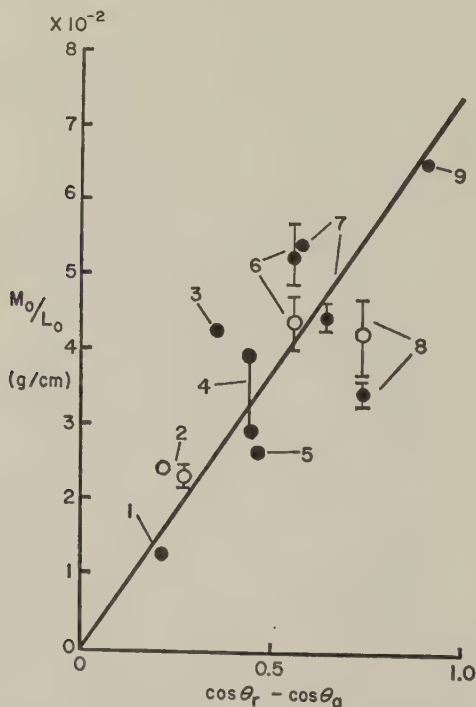


FIG. 7. Comparison of theory with the experimental data. ● from the author's data; ○ from the data of Uriu *et al.*; solid line from theory.

① paraffin; ② polystyrene; ③ trifluoromonoethoxyethylene; ④ polytetrafluoroethylene; ⑤ polyethylene; ⑥ polymethyl methacrylate; ⑦ phenol resin; ⑧ polyvinyl chloride; ⑨ polyvinyl acetate.

Furthermore we consider the sliding motion of water drops on a vertical wall. Let  $M_0$  be the value of  $M$  at which sliding of water drops along a vertical wall is prevented. For this case Eq. [5] reduces to

$$M_0 g = L_0 \sigma_l (\cos \theta_r - \cos \theta_a), \quad [6]$$

where  $L_0$  is the width of a water drop (having mass  $M_0$ ) perpendicular to the moving direction. In order to test Eq. [6], values of  $M_0$  and contact angle for polymers are given in Table I (2, 4, 5), and  $M_0/L_0$  is plotted in Fig. 7 versus  $\cos \theta_r - \cos \theta_a$ . The experimental results are in good agreement with theoretical values.

By introduction of a roughness factor of the solid surface into Eq. [5] by a treatment similar to that of Bikerman, a more general equation is obtained:

$$\begin{aligned} Mg \cdot \sin \alpha &= \beta L \sigma_l (\cos \theta_r - \cos \theta_a) \\ &= K \cdot L \cdot \sigma_l \end{aligned} \quad [7]$$

$$K \equiv \beta (\cos \theta_r - \cos \theta_a).$$

This equation is very similar to Eq. [2] given by Bikerman.

The author would like to thank Dr. T. Sasaki, Tokyo Metropolitan University, and Dr. J. J. Bikerman, Massachusetts Institute of Technology, for their helpful comments. He is also indebted to Dr. T. Matsumoto, Kobe University, for his measurements of  $\theta_a$  and  $\theta_r$ .

#### REFERENCES

1. BIKERMAN, J. J., *Proc. Roy. Soc. (London)* **A170**, 130 (1939).
2. KAWASAKI, K., *Bull. Electrotech. Lab. (Tokyo)* **16**, 179 (1952).
3. BIKERMAN, J. J., *J. Colloid Sci.* **5**, 349 (1950).
4. URIU, T., *et al.*, *J. Chem. Soc. Japan (Ind. Chem. Sect.)* **62**, 862 (1959).
5. Values of  $\theta_a$  and  $\theta_r$  in the table are cited from a private communication by Dr. Matsumoto.



## APPARATUS FOR THE MEASUREMENT OF LIGHT SCATTERING IN LIQUIDS

### MEASUREMENT OF THE RAYLEIGH FACTOR OF BENZENE AND OF SOME OTHER PURE LIQUIDS

D. J. Coumou

*Koninklijke/Shell-Laboratorium, Amsterdam, Holland  
(Shell Internationale Research Maatschappij N.V.)*

*Received January 19, 1960*

#### ABSTRACT

The construction of an apparatus for measuring the scattering of light in colloidal solutions and its angular dependence is described. The optical part is designed in such a way that the photometer measures the flux of scattered light originating from a well-defined volume of liquid within a well-defined solid angle. The intensity of the scattered light is compared with a part of the primary beam in a compensator with a sensitive null-amplifier.

For comparing fluxes of light scattered in different media the corrections for volume and solid angle can be combined into one refractive-index correction. Its value, for cylindrical as well as for rectangular liquid cells, is equal to the square of the ratio of the refractive indices.

Absolute measurements of the Rayleigh factor of benzene with a precision of about 2.5% were made using light of three different wavelengths. Rayleigh factors of some other pure liquids were also determined. The value of Avogadro's number calculated from these results with the aid of the Einstein formula shows the reliability and accuracy of the instrument for absolute light-scattering measurements.

#### INTRODUCTION

In practice the absolute light scattering by a liquid or a solution is determined by comparison with a standard liquid, the scattering power of which has been previously established. If the refractive indices of the liquids to be compared are different, corrections are necessary because

- (a) the volumes from which the scattering is measured are different, and
- (b) the solid angle within which the scattered light received by the measuring device is contained, varies.

In some of the instruments described in the literature these corrections are rather complicated.

The absolute scattering of light by a liquid can be characterized by the Rayleigh factor,  $R(\theta)$ , representing the flux of light scattered per unit solid angle, and per unit volume:

$$R(\theta) = \frac{J(\theta)}{I_0 V} \text{ (cm}^{-1}\text{)},$$

where  $I_0$  = irradiance of the primary light beam illuminating the liquid;  
 $J(\theta)$  = radiant intensity of scattering in a direction making an angle  $\theta$   
 with the primary beam;

$V$  = volume of which the scattering is measured.

In a light-scattering apparatus the photometer measuring the scattered light should therefore exactly define:

(a) the volume  $V$ ; and

(b) the solid angle  $\omega$  of the cone of scattered light accepted by the photometer from any point within  $V$ .

If these requirements are met a well-defined flux,  $L(\theta)$ , of scattered light of magnitude

$$L(\theta) = J(\theta)\omega = R(\theta)I_0V\omega \quad [1]$$

is measured.

In the construction of the light-scattering apparatus described here we specially paid attention to a good definition of  $V$  and  $\omega$  by the photometer. The refractive index corrections to be applied in this instrument for absolute measurements will be shown to be relatively simple.

The reliability of our instrument was first demonstrated by the determination of the Rayleigh factor  $R_{90}$ —in the direction perpendicular to the primary beam—of benzene. Further the Rayleigh factors of carbon tetrachloride and of some normal paraffins were measured by comparing their scattering at  $90^\circ$  with that of benzene.

## APPARATUS

### *Optical part*

A layout (top view) of the instrument is shown in Fig. 1. The light source  $S$  is a Philips mercury lamp, type 103107 (125 watt) which is stabilized for "hot spot jumping." By using a narrow slit  $S_1$  in the focus of lens  $L_2$  (a low-power microscope objective), and by making it pass a number of other slits  $S_2$ ,  $S_3$ , and  $S_4$ , the divergence of the primary beam illuminating the liquid in the cell  $LC$  could be reduced to less than one degree. The edges of slit  $S_4$  do not touch the light beam; however,  $S_4$  prevents stray light from the edges of  $S_2$  and  $S_3$  from entering the chamber  $K$ . Having traversed the liquid cell the primary light is completely absorbed in a light trap. Before passing the defining slits the central part of the primary beam passes a rectangular opening in the plate  $P$ , whereas the other part of the light is diffusely reflected to the reference photomultiplier  $P_2$ .

The construction of the photometer should meet the requirements for a good definition of the geometry, as stated in the Introduction. The amount of light transmitted by an optical instrument is generally determined by two series of pupils realized by material stops and their "virtual" images formed by the optical system, and known as the field stops and the aperture stops (1). Carr and Zimm (2) have already used this principle in the design

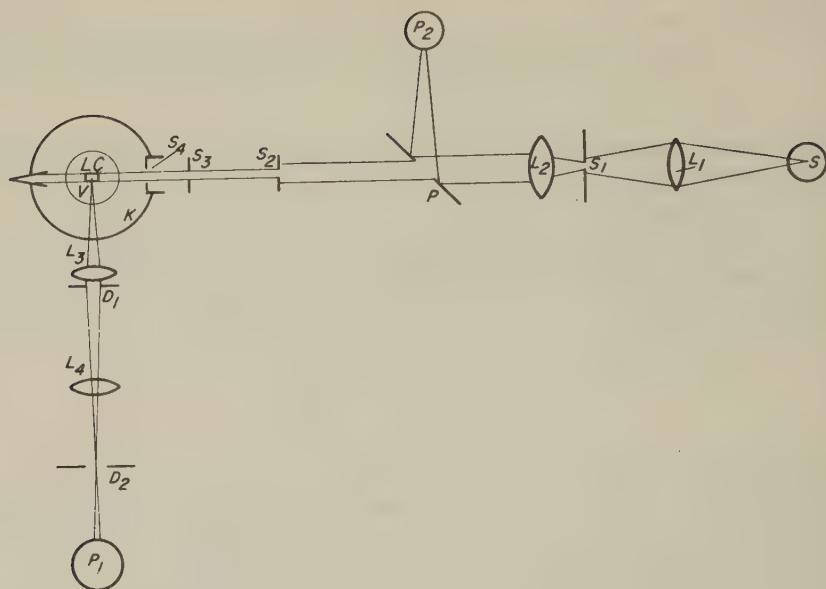


FIG. 1. Principle of light-scattering apparatus (top view).

of their apparatus for the determination of the absolute scattering of benzene. It is, however, not generally applied in the construction of light-scattering instruments. Probably its several advantages have not generally been recognized.

In the photometer of our instrument the first series consists of the rectangular diaphragm  $D_2$  and its image formed in the liquid cell  $LC$  by the lens system  $L_3, L_4$ . The surface  $O_2 = b \times h$  (width  $\times$  height) of this image defines the volume  $V$  "seen" by the photometer, the third dimension of this volume being the depth  $d$  of the primary beam;  $V = b \times h \times d$ . The diaphragm image is completely confined within the height of the primary beam, so that the photometer "does not see past the edges of this beam" (3).

On the other hand the iris diaphragm  $D_1$  forms the aperture stop of the instrument. It is imaged on the cathode surface of the sample photomultiplier  $P_1$  by the lens  $L_4$ . The surface  $O_1$  of  $D_1$  exactly defines the solid angle  $\omega$  of the cone in which the photometer receives scattered light from each point of the volume  $V$ . If  $a$  is the (angular) aperture = plane semi-angle of the cone,  $\omega = \pi a^2$ . Thus the diaphragms  $D_1$  and  $D_2$  together determine the flux of scattered light  $L$  (Eq. [1]) measured by the photometer. Filters and a polarizer can be inserted in the primary beam as well as in the photometer. For depolarization measurements a Glan-Thompson prism is used.

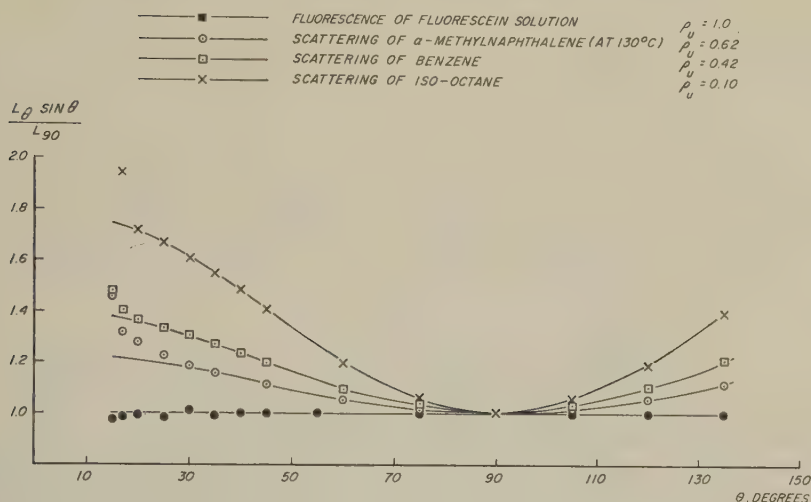


FIG. 2. Angular dependence of scattering (fluorescence) in cylindrical cells.

The angular dependence of the scattered light can be measured by rotating the photometer around an axis in the center of the chamber *K* containing the liquid cell. For these measurements cylindrical cells of the type as described by Witnauer and Scherr (4) are used. Stray light originating in the walls of these cells could be eliminated by cementing the flat entrance and exit windows from the primary beam with a black cement. Figure 2 shows the angular dependence of *L* for different cases, the calculated curves representing the formula

$$L_{\theta} \sin \theta = L_{90} \left( 1 + \frac{1 - \rho_u}{1 + \rho_u} \cos^2 \theta \right)$$

where  $\rho_u$  = depolarization of the radiation at  $\theta = 90^\circ$  for unpolarized incident light. It may be seen that measurements at angles as small as  $20^\circ$  with respect to the primary beam are sometimes possible; the minimum angle depends strongly on a careful cleaning of the liquids.

#### *Electronic detector<sup>1</sup>*

The photomultipliers  $P_1$  and  $P_2$  are identical (R.C.A.-IP 21) and have a common power supply, so that a very good stability of the electronic detector is obtained. A block diagram of the detector is shown in Fig. 3.

As the light source is connected to the mains voltage, its intensity and thus the output currents of the photomultipliers fluctuate with a frequency of 100c.p.s. The ratio of the sample signal to the reference signal is measured in a compensator forming the load of the sample photomultiplier  $P_1$ . The compensator is adjusted for bal-

<sup>1</sup> The author expresses his indebtedness to his colleague A. Bijl, who constructed the electronic detector.

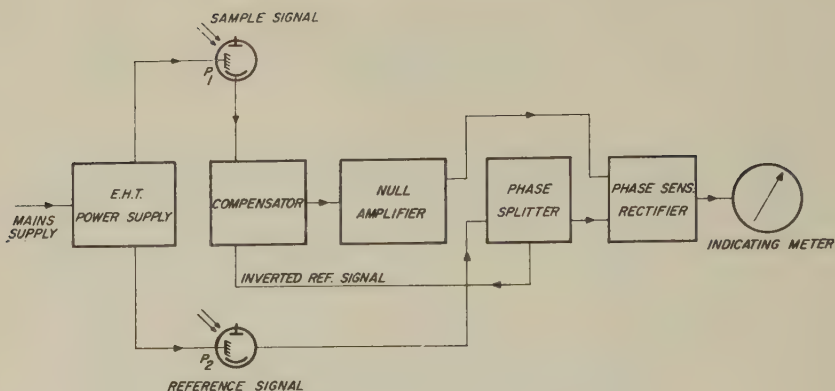


FIG. 3. Block diagram of electronic detector.

ance with a 10-turn Helipot potentiometer, the balance condition being determined with a null-amplifier. The phase opposition required by the compensator is obtained by a phase inversion in the null-amplifier. This amplifier further contains a parallel T-filter tuned to the signal frequency.

The current output of  $P_2$  is kept constant at 10  $\mu$ amp., so that the reading of the potentiometer is a measure for the current output of  $P_1$ . The linearity of the output of  $P_1$  with the incident light flux has been checked for currents of up to 10  $\mu$ amp.

The null-amplifier is a 3-stage amplifier with automatic gain control, the gain being maximum at zero input voltage. This obviates the necessity of manual gain control and greatly simplifies the operation of the instrument. The gain without automatic gain control is approximately  $5 \times 10^{-5}$ ; the noise is 0.2  $\mu$  v. referred to the input terminals of the amplifier, at a band width of 2 c.p.s.

### REFRACTIVE INDEX CORRECTION

The Rayleigh factor of a liquid can be calculated from Eq. [1], if the magnitudes of  $L$ ,  $I_0$ ,  $V$ , and  $\omega$  have been exactly determined. In practice  $R$  is determined by comparing the light flux  $L$  from the liquid to that from a standard liquid. Measuring in the direction perpendicular to the primary beam ( $\theta = 90^\circ$ ) we have

$$\frac{L}{L_b} = \frac{R_{90}}{R_{90,b}} \frac{V\omega}{(V\omega)_b}, \quad [2]$$

where the ratio  $L/L_b$  equals the ratio of the currents given by the photomultiplier  $P_1$ . The index  $b$  refers to the standard, for which benzene is generally used. The ratio  $V\omega/(V\omega)_b$  originates from the difference both in volume  $V$  "seen" by the photometer and in the solid angle  $\omega$  when liquids with different refractive indices are used.

If we write:  $\omega = \pi a_h a_v$ , where  $a_h$  and  $a_v$  are the angular apertures of the cone in the horizontal and in the vertical cross section, respectively, we have  $V\omega = \pi d \times a_h b \times a_v h$ . In Fig. 4 it can be seen how in the horizontal



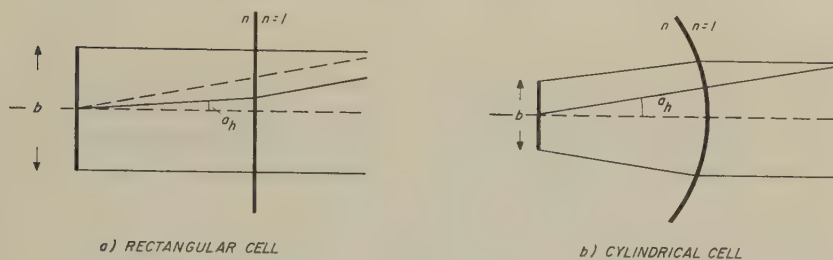


FIG. 4. Change of volume and solid angle (horizontal cross section).

cross section the values of  $a_h$  and  $b$  are changed in rectangular or in cylindrical cells owing to the refraction at the boundary.

Considering the formation of the "virtual" image of the diaphragm  $D_2$  separately in the horizontal and in the vertical plane, we may apply the theorem of Helmholtz-Lagrange (5) in each of these two cross sections. According to this we have:

$$na_h b = \text{constant}, \text{ and } na_v h = \text{constant}$$

if  $n$  = refractive index of the liquid in the cell. Thus the factor  $V\omega$  will be proportional to  $1/n^2$ . This will be true regardless of the shape of the liquid cell. The light fluxes measured in our equipment from the same liquid in a rectangular and a cylindrical cell indeed were equal within the precision of the experiment.

When comparing liquids of different refractive indices Eq. [2] thus becomes

$$\frac{L}{L_b} = \frac{R_{90}}{R_{90,b}} \left( \frac{n_b}{n} \right)^2. \quad [2^a]$$

This refractive-index correction is very simple as compared to those given in the literature.

In order to demonstrate the validity of the derivation of Eq. [2<sup>a</sup>] we have determined experimentally the dimensions of the volume  $V$  in the two types of cells. The photomultiplier  $P_1$  was replaced by a small light source illuminating  $D_2$ . Pieces of photographic film were immersed in the liquid cell at  $V$  (Fig. 1) perpendicular to the direction of the photometer. Exposure by the small light source gives the image of  $D_2$  on the film. After development the dimensions of the illuminated area were measured with a micrometer microscope.

It was found that there is no influence of the refractive index on:

- the width of the image,  $b$ , in rectangular cells;
- the product  $nb$ , in cylindrical cells;
- the height,  $h$ , in either type of cells.

These facts can be understood by an image formation as sketched in Fig. 4: a practically parallel light beam incident on a flat boundary (rectangular cells) gives no change of the linear dimensions of the image, but the apertures  $a_h$  and  $a_v$  each are proportional to  $1/n$ ; in the cylindrical cell  $a_h = \text{constant}$ , but  $b$  is proportional to  $1/n$ , whereas in the vertical cross section  $h = \text{constant}$  but  $a_v$  is proportional to  $1/n$ .

## EXPERIMENTAL

*Materials*

Commercial benzene (Analar) showed some fluorescence in light of the 366-m $\mu$  mercury line. It was purified by washing with concentrated sulfuric acid and with sodium hydroxide solution. After drying over calcium chloride it was sharply fractionated. No fluorescence was present in the middle fractions.

Carbon tetrachloride (Analar) was dried over calcium chloride; a single distillation appeared to be sufficient to free it from fluorescence. Dust-free samples were obtained by distillation, immediately before measurement, of benzene or CCl<sub>4</sub> directly into the liquid cell of the instrument.

Normal octane and *n*-decane were Phillips Petroleum Comp. products of Research Grade; *n*-hexadecane was of Pure Grade and was further purified by crystallization. Traces of fluorescent impurities were removed by percolation over silica. These paraffins were filtered through a millipore filter, type HA.

*Determination of  $R_{90}$  of Benzene*

The Rayleigh factor of benzene was obtained by measuring the ratio of the light flux  $L_b$  received by the photometer from scattering in this liquid to the light flux  $L_m$  received from an ideal diffuse surface illuminated by the same primary beam. The surface of a freshly prepared magnesium oxide layer of at least 2 mm. thickness was used as such a diffuser (6). This surface was illuminated at an angle of about 45°. For an ideal diffuser  $L_m$  is independent of this angle of illumination, and proportional to  $\cos \alpha$ , when the diffuse reflection is measured in a direction making an angle  $\alpha$  with the normal on the surface (Lambert's cosine law for an ideal diffuse surface).

The Rayleigh factor can then be calculated from the equation:

$$R_{90} = \frac{n_b^2 r \cos \alpha}{\pi b_a} \frac{L_b}{L_m} \quad [3]$$

where  $r$  = reflectance of the MgO surface. The refractive index correction  $n_b^2$  occurs in this equation because of the fact that the light flux  $L_b$  originates in a medium with refractive index  $n_b$ , whereas the flux  $L_m$  originates in air, a medium for which  $n = 1$ . The only linear dimension to be known is  $b_a$ , the width of the image of diaphragm  $D_2$  in air.

The scattering of benzene was measured in the direction perpendicular to the primary beam, the diffuse reflection of the magnesium oxide in the direction perpendicular to the surface ( $\alpha = 0^\circ$ ). The measurements were carried out for three wavelengths given by the mercury arc: 366 m $\mu$  (isolated by a Chance OX 1 filter), 436 m $\mu$ , and 546 m $\mu$  (isolated by interference filters).

The ratio of the two light fluxes being very large, the multiplier output must be reduced in a measurable ratio. This was carried out in two ways:

I. With the aid of neutral filters. The attenuation factors of these filters were obtained by means of reference scatterers the scattering of which lay in between the diffuse reflection of MgO and the scattering of benzene. The ratio  $L_m/L_b$  is then obtained in at least four steps.

II. With the aid of a fixed and a rotating polarizer in the primary beam. The light-flux ratio can now be obtained in two steps only. It is, however, the Rayleigh factor  $R_{90,v}$  for vertically polarized light which is thus determined. The following relation holds between  $R_{90,v}$  and  $R_{90,u}$  for unpolarized light:

$$R_{90,u} = R_{90,v} \frac{1 + \rho_u}{2}, \quad [4]$$

where  $\rho_u$  = depolarization of the scattered light for unpolarized incident light.

#### *Absolute Scattering of Other Pure Liquids*

The light scattered at  $90^\circ$  by carbon tetrachloride and by *n*-octane, *n*-decane, and *n*-hexadecane was compared to that from benzene, and  $R_{90}$  was calculated with the aid of Eq. [2<sup>a</sup>]. All measurements were made at a temperature of  $23^\circ\text{C}$ . ( $\pm 0.5^\circ$ ). The scattering in the hydrocarbons was determined with unpolarized as well as with vertically polarized incident light. The relation [4] appeared to hold within 2%.

For carbon tetrachloride the normal light source was replaced by a Philips water-cooled mercury lamp, SP 500, and measurements were made in unpolarized light only.

#### RESULTS

The results of our scattering and depolarization measurements on pure liquids are summarized in the columns 3 and 4 of Table I. The refractive indices needed for the application of Eqs. [3] and [2<sup>a</sup>] were determined for the visual wavelengths with a Bausch and Lomb Precision Refractometer; for the ultraviolet wavelength the refractive index was found by extrapolation according to the Cauchy formula

$$n = A + \frac{B}{\lambda^2}.$$

For the calibration of benzene [Eq. 3] we further used values for the reflectance  $r$  of the MgO-surface reported by Benford, Lloyd, and Schwarz (7). In the experiments I (with unpolarized light)  $b_a$  was 0.695 cm., in the experiments II (with vertically polarized light)  $b_a$  was 0.608 cm.

The repeatability of the measurement of the flux of light scattered by a liquid is better than 1%. The precision of the  $R_{90}$  values for benzene is

TABLE I

*Absolute Light Scattering in Pure Liquids—Calculation of Avogadro's Number*

Liquid	Wavelength ( $m\mu$ )	$R_{90u} \cdot 10^6$ ( $cm^{-1}$ )	$\rho_u$	$n_{23}^\circ$	$\frac{\partial n}{\partial T} \cdot 10^6$ per degree <sup>a</sup>	$\kappa \left( \frac{cm^2}{dyne} \right)$	$\alpha \cdot 10^3$ per degree	$N_A \cdot 10^{-23}$
Benzene	546	15.8	0.41	1.503	64	$95 \cdot 10^{-12}$	$1.18^b$	5.95
	436	45.6	0.42	1.521	$66_5$			5.79
	366	100	0.44	1.541	69			6.24
<i>n</i> -Octane	546	$4.8_5$	0.12	1.398	47	$125 \cdot 10^{-12}$	$1.15^b$	6.11
	436	13.2	$0.12_5$	1.405	48			5.90
	366	25.7	$0.12_5$	1.413	$48_5$			6.18
<i>n</i> -Decane	546	$4.9_5$	0.15	1.413	45	$105 \cdot 10^{-12}$	$1.04^b$	6.13
	436	13.5	0.16	1.420	46			5.84
	366	26.4	$0.16_5$	1.428	46			6.23
<i>n</i> -Hexadecane	546	$5.7_5$	0.26	1.435	$40_5$	$83 \cdot 10^{-12}$	$0.90^b$	5.94
	436	15.6	$0.26_5$	1.443	42			5.95
	366	30.3	0.27	1.452	42			6.34
Carbon tetra- chloride	546	5.5	0.05	1.463	$58_5$	$108 \cdot 10^{-12c}$	$1.21_5^c$	5.89
	436	14.8	0.05	1.472	60			5.81
	366	28.9	$0.05_5$	1.484	61			6.37

mean =  $6.04 \pm 0.19$ <sup>a</sup> Determined with a Bausch and Lomb Precision Refractometer.<sup>b</sup> Derived from density data given by the A.P.I. (13).<sup>c</sup> Data reported by Freyer *et al.* (14).

mainly determined by that of the determinations of the light flux ratios  $L_b/L_m$ . This standard deviation was  $\pm 3\%$  in the experiments *I*, and it was improved to better than  $2\%$  where the ratio  $L_b/L_m$  was found in two steps only.

The  $R_{90}$  values of benzene found in this investigation for green and blue mercury light are somewhat lower than those originally published by Carr and Zimm (2), and by Brice and co-workers (8); the value for  $436 m\mu$  corresponds very well to that mentioned by Kushner (9), by Kremen and Saphiro (10), and by Stamm and Button (11). For  $366 m\mu$  only Cantow (12) has published a value ( $103 \times 10^{-6} cm^{-1}$ ), which is in good agreement with our result.

#### CALCULATION OF AVOGADRO'S NUMBER

The theory of the scattering of light in pure liquids has been given by Einstein (15). Zimm (2) has modified the formula of Einstein into

$$R_{90} = \frac{2\pi^2}{\lambda^4 N_A} RT \kappa \left( \frac{n}{\alpha} \frac{\partial n}{\partial T} \right)^2 \frac{6 + 6\rho_u}{6 - 7\rho_u}, \quad [5]$$



where  $N_A$  = Avogadro's number;

$T$  = absolute temperature;

$\kappa$  = isothermal compressibility of the liquid;

$\alpha$  = volume expansion coefficient of the liquid.

The validity of this equation has been checked by measurements of the scattering power of some liquids, and calculating Avogadro's number (2, 12, 16). We applied this method as a test on the performance of our light-scattering apparatus, using the  $R_{90}$  values of Table I.

This table further contains the additional data necessary for the application of Eq. [5]. The isothermal compressibilities of benzene and the hydrocarbons were determined in this laboratory.<sup>2</sup> The last column gives the values for Avogadro's number calculated from our light-scattering measurements. These results prove the reliability and accuracy of our instrument for absolute measurements. The precision in the Avogadro number corresponds to that derived from the precision in each of the quantities involved in the calculation.

#### ACKNOWLEDGMENTS

The author expresses his gratitude to Dr. E. L. Mackor for valuable discussions and criticism, and to Mr. H. Verheijke for his careful execution of the measurements.

#### REFERENCES

1. e.g. BROWN, E. B., "Optical Instruments," p. 105. Chemical Publishing Co., Brooklyn, 1945. HABELL, K. J., AND COX, A., "Engineering Optics," p. 47. Sir Isaac Pitman and Sons, London, 1948.
2. CARR, C. I., AND ZIMM, B. H., *J. Chem. Phys.* **18**, 1616 (1950).
3. HERMANS, J. J., AND LEVINSON, S., *J. Opt. Soc. Amer.* **41**, 460 (1951).
4. WITNAUER, L. P., AND SCHERR, H. J., *Rev. Sci. Instr.* **23**, 99 (1952).
5. GRIMSEHL, E., A Textbook of Physics, Vol. 4, p. 77. Blackie and Son, London and Glasgow, 1933.
6. Letter Circular L.C.547. National Bureau of Standards, Washington, 1939.
7. BENFORD, F., LLOYD, G. P., AND SCHWARZ, S., *J. Opt. Soc. Amer.* **38**, 445, 964 (1948).
8. BRICE, B. A., HALWER, M., AND SPEISER, R., *J. Opt. Soc. Amer.* **40**, 768 (1950).
9. KUSHNER, L. M., *J. Opt. Soc. Amer.* **44**, 155 (1954).
10. KREMEN, J., AND SAPHIRO, J. J., *J. Opt. Soc. Amer.* **44**, 500 (1954).
11. STAMM, R. F., AND BUTTON, P. A., *J. Chem. Phys.* **23**, 2456 (1955).
12. CANTOW, H. J., *Makromol. Chem.* **18/19**, 367 (1956).
13. Selected Values of Properties of Hydrocarbons, A.P.I. Research Project 44. Carnegie Press, Pittsburgh, Pennsylvania, 1953.
14. FREYER, E. B., HUBBARD, J. C., AND ANDREWS, D. H., *J. Am. Chem. Soc.* **51**, 759 (1929).
15. EINSTEIN, A., *Ann. Physik* **33**, 1275 (1910).
16. MARON, S. H., AND LOU, L. H., *J. Polymer Sci.* **14**, 273 (1954).

---

<sup>2</sup> The author is indebted to Mr. J. W. M. Boelhouwer for communicating the results of his measurements.



## THE HYDROTHERMAL GROWTH OF MOLYBDENA WHISKERS ON $\text{MoO}_3$ - $\text{SiO}_2$ SUBSTRATE<sup>1</sup>

James L. Callahan,<sup>2</sup> Ralph H. Petrucci, and Charles A. Brown

*Received January 21, 1960; revised April 25, 1960*

### ABSTRACT

The following variables have been studied in the growth of  $\text{MoO}_3$  whiskers on a  $\text{MoO}_3$ - $\text{SiO}_2$  substrate under hydrothermal conditions: steam pressure, temperature,  $\text{MoO}_3$  concentration, silica surface area, molybdenum oxidation state, and the effect of added metal oxides. The diffusion of  $\text{MoO}_3$  over silica films has also been investigated. An hypothesis for the mechanism of the transport and whisker growth processes has been formulated. Transport is believed to be a surface process which occurs via a slightly stable silicomolybdic acid-like complex. Decomposition of the surface complex with deposition of  $\text{MoO}_3$  at preferred surface sites is believed to result in the observed whisker growth.

### INTRODUCTION

The growth of  $\text{MoO}_3$  whiskers from  $\text{MoO}_3$ - $\text{SiO}_2$  substrates under hydrothermal conditions has been reported previously (1). This present work represents an attempt to elucidate the mechanism of the mobility processes and the resulting crystal growth in the  $\text{MoO}_3$ - $\text{SiO}_2$ - $\text{H}_2\text{O}$  system. The determined response to certain variables affecting  $\text{MoO}_3$  whisker growth and pertinent literature data are employed in the formulation of a growth mechanism hypothesis.

### EXPERIMENTAL

#### *Substrate Preparation*

$\text{MoO}_3$ - $\text{SiO}_2$  substrates were prepared by dissolving ammonium heptamolybdate at various concentrations in ammonia-stabilized "Ludox" (silica sol, containing 28 %  $\text{SiO}_2$  obtained from the E. I. duPont de Nemours Co.) and "flash drying" the resulting solutions by delivering them, a drop at a time, into a platinum crucible heated to a dull-red color. Samples of the solid so prepared (approximately 3 %  $\text{MoO}_3$ -97%  $\text{SiO}_2$ ) gave no detectable X-ray diffraction pattern, even after several hours exposure.

<sup>1</sup> Taken from the thesis submitted by J. L. Callahan in partial fulfillment of the requirements for the Ph.D. degree at Western Reserve University, November, 1957. This investigation was supported in part by the grant of an educational assignment by the Standard Oil Company (Ohio).

<sup>2</sup> Present address: Sohio Research Laboratory, Cleveland, Ohio.

### *Hydrothermal Treatment*

Open-end glass tubes containing the  $\text{MoO}_3$ - $\text{SiO}_2$  solids and capillaries filled with the desired amounts of water were sealed in glass ampules. In most experiments the ampules were flushed with oxygen and sealed off in such a way as to give known internal free volumes. The sealed ampules were inserted into lengths of steel pipe and placed into a temperature-controlled furnace ( $\pm 5^\circ\text{C}$ .) for the desired time intervals. Steam pressures were calculated from the known weights of water, the free volumes of the ampules, and furnace temperatures.

### *Whisker Detection and Determination*

An X-ray diffractometer technique was used to determine semi-quantitatively the crystalline  $\text{MoO}_3$  concentration in the amorphous  $\text{MoO}_3$ - $\text{SiO}_2$  substrates in the concentration range 0.5–3.0 wt. %  $\text{MoO}_3$ . Suitable standards for this method were prepared by subjecting  $\text{SiO}_2$  samples containing 0.5–3.0 wt. %  $\text{MoO}_3$  to hydrothermal whisker-growing conditions for 1 week, a length of time which assured substantially complete conversion of the amorphous  $\text{MoO}_3$  to whiskers. This assurance was afforded by a plot to band height ( $2\theta = 27.4^\circ$ ) versus time of hydrothermal treatment at  $375^\circ\text{C}$ . and 4.84 atm. steam pressure. Band height leveled off after 100 hours and remained constant to 340 hours (2 weeks). Therefore, the 1-week treatment which the standards received seemed to have resulted in the complete transformation of amorphous  $\text{MoO}_3$  to whiskers.

The X-ray diffractometer method could not be used for the determination of whisker concentration in  $\text{MoO}_3$ - $\text{SiO}_2$  substrates rich in  $\text{MoO}_3$ . At high concentrations, the  $\text{MoO}_3$  gave a strong diffraction, even before whisker growth. In these cases the average of several whisker counts, each on  $0.01\text{ mm.}^2$  of substrate surface, was obtained microscopically. Individual counts on different regions of the surface of the same sample were found to vary by as much as a factor of two. However, the average of 10 or more counts gave reasonably reproducible results. This average count was taken as a relative measure of whisker concentration.

### *$\text{MoO}_3$ and $\text{SiO}_2$ Film Preparation*

Films of  $\text{SiO}_2$  and  $\text{MoO}_3$  were prepared by spreading  $\text{SiO}_2$ - $\text{H}_2\text{O}$  and  $\text{MoO}_3$ - $\text{H}_2\text{O}$  pastes on microscope or platinum foil slides. The paste films were rapidly dried in a furnace at  $480^\circ\text{C}$ . The slides supporting the films were then subjected to the usual hydrothermal treatment in sealed ampules. In some experiments glass rods were employed as supports for  $\text{SiO}_2$  and  $\text{MoO}_3$  films.

## RESULTS

### *Chemical Identity of the Whiskers*

The chemical identity of the whiskers grown from  $\text{MoO}_3$ - $\text{SiO}_2$  substrates under hydrothermal conditions has already been established (1). The X-ray

diffraction pattern and infrared spectrum of the whiskers were shown to be identical to samples of pure  $\text{MoO}_3$ . The emission spectrum established that the whiskers were of high purity.

Figure 1 is an electronmicrograph of a sample of  $\text{MoO}_3$  whiskers at 2400 diameters magnification. The apparent high degree of crystallinity of the whiskers, as evidenced by their uniform surfaces, indicates that they may be single crystals.

#### *Migration of $\text{MoO}_3$ on $\text{SiO}_2$ Films*

In one experiment, a glass rod was covered with a silica film 15 cm. long and 1 mm. thick. A film of molybdena, 3 cm. long and 1 cm. thick, was placed in contact with one end of the silica film. The rod supporting the films was subjected to hydrothermal treatment (400°C. and 4.45 atm. steam pressure) for 72 hours and then examined with a microscope. Starting at the  $\text{MoO}_3$ - $\text{SiO}_2$  boundary, the first 1.2 cm. of the  $\text{SiO}_2$  film was found to be essentially whisker-free. This zone was followed by a zone, 3.8 cm. in length, containing whiskers and the remaining portion of the  $\text{SiO}_2$  film was whisker-free.

Bands of the  $\text{SiO}_2$  film, 1–2 cm. in length, were removed from the rod and were subjected to emission spectrographic analysis. The zone in which the whiskers were observed contained about 0.3–1.0 wt. %  $\text{MoO}_3$ . The whisker-free zone, adjacent to the boundary, was highest in  $\text{MoO}_3$  concentration, being 1.0 wt. %  $\text{MoO}_3$ . (The spectrographic method determined both crystalline and amorphous  $\text{MoO}_3$  content in the  $\text{SiO}_2$  film. Microscopic examination reveals only crystalline  $\text{MoO}_3$ -whiskers.)



FIG. 1. Electronmicrograph (2800  $\times$ ) of  $\text{MoO}_3$  whiskers.

In the spectrographic analyses of the  $\text{SiO}_2$  film sections it was observed that there were some alkali and alkaline earth lines which did not appear in the standards. The lines were most intense in the sections of silica film taken from the whisker-free zone adjacent to the boundary. It was hypothesized that these metal ions were being extracted from the glass surface by reaction with the silica film. That these ions react rapidly with amorphous silica under hydrothermal conditions to form silicates has been established by Assarasson and Rydberg (2) and others (3). Once in the silica film, the ions might diffuse over the surface toward the  $\text{MoO}_3$  boundary where they could react with the more acidic  $\text{MoO}_3$  to yield relatively immobile molybdates (4).

In order to test this hypothesis, it was predicted that  $\text{MoO}_3\text{-SiO}_2$  films in contact on a platinum surface would display no whisker-free zone, and this indeed was found to be the case in actual experiments. Furthermore it was predicted that if an appropriate concentration of  $\text{MgO}$  were added to the silica, a whisker-free zone should be produced, even on a platinum support. Samples of silica gel containing 0.5–1.0 wt. % added  $\text{MgO}$  were laid down as films in contact with  $\text{MoO}_3$  on platinum surfaces and were hydrothermally treated. It was found that the addition of  $\text{MgO}$  caused an increase in the length of the whisker-free zone; but if  $\text{MgO}$  in excess of about 0.6 wt. % was added, no whiskers were found over the entire length of the silica film.

Silica films containing  $\text{CuO}$ ,  $\text{BaO}$ , and  $\text{CaO}$  were prepared in contact with  $\text{MoO}_3$  films. When these preparations were subjected to hydrothermal treatment a whisker-free silica zone was observed adjacent to the boundary in each case.

These data indicate that magnesium ion and other mobile ions in the silica substrate are responsible for producing whisker-free zones on silica films in contact with  $\text{MoO}_3$  films under hydrothermal conditions; this process seems similar to rhythmic banding in gels.

#### *MoO<sub>3</sub> Transport Phase*

The results of experiments on the diffusion of  $\text{MoO}_3$  on  $\text{SiO}_2$  films strongly indicated a solid phase mobility mechanism. However, it was desired to establish this point more clearly.

Two parallel silica films, 2 mm. in width, 3 cm. long, and separated by a distance of about 3 mm., were laid down on a platinum surface. A molybdena film, 3 mm. square, was placed such that it contacted the end of one silica film but not the other. The distance between the molybdena film and the closest point of the nonadjacent silica film was about 2 mm. This specimen was placed in an ampule and subjected to hydrothermal treatment at  $400^\circ\text{C}$ . for 72 hours. Microscopic examination revealed that the silica film in contact with the  $\text{MoO}_3$  film contained whiskers over its entire length. No whiskers were observed on the silica film which did not contact the



MoO<sub>3</sub> film. Therefore, any vapor transport of MoO<sub>3</sub> must have been quite small relative to transport via the solid phase.

### *Variables Affecting Whisker Growth*

*Steam Pressure.* The temperature (400°C.), solid composition (3 wt. % MoO<sub>3</sub>-97 wt. % SiO<sub>2</sub>), and hydrothermal treatment time (72 hours) were maintained constant while steam pressure was varied in the range 0.0-27.82 atm. The resulting samples were analyzed quantitatively for MoO<sub>3</sub> whisker concentration using the X-ray diffractometer method. In Fig. 2, MoO<sub>3</sub> whisker concentration is plotted against steam pressure. It is seen that the rate of whisker growth was very sensitive to steam pressure in the range 1-5 atm. Pressures less than about 1 atm. gave greatly reduced growth rates. Microscopic examination, which enables the determination of even traces of whiskers, disclosed that a sample containing no water was completely whisker-free.

*Temperature.* The effect of temperature on whisker growth was studied by maintaining the variables solid composition (3 wt. % MoO<sub>3</sub>), time (72 hours), and steam pressure (4.10-5.78 atm.) constant while the tempera-

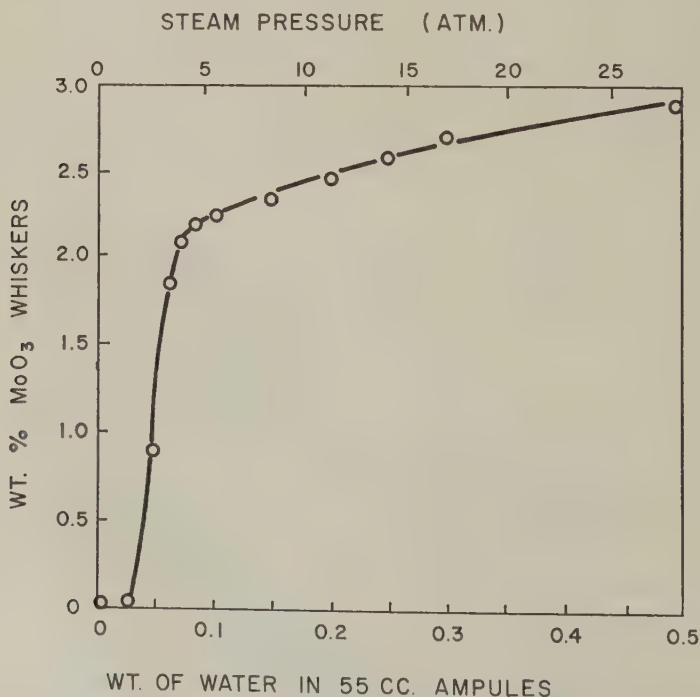


FIG. 2. Effect of steam pressure on MoO<sub>3</sub> whisker growth (3 wt. % MoO<sub>3</sub>-97 wt. % SiO<sub>2</sub>; 72 hours at 400°C.).



ture was varied over the range 250°–500°C. in 25°C. increments. The X-ray diffractometer method was used for  $\text{MoO}_3$  whisker concentration determinations. Figure 3 is a plot of  $\text{MoO}_3$  whisker concentration versus temperature in the range 250°–500°C. A definite optimum temperature was found for whisker growth at about 375°C., indicated by the broad maximum in the curve in this range. The whisker concentration falls off and approaches zero on either side of the maximum.

*MoO<sub>3</sub> Concentration.* A series of "flash-dried"  $\text{MoO}_3$ - $\text{SiO}_2$  solids was prepared with  $\text{MoO}_3$  concentrations in the range 0.01–90 wt. %. These samples were subjected to whisker growth and an average whisker count on 0.01 mm.<sup>2</sup> of substrate surface was taken as a measure of whisker concentration. Figure 4 is a plot of whisker count versus concentration of  $\text{MoO}_3$  in the silica substrate. A broad maximum in whisker concentration appeared in the region 10–30 wt. %  $\text{MoO}_3$ . At 90 wt. %  $\text{MoO}_3$ , the whisker growth dropped off to such an extent that only traces of whiskers were observed (growth limited by  $\text{SiO}_2$  surface), while as little as 0.1 wt. %  $\text{MoO}_3$  gave some whisker growth.

*Silica Surface Area.* Samples of Ludox-derived silica gel were sintered at elevated temperatures for various lengths of time to obtain substrate samples with a range of surface areas. The BET nitrogen adsorption method (5) was employed in determining the surface areas. The sintered silica

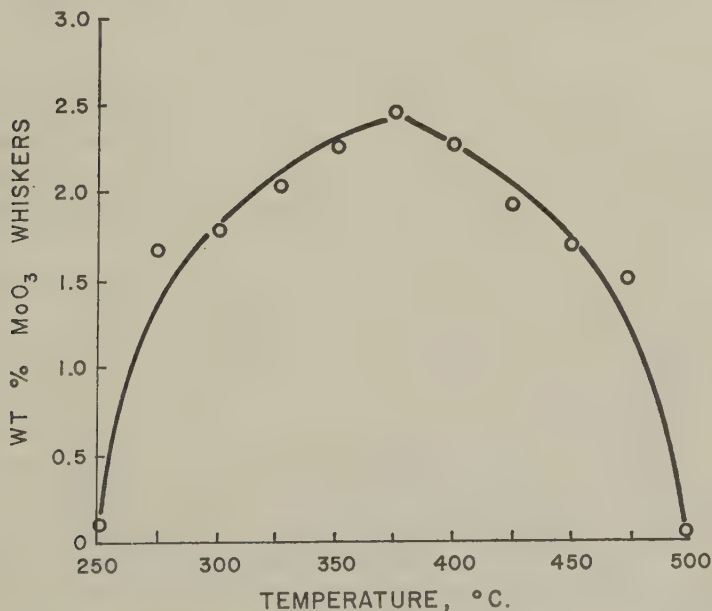


FIG. 3. Effect of temperature on  $\text{MoO}_3$  whisker growth (72 hours at 4.10–5.78 atm. steam pressure, 3 wt. %  $\text{MoO}_3$ –97 wt. %  $\text{SiO}_2$ ).

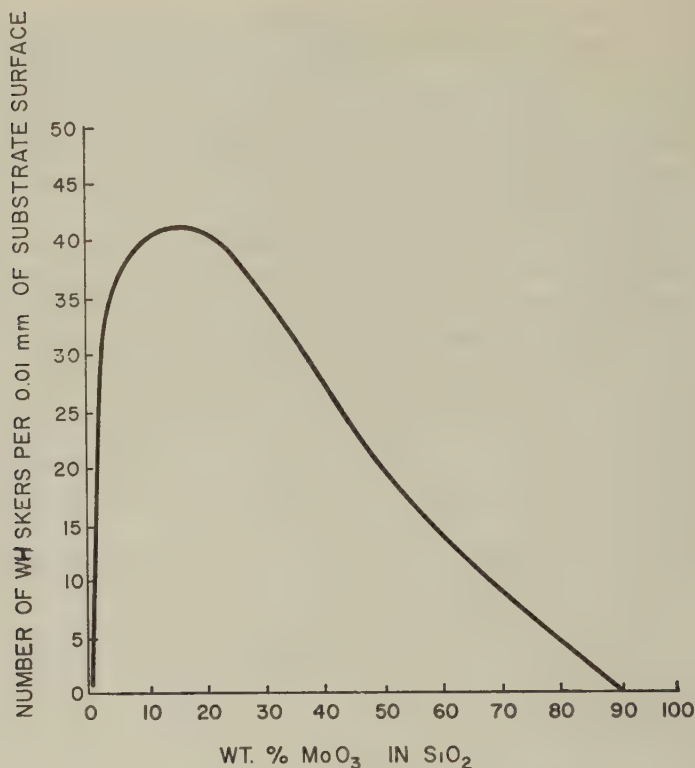


FIG. 4. Effect of MoO<sub>3</sub> concentration on MoO<sub>3</sub> whisker growth.

samples were impregnated with ammonium heptamolybdate solution to obtain solids of composition, 3 wt. % MoO<sub>3</sub>-97 wt. % SiO<sub>2</sub>. Each sample was subjected to hydrothermal treatment under identical conditions and an average whisker count on 0.01 mm.<sup>2</sup> of substrate surface was made. The extent of whisker growth decreased as the silica substrate surface area decreased, especially so in the case of the smaller surface areas.

*Substrate.* The effect on whisker growth of replacing the silica substrate with alumina was investigated. Under conditions which would have produced whisker growth on a silica substrate, no trace of whisker growth was observed on an alumina substrate.

It was also found that the addition to the MoO<sub>3</sub>-SiO<sub>2</sub> solid of several metal oxides such as Na<sub>2</sub>O, K<sub>2</sub>O, Cs<sub>2</sub>O, CuO, MgO, CaO, Fe<sub>2</sub>O<sub>3</sub>, and NiO in concentrations sufficient to form the corresponding molybdates, completely suppressed whisker growth. Additions of small quantities of these oxides, i.e., quantities less than those required for stoichiometric reaction with MoO<sub>3</sub>, resulted only in reduced whisker growth.

*Oxidation State of Molybdenum.* A sample of 3 wt. % MoO<sub>3</sub>-97 wt. %

$\text{SiO}_2$  was reduced with hydrogen at  $480^\circ\text{C}$ . When a portion of this solid was subjected to hydrothermal treatment in the presence of hydrogen, no whiskers were observed, indicating that, under hydrothermal conditions, whisker growth on a silica substrate is limited to the higher oxide of molybdenum,  $\text{MoO}_3$ .

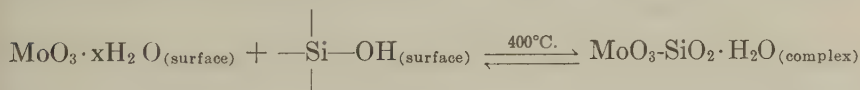
### DISCUSSION

The following hypothesis is suggested as a mechanism for the mobility of  $\text{MoO}_3$  on a silica substrate: As the first step, a molybdic acid is formed by the reversible hydration of  $\text{MoO}_3$ ,



The equilibrium constant for this reaction is assumed to be such that a substantial portion of the  $\text{MoO}_3$  in the surface is not hydrated. The following evidence for the occurrence of this reaction at the surface of solid  $\text{MoO}_3$  in the presence of steam leaves little doubt that it actually takes place: Balareff (6) and Tammann and Westerhold (4) have pointed out the strong promotional effect of steam on the solid state reaction of  $\text{MoO}_3$  with other metal oxides to form molybdates. Jander and Stamm (7) have found that water vapor affects the extent of reaction of  $\text{CaCO}_3$  with  $\text{MoO}_3$  to form  $\text{CaMoO}_4$ . Cornelius and co-workers (8) find a high rate of deuterium exchange for hydrogen when  $\text{D}_2\text{O}$ - $\text{H}_2\text{O}$  gas mixtures are in contact with metal oxide catalysts in general. They also call attention to the fact that the chemisorption of  $\text{H}_2\text{O}$  on a metal oxide surface can be demonstrated by attempts at measuring the surface area using water vapor in the BET method. Finally, Millner and Neugebauer (9) have indicated that  $\text{MoO}_3$  forms a hydrate in the gas phase in the temperature range  $600^\circ$ - $700^\circ\text{C}$ .

The second step involves the reaction of molybdic acid with the silanol surface of the silica substrate to form a silicomolybdic acid-like complex:

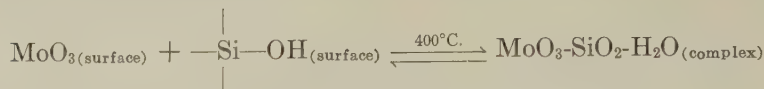


Khitarov and Ivanov (10) found that if gelatinous silica was added to a sodium molybdate solution and the mixture heated in an autoclave at  $400^\circ$ - $430^\circ\text{C}$ . and above the critical pressure, a large transport of  $\text{MoO}_3$  to  $\text{PbO}$  or  $\text{CaO}$  placed in platinum boats in the upper part of the autoclave was obtained. When the same experiment was conducted without the addition of silica gel, very little transport of  $\text{MoO}_3$  resulted. Formation of a complex between  $\text{MoO}_3$  and  $\text{SiO}_2$  was postulated.

In the present work it is believed that the mobility of  $\text{MoO}_3$  might be derived by reaction to form the  $\text{MoO}_3$ - $\text{SiO}_2$ - $\text{H}_2\text{O}$  complex followed by decomposition of the complex. Through a process of successive reaction and

decomposition, the  $\text{MoO}_3$  might be macroscopically displaced on the silica substrate.

The growth of whiskers is assumed to occur because the equilibrium in the overall reaction:



is such that it substantially displaced toward the left.

West and Audrieth (11) have carried out differential thermal analysis studies on several heteropoly acids. They found that silicomolybdic acid displayed an exothermic break in the temperature range  $340^\circ\text{--}360^\circ\text{C}$ . X-ray analysis confirmed that the silicomolybdic acid crystal structure had broken down into a mixture of  $\text{MoO}_3$  and  $\text{SiO}_2$  at the point of exothermic transition. These observations lend support to the postulate that  $\text{MoO}_3$  transport may occur via a silicomolybdic acid-like complex of slight stability in the temperature range where  $\text{MoO}_3$  whisker growth was observed.

When the silicomolybdic acid-like complex decomposes, the  $\text{MoO}_3$  fragments would be expected to take up positions on the substrate where the surface energy is high. The ends of emergence of dislocation lines or similar defect areas might correspond to such energy-rich regions. Such high-energy "islands" on the surface are assumed to be the sites from which the whiskers grow. Thus growth is postulated to take place at the base of the whisker by the accumulation of  $\text{MoO}_3$  from the decomposition of the surface complex.

#### REFERENCES

1. CALLAHAN, J. L., PETRUCCI, R. H., AND BROWN, C. A., *Science* **128**, 841 (1958).
2. ASSARASSON, G. O., AND RYDBERG, E., *J. Phys. Chem.* **60**, 397-404 (1956).
3. CARLSON, E. T., PEPPLER, R. B., AND WELLS, L. S., *J. Research Natl. Bur. Standards* **51**, 179-184 (1953).
4. TAMMANN, G., AND WESTERHOLD, FR., *Z. anorg. u. allgem. Chem.* **149**, 21-34 (1925).
5. BRUNAUER, S., EMMETT, P. H., AND TELLER, E. J., *J. Am. Chem. Soc.* **60**, 309-319 (1938).
6. BALAREFF, D., *Z. anorg. Chem.* **136**, 216-220 (1924).
7. JANDER, W., AND STAMM, W., *Z. anorg. u. allgem. Chem.* **190**, 65-78 (1930).
8. CORNELIUS, E. B., MILLIKEN, T. H., MILLS, G. A., AND OBLAD, A. G., *J. Phys. Chem.* **59**, 809-813 (1955).
9. MILLNER, T. A., AND NEUGEBAUER, J., *Nature* **163**, 601-602 (1949).
10. KHITAROV, N. I., AND IVANOV, L. A., *Compt. rend. acad. sci. U.R.S.S.* **27**, 694-696 (1940).
11. WEST, S. F., AND AUDRIETH, L. F., *J. Phys. Chem.* **59**, 1069-1072 (1955).

## AN EVALUATION OF THE ELECTROSTATIC FREE ENERGY OF MICELLE FORMATION

Arthur Veis and Charles W. Hoerr

*Research Division, Armour and Company  
Chicago, Illinois*

*Received November 2, 1959; revised January 25, 1960*

### ABSTRACT

The acid dissociation constants,  $K$ , of decyl- and dodecylammonium chloride were determined from pH measurements, in the absence of added salt, just above and just below the critical micelle concentration. The change in  $K$  is related to the electrostatic work of forming the micelle. This work is  $2.53 kT$  and  $3.75 kT$ , respectively, for the  $C_{10}$  and  $C_{12}$  salts. Upon comparing these values with similar values obtained by other means for different micelle-forming molecules of equal hydrocarbon chain length, one finds a correlation between the change in  $K$  and the specific character of the ionizable group. This specific effect is discussed in terms of the surface geometry of the micelle and the transmission of electrostatic effects through the micelle hydrocarbon cavity of low dielectric constant.

The thermodynamic approaches to an understanding of the factors that control micelle size and shape have emphasized the crucial role of electrostatic repulsive forces at the micelle surface (1-3). These repulsive forces balance the van der Waals' cohesive forces of the non-polar parts of the micelle-forming molecules (MFM) (1), or the change in surface energy on the formation of the micelle (2), or both (3). Ooshika (2, 4), for example, has formulated the energy per micelle,  $w$ , as

$$w = n^{3/2}w_e + n^{1/2}w_s - nw_m \quad [1]$$

in which  $n$  is the aggregation number (MFM per micelle). Here  $w_e$  is the electrostatic term related to the work required to overcome the electrostatic repulsions at the micelle surface. This is a constant for any given MFM species. Similarly,  $w_s$  is a constant describing the work required to create the micelle surface and  $w_m$  is the energy gained from attractive van der Waals' interactions.

Essentially, two paths have been taken for the evaluation of these energy constants. The free energy equation concerned with the equilibrium between the micelle and the solution has been written in such a way as to include both Eq. [1] and the concentration of the MFM. This expression has been minimized and solved to give a relationship between the critical



micelle concentration (CMC),  $w$  and  $n$  (2-4). Knowing the CMC and  $n$ , one could calculate  $w$ , and by studying the effect of ionic strength on the CMC and  $n$ , one could determine  $w_e$ .

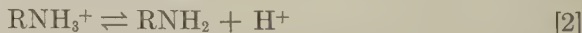
Alternatively, Overbeek and Stigter (5) computed  $\Delta F_e$  from a theoretical analysis of the Poisson-Boltzmann distribution of counter-ions about the micelle. Debye (1) and Hobbs (6) made similar computations with somewhat different assumptions.

Using the first method of analysis, Shinoda (7) found that  $\Delta F_e/kT$  varied from 2.6 for the potassium soap of the  $C_8$  carboxylic acid to 6.7 for the  $C_{18}$  soap. The cohesive energy was  $7.6 kT$  and  $18.4 kT$ , respectively, for these two examples. Overbeek and Stigter (5) analyzed data on sodium lauryl sulfate in terms of their treatment as a function of salt concentration and found  $\Delta F_e/kT$  to vary from 3.4 in the absence of salt to 0.6 in  $0.4 M$  NaCl. One obtains values of  $\Delta F_e$  of the same order of magnitude by either treatment, but both have a common failing. In order to compute  $\Delta F_e$  one must know  $n$  and, in addition, estimate the size and shape of the micelle to obtain some other parameters appearing in the complete free energy equations.

It occurred to us that an alternative approach, which did not require the knowledge of  $n$  nor any approximations as to micelle shape, might provide more nearly direct experimental values for the electrostatic interaction term.

#### CHANGES IN IONIZATION EQUILIBRIA ON MICELLE FORMATION

The cationic long-chain ammonium ions can be treated as acids that dissociate reversibly in aqueous solution, e.g.,



with a characteristic acid dissociation constant,  $K_a$ , given by Eq. [3].

$$K_a = \frac{[RNH_2][H^+]}{[RNH_3^+]} \quad [3]$$

The bracketed terms in this equation represent the concentration of each moiety. It is not necessary to include activity coefficients for the estimates to be made shortly. When the hydrocarbon chain  $R$  is large enough and when  $\{[RNH_3^+] + [RNH_2]\}$  is sufficiently great for micelles to form,  $K_a$  becomes a composite of two ionization equilibria. If we set

$n_T$  = total number of MFM in the system of volume  $V$ ;

$n_f$  = number of single MFM in  $V$ ;

$n_m$  = number of micelles in  $V$  each with aggregation number  $n$ ;

then

$$n_T = n_f + n \cdot n_m, \quad [4]$$

and the hydrogen-ion equilibria are

$$K_f = \frac{n_f^0 [\text{H}^+]}{n_f^+}; \quad [5]$$

$$K_m = \frac{\alpha n \cdot n_m [\text{H}^+]}{(1 - \alpha) n \cdot n_m}, \quad [6]$$

where  $\alpha$  is the fraction of unionized MFM in the micelle. This formulation of the equilibria implies that we anticipate that the molecules in the micelle will have a different ionization constant from that of the free molecules. We still assume, however, that we can treat the ionization of each MFM in the micelle independently. That is,  $K$  is to be modified by the same average effect for each ionizable group, so we can write

$$K_m = K_f e^{\Delta F_e / RT}. \quad [7]$$

As with polyelectrolyte systems, we assume that the major effect is the mutual electrostatic repulsive force of the nearby ionized groups and that we can identify  $\Delta F \approx \Delta F_e = w_e$ .

Thus,  $w_e$  can be evaluated through determinations of  $K_f$  and  $K_m$ . If an apparent  $K_f$  is measured in the region just below the CMC and the  $K_m$  is obtained just above the CMC, concentrations can be used in place of activities since we are interested in the  $K_m/K_f$  ratio. This method of calculation puts all deviations in the activity coefficient of each ion, because of environmental differences in the micelle and in the free state, into the term for  $\Delta F_e$ . The acid dissociation constant of the amine hydrochloride,  $K_f$ , is very small,  $\sim 10^{-11}$ , and the effective change is not very great. Thus, we are dealing with small degrees of dissociation both in the free state and in the micelle. Otherwise, the  $K_m$  value calculated through Eq. [6] would not be expected to be constant. As found from the measurements  $K_m$  is the dissociation constant of the first  $\text{H}^+$  ion leaving the micelle and  $\Delta F_e$  relates to that process. This electrostatic free energy is not the same as the average value of  $\Delta F_e$  obtained by the method of Overbeek and Stigter (5). The  $\Delta F_e$  that we calculate is the limiting value and corresponds to the work,  $w_e$ , required to form the first micelle in the environment of the MFM at the CMC. The values of  $K_m$  and  $K_f$  have been arrived at through careful pH determinations in the region of the CMC for dodecylammonium chloride ( $\text{C}_{12}\text{H}_{25}\text{NH}_3\text{Cl}$ ) and for decylammonium chloride ( $\text{C}_{10}\text{H}_{21}\text{NH}_3\text{Cl}$ ).

#### pH DETERMINATIONS

The pH of each of the ammonium salt solutions fell between 7.0 and 5.0. Therefore, every precaution had to be taken to carry out the measurements in the absence of  $\text{CO}_2$ . The apparatus used for these determinations

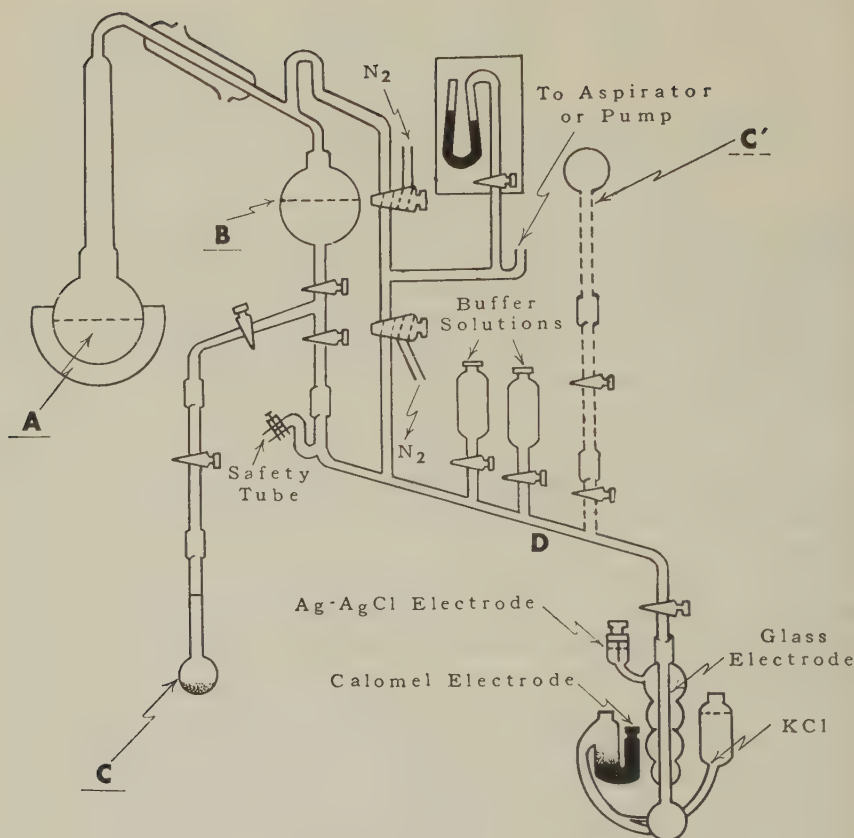


FIG. 1. Apparatus for  $\text{CO}_2$ -free pH determination (see text for explanation).

is shown in Fig. 1. After the system was flushed with  $\text{CO}_2$ -free  $\text{N}_2$ , water was distilled from flask A to storage flask B. A weighed amount of amine salt was put into flask C, the air was evacuated, and the solution made up by weight with water from B. The solution was then transferred to position C' and, after again flushing the system with  $\text{N}_2$ , was drained into the closed assembly of a Cambridge pH electrode system. There was a slight but decided time lag before the glass electrode became equilibrated with the solution so, as a matter of routine, at least 8 minutes contact time was allowed before readings were taken. A second reading was taken about 10 minutes later. The results are given in Figs. 2 and 3 for  $\text{C}_{12}\text{H}_{25}\text{NH}_3\text{Cl}$  and  $\text{C}_{10}\text{H}_{21}\text{NH}_3\text{Cl}$ , respectively. Each point on these diagrams represents an entirely independent measurement (weighed sample, weighed solvent, pH measurement, and meter calibration<sup>1</sup>). It is evident that an abrupt decrease

<sup>1</sup> The measurements were carried out by Mr. H. Hausman.

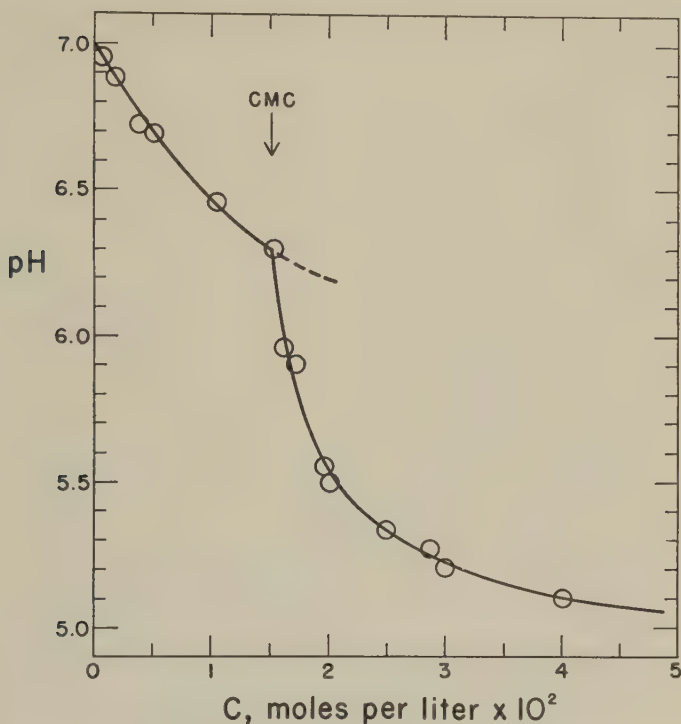


FIG. 2. The pH of dodecylammonium chloride solutions as a function of concentration.

in pH did occur in the region of the CMC as the amine salt concentration was increased. Similar pH measurements were carried out on hexylammonium chloride, Fig. 4, in the same concentration range. The  $C_6H_{13}NH_3Cl$  does not form micelles and no sharp variations in pH could be detected in the pH vs.  $C$  plots.

#### EVALUATION OF $w_e$

Values of  $K_f$  were determined through Eq. [5] from the pH measurements immediately below the CMC. It was then assumed that in the region just above the CMC  $K_f$  did not change appreciably. With  $K_f$ ,  $n_f$  (from the CMC), and the measured pH known,  $n_f^0$  and  $n_f^+$  were calculated with the aid of Eq. [5]. The number of MFM held in the micelles ( $nn_m$ ) is known from the difference between the total MFM concentration and the CMC and the fraction of these ionized can be calculated from the stoichiometric hydrogen ion balance. The contribution of  $H^+$  ions from the water can be included in these calculations but result in negligible corrections. With these data, since  $n$ , the aggregation number, cancels in Eq. [6],  $K_m$  can be

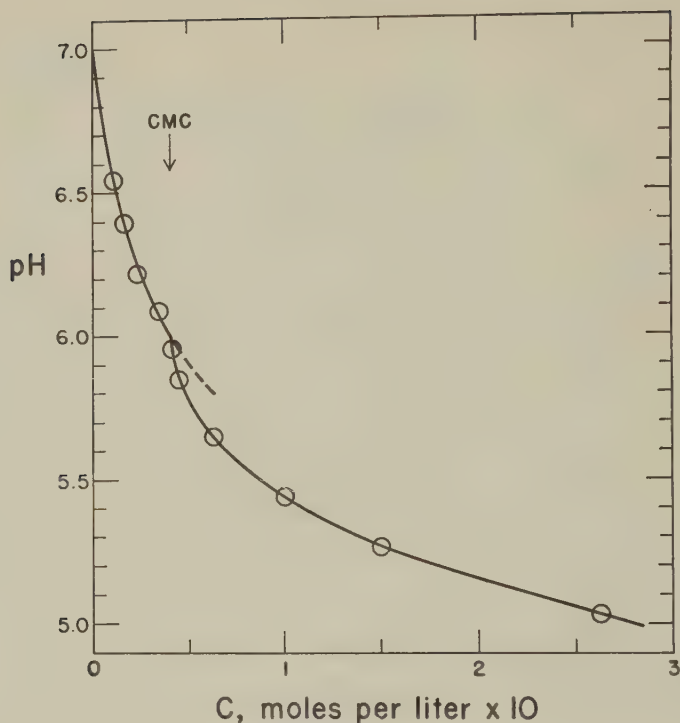


FIG. 3. The pH of decylammonium chloride solutions as a function of concentration.

evaluated without knowing the micelle size. The results are shown graphically in Fig. 5, in which the negative logarithms of  $K_f$  and  $K_m$  ( $pK$ ) are plotted versus the total amine salt concentration. Extrapolating these data a short distance to the CMC, one finds  $\Delta pK_{C_{12}} = -1.63$  and  $\Delta pK_{C_{10}} = -1.10$  ( $pK_m = pK_f$ ). These values correspond to  $(w_e)_{C_{12}} = 3.75 kT$  and  $(w_e)_{C_{10}} = 2.53 kT$  for the salt-free micelles at the ionic strength indicated by the CMC. The calculations for  $pK_m$  very close to the CMC were not very precise for the  $C_{10}$  amine salt because of the relatively smaller change in pH in that region. The extrapolated  $\Delta pK$  value was taken from points at significantly higher concentrations. The  $\Delta pK$  in this case is probably a maximum value.

It is instructive to compare the values of  $w_e$  and CMC for different MFM of similar hydrocarbon chain length. Such values are assembled in Table I as far as available data permit. The  $w_e$ 's for the sulfate and carboxylate MFM are essentially experimental values determined from the variation of the CMC with ionic strength. The tabulated data for the  $C_{11}$  and  $C_{13}$  carboxylic acids were obtained from a plot of Shinoda's estimates



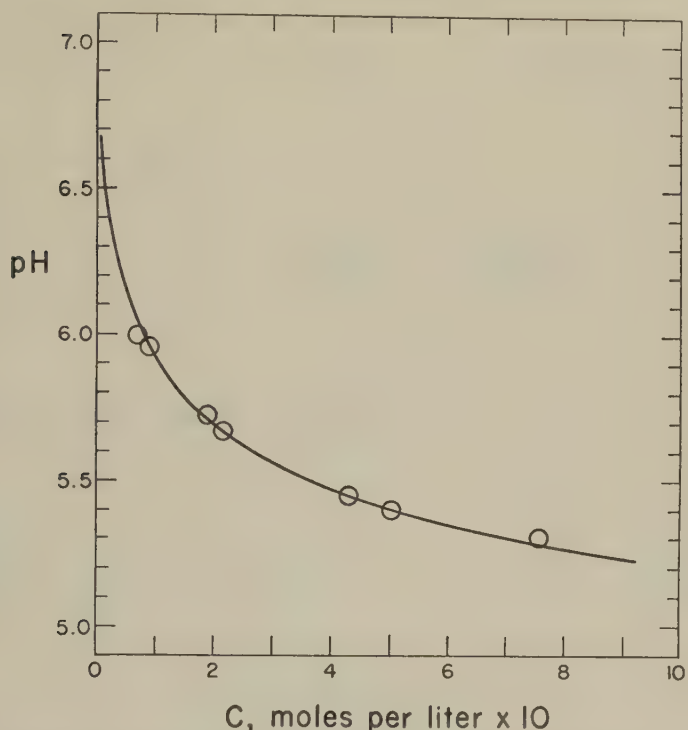


FIG. 4. The pH of hexylammonium chloride solutions as a function of concentration.

of  $w_e$  vs. chain length (7). The carboxylate CMC's are the values of Herzfeld (8). It is evident that the  $w_e$  obtained from our treatment of the changes in  $K_a$ , without resorting to any models of micelle shape or knowledge of micelle size, fits very well with the  $w_e$  values obtained by using different approaches. A more important observation can be made, however. From Shinoda's work (7) one can see that in a homologous series of any MFM type,  $w_e$  decreases as the CMC increases. Since the work required to add a charge to the micelle is proportional to the square of the total micelle charge,  $w_e$  should decrease as the micelle becomes smaller. In addition, it is also reasonable to ascribe part of the decrease in  $w_e$  with decreasing chain length to the fact that the ionized free MFM provide the ionic atmosphere for the charge shielding in the micelle layer. The interesting point is that just the opposite effect is noted in comparing the CMC's and  $w_e$  values for the  $C_{10}$  and  $C_{12}$  chain length MFM of varying charge types within the limitations of the available data. The value of  $w_e$  is found to decrease as the CMC decreases.

For the MFM listed in each part of Table I the hydrocarbon chain

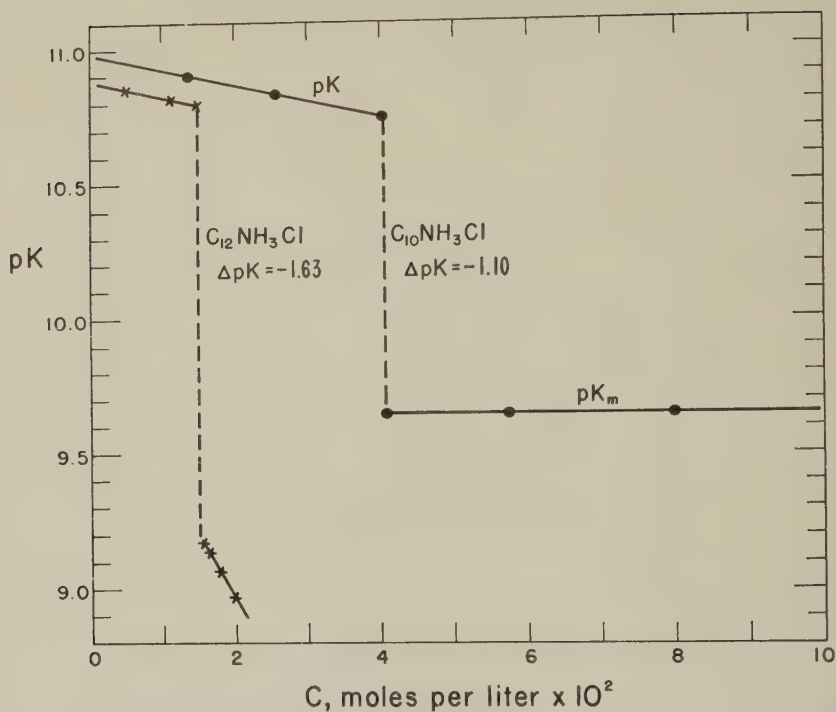


FIG. 5. Calculated pK values as a function of amine salt concentration. ●—C<sub>10</sub> salt; ×—C<sub>12</sub> salt.

lengths are the same and  $m$  is nearly identical in each case (9). Thus, to a good first approximation the  $nw_m$  and  $n^{1/2}w_s$  terms of Eq. [1] will also be identical for each micelle species. The information in Table I therefore directly illustrates the effect of  $w_e$  on the CMC, or more exactly on the equilibrium between the micelles and the free micelle-forming ions. Furthermore, since the C<sub>12</sub> micelles are of similar total charge and surface charge density the differences in  $w_e$  must be due to the specific ways in which the ionic groups are situated in the surface of the micelle. As Tartar points out (9), there is no question of steric interference of the ionic groups in the micelle surface since these groups are so widely separated.

Figure 6 illustrates schematically the differences in surface configuration. The dimensions of each ion have been taken into account in the drawing. The principal difference appears to be in the extension of the charged groups into the aqueous phase, or conversely, in the degree to which they are buried in the hydrocarbon medium of the micelle interior. These structural differences result in variations in the extent of hydration of each ion and in the effective dielectric constant of the immediate surroundings of each ion. This latter effect seems to us to be the most logical explanation for the differences in  $w_e$ .

TABLE I

Comparative Values of the Electrostatic Free Energy for Different MFM in Salt-free Systems

MFM	CMC (moles/ liter)	$w_0/kT$	Method	Reference
$C_{12}H_{25}COOK$ . . . . .	0.013	4.6	Flat electrical double layer + variation of CMC with salt	Shinoda (7)
$C_{12}H_{25}NH_3Cl$ . . . . .	0.013	3.75	$\Delta pK_a$	This paper
$C_{12}H_{25}SO_4Na$ . . . . .	0.008	3.4	Poisson-Boltzmann distribu- tion of counterions + vari- ation of CMC with salt	Overbeek and Stig- ter (5)
$C_{10}H_{21}COOK$ . . . . .	0.05	3.85	Flat electrical double layer + variation of CMC with salt	Shinoda (7)
$C_{10}H_{21}NH_3Cl$ . . . . .	0.04	2.53	$\Delta pK_a$	This paper
$C_{10}H_{21}SO_4Na$ . . . . .	0.031	—	—	Tartar (9)

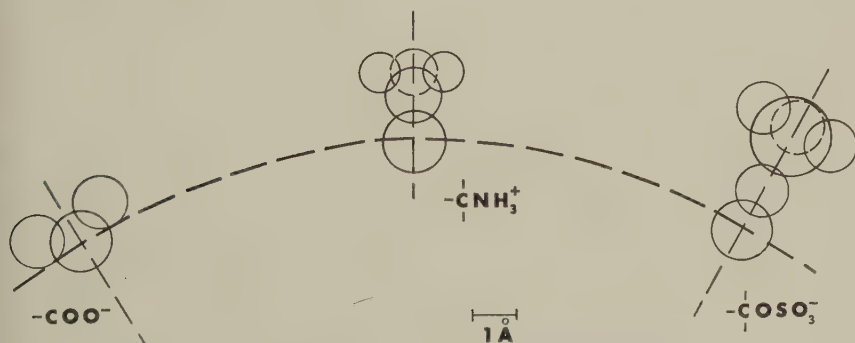


FIG. 6. Schematic diagram of the relative spatial arrangements of ionic groups on a  $C_{12}$  micelle surface. Intergroup distances and ionic radii are drawn to scale.

The situation is analogous to that treated by Kirkwood and Westheimer (10). They considered the effect of charged substituents on the ionization constants of another ionizable group in the same molecule. The direct effect of the new electric field through the solvent was the greater, but the secondary effect of the transmission of the electrical field through the molecular cavity of low dielectric constant was pronounced. This treatment enables us to put the effects noted in micelles into quantitative terms. There is transmission of electrostatic effect through the aqueous phase ( $D \sim 80$ ) which surrounds the micelle. There is also transmission of these effects through the hydrocarbon interior of the micelles ( $D \sim 2$ ). From Fig. 6, we anticipate the effective dielectric constant,  $D_E$ , to vary in the order

$(D_E)_{-COO^-} < (D_E)_{NH_3^+} < (D_E)_{-OSO_3^-}$ . Using the Kirkwood-Westheimer equation (10)

$$\Delta pK = \frac{N\epsilon^2}{2.303 RT\tau D_E} \quad [8]$$

and assuming that the interionic distance,  $r$ , along the micelle surface is constant, one can calculate the ratios  $(D_E)_{COO^-}/(D_E)_{OSO_3^-}$  and  $(D_E)_{NH_3^+}/(D_E)_{OSO_3^-}$ , which have the value 0.79 and 0.87, respectively. It is not possible to calculate  $D_E$  in absolute terms at the present time.

### CONCLUSIONS

The CMC's of molecules of the same hydrocarbon chain length but with different ionized end groups vary directly in relation to the electrostatic work required to form the micelle. This work, in turn, is related to the spatial arrangement of the ionic groups on the micelle surface. According to the above discussion, the primary consequence of the ionic group-surface configuration is, electrostatically, the result of a change in the effective dielectric constant along the micelle surface for each particular type of ion. Furthermore,  $D_E$  is less than  $D_{\text{solvent}}$  in every case. Thus, an irreducible electrostatic repulsion will always be transmitted through the micelle hydrocarbon cavity, again specific for each type of ion. From this, one would predict that the effect of added salt on the CMC would be greater whenever the  $D_E/D_{\text{solvent}}$  ratio is greater. For example, one would predict from Table I that salt would lower the CMC of the  $C_{12}H_{23}OSO_3Na$  much more than it would that of the  $C_{11}H_{23}COOK$ . This, of course, has been found experimentally, as Harkins (11) has summarized, "It is apparent that the lower the critical concentration, i.e. the greater the tendency toward aggregation, the greater is the lowering of the critical concentration by equal amounts of salt." In our terms, the "tendency toward aggregation" for a given chain length is determined by the intrinsic  $w_e$ . Other predictions on micelle-environment interaction can also be made on this basis.

### REFERENCES

1. DEBYE, P., *Ann. N. Y. Acad. Sci.* **51**, 575 (1949); *J. Phys. Chem.* **53**, 1 (1949).
2. OOSHIMA, Y., *J. Colloid Sci.* **9**, 254 (1954).
3. K. SHINODA AND K. KIMOSHITA, *Bull. Chem. Soc. Japan* **27**, 73 (1954).
4. Y. OOSHIMA AND Y. IKEDA, *Kolloid-Zeitschrift* **145**, 3 (1956).
5. J. TH. G. OVERBEEK AND D. STIGTER, *Rec. trav. chim.* **75**, 1263 (1956).
6. HOBBS, M. E., *J. Phys. Chem.* **55**, 675 (1951).
7. SHINODA, K., *J. Phys. Chem.* **60**, 1439 (1956).
8. HERZFELD, S. H., *J. Phys. Chem.* **56**, 959 (1952).
9. TARTAR, H. V., *J. Colloid Sci.* **14**, 115 (1959).
10. KIRKWOOD, J. G., AND WESTHEIMER, F. H., *J. Chem. Phys.* **6**, 506, 513 (1938).
11. HARKINS, W. D., *J. Am. Chem. Soc.* **69**, 683 (1947).

## ELECTROPHORETIC MOBILITY AND ELECTROCHEMISTRY OF LATEX SYSTEMS

C. L. Sieglauff and J. Mazur\*

*Polymer Research Laboratory, The Dow Chemical Company, Midland, Michigan*

*Received April 29, 1960*

### ABSTRACT

The electrophoretic behavior of a polystyrene latex measured at various soap and salt concentrations is explained on the basis of the Stern theory of the double layer. It was found that the direct application of the Stern theory agrees well with the experimental findings only for latex systems characterized by highly covered surfaces. A modified Stern theory is presented to account for the electrophoretic behavior of latex particles characterized by lightly covered surfaces. This is done by assuming that the potential at the slipping plane (zeta potential) differs from the surface potential, and that the potential drop in the Stern layer depends on the ionic strength of the solution. A theoretical explanation of the variation in mobility with change in soap and salt concentrations and of the conditions for maximum mobility is given.

### INTRODUCTION

Current theories of the stability of colloids involve the electrostatic interactions between the charges on the colloidal particles, which lead to a net repulsion, and the nonelectrostatic attractions between these particles (1). Basic to the theory of the stability of latex systems is the understanding of the structure of the electric double layer which surrounds a latex particle. Such physical quantities as the potential of adsorption of the soap ions on the latex particles, the number of adsorption sites per unit area of the particle, and the potential at the interface are of primary importance in the problem of the interaction between the latex particles, and consequently, in the problem of latex stability. The electrophoretic mobilities of a latex particle present a method of obtaining this information about the structure of the double layer.

This and a forthcoming paper are devoted to an analysis of the experimental electrophoretic mobilities of a polystyrene latex measured at various soap and salt concentrations. In the present paper, the effects of salt and soap concentrations on the structure of the double layer are analyzed. Later, the effect of the nature of the soap molecule upon the structure of the double layer will be treated by comparing electrostatic mobilities with various soaps.

\* Present address: National Bureau of Standards, Washington 25, D. C.



Let us review briefly the theory of the double layer. The electrical double layer is an array of charged particles and oriented dipoles which exists at a phase boundary. This double layer is composed for completely non-ionogenic particles of a layer of adsorbed soap ions (Stern layer) and of a diffuse layer which consists of an equivalent amount of ionic charge of opposite sign. In the ionic atmosphere, ions of one sign are in an excess of their average concentration in the solution, whereas the oppositely charged ions are in relative deficiency. This condition of abnormal concentrations of ions diminishes with distance from the surface of the adsorbing particle.

The proposed model is restricted to latex particles without intrinsic charges, and therefore to cases where the total charge of the double layer must be zero. In other words, the total space charge of the diffuse part of the double layer must be oppositely equal to the total charge of the adsorbed layer. The adsorbed, or the "compact" layer, consists in part of a monolayer of adsorbed ions. In the original theory of Stern (2) it was assumed that this monolayer constitutes the whole of the "compact" layer. More recent investigations of electrocapillary phenomena of mercury electrodes have led to the belief that the "adsorbed" layer includes in addition to the adsorbed ions displaced solvent molecules (3). We shall return later to this possibility when we discuss the experimental results. In the proposed theoretical model only the monolayer of adsorbed soap anions contributes to the total charge of the "adsorbed" layer. For this reason the total space charge of the *diffuse* part of the double layer must be oppositely equal to the total *surface* charge. It is convenient to employ the space and the surface charges in units of volume and area, respectively. Mathematically, this means that

$$\int_{\delta}^{\infty} \rho \, dx = \sigma_2, \quad [1]$$

where  $\sigma_2$  is the surface charge in a column of liquid of unit cross section, from the plane with  $x = \delta$ , into the plane where the potential is zero. Here  $\delta$  is the thickness of the Stern Layer which includes the monolayer.<sup>1</sup>

The proposed model states that  $\sigma_2 = -\sigma_1$ , where  $\sigma_1$  is the surface charge of a unit surface of the latex particle. The value of  $\sigma_1$  is therefore given by two equations:  $\sigma_1$  can be obtained from Eq. [1] and from the adsorption equilibrium on the surface of the particle. The surface charge,  $\sigma_2$ , will be obtained from the theory of the diffuse double layer.

The equation for the surface charge in a column of liquid,  $\sigma_2$ , has been derived and has been applied by many investigators to problems which

<sup>1</sup> It should be pointed out, that for the extremely large particles that we are dealing with  $\kappa a$  ( $\kappa$  is the Debye-Hückel constant,  $a$  is diameter of the particle) is large enough to justify the flat double layer treatment, as implied by Eq. [1].

involve the electric double layer (1):

$$\sigma_2 = \left( \frac{2DkTN_0}{\pi 10^3} \right)^{1/2} \Gamma^{1/2} \sinh \frac{ze\psi_\delta}{2kT}. \quad [2]$$

In this equation,  $\Gamma = \sum_i c_{oi}$ , where  $c_{oi}$  are the concentrations in moles per liter of the electrolytes;  $N_0$  stands for Avogadro's number. Since we are dealing with uni-univalent electrolytes,  $\Gamma$  will be designated as the ionic strength of the solution. In the derivation of the equation for  $\sigma_2$  it has been assumed that the dielectric "constant"  $D$  is really a constant independent of  $x$ , the distance from the surface. It would be expected that  $D$  is not a constant in the vicinity of the particle. Presently, we will have to accept Eq. [2] as being reasonably valid up to the point where  $\psi = \psi_\delta$ .

There is a problem of the sign in front of the right-hand side of Eq. [2]. Obviously both  $\sigma_2$  and  $\psi_\delta$  must be of the same sign. For this reason there is a positive sign in front of the right-hand side of Eq. [2]. In the present cases, both  $\sigma_1$  and  $\psi_\delta$  are negative.

According to the Stern Langmuir theory [3]

$$\sigma_1 = \frac{N_1 e v_1}{1 + \frac{\lambda_1}{c} e^{w_1/kT}} \quad [3]$$

where  $N_1$  denotes the number of adsorption sites on  $1 \text{ cm.}^2$  of the surface,  $v_1 e$  is the charge of the adsorbed soap ion, and  $c$  is the concentration of the soap molecules. Here  $\lambda_1$  is a constant which according to Stern is proportional to the number of available positions per cubic centimeter in the liquid;  $w_1$  is the amount of work required to move an ion from the bulk of the solution to the surface of the particle. It is composed of two parts: (1) the electrostatic work and (2) the chemical work assumed to be independent of the electrostatic properties of the system. For adsorbed univalent anions the work will be given by:

$$w_1 = v_1 e \psi_0 - \varphi_1 = -e \psi_0 - \varphi_1, \quad [4]$$

where  $\psi_0$  is the (negative) potential at the surface. The adsorption potential of the soap anion,  $\varphi_1$ , will be included with  $\lambda_1$ , into one comprehensive constant  $\lambda$ .

$$\lambda = \lambda_1 e^{-\varphi_1/kT}.$$

This constant is characteristic of the chemical structure of the soap molecules and the nature of the latex particle, but it is supposed to be independent of the soap and salt concentrations. This assumption will be re-examined later.

Since the Stern model of the double layer does not picture any additional layers besides the diffuse layer and the *monolayer*, it is required that  $\psi_0 = \psi_\delta$

and accordingly

$$\sigma_1 = \frac{-N_1 \epsilon}{1 + \frac{\lambda}{c} e^{+|\epsilon \psi_\delta|/kT}} = A \Gamma^{1/2} \sinh \frac{ze\psi_\delta}{2kT}; \quad [5]$$

$$A = \left( \frac{2DkTN_0}{1000\pi} \right)^{1/2}.$$

If this theory fails, it will be assumed that  $\psi_0 \neq \psi_\delta$ , and  $\psi_0$  will be calculated as a function of the physical parameters of the system. Before proceeding, Eq. [5] will be simplified by removing the charge valences. Since all electrolytes in the system are 1-1 valent,  $|v| = 1$ . Equation [5] is rewritten as follows:

$$\frac{N_1 \epsilon}{1 + \frac{\lambda}{c} e^{\epsilon|\psi_0|/kT}} = A \Gamma^{1/2} \sinh \frac{\epsilon|\psi_\delta|}{2kT}. \quad [5a]$$

In order to determine  $\psi_0$  from the electrophoretic mobilities, one has to give a kinetic meaning to the double layer. It is customary to identify the diffuse part of the double layer with the mobile part of the double layer. The compact part of the double layer is "attached" to the particle. The potential between these two kinetic units is the  $\zeta$ (zeta) potential, which is actually the potential of the slipping plane between the layer which is fixed to the particle and the mobile part of the double layer. Therefore,  $\psi_\delta = \zeta$ , or if the Stern model is assumed,  $\psi_0 = \zeta$ . The relation between mobility and zeta potential for large nonconducting spheres is obtainable from the theory of electroosmosis, since, in a way, electrophoresis is the reverse of electroosmosis.

$$\zeta = \frac{4\pi\eta u}{DE}. \quad [6]$$

Here  $E$  denotes the strength of the applied electric field,  $\eta$  is the coefficient of viscosity, and  $u$  is the velocity of the particle.

Another quantity which has to be discussed is the ionic strength,  $\Gamma$ , of the solution. First of all, it is assumed that the soap molecules are completely dissociated at the working conditions and that their activity coefficients are equal to unity. This assumption is not valid for all soaps, but for caprate it will not lead to large errors. In order to find the concentration of soap molecules in the diffuse layer, it is necessary to know the concentration of soap molecules which are adsorbed on the latex particles. It is assumed for the moment that the surface is completely covered. The number of adsorption sites per square centimeter of the surface is approximately  $2 \times 10^{13}$  (see below). The system has 1 c.c. of a polystyrene latex per liter. Since this latex is approximately 20% solids, and since the

radius of the latex particle is known to be  $8.5 \times 10^{-5}$  cm., the total surface of latex particles per liter of solution is  $7 \times 10^3$  cm.<sup>2</sup>. Therefore, the total concentration of adsorbed soap ions is only about  $2 \times 10^{-7}$  mole/l., which is a negligible amount compared to the soap concentrations employed. For this reason the ionic strength is simply the sum of the salt and soap concentrations. The unknowns in the basic equation [5a] are  $N_1$  and  $\lambda$ , and both are by hypothesis constants for the given systems (i.e., independent of the soap and salt concentrations). If the Stern theory were invalid in the sense that  $\psi_0 \neq \psi_\delta$ , while  $\zeta = \psi_\delta$ , the quantity  $\lambda e^{\psi_0/kT}$  of Eq. [5a] is an unknown function of soap and salt concentrations. The right-hand side of Eq. [5a] is assumed to be completely determined from the measured physical quantities, because the assumption that the potential at the surface end of the *diffuse* double layer is equal to the zeta potential is not being questioned. The validity of the Stern model can be at once tested from the experimental data.

## EXPERIMENTAL

### *Apparatus*

A microelectrophoresis cell (Fig. 1) was used to measure the electrophoretic mobility of the latex particles. The cell was fabricated from Pyrex glass. The observation windows (center section) were made from 0.5 mm. Pyrex plate and were made as parallel as possible. The thickness of the cell varied from 600 to 700 microns. The platinized-platinum electrodes were mounted in 18/9 spherical joints and clamped to the cell. The cell with attached electrodes was clamped to the stage of a microscope.

The microscope and cell were positioned so that the applied electrical field would cause the particles to move in a vertical direction. The microscope was fitted with a 20 $\times$  objective and a 25 $\times$  compensating eyepiece containing a calibrated grid. The light source was a 300 watt zirconium arc. These optics limit the study to particles larger than 1 micron in diameter.

A 0-150 volt variable voltage D.C. power supply was used to apply the potential to the cell. The potential gradient is obtained by calculation from Ohm's law. Thus  $X = IR_{sp.}/A$ , where  $I$  is the measured current flowing through the cell,  $R_{sp.}$  is the specific resistance of the liquid, and  $A$  is the cross-sectional area of the cell at the point of observation. The current was measured using a  $\pm 2\%$  milliammeter. A sensitive conductivity bridge was used to measure the specific resistance of the liquid.

### *Materials*

The latex studied in this investigation was a monodisperse, 1.7 micron polystyrene latex prepared by Dr. J. W. Vanderhoff of the Physical Re-

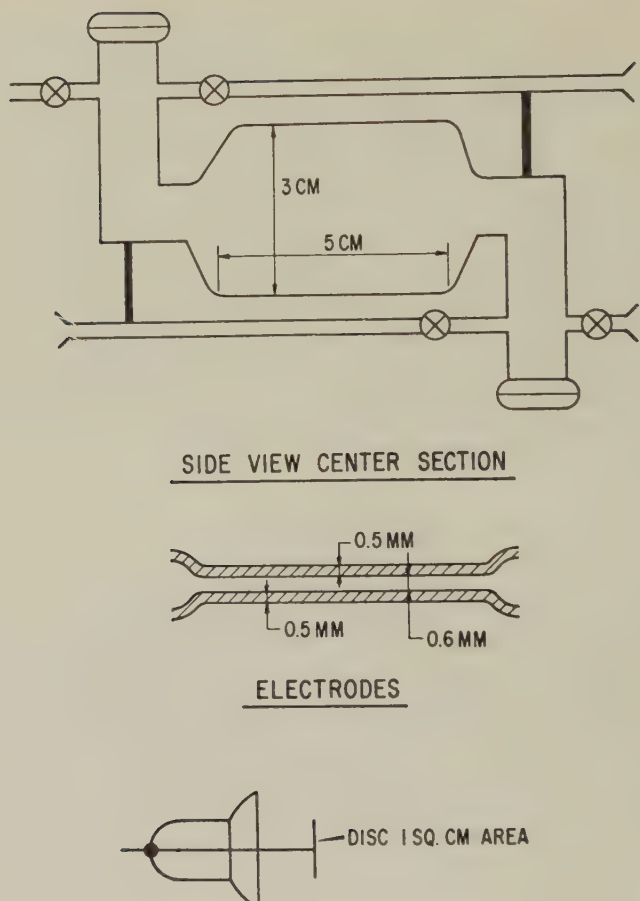


FIG. 1. Microelectrophoresis cell.

search Laboratory, The Dow Chemical Company. This latex was dialyzed against a 2.5% sodium caprate solution. The sodium caprate was prepared by neutralizing pure capric acid with a stoichiometric amount of sodium hydroxide. The resultant material was extracted with xylene and dried.

#### *Procedure*

The dialyzed latex containing 20% total solids was diluted by addition to a solution containing the desired soap and salt concentration. The suspension was allowed to stand for 48 hours to insure equilibrium. The cell was then filled and the solution was allowed to equilibrate with the walls of the cell before any measurements were made.

The microscope was focused on the front edge of the cell, and the time



for the particles in focus to transverse the grid was measured. The polarity of the cell was then changed and the measurement was repeated. Thus, the particles were timed going alternately with the gravitational field and against it. Several measurements were taken in each direction and the average velocity was calculated. The microscope was then racked down 90 microns, and the measurements were repeated. This procedure was continued until the back edge of the cell was reached. A plot was made of the velocity vs. depth in the cell and then the area under the curve was ob-

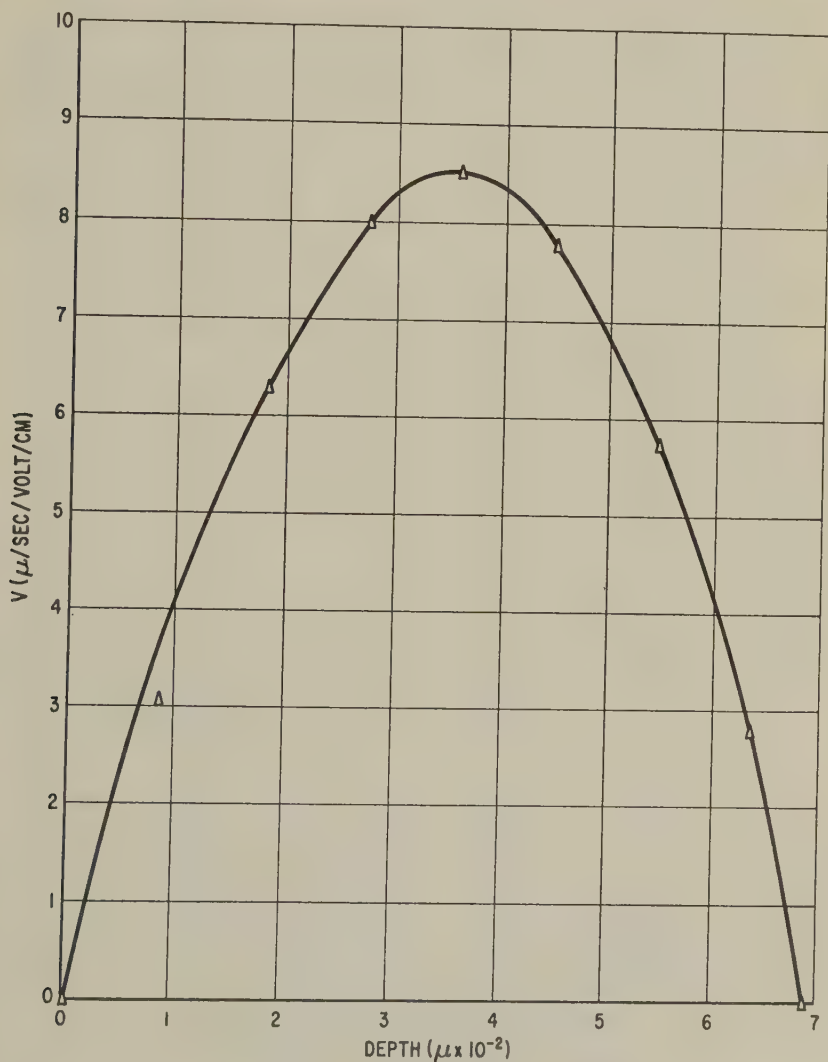


FIG. 2. Typical velocity vs. depth in cell curve.

tained (Fig. 2). From the area and the thickness of the cell it is possible to calculate the mean velocity, i.e., the velocity corresponding to the level at which the electroosmotic velocity is zero. This velocity is then the true electrophoretic velocity.

The above method, although more time consuming than the use of the stationary levels in the cell, yields more accurate data. In the case when the rate of change of the observed velocity with depth is large, a small

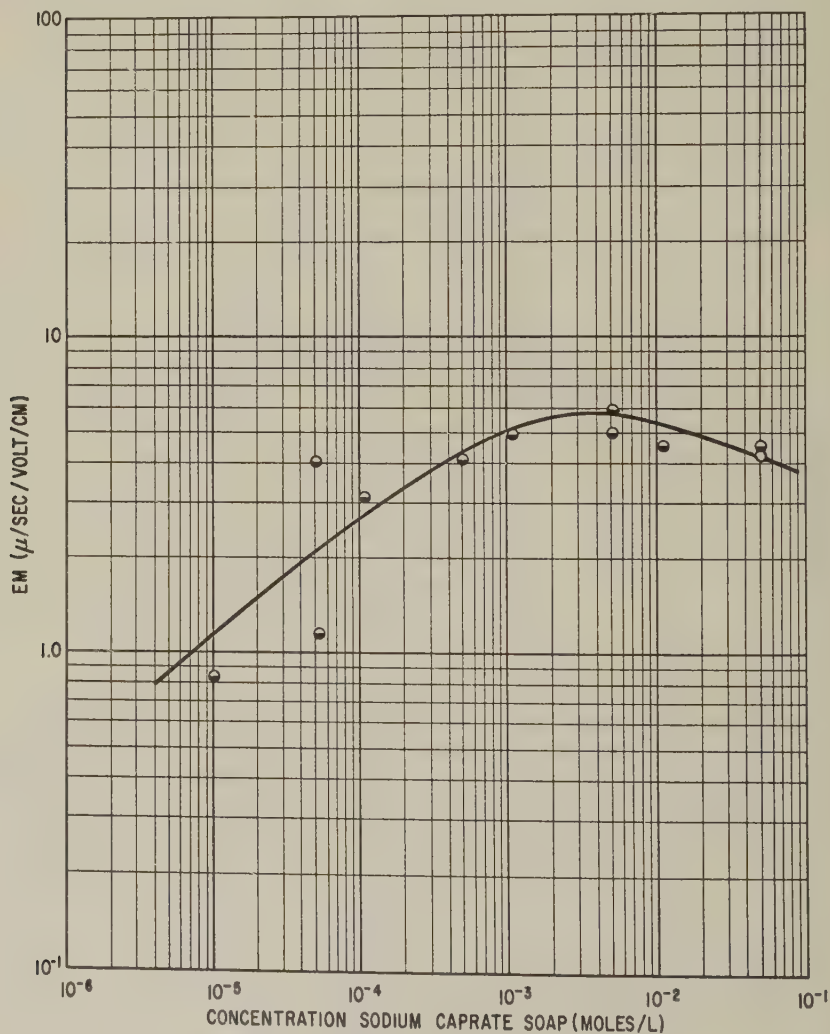


FIG. 3. Mobility vs. soap concentration.

error in focusing at the stationary level can lead to large errors in the electrophoretic velocity. The use of the complete velocity profile allows one to average out small focusing errors.

The intercept of the velocity vs. depth curve (Fig. 2) depends upon the ionic environment. At low ionic strength, i.e., low soap and salt, the intercept was negative; at high ionic strength the intercept was positive. Figure 2 was chosen not as an example of a typical intercept but only to show the typical scatter and shape of the curves.

## RESULTS

The cell employed in making these measurements did not isolate the electrodes from the measuring chamber. It is believed that at low ionic concentrations ( $<10^{-2} M$ ) the electrode products will have a negligible influence on the mobility measurements. This was checked by repeating measurements several times on the same sample and observing little deviation from the original measurement.

The variables studied in this latex system were soap concentration and ionic strength. The relationship between electrophoretic mobility and both of these variables will be discussed separately.

### *Soap Concentration*

The soap concentration was varied from  $10^{-5}$  to  $5 \times 10^{-2}$  mole/l. The lowest concentration was obtained by adding the latex to deionized water in the ratio of approximately 1 volume to 1000 volumes. The concentration of soap was estimated from the specific resistance of the resulting solution. Figure 3 is a log-log plot of the electrophoretic mobility vs. the concentration of sodium caprate soap. The mobility of the latex particles is small at a low concentration of soap, increasing with increasing soap until a concentration of soap of approximately  $3 \times 10^{-3}$  moles/l. is reached. After this soap concentration is reached the mobility decreases with increasing concentration of soap.

### *Ionic Strength*

The mobilities of the polystyrene latex particles were measured in solutions containing three different concentrations of soap and KCl salt concentrations varying from  $10^{-4}$  to  $10^{-1} N$ . The latex particles in solutions containing  $5.15 \times 10^{-4} M$  soap show an increase in mobility when the KCl concentration is increased. (See Fig. 4.) Also, the mobility in solutions containing  $5.15 \times 10^{-3} M$  soap increases as the concentration of salt is increased. When the soap concentration is raised to  $2.57 \times 10^{-2} M$  the electrophoretic velocity decreases upon the addition of KCl.

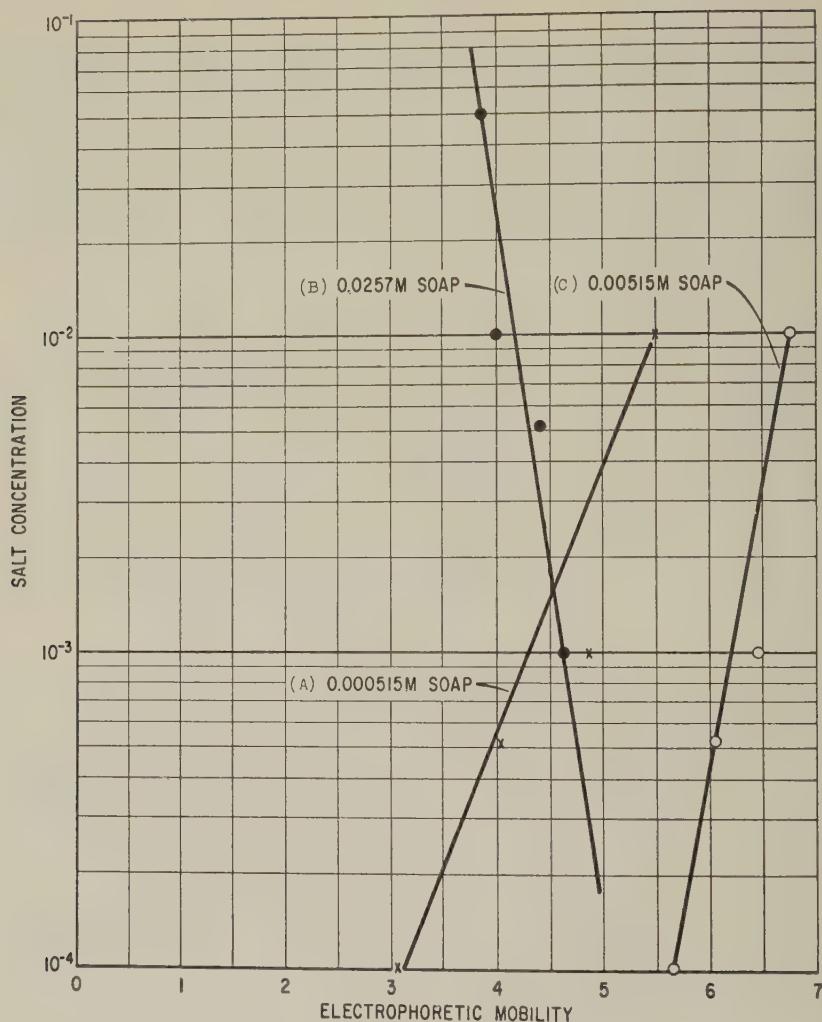


FIG. 4. Mobility vs. salt concentration.

## DISCUSSION

The three salt concentration versus electrophoretic mobility curves for the polystyrene-latex-sodium caprate-KCl systems (Fig. 4) will be discussed. The three curves, designated here as (A), (B), and (C) are typical of three limiting cases. In case (A), the soap concentration is  $5.15 \times 10^{-4}$  m./l. The surface is very lightly covered by soap ions, and it might be assumed that:

$$|\sigma_1| = \frac{N_1 \epsilon c}{\lambda} e^{-\epsilon |\psi_\delta| / kT} \quad [7]$$

(except for high salt concentrations when the surface coverage is close to its saturation value even at low soap concentrations). In case (B), the soap concentration is  $2.57 \times 10^{-2}$  m./l. The surface is completely saturated, and therefore:

$$-\sigma_1 = N_1\epsilon = \text{constant.}$$

In case (C), the soap concentration is  $5.15 \times 10^{-3}$  m./l. At this soap concentration the mobility is at its maximum. It was found that whereas this maximum mobility is a function of the salt concentration, the value of the soap concentration for which this mobility has a maximum is practically independent of the salt concentration.

Since the surface is saturated in the whole range of ionic strengths in case (B), it is not possible to find the surface potential from these measurements. However, from the fact that along the entire curve (B),  $\sigma_2$  is a constant, the following relation is obtained:

$$\frac{\sinh \frac{\epsilon |\zeta_2|}{2kT}}{\sinh \frac{\epsilon |\zeta_1|}{2kT}} = \sqrt{\frac{\Gamma_1}{\Gamma_2}},$$

where 1 and 2 denote two different measurements. Therefore, this case offers a check of the assumption that  $\zeta = \psi_\delta$ , or that the slipping plane is located at the boundary between the compact part of the double layer and the diffuse part of the double layer. Take the two measurements at  $n = 5 \times 10^{-2}$  and  $n = 10^{-3}$ .

$$\sqrt{\frac{\Gamma_1}{\Gamma_2}} = 1.67.$$

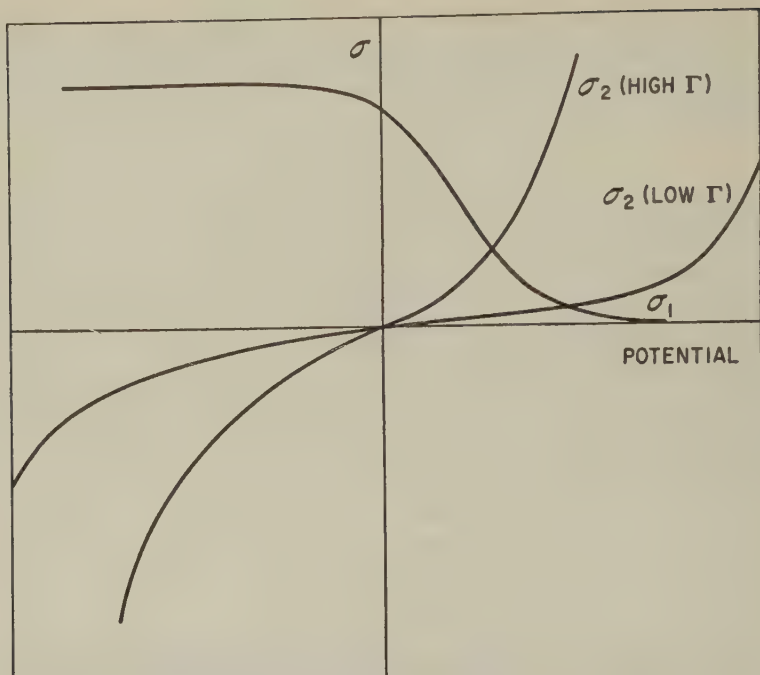
From the corresponding mobilities,  $\epsilon |\zeta_1| = 1.8 kT$ ,  $\epsilon |\zeta_2| = 2.30 kT$ , or

$$\frac{\sinh \frac{\epsilon |\zeta_2|}{2kT}}{\sinh \frac{\epsilon |\zeta_1|}{2kT}} = 1.39.$$

This agreement is good. This is especially so, since it was assumed that  $|\zeta| = |\psi_\delta|$ . It is reasonable to suspect that  $|\zeta| < |\psi_\delta|$ ; therefore, the assumption of equality would lead to a lower value for the ratio of hyperbolic sines, as found for this case.

Curve (B) permits finding of  $N_1$ . This number, averaged over the entire curve, is  $1.9 \times 10^{13}$ . According to the simple theory we were using,  $N_1$  should denote the number of adsorption sites on 1 cm.<sup>2</sup> of the surface. For a smooth, close-packed surface, this value of  $N_1$  would lead to a rather high value of the area of the soap molecule (in the vicinity of 500 Å.<sup>2</sup>). However, we have to bear in our mind that owing to the nearest neighbor repul-



FIG. 5. Plots of  $\sigma_1$  and  $\sigma_2$  vs. potential.

sions, the surface might not be closely packed, even at maximum coverage. Also, a possible hydrolysis, inhomogeneity in the surface, formation of acid salts, and other possible side effects complicate the situation to such a degree that no conclusion about the exact meaning of  $N_1$  should be made at the present state of investigation. The fact, however, that  $N_1$  depends directly, among other things, also on the area of the soap molecule, will make it vary with the nature of the soap molecule we are employing. This variation is treated in the second paper of this series.

Having thus determined  $N_1$ , and having proved that  $|\zeta| \sim |\psi_s|$ , we can now discuss curve (A).

Curve (A) shows that the mobility increases with increasing ionic strength. According to the Stern model, an *increase* in ionic strength should bring a *decrease* in mobility. In order to show the expected velocity versus concentration dependence, a diagram of  $\sigma_1$  versus  $\psi_0$  (from Eq. [3]) and of  $\sigma_2$  versus  $\psi_s$  (from Eq. [2]) at constant salt and soap concentration is plotted (Fig. 5). The intersection of these curves gives the potential and the charge density which satisfy the requirement that  $\sigma_1 = -\sigma_2$ . If the ionic strength is increased while keeping the soap concentration constant, the  $\sigma_1$  versus  $\psi_0$  curve will be unchanged while the  $\sigma_2$  versus  $\psi_s$  curve will

be shifted toward higher values of  $\sigma_2$ . The new  $\sigma_2$  versus  $\psi_\delta$  curve will intersect the  $\sigma_1$  versus  $\psi_0$  curve at lower potential values.

Equation [5a] can be rewritten as follows

$$\frac{N_1 \epsilon}{1 + \frac{\lambda}{c} e^{\epsilon |\psi_0| / kT}} = A \Gamma^{1/2} \sinh \frac{\epsilon |\zeta|}{2kT}; \quad [8]$$

and the following quantities:

$$\frac{\lambda}{c} e^{\epsilon |\psi_0| / kT}, \quad \frac{\lambda e^{\epsilon |\psi_0 - \zeta| / kT}}{c}, \quad \text{and} \quad \lambda e^{\epsilon |\psi_0 - \zeta| / kT}$$

can be calculated for several values of ionic strength, using the experimentally determined mobilities and salt concentrations. The results are shown in Table I.

Many explanations can be given to the reason why  $\psi_0 - \zeta$  should depend on the ionic strength. One can assume that the adsorption potential depends on the ionic properties of the system as well as it could depend on the coverage of the latex particle. A simple assumption that slipping plane ( $\psi = \zeta$ ) is at some distance from the plane where  $\psi = \psi_0$  makes  $\psi_0 - \zeta$  a function of the ionic content of the system.

It is of interest to calculate the approximate value of the adsorption potential. On the assumption that: (1) the last line of Table I represents conditions when  $\psi_0 = \zeta$  and (2)  $\lambda = \frac{10^3}{18} e^{-\varphi / kT}$  (according to Stern) the adsorption potential of caprate ions to the polystyrene latex is

$$\varphi = 10.65 kT \quad \text{or} \quad \varphi = 6.4 \text{ kcal./mole.}$$

The direct analysis of curve (C) is of uncertain value. From the calculated right-hand side of Eq. [15] it is noticed that the denominator of the left-hand side of this equation fluctuates between 0.5 and 2. Since these values are close to unity, a small error in the measured  $\zeta$  value can cause a large error in the calculated value of  $\lambda/c e^{\epsilon |\psi_0| / kT}$ . However, this difficulty can be overcome as follows: Assume that the entire curve (C) represents

TABLE I  
Numerical Analysis of Curve (A), Fig. 4

$n$	$\Gamma$	$\frac{\epsilon  \zeta }{kT}$	$\frac{c}{\lambda} e^{-\epsilon  \psi_0  / kT}$	$\frac{c}{\lambda} e^{-\epsilon  \psi_0 - \zeta  / kT}$	$\frac{1}{\lambda} e^{-\epsilon  \psi_0 - \zeta  / kT}$
$10^{-2}$	$10^{-2}$	2.70	1.997	29.73	$5.773 \times 10^4$
$10^{-3}$	$1.5 \times 10^{-3}$	2.35	0.2658	2.787	$5.412 \times 10^3$
$5 \times 10^{-4}$	$10^{-3}$	1.95	0.1536	1.080	$2.097 \times 10^3$
$10^{-4}$	$6 \times 10^{-4}$	1.53	0.0827	0.382	$0.742 \times 10^3$

TABLE II  
Numerical Analysis of Curve (C), Fig. 4

$n$	$\Gamma$	$1 + \frac{c}{c + 2n}$	$\frac{N_1\epsilon}{A} \left( \Gamma^{1/2} \sinh \frac{\epsilon \xi }{2kT} \right)^{-1}$
$10^{-2}$	$1.5 \times 10^{-2}$	1.205	0.706
$10^{-3}$	$6.5 \times 10^{-3}$	1.720	1.305
$5 \times 10^{-4}$	$5.6 \times 10^{-3}$	1.837	1.563
$10^{-4}$	$5.25 \times 10^{-3}$	1.963	1.838

conditions under which the mobility is at its maximum. Moreover, assume that  $|\psi_0 - \xi|$  does not depend on soap concentration in the neighborhood of this maximum. A typical curve of mobility versus soap concentration at constant salt concentration is shown in Fig. 3. (In this particular case no added electrolyte was present in the solution.) Then, from  $(d\psi_0/dc)_{n=\text{constant}} = 0$ :

$$\frac{c^* e^{-\epsilon|\psi_0^*|/kT}}{\lambda} = \frac{c^* + 2n}{c^*} \quad [9]$$

( $n$  = salt concentration).  $c^*$  and  $\psi_0^*$  are the concentration and potential at maximum mobility.

The fraction of the surface covered is equal to  $|\sigma_1|/N_1\epsilon$ . Obviously, when  $n = 0$ , the surface is only one half covered, whereas when  $n \gg c$ , the surface is practically saturated at the maximum mobility of the particle.

From the experimental data of curve (C)

$$\left( \frac{N_1\epsilon}{A} \right), \quad \left( \frac{1}{\Gamma^{1/2} \sinh \frac{\epsilon|\xi|}{2kT}} \right)$$

and  $\left( 1 + \frac{c}{c + 2n} \right)$  are calculated as functions of  $n$ . The results are shown in Table II. The values for  $\left( 1 + \frac{c}{c + 2n} \right)$  are similar to those for the last column and the agreement is especially good for low salt concentrations. From the last two lines of Table II, we can calculate directly

$$\frac{c}{\lambda} e^{-\epsilon|\psi_0|/kT} = 1.11 (\Gamma \cong 5.5 \times 10^{-3} \text{ m./l.});$$

and therefore,

$$\frac{e^{-\epsilon|\psi_0 - \xi|/kT}}{\lambda} \cong 0.86 \times 10^4.$$

Comparison with the corresponding data from Table I indicates that the soap concentration by itself does not affect greatly the deviation of  $|\psi_0|$

from  $\zeta$ , and that  $|\psi_0 - \zeta|$  depends primarily on the ionic strength of the solution.

### CONCLUSIONS

In the case of polystyrene latex particles having surfaces highly covered by soap molecules, the electrophoretic mobility can be explained using Stern's treatment of the diffuse double layer.

For the systems containing low soap and low salt concentrations, i.e., low surface coverage, the Stern theory has to be modified. The experimental mobilities at low coverage can be explained by assuming that the slipping plane is not located at the interface.

The adsorption potential for sodium caprate soap on polystyrene latex particles was found within our approximation to be 6.4 kcal./mole.

### REFERENCES

1. VERWEY, E. J. W., AND OVERBEEK, J. TH. G., "Theory of the Stability of Lyophobic Colloids," Elsevier, Amsterdam, 1948.
2. STERN, O., *Z. Electrochem.* **30**, 508 (1924).
3. GRAHAME, D. L., *Chem. Revs.* **41**, 441 (1947).
4. BIKERMAN, J. J., *Phil. Mag.* **33**, 384 (1942).

## POLYELECTROLYTE EXPANSION OF A LIGNIN SULFONATE MICROGEL

A. Rezanowich and D. A. I. Goring

*The Physical Chemistry Division, Pulp and Paper Research Institute of Canada,  
McGill University, Montreal, Quebec*

*Received February 1, 1960; revised April 27, 1960*

### ABSTRACT

The polyelectrolyte expansion of selected fractions of sodium lignin sulfonate has been measured viscometrically and by light scattering. Isoionic dilution techniques were used. The light-scattering radius of gyration,  $\bar{S}$ , and the intrinsic viscosity,  $[\eta]$ , increased with decrease in ionic strength  $I_E$  and with  $\bar{S}$  proportional to  $[\eta]^{1/3}$ . These results supported a microgel model for the macromolecule. The increase of  $[\eta]$  with decrease in  $I_E$  was not in quantitative accord with the theories of Flory or with those of Hermans and Overbeek. A new theory was developed in which the molecule was assumed to have free charges only on the surface. The elastic energy of the expanding network was equated to the electrostatic energy in the double layer. The resulting equation was found to apply to the first part of the expansion, but at very low values of  $I_E$  the expansion was less than predicted theoretically.

### INTRODUCTION

Gardon and Mason (1) were the first to show that lignin sulfonates behaved as swelling polyelectrolytes in aqueous solution. In a recent review Goring (2) pointed out that any water-soluble lignin might be expected to show some of the properties of polyelectrolytes in aqueous solvents. Subsequently, Gupta and Goring (3) showed that alkali lignin was a polyelectrolyte. The present work is a somewhat more detailed study of the polyelectrolyte expansion of certain sodium lignin sulfonates. The techniques of light scattering and viscosity were used.

The long-term purpose of the work is to elucidate the configurational behavior of the lignin macromolecule in aqueous solution and also to detect any configurational differences in different lignins. For example, the polyelectrolyte expansion should be sensitive to the degree of crosslinking or branching in the macromolecule. Observed differences in the degree of expansion might be used to measure the molecular weight,  $M_c$ , between crosslinks in the same manner that  $M_c$  can be deduced from the macroscopic swelling of crosslinked gels (4). In the present paper the results were treated quantitatively by means of the well-known equations derived by Flory (4) and by Hermans and Overbeek (5) for the expansion of single,



flexible polyelectrolyte chains. However, a new and somewhat simpler theory based on a microgel model of the lignin macromolecule was found to fit the experimental data more closely.

Some of the lignin sulfonates used in the present work have been described in a previous investigation (6) in which spruce periodate lignin was made soluble by 14 successive stages of sulfonation. The fractions thus obtained were identical in several characteristic properties of lignin, e.g., methoxyl content and UV absorption. For the present study, fractions were selected from various stages of the cook in order to see if these chemically similar macromolecules showed differences in their polyelectrolyte behavior.

For the viscosity and light-scattering experiments, considerable care was taken to dilute by the isoionic technique. This technique ensured that the negatively charged lignin sulfonate macromolecule was kept in an environment of constant cationic strength. Under such conditions, the usual linear concentration dependence of the viscosity and light-scattering parameters was obtained. In viscosity, however, an unusually large increase of the Huggins coefficient,  $k'$ , was found on decrease of the ionic strength. A semiquantitative treatment of this phenomenon has been developed and used to explain some of the characteristics of the classical concentration dependence of the viscosity of polyelectrolytes in aqueous solutions. Because of the more general nature of this part of the work it has been reported in a separate paper (7).

## EXPERIMENTAL

### *Materials*

Some of the lignin sulfonate fractions have already been described (6). These were Fractions S-7 and S-14, which were prepared by successive sulfonation of spruce periodate lignin and which were purified by centrifugation, ion exchange, and freeze drying.

For the more detailed light-scattering study with Fractions PS-5 and PB-3b, a more rigorous purification was necessary. Fraction PS-5 was prepared from the previously described Fraction S-5 (6) by centrifugation at 100,000  $g$  in 0.01  $M$  NaCl, followed by filtration through fine sintered glass, ion exchange, and freeze drying.

Fraction PB-3b was selected from a subfractionation of a recooked mixture of Fractions S-10, S-11, S-12, S-14, and S-16 described in an earlier paper (6). Fractionation was achieved by the addition of ethanol to a 2% solution of the barium salt of the lignin sulfonate. PB-3b was the third of six fractions and was 30% by weight of the original mixture. Fraction PB-3b was purified in a similar manner to Fraction PS-5. The sulfur content, neutralization equivalent ( $N_e$ ), and methoxyl content of the fractions are given in Table I.

TABLE I  
*Sulfur Content, Neutralization Equivalent, and Methoxyl Content  
 of the Lignin Sulfonate Fractions*

Fraction	Sulfur content (%)	<i>Ne</i> (meq. g. <sup>-1</sup> )	Methoxyl content (%)
S-7	3.5	2.2	11.4
S-14	4.5	3.1 <sup>a</sup>	11.4
PS-5	2.8	1.54	11.2
PB-3b	4.4	1.76	10.7

<sup>a</sup> Incorrectly high because of insufficient purification.

Laboratory distilled water (specific conductivity =  $2 \times 10^{-6}$  mho.cm.<sup>-1</sup>) was used in the preliminary experiments with Fractions S-7 and S-14. In the more precise measurements of Fractions PS-5 and PB-3b, the distilled water was passed through an Amberlite (MB-1) mixed bed column which resulted in a conductivity of less than  $1 \times 10^{-6}$  mho.cm.<sup>-1</sup>. The sodium chloride was reagent grade.

#### *Viscosity*

Viscosity was measured in Craig-Henderson viscometers (8) at 25°C. with a relative temperature control of  $\pm 0.002^\circ\text{C}$ . For the extremely dilute solutions the bulb volume of the viscometer was increased by a factor of 10, increasing the flow time from 155 to 1730 sec. Shear dependence was considered negligible. This was justified both by the low values of  $\eta_{sp}/c$  and by the small range of shear encountered (650–950 sec.<sup>-1</sup>).

#### *Light Scattering*

Light-scattering measurements were made with a Brice-Phoenix photometer by the method described previously (9). The wavelength was 5460 Å. Solutions were clarified by ultracentrifugation in special light-scattering cells which were transferred directly from the rotor to the photometer. Concentrations were measured before and after ultracentrifugation; the loss in no case exceeded 6% and was on the average 3%. Reduced Rayleigh ratios were obtained for the angular range 35°–135°. The fluorescent emission of the lignin was eliminated by inserting a combination of Corning filters No. 4305 (C.S. 471) and 5120 (C.S. 1–60) in the nose-piece of the photometer. The details of this technique are described in a previous publication (10). The data were processed by Zimm's method (11) in which the weight-average molecular weight  $M_w$ , the Z-average radius of gyration  $\tilde{S}_z$ , and the second virial coefficient  $A_2$  were determined by the usual extrapolation procedures.

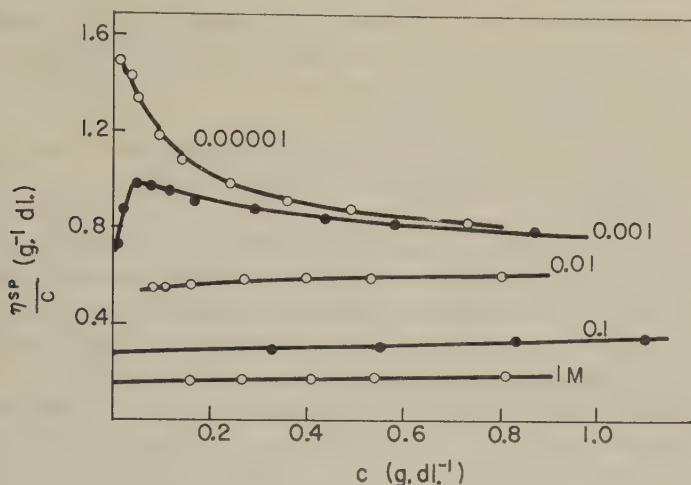


FIG. 1. Fraction S-14:  $\eta_{sp}/c$  vs.  $c$  by solvent dilution at various ionic strengths of NaCl.

### RESULTS

The initial viscosity measurements on Fractions S-7 and S-14 were made by the usual procedure of diluting the solution with the solvent. For both fractions rather typical polyelectrolyte data were obtained. As shown in Fig. 1 for Fraction S-14, the reduced viscosity graphs were linear at high ionic strength. The characteristic upward curvature was found at low ionic strength with a maximum in  $\eta_{sp}/c$  in some cases. Similar maxima have been reported in the literature for other polyelectrolytes (12-16), and a more detailed discussion of this effect is presented in a further publication (7).

Intrinsic viscosities for ionic strengths less than 0.01  $M$  were inaccessible from the results described above. Therefore, the isoionic dilution technique of Pals and Hermans (17) as modified by Terayama and Wall (18) was adopted. The free counter ion supplied by the polyelectrolyte was assumed to contribute to the total counter-ion concentration. However, only a fraction of the  $\text{Na}^+$  ions associated with the lignin sulfonates were free counter ions in solution. The total effective ionic strength  $I_E$  of the counter ions was given by

$$I_E = I + I_L = I + \frac{cR N_e}{100}, \quad [1]$$

where

- $I$  = ionic strength of  $\text{Na}^+$  supplied by the sodium chloride (moles/l.);  
 $I_L$  =  $\text{Na}^+$  contributed to the solution by the ionization of the sodium lignin sulfonate (NaLS) (moles/l.);  
 $c$  = NaLS concentration (g./dl.);  
 $R$  = fraction of  $\text{Na}^+$  from the NaLS which are free in solution;  
 $N_e$  = neutralization equivalent of the lignin sulfonic acid (milli-equiv./g.).

As pointed out by Terayama and Wall (18),  $R$  is approximately constant regardless of changes in the concentration of the polyelectrolyte and the total ionic strength of the solution. Therefore if  $R$  is known, isoionic dilutions can be made by using an NaCl concentration determined from Eq. [1].

To find the degree of ionization, a value of  $R$  was assumed. A 0.3% solution of sodium lignin sulfonate was made up in distilled water and the viscosity was measured for a series of dilutions. The ionic strength of the diluting NaCl solution was  $0.003 N_e R$ . In the resulting  $\eta_{sp}/c$  vs.  $c$  plot, if the line was concave to the  $c$ -axis,  $R$  was chosen too small; a line convex to the  $c$ -axis indicated that  $R$  was too large. Thus by trial and error, as shown in Fig. 2, an  $R$  value to yield a linear plot of  $\eta_{sp}/c$  vs.  $c$  was found. The degree of ionization thus obtained was then assumed to apply at all ionic strengths. Linear viscosity curves at various ionic concentrations were obtained by making up the appropriate concentration of lignin sulfonate (plus salt if necessary) and diluting this initial solution with an isoionic ( $\text{Na}^+$ ) solution the concentration of which was calculated from Eq. [1].

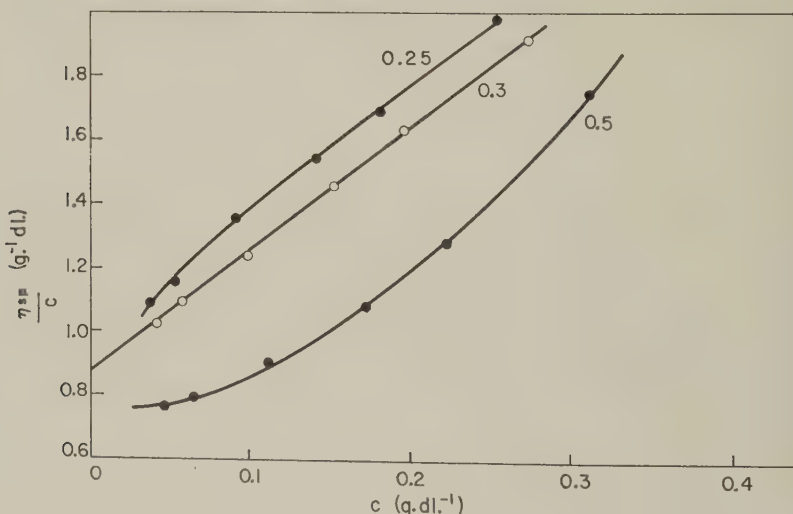


FIG. 2. Fraction PB-3b:  $\eta_{sp}/c$  vs.  $c$  by isoionic dilution assuming  $R = 0.25, 0.3$  and  $0.5$ .

No adjustment was necessary at 0.1  $M$  and 1  $M$  because the high salt concentration swamped the counter ions from the lignin.

For Fractions PS-5 and PB-3b (Fig. 3), linear viscosity plots were obtained by this technique for ionic strengths greater than  $3 \times 10^{-4} M$ . With Fraction PB-3b an attempt was made to study even lower ionic strengths. Here the limiting factor was the very low initial concentration of lignin sulfonate in distilled water which was necessary because of the low ionic strength required. To overcome this difficulty, the more sensitive viscometer with the larger bulb volume was used in all measurements with  $I_E < 10^{-3} M$ . For PB-3b,  $R$  did not remain constant at very low ionic strengths. In the range  $I_E = 10^{-3}$  to 1  $M$ , the value  $R = 0.30$  gave linear  $\eta_{sp}/c$  vs.  $c$  graphs. At  $I_E = 2.4 \times 10^{-4} M$ , however, a slight curvature was apparent, and it was estimated (by a method not reproduced here) that  $R = 0.35$  would have given a linear  $\eta_{sp}/c$  vs.  $c$  graph. For  $I_E = 1.6 \times 10^{-4} M$  an  $R$  value of 0.45 was necessary. As shown in Fig. 4, the lower  $R$  value of 0.35 gave a markedly curved viscosity graph at  $I_E = 1.2 \times 10^{-4} M$ . Finally at  $I_E = 2 \times 10^{-5} M$ ,  $R$  was equal to 0.75. These results indicated clearly that at very low ionic strengths the degree of ionization of Fraction PB-3b increased considerably.

Intrinsic viscosities obtained by extrapolation of the linear graphs of  $\eta_{sp}/c$  vs.  $c$  at various ionic strengths are given in Table II. Also included are values of  $R$  and of the radius,  $r_\eta$ , of the equivalent Einstein sphere

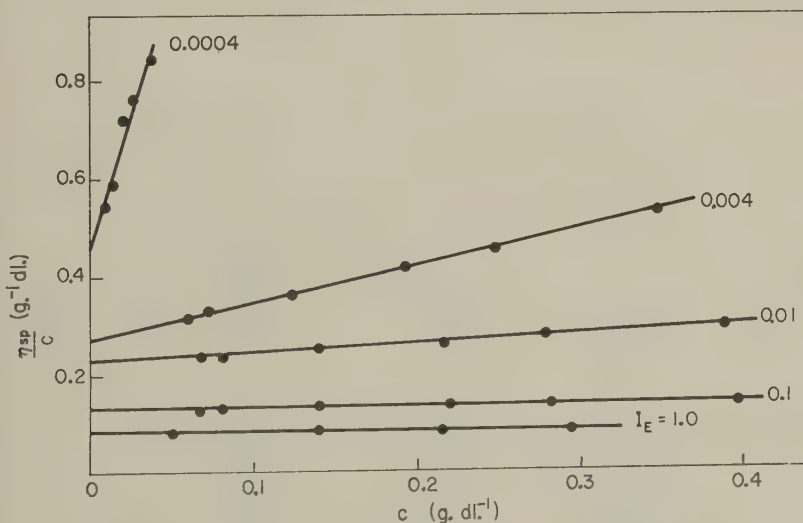


FIG. 3. Fraction PS-5:  $\eta_{sp}/c$  vs.  $c$  by isoionic dilution at various values of  $I_E$ .  $R = 0.75$ . Similar data were obtained for PB-3b with  $R = 0.30$ .



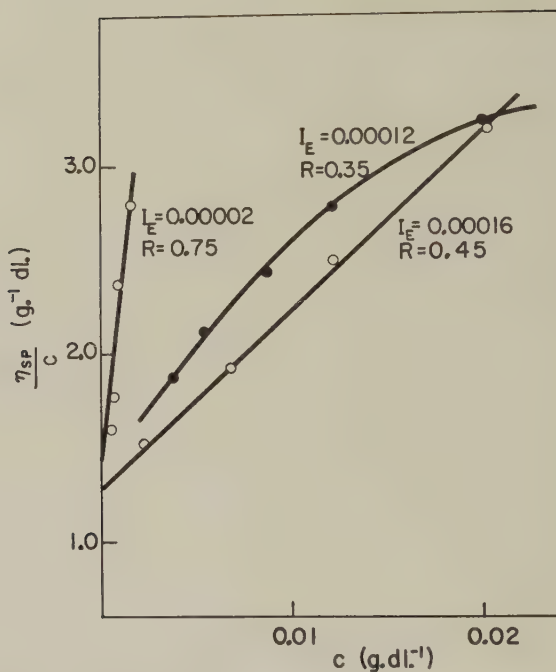


FIG. 4. Fraction PB-3b:  $\eta_{sp}/c$  vs.  $c$  by isoionic dilution at low  $I_E$ . Note the increase in  $R$  required to give a linear graph.

TABLE II

Values of  $[\eta]$  and  $r_\eta$  Obtained by Isoionic Dilution for Fractions PS-5 and PB-3b

	$I_E$ (moles $Na^+$ l. <sup>-1</sup> )	$[\eta]$ (g. <sup>-1</sup> dl.).	$r_\eta$ (Å)	$R$
Fraction	1	0.062	117	0.75
PS-5	0.1	0.129	148	0.75
	0.01	0.228	179	0.75
	0.00401	0.274	190	0.75
	0.00044	0.442	223	0.75
Fraction	1	0.153	171	0.30
PB-3b	0.1	0.242	199	0.30
	0.01	0.462	248	0.30
	0.00145	0.868	306	0.30
	0.00024	1.10	330	0.35
	0.00016	1.28	348	0.45
	0.00002	1.45	362	0.75

computed from

$$r_{\eta} = \left[ \frac{30M_w [\eta]}{\pi N} \right]^{1/3}, \quad [2]$$

where  $N$  is Avogadro's number,  $M_w$  is the light-scattering molecular weight, and the units of  $r_{\eta}$  and  $[\eta]$  are cm. and dl.g.<sup>-1</sup>, respectively.

The Huggins parameter of the concentration dependence,  $k'$ , was also measured, but discussion of this is reserved for a later publication (7).

In light scattering, full Zimm plots were made for Fraction PB-3b at various ionic strengths. An example is shown in Fig. 5. Dilution was made by the isoionic technique using the values of  $R$  determined viscometrically. At all ionic strengths the relationship between  $K_c/R_{\theta}$  and  $c$  was linear. Values of  $M_w$ ,  $\bar{S}_z$ , and  $A_2$  are given in Table III.

With Fraction PS-5 a shorter method was used. Light scattering was measured over a range of ionic strengths for a single concentration of 0.04%;  $K_c/R_{\theta}$  was then plotted against  $\sin^2 (\theta/2)$  and extrapolated to  $\theta = 0$ . From the initial slope of this line,  $\bar{S}_z$  was calculated using the mean intercept from the graphs for  $I_E = 1$  and  $0.1M$ ;  $M_w$  values from the intercepts at  $I_E = 1$  and  $0.1M$  and  $\bar{S}_z$  at all ionic strengths are given in Table III.

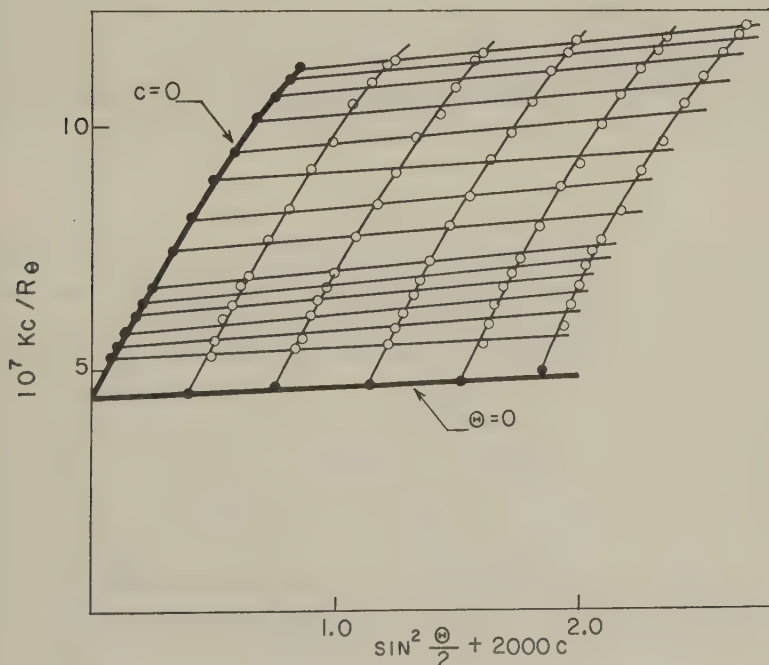


FIG. 5. Fraction PB-3b: Zimm plot at  $I_E = 0.01M$  NaCl.

TABLE III  
*Values of Molecular Parameters from Light Scattering at Different  
 Ionic Strengths for Fractions PS-5 and PB-3b*

	$I_E$ (moles $Na^+$ $l^{-1}$ )	$M_w$ $\times 10^{-6}$	$S_z$ ( $\text{\AA}$ )	$A_2$ $\times 10^6$
Fraction	1	1.64	479	—
PS-5	0.1	1.51	583	—
	0.0105	—	703	—
	0.00147	—	839	—
	0.000476	—	884	—
Fraction	1	2.17	521	-0.3
PB-3b	0.1	2.25	677	1.1
	0.01	2.25	806	1.8
	0.001	2.10	990	10.2
	0.000224	1.94	1070	57

There was fair justification for the shorter procedure described above. The Zimm plots for PB-3b showed that  $A_2$  (Table III) was nearly zero at  $I_E = 1$  and  $0.1M$ . On the assumption of similar behavior in PS-5, the molecular weight based on  $(K_c/R_\theta)_{\theta=0}$  at the low, finite concentration of  $0.04 \text{ g.dl.}^{-1}$  would differ negligibly from the value based on extrapolation to  $c = 0$ . Also, for PB-3b at any ionic strength, the initial slopes of the  $K_c/R_\theta$  vs.  $\sin^2 \theta/2$  lines were independent of the concentration of lignin sulfonate, the average error in using  $\bar{S}_z$  at  $c = 0.04 \text{ g.dl.}^{-1}$  instead of  $c = 0$  being  $\pm 2\%$ .

## DISCUSSION

Before a detailed analysis of the results is presented it may be useful to consider what starting model is most suitable for the lignin sulfonate macromolecule. Physicochemical discussions of polymeric behavior are usually based on the Gaussian coil, i.e., a linear, flexible string coiled randomly in solution. Lignin in wood is believed to be a highly crosslinked (or branched) network of polyphenylpropane chains (2). Thus, lignin sulfonate molecules are soluble fragments of the network, cut out by the hydrolyzing action of the cooking liquor and made soluble by the attachment of hydrophilic sulfonate groups. For such molecules, a microgel (19-21) is probably a more satisfactory starting model than a random coil. The model assumed is, therefore, a compact colloidal particle, made up of crosslinked material, almost completely non-free draining but capable of limited swelling. The compactness of the molecule is illustrated by the small values of  $[\eta]$  (Table II) for the high molecular weights (Table III). The microgel model is also supported by a recent study on alkali lignin (10) which indicated that the

configuration of the molecule was between that of an Einstein sphere and a random coil.

The intrinsic viscosity at various ionic strengths may now be compared with the size of the molecule as determined by light scattering. For this,  $[\eta]$  values are needed which correspond to the ionic strength at which light-scattering measurements were made. It was found empirically that a plot of  $[\eta]^{1/3}$  vs.  $\log I_E$  was approximately linear, from which values of  $[\eta]$  could be read off for particular values of  $I_E$ ;  $\bar{S}_z$  could then be compared directly with  $[\eta]$ . As shown in Fig. 6,  $[\eta]$  vs.  $\bar{S}_z^3$  gave a straight line through the origin for Fractions PS-5 and PB-3b.

The proportionality of  $[\eta]$  and  $\bar{S}_z^3$  is exactly what would be expected for a swelling microgel. The particle in its various states of swelling could be regarded as an Einstein sphere of varying volume. Thus  $[\eta]$  would be directly proportional to the volume of the sphere and therefore to  $\bar{S}_z^3$ . On the other hand, for an expanding randomly coiled polyelectrolyte, the relationship between  $[\eta]$  and  $\bar{S}_z$  is not so clearly defined. If the degree of free draining and the overall statistical distribution remain unchanged,  $[\eta]$  would be expected to vary as  $\bar{S}_z^3$  (4). If on expansion the molecule became more free draining,  $[\eta]$  would increase more slowly than  $\bar{S}_z^3$  even if the coil retained its essential Gaussian character. Such behavior has been reported for carboxymethyl cellulose where  $[\eta]$  varies as  $\bar{S}_z^2$  (22).

In terms of the microgel model, however, the data in Fig. 6 reveal an interesting discrepancy, i.e., the particle radius obtained by light scattering is several times that computed from  $[\eta]$ . The particle radius from viscosity,  $r_\eta$ , is given by the Einstein relationship in Eq. [2].

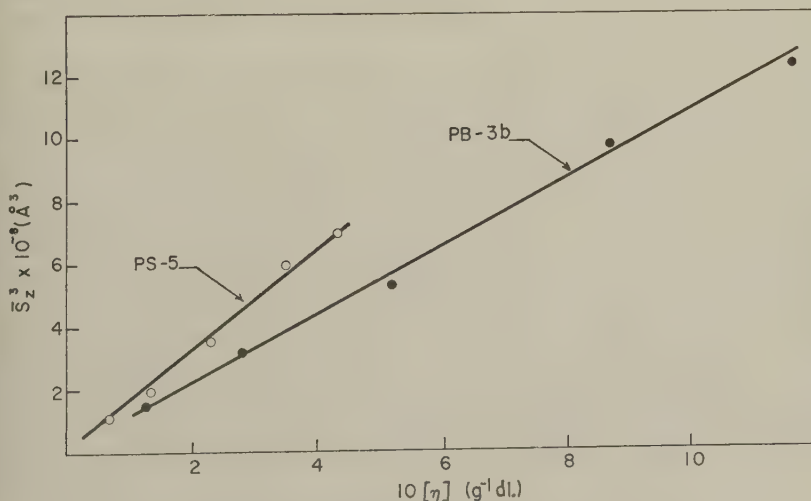


FIG. 6.  $[\eta]$  vs.  $\bar{S}_z^3$  for Fractions PS-5 and PB-3b.

The relationship between the radius of a sphere and its radius of gyration is given by

$$r_z = 1.29 \bar{S}_z. \quad [3]$$

Combining Eqs. [2] and [3]

$$\frac{r_z}{r_\eta} = \left( \frac{0.0716 \pi N \bar{S}_z^3}{M_w [\eta]} \right)^{1/3}, \quad [4]$$

by means of which  $r_z/r_\eta$  can be calculated from the slopes of the lines in Fig. 6. This ratio for Fraction PS-5 and PB-3b was 5.2 and 4.1, respectively. The radius  $r_z$  is a Z-average, whereas  $r_\eta$  calculated from  $M_w$  and  $[\eta]$  will be between a number and a weight average. Thus  $r_z$  would be expected to be greater than  $r_\eta$ , the ratio  $r_z/r_\eta$  depending on the polydispersity of the sample. Soluble lignin derivatives are probably produced by the random degradation of a three-dimensional network and therefore would be expected to be appreciably polydisperse (4). Several investigations have demonstrated polydispersity. Gardon and Mason (23) reported molecular weights of 60,000 to 4,000 for fractions of a commercial lignin sulfonate. Similarly, McCarthy and co-workers (24) found a range of 138,000 to 8,000 in fractions of lignin sulfonate. In a recent study of alkali lignins, Gupta and Goring (10) prepared fractions with  $M_w$  values ranging from 50,000 to  $50 \times 10^6$ . Sedimentation constants in any single fraction could range from 1–400  $S$  and the polydispersity was not significantly decreased by fractionation (25). For such systems,  $M_w/M_n$  ratios as high as 100 are possible (26). It is very likely that the fractions used were highly polydisperse; this would explain the discrepancy between  $r_z$  and  $r_\eta$ . The lower value of  $r_z/r_\eta$  for PB-3b is probably due to a small decrease in polydispersity on fractionation.

Implicit in the above discussion is the assumption that the double layer itself has only a negligible effect on  $[\eta]$  and  $\bar{S}_z$ . Changes in these parameters are considered to arise solely from the swelling of the particle. Here, it is useful to distinguish between primary and secondary effects. Primary effects may be defined as variations in intrinsic parameters, i.e., quantities such as  $[\eta]$ ,  $M_w$ , or  $\bar{S}_z$ , which are obtained by extrapolation to zero concentration. On the other hand, changes in parameters which define concentration dependence (e.g.,  $k'$  or  $A_2$ ) may be termed secondary effects.

The primary electroviscous effect has been treated in detail by Booth (27). Compared with the changes in  $[\eta]$  due to polyelectrolyte swelling, the magnitude of the effect is small and has usually been neglected by workers in this field. From calculations not reproduced in detail here, the increase in  $[\eta]$  expected from Booth's theory was less than 6% for Fraction PB-3b at  $I_E = 2 \times 10^{-5} M$ , and the size of the effect decreased by approximately an order of magnitude for each 10-fold increase in  $I_E$ . The primary electro-



viscous effect was therefore assumed negligible in contrast to the secondary electroviscous effect which produced large changes in  $k'$  as discussed in a subsequent publication (7).

As far as is known, the primary effect of the double layer in light scattering has not been considered in detail. Doty and Steiner (28) have outlined the problem and for most conditions consider the effect negligible. In the present work, the total contribution of the individual  $\text{Na}^+$  counter ions would be  $\sim 10^{-5}$  of the scattering of the macromolecule. If, however, the refractive index increment of the water molecules is altered by the substantial electrical fields in the double layer, much more serious changes in  $M_w$  and  $\tilde{S}_z$  with ionic strength would be expected. The constancy of  $M_w$  for Fraction PB-3b in Table III suggests that this effect is negligible and thus that variation of  $\tilde{S}_z$  (like that of  $[\eta]$ ) is due only to swelling of the microgel. The secondary effect of the double layer on light scattering has been treated by several authors by means of the fluctuation theory (29-31). The theory predicts that  $A_2$  will increase with decrease in  $I_E$ , and such an increase was found for PB-3b as shown in Table III. Further quantitative treatment of the concentration dependence of light scattering will not be given in the present study.

The change of  $[\eta]$  with ionic strength may now be compared quantitatively to that predicted by some of the theories of polyelectrolyte expansion. According to Flory and Osterheld (32),  $(\alpha^5 - \alpha^3)$  should give a linear plot against  $1/I_E$ , where  $\alpha^3$  is the ratio of the intrinsic viscosity at  $I_E$  to the value at the ionic strength corresponding to the  $\theta$ -point of the system (4). Here,  $\alpha$  was obtained from

$$\alpha^3 = \frac{[\eta]_{I_E}}{[\eta]_{1M}}. \quad [5]$$

This procedure is justified by the zero value for the second virial coefficient ( $A_2$ ) of light scattering in 1 *M* NaCl (Table III). As shown in Fig. 7,  $(\alpha^5 - \alpha^3)$  vs.  $1/I_E$  was not linear even near the origin and showed marked downward curvature at low ionic strength. From the theory by Hermans and Overbeek (5), the intrinsic viscosity (or  $\alpha^3$ ) is a linear function of the Debye radius (33) which for a uni-univalent electrolyte is given in Angstroms by  $3/\sqrt{I_E}$  when the units of  $I_E$  are moles/l. The graph of  $\alpha^3$  vs.  $3/\sqrt{I_E}$  is given in Fig. 8, and for both fractions, curvatures similar to those in Fig. 7 were found. Evidently the increase of  $[\eta]$  at low ionic strength was less than that predicted by either treatment. Katchalsky and Lifson (34, 35) have also proposed a theory of polyelectrolyte expansion based on the electrostatic interaction of individual charges on the chain. No attempt was made to apply this treatment to the present data (*cf.* Schneider and Doty (33)).

In the above theories, the charge is assumed to be present throughout

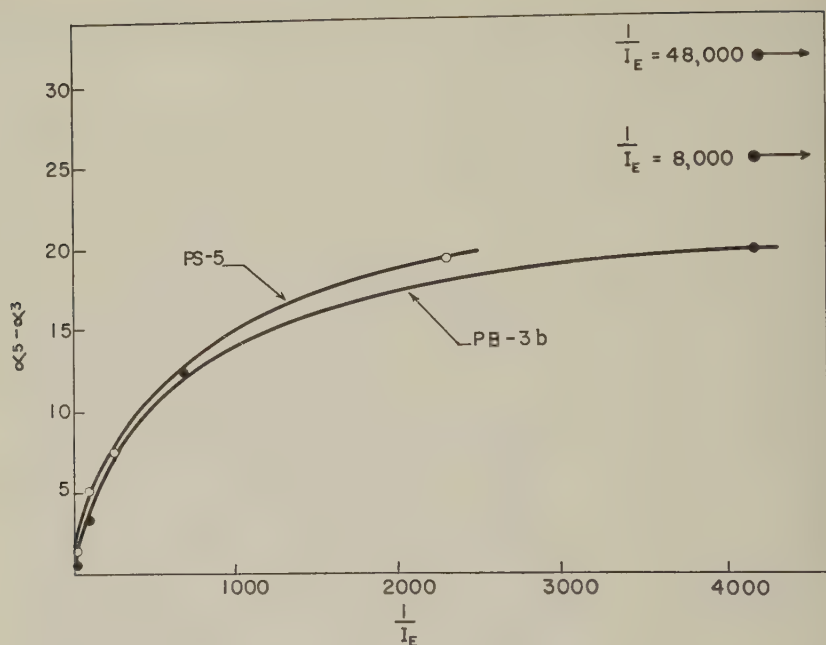


FIG. 7.  $\alpha^5 - \alpha^3$  vs.  $1/I_E$  for Fractions PS-5 and PB-3b. The points corresponding to the two lowest ionic strengths with PB-3b are plotted on a reduced abscissa scale.

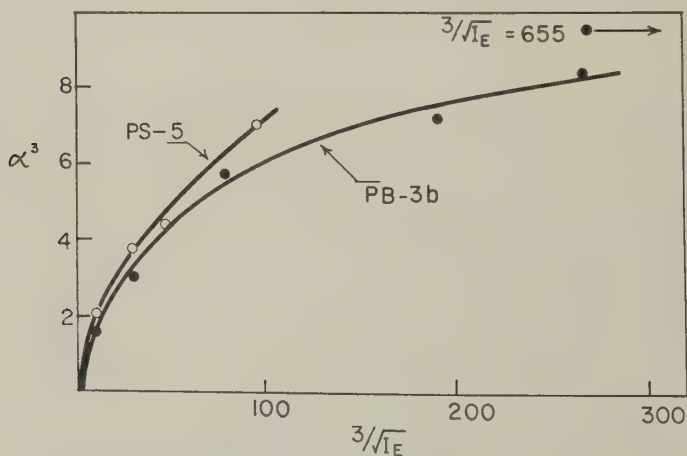


FIG. 8.  $\alpha^3$  vs.  $3/\sqrt{I_E}$  for Fractions PS-5 and PB-3b. The point corresponding to the lowest ionic strength with PB-3b is plotted on a reduced abscissa scale.

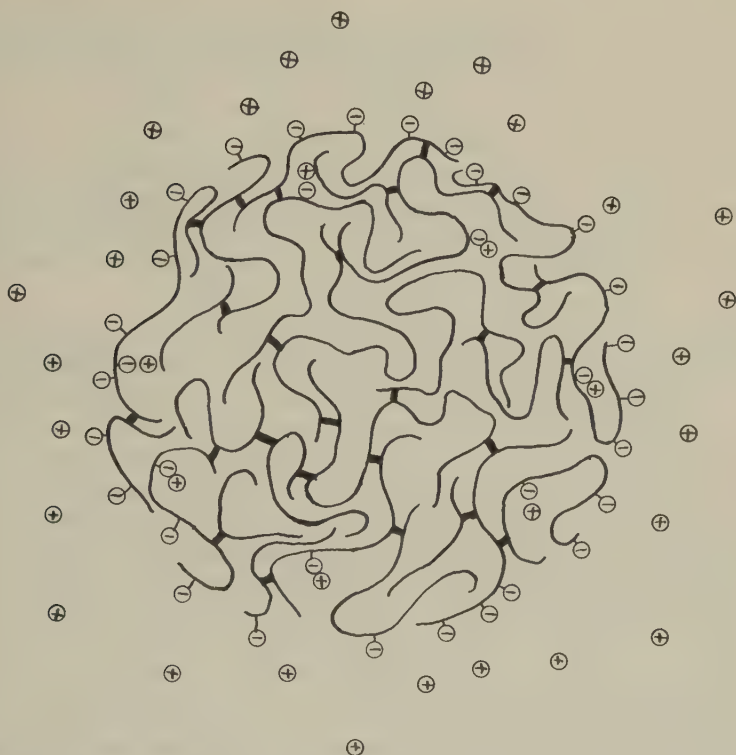


FIG. 9. Idealized spherical model of the spruce lignin sulfonate macromolecule.

the volume of the molecular domain. It seemed possible that the lignin sulfonate microgel might resemble more closely certain inorganic colloids which have the charge on the surface with a relatively charge-free interior. Such a model is shown in Fig. 9. The bulk of the molecule is assumed to be made up of crosslinked, polyaromatic chains which are randomly coiled in the unexpanded state. The negatively charged sulfonate groups are mainly on the surface or near the surface of the particle. A double layer of counter ions ( $\text{Na}^+$ ) is present in the solvent in the characteristic Boltzmann distribution. Figure 9 must be regarded as an idealized model which permits a quantitative theoretical treatment of the data. In practice, lignin sulfonate probably exists in solution as irregularly shaped, submicroscopic particles in a wide polydispersity of size.

In an uncharged, swollen, crosslinked network, the free energy of the system is given by

$$F = F_m + F_e, \quad [6]$$

where  $F_m$  is the free energy of mixing the polymer chains with the imbibed liquid and  $F_e$  is the elastic free energy released when the crosslinked chains are stretched beyond their most probable configuration (36). In the following treatment  $F_m$  will be assumed negligible compared to  $F_e$ . The justification for this is that the microgel is already swollen in 1 *M* NaCl. For PS-5 and PB-3b the volume  $\frac{4}{3}\pi r_\eta^3$  is respectively 4 and 9 times the volume based on the light-scattering molecular weight and a lignin density of 1.4 g.ml.<sup>-1</sup>. Thus the further swelling due to the polyelectrolyte expansion will be regulated mainly by the elastic recovery of the stretched chains rather than by energy of further dilution with solvent.

Because the charge is assumed to be on the surface only, there are no free ions within the molecule. Accordingly, the osmotic term in the treatment of Flory and Osterheld (32) will be zero. One objection may be that only a fraction,  $R$ , of the ions required for neutralization are hydrodynamically free. It will be assumed that the counter ions which are not hydrodynamically free form ion pairs, are thereby immobilized, and do not cause osmotic expansion of the molecule. This concept of strong ion binding is supported by the transference studies of Wall *et al.* (37, 38) and has been favored by several authors recently (33, 39).

Thus two primary forces are assumed to be in equilibrium in the swollen molecule:

- a. The expansion force produced by the electrical double layer at the surface of the molecule.
- b. The elastic contractile force produced by the decrease in entropy of the stretched chains.

At equilibrium the electrostatic energy will be balanced against the work done in stretching the network. The electrostatic energy is  $\frac{1}{2}Qe\zeta$  where  $Q$  is the number of charged groups on the molecule,  $e$  is the electronic charge, and  $\zeta$  is the electrical potential between the surface of the particle and the solvent. The mechanical potential energy may be derived from a negative hydrostatic pressure,  $p$ , which Treloar (36) relates to the properties of the network by

$$\frac{RT}{V_0} \left[ \log(1 - v_2) + v_2 + \mu v_2^2 + \frac{\rho V_0}{M_c} v_2^{1/3} \right] = p, \quad [7]$$

in which

$R$  = molar gas constant;

$T$  = absolute temperature;

$V_0$  = molar volume of solvent;

$v_2$  = volume fraction of polymer;

$\mu$  = thermodynamic parameter;

$\rho$  = density of the polymer; and

$M_c$  = molecular weight of the chain between crosslinks.

The first three terms in Eq. [7] are for the energy of mixing of polymer solvent which we are assuming zero. The last term is the approximate elastic entropy expression. For a single microgel

$$v_2 = \frac{M_w}{N\rho v}, \quad [8]$$

where  $v$  is the volume of the molecule.

Substituting in Eq. [7]

$$p = \frac{RT\rho^{2/3}M_w^{1/3}}{M_cN^{1/3}v^{1/3}}. \quad [9]$$

At swelling equilibrium the electrostatic and mechanical potential energies are equal.

Thus

$$\frac{1}{2} Qe\zeta = \int_{v_0}^v p \, dv, \quad [10]$$

where  $v_0$  is the volume of the molecule when  $\zeta = 0$ .

For a uni-univalent electrolyte the  $\zeta$ -potential is related to the charge by

$$\zeta = \frac{Q}{Nr_\eta^2} \left( \frac{125RT}{\pi DI_E} \right)^{1/2} \quad [11]$$

where  $D$  is the dielectric constant of the solvent and the Debye-Hückel approximation is made (40).

Substituting for  $p$  (Eq. [9]) in Eq. [10], integrating, and replacing  $v$  by  $\frac{4}{3}\pi r_\eta^3$  and  $\zeta$  by Eq. [11], we have

$$\frac{5Q^2eM_c}{2\pi} \left( \frac{5}{DRT} \right)^{1/2} \left( \frac{1}{6\sqrt{\pi}N^2\rho^2M_w} \right)^{1/3} \frac{1}{r_\eta^2\sqrt{I_E}} = r_\eta^2 - r_\eta^{\circ 2}, \quad [12]$$

in which  $r_\eta^\circ$  is the Einstein radius corresponding to  $v_0$ .

At 25°C., for  $r_\eta$  in Angstroms and with the assumption that  $\rho = 1.4 \text{ g.ml.}^{-1}$  Eq. [12] reduces to

$$\frac{3.1Q^2M_c}{M_w^{1/3}} \frac{1}{r_\eta^2\sqrt{I_E}} = r_\eta^2 - r_\eta^{\circ 2}, \quad [13]$$

which yields a linear relation between  $r_\eta^2$  and  $1/r_\eta^2\sqrt{I_E}$ . Such plots are shown in Fig. 10 for Fractions PS-5 and PB-3b. In the case of PB-3b the first four points are almost exactly linear while the remaining three fall well below the initial straight line in a manner which is best fitted by a second straight line of smaller slope. The results for PS-5 are similar although the slope of the initial line is smaller. No isoionic dilutions were made with Fractions S-14 and S-7. Fujita and Homma (16) have shown that it is



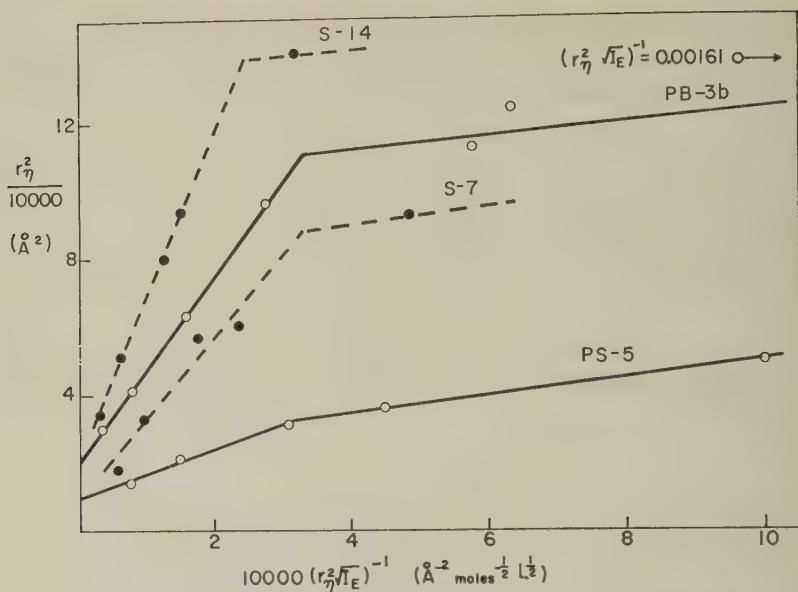


FIG. 10.  $r_\eta^2$  vs.  $1/r_\eta^2 \sqrt{I_E}$  for Fractions PS-5 and PB-3b. The point corresponding to the lowest ionic strength with PB-3b is plotted on a reduced abscissa scale. The nearly horizontal portion of the graph for PB-3b passes through this point if produced. The dotted lines are data for Fractions S-7 and S-14 based on an analysis of non-isoionic dilution data as shown in Fig. 1.

possible, by a method of trial and error, to derive from curves such as those shown in Fig. 1, linear  $\eta_{sp}/c$  vs.  $c$  graphs corresponding to isoionic dilutions such as those shown in Fig. 3. A similar analysis was made for Fractions S-7 and S-14, and the results are plotted as  $r_\eta^2$  vs.  $1/r_\eta^2 \sqrt{I_E}$  in Fig. 10. These data, though not as extensive, fall into the same general pattern as that for PB-3b and PS-5.

First, let us consider only the initial linear portion of the  $r_\eta^2$  vs.  $1/r_\eta^2 \sqrt{I_E}$  graphs. This linearity, even though only approximate, supports the model shown in Fig. 9, in favor of models in which the charge is distributed throughout the sphere. Some further support arises from the values of  $M_c$  calculated from the slopes of the line and shown in Table IV. If the monomer of spruce protolignin is assumed to be the guaiacylpropane unit (M.W. = 164), the number of units between crosslinks (D.P.)<sub>c</sub> is 53 and 5, respectively, for PB-3b and PS-5. Ignoring their difference for the moment, we see that these values are probably in the correct range. It has been estimated by means of end group analysis that the average D.P. of the primary chain is 15 (41). If there are two crosslinks per chain this leads to approximately 5 units between crosslinks. On the other hand, longer primary chains with fewer crosslinks could produce as with PB-3b a (D.P.)<sub>c</sub> of

TABLE IV  
*Values of  $Q$ ,  $r_{\eta}^0$ , and  $M_c$  from Data in Fig. 10*

Fraction	$Q$	$r_{\eta}^0(A.)$	$M_c$
PS-5	1823	100	860
PB-3b	1150	140	8620

53. Thus, the initial linearity of the  $r_{\eta}^2$  vs.  $1/r_{\eta}^2 \sqrt{I_E}$  graph and the reasonable values found for  $M_c$  provide some justification for the assumptions made in deriving Eq. [13].

The less-than-theoretical expansion at low ionic strengths seems to be a general phenomenon in physicochemical studies of polyelectrolytes. In the present instance it may be due to chain stretching beyond the extension at which Gaussian statistics apply. In the case of PS-5 with  $(D.P.)_c = 5$  this seems likely even for a small increase in the volume of the molecule. The "netting" effect as described by Medalia (20) may also be important here. In the original tetrahedral model on which the entropy term in Eq. [7] is based, Flory and Rehner (42) do not consider the effect of large, closed circuits. These may have no effect during the initial swelling at high ionic strength, but as soon as a volume is reached such that the circuits are strained, the expansion of the gel will be less than predicted theoretically. In a highly crosslinked polymer such as lignin, "netting" is probably quite common and could be expected to restrain the expansion, thereby producing the smaller slope at low  $I_E$  values as shown in Fig. 10. In PB-3b at low ionic strength, interpretation is further complicated by the increased ionization of the effective charge groups on the molecule. Increased ionization will favor increased extension and so, for this fraction, the decreased extension occurs in spite of an increase in  $Q$ . However, for both PB-3b and PS-5,  $R$  remains constant over the initial linear portion of the curve.

Finally we may consider any differences which have been revealed between lignin sulfonates made soluble early and late in the sulfonation process. Fraction PS-5 was made soluble during the first part of the sulfonation, and Fraction PB-3b may be regarded as coming from the last part of the cook.

One clear-cut difference is the degree of ionization of the molecule. The  $R$  value of 0.30 for PB-3b is considerably smaller than the value of 0.75 for PS-5. The reason may be that a greater proportion of the ionizable groups in PB-3b are below the effective surface of the molecule, thereby causing more site binding and decreased counterion activity. Such a distribution would be expected after prolonged sulfonation. It is interesting to note, however, that, if one charge-bearing group per guaiacylpropane unit is assumed possible, less than  $1/3$  of the monomer units of PB-3b are carrying ionizable sites. These could occur within an outer shell of thickness less

than 10% of the radius of the microgel. It is possible, therefore, that even with PB-3b the charge is on or near the surface of the microgel particle.

A second difference lies in the values of  $M_c$  in Table IV. If the treatment is correct, there is considerably less crosslinking in PB-3b than in PS-5. A similar detailed analysis was not possible for S-7 and S-14 but the slopes of the initial linear  $r_\eta^2$  vs.  $1/r_\eta^2 \sqrt{I_E}$  plots fit the trend of increase in  $M_c$  with time of cooking. From somewhat different evidence Sarkanen (43) has suggested that protolignin is solubilized during acid cooking by the progressive breaking of acid-sensitive crosslinks. The results of the present work support this concept. However, it is realized that the numerical values of  $M_c$  in Table IV must be considered very approximate. More exact data will depend on subsequent experiments with more carefully fractionated samples.

#### ACKNOWLEDGMENT

The authors wish to thank Mr. J. Jaworzyn for his assistance, particularly for the carefully made light-scattering measurements.

#### REFERENCES

1. GARDON, J. L., AND MASON, S. G., *Can. J. Chem.* **33**, 1491 (1955).
2. GORING, D. A. I., *Pulp & Paper Mag. Can.* **58**(5), 165 (1957).
3. GUPTA, P. R., AND GORING, D. A. I., *Can. J. Chem.* **38**, 248 (1960).
4. FLORY, P. J., "Principles of Polymer Chemistry." Cornell University Press, Ithaca, New York, 1953.
5. HERMANS, J. J., AND OVERBEEK, J. T. G., *Rec. trav. chim.* **67**, 762 (1948).
6. GORING, D. A. I., AND REZANOWICH, A., *Can. J. Chem.* **36**, 1653 (1958).
7. GORING, D. A. I., AND REZANOWICH, A., *J. Colloid Sci.* **15**, 472 (1960).
8. CRAIG, A. W., AND HENDERSON, D. A., *J. Polymer Sci.* **19**, 215 (1956).
9. HUQUE, M. M., JAWORZYN, J., AND GORING, D. A. I., *J. Polymer Sci.* **39**, 9 (1959).
10. GUPTA, P. R., AND GORING, D. A. I., *Can. J. Chem.* **38**, 270 (1960).
11. ZIMM, B. H., *J. Chem. Phys.* **16**, 1093, 1099 (1948).
12. FUOSS, R. M., AND STRAUSS, U. P., *J. Polymer Sci.* **3**, 602 (1948).
13. PALS, D. T. F., AND HERMANS, J. J., *J. Polymer Sci.* **5**, 733 (1950).
14. BASU, S., AND DAS GUPTA, C., *J. Colloid Sci.* **7**, 53 (1952).
15. MASSON, C. R., AND CAINES, G. W., *Can. J. Chem.* **32**, 51 (1954).
16. FUJITA, H., AND HOMMA, T., *J. Polymer Sci.* **15**, 277 (1955).
17. PALS, D. F. T., AND HERMANS, J. J., *Rec. trav. chim.* **71**, 433 (1952).
18. TERAYAMA, H., AND WALL, F. T., *J. Polymer Sci.* **16**, 357 (1955).
19. BAKER, W. O., *Ind. Eng. Chem.* **41**, 511 (1949).
20. MEDALIA, A. I., *J. Polymer Sci.* **6**, 423 (1950); also MEDALIA, A. I., AND KOLTHOFF, I. M., *ibid.* **6**, 433 (1950).
21. SHASHOUA, V. E., AND VAN HOLDE, K. E., *J. Polymer Sci.* **28**, 395 (1958).
22. TRAP, H. J. L., AND HERMANS, J. J., *J. Phys. Chem.* **58**, 757 (1954).
23. GARDON, J. L., AND MASON, S. G., *Can. J. Chem.* **33**, 1477 (1955).
24. MOACANIN, J., FELICETTA, V. F., HALLER, W., AND MCCARTHY, J. L., *J. Am. Chem. Soc.* **77**, 3470 (1955).
25. GUPTA, P. R., ROBERTSON, R. F., AND GORING, D. A. I., *Can. J. Chem.* **38**, 259 (1960).

26. ERLANDER, S., AND FRENCH, D., *J. Am. Chem. Soc.* **80**, 4413 (1958).
27. BOOTH, F., *Proc. Roy. Soc. (London)* **A203**, 533 (1950).
28. DOTY, P., AND STEINER, R. F., *J. Chem. Phys.* **20**, 85 (1952).
29. BRINKMAN, H. C., AND HERMANS, J. J., *J. Chem. Phys.* **17**, 574 (1949).
30. EDSALL, J. T., EDELHOCK, H., LONTIE, R., AND MORRISON, P. R., *J. Am. Chem. Soc.* **72**, 4641 (1950).
31. MYSELS, K. J., *J. Phys. Chem.* **58**, 303 (1954).
32. FLORY, P. J., AND OSTERHELD, JEAN E., *J. Phys. Chem.* **58**, 653 (1954).
33. SCHNEIDER, N. S., AND DOTY, P., *J. Phys. Chem.* **58**, 762 (1954).
34. KATCHALSKY, A., *J. Polymer Sci.* **7**, 393 (1951).
35. KATCHALSKY, A., AND LIFSON, S., *J. Polymer Sci.* **11**, 409 (1953).
36. TRELOAR, L. R. G., in H. A. Stuart, ed., "Die Physik der Hochpolymeren," Vol. 4, Chap. 5, Springer-Verlag, Berlin, 1956.
37. HUIZENGA, J. R., GRIEGER, P. F., AND WALL, F. T., *J. Am. Chem. Soc.* **72**, 2636 (1950).
38. WALL, F. T., *J. Phys. Chem.* **61**, 1344 (1957).
39. HARRIS, F. E., AND RISE, S. A., *J. Phys. Chem.* **61**, 1360 (1957).
40. ELTON, G. A. H., AND HIRSCHLER, F. G., *J. Chem. Soc.* 2953 (1952).
41. GUSTAFSSON, C., AND ANDERSEN, L., *Paperi ja Puu* **37**, 1 (1955).
42. FLORY, P. J., AND REHNER, J., *J. Chem. Phys.* **11**, 512 (1943).
43. SARKANEN, K. V., Literature Review on Lignin, Cellulose Research Institute, State College of Forestry at Syracuse University, to be published as a chapter in "Wood Chemistry," edited by B. L. Browning, Interscience Publishers.

## THE HUGGINS VISCOSITY COEFFICIENT FOR A POLYELECTROLYTE MICROGEL

D. A. I. Goring and A. Rezanowich

*The Physical Chemistry Division, Pulp and Paper Research Institute  
of Canada, McGill University, Montreal, Quebec*

*Received February 1, 1960; revised April 27, 1960*

### ABSTRACT

The Huggins coefficient,  $k'$ , was measured for certain lignin sulfonate fractions by isoionic dilution over a range of ionic strengths. Gross increases of  $k'$  were found with decreasing ionic strength. This effect was interpreted quantitatively in terms of the secondary electroviscous effect in which the electrokinetic double layer contributed to the collision diameter of the macromolecule. The concept of the collision diameter was then used to give a semiquantitative treatment of the familiar maxima in  $\eta_{sp}/c$  found on dilution of polyelectrolytes at low ionic strength. Theoretical prediction of the positions of the maxima agreed fairly well with experiment for sodium lignin sulfonate and sodium carboxymethyl cellulose.

### INTRODUCTION

In comparison with the data available for synthetic polymers in organic solvents there have been relatively few measurements of the Huggins viscosity coefficient,  $k'$ , on polyelectrolytes at various ionic strengths. With the normal type of dilution, in which the dissolving solvent is the diluent, curved  $\eta_{sp}/c$  plots are obtained at lower values of the ionic strength (1-3). Measurement of  $k'$  is then not possible. Linear graphs of  $\eta_{sp}/c$  can be obtained if the dilution is isoionic, i.e., if the total concentration of free counter ions in solution is kept constant at all concentrations of the polyelectrolyte (2-4). The parameter,  $k'$ , can then be computed by means of the familiar Huggins equation

$$\frac{\eta_{sp}}{c} = [\eta] + k'[\eta]^2 c, \quad [1]$$

in which the symbols have their usual significance.

In work described in a previous paper (2), viscometric measurements were made on solutions diluted by a carefully controlled isoionic technique. The polyelectrolyte was sodium lignin sulfonate, which demonstrated the behavior expected for a soluble polyelectrolyte microgel. The present paper is an attempt to explain the somewhat unusual values of  $k'$  found in this study.

Nawab and Mason (5, 6) have recently described certain experimental



TABLE I  
Data for Fractions PS-5 and PB-3b

Fraction	$I_E$ (moles $\text{Na}^+$ /l.)	$[\eta]$ ( $\text{g.}^{-1} \text{ dl.}$ )	$r_\eta$ ( $\text{\AA.}$ )	$k'$	$\delta$ ( $\text{\AA.}$ )
PS-5	1	0.062	117	1.0	0
	0.1	0.129	146	1.4	8
	0.01	0.228	177	3.3	39
	0.00401	0.274	188	9.8	87
	0.000435	0.442	221	55.6	211
PB-3b	1	0.153	173	0.9	0
	0.1	0.242	202	1.5	18
	0.01	0.462	251	2.7	50
	0.00145	0.868	309	5.1	103
	0.000239	1.10	334	37.7	288
	0.000161	1.28	352	57.0	350
	0.000021	1.45	367	398	645

complications in empirical relationships for the concentration dependence of the viscosity of emulsions and suspensions of macroscopic rods. There is, however, no general theory for the concentration dependence of viscosity, and the theoretical solution of the absolute value of  $k'$  in macromolecule systems is beyond the scope of the present paper. Instead, a quantitative explanation is attempted for the relative changes in  $k'$  due to the polyelectrolyte nature of the macromolecule. This concept is further developed to explain the familiar maxima found in  $\eta_{sp}/c$  when a polyelectrolyte is dissolved in and diluted with aqueous solvents of low ionic strength.

#### EXPERIMENTAL AND RESULTS

Viscosity measurements were made in capillary viscometers at 25°C. by isoionic dilution with aqueous NaCl. Materials, preparation of lignin sulfonate fractions, viscometric and dilution techniques, and graphical representation of the data are all given in a previous paper (2). The values of  $[\eta]$  and  $k'$  shown in Table I were computed from the linear graphs of  $\eta_{sp}/c$  vs.  $c$  by means of Eq. [1]. The ionic strength,  $I_E$ , is the sum of the  $\text{Na}^+$  ions supplied by the lignin sulfonate and the sodium chloride (see Eq. (1) in reference 2).

#### DISCUSSION

The most obvious feature of the results is the increase of  $k'$  at low ionic strength by two orders of magnitude as shown in Table I. We believe that the value of 398 for PB-3b at  $I_E = 2 \times 10^{-5} M$  is unique in being the largest value of  $k'$  ever reported. It is interesting to contrast such gross changes with the relative constancy of this parameter for solutions of

nonionic polymers where differences between such  $k'$  values as 0.35 and 0.5 are considered significant in assigning the configuration of the macromolecule (7).

Other workers have reported an increase in  $k'$  with decrease in ionic strength. Pals and Hermans (3), who studied a sodium pectinate and several sodium carboxymethyl cellulose fractions, observed that  $k'$  was inversely proportional to the ionic strength. Their values of  $k'$  ranged from 0.5 to 10. Similar increases in  $k'$  have been reported for potassium cellulose sulfonate and potassium polyacrylate (4). With sodium carboxymethyl cellulose, Fujita and Homma (8) found that  $k'$  increased linearly from 0.4 to 4 when plotted against the reciprocal of the ionic strength. As shown in Table I, a considerably wider range of  $k'$  was found in the present work, probably because a wider range of ionic strengths was studied. Also the relationship between  $k'$  and  $1/I_E$  (Fig. 1) was approximately linear as noted by previous workers.

Before considering in detail the variation in  $k'$  let us briefly recount the physical significance of  $k'$  in a colloidal solution. A spherical macromolecule increases the effective viscosity of the solvent by distorting the field of laminar shear flow in the region surrounding the particle in such a way as to increase the local velocity gradient and hence the rate of dissipation of energy. As a result of the velocity gradient, the spheres rotate. At finite concentrations, some of the individual macromolecules will undergo

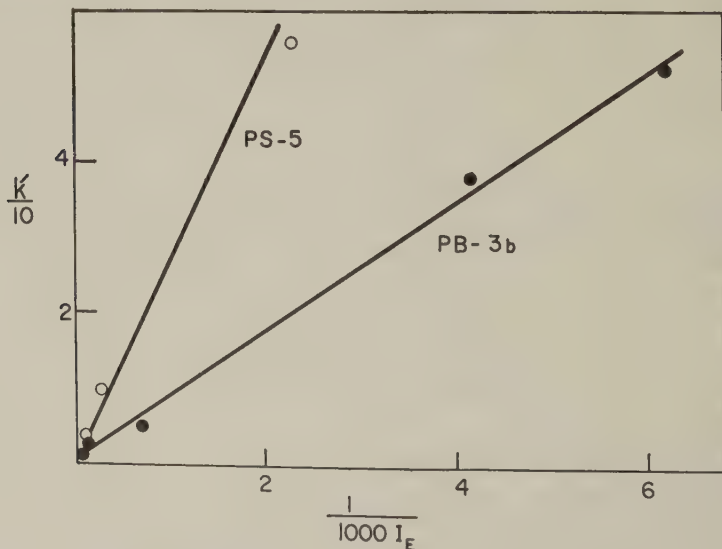


FIG. 1.  $k'$  vs.  $1/I_E$  for Fractions PS-5 and PB-3b. The point corresponding to PB-3b at lowest ionic strength falls on the line but was not included because of the larger scale required.

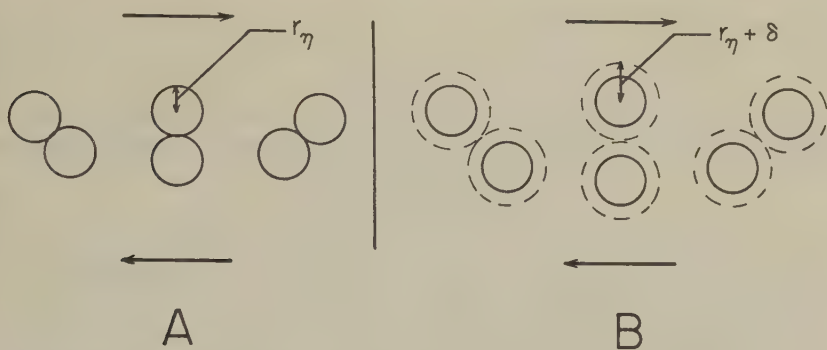


FIG. 2. Two-bodied collisions (A) without and (B) with the interacting double layer. The arrows indicate the direction of the shear field.

two-body collisions and thus form doublets which will rotate in the manner shown by Manley and Mason (9) and represented in Fig. 2. The energy dissipation due to the doublet exceeds that of the two spheres isolated from one another.

Therefore a collision will momentarily cause an increase in the viscosity of the solution over and above the viscosity imparted by the two particles when spinning separately. Since collision frequency is a function of the concentration, this effect results in the usual increase of  $\eta_{sp}/c$  with  $c$ . The Huggins coefficient  $k'$  is an empirical measure of this effect. For a given polymer/solvent system,  $k'$  is generally considered to be independent of molecular weight (10).

Let us now consider the effect of the electrical double layer on these processes. The microgel particle may be regarded as a sphere having a layer of gegen ions around it in solution. As the ionic strength decreases, (a) the particle swells, and (b) the double layer expands. As mentioned previously, the gegen ion layer appears to have a negligible effect on the intrinsic viscosity (2). This means that the isolated rotating sphere is not appreciably affected by changes in the thickness of the electrical double layer. The "primary" electroviscous effect is therefore small (2).

What effect might the double layer be expected to have on  $k'$ ? Owing to electrostatic repulsion the effective collision diameter of the particle will increase with increase in the width of the double layer. Thus, not only will more collisions occur but the rate of energy dissipation per doublet will be greater because of the greater effective volume of the doublet resulting from the increased separation of centers of the colliding spheres (Fig. 2). This causes the slope of the  $\eta_{sp}/c$  vs.  $c$  plot to increase markedly, producing the observed changes in  $k'$ . The parameter,  $k'$ , therefore becomes a rather sensitive measure of the "secondary" electroviscous effect.

In this context, an interesting dimension of the microgel particle is a

"collision radius,"  $r_c$ , given by

$$r_c = r_\eta + \delta \quad [2]$$

where  $\delta$  is one-half the distance between the surfaces of colliding microgels and  $r_\eta$  is the radius of the equivalent Einstein sphere;  $r_\eta$  is given in cm. by

$$r_\eta = \left( \frac{30M [\eta]}{\pi N} \right)^{1/3}, \quad [3]$$

in which  $M$  is the molecular weight of the particle,  $N$  is Avogadro's number, and the units of  $[\eta]$  are in dl. g.<sup>-1</sup>.

It is possible to calculate the distance  $\delta$ , from a comparison of  $k'$  at low ionic strengths with  $k'$  obtained when the effect of the double layer is small. From Eqs. [1] and [3]

$$k' = \frac{\Delta \frac{\eta_{sp}}{c} / \Delta c}{A r_\eta^6} \quad [4]$$

where

$$A = \left( \frac{\pi N}{30M} \right)^2.$$

The increase of  $k'$  at low ionic strengths is due to the incorrectly low value of  $r_\eta$  in Eq. [4]. If  $r_\eta + \delta$  were substituted for  $r_\eta$  in Eq. [4], it would be expected that the Huggins coefficient thus obtained would be equal to the value found when the effect of the double layer is negligible, i.e., at high ionic strength. Thus

$$\left( \frac{r_\eta + \delta}{r_\eta} \right)^6 = \frac{k'}{k'_0}, \quad [5]$$

where  $k'_0$  is the Huggins coefficient at an ionic strength high enough to eliminate the effect of the double layer. By extrapolation of the linear relationships shown in Fig. 1, it can be shown that the change of  $k'$  between  $1/I_E = 1$  and 0 is negligible. Thus  $k'_0$  was assumed to be  $(k')_{I_E=1M}$ . The values of  $\delta$  at various ionic strengths were then computed from Eq. [5] and are given in Table I.

As shown in Table I,  $\delta$  increased markedly at lower ionic strengths, becoming comparable with the radius of the swollen particle. It is interesting to compare  $\delta$  with the Debye thickness of the double layer which is given by  $3/\sqrt{I_E}$  for the present experimental conditions. In Fig. 3,  $\delta$  is plotted against  $3/\sqrt{I_E}$  and, except for the lowest ionic strength with PB-3b, a linear relationship was obtained. The slope of the line, which gives the ratio of  $\delta$  to the Debye double layer thickness, is 1.5 over a wide range of ionic strengths. Theoretically  $\delta$  will depend on the equilibrium between

the hydrodynamic force pushing the two spheres together and the electrostatic repulsion keeping them apart. Thus  $\delta$  will be a function of variables such as shear rate, solvent viscosity, zeta potential, and the width of the double layer. The results in Fig. 3 suggest that the latter is rather important in delineating  $\delta$ . A more detailed theoretical treatment of the size of the doublet is reserved for a later publication.

On solvent dilution (i.e., dilution with the solvent used for solution), a polyelectrolyte gives characteristic, upward curving graphs of  $\eta_{sp}/c$  vs.  $c$  with maxima at low concentrations. The curves become steeper and the maxima occur at lower concentrations when the ionic strength of the diluting solvent is decreased. A series of such maxima is shown in Fig. 4 for Fraction S-7, a lignin sulfonate described in previous publications (2, 11). Similar behavior with different polyelectrolytes has been noted by other workers (1, 3, 8, 12, 13). Conway (14) has suggested that the maxi-

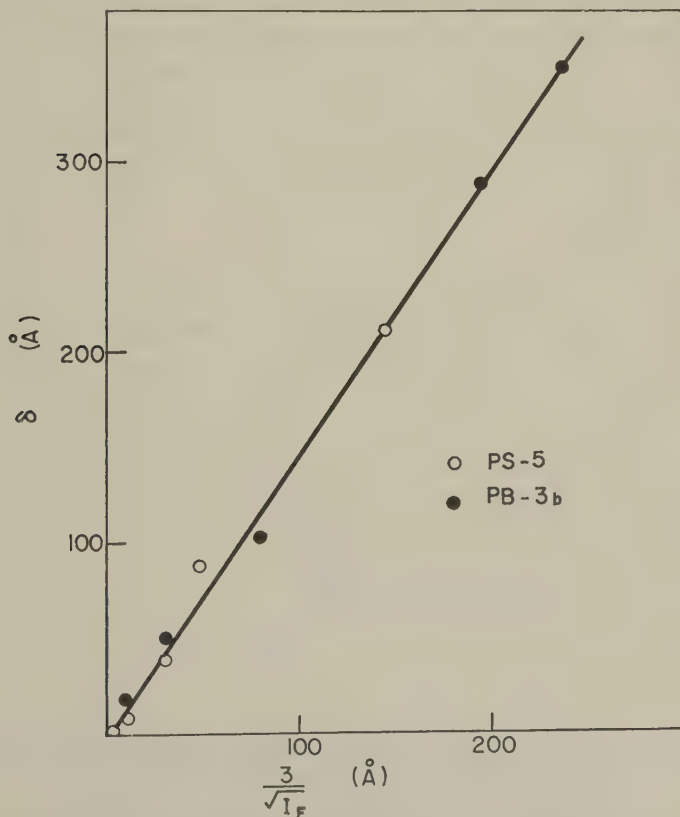


FIG. 3.  $\delta$  vs.  $3/\sqrt{I_E}$  for Fractions PS-5 and PB-3b. The point corresponding to PB-3b at lowest ionic strength was not included because of the larger scale required. It falls somewhat off the line at  $\delta = 645$  Å and  $3/\sqrt{I_E} = 655$  Å.



imum is due to a combination of the interaction effect and molecular expansion on dilution and he was able to predict the concentration at which the maximum occurred for sodium polymethacrylate dissolved in water. As a development of Conway's original idea, a semiquantitative treatment is possible based on the concept of the collision radius of the particle introduced above. The proposal is that a concentration,  $c_m$ , in the vicinity of the maximum bending of the curves, corresponds to the packing of the solution with spheres the size of the collision volume of the particles, i.e., spheres of radius  $r_c$ . At polyelectrolyte concentrations above  $c_m$  the double layer is compressed and  $\eta_{sp}/c$  decreases. At concentrations below  $c_m$ , the particles begin to move freely in solution and as  $I_E$ ,  $[\eta]$ , and  $k'$  approach their limiting constant value,  $\eta_{sp}/c$  decreases with decrease in  $c$  in the usual manner.

The above idea was tested by analyzing the data for Fraction S-7. The procedure consisted in predicting theoretically the concentration,  $c_p$ , at which the particles would be close-packed with respect to the collision radius and comparing this with  $c_m$  determined from the curves of  $\eta_{sp}/c$  vs.  $c$ .

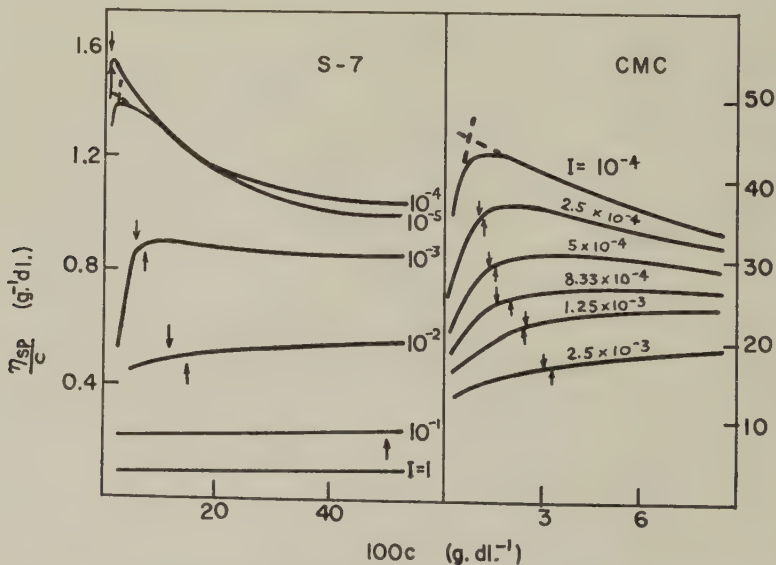


FIG. 4.  $\eta_{sp}/c$  vs.  $c$  on solvent dilution of polyelectrolytes with various molarities of NaCl. The upward pointing arrows are the computed values of  $c_p$ . Downward pointing arrows are the abscissae corresponding to experimentally determined values of  $c_m$ . The extrapolation method of determining  $c_m$  is shown for curves at  $I = 10^{-4} M$ . No explanation is offered for the inversion of the  $10^{-4} M$  and  $10^{-5} M$  plots at higher concentrations for Fraction S-7. The CMC data were taken directly from Fujita and Homma (8) for a sample (D.P. = 417, degree of substitution 0.73) in solutions of sodium chloride at 25° C.

shown in Fig. 4. If the theory is correct,  $c_m \simeq c_p$ . The position of the maximum was ill-defined at higher ionic strengths, and therefore  $c_m$  was defined as the concentration corresponding to the intersection obtained by extrapolating the approximately linear portions before and after the curvature. All values of  $c_m$  were determined in this manner before  $c_p$  was calculated as described immediately below.

The value of  $r_c$  was computed from Eq. [2] for each concentration of lignin and added electrolyte. For this purpose, the variation of  $[\eta]$  with  $I_E$  for Fraction S-7 was required. Such data were not available directly because the isoionic dilution technique was not applied in the case of S-7. As mentioned in the previous paper (2), isoionic dilution curves were derived by the method of Fujita and Homma (8) from the data in Fig. 4. Thus  $[\eta]$  and therefore  $r_\eta$  for any particular value of  $I_E$  could be computed. The calculation of  $r_c$  for any point in a solvent dilution curve was as follows:

1. The value of  $I_E$  was calculated from the NaCl concentration, the lignin concentration, and its degree of ionization (Eq. [1], reference 2).
2. The  $[\eta]$  value corresponding to  $I_E$  was deduced by the method of Fujita and Homma (8).
3. The value of  $r_\eta$  was computed from  $[\eta]$  from Eq. [3]. For this purpose an  $M_w$  value of  $1.83 \times 10^6$  was used which was obtained by interpolation

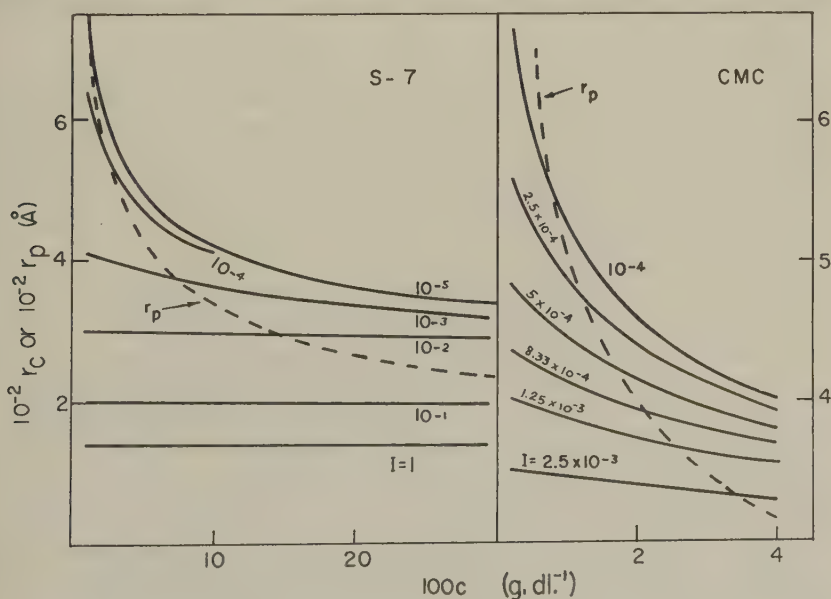


FIG. 5. Theoretically derived curves of  $r_c$  vs.  $c$  for polyelectrolytes dissolved in and diluted with various molarities of NaCl. The superimposed dotted line is the curve  $r_p$  vs.  $c$ . The concentrations corresponding to the points of intersection are reproduced as the upward pointing arrows in Fig. 4.

with two fractions of similar intrinsic viscosities for which  $M_w$  was measured by light scattering. Small errors in  $M_w$  do not affect the argument.

4. Here Fig. 3 was used to obtain  $\delta$  for any value of  $I_E$ .

5. Finally  $r_c$  was calculated from  $r_\eta$  and  $\delta$  by means of Eq. [2].

In Fig. 5, calculated values of  $r_c$  are plotted against the lignin concentrations for dilution with solvents having ionic strengths ( $I$ ) from 1.0 to  $10^{-5}$   $M$ . (N.B.,  $I$  is the solvent ionic strength. At finite lignin sulfonate concentration,  $I$  is always less than  $I_E$ , which is the cationic strength of the solvent + free cations from the polyelectrolyte.)

The next step in the analysis is the deduction of the radius required for close packing at any particular concentration of lignin. If we assume cubic close packing, the close-packed radius,  $r_p$ , is given by

$$r_p = \frac{B'}{c^{1/2}} \quad [6]$$

where  $B'$  is a constant.

In order to obtain a value for  $B'$ , the  $\eta_{sp}/c$  vs.  $c$  graph for  $I = 10^{-4}$   $M$  in Fig. 4 was used. The  $c_m$  value of 0.023 % lignin sulfonate was assumed to correspond to a cubic close-packed arrangement. From Fig. 5,  $r_c = 558$  A. Substituting 558 A for  $r_p$  and 0.023 % for  $c$  in Eq. [6], we find  $B' = 156$ ;  $r_p$  can then be calculated for any value of  $c$  and is shown by the dotted line in Fig. 5.

From the above it is clear that  $c_p$  at any ionic strength will be the point at which the  $r_p$  vs.  $c$  curve intersects the appropriate  $r_c$  vs.  $c$  curve. These points are reproduced in Fig. 4 by the upward pointing arrows. Values of  $c_m$  are indicated by the downward pointing arrows. The abscissal alignment between the two sets of arrows is fairly good and may be regarded as support for the theory given above.

Fujita and Homma (8) have published somewhat more complete  $\eta_{sp}/c$  vs.  $c$  data for sodium carboxymethyl cellulose at a variety of ionic strengths (Fig. 4). A similar analysis was made using their values of molecular weight, degree of substitution and ionization and  $[\eta]$  at various  $I_E$  to construct the curves of  $r_c$  vs.  $c$  shown in Fig. 5. Using the  $\eta_{sp}/c$  vs.  $c$  curve at  $I = 10^{-4}$   $M$  in Fig. 4 as a reference,  $c_m$  was found to be 0.0075 % corresponding to  $r_c = 552$  A. Substituting in Eq. [6],  $B'$  was found to be 108, from which the dotted curve of  $r_p$  vs.  $c$  shown in Fig. 5 was drawn. The intersections of  $r_p$  vs.  $c$  and  $r_c$  vs.  $c$  in Fig. 5 are given as upward pointing arrows in Fig. 4. As with lignin sulfonate, values of  $c_m$  (downward pointing arrows) were obtained by the extrapolation method. Here the abscissal alignment is better than obtained with NaLS, suggesting that the treatment can also be applied to linear polyelectrolytes such as CMC. In this respect it is interesting to note that no assumptions were necessary concerning the internal arrangement within the molecular domain. Pro-

vided the molecule is roughly spherical and remains spherical in its expanded state, the theory would be expected to apply. Thus, in addition to lignin sulfonate and CMC, synthetic polyelectrolytes might be expected to behave in a similar manner.

If the theory presented above is correct, certain currently accepted interpretations of the concentration dependence of viscosity of polyelectrolytes are incorrect. The extremely high values of  $k'$  at low ionic strength affect the validity of the extrapolation of the well-known equation of Fuoss and Strauss (1)

$$\frac{\eta_{sp}}{c} = \frac{A}{1 + Bc^{1/2}} + D, \quad [7]$$

where  $A$ ,  $B$ , and  $D$  are constants.

This empirical equation has been shown to represent the viscosity behavior of a wide variety of polyelectrolytes when diluted with water. The data are usually plotted as  $\frac{1}{\eta_{sp}/c} - D$  vs.  $c^{1/2}$ , where  $D$  is  $\eta_{sp}/c$  measured at a concentration high enough to make  $A/(1 + Bc^{1/2})$  negligible. Extrapolation of the straight line enables  $A$  and  $B$  to be evaluated. (It is interesting that Gardon and Mason (13) could obtain linearity for sodium lignin sulfonates only when  $\frac{1}{\eta_{sp}/c} - D$  vs.  $c^{0.7}$  was plotted.) The quantity  $A + D$  is then regarded as the intrinsic viscosity of the expanded macromolecule while  $D$  is the intrinsic viscosity of the coiled macromolecule. Clearly this procedure is not justified. Before zero concentration is reached, the macromolecule and its double layer must cease expanding. Because of the large value of  $k'$ ,  $\eta_{sp}/c$  will then fall rapidly to give a value of  $[\eta]$  which will be considerably less than  $A + D$ . At high concentrations the interaction between the electrical double layers will be so pronounced that  $D$  cannot be related to the viscometric behavior of the isolated macromolecule. Equation [7] must therefore be regarded as an empirical equation describing the rising portion of curves such as those shown in Fig. 4. No theoretical significance can be attached to the constants  $A$ ,  $B$ , and  $D$ .

As mentioned earlier, much significance has been placed on  $k'$  as a measure of the degree of branching for polymers in nonaqueous solvents. Such polymers seldom contain groups capable of formal ionization and, even if present, these would not ionize because the solvent is usually unable to support dissolved ions. However, electrical fields are certain to be present across the boundary between the molecular domain and the surrounding solvent. There is no reason why such fields should not influence  $k'$  in the same manner that an extended double layer increases this parameter, although the effect in the former case would probably be smaller. Thus, when interpreting the concentration dependence of viscosity in nonaqueous

solvents the polar nature of the macromolecule should be taken into account in addition to its shape and configuration.

#### ACKNOWLEDGMENT

The authors wish to thank Dr. S. G. Mason, whose interest and helpful suggestions were an essential part of the interpretation of the data.

#### REFERENCES

1. FUOSS, R. M., AND STRAUSS, U. P., *J. Polymer Sci.* **3**, 602 (1948).
2. REZANOWICH, A., AND GORING, D. A. I., *J. Colloid Sci.* **15**, 452 (1960).
3. PALS, D. F. T., AND HERMANS, J. J., *Rec. trav. chim.* **71**, 433 (1952).
4. TERAYAMA, H., AND WALL, F. T., *J. Polymer Sci.* **16**, 357 (1955).
5. NAWAB, M. A., AND MASON, S. G., *Trans. Faraday Soc.* **54**, 1712 (1959).
6. NAWAB, M. A., AND MASON, S. G., *J. Phys. Chem.* **62**, 1248 (1958).
7. CRAGG, L. H., AND FERN, G. R. H., *J. Polymer Sci.* **10**, 185 (1953).
8. FUJITA, H., AND HOMMA, T., *J. Polymer Sci.* **15**, 277 (1955).
9. MANLEY, R. ST. J., AND MASON, S. G., *J. Colloid Sci.* **7**, 354 (1952).
10. FLORY, P. J., "Principles of Polymer Chemistry." Cornell University Press, Ithaca, New York, 1953.
11. GORING, D. A. I., AND REZANOWICH, A., *Can. J. Chem.* **36**, 1653 (1958).
12. MASSON, C. R., AND CAINES, G. W., *Can. J. Chem.* **32**, 51 (1954).
13. GARDON, J. L., AND MASON, S. G., *Can. J. Chem.* **33**, 1491 (1955).
14. CONWAY, B. E., *J. Polymer Sci.* **18**, 257 (1956).



COMMENT ON THE PAPER "DIFFUSION OF STRONTIUM IN  
ION-EXCHANGE MEMBRANES" BY J. DE  
LOPEZ-GONZALES AND H. JENNY

In a recent issue of this Journal, J. de Lopez-Gonzales and H. Jenny have reported measurements of diffusion in ion-exchanger membranes (1). The measurements were made with cation-exchanger membranes and  $\text{Sr}^{++}$  and  $\text{H}^+$  as the counter ions. Self-diffusion coefficients of (radioactive)  $\text{Sr}^{++}$  and interdiffusion coefficients of the exchange  $\text{Sr}^{++}/\text{H}^+$  were calculated. One effect, in particular, emerges clearly from the results: with progressing conversion of the membranes to the  $\text{Sr}^{++}$ -form the *self-diffusion coefficient* of  $\text{Sr}^{++}$  *decreases*, whereas the *interdiffusion coefficient* of the  $\text{Sr}^{++}/\text{H}^+$  exchange *increases*.

Similar variations of self-diffusion coefficients have been observed previously, as quoted by the authors, and can be explained in a number of ways. The fact that the interdiffusion coefficient varies in just the opposite way may seem surprising at first sight. However, this variation is exactly as predicted by the theory of ionic interdiffusion in ion exchangers (2, 3). According to this theory, the interdiffusion coefficient depends on the relative amounts of the interdiffusing ions. The general rule has been derived that the interdiffusion coefficient is more strongly affected by the ion which is *in the minority*, and approaches the self-diffusion coefficient of this ion when the concentration of the ion approaches zero. This behavior is a consequence of the electric potential gradient (diffusion potential) which arises in any diffusion process involving ions of different mobilities. The phenomenon is a general one, and its explanation does not require assumptions about the molecular structure of the system. The system studied by de Lopez-Gonzales and Jenny behaves as predicted: with progressing replacement of the much faster  $\text{H}^+$  by  $\text{Sr}^{++}$  the interdiffusion coefficient increases, even though the self-diffusion coefficient of  $\text{Sr}^{++}$  (and conceivably also that of  $\text{H}^+$ ) decreases.

The theory of ionic interdiffusion has been quantitatively confirmed by measurements in steady-state membrane systems (3). The results now obtained by de Lopez-Gonzales and Jenny are, it seems, the first qualitative confirmation of its validity in nonstationary systems.

REFERENCES

1. DE LOPEZ-GONZALES, J., AND JENNY, H., *J. Colloid Sci.* **14**, 533 (1959).
2. HELFFERICH, F., *Discussions Faraday Soc.* **21**, 83 (1956); HELFFERICH, F., AND

PLESSET, M. S., *J. Chem. Phys.* **28**, 418 (1958); HELFFERICH, F., "Ionenaustauscher," p. 253. Verlag Chemie, Weinheim/Bergstr., 1959.

3. HELFFERICH, F., AND OCKER, H. D., *Z. physik. Chem. (Frankfurt)* **10**, 213 (1957).

*Shell Development Company,  
Emeryville, California*

FRIEDRICH HELFFERICH

*Received April 12, 1960*

*A New Journal*

*... serving biochemistry, biophysics, and  
related areas of experimental biology*

# Analytical Biochemistry

*Volume 1, Number 1, June 1960*

AN INTERNATIONAL JOURNAL

*Edited by* ALVIN NASON

ADVISORY BOARD

SAMUEL P. BESSMAN  
HARRY P. BROQUIST  
MELVIN CALVIN  
OSAMU HAYAISHI  
ROLLIN D. HOTCHKISS  
WALTER L. HUGHES  
VERNON M. INGRAM  
OLOV LINDBERG  
HUGH J. McDONALD  
EDWARD F. MacNICHOL, Jr.  
MANFRED M. MAYER  
HOWARD K. SCHACHMAN  
DONALD D. VAN SLYKE  
SIDNEY UDENFRIEND  
THEODOR WIELAND  
LEMUEL D. WRIGHT

ANALYTICAL BIOCHEMISTRY is intended to serve as a central, international source of information on new and improved methods in the various fields of biochemistry, biophysics, and related areas of experimental biology. It is designed to meet the need for a publication devoted solely to papers describing methods in these areas.

The new journal will publish detailed accounts of fundamental contributions on analytical and preparative procedures. It will include papers on qualitative and quantitative techniques based on chemical, physical, and biological principles; methods of preparation, purification, characterization, isolation and separation of biological substances and related materials; and instrumentation.

Short communications will also be considered.

Manuscripts and queries concerning editorial policy should be sent to the Editor:

DR. ALVIN NASON  
McCollum-Pratt Institute  
The Johns Hopkins University  
Baltimore 18, Maryland

Subscription orders should be sent to the publishers.

*Volume 1, 1960, \$15.00*



ACADEMIC PRESS, *New York and London*

111 Fifth Avenue, New York 3, N. Y.

17 Old Queen Street, London, S.W. 1

# Journal

Editor-in-chief: J. C. Kendrew  
Peterhouse, Cambridge, England

VOLUME 1 1959, \$14.00

- Geoffrey Zubay and Paul Doty. The Isolation and Properties of Deoxyribonucleoprotein Particles Containing Single Nucleic Acid Molecules
- V. Moses, O. Holm-Hansen, J. A. Bassham and M. Calvin. The Relationship between the Metabolic Pools of Photosynthetic and Respiratory Intermediates
- I. M. Dawson and D. H. Watson. An Electron Microscope Study of the Structure of Crystalline Ribonuclease
- Robert L. Sinsheimer. Purification and Properties of Bacteriophage  $\phi$ X174
- Robert L. Sinsheimer. A Single-Stranded Deoxyribonucleic Acid from Bacteriophage  $\phi$ X174
- D. W. Green and R. Aschaffenburg. Twofold symmetry of the  $\beta$ -lactoglobulin Molecule in Crystals
- M. S. Santanam. Calcification of Collagen
- Pauline M. Harrison. The Structures of Ferritin and Apoferritin: Some Preliminary X-Ray Data
- C. O. Doudney and F. L. Haas. Gene Replication and Mutation Induction in Bacteria
- R. W. Horne, S. Brenner, A. P. Waterson, P. Wildy. The Icosahedral Form of an Adenovirus
- Ernest Freese. The Specific Mutagenic Effect of Base Analogues on Phage T4
- Jacques R. Fresco. Polynucleotides II: The X-Ray Diffraction Patterns of Solutions of the Randomly Coiled and Helical Forms of Polyriboadenylic Acid
- Benjamin D. Hall and Paul Doty. The Preparation and Physical Chemical Properties of Ribonucleic Acid from Microsomal Particles
- V. Luzzati and A. Nicolaieff. Etude par Diffusion des Rayons X aux Petits Angles des Gels d'Acide Désoxyribonucléique et de Nucléoprotéines: (Note Préliminaire)
- Gunther S. Stent, Gordon H. S. Shewen, Niels K. Jerne. Dispersal of the Parental Nucleic Acid of Bacteriophage T4 among its Progeny
- Endre A. Balazs, Aksel A. Bothwell and John Gergely. Proton Magnetic Resonance Studies on Water in the Presence of Various Macromolecular Substances
- R. E. Burge and R. D. Hynes. Thermal Denaturation of Collagen in Aqueous Solution and its Structural Implications
- Arthur B. Pardee, François Jacob, Jacques Monod. The Genetic Control of "Cytoplasmic Expression of Inducibility" in the Synthesis of Lactosidase by *Escherichia coli*
- M. H. F. Wilkins, G. Zubay and D. Wilson. X-Ray Diffraction Studies of the Molecular Structure of Nucleosomes and Chromosomes
- Geoffrey Zubay. The Transition between Straight and Coiled-Coil Configurations of the  $\alpha$ -Helix
- Richard S. Morgan and Ray Byrne. "Alkaline" Polyadenylation
- Hideo Kon and Norman Davidson. Nuclear Magnetic Relaxation of Protons by Ferrihemoglobin and Ferrimyoglobin
- Cecil E. Hall, Elizabeth C. MacLennan, Irwin Tessman. Structure and Functions of Bacteriophage  $\phi$ X174. Electron Microscopy
- Ellen Borenfreund, Herbert S. Kranz and Aaron Bendich. Studies on the Release of Deoxyribonucleic Acid after Exposure to Tritium Gas
- Masayasu Nomura and J. D. Watson. Ribonucleoprotein Particles Inhibited by Chloromycetin in *Escherichia coli*
- Robert L. Sinsheimer. Is the Genetic Message in a Two-Symbol

# Molecular Biology

Board: P. Doty, A. F. Huxley, R. L. Sinsheimer,  
J. D. Watson, M. H. F. Wilkins

- ères, J. D. Watson, D. Schlesinger and B. R. Hollingworth. Ribonucleoprotein Particles from *Escherichia coli*
- Horne, G. E. Russell and A. R. High Resolution Electron Microscopy of Beet Yellows Virus Filaments
- Mahr and A. Tissières. Nucleotide Composition of Ribonucleoprotein Particles from *Escherichia coli*
- ne Grunberg-Manago. Phosphorylation and Configuration Macromolecules des Polyribonucleotides Synthétiques et des Acides Ribonucléiques
- and Koch and A. D. Hershey. Synthesis of Phage-Precursor Protein in Bacteria Infected with T2
- h M. Smith and G. J. Hills. Electron Microscopy of the *Tipula* Iridescent Protein
- er, G. Streisinger, R. W. Horne, J. Champe, L. Barnett, S. Benzer and T. W. Rees. Structural Composition of Bacteriophage
- . Donovan, Michael Laskowski, and Harold A. Scheraga. Carboxyl-Group Interactions in Lysozyme
- L. Hayes, Jack C. Murchio, and T. Lindgren and Alex. V. Ts. A Determination of Lipoprotein Molecular Weight by use of the Electron Microscope
- and Lacks and François Gros. A Polyelectrolytic Study of the RNA-Amino Acid Complexes in *Escherichia coli*
- in S. Friesen and Robert L. Sinsheimer. Partition Cell Analysis of Tobacco Mosaic Virus Nucleic Acid
- C. E. Hall and H. S. Slayter. Electron Microscopy of Ribonucleoprotein Particles from *Escherichia coli*
- R. W. Horne and J. Nagington. Electron Microscope Studies of the Development and Structure of Poliomyelitis Virus
- E. A. Barnard and W. D. Stein. Histidine Residue in the Active Center of Ribonuclease. I: A Specific Reaction with Bromoacetic Acid
- W. D. Stein and E. A. Barnard. Histidine Residue in the Active Center of Ribonuclease. II: The Position of this Residue in the Primary Protein Chain
- Kazutomo Imahori and Jiro Tanaka. Ultraviolet Absorption Spectra of Poly-L-Glutamic Acid
- A. Tissières. Some Properties of Soluble Ribonucleic Acid from *Escherichia coli*
- Murray Vernon King. The Unit Cell and Space Group of Cubic Glucagon
- J. Weigle, Matthew Meselson and Kenneth Paigen. Density alterations Associated with Transducing Ability in the Bacteriophage Lambda
- R. D. B. Fraser and T. P. MacRae. Molecular Organisation in Feather Keratin
- C. R. Worthington. Large Axial Spacings in Striated Muscle
- M. F. Perutz, L. K. Steinrauf, Anne Stockell and A. D. Bangham. Chemical and Crystallographic Study of the two Fractions of Adult Horse Haemoglobin
- Index.



# INFRARED METHODS

**Volume 7 of Physical Chemistry: A Series of Monographs**  
**edited by Eric Hutchinson and P. Van Rysselberghe**

*By G. K. T. CONN, The University, Exeter*  
*and D. G. Avery, Atomic Energy Authority, Copenhurst Works*

*August 1960, 203 pp., illus., \$6.80*

This book is a critical guide for the choice and evaluation of infrared methods. It is intended for the scientist in any field to whom a concise, reliable manual is important. The longer of the two parts, Principles, discusses the chief components used in exploring the infrared region: Sources of Radiation, Optical Materials, Detectors, Amplifiers, and Dispersive Systems. The second part, Practical Applications, is an introduction to specific techniques and the types of experiments for which they are suited. The chapters in this section are: Calibration of Detectors, A Simple Monochromator, Instruments for Gas Analysis and Plant Control, and Radiation Pyrometry.

# INFRARED ABSORPTION SPECTRA Index for 1945-1957

*By HERBERT M. HERSHENSON, Baird-Atomic, Inc.*

*1959, 111 pp., 8½ x 11", \$7.00*

This index gives the location of infrared absorption spectra published in thirty-two representative American and European journals during the thirteen-year period from 1945 through 1957. It will greatly simplify the problems of locating infrared spectra and will in many instances eliminate the necessity of obtaining a pure specimen of a compound in order to determine its absorption characteristics.



**Academic Press, New York and London**

**111 Fifth Avenue, New York 3, New York**

**17 Old Queen Street, London, S.W. 1**

## SELF-DIFFUSION OF CALCIUM IONS IN CALCIUM MONTMORILLONITE GELS<sup>1</sup>

G. E. Fletcher and W. H. Slabaugh

*Department of Chemistry, Oregon State College, Corvallis, Oregon*

*Received April 19, 1960*

### ABSTRACT

Self-diffusion constants of  $\text{Ca}^{++}$  in gels of calcium montmorillonite have been measured by means of radiotracer methods. The labyrinth factors,  $g$  and  $h$ , which reveal a structural aspect of the gel, were calculated and compared to similar factors reported by Bloksma, who examined the self-diffusion of  $\text{Na}^+$  and  $\text{I}^-$  in similar gels. The eccentricity of the gel particles, essentially the clay micelles, based upon the present data, are in good agreement with independently derived values.

In a previous work, Bloksma (1) studied the diffusion of sodium and iodide ions and of urea in sodium montmorillonite and kaolinite pastes and calculated two labyrinth factors,  $h$  and  $g$ ; he found the mobility of non-exchangeable ions (anions) and molecules to be a fraction  $h$  of their mobility in aqueous solutions, and the mobility of exchangeable ions (cations) to be a fraction  $g$  of their mobility in aqueous solutions.

In infinitely dilute solutions, the relationship (2) between the self-diffusion coefficient  $D_i^0$ , the mobility  $w_i^0$ , and the limiting equivalent ionic conductance  $\lambda_i^0$  of the ion  $i$  is

$$D_i^0 = kTw_i^0 = \frac{\lambda_i^0 RT}{|z_i| F^2}, \quad [1]$$

where  $k$  is Boltzmann's constant,  $R$  is the gas constant,  $T$  is the absolute temperature,  $F$  is the Faraday, and  $z_i$  is the valency of  $i$ .

In porous materials such as clay gels, diffusion is affected by electrical charges on the clay particles and by the geometry of the diffusion path. For the diffusion of anions, allowance is made for the diffusion path geometry by adding the labyrinth factor  $h$  to the second term in Eq. [1]:

$$D_i = kTw_i h. \quad [2]$$

The model adopted for the diffusion of the cation involves two aspects.

<sup>1</sup> Taken in part from the thesis submitted by G. E. Fletcher in partial fulfillment of requirements for the Master of Science degree at Oregon State College and supported by a grant from the Baroid Division of the National Lead Company.

There is, first, the diffusion of soluble cations independent of those in the exchange sites. To these cations in solution, the concentration of which is  $n$  moles per liter, is assigned the labyrinth factor  $h$ . Secondly, there are cations in exchange positions the diffusion of which is affected not only by diffusion path geometry but also by the negative electrical charges on the clay particles. Consequently, the labyrinth effect is composed of two factors, and Eq. [2] becomes

$$D_i = kTw_i \left( \frac{nh + sg}{n + s} \right), \quad [3]$$

where  $D_i$  is the diffusion coefficient for cations,  $s$  is the concentration, and  $g$  is the labyrinth factor for these exchangeable cations.

Bloksma evaluated  $h$  directly through Eq. [2] by determining  $D_{\text{urea}}$  and  $D_i$  experimentally, and then calculated  $g$  for  $\text{Na}^+$  by determining  $D_{\text{Na}^+}$  experimentally and substituting into Eq. [3]. In this study, however,  $h$  and  $g$  were both evaluated through Eq. [3] by determining  $D_{\text{Ca}^{++}}$  experimentally and using three sets of clays with different values of  $n/s$  including  $n/s = 0$  (or  $n = 0$ ) (3,4). It is to be noted that when  $n = 0$ , the labyrinth factor reduces simply to  $g$ , which, according to the present model, describes the joint effects of diffusion path geometry and electrical charges on the mobility of the exchangeable cation in the calcium clay gels.

Crank has shown (5) that

$$C = \frac{1}{2} C_0 \operatorname{erfc} \frac{x}{2\sqrt{Dt}} \quad [4]$$

is a solution of the diffusion equation for the initial and boundary conditions used in this study.

Equation [4] takes the form

$$\frac{2Cl}{C_0} = \int \left( \operatorname{erfc} \frac{x}{2\sqrt{Dt}} \right) dx, \quad [5]$$

where  $l$  is the length of the cylinder (or the width of the plates) measured in direction  $x$ ,  $t$  is time, and  $C$  and  $C_0$  are concentrations of diffusate and are proportional to the measured activities of the samples.

The three calcium montmorillonite gels were prepared by passing a 1% suspension of Wyoming bentonite through ion exchange columns packed with the calcium form of Amberlite IR-120, adding sufficient  $\text{CaCl}_2$  so that  $n/s$  equalled 0, 0.1, and 1.0, and then drying at  $80^\circ\text{C}$ . until a fairly thick paste was obtained. Three other clays were prepared similarly, except that calcium-45 was used.

The apparatus was similar to that used by Bloksma, except that it was made of Plexiglas and utilizes two additional plates, or a total of six plates,

four of which contained the gel and two of which served as covers for each diffusion cell.

The ordinary calcium gels were loaded into the cylindrical holes of plates numbered four and five, and the corresponding calcium-45 gels into plates numbered two and three, and diffusion was initiated by aligning the holes. After diffusion at  $24^\circ \pm 1^\circ\text{C}$ ., the gels from the compartments of plates four and five were removed and separately shaken with ammonium acetate solution to remove the calcium from the clay, and the clay was removed by centrifugation. Additional calcium chloride was added and the calcium was precipitated as the oxalate in a uniform layer on planchets. The samples were then counted with a G-M thin mica window counter, and the counting rates were corrected for coincidence loss and self absorption.

TABLE I  
*Self-Diffusion Constants of  $\text{Ca}^{++}$  in Calcium Bentonite Gels*

Run no.	Plate no.	Number of determinations	Clay conc. (wt. %)	$n/s$	$t \times 10^{-5}$ (sec.)	$D \times 10^5$ ( $\text{cm}^2 \text{sec}^{-1}$ )	Error std. dev. (%)
1	4	3	4.91	0	2.608	0.0519	3.25
	5	3				0.0706	0.58
2	4	3	7.90	0	3.117	0.0469	4.3
	5	3				0.0622	5.0
3	4	3	10.6	0.1	4.418	0.0641	1.6
	5	3				0.0880	5.1
4	4	3	9.02	0.1	3.547	0.0774	9.1
	5	3				0.1234	8.9
5	4	3	5.72	1.0	2.895	0.171	21.7
	5	2				0.243	0.62
6	4	3	8.20	1.0	2.612	0.283	17.7
	5	3				0.264	0.53

TABLE II  
*Constants Calculated from Experimental Results*

From $\text{Ca}^{++}$ diffusion in Ca-montmorillonite		From $\text{Na}^+$ and $\text{I}^-$ diffusion in Na-montmorillonite (Bloksma)	
$g$	$h$	$g$	$h$
0.084 <sup>a</sup>	0.630 <sup>b</sup>	0.37	0.49
	0.557 <sup>c</sup>		
	0.590 (Av.)		

<sup>a</sup> From runs one and two.

<sup>b</sup> From runs three and four.

<sup>c</sup> From runs five and six.

To obtain  $D$  from the experimentally determined value of  $2Cl/C_0$ , Eq. [5] was integrated graphically and a curve obtained for  $2Cl/C_0$  vs.  $Dt$ ; a value of  $Dt$  was thus read from the curve for the corresponding experimentally determined value of  $2Cl/C_0$ , and since the diffusion time,  $t$ , was also measured,  $D$  was readily calculated.

Values of  $D$  for six runs appear in Table I. The values of the concentrations are the averages of the concentrations of the two clays used in each run. The errors represent the standard deviation of the values of  $D$  calculated for each plate from the average value for that plate.

The calculated labyrinth factors appear with those obtained by Bloksma in Table II. Average values of  $D$  from plate number five were used in the calculations since the average of the standard deviations for plate number four is 9.6% and the average for plate number five is 3.5%.

The value of  $g$  is seen to be much lower for  $Ca^{++}$  than for  $Na^+$  as would be expected. The difference in values for  $h$  for the two systems may be attributed to experimental error, to differences in structure among various clays, and particularly to the different type of cation in the exchange position on the clay.

Following the method of de Vries (6), the eccentricity of the oblate spheroids that may serve as a model for the particles in the calcium clay gel was calculated. An average value of  $h$  along with a pore fraction based upon a density of 2.65 g./cm.<sup>3</sup> for the clay gave an eccentricity of approximately 100. This value agrees well with the range of 10 to 100 obtained by shadow cast electronmicrographs (7).

The assistance of Dr. Chih H. Wang by way of discussions of the tracer techniques used in this study is gratefully acknowledged.

#### REFERENCES

1. BLOKSMA, A. H., *J. Colloid Sci.* **12**, 40 (1957).
2. HARNED, H. S., AND OWEN, B. B., "The Physical Chemistry of Electrolytic Solutions," p. 86. Reinhold, New York, 1943.
3. MARSHALL, C. E., AND CHATTERJEE, B., *J. Phys. & Colloid Chem.* **54**, 671 (1950).
4. CHAO, T., Master's thesis, Oregon State College, 1959.
5. CRANK, J., "The Mathematics of Diffusion," p. 103. Oxford University Press, London, 1956.
6. DE VRIES, D. A., *Trans. 4th Intern. Congr. Soil Sci.* **2**, 41 (1950).
7. GRIM, RALPH E., "Clay Mineralogy," p. 116. McGraw-Hill, New York, 1953.



## STABILITY OF EMULSIONS OF WATER IN OIL

### III. FLOCCULATION AND REDISPERSION OF WATER DROPLETS COVERED BY AMPHIPOLAR MONOLAYERS

W. Albers<sup>1</sup> and J. Th. G. Overbeek<sup>2</sup>

*van't Hoff Laboratory, University of Utrecht, Utrecht, Netherlands*

*Received April 20, 1960*

#### ABSTRACT

Theoretical calculations demonstrate that emulsions of water in oil cannot be sufficiently protected against flocculation by an adsorbed layer of amphipolar molecules with an oleophilic chain of about 20 Å. It is, however, expected that such flocculated emulsions can be redispersed by moderate rates of shear. This is confirmed by viscosity measurements. Non-Newtonian behavior found at low rates of shear is a consequence of flocculation. From the minimum rate of shear to reach the Newtonian region, i.e., to cause complete redispersion, the effective van der Waals' constant between the water droplets can be estimated. The rather low value of  $A = 0.4 \times 10^{-14}$  erg is found.

#### INTRODUCTION

It was shown in a previous communication (1) that electric charges cannot be expected to stabilize water-in-oil (W/O) emulsions of more than extremely low concentration. In this paper we shall investigate whether a layer of oleophilic chains on the water droplets may prevent their flocculation.

When the surface of the water droplets is densely covered with stabilizer molecules of high desorption energy the surfaces of the droplets can approach each other only to a distance that equals twice the length of the stabilizer molecules. If the energy of the van der Waals' attraction at this distance is larger than a few times  $kT$  flocculation will occur. If not, the emulsion will be stable.

For the usual stabilizers the oleophilic chain is not longer than 20 Å. Consequently the minimum distance between the water droplets is 40 Å.

<sup>1</sup> Present address: Philips Research Laboratories, Eindhoven, Netherlands.

<sup>2</sup> Presently: Visiting Professor of Chemistry, University of Southern California, Los Angeles 7, California.

TABLE I  
*Van der Waals' Energy between Two Spheres at a Distance of 40 Å.  
 Expressed as Multiples of  $kT$  ( $4 \times 10^{-14}$  erg)*

Radius $a$	$A = 10^{-12}$ erg	$A = 10^{-13}$ erg	$A = 10^{-14}$ erg
0.1 $\mu$	50	5	0.5
1.0 $\mu$	500	50	5
10 $\mu$	5000	500	50

The van der Waals' energy between two spheres of radius  $a$  at a distance  $d$  is given by:

$$V_{\text{van der Waals}} = -\frac{Aa}{12d},$$

when  $d \ll a$  and  $A$  is the van der Waals' constant (2).

Table I shows that for the usual range of droplet sizes and normal values of the constant  $A$  the energy at contact, i.e.,  $d = 40$  Å, is much larger than  $kT$  except perhaps for the smallest particles at an exceptionally low value of  $A$ . Therefore W/O emulsions are not stabilized against flocculation when the adsorbed stabilizers have a hydrocarbon chain of 20 or less carbon atoms.

#### CHARGED DROPLETS

It may be argued that if an electric charge or a layer of oleophilic chains are unable to stabilize W/O emulsions a combination of the two may perhaps lead to stabilization. The repulsion due to the electric double layer, however, has a very long range, and the maximum in the potential energy vs. distance curve (*cf.* Fig. 1 of paper I (3) in this series) is always situated at a larger separation than 40 Å. Consequently the action of the oleophilic chains does not support that of the double layer and vice versa.

In general W/O emulsions containing droplets with a radius  $\geq 1\mu$  will therefore be either broken or flocculated, depending on their stability against coalescence (1, 3). If they are not stabilized against coalescence, they will flocculate and break. If, however, they are stable against coalescence the flocculation may conceivably be prevented or reversed by mechanical action, e.g., by stirring the emulsion.

#### BEHAVIOR OF BINARY AGGREGATES IN LAMINAR FLOW

In order to investigate whether a flocculated system can be redispersed to the primary particles by shaking, we shall consider the behavior of aggregates in a laminar field of flow.

Two points have to be considered:

First: what is the minimum rate of shear,  $D$ , to surmount the van der

Waals' attraction by which the particles are held together in the aggregate, if the minimum distance between the surfaces of the water droplets equals  $d$  ( $d$  is twice the length of the hydrocarbon chain of the stabilizing molecule adsorbed at the interface)?

Second: will the period during which the shearing force is acting last long enough to allow the redispersed particle to be removed to such a distance from the aggregate that it will not be caught back during the rotation of the aggregate?

#### CALCULATION OF THE RATE OF SHEAR NECESSARY TO OVERCOME THE VAN DER WAALS' FORCE IN THE AGGREGATE

Big aggregates may be expected to fall apart more easily than small ones. For a given rate of shear, the redispersing force (see Eq. [4] for  $d \ll a$ ) and the number of contact points to be broken will both on the average be proportional to the  $2/3$ rd power of the number of primary globules in the aggregate. But the breaking of the aggregate may occur along the weakest plane by breaking the contact points one by one. This wedge effect is absent in a doublet. Consequently the splitting of the smallest aggregate, a complex consisting of two particles only, is the last and the most difficult step to complete redispersion. For this reason we shall investigate the behavior of a two-particle aggregate under the influence of a shearing force.

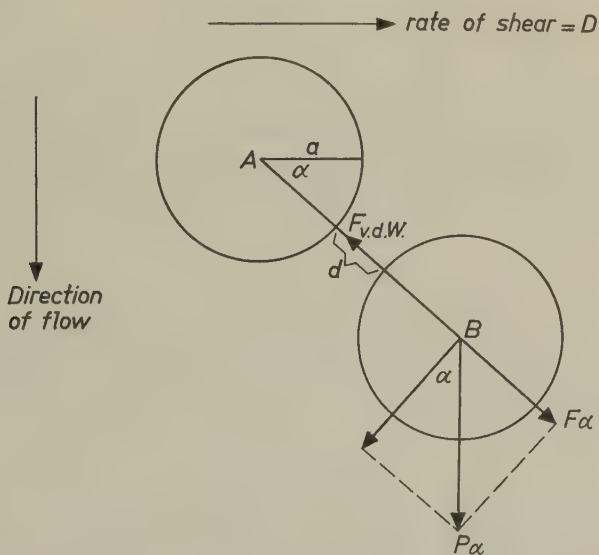


FIG. 1. Rotation of a two-particle aggregate under influence of a shearing force. Here  $a$  = radius of the globule,  $d$  = distance between the surfaces of the globules,  $F_{vdW}$  = van der Waals' force,  $F\alpha$  = shearing force acting on particle  $B$ , as caused by the hydrodynamic flow.

In general the line connecting the centers of the two droplets will make an angle with the plane defined by the direction of flow and the direction of shear. When the flow starts this line will describe a rather complicated trajectory, but finally it will become parallel to the plane indicated above (at least if the aggregate has not been broken up before). Therefore we shall consider only a binary aggregate  $AB$  built up from two spherical droplets  $A$  and  $B$ , and situated in the plane of flow and shear (see Fig. 1). The line connecting the particles makes an angle  $\alpha$  with the direction of shear; the distance between the surfaces is  $d$ . The difference in rate of flow between the centers of the droplets  $A$  and  $B$  is equal to

$$\Delta v = (2a + d)D \cos \alpha. \quad [1]$$

A part of this flow, viz.,  $\Delta v \cos \alpha$  leads to a rotation of the droplets around their center of gravity with a rate

$$d\alpha/dt = D \cos^2 \alpha. \quad [2]$$

The remaining part of the flow, viz.  $\Delta v \sin \alpha$  results in a tension  $F_\alpha = P_\alpha \sin \alpha$  tending to force the particles apart.

This tension  $F_\alpha$  is determined by the entire flow pattern around the two spheres. As a very first approximation we may put it equal to the force calculated from Stokes' law. This results in

$$F_\alpha = 6\pi\eta a \frac{\Delta v}{2} \sin \alpha = 3\pi\eta a(2a + d)D \sin \alpha \cos \alpha. \quad [3]$$

During the rotation of the aggregate from  $\alpha = 0$  to  $\alpha = 90^\circ$  the tension  $F_\alpha$  increases from zero to a maximum value at  $\alpha = 45^\circ$  and decreases again to zero for  $\alpha = 90^\circ$ . Separation of the aggregate and redispersion may occur when the value of  $F_\alpha$  is larger than the van der Waals' attraction  $F_{\text{vdw}}$ , starting at some angle  $\alpha_{\text{crit.}} < 45^\circ$  and extending to  $\alpha = 90^\circ$

$$F_{\alpha_{\text{crit.}}} = \frac{3}{2}\pi\eta a(2a + d)D \sin (2\alpha_{\text{crit.}}) = F_{\text{vdw}}. \quad [4]$$

We are interested in cases where  $d$  starts at a value (e.g., 40 Å.) much smaller than  $a$  (e.g., 1  $\mu$ ). In these cases, according to Hamaker (2) the van der Waals' force is given by

$$F_{\text{vdw}} = \frac{Aa}{12d^2}. \quad [5]$$

The condition for redispersion is, therefore, neglecting  $d$  in comparison with  $a$

$$3\pi\eta a^2 D \sin (2\alpha_{\text{crit.}}) > \frac{Aa}{12d^2} \quad [6]$$

TABLE II

*Critical Rates of Shear in sec.<sup>-1</sup> for Redispersion of Particles Separated by a Layer of 40 Å. Thickness as a Function of van der Waals' Constant, A, and Particle Radius a.*

Radius $a$	$A = 10^{-12}$ erg	$A = 10^{-13}$ erg	$A = 10^{-14}$ erg
0.1 $\mu$	$10^6$	$10^5$	$10^4$
1 $\mu$	$10^5$	$10^4$	$10^3$
10 $\mu$	$10^4$	$10^3$	$10^2$

or

$$D > \frac{A}{36\pi\eta a d^2 \sin(2\alpha_{\text{crit.}})} \quad [7]$$

Inserting the value 40 Å. for  $d$  and 0.006 poise for  $\eta$  (e.g., benzene at 25°C.) and 30° for  $\alpha_{\text{crit.}}$  (see below), we obtain

$$D > \frac{A}{a} \times 10^{13}. \quad [8]$$

Table II gives values for the critical rate of shear,  $D_{\text{crit.}}$ , calculated with Eq. [7] for a number of representative cases.

#### ESTIMATION OF THE CRITICAL ANGLE, $\alpha_{\text{crit.}}$ , FOR DISPERSION

We shall now show that redispersion occurs in a very short time, if the rate of shear is larger than  $D_{\text{crit.}}$ . During rotation of the aggregate between  $\alpha = 0$ , and  $\alpha = 90^\circ$  the excess of the tension  $F_\alpha$  over the van der Waals' attraction,  $F_{\text{vdw}}$ , will force the particles apart. Mooney (4) has calculated the friction factor for the motion of two solid spheres along the line connecting their centers. For small distances,  $p$ , between the surfaces the relative axial velocity  $v_{\text{rel.}}$  under the influence of an axial force  $F$  on each of the spheres is given by

$$v_{\text{rel.}} = \frac{4p \left(1 + \frac{p}{2a}\right)^2}{3\pi\eta a^2} F. \quad [9]$$

If the separation is large Stokes' law holds and then

$$v_{\text{rel.}} = \frac{2F}{6\pi\eta a}. \quad [10]$$

The transition between the validity regions of Eqs. [9] and [10] will be situated roughly at

$$\frac{4p \left(1 + \frac{p}{2a}\right)^2}{a} \sim 1 \quad \text{or} \quad \frac{p}{a} \sim 0.215. \quad [11]$$



There are a number of uncertainties in applying Mooney's equation [9] to our case. Emulsion droplets are liquid and so deformation of the particles and flow inside the droplets may play a role. A more serious difficulty is presented by the choice of a relation between  $p$ , the gap through which flow with a viscosity  $\eta$  is possible, and  $d$ , the distance between the water droplets. The extreme view that  $p$  is equal to  $d$  minus twice the length of a stabilizer chain would lead to the conclusion that the droplets would not be separated by any finite rate of shear, because then at the start  $p$  would be zero and according to Eq. [9]  $v_{rel.}$  would be and remain zero as well.

However, the layer of stabilizing chains is certainly not rigid and not impermeable to the oil phase. Consequently we should assume that  $p$  at the start has a finite value between 0 and  $d$ . If  $d$  is 40 A.,  $p$  will very probably be between 2 and 20 A. In the region where Mooney's expression [9] is applicable the rate of separation of the droplets can be approximately described by

$$\frac{dd}{dt} = \frac{4p}{3\pi\eta a^2} \left[ 6\pi\eta a^2 D \sin \alpha \cos \alpha - \frac{Aa}{12d^2} \right], \quad [12]$$

with Eq. [2] giving the relation between  $\alpha$  and  $t$ . We carried out a few numerical integrations of Eq. [12]. They showed that for an initial value of  $p = 2$  A. the critical angle  $\alpha_{crit.}$  was about  $27^\circ$ ; for  $p = 6$  A. it was about  $32^\circ$ . In Eq. [7] the critical angle occurs as  $\sin 2\alpha$ . As  $\sin 2\alpha$  is already 0.80 for  $\alpha = 27^\circ$  and can never be larger than 1, the precise value of  $\alpha_{crit.}$  is of little importance for our problem.

Consequently when the rate of shear exceeds the value given by Eq. [7] agglomerates will be broken up into single particles in less than the time required for half a revolution, i.e., in less than  $2\pi/D$  sec. Table II shows that droplets of  $1\mu$ , protected by an oleophilic layer of 20 A. each, may be separated by a rate of shear of about  $1000 \text{ sec.}^{-1}$  when the van der Waals' constant is low. For a high value of this constant the rate of shear must be higher.

#### DEPENDENCE OF THE VISCOSITY OF AN EMULSION ON THE STATE OF AGGREGATION OF THE DISPERSED PHASE

In a flocculated emulsion part of the continuous phase is immobilized in the aggregates, so that the volume fraction  $\varphi$  of the dispersed phase, and consequently also the viscosity of the emulsion, is increased. Redispersion of an emulsion may therefore be investigated by means of viscosity measurements.

Under the influence of an increasing hydrodynamic force, i.e., by increasing the rate of shear, a flocculated aggregate redisperses gradually as is schematically represented in Fig. 2. During disaggregation, immobilized medium is set free and the viscosity decreases. As soon as all aggregates are redispersed into original globules the viscosity remains constant in spite of further increase in the rate of shear. This is expressed by the  $D\tau$

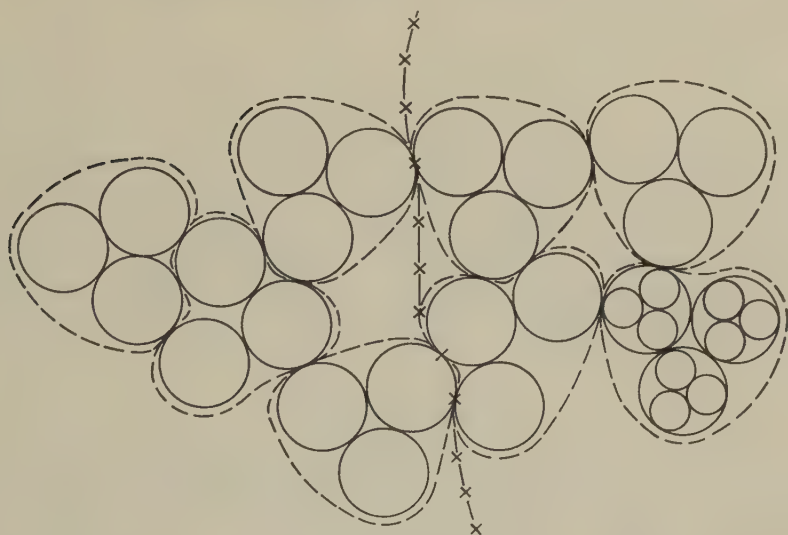


FIG. 2. Under influence of a shearing force the aggregates redisperse first along the crossed line, secondly along the broken lines, and finally along the solid lines.

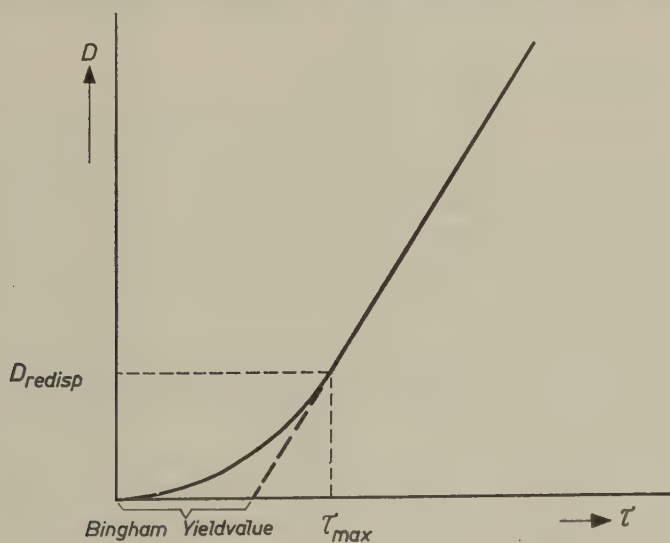


FIG. 3. Schematic representation of the  $D$ - $\tau$  curve of an agglomerated emulsion, as expected on the basis of the theory presented. Complete redispersion results if  $D$  and  $\tau$  are greater than  $D_{\text{redisp.}}$  and  $\tau_{\text{max.}}$ , respectively.

(rate of shear, shear stress) diagram of Fig. 3, where a straight line is found beyond the critical point  $\tau_{\text{max.}}$ ,  $D_{\text{redisp.}}$ .<sup>3</sup>

<sup>3</sup> See the discussions on this subject given by J. J. Hermans in "Flow Properties of Disperse Systems," pages 26 and 27. North-Holland Publishing Company, Amsterdam, 1953.

According to Eq. [6]

$$D_{\text{redisp.}} = \frac{A}{36\pi\eta a d^2 \sin(2\alpha_{\text{crit.}})} \quad [13]$$

To obtain  $D_{\text{redisp.}}$  from viscosity measurements the concentration of the emulsion should be high enough to have a sufficiently pronounced non-Newtonian behavior. On the other hand, it should be low enough to allow a redispersing droplet to move away far enough from the rotating aggregate to move out of the van der Waals' attraction field without being caught immediately by a neighboring aggregate. Concentrations between 10 % and 30 % by volume are suitable.

### THE VISCOMETER

An Ostwald type viscometer with a capillary of radius  $r = 0.032$  cm. and length  $L = 17.4$  cm. and with two flow bulbs situated about 10 cm. above each other (see Fig. 4) was used (5). Different levels of filling can be chosen. For each level two different average rates of shear are available. A cathetometer was used to determine the (average) hydrostatic head and to reproduce the levels of filling. Water was used for the calibration. The viscometer was rigidly mounted in a constant-temperature bath at *ca.* 21°C. with a fluctuation of less than 0.02°C.

The flow time,  $t$ , varied between 50 and 1000 sec. and was determined with an accuracy of 0.1 sec. No corrections were applied for the influence of surface tension, of incomplete drainage (6), and of the Hagenbach correction (7). The latter equals about 0.5 % in the most unfavorable cases.

In order to prevent creaming of the emulsion during the rather long waiting and measuring periods, the density of the benzene phase was adjusted to the density of water by addition of about 15 % carbon tetrachloride.

Diagrams of  $D$ - $\tau$  were derived from the data in the following way (8).

The shear stress at the wall of the capillary is calculated from

$$\tau = \frac{rgh\rho}{2L}, \quad [14]$$

and the rate of shear at the wall from

$$D = \frac{rg}{8L} \frac{\rho_0 h_0 t_0}{\eta_0} \left[ \frac{3}{t} + \frac{h}{dh} d\left(\frac{1}{t}\right) \right], \quad [15]$$

where  $g$  = the acceleration due to gravity,  $h$  = the average value of the hydrostatic head, and  $\rho$  = the density of the emulsion. The values with subscript 0 refer to the calibration experiment with water.

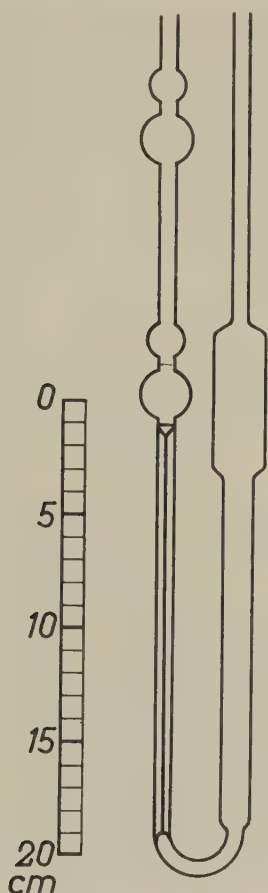


FIG. 4. Viscometer. Radius of capillary  $r = 0.032$  cm.

#### EFFICIENCY OF REDISPERSION IN THE CAPILLARY OF THE VISCOMETER

Equation [15] is based upon the assumption that the rate of shear,  $D$ , is a unique function of the shear stress,  $\tau$ . This implies that, if aggregates are broken up, this disentangling takes place in a short time as compared to the total time of travel in the capillary. It will now be shown that this is the case in our experiments.

It has already been pointed out that fission of a binary aggregate will occur in a fraction of the time of rotation of the aggregate, if it occurs at all. Therefore the time of rotation  $T_r$  should be small compared to the traveling time  $T_c$  of the aggregate in the capillary. In a field with a rate of shear  $D$ , the time of rotation is equal to

$$T_r = \frac{2\pi}{d\alpha/dt} = \frac{2\pi}{D \cos^2 \alpha} = \frac{4\pi}{D}. \quad [16]$$

From the center to the wall of the capillary the velocity decreases and the rate of shear increases. Conditions in the axis are therefore unfavorable for redispersion, whereas they are most favorable near the wall of the capillary. More or less arbitrarily we shall consider the conditions at  $\frac{1}{3}r$  from the axis because 80 % of the liquid travels and 90 % of the friction is generated between  $\frac{1}{3}r$  and  $r$ .

At  $\frac{1}{3}r$  from the axis the rate of shear is (assuming for simplicity strict Newtonian behavior)

$$D = \frac{rgh\rho}{6\eta L}. \quad [17]$$

The velocity  $v$  of the liquid at  $\frac{1}{3}r$  is given by

$$v = \frac{2r^2gh\rho}{9\eta L}, \quad [18]$$

and the total time of flow through the capillary

$$T_c = \frac{L}{v} = \frac{9\eta L^2}{2r^2gh\rho}. \quad [19]$$

From Eqs. [16], [17], and [19] we find:

$$\frac{T_r}{T_c} = \frac{16\pi r}{3L} = 0.03, \quad [20]$$

substituting the actual values for  $r = 0.032$  cm. and  $L = 17.4$  cm.

Consequently, if the rate of shear is high enough to redisperse the aggregates, redispersion will be complete in the first few millimeters of the capillary.

#### MEASUREMENTS

Emulsions of water in benzene (+15 % carbon tetrachloride) were prepared as described in part I of this series (3). Measurements were made on emulsions in which one of the following stabilizers had been dissolved.

- I. 1 %  $\text{Cu}^{\text{II}}$ -oleate.
- II. 1 % emulgid W.O.L. = partial ester of triglycerol and polycondensed ricinoleic acid.
- III. 1 % SPAN 85 = sorbitan trioleate.
- IV. 1 % SPAN 60 = sorbitan monostearate.
- V. 1 % magnesium-petroleum sulfonate = magnesium salt of didodecylbenzene (naphthene) sulfonic acid.
- VI. 1 % mixture of magnesium-petroleum sulfonate and Ca-didodecylsalicylate, while at the same time 18 % calcium acetate has been dissolved in the water phase.
- VII. Like VI, but a slightly more concentrated emulsion.



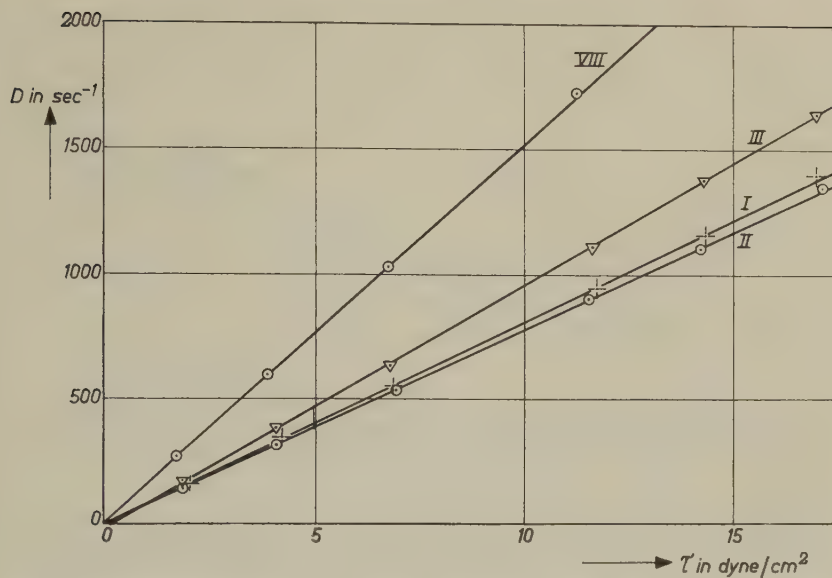


FIG. 5. Rheological behavior of benzene and water in benzene (+15%  $\text{CCl}_4$ ) emulsions.

Curves I, II, and III represent water in benzene emulsions stabilized with  $\text{Cu}^{\text{II}}$ -oleate, emulgid W.O.L., and SPAN 85, respectively. Curve VIII shows the behavior of pure benzene.

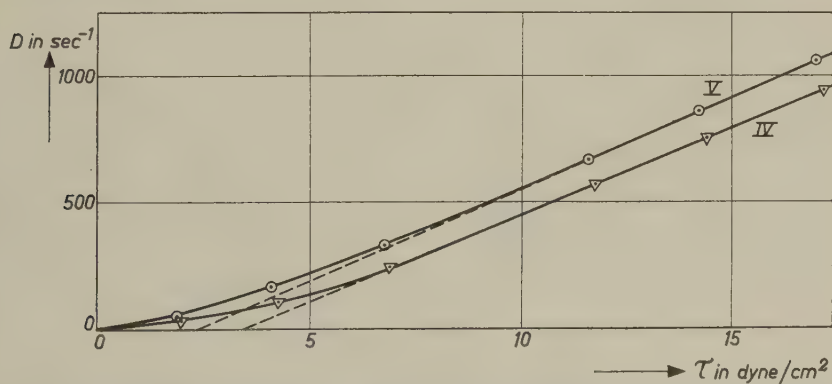


FIG. 6. Rheological behavior of water (+18% Ca-acetate) in benzene (+15%  $\text{CCl}_4$ ) emulsions, stabilized with a mixture of Mg-petroleum-sulfonate and Ca-didodecyl-salicylate.

For comparison viscosity measurements were also done on VIII, pure benzene.

Figures 5, 6, and 7 show the relation between shearing stress  $\tau$  and rate of shear  $D$  for these emulsions as calculated from Eqs. [14] and [15]. The relevant data for these emulsions were collected in Table III.

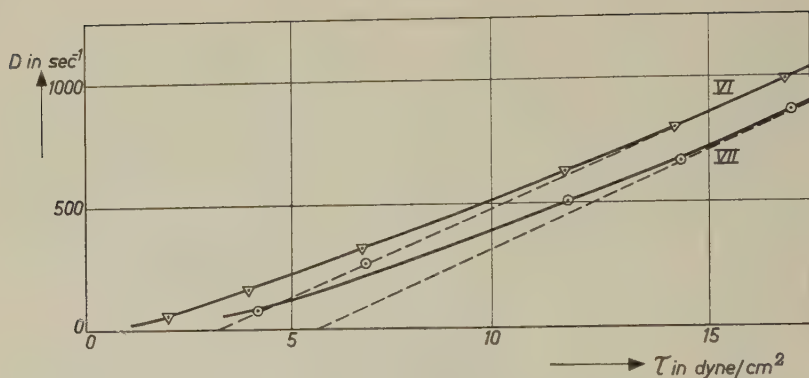


FIG. 7. Rheological behavior of water in benzene (+15%  $\text{CCl}_4$ ) emulsions, stabilized with SPAN 60 (curve IV) and Mg-petroleum-sulfonate (curve V).

TABLE III

Comparison between the Calculated and the Measured Critical Rate of Shear,  $D_{\text{redisp.}}$

1	2	3	4	5	6	7
Emulsion number	Volume fraction $\phi$	Most frequent radius $a$ ( $\mu$ )	$\left(\frac{d\tau}{dD}\right)_{\text{lin}} = (\eta_{\text{Newton}})_{\text{centi-poise}}$	$D_{\text{redisp.}}$ observed from $D$ - $\tau$ diagram ( $\text{sec}^{-1}$ )	$D_{\text{redisp.}}$ calculated from Eq. [13] ( $\text{sec}^{-1}$ ); $A = 0.4 \times 10^{-14}$ erg	Number of carbon atoms in oleophilic chain of the stabilizer
I	0.17	3.5	1.24	<50	100	17 (but hydrolyzed)
II	0.17	4.5	1.29	<50	4	78
III	0.14	5.5	1.04	<100	70	17
IV	0.175	3.5	1.41	200	100	18
V	0.17	1.5	1.35	550	500	12
VI	0.15	1	ca. 1.27	>1400	750	12
VII	0.17	1	ca. 1.20	>1400	750	12
VIII	0.00	—	0.65	<50	0	—

### DISCUSSION OF RESULTS

Figures 5, 6, and 7 indicate that all the curves pass through the origin or come very near to it. There is no yield value or only a very small one. Some of the curves are straight (I, II, and VIII); the others are more or less curved, indicating a plastic behavior of the emulsions. The upper straight parts of the curves indicate situations where the emulsions behave as Newtonian liquids, i.e., where complete redispersion has taken place. The rate of shear where the straight part passes into the curved part is the minimum rate of shear sufficient for complete redispersion,  $D_{\text{redisp.}}$ .

The theoretical value for  $D_{\text{redisp.}}$  was calculated from Eq. [13]. The most

frequent radius as mentioned in column 3 of Table III was used for  $a$ , and twice the hydrocarbon chain length (1.2 Å. per carbon atom) of the stabilizer for  $d$ . The value of  $\alpha_{\text{crit.}}$  was put equal to  $30^\circ$ . A reasonable agreement between the experimental and theoretical values for  $D_{\text{redisp.}}$  is obtained by choosing  $A = 0.4 \times 10^{-14}$  erg for the van der Waals' constant.

The difference between the two values for emulsion I suggests a larger  $d$  than the length of an oleate chain can account for. This corresponds with the view that this emulsion is not stabilized by the oleate chains but by products of hydrolysis which act as solid particle stabilizers, as has been pointed out in a preceding paper (3). The experimental value for emulsion III is quite low. However, emulsion III is definitely non-Newtonian, whereas emulsion I is not; this indicates a greater tendency to flocculation in emulsion III, as has been confirmed by microscopic observation.

There is a striking difference between emulsions III and IV, though the hydrocarbon chains are approximately of the same length. However, the rapid flocculation of emulsion IV can easily be explained by the fact that in this case only one stearic chain per sorbitan molecule is present, whereas the stabilizer of emulsion III contains three oleate chains per sorbitan molecule. The surface of the water globules of emulsion III is therefore notably more densely covered with oleophilic chains than that of emulsion IV. Thus, on the mutual approach of the water globules of emulsion IV, the stearic chains may partially double up or slip alongside each other instead of mutually colliding with their extremities as occurs in the case of emulsion III, so that the effective length is less than 18 C-atoms. The experimental value of  $D_{\text{redisp.exp.}}$  actually appears to be notably higher than the theoretical value of  $D_{\text{redisp.th.}}$  for 18 C-atoms.

Once more it becomes obvious that water-in-oil emulsions at rest are not stable to flocculation in spite of a surface potential of about 100  $mV$  as is shown clearly by curves V, VI, VII, represented in Figs. 6 and 7. Moreover microscopic observations proved all emulsions except I and II to be aggregated to a large extent.

#### THE VAN DER WAALS' CONSTANT

A value of the order of  $10^{-14}$  erg has to be taken for the van der Waals' constant  $A$  to obtain agreement between experiment and theory in the redispersion experiments (column 5 and 6 of Table III). This is much lower than the values commonly used for suspensions in aqueous media ( $A \approx 10^{-12}$  erg) and also lower than the values to be expected from theory, although these are admittedly rather uncertain.

Some possible explanations for the low value of  $A$  that have to be considered are:

1. The van der Waals' constants for water and the mixture of benzene and carbon tetrachloride might be nearly the same, so that the mutual

van der Waals' constant would be quite small. This, however, would be quite accidental and would also make it hard to explain why the stability of emulsions with and without  $\text{CCl}_4$  is so similar.

2. Double layer repulsions will in principle promote further redispersion and if left out of account simulate too low a van der Waals' constant. Quantitative calculations as given in parts I and II of this series (1, 3) prove that the force of the double layer repulsion is only a small fraction of that of the van der Waals' attraction and could never explain that the van der Waals' constant is one to two orders of magnitude smaller than expected.

3. Incomplete redispersion at the limit where the  $D$ - $\tau$  curve is already straight might be partly responsible for the discrepancy. It would increase the value of  $a$  in Eq. [13] and thus lead to a larger value of  $A$ . But more than a factor 2 or 3 would not be expected from this source.

4. The retardation effect. For the relatively large particles and inter-particle distances considered here retardation (2) of the van der Waals' force has to be taken into account. However, if the typical retardation wavelength is put equal to 1000 Å. the retardation factor is between 1 and 0.5, and again the discrepancy between  $A = 10^{-14}$  and  $A = 10^{-12}$  remains unexplained.

We must conclude either that the van der Waals' constant in these emulsions is rather low indeed, or that the minimum distance between the emulsion droplets is larger than we realize.

#### ACKNOWLEDGMENT

The authors wish to express their gratitude to the two referees, who by their remarks have substantially contributed to improvement of this paper.

#### REFERENCES

1. ALBERS, W., AND OVERBEEK, J. TH. G., *J. Colloid Sci.* **14**, 510 (1959).
2. HAMAKER, H. C., *Physica* **4**, 1058 (1937).  
See also H. R. Kruyt, ed., "Colloid Science," Vol. 1, p. 270. Elsevier, New York, Amsterdam, 1952.
3. ALBERS, W., AND OVERBEEK, J. TH. G., *J. Colloid Sci.* **14**, 501 (1959).
4. MOONEY, M., *J. Colloid Sci.* **12**, 575 (1957).
5. FOX, T. G., FOX, J. C., AND FLORY, P. J., *J. Am. Chem. Soc.* **73**, 1901 (1951).
6. SPROKEL, G. J. M., Thesis, Utrecht, 1952.
7. HAGENBACH, E., *Poggendorfs Ann.* **109**, 385 (1860).
8. See, for example, LOHMANDER, U., *Arkiv Kemi* **13**, 385 (1958).

## THE MEASUREMENT OF THE SURFACE TENSION OF PURE LIQUIDS AND SOLUTIONS<sup>1</sup>

J. F. Padday and D. R. Russell

*Research Laboratories, Kodak Ltd., Wealdstone, Harrow, Middlesex, England*

*Received February 1, 1960; revised April 29, 1960*

### ABSTRACT

The surface tensions of some pure liquids and solutions of surface-active agents have been measured by methods either involving or not involving rupture of the liquid-air surface. It is shown that rupture of the surface can produce serious errors in measurement with solutions, especially when the surface tension is slow in reaching a steady value. The Wilhelmy-plate method does not suffer from these errors because the plate is never pulled from the surface.

### INTRODUCTION

The measurement of the surface tension of pure liquids and solutions has been studied extensively. However, surface-tension measurements of solutions of capillary-active substances (surface-active agents), as reported in the literature, reveal differences according to the method of measurement.

Adam (1) and Bikerman (2) list some twelve methods of surface-tension measurement many of which have been modified. To this list may be added the Dognon-Abribat-Wilhelmy plate, as modified by Padday (3). Of these methods, most involve stretching the liquid-air surface at the instant of measurement: such methods as the drop weight and the Du Noüy ring inevitably stretch the surface at the moment of measurement as detachment takes place.

Omitting "dynamic" methods and those involving stretching a surface, three basic methods remain: the Wilhelmy plate (4), the sessile drop (5), and the capillary height (6-8). All these methods should measure the true equilibrium surface tension, provided sufficient time is allowed for adsorption of the surface-active agent in the surface to become complete. The sessile-drop method can be inaccurate because it is difficult to determine position on a curved surface. Capillary-height measurements can be very accurate, provided the apparatus is calibrated empirically and, with solutions, provided very long aging times are allowed. The Wilhelmy-plate principle offers the advantage over all the other methods of being a true equilibrium method which is both accurate and easy to operate.

<sup>1</sup> Communication No. 2068H from the Kodak Research Laboratories.



In this study, a direct comparison has been made between detachment methods and equilibrium methods. Comparison of the methods with pure liquids showed their general accuracy. With solutions of surface-active agents, the methods showed differences which were attributed to sudden expansions of the surface.

### METHODS

Surface-tension measurements of pure liquids were obtained in six different ways but basically only three principles were involved: capillary rise, Wilhelmy plate, and ring detachment from the surface. The methods used were as described in the next section.

#### *"Equilibrium" Methods*

1. *Capillary rise.* The surface tension of a liquid can be expressed in terms of the difference  $\Delta H$  in height of the capillary rises ( $H_1 - H_2$ ) in two tubes of radius  $R_1$  and  $R_2$ , according to Rayleigh's formula (9, 10). In this investigation,  $R_1$  and  $R_2$  could not be determined with sufficient accuracy. They were found, therefore, by assuming the surface tension of water to be 72.75 dynes/cm. and calculating them approximately by the simple capillary formula,

$$RH\rho g = 2\gamma.$$

This enabled the small correction terms to be calculated with sufficient accuracy.

The approximate radii of the capillary tubes used were 0.023 cm. and 0.086 cm.

2. *Plate equilibrium.* Measurements were made according to the method and apparatus previously described (3). By this method the force required to balance a depolished platinum Wilhelmy plate is calibrated in such a way as to give a direct reading of surface tension, calculated from the blade dimensions. The plate is never pulled from the surface during measurement.

#### *Detachment Methods*

To avoid the effect of meniscus shape on surface tension, variations of the detachment method were used.

3. *Plate detachment.* The plate equilibrium surface-tension balance was set up and calibrated exactly as before, but this time the surface tension was obtained from the force which caused *detachment* of the 2-cm. blade from the surface as the beam reached its zero position.

4. *Ring detachment.* Here the plate equilibrium surface-tension balance was set up and the platinum blade was replaced by a small platinum ring (radius of ring = 0.34 cm., and radius of wire forming ring = 0.0235 cm., these dimensions being such as to produce conditions at the meniscus equivalent to those pertaining to the 2-cm. plate). The ring was calibrated

empirically as it was not possible to do so from first principles, the corrections of Harkins and Jordan (11) not applying to a ring of such small dimensions. The calibration was carried out by initially balancing the dry ring. Wetting the ring first before balancing it has been suggested (12), but this procedure led to inaccuracies.

5. *Ring-detachment method of Du Noüy.* Measurements by this method were made on the standard apparatus built by the Cambridge Instrument Company (Cambridge, England) following carefully the makers' instructions, except that the ring was initially balanced dry. Calibration was obtained by assuming the surface tensions of the three liquids: water, ethyl alcohol, and formic acid. The dimensions of the ring were: radius of the ring = 0.635 cm. and radius of the wire = 0.015 cm.

6. A further set of results with the Du Noüy apparatus was obtained by calculating the calibration curve from the dimensions of the ring, the well-known formula, and the corrections of Harkins and Jordan (11) and Freud and Freud (13).

The surface tensions of solutions of surface-active agents were measured by the plate-equilibrium, the plate-detachment, the Du Noüy tensiometer, and the capillary-rise methods. Eight surface-active agents were used, anionic, cationic, nonionic, and ampholytic, and measurements were made on solutions of each agent in concentrations of 0.1 % and 0.01 % wt./vol.

### *Materials*

Tap water, once distilled in an all-glass still and subsequently kept free from contamination, was used. Other liquids were of Analar quality and were not purified further. The surface-active agents were all commercially available and were used as supplied. Many of them showed the surface tension-concentration curve typical of an impure agent.

### *Aging*

Solutions of surface-active agents take a finite time for their surfaces to reach equilibrium concentration. The plate method was used to determine the effect of age on surface tension, because, by this method, surface tension was measured on an undisturbed surface. Attempts were made to study the surface tension of solutions of surface-active agents by capillary rise, but the aging times were, in many cases, prohibitively long.

### *Temperature Control*

1. *Capillary rise.* The apparatus was immersed in a thermostat kept at  $20^{\circ} \pm 0.01^{\circ}\text{C}$ .

2. *Other methods.* (1) Pure liquids were cooled to  $20^{\circ} \pm 0.1^{\circ}\text{C}$ . (2) Solutions were cooled to  $20^{\circ} \pm 0.2^{\circ}\text{C}$ .

With solutions, detachment and plate-equilibrium determinations were carried out on the same solution simultaneously.

## RESULTS

The precision of each method was estimated by calculating the standard deviation, and the accuracy was estimated by comparing the surface tension of pure liquids with the literature values. By choosing pure liquids, the performance of each method was assessed independently of aging effects. The methods found to give the best performance with pure liquids were then applied to measure the surface tensions of solutions of the surface-active agents.

*Pure Liquids*

The results for pure liquids are shown in Table I. All measurements were made at least three, and often six to eight, times.

TABLE I  
*Surface-Tension Measurements of Pure Liquids*

Liquid	Capillary rise (dynes/cm.)	Plate equilibrium (dynes/cm.)	Plate detachment (dynes/cm.)	Ring detachment (dynes/cm.)	Du Noüy		Literature value (dynes/cm.)
					Calcd. <sup>a</sup> (dynes/cm.)	Empirical (dynes/cm.)	
Water.....		72.72	72.79		71.95		72.55
		±	±		±		-
		0.03	0.03		0.1		72.91
Ethanol.....	22.26	22.30	22.34		22.05		22.32
		±	±		±		
		0.05	0.05		0.08		
Benzene.....	28.63	28.65	28.70	28.2	28.65	28.60	28.88
		±	±		±	±	
		0.10	0.03		0.08	0.08	
Acetone.....	23.30	23.35	23.40	23.3	23.34	23.52	23.32
		±	±		±	±	
		0.13	0.14		0.03	0.03	
Nitrobenzene....	43.46	43.30	43.50	0.06	43.10	43.22	43.35
		±	±		±	±	
		0.10	0.29		0.05	0.05	
Formic acid.....	37.62	37.68	37.75	37.7	37.30		37.58
		±	±		±		
		0.08	0.08		0.16		
Acetic acid.....	27.35	27.60	27.65	27.8	27.23	27.70	27.42
		±	±		±	±	
		0.03	0.03		0.05	0.05	
Average standard deviations (precision).....	±0.1	±0.07	±0.10	±0.06	±0.08	±0.05	

<sup>a</sup> The precision here does not include inaccuracies derived from errors in measuring the dimensions of the ring.

The precision of reproducibility of each method was assessed by statistical analysis, and the errors quoted are the standard deviations. The standard deviations in the last row are a mean for all liquids by each method and indicate that all methods behaved equally well, with a reproducibility better on average than  $\pm 0.1$  dyne/cm., except in the case of the calculated Du Noüy calibration, where considerable errors are introduced in finding the correction term,  $KR^3/V$ . The comparatively large standard deviations quoted arise, to a large extent, from the estimated errors of the correction terms. Slight departures from standard techniques immediately produced greater errors.

The accuracy of the results (i.e., agreement with literature values) varied rather more than the precision. Table I shows that, except for benzene, the capillary-rise and the plate-equilibrium methods agree with the literature values (14) reasonably well. The values for benzene are lower than the well-authenticated literature value, suggesting that the benzene sample used might not have been completely pure. With the pure liquids, the calculated Du Noüy ring results were all slightly lower than the literature values and the scatter was rather greater. By calibration from assumed values of water, ethanol, and formic acid, better agreement was obtained. Observations on the meniscus at the moment of detachment suggested that the liquid affected greatly the way in which the ring broke from the surface. The ring- and plate-detachment methods behaved similarly to the Du Noüy ring, both showing less accuracy than the plate-equilibrium method.

The performances with pure liquids showed that all methods were precise to  $\pm 0.1$  dyne/cm. and that the plate-equilibrium method was more accurate than the detachment methods. With the Du Noüy ring, low values of surface tension were obtained when calibrating from first principles using Harkins and Jordan's (11) corrections, owing to an uncertainty in the measured radius of the ring. Therefore, in subsequent measurements with solutions, the Du Noüy ring was first calibrated empirically.

### *Solutions of Surface-Active Agents*

Measurement of the surface tension of solutions differs from the measurement of pure liquids because an aging time is required for the surface of the solution to reach its equilibrium concentration. With some surface-active agents, many minutes are required to reach this equilibrium. Accordingly, the surface tensions of some solutions were measured by the different methods at different aging times to ensure that a steady state had been reached.

The ring-detachment method, with solutions, gave a wide scatter of results which may have been due to the small diameter of the ring; therefore, accurate measurement of solutions by this method was not attempted.



TABLE II  
*Surface-Tension Measurements of Solutions of Surface-Active Agents*

Agent	Concn. %	Plate equilibrium	Plate detachment	Du Noüy tensiometer	Capillary rise (dynes/cm.)
Aerosol OT	0.1	25.9 (5)	26.0 (5)	26.7	
	0.01	40.9 (5)	41.8	41.5	
Alkanol B	0.1	46.0	46.5	46.7	
	0.01	58.5	59.3	59.9	
Lissapol N.X	0.1	30.2	30.3 (5)	30.3	30.3
	0.01	30.6	31.1	31.7	
Igepon T	0.1	29.2	29.7	29.7	
	0.01	33.7	34.5	34.5	
C.T.A.B.	0.1	34.4	34.7	34.3	34.0
	0.01	44.2	44.7	44.8	
Saponin	0.1	36.8	40.1	42.0	37.0
	0.01	43.3	45.4	47.7	
Tergitol NPX	0.1	29.8	30.1 (5)	29.9	29.6
	0.01	29.7	30.0	29.8	
Teepol	0.1	32.0	33.0	34.3	
	0.01	45.3	47.0	49.1	

Capillary-rise heights were found to be affected by aging of the surfaces over considerable periods, 30 to 60 hours; therefore, the results are quoted more out of interest than independent confirmation, because so few of the measurements reached equilibrium.

The surface-tension measurements of the solutions of surface-active agents are shown in Table II. They indicate that, in some cases, the agreement is fairly good but that, in other cases, the two detachment methods give greater values than the plate-equilibrium method. In fact, with saponin (*Quillaia*) and Teepol, the values are considerably greater.

The lack of independent confirmation of either method with solutions of surface-active agents suggested that either the plate-equilibrium method gave low results or the Du Noüy method gave high results. However, when the plate was detached from the surface (plate-detachment method), higher surface-tension values similar to those of the Du Noüy method were obtained. As the act of detachment could give a high result but lack of detachment could not in itself give a low result, it seemed that the detachment methods were likely to be in error. Low surface-tension values by the plate method due to poor wetting were not possible as the blade was seen to be completely wetted during each reading. Surface-active agents that contaminate a depolished platinum blade were not used in this investigation. These considerations indicated that the act of detachment was the likely source of error.



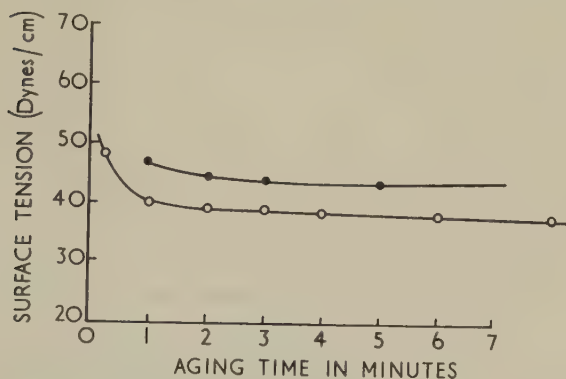


Fig. 1. The effect of the method of measurement on the surface-tension/aging-time curve for 0.1% saponin solution: ● Du Noüy ring; ○ plate.

### DISCUSSION

The measurements of surface tension of pure liquids by all methods gave results that were not seriously in error, but when these methods were applied to solutions, large differences were found in some cases. Furthermore, the measurements of surface tension of solutions suggested that detachment methods of measuring surface tension sometimes gave rise to values that were too high.

Figure 1 shows the results obtained by the Du Noüy ring and the plate-equilibrium methods when the surfaces were allowed to age. From this and other results it seemed that, even after very long periods, the Du Noüy ring results would never quite reach those of the plate-equilibrium method. Furthermore, the curves of Figs. 1 and 2 show that the error of the Du Noüy ring depended very much on the agent, the values being too high by 5 dynes/cm. for saponin and 0.7 dyne/cm. for Aerosol OT.

The following experiment suggests that the act of pulling the ring out of a surface could give rise to serious errors: The plate method was used to measure the surface tension of both saponin and Teepol solutions before and after a Du Noüy ring had been detached from their solution-air surfaces. With both solutions, the removal of the ring from the surface increased the surface tension by several dynes. Some of this change may have occurred before the instant of measurement. If so, then the magnitude of the difference ( $\gamma_{\text{Du Noüy}} - \gamma_{\text{plate}}$ ) between the Du Noüy and plate methods would be related to the rate of aging of the solution of surface-active agent. Figure 3 shows the difference plotted against the aging rate, measured as the difference between the 15-sec. and 1-min. values by the plate method. If the solution ages very quickly, the difference between the 15-sec. and 1-min. readings is small, but if the aging is slow, then a large difference results. The plate-equilibrium curves in Figs. 1 and 2 demonstrate the slow aging of 0.1 % saponin solution and fast aging of 0.1 % Aerosol OT solution, giving large and small differences between the 15-sec. and 1-min. readings,

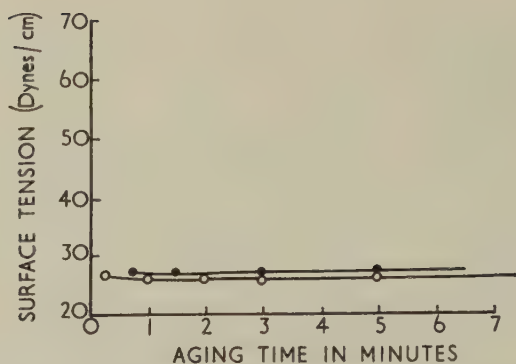


FIG. 2. The effect of the method of measurement on the surface-tension/aging-time curve for 0.1% Aerosol OT solution: ● Du Noüy ring; ○ plate.

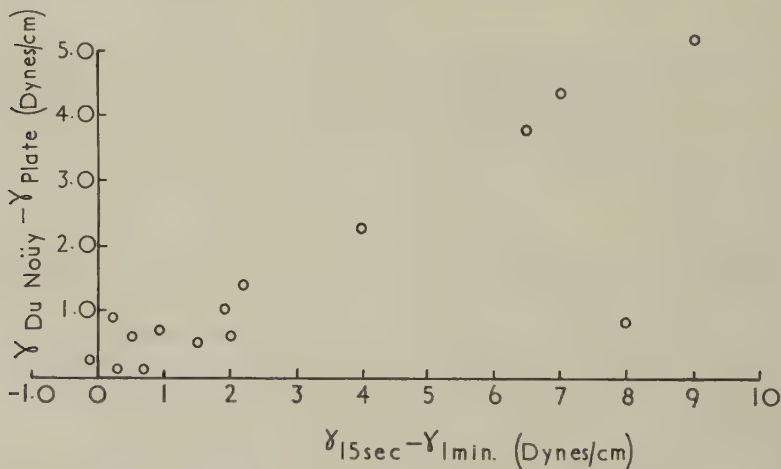


FIG. 3.  $(\gamma_{\text{Du Noüy}} - \gamma_{\text{plate}})$  as a function of aging effect.

respectively. The correlation between aging rate and divergence of the Du Noüy method is shown by Fig. 3, which indicates that the Du Noüy method will give correct results with solutions only when the aging rate of the solution is rapid. For solutions which age slowly, errors as great as 5 dynes/cm. are possible. We consider the error of the Du Noüy method, associated with solutions of long aging times, to be fundamental to the process of detachment which stretches the surface at the moment of measurement.

Ross (15) calculated that the static surface tension of pure liquids is reached in  $5 \times 10^{-3}$  sec. and probably much less ( $10^{-9}$  sec.). Therefore, it is expected that detachment methods should agree well with other methods for surface-tension measurement. Bond and Puls (16) calculate that all solutions should reach equilibrium with the surface in less than a second,

but McBain, Ford, and Mills (17) found experimentally that the time of 1 sec. is often exceeded.

Several workers (18-21) have reported that the Du Noüy ring gave errors with solutions, although Nutting, Long, and Harkins (22) state that agitation of the surface did not produce errors with sodium lauryl sulfate. However, it appears that it is not agitation but the pulling of the ring from the surface that destroys the surface equilibrium, a surface deficiency being created in the region formerly occupied by the ring. This deficiency is not made up quickly with some agents; hence a high "apparent" surface tension is obtained.

Experiments were attempted to measure surface tension by a "ring-equilibrium" method, whereby the ring was never pulled from the surface. These experiments failed because the position of the ring in relation to the liquid surface could not be kept fixed.

#### ACKNOWLEDGMENT

The authors gratefully acknowledge the help of Mrs. F. Tabor in carrying out a comprehensive statistical analysis of the results.

#### REFERENCES

1. ADAM, N. K., "The Physics and Chemistry of Surfaces," 3rd ed., Clarendon Press, Oxford, 1941.
2. BIKERMAN, J. J., "Surface Chemistry for Industrial Research," p. 4, Academic Press, New York, 1947.
3. PADDAY, J. F., "Proc. 2nd Intern. Congr. Surface Activity," p. 1, Butterworth's, London, 1957.
4. WILHELMY, L., *Ann. Physik (Leipzig)* **119**, 177 (1863).
5. VERSCHAFFELT, J. E., *Proc. Koninkl. Akad. Wetenschap. Amsterdam* **21**, 357 (1919).
6. RICHARDS, T. W., AND COOMBS, L. B., *J. Am. Chem. Soc.* **37**, 1656 (1915).
7. RICHARDS, T. W., AND CARVER, E. K., *J. Am. Chem. Soc.* **43**, 827 (1921).
8. HARKINS, W. D., AND BROWN, F. E., *J. Am. Chem. Soc.* **41**, 499 (1919).
9. RAYLEIGH, LORD, *Proc. Roy. Soc. (London)* **A92**, 184 (1916).
10. ADAM, N. K., "The Physics and Chemistry of Surfaces," 3rd ed., p. 367, Clarendon Press, Oxford, 1941.
11. HARKINS, W. D., AND JORDAN, H. F., *J. Am. Chem. Soc.* **52**, 1751 (1930).
12. KLOPSTEG, P. E., *Science* **60**, 319 (1924); HARKINS, W. D., AND JORDAN, H. F., *J. Am. Chem. Soc.* **52**, 1763 (1930); "Instruction Manual for Du Noüy Tensiometer," Cambridge Instrument Co., Cambridge, England.
13. FREUD, B. B., AND FREUD, H. Z., *J. Am. Chem. Soc.* **52**, 1772 (1930).
14. "International Critical Tables," McGraw-Hill, New York, 1933.
15. ROSS, S., *J. Phys. Chem.* **49**, 377 (1945).
16. BOND, W. N., AND PULS, H. O., *Phil. Mag.* **24**, 864 (1937).
17. MCBAIN, J. W., FORD, T. F., AND MILLS, G. F., *J. Am. Chem. Soc.* **62**, 1319 (1940).
18. DOSS, K. S. G., *Kolloid-Z.* **86**, 205 (1939).
19. WAKSMUNDZKI, A., *Ann. Univ. Mariae Curie-Skłodowska, Lublin-Polonia. Sect. AA*, **2**, 125 (1947).
20. RUYSSSEN, R., *Rec. trav. chim.* **65**, 580 (1946).
21. DERVICHIAN, D. G., AND CLARK, C., *Compt. rend.* **207**, 277 (1938).
22. NUTTING, G. C., LONG, F. A., AND HARKINS, W. D., *J. Am. Chem. Soc.* **62**, 1496 (1940).

## STUDIES ON A FLOW METHOD FOR PARTICLE COUNTING IN COLLOIDAL SYSTEMS

R. H. Ottewill and D. J. Wilkins

*Department of Colloid Science, University of Cambridge, Cambridge, England*

*Received January 4, 1960; revised May 26, 1960*

### ABSTRACT

An apparatus is described for the accurate and rapid evaluation of particle numbers per unit volume which depends upon counting the number of particles emitted from the end of a fine capillary per unit of time. The accuracy of the method has been checked, using polystyrene latex particles and a monodisperse silver iodide sol, by comparison with particle counts using turbidity measurements, hemocytometer chamber counts, dry weight determinations in combination with the electron microscopic determination of particle radius, and the spray drop method. The apparatus has been successfully employed to study the kinetics of coagulation of an arachidic acid sol.

Many problems of a colloidal nature require the accurate evaluation, either directly or indirectly, of the number of particles contained per unit volume of sol. Often, moreover, as in the study of coagulation phenomena, it is necessary to know how this number changes with time.

Of the indirect methods available light scattering provides a convenient means for studying sols of particle size of diameter less than about 500 Å., i.e., in the region where simple Rayleigh theory can be applied (1), and apparatus can be constructed for the automatic recording of rate processes (2, 3); greatest accuracy is achieved in the determination of particle numbers when the sol is monodisperse. The method can also be applied to monodisperse sols of larger particles but the necessity of employing Mie theory (4) in this case often involves laborious computations, unless tables of total Mie scattering functions are already available.

In the case of direct methods of particle counting both electron and optical microscopy can be used. In the former case two procedures have been employed. The first method is to determine the number of particles in drops of suspensions which have been sprayed on to a grid with a high pressure nebulizer (5-7). Alternatively, in a monodisperse system the electron microscope may be used to determine the particle diameter whence from a knowledge of the weight concentration of the sol and the density of the particle, the particle number is easily calculated (5). Both methods have been used, especially for biological problems; however, caution must



be exercised since it is not easy to determine drop diameters accurately, and the second method may yield spurious results either because of particle shrinkage or because of the fact that the particles do not have a well-defined geometrical shape.

Optical microscopy can be used for particle counting in conjunction with a hemocytometer blood-counting chamber. This requires that the particles should be large (*ca.* 10  $\mu$ ) with a density greater than that of the suspending medium, and a large number of particles must be counted in order to achieve accurate results. This method has been mainly employed for studies on blood cells and emulsions (8–10) but can be extended to smaller particles by the use of a dark-ground condenser. The method has also been successfully used by the authors with a hemocytometer cell which was optically ground so that the known distance between the counting grid and the coverslip was the same as the depth of focus of the viewing microscope. Under the latter conditions it was found more convenient to calibrate a graticule in the eyepiece against the hemocytometer grid. In practice, however, the method is tedious and time consuming. The classical ultramicroscopic method of Zsigmondy (11) has been used extensively, but this suffers from the disadvantage that for accurate results extrapolation to infinite slit-width is required (12).

In work in progress on the coagulation of arachidic acid sols the particle diameters were of the order of 0.2–0.5  $\mu$ , and the sols were polydisperse. These are conditions in which light scattering is not easily applicable, and the classical methods appeared unnecessarily tedious and not sufficiently accurate. A method which enabled reliable results to be obtained quickly was required, and the earlier work of Gucker *et al.* (13), Derjaguin and Wlacenki (14), Lee and La Mer (12), and Watillon and Grunderbeeck (15) showed that flow methods had produced promising results.<sup>1</sup> The earlier authors counted the number of particles per unit volume of aerosols and Watillon and Grunderbeeck the number density of selenium sols. In principle this method depends upon counting the number of particles emitted from the end of a capillary, illuminated as for ultramicroscopy, per unit of time. Since the capillary diameter can be measured accurately, the volume of sol can easily be calculated.

Although the apparatus described by Watillon and Grunderbeeck (15) has also been used to follow the coagulation of sols (16), the procedure employed involved the removal of the capillary, for cleaning and recharging, for every count. The method described in this communication was developed to obviate this maneuver and to incorporate a device for clean-

<sup>1</sup> An apparatus is also available commercially, based on the flow method, which employs the change in conductivity as a nonconducting particle passes through a small orifice as a means of counting particles (17). This instrument is manufactured by Coulter Industrial Sales Co., Elmhurst, Illinois.



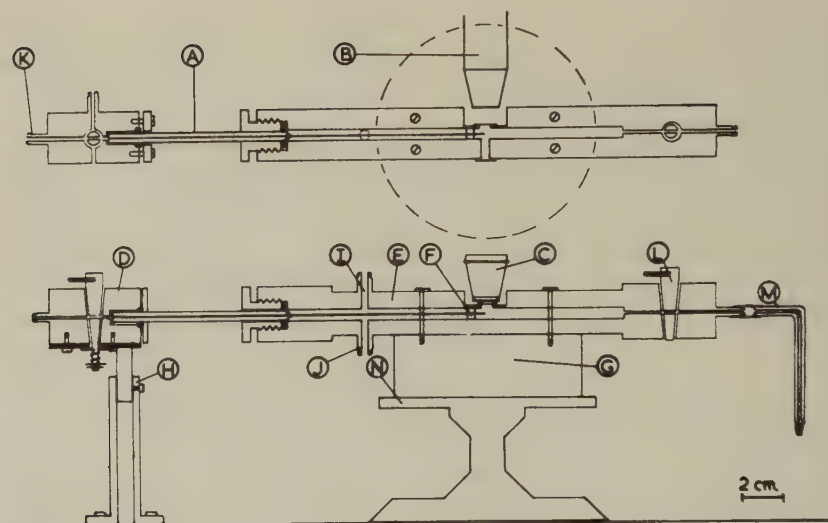


FIG. 1. Particle counting apparatus. A, capillary tube; B, ultramicroscope objective; C, viewing objective; D, injection unit; E, counting cell; F, Perspex collar; G, Perspex block; H, adjustable support; I, point of attachment of the reservoir for optically clear water; J, outlet; K, point of attachment of pressure system; L, flow control tap; M, outlet capillary tube; N, microscope stage.

ing the capillary *in situ*. Moreover, fixing the capillary firmly in the apparatus prevented possible damage and facilitated optical adjustment. These modifications rendered the apparatus much more suitable for the study of coagulation rates.

## EXPERIMENTAL

### *Description of the Apparatus*

The apparatus, shown in Fig. 1, consisted essentially of a fine capillary A through which the sol was streamed into a flowing system of optically clear water. The emergent particles were illuminated by the ultramicroscopic system B and viewed by the microscope C. The capillary was constructed from a piece of Veridia glass of internal diameter  $373\ \mu$  (determined by weighing a thread of mercury); this was pulled out to give a length of approximately 10 cm. of fine capillary at one end, of internal diameter  $30\ \mu$ . The tip was tapered to a cone by grinding with emery paper after embedding in paraffin wax to ensure rigidity; an electric motor was used to rotate the tube. The other end was ground square and held to the injection unit D by means of a brass plate and rubber washer. The tube was held in the counting cell E by means of a Perspex threaded cylinder and rubber washer. The tip was held rigid by means of a Perspex collar F, cemented in position. The counting cell E, which was also constructed

from Perspex, consisted of a rectangular block which had a longitudinal hole of diameter 3.5 mm. This was firmly held to the stage of the microscope. For viewing and illuminating the tip of the capillary *A* two holes were drilled into the central hole at right angles; these were sealed with coverslips which were cemented on with Araldite.

The optically clear water supply was connected to *I*; *J* was closed by a short length of polyvinyl chloride tubing and an artery clip. The pressure supply was connected to *K*.

The ultramicroscope consisted of a petrology microscope fitted with an adjustable slit, in place of the ocular, which was illuminated by a microscope lamp. The slit image was focused with a  $\times 10$  objective. The ultramicroscope, the viewing microscope, and the adjustable support *H* for the injection unit were all screwed firmly to the bench.

Owing to the low refractive index of the particles under investigation it was necessary to avoid stray light entering the counting cell, and hence the apparatus was set up in a dark room.

#### *Pressure System*

This consisted essentially of a nitrogen cylinder, fitted with a reduction head, which was connected to a water manostat linked with a reservoir. The latter was introduced into the system in order to minimize minor pressure fluctuations. The pressure was measured with a mercury manometer. Two three-way taps were used, one to allow the pressure to be released quickly, and one connected to a vacuum line (water pump) for cleaning purposes (see later). A trap was included to prevent used sol and cleaning liquid from entering the vacuum system.

#### *Preparation of Optically Clear Water*

Ordinary distilled water was passed over a column of Bio-deminrolit ion-exchange resin and then redistilled in an all Pyrex apparatus. It was then clarified by the procedure used for light-scattering measurements (3) by filtration through a selected Pyrex filter (pore size *ca.*  $1\ \mu$ ) using a pressure of about 10 cm. of mercury. The water was stored in a Pyrex bottle with an inverted ground-glass stopper.

#### *Assembly and Operation of the Apparatus*

It was first necessary to obtain a calibration curve for the rate of flow of the sol along the capillary tube against the applied pressure at *K*. The sol was injected into *D* with a tapered polythene pipet and the tap turned through  $90^\circ$  so that the sol was forced along the capillary tube. The hole in the barrel of the tap in the injection unit *D* was accurately drilled so that the volume of sol which it contained just filled the capillary. The rate of flow was determined by observing the rate of movement of the

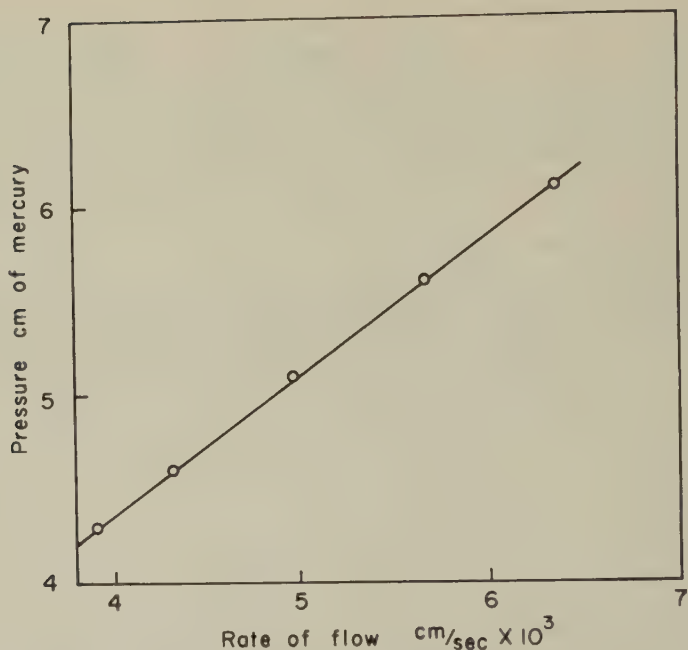


FIG. 2. Calibration curve of rate of flow in capillary tube against applied pressure.

meniscus in the capillary *A*, with a traveling microscope, at different pressures; the pressure was varied by altering the liquid level in the manostat. This gave a good linear plot (Fig. 2); hence from a knowledge of the pressure and the radius of the capillary it was possible to calculate the volume of sol issuing from the tip in a known time. The calibration was carried out under experimental conditions in that the counting cell was filled with optically clear water at a constant head of pressure. This was achieved by attaching the reservoir to *I* and controlling the rate of flow by the tap *L* and the capillary tube *M*.

Initially the illuminating beam was focused on the tip of the capillary. It was then moved to one side so that perfect dark-ground illumination was obtained. The sol particles emerging from the capillary were hence observed as individual flashes of light which were easily counted, using a hand tally counter and stop watch, as they entered the controlled flow of optically clear water. It was necessary to dilute the sol with optically clear water and to adjust the pressure applied at *K* to obtain a suitable rate for counting, i.e., about 1 particle per second. Approximately 100 particles were counted and five to ten readings taken for each value. If erratic results were obtained the apparatus was recleaned and the run repeated.

The capillary was rapidly and efficiently cleaned out between runs by

means of the three-way tap to vacuum. By turning through  $90^\circ$  the pressure was cut off, the sol was sucked out of the capillary tube, and optically clear water was drawn through. The cell was then emptied of water through the outlet  $J$  and air was drawn through the tube; thus the tube was dried and made ready for refilling.

### *Depth of the Field of the Viewing Microscope*

For the successful operation of the apparatus two criteria must be established for the viewing microscope. Firstly, the resolution of the microscope must be such that all particles in the sol are visible; i.e., the method cannot be used for very small particles or for those with a refractive index very close to that of the suspending medium. Secondly, the depth of field of the microscope must be sufficient to maintain in focus all the particles emitted from the capillary, i.e., it must be greater than the diameter of the capillary.

### *Calculation of the Depth of Field*

The calculation of the depth of field of a microscope depends to some extent on a set of assumptions. However, since this factor is of major importance it is essential to obtain an estimate of the order of magnitude of this depth in order that a suitable optical system may be chosen. The depth of field can be divided into two main components, firstly, the sharp depth of field  $d$ , which is the depth of field which would be in focus if the image were formed on a photographic plate, and, secondly, the depth of field  $x$  due to accommodation of the eye. Thus the total depth of field  $T$  is given by

$$T = d + x.$$

According to Hardy and Perrin (18),

$$d = \frac{2z'n}{M(\text{N.A.})}$$

where  $z'$  = the circle of confusion in millimeters,  $n$  = the refractive index of the medium,  $M$  = the total magnification, and N.A. is the numerical aperture of the objective. The value of  $z'$  chosen is somewhat arbitrary, but a reasonable value would appear to be 0.25 mm. (19).

The depth of field due to accommodation of the eye is given by Hardy and Perrin (18) as,

$$x = \frac{(250)^2}{M^2 x'} \text{ mm.},$$

where  $x'$  is the near point distance of the eye. Again the value to be chosen for  $x'$  is somewhat arbitrary, particularly as this is a distance which varies

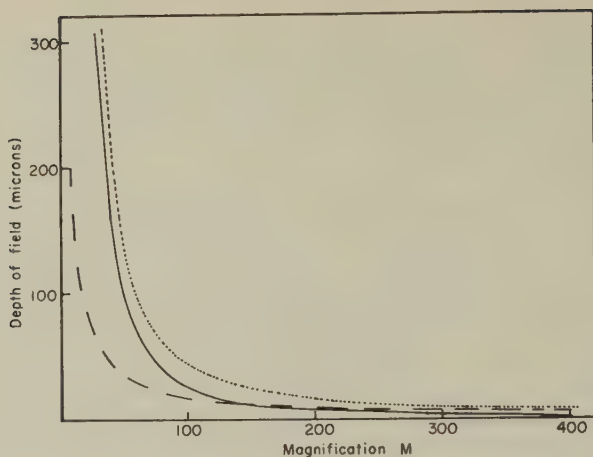


FIG. 3. Depth of field of viewing microscope against magnification. . . . . total depth of field; ——— depth of field due to eye accommodation; - - - - depth of field without accommodation.

with the age of the observer (18). The value normally assigned to this in optical treatments is 250 mm. (it would appear advisable also to underestimate the depth of field rather than overestimate it); whence

$$x = \frac{250}{M^2} \text{ mm.}$$

Values of the depth of field in microns as a function of the magnification of the optical system, taking  $n = 1$ ,  $z' = 0.25$  mm., are given in Fig. 3; for the purposes of calculation a constant N.A. of 0.3 was assumed.

For viewing a combination of a  $\times 10$  objective (N.A. 0.28) with a  $\times 7.5$  ocular was used. From Fig. 3 it can be seen that this corresponds to a depth of field of  $67 \mu$ . The diameter of the capillary outlet was found to be  $30 \mu$  so that this lens combination covered the field adequately and also gave a sufficiently high magnification to ensure that all sol particles were visible. It was found that a low-powered objective ( $\times 5$ ) and a higher powered objective ( $\times 20$ ) both gave an apparent decrease in particle numbers. The former was due to insufficient magnification, and the latter was due to a decrease of the depth of field ( $24 \mu$  from Fig. 3).

## RESULTS AND DISCUSSION

### *Check of the Accuracy of the Apparatus*

In order to establish that the apparatus was giving accurate and reproducible determinations of particle numbers per unit volume, measurements were carried out on three different systems and the results checked



TABLE I

*Representative Data Obtained with Particle Counter for Monodisperse Silver Iodide Sols*

$N$ (no. of particles counted)	$t$ (sec.)	$N/t$	$n \times 10^{-5}$ (no. of particles per ml.)
68	66.0	1.030	1.398
68	63.8	1.066	1.446
82	78.0	1.052	1.427
57	56.0	1.018	1.381
80	67.6	1.184	1.606
71	59.1	1.201	1.630
85	71.6	1.187	1.611
59	60.0	0.983	1.335

Mean  $n = 1.479 \times 10^5$  per ml.Standard error of the mean =  $\pm 0.039 \times 10^5$ .Standard deviation =  $0.110 \times 10^5$ .

Coefficient of variation = 7.45%.

by a number of independent methods. The systems chosen were all monodisperse and consisted of two samples of Dow spherical polystyrene latex particles<sup>2</sup> (quoted diameters  $0.264 \mu$  and  $1.171 \mu$ ) and a silver iodide sol (20). For convenient counts particle numbers of the order of  $10^5$  per milliliter were found most convenient, and hence the Dow material was diluted to give this order of particle numbers. In the case of silver iodide the prepared sol was diluted by  $10^2$  for particle counting. The results for a typical set of counts on a silver iodide sol are given in Table I.

In Table II results obtained with the particle-counting apparatus are compared with those obtained by other methods.

Turbidity measurements were carried out with a Unicam SP 500 spectrophotometer, using cells of either 10 cm. or 4 cm. path length, over a range of wavelengths. The stock suspensions of polystyrene latex were diluted by a factor of  $10^4$  for measurement. The numbers of particles per milliliter were calculated from the interpolated turbidity at a wavelength (in air) of 5600 Å. using the total Mie scattering coefficients tabulated by Pangonis, Heller, and Jacobson (21). Calculations were carried out using both the particle radius given by Dow and that determined by electron microscopy. The electron micrographs were taken with a Siemens Elmiskop I electron microscope, and the particle diameter was taken as the mean of a number of measurements of single particles on a number of plates; this included plates taken at several different magnifications. Low beam intensities were employed in order to avoid shrinkage of the particles. The particles in the

<sup>2</sup> Kindly supplied by Dow Chemical Corporation Ltd., through the courtesy of Dr. J. W. Vanderhoff. The  $0.264 \mu$  diameter material was run no. LS-057-A and the  $1.171 \mu$  diameter material run no. LS-067-A.

TABLE II  
*Comparison of Particle Counts by Various Methods. Number of Particles per Milliliter*

System	Particle diam. ( $\mu$ )	Particle counter	Turbidity measurements	Dry wt.	Hemocytometer	E.M. spray method
Dow polystyrene latex	0.264 <sup>a</sup>	$1.90 \times 10^{13}$	$9.43 \times 10^{12c}$	$1.12 \times 10^{13e}$	—	$5.6 \times 10^{14}$
	0.216 <sup>b</sup>	—	$2.53 \times 10^{13d}$	$1.93 \times 10^{13f}$	—	—
Dow polystyrene latex	1.171 <sup>a</sup>	$2.01 \times 10^{11}$	$9.07 \times 10^{10c}$	$1.19 \times 10^{11e}$	$3.40 \times 10^{11}$	—
	1.029 <sup>b</sup>	—	$1.26 \times 10^{11d}$	$1.76 \times 10^{11f}$	—	—
Monodisperse silver iodide sols	—	$1.48 \times 10^7$	$1.40 \times 10^7$	$1.70 \times 10^7$	$1.08 \times 10^7$	—

<sup>a</sup> Particle diameter quoted by Dow.

<sup>b</sup> Particle diameter determined by electron microscopy.

<sup>c</sup> Calculated using diameter<sup>a</sup>.

<sup>d</sup> Calculated using diameter<sup>b</sup>.

<sup>e</sup> Calculated from determined dry weight using diameter<sup>a</sup>.

<sup>f</sup> Calculated from determined dry weight using diameter<sup>b</sup>.

sols of silver iodide were shown by electron microscopy to be very close to cubes of side  $0.24 \mu$ . The number of particles per milliliter was calculated from the turbidity at a wavelength of 5600 Å., on the assumption that the particles were spheres of diameter equal to the length of the diagonal of the cube, using a value for the Mie scattering coefficient interpolated from the values given by Luvalle and Jackson (22). It must be admitted, however, that the assumptions used to determine the number of particles of silver iodide per milliliter from turbidity measurements render these data somewhat more uncertain than those for polystyrene.

The dry weights of the  $0.264 \mu$  and  $1.171 \mu$  polystyrene samples were determined by drying aliquots of the samples at  $66^{\circ}\text{C}.$ ; these gave the percentages of solid material as 10.84% and 12.44%, respectively, on a weight/volume basis. The numbers of particles per milliliter of the original stock solutions were calculated from these dry weights using both the Dow radii and those determined by electron microscopy.

The hemocytometer counts on the silver iodide sols were carried out using a cell with a Neubauer ruling in conjunction with dark-ground illumination; 10–15 min. were allowed for the particles to settle on to the grating. In the case of the  $1.171 \mu$  polystyrene sample, a cell was used which had been ground down to give a total depth of 0.01 mm.; this had a Thoma ruling.

The electron microscope counts were carried out by spraying a one hundredth dilution of the  $0.264 \mu$  polystyrene sample, with a Vaponefrin nebulizer, on to grids covered with a supporting nitrocellulose membrane. Micrographs were taken at magnifications of  $\times 8000$ , the number of particles per drop was counted, and then the number of particles per milliliter was calculated from the diameter of the "dried" drop (5, 6).

In Table II all particle counts have been multiplied by a factor to give the number of particles per unit volume of the initial stock solution. Using the determined values for the radius of the polystyrene particles agreement is obtained between particle numbers obtained from the counting apparatus and those from dry weight determinations. The agreement between the results from turbidity measurements and from the particle counter is also reasonable; as the spectrophotometer was not modified for absolute turbidity measurements (see 23, 24), this method may not yield results as accurate as the dry weight method. The hemocytometer method appears to give somewhat high results for polystyrene but quite reasonable results for silver iodide. This may well be associated with the easier sedimentation of the latter and the higher refractive index difference between particle and solvent. The results obtained using the electron microscope spray drop method are an order of magnitude higher than the other data. It is clear that this method must obviously be used with considerable caution if reliable physical data are required. In view of the large dilutions

involved for particle counting on the polystyrene samples, some small errors might be expected, and it is noticeable that in the case of the silver iodide sols, where the dilutions involved were small, much better all-round agreement was obtained.

The evidence obtained indicates that the particle counting apparatus is capable of yielding accurate results, confirming the earlier work of Watillon and Grunderbeeck (15).

#### *The Determination of Coagulation Rates*

One of the primary reasons for constructing the apparatus was to obtain a method suitable for the rapid study of the kinetics of coagulation of particles in the size range of  $1\ \mu$ . In this connection the apparatus has been used to study the coagulation of sols of arachidic acid by various cations. This work will be reported in detail elsewhere, but some preliminary results will be quoted here to demonstrate the method of following coagulation.

The procedure employed was as follows: 10 ml. of a  $10^{-5}M$  arachidic acid sol were pipetted into a test tube and 0.1 ml. of the cation solution added. At 10-min. intervals 0.1 ml. samples of this solution were removed

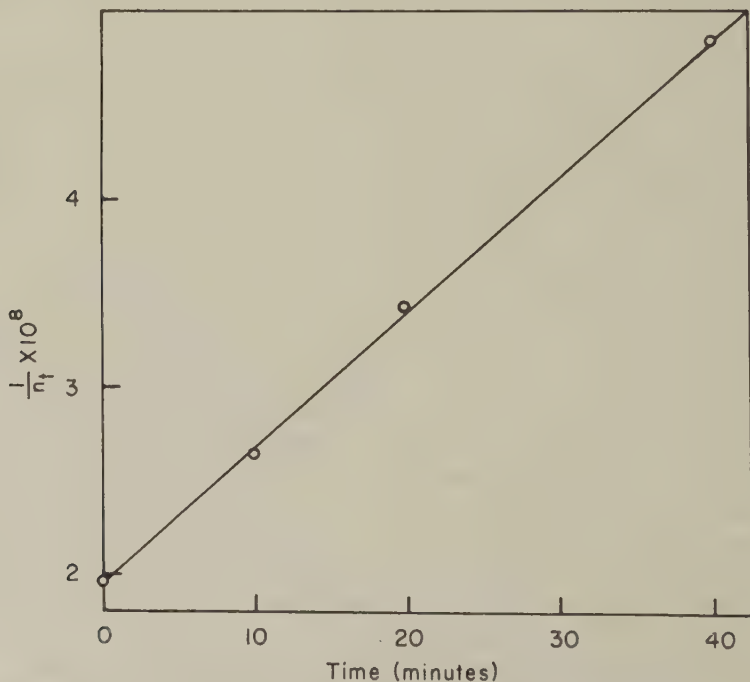


FIG. 4. Reciprocal particle concentration per milliliter against time for coagulation of an arachidic acid sol by  $10^{-6}M$  thorium nitrate.

and the coagulation was quenched by adding this to 50 ml. of ultrafiltered water. Particle counts were then carried out on each of these solutions, and thus the decrease in particle numbers with time at a known cation concentration was obtained. The experiments were then repeated for different cation concentrations. The average rate of shear in the capillary was of the order of  $100 \text{ sec.}^{-1}$ , and it is unlikely that any errors would arise owing to deflocculation by this cause.

A typical result, that for rapid coagulation of an arachidic acid sol with thorium nitrate, is shown in Fig. 4, as a curve of  $1/n_t$  (reciprocal particle number per milliliter after time  $t$ ) against time. As predicted by Smoluchowski (25), a good linear plot is obtained.

### General Conclusions

The apparatus has been shown to provide an effective method for obtaining absolute particle counts and for following coagulation rates. The main advantages of the method are (1) polydisperse systems can be used; (2) the time required for observation is comparatively short; (3) absolute particle numbers are obtained directly without subsidiary information on particle radius, etc.; (4) only small volumes are required; and (5) errors due to sedimentation can be minimized. Further developments of the apparatus for automatic counting and for the counting of biological cells are envisaged.

### ACKNOWLEDGMENTS

The authors wish to thank Dr. A. Watillon for much helpful advice and discussion, Mr. R. W. Horne for much helpful discussion on electron microscopy and for taking the electron micrographs, and Mr. L. Sagers for much of the constructional work on the apparatus. One of us (D.J.W.) wishes to thank the Agricultural Research Council for financial assistance.

### REFERENCES

1. RAYLEIGH, LORD, *Phil. Mag.* **41**, 107, 447 (1871).
2. OTTEWILL, R. H., AND SIRS, J. A., *Bull. Photoelectric Spectrometry Group* **10**, 262 (1957).
3. OTTEWILL, R. H., AND PARREIRA, H. C., *J. Phys. Chem.* **62**, 912 (1958).
4. MIE, G., *Ann. Physik* **25**, 377 (1908).
5. BACKUS, R. C., AND WILLIAMS, R. C., *J. Appl. Phys.* **21**, 11 (1950).
6. WILLIAMS, R. C., AND BACKUS, R. C., *J. Am. Chem. Soc.* **71**, 4052 (1949).
7. GEROULD, C. H., *J. Appl. Phys.* **21**, 183 (1950).
8. OLIVER, J., AND SMITH, P., *J. Phys. Chem.* **30**, 1 (1926).
9. LAWRENCE, A. S. C., AND MILLS, O. S., *Discussions Faraday Soc.* **18**, 98 (1954).
10. VAN DEN TEMPEL, M., *Rec. trav. chim.* **72**, 419 (1953).
11. ZSIGMONDY, R., *Z. physik. Chem.* **92**, 600 (1918).
12. LEE, P. K., AND LA MER, V. K., *Rev. Sci. Instr.* **24**, 1004 (1954).
13. GUCKER, F. T., O'KONSKI, C. T., PICKARD, H. B., AND PITTS, G. N., *J. Am. Chem. Soc.* **69**, 2422 (1947); GUCKER, F. T., AND O'KONSKI, C. T., *J. Colloid Sci.* **4**, 541 (1949).



14. DERJAGUIN, B., AND WLACENKI, G., *Doklady Akad. Nauk S.S.S.R.* **63**, 155 (1948).
15. WATILLON, A., AND VAN GRUNDERBEECK, F., *Bull. soc. chim. Belges* **63**, 115 (1954).
16. WATILLON, A., ROMEROWSKI, M., AND VAN GRUNDERBEECK, F., *Bull. soc. chim. Belges* **68**, 450 (1959).
17. COULTER, W. H., U. S. Patent No. 2,656, 508 (1953).
18. HARDY, A. C., AND PERRIN, F. H., "The Principles of Optics," p. 510. McGraw-Hill, New York, 1932.
19. KRUYT, H. R., AND VAN GILS, G. E., *Kolloid-Beih.* **45**, 60 (1937).
20. OTTEWILL, R. H., AND WOODBRIDGE, R. F., to be published.
21. PANGONIS, W. J., HELLER, W., AND JACOBSON, A., "Tables of Light Scattering Functions for Spherical Particles." Wayne State University Press, Detroit, 1957.
22. LUVALLE, J. E., AND JACKSON, J. M., *J. Phys. Chem.* **61**, 1216 (1957).
23. HELLER, W., AND TABIBIAN, R. M., *J. Colloid Sci.* **12**, 25 (1957).
24. BATEMAN, J. B., WENECK, E. J., AND ESHLER, D. C., *J. Colloid Sci.* **14**, 308 (1959).
25. SMOLUCHOWSKI, M. VON, *Z. physik. Chem.* **92**, 129 (1917).

## THE RATE OF NUCLEATION AT HIGH PRESSURES

R. S. Bradley

*Department of Inorganic & Structural Chemistry, The University of Leeds, England**Received June 10, 1959; revised February 4, 1960*

## ABSTRACT

Formulas are derived for the effect of pressure on the rate of formation of liquid and solid nuclei from the vapor and of solid nuclei from the melt and from another solid. The nucleation process in the formation of diamond is discussed, and it is considered likely that nucleation occurs on a foreign inclusion.

The effect of pressure on the thermodynamics of phase transitions has recently attracted much attention, especially from geochemists. Less has been published on the kinetic aspects, such as rates of nucleation and crystal growth, although these must also be of considerable geological interest. In this paper the effect of high pressure on the rate of nucleation is studied theoretically, first for the appearance of a new phase from a gas, and then for condensed phases. It will appear that the effects of pressure may be surprisingly large.

## THE FORMATION OF A NUCLEUS FROM A GASEOUS PHASE AT HIGH PRESSURE

Suppose that a vapor of a substance  $X$  at pressure  $p$  is in the presence of an inert gas  $Y$  at pressure  $P$  where  $P \gg p$ . The Gibbs free energy of formation of a spherical liquid nucleus of radius  $r$  from the vapor at pressure  $p$  is given by

$$\Delta G = -\frac{4}{3}\pi r^3 \frac{\rho(P)}{M} RT \ln [p/p_0(P)] + 4\pi r^2 \sigma(P), \quad [1]$$

where  $\rho(P)$ ,  $\sigma(P)$ , and  $p_0(P)$  are the density, surface tension, and vapor pressure of the liquid at pressure  $P$  and  $M$  is the molecular weight (1). To a first approximation the value of  $p_0(P)$  is given by the Poynting equation

$$\ln [p_0(P)/p_0(0)] = PV_l(P)/(RT), \quad [2]$$

where  $V_l(P)$  is the molar volume of the liquid at pressure  $P$ .

Hence

$$\Delta G = -\frac{4}{3}\pi r^3 \rho(P)[RT \ln \alpha - PV_l(P)]/M + 4\pi r^2 \sigma(P), \quad [3]$$

where  $\alpha = p/p_0(0)$ . For constant  $P$  the critical radius  $r_c$  is given by

$$(\partial \Delta G / \partial r)_{P,T} = 0$$

and hence

$$r_c(P) = 2\sigma(P)M/\{\rho(P)[RT \ln \alpha - PV_l(P)]\}. \quad [4]$$

If  $p$  is kept constant and  $P$  varied there will be a limiting pressure  $P_c$  given by

$$P_c = RT \ln \alpha / V_l(P), \quad [5]$$

above which  $\Delta G$  becomes positive for all values of  $r$ , and above which there is no maximum in  $\Delta G$  and no critical nucleus. This arises from the effect of  $P$  on the vapor pressure  $p_0(P)$ , i.e., an increase in  $P$  at constant  $p$  can convert a supersaturated to an undersaturated vapor. Suppose, for example, that for water vapor  $\alpha = 2$ ; then, neglecting the compressibility of liquid water  $P_c = 940$  atm. at  $25^\circ\text{C}$ .; i.e., the application of a pressure of 940 atm. will destroy this supersaturation at  $25^\circ\text{C}$ .

It would be expected that the rate of nucleation would gradually decrease to zero with increase in pressure, and this is clear from the change with pressure of the controlling term on the rate, namely,  $e^{-\Delta G_{\max.}/(kT)}$ , where  $\Delta G_{\max.}$  is given by

$$\Delta G_{\max.} = \frac{4}{3}\pi r_c^2 \sigma(P) \quad [6]$$

$$= 16\pi\sigma(P)^3 M^2 \{3\rho(P)^2 [RT \ln \alpha - PV_l(P)]^2\} \quad [7]$$

It follows that [5] gives the condition of zero velocity.

Similar considerations will apply when a crystal nucleus is formed from the vapor, with minor changes in the formulas to allow for the change in geometry. Equation [3] becomes for a cubic nucleus

$$\Delta G = -l^3 \rho(P)[RT \ln \alpha - PV_s(P)]/M + 6l^2 \sigma(P), \quad [8]$$

where  $V_s(P)$  is the molar volume of the crystal, of edge  $l$ , at  $P$  and  $\rho_s(P)$  is the density of the crystal at  $P$ . Equation [4] becomes

$$l_c(P) = 4\sigma(P)M/\{\rho_s(P)[RT \ln \alpha - PV_s(P)]\}. \quad [9]$$

Equation [7] becomes

$$\Delta G_{\max.} = 32\sigma(P)^3 M^2 / \{\rho_s(P)^2 [RT \ln \alpha - PV_s(P)]^2\}. \quad [10]$$

It might be thought that the application of the usual nucleation theory, as developed by Becker, Döring, and others (2), is unreal at high pressures, since diffusion constants do not enter into the formulas, which contain expressions for the collision number per  $\text{cm}^2$  per second from the gas to surface of the same type as if the gas  $X$  were at low pressure and the medium a vacuum. Unless, however, the pressure is so high that the system, although called a gas, is virtually a condensed phase, in which event the discussion below applies, the nuclei will in fact grow by a nondiffusion mechanism. This follows, at any rate for the formation of liquid droplets,

by the application of the theory given by Fuchs (3) and studied by the writer and others (4). This theory deals with droplet evaporation in an undersaturated medium, but will obviously apply equally well to the growth of droplets from supersaturated vapor. If the droplet diameter and mean free path in the gas phase are comparable the drop will grow largely by a process of "molecular distillation" rather than diffusion, another example of the fact that Knudsen or "molecular" phenomena in gases can be observed at atmospheric or higher pressures provided that the dimensions of the body studied are comparable with the mean free path. In fact the rate of growth of a micro drop will be given by (4)

$$dM/dt = 4\pi r D(p - p_0(P))M / \{RT[D/(r\nu\beta) + r/(r + \Delta)]\} \text{g. sec.}^{-1} \quad [11]$$

where  $D$  is the diffusion coefficient of  $X$  in  $Y$  at pressure  $P$ ,

$$\nu = (RT/2\pi M)^{1/2},$$

$\beta$  is the condensation coefficient for condensation of vapor on the surface of the liquid, and  $\Delta$  is approximately equal to the mean free path. Clearly, when  $r$  becomes small enough we have

$$dM/dt = 4\pi r^2(p - p_0(P))M\nu\beta/(RT), \quad [12]$$

as for growth in the complete absence of  $Y$ .

We may note that the Poynting equation may be generalized to the more exact form

$$\ln f(P)/f(0) = PV_i(P)/RT, \quad [13]$$

where the  $f$ 's are fugacities, and the Eqs. [3] and [4] will apply in general if the supersaturation is expressed in terms of fugacities.

The correction to allow for the compressibility of the solid or liquid phase is small. The correction for the influence of  $P$  on  $\sigma$  is obscure, since it is unreal to imagine that  $Y$  is insoluble in liquid  $X$ , and the effect on surface concentration must be considered. However, the correction is likely to be small.

#### THE FORMATION OF A NUCLEUS IN CONDENSED PHASES

In contrast to the considerations above it is possible for the rate of nucleation to be increased by increase in pressure when the nucleus is formed in a condensed phase. This may occur when the new phase has a smaller specific volume than the old, as will generally apply for solidification of a melt (water, except at very high pressures, and germanium being exceptions). Instead of Eq. [8] we may write for the formation of a cubic crystal nucleus from a melt

$$\Delta G = -l^3\rho_s(P)[(RT \ln \alpha)/M - P(1/\rho_s - 1/\rho_l)] + 6l^2\sigma(P), \quad [14]$$

where by  $\alpha$  we now mean the ratio of the vapor pressures of liquid and solid at pressure  $P$ , i.e.,  $p_l(P)/p_s(P)$ . Equation 14 follows by applying equation 2 to the liquid and solid, or by the use of  $(\partial\Delta G/\partial P)T = -\Delta V$ . Hence the critical size is given by  $(\partial\Delta G/\partial l)_{P,T} = 0$  i.e.

$$l_c = 4\sigma(P)/\{\rho_s(P)[(RT \ln \alpha)/M - P(1/\rho_s - 1/\rho_l)]\} \quad [15]$$

Similarly

$$\begin{aligned} \Delta G_{\max.} &= 2\sigma(P)l_c^2 \\ &= 32\sigma(P)^3/\{\rho_s(P)^2[(RT \ln \alpha)/M - P(1/\rho_s - 1/\rho_l)]^2\}. \end{aligned} \quad [16]$$

Since the effect of  $\Delta G_{\max.}$  on the rate is given by the term  $e^{-\Delta G_{\max.}/(kT)}$ , it is clear that so far as this term is concerned the rate of nucleation will be increased if the specific volume of the liquid is greater than that of the solid. Although the assumption of a cubic nucleus is naive, this assumption will not affect the general argument and may lead to equations incorrect merely by a numerical factor.

However, the kinetic factor for condensed phases differs from that for gases, and allowance must be made for an activation energy for diffusion or viscous flow. This will also apply in the case of a so-called gas at sufficiently high pressures to show activated diffusion of the cell type (5). The main effect of pressure on viscosity is covered by a factor  $e^{P\Delta V^*(P)/(kT)}$ , where  $\Delta V^*(P)$  is the increase in volume associated with the activation process for flow, and very large increases in viscosity may occur. For water, however, there is an initial decrease in viscosity as the pressure rises, owing to the breakup of structure. It follows that the overall effect may be a decrease in nucleation velocity as the pressure is increased; if the effect of pressure on viscosity is known a fair estimate may be made of the direction of the change.

Similar considerations apply to the transformation solid  $\rightarrow$  solid. We should expect the kinetic factor to be of the nature of a vibration, and the rate of nucleation to be given by

$$I = n_s \nu' e^{-E/kT} e^{-\Delta G_{\max.}/(kT)} e^{-\phi/kT} \quad [17]$$

where  $n_s$  is the number of atoms or molecules of the old phase per square centimeter of the interface between the two phases,  $E$  is an activation energy for molecular jumping between the two phases, and  $\phi$  is a strain energy;  $\nu'$  is a vibration frequency. A good example which brings out the various factors is the transformation of graphite to diamond or vice versa. The high value of the total surface energy of diamond estimated by Harkins for the 111 face at  $5,655 \text{ ergs cm.}^{-2}$  for a C—C bond energy of 90 kcal. per g. atom (6) will make the rate of nucleation from the vapor extremely low, since the surface energy occurs as the cube power in  $\Delta G_{\max.}$ . This calcula-



tion for  $\sigma$  is, however, somewhat unreal, since the cleavage of the 111 planes will either leave some kind of unsaturated bond for cleavage *in vacuo*, or else the free valencies, if the diamond is cleaved in air, will become saturated with oxygen. The free valencies occur on alternate carbon atoms, so that the surface unsaturation will not in fact be benzenoid. As a generous allowance for this rearrangement of electron orbitals we may drop  $\sigma$  by a factor of  $\frac{1}{2}$ . The surface energy of graphite in the cleavage plane is much less. As shown by Cleasby (7) and the writer, the lattice energy of various fused ring aromatic hydrocarbons is approximately 1.75 kcal. per g. atom of carbon, and this value will give a reasonable estimate of the  $\pi$  bonding in graphite, per g. atom. It follows that the surface energy of graphite is only a few per cent of that of diamond and a rough estimate of the interfacial energy graphite-diamond may be made by equating this to the (corrected) surface energy of diamond, say 2500 ergs cm.<sup>-2</sup>.

The rate of graphitization of diamond is decreased by the application of pressure (8) and in fact will be reversed above the equilibrium pressure. The reaction is nucleated on the surface (9), probably because the increase in volume would cause a large strain energy for nucleation in the interior. The nucleation process in the reverse transformation graphite  $\rightarrow$  diamond is unknown, but could well occur in the interior of the graphite crystal. The application of the theory above requires, however, allowance for the fact that diamond is not stable, unless the pressure is high, 13,500 atm. at 0°K. and 34,000 atm. at 1000°K. (10). Equation [14] becomes, assuming for simplicity a cubic nucleus, for graphite  $\rightarrow$  diamond

$$\Delta G = -l^3 \rho_D(P)(P - P_E)(1/\rho_G(P) - 1/\rho_D(P)) + 6l^2 \sigma(P) \quad [18]$$

where  $P_E$  is the equilibrium pressure and  $\rho_D$  and  $\rho_G$  are the respective densities of diamond and graphite at pressure  $P$ . This gives

$$l_c(P) = 4\sigma(P)\rho_G(P)/[(P - P_E)(\rho_D(P) - \rho_G(P))] \quad [19]$$

$$\Delta G_{\max.} = 32\sigma(P)^3 \rho_G(P)^2 / [(P - P_E)^2 (\rho_D(P) - \rho_G(P))^2]. \quad [20]$$

At 50,000 atm. at 1000°K.  $\Delta G_{\max.}/(kT) = 4.2 \times 10^4$ ; at 75,000 atm.  $\Delta G_{\max.}/(kT) = 6.5 \times 10^3$  taking  $\sigma = 2,500$  ergs. cm.<sup>-2</sup>. Although this increase in pressure corresponds to an enormous kinetic factor, the value of  $\Delta G_{\max.}/(kT)$  is even at 75,000 atm. so large that the rate of nucleation will be practically zero, mainly because of the high value of the interfacial energy. It follows that nucleation in the interior of graphite to produce diamond is likely to occur on a foreign inclusion.

#### REFERENCES

1. VOLMER, M., "Kinetik der Phasenbildung." Steinkopff, Dresden and Leipzig, 1939. BRADLEY, R. S., *Quart. Revs (London)* **5**, 315 (1951). REISS (*J. Chem.*

- Phys.* **18**, 840, 1950; *ibid.* **18**, 996, 1950) and REISS AND FRIEDMAN (*J. Chem. Phys.* **19**, 253, 1951) have considered nucleation in binary systems where the nucleus contains two components. In this paper the second component  $Y$  is used merely to transmit the pressure.
2. BECKER, R., AND DÖRING, W., *Ann. Phys.* **24**, 719 (1935).
  3. FUCHS, N., *Phys. Z. Sowjet* **6**, 225 (1934).
  4. BRADLEY, R. S., *J. Colloid Sci.* **10**, 571 (1955).
  5. TIMMERHAUS, K. D., AND DRICKAMER, H. G., *J. Chem. Phys.* **20**, 981 (1952).
  6. HARKINS, W. D., *J. Chem. Phys.* **10**, 268 (1942).
  7. BRADLEY, R. S., AND CLEASBY, T. G., *J. Chem. Soc.* **1953**, 1681.
  8. BRIDGMAN, P. W., *J. Chem. Phys.* **15**, 92 (1947).
  9. SEAL, M., *Nature* **182**, 1264 (1958).
  10. BERMAN, R., AND SIMON, F. E., *Z. Elektrochem.* **59**, 333 (1955).

## OIL-SOLUBLE SURFACE-ACTIVE COPOLYMERS OF ALKENES AND POLAR MONOMERS<sup>1</sup>

F. M. Fowkes, M. J. Schick,<sup>2</sup> and A. Bondi

*Shell Development Company, Emeryville, California*

*Received December 22, 1959; revised May 23, 1960*

### ABSTRACT

Oil-soluble surface-active copolymers have been prepared by copolymerizing  $C_8$ - $C_{18}\alpha$ -olefins with polar monomers. Polyacetates, polyalcohols, and a polynitrile with 1 to 5 polar groups per hydrocarbon chain and with molecular weights from 10,000 to 40,000 were obtained. Sedimentation, diffusion, and viscosity measurements showed the polymers to be most expanded in polar organic solvents and to contract and form aggregates of 10 or more molecules in hydrocarbon solutions. Studies with adsorbed and insoluble monolayers showed that these polymers adsorb onto water, glass, or carbon surfaces as thin monolayers with nearly all the polar groups attached. These polymers are unusually effective dispersants for solids in oil.

### INTRODUCTION

Surface-active oil-soluble copolymers with acetate, alcohol, and nitrile groups are found to be useful dispersants for solids in organic media. The results of having highly polar groups in oil-soluble polymers are evident in the unusual tendency to be soluble in a wide range of solvents, to aggregate in nonpolar solvents, to adsorb on polar substrates as completely unrolled molecules, and to deflocculate oil suspensions of solids at unusually high temperatures. This paper is concerned with the behavior of these new dispersants in all these phenomena.

### MATERIALS

Oil-soluble polymeric dispersants have been prepared by copolymerization of long-chain  $\alpha$  olefins with simple polar vinyl monomers (1). The mixture of long-chain  $\alpha$ -olefin (most often octadecene) and vinyl acetate (or other polar monomer) was polymerized at 80° to 130°C. with 0.5% to 1.0% benzoyl peroxide, or other free radical chain initiators, to conversions ranging between 10% and 50%. Excess monomers were dis-

<sup>1</sup> Presented at the 134th Meeting of the American Chemical Society in Chicago, September 11, 1958.

<sup>2</sup> Present address: Research and Development Center, Lever Bros. Co., Edgewater, New Jersey.



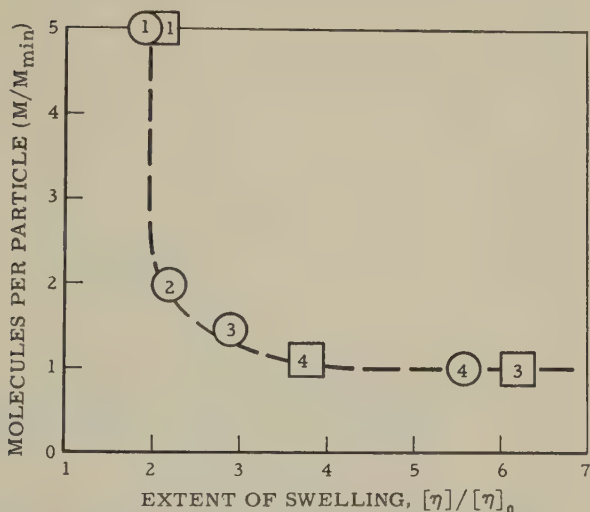


FIG. 1. Effect of solvent "goodness" on aggregation of polyalcohols and polyacetates. 1.  $n\text{-C}_7\text{H}_{16}$ ; 2.  $\text{CS}_2$ ; 3.  $\text{CHCl}_3$ ; 4.  $(\text{C}_2\text{H}_5)_2\text{NH}$ ;  $\circ$  Polyalcohol;  $\square$  Polyacetate.

gated in hydrocarbon solutions. The polyalcohols require a hydrogen-bonding solvent (diethylamine) to avoid aggregation. Figure 1 illustrates with intrinsic viscosity measurements that the least aggregation occurs in the best solvents (largest values of  $[\eta]$ ). The details are reported in Table I.

An acrylonitrile-octadecene copolymer (1.7/1) was found to have an  $M_{s\eta}$  of 11,400 and  $[\eta]$  of 0.081 in chloroform solutions. The value of  $[\eta]$  indicates the coils to be only slightly swollen with solvent.

Figure 2 illustrates the concentration dependence of inter-polymer interactions. The slope gives  $A_2$ , an approximate weight-average second virial coefficient, for

$$\frac{M(1 - \bar{v}\rho)D}{RT_s} = 1 + 2A_2 M_{c_2} + 3A_3 M_{c_2}^2 + \dots$$

The positive slopes indicate repulsion between molecules and the negative slope aggregation. Values of  $A_2$  may be used to compare polymer-solvent versus polymer-polymer interaction. If (as with homopolymers) zero values of  $A_2$  indicate these interactions to be equal (as in a  $\theta$ -solvent), then the configuration of the polymer in such a solvent is nearly a random coil. The polyalcohol has a zero-value for  $A_2$  in carbon disulfide where the degree of swelling is slight;  $[\eta]/[\eta]_0$  is 2.2. In better solvents values of  $[\eta]/[\eta]_0$  are greater than 6; these solvents swell polymer molecules to equivalent hydrodynamic volumes about three times greater than random coils. With the polyalcohols the degree of swelling increased with polarity of the solvent, whereas with the polyacetates diethylamine was too polar and maximum swelling was observed with chloroform.



TABLE I  
Molecular Weights and Solution Behavior of Olefin-Vinyl Acetate and Olefin-Vinyl Alcohol Copolymers—25°C.

Vinyl acetates per olefin	Solvent	$[\eta]$	$k_s$	$s_0(\times 10^{13})$	$D_0$ ( $\times 10^6$ )	$M_{SD}$	$M_{\eta}$	$\frac{[\eta]}{[\eta]_0}$	$\left(\frac{[\eta]}{[\eta]_0}\right)^{1/3}$	$f/f_0$	$\beta$ ( $\times 10^{-6}$ )
3.2 <sup>a</sup>	(C <sub>2</sub> H <sub>5</sub> ) <sub>2</sub> NH	0.054	0.24	5.24	2.9	15,100	16,600	2.2	1.30	1.2	2.28
	CHCl <sub>3</sub>	0.133	0.40	-4.0 <sup>b</sup>	1.2	17,000	13,600	5.3	1.74	1.9	2.57
3.95	<i>n</i> -C <sub>6</sub> H <sub>14</sub> —two equal sedimentation peaks corresponding to 15,000 and 210,000										
	(C <sub>2</sub> H <sub>5</sub> ) <sub>2</sub> NH	0.095	0.38	8.0	2.4	28,000	37,400	3.8	1.56	1.2	2.40
	CHCl <sub>3</sub>	0.155	0.96	-7.7 <sup>b</sup>	1.10	38,000	38,000	6.2	1.84	1.8	2.63
3.0 (85% hydrolyzed)	<i>n</i> -C <sub>7</sub> H <sub>16</sub> —extremely broad sedimentation peak										
	(C <sub>2</sub> H <sub>5</sub> ) <sub>2</sub> NH	0.140	0.64	4.84	2.1	18,200	18,000	5.6	1.78	1.8	2.56
	CHCl <sub>3</sub>	0.072	0.04	-7.6 <sup>b</sup>	1.45	26,100	25,600	2.9	1.42	1.4	2.37
	CS <sub>2</sub>	0.055	0.03	-8.6 <sup>c</sup>	2.1	36,600	37,000	2.2	1.30	1.3	2.32
3.95 (92% hydrolyzed)	<i>n</i> -C <sub>7</sub> H <sub>16</sub>	0.047	0.52	17.2	1.25	107,000	92,000	1.9	1.24	1.4	2.28
	<i>n</i> -C <sub>7</sub> H <sub>16</sub> (+1% H <sub>2</sub> O) <i>s</i> (at 1%) = 19, corresponding to 200,000										
	(C <sub>2</sub> H <sub>5</sub> ) <sub>2</sub> NH	0.133	0.144	3.67	2.7	10,700	11,700	5.3	1.74	1.6	2.55
	moist <i>n</i> -C <sub>7</sub> H <sub>16</sub>	0.043	-0.67	6.0	—	—	26,000	1.7	1.2	—	—
	dry <i>n</i> -C <sub>7</sub> H <sub>16</sub>	0.063	0.02	15.1	1.61	73,000	84,000	2.5	1.36	1.2	2.32

<sup>a</sup> Molecular weight by light scattering—13,700.

<sup>b</sup> Sedimentation constant increased 23% to compensate for increased viscosity at 360 kg./cm.<sup>2</sup>.

<sup>c</sup> Sedimentation constant increased 12% for pressure of 300 kg./cm.<sup>2</sup>.

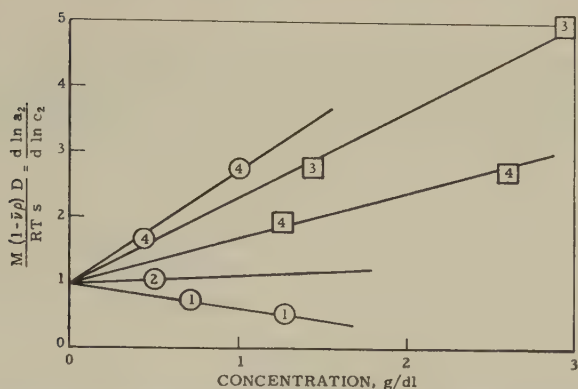


FIG. 2. Concentration dependence of thermodynamic activity of polymers as determined by diffusion and sedimentation measurements. 1.  $n\text{-C}_7\text{H}_{16}$ ; 2.  $\text{CS}_2$ ; 3.  $\text{CHCl}_3$ ; 4.  $(\text{C}_2\text{H}_5)_2\text{NH}$ ;  $\circ$  Polyalcohol;  $\square$  Polyacetate.

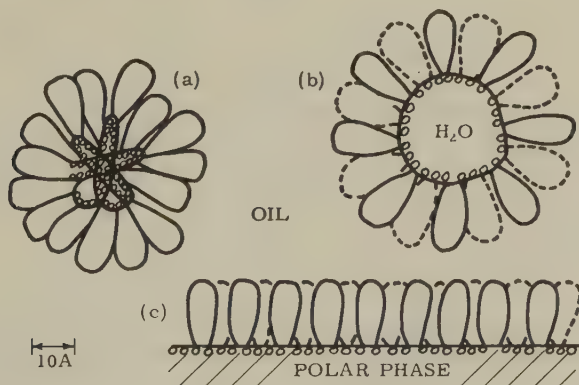


FIG. 3. Configuration of copolymers. (a) In hydrocarbon solution; (b) Swollen with solubilized water; (c) Adsorbed onto polar substrate.

The configuration of molecules in solution is indicated by the  $\beta$ -value (2) calculated from  $M_{sD}$  in Table I to be swollen coils in good solvents and nearly solvent-free spheres in poor solvents. Added water increases the apparent particle weights sufficiently to suggest that each particle or molecule swells to spherical shape with a monolayer of polymer surrounding it (see Fig. 3).

Polar dispersants in nonpolar media are known to aggregate into micelles (soaps, etc.) or into dimers (fatty acids). This tendency to aggregate is a measure of the ability of the dispersant to bond to other polar groups (including polar solids). These oil-soluble polar polymers demonstrate a wide range of interactions between polar groups, from weak interactions such as those leading to polymer molecules occupying less than the fully extended volume to those involving the squeezing out of nearly all the

solvent and the aggregation of molecules into clumps of ten or more molecules. The greater interaction of the polyalcohols resulting in aggregation may be an indication of a good dispersant. We, therefore, would expect the polyalcohols to be good dispersants, especially in hydrocarbon solvents.

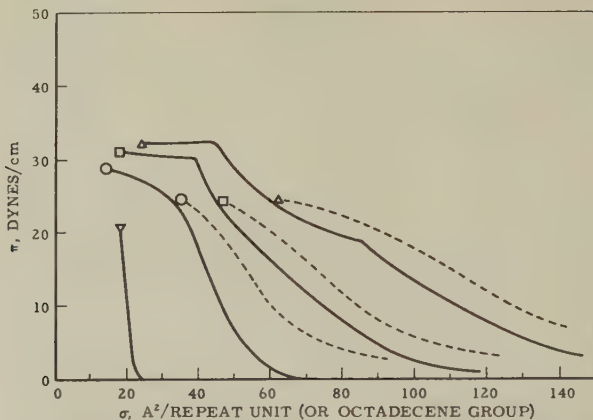


FIG. 4. Surface pressure vs. area curves of copolymers of octadecene and vinyl acetate on 0.01 *N* HCl. Solid lines—copolymers of vinyl acetate; broken lines—octadecyl acetate plus corresponding ratio of polyvinyl acetate (computed). ○ 2.9 vinyl acetates per alkene; □ 3.41 vinyl acetates per alkene; △ 5.69 vinyl acetates per alkene; ▽ Octadecyl acetate.

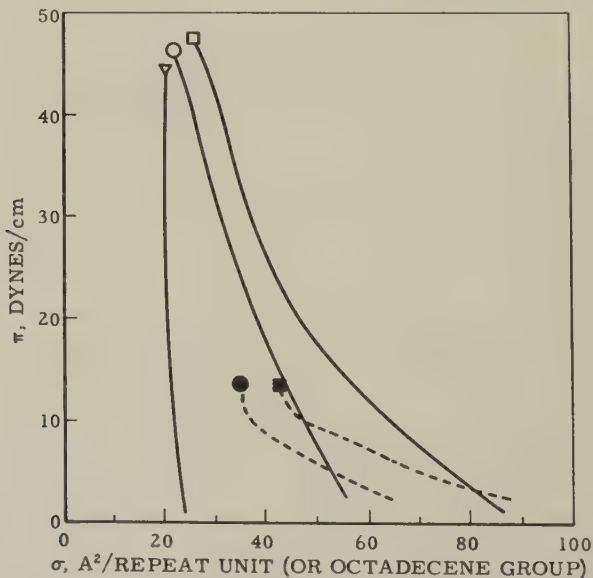


FIG. 5. Surface pressure vs. area curves of hydrolyzed octadecene-vinyl acetate copolymers on 30%  $\text{NaNO}_3$  at 25°C. Solid lines—copolymers of vinyl alcohol; broken lines—octadecanol plus corresponding ratio of polyvinyl alcohol (computed). ○ 2.19 vinyl alcohols per alkene; □ 3.41 vinyl alcohols per alkene; ▽ *n*-octadecanol.

*Monolayers at the Air/Water Interface*

Monolayers of polyalcohols, polyacetates, and a polynitrile were spread on the surface of water from hexane solution. The dependence of film pressure and surface potential on the area of film per alkyl chain was determined with the film balance (Fig. 4-7).

It is evident from both pressure and potential measurements that at low film pressures *all* the vinyl acetate or vinyl alcohol groups are in the surface, occupy the same area as if the alkyl groups were not present, and give the same surface potential as if the monolayers were polyvinyl acetate

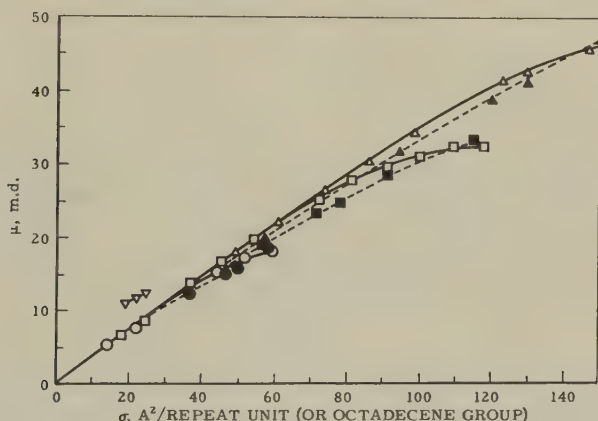


FIG. 6. Surface moment vs. area curves of copolymers of octadecene and vinyl acetate on 0.01 *N* HCl. Solid lines—copolymers of vinyl acetate; broken lines—polymers of vinyl acetate computed for the corresponding number of vinyl acetates. ○ 2.19 vinyl acetates per alkene; □ 3.41 vinyl acetates per alkene; △ 5.69 vinyl acetates per alkene; ▽ *n*-Octadecyl acetate.

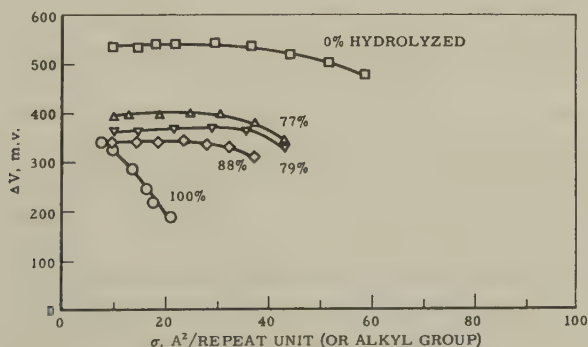
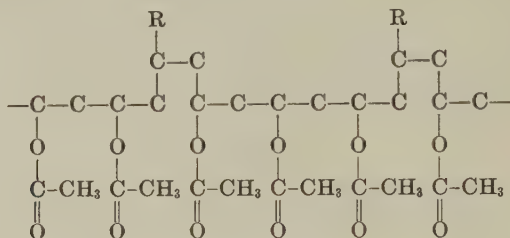


FIG. 7. Surface potential vs. area curves of copolymers of alkenes and hydrolyzed vinyl acetate. ○ Polyvinyl alcohol; □ Copolymer of octadecene and vinyl acetate 1:2.19, 1:3.41, 1:5.69; △ Copolymer of octadecene and vinyl alcohol 1:2.19; ▽ Copolymer of octadecene and vinyl alcohol 1:3.41; ◇ Copolymer of dodecene and vinyl alcohol 1:2.23.

or polyvinyl alcohol. In the case of the polyacetates, Fig. 4 shows with dashed lines the area per molecule expected if each alkyl group occupied 20 A.<sup>2</sup> of the surface in addition to the area occupied by the vinyl acetate groups. At low pressures the experimental areas are 20 A.<sup>2</sup> less than this dashed line, demonstrating that only the vinyl acetate groups are in the water surface with the alkyl group pushed out:



The same conclusion may be drawn from Fig. 5 for the polyalcohol where the area per alkyl chain at low pressures is directly proportional to the number of vinyl alcohols per alkyl chain (27 A.<sup>2</sup> per vinyl alcohol at zero pressure). Figures 6 and 7 confirm these conclusions by showing that the copolymers have about the same surface potential as polyvinyl acetates or alcohols.

Compression of the copolymer films reduces the area per polar monomer to a minimum value (26 A.<sup>2</sup> for vinyl acetate, 23 A.<sup>2</sup> for vinyl alcohol). Further compression reduces the total area by squeezing the vinyl acetate or alcohol groups out of the surface into the substrate, but the remaining groups retain their minimum area of surface as evidenced by the constant surface potential (Fig. 6 and 7). The energy required to squeeze a polar monomer group out of the surface can be calculated from the average film pressure and the minimum area per polar monomer group. These values varied from 200 to 600 calories per mole; they are lowest for squeezing out the first polar group of a copolymer having a high ratio of polar to alkyl groups.

High film pressures tend to reduce the area per alkyl chain to about 30 A.<sup>2</sup> regardless of the ratio of polar to alkyl groups. However, Fig. 4 shows that the polyacetate films collapse at 25–30 dynes/cm. before attaining as tight packing as encountered with the polyalcohols. This is a reversible collapse, however, as the polyacetates are squeezed from the film into droplets which can spread again if the area is increased. The higher collapse pressures of the polyalcohols indicate stronger adhesion to the substrate and suggest that these would be better dispersants than the polyacetates; this indeed has proved to be the case.

A polynitrile monolayer has about the same pressure-area curve as the polyalcohols; it too is a better dispersant than the polyacetate.



*Interfacial Tensions*

The interfacial tensions of oil solutions of polyalcohols were measured at the oil/water interface. With increasing concentration the interfacial tensions fell rapidly at first but leveled off to constant values with concentrations in excess of 0.5%. Lower interfacial tensions were obtained with copolymers having the larger ratio of polar to alkyl groups. This indicates that the adhesion of dispersants to polar phases should increase with this ratio; optimum dispersant qualities may be expected at the highest ratios compatible with the solvent.

*Adsorption on Solids*

(Work of A. E. O'Donnell)

Solutions of polyalcohols in various solvents were found to adsorb quantitatively onto various solids such as zinc dust, glass beads diatomaceous earth, and magnesia. This suggests that these copolymers may be useful dispersants for a wide variety of polar solids. Glass beads in a chromatographic column have been used for quantitative measurements of adsorption of the polyalcohol using methylene blue as an after treatment to dye the beads which have no adsorbed copolymer and thus show how far down the column the copolymer solution traveled before it was exhausted of polyalcohol. Table II shows the results of these measurements with various solvents. The area of surface per alkyl chain (repeating unit) varied with solvent from 36 to 70 A.<sup>2</sup>, being greater in wet than in dry solvents. These values correspond to a completely unrolled monolayer similar to that obtained on the surface of water. The smaller areas may be the result of tighter packing but probably are the result of incomplete spreading. The latter is surely the cause of the small areas obtained with acetone solutions.

TABLE II  
*Adsorption of Vinyl Alcohol/Octadecene Copolymer<sup>a</sup> on Glass Beads  
Out of Various Solvents*

Area calculation:		Geometric area	Krypton adsorption
Specific area of beads, cm. <sup>2</sup> /gm.		330	500
On glass beads:			
Out of CHCl <sub>3</sub> (H <sub>2</sub> O sat'd),	A. <sup>2</sup> per alkyl group	46.5	70.5
Out of benzene (H <sub>2</sub> O sat'd.),	A. <sup>2</sup>	44	67
Out of benzene (dry)	A. <sup>2</sup>	32	48.5
Out of CHCl <sub>3</sub> (dry),	A. <sup>2</sup>	24	36.5
Out of acetone			
(with 0.29% H <sub>2</sub> O),	A. <sup>2</sup>	8	12

<sup>a</sup> Composition of this sample: 4.6 hydroxyl groups per alkyl side chain.

*Deflocculation of Carbon Blacks in Oil*

Evaluation of the polyalcohols, polyacetates, and polynitriles as dispersants for carbon black is based on measurements of the electrical conductivity of oleogels. Briefly, the principle of the method is the comparison of the electrical resistance of a carbon black oleogel containing the adsorbable compound with that of a suspension of the same carbon black in medicinal white oil (4, 5). Since the adsorbed agent acts as an electrical insulator around the otherwise conducting particles, it increases the resistance of the carbon gel by factors as large as  $10^4$ . The degree of deflocculation is expressed in logarithmic units ( $pD_{10}^w$ ), as defined earlier. The neutral graphitized acetylene black is essentially nonporous and all of its  $53 \text{ m.}^2/\text{g.}$  of surface (measured by nitrogen adsorption) is believed available for adsorption of polymer. However, in the case of the acidic, less graphitic channel black, the surface area available to polymer is probably only 60%–70% of the  $110 \text{ m.}^2/\text{g.}$  available to nitrogen, as has been demonstrated

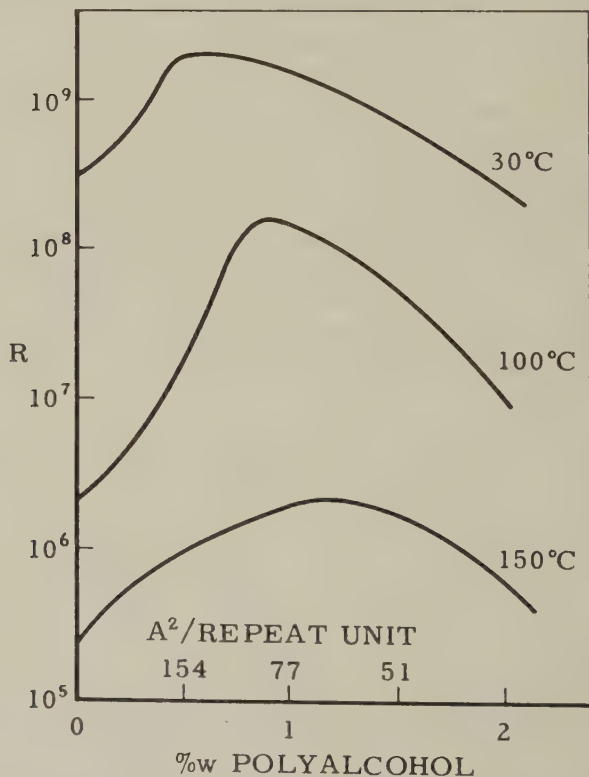


FIG. 8. Electrical resistance vs. concentration curve (taken at  $10 \text{ sec.}^{-1}$  shear rate) of a 10% w channel black suspension in refined lubricating oil as function of polyalcohol ( $R = C_{18}$ ,  $r = 3.9$ ,  $n = 24$ ) concentration.

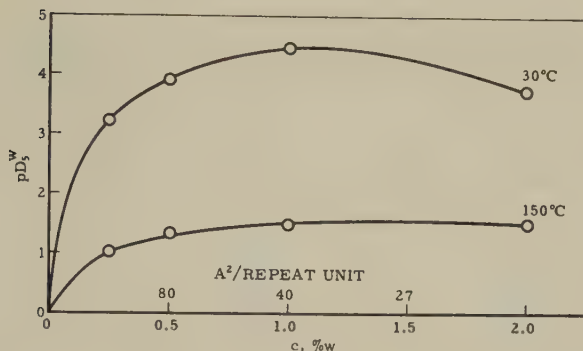


FIG. 9. Degree of deflocculation of acetylene black as function of concentration. Polyalcohol ( $R = C_{12}$ ,  $r = 2.2$ ,  $m = 20$ ) in refined lubricating oil.

with adsorption of fatty acids (6) and by electron microscopy (7). The area per alkyl group of the copolymer is reported on the basis of the entire  $110 \text{ m}^2/\text{g}$ ; the indicated correction would give areas 60%–70% of those reported.

A large number of copolymers were tested for carbon black deflocculation. Properties of the polymer and test conditions were systematically varied. For ease in indicating variations in polymer structures the formula  $(RX_r)_m$  is used, where  $R$  is the olefin,  $X$  the polar monomer,  $r$  the ratio of polar to alkyl groups, and  $m$  the number of "repeat units" in an average molecule. All polymers were tested in a neutral refined lubricating oil.

All combinations of copolymers and carbon black were tested at a number of concentrations of the copolymer (always with 10% of carbon black), and at several temperatures. At every temperature there was found a maximum in the resistance (or  $pD_5^w$ ) as a function of concentration (Figs. 8 and 9). This maximum occurs at the concentration where the carbon black surface is saturated with copolymer (4), so from this concentration the area per adsorbed molecule (or per adsorbed repeat unit) may be calculated. In Figs. 8 and 9 the maximum occurs at polyalcohol concentrations corresponding to  $40 \text{ A}^2$  per alkyl group with the acetylene black and  $40$ – $90 \text{ A}^2$  per alkyl group with the channel black (after correction). These values agree very well with those obtained on the water surface ( $30$ – $60 \text{ A}^2$  for the polymer used with acetylene black,  $30$ – $105 \text{ A}^2$  for the polymer used with channel black). Similar results were obtained with polyacetates and a polynitrile (Table III). This leads to the conclusion that on carbon blacks, just as on glass, these copolymers are completely spread out as unimolecular layers with a thickness no greater than  $20 \text{ A}$ . This conclusion appears to be contradictory to some theoretical (8) and experimental (9) studies of the adsorption of polymers at the oil/solid interface. However, in these latter studies the solvent molecules were about as strongly attracted

TABLE III  
Area per  $RX_r$  Group from Deflocculation Data (at 30°C.)

Copolymer	$r$	Molecular area per $RX_r$ group at		
		Air/water interface ( $\text{\AA}^2$ )	Acetylene black oil interface ( $\text{\AA}^2$ )	Channel black oil interface ( $\text{\AA}^2$ )
Octadecene-vinyl alcohol	3.5	30-95	42	116 (81 <sup>a</sup> )
Dodecene-vinyl alcohol	2.2	30-60	29	—
Octadecene-acrylonitrile	1.9	20-30	~15	—
Octadecene-vinyl acetate	4.1	45-120	≤ 54	—

<sup>a</sup> Corrected for "roughness."

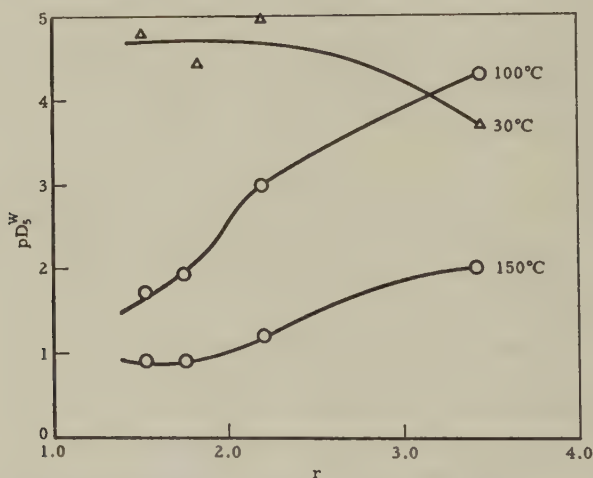


FIG. 10. Effect of vinyl alcohol to alkene ratio  $r$  (at approximately constant molecular weight 5-8000) upon deflocculation at 2% w in refined lubricating oil.

to the solid surface as the individual monomer residues in the polymers, whereas in our studies the adsorbed monomer residues are very much more strongly bonded to the surface than the solvent molecules. Consequently there is sufficient energy of adsorption per segment to more than offset the loss in entropy involved in bonding each segment to the surface. This conclusion has already been reached in some more recent studies (10, 11).

The effect of temperature on the ability of the various copolymers to deflocculate carbon black oleogels has been of particular interest and is illustrated in Figs. 8, 9, and 10 and in Tables IV and V. The maximum attainable degree of deflocculation decreases and the additive concentration at which the maximum occurs increases with the temperature. This effect is most marked with polyacetates or with copolymers having a low

TABLE IV

*Comparison of Maximum Degree of Deflocculation Achieved with Different Additives (in Refined Lubricating Oil) for Typical Carbon Black Types*

Additive	Temp., °C.	Acetylene black $pD_5^w$	Channel black $pD_5^w$
Copolymer ( $r = 3.5$ ) of octadecene-vinyl alcohol	30	>5	3.3
	150	4.3	2.4
Neutral calcium petroleum sulfonate	30	2.8	2.6
	150	2.3	2.1

TABLE V

*Effect of Polar Group on Deflocculation (at 1%(w) Polymer Concentration in Refined Motor Oil)*

Copolymer	$r$	$m$	Temp. (°C.)	$pD_5^w$ Acetylene black
Octadecene-vinyl acetate	4.1	33	30	2.6
			100	1.2
			150	0.9
Octadecene-vinyl alcohol	4.1	33	30	4.9
			100	5.6
			150	4.4
Octadecene-acrylonitrile	1.9	35	30	4.6
			100	3.0
			150	1.8
Octadecene-vinyl alcohol (for comparison)	2.2	18	30	5.0
			100	2.3
			150	1.0

ratio of polar to alkyl groups. However, a negligible decrease in deflocculating ability with temperature is observed with the polyalcohols having large ratios of polar to alkyl groups (note especially Table V). These latter copolymers are outstanding dispersants and outperform (in these tests) a typical monomeric deflocculant, neutral calcium petroleum sulfonate (Table IV). The shift of the maximum electrical resistance to larger areas per repeat unit with decrease in temperature (Figs. 8 and 9) may be the result of a greater water content of the oil and carbon at the lower temperature; this results in more efficient adsorption of these polymers on solids (as illustrated in Table II).

The ratio of polar groups to side chains determines in principle the



strength of adhesion of the adsorbed molecule to the oil/solid interface. The effect is twofold in nature, as the increased concentration of polar groups raises both the activity coefficient of the polymer in the solution and the adhesion to the interface. The upper limit of the polar group ratio is determined by the onset of insolubility, and depends therefore on the solvent as well as on the nature of the polar group. The net effect of the polar group ratio on the deflocculating ability of the octadecene-vinyl alcohol copolymer is illustrated in Fig. 10.

The nature of the polar group affects the ability of the copolymers to deflocculate carbon black oleogels as illustrated in Table V. The poly-nitriles and polyalcohols appear about equal, and both are more effective than the polyacetates.

### SUMMARY

1. Oil-soluble surface-active polymers have been prepared by copolymerizing  $\alpha$ -olefins and polar monomers.

2. These polymers are soluble in an unusually wide range of solvents, are most extended in polar organic solvents, and are most compact in hydrocarbon solvents. Polyalcohols are most extended in hydrogen-bonding solvents.

3. In poor solvents these polymers form aggregates with 10 or more molecules each.

4. Monolayers spread on the surface of water or adsorbed onto glass or carbon blacks are monomolecular in thickness (10–20 Å.) with nearly all polar groups attached to the polar phase.

5. The presence of traces of water nearly doubled the area of polyalcohols adsorbed on glass. The increased coverage of polyalcohols on carbon blacks at temperatures below 100°C. may also result from the presence of water.

6. Electrical resistance measurements have demonstrated that the adsorption of polyalcohols increases with high ratios of alcohol groups to paraffin chains, and with ratios of 4/1 nearly all the polyalcohol in solution is adsorbed even at temperatures as high as 150°C.

7. These copolymers are found to be unusually effective dispersants for carbon blacks in oil.

### ACKNOWLEDGMENTS

The authors wish to acknowledge their indebtedness to the many contributors to this investigation: H. A. Newey, E. E. Ryder, and co-workers for preparation of the copolymers; E. Wasserman for film balance measurements; M. W. Wales for advice on sedimentation studies; S. Beckley, S. J. Rehfeld, and G. H. Chakeris for sedimentation and related measurements; R. E. Fraatz for the deflocculation measurements; and A. E. O'Donnell for permission to include his adsorption study.

## REFERENCES

1. BONDI, A., AND SCOTT, L. B., U. S. Patent No. 2,800,453 (1957) (to Shell Development Company).
2. SCHERAGA, H. A., AND MANDELKERN, L., *J. Am. Chem. Soc.* **75**, 179 (1953).
3. SCHICK, M. J., *J. Polymer Sci.* **25**, 465 (1957).
4. BONDI, A., AND DIAMOND, H., *J. Colloid Sci.* **12**, 510 (1957).
5. BONDI, A., AND PENTHER, C. J., *J. Phys. Chem.* **57**, 72, 540 (1951).
6. MARON, S. H., BOBALEK, E. G., AND SHIN-MING FOK, *J. Colloid Sci.* **11**, 21 (1956).
7. ANDERSON, R. B., AND EMMETT, P. H., *J. Appl. Phys.* **19**, 367 (1948).
8. SIMHA, R., FRISCH, H. L., AND EIRICH, F. R., *J. Phys. Chem.* **57**, 584 (1953).  
FRISCH, H. L., AND SIMHA, R., *ibid.* **58**, 507 (1954).  
FRISCH, H. L., *ibid.* **59**, 633 (1955).
9. KORAL, J., ULLMAN, R., AND EIRICH, F. R., *J. Phys. Chem.* **62**, 541 (1958).
10. FRISCH, H. L., AND SIMHA, R., *J. Chem. Phys.* **27**, 705 (1957).
11. BINFORD, J. S., AND GESSLER, A. M., *J. Phys. Chem.* **63**, 1376 (1959).

## THE AEROSOL EFFICIENCY AND PRESSURE DROP OF A FIBROUS FILTER AT REDUCED PRESSURES<sup>1</sup>

S. C. Stern, H. W. Zeller, and A. I. Schekman

*Mechanical Division of General Mills, Inc., Minneapolis, Minnesota*

*Received August 13, 1959, revised June 13, 1960*

### ABSTRACT

The collection efficiency of an Institute of Paper Chemistry fibrous filter for mono-dispersed aerosols of  $0.026\ \mu$  to  $1.71\ \mu$  diameter and the resistance to flow through the filter were investigated experimentally at reduced pressures which simulate air densities in the stratosphere. Single fiber efficiencies in the diffusion and impaction regimes were calculated and compared with theory. Resistance to flow through the mat was analyzed in terms of a drag coefficient of a single fiber imbedded in a mat or flow through a bed composed of capillary tubes. The experimental results show the dominant effects of slip flow in increasing collection efficiency and reducing pressure drop through the filter at reduced pressures.

### INTRODUCTION

The injection of radioactive debris into the stratosphere as a result of nuclear weapons tests has made it mandatory to monitor the concentration of specific radioactive species in the stratosphere in order to determine long-range potential hazards due to fall out. The aerosol collection efficiency and pressure drop of a fibrous mat as a function of free stream velocity and reduced pressure are, therefore, prerequisites that must be determined before a stratospheric sampling device employing a filter mat can be designed. Additional filter mat requirements are a high collection efficiency for micron sized particles concurrent with a minimum pressure drop across the filter at high flow rates.

Both efficiency of collection and pressure drop are intimately related to linear velocity of sampling, filter porosity, fiber diameter, and mat thickness. An understanding of the mechanisms involved in particle collection on a fiber and flow about a fiber is fundamental in the final selection or design of a fibrous mat for collecting the particulates resident in the stratosphere. The mechanisms considered responsible for aerosol filtration are diffusion, interception, and inertial impaction (1). The mechanism of diffusion postulates that the Brownian motion of a very small particle, embedded and moving in a fluid at low velocities, is sufficient to cause a

<sup>1</sup> This work was sponsored by the U. S. Atomic Energy Commission under Contract AT(11-1)-401.

particle not to follow its initial streamline flow and to deposit and adhere to a fiber on contact. Inertial impingement against fibers is a removal mechanism for large particles moving in an air stream at high velocities. Owing to inertia, impingement on an obstruction occurs because particles resist directional change and tend to continue along paths independent of streamline flow. Interception is the removal mechanism for particles, moving along streamlines of a fluid, that approach within a distance of a fiber equal to the radius of the particle. La Mer (2) and Gallily (3) have shown that efficiency is also affected by charged aerosol particles and "bounce off" of particles from the surfaces of fibers at critical velocities. These mechanisms were not considered in this study, and their effects, if they exist for the solid particles and filter mat used in this study, are masked.

Although a theory of filtration does not exist for all particle sizes and filter face velocities, mathematical models have been proposed to predict for diffusion and inertial impaction regimes (1) the efficiency of a single fiber embedded in a filter, (2) isolated single fiber efficiency, and (3) total filter mat efficiency. These advances in the present knowledge of aerosol filtration by fibrous mats can be credited to Wong (4), Davies (5), Chen (6), Langmuir (7), Friedlander (8), Ramskill and Anderson (9), and La Mer (10).

A number of theories have been advanced to predict pressure drop across filters based on the following models: (a) a model (11) in which the filter is considered to be a series of interconnected channels and in which the pressure drop through these channels obeys Darcy's law (12), and (b) a model (6) in which the pressure drop across a unit thickness of a filter is the total aerodynamic drag on the fibers in a unit volume of the filter. An appraisal of these theories and a comparison with experimental data from mats with well-defined physical characteristics have been made by both Wong (4) and Chen (6).

In the main, filter efficiency and pressure drop at reduced pressures have received only slight experimental or theoretical attention (13). Since this laboratory is concerned with the sampling of particulate matter in the stratosphere, experimental procedures have been developed to study filtration with monodispersed aerosols and pressure drop through fibrous mats under simulated stratospheric densities. These experimental techniques, the efficiency results obtained with a viscose fiber filter mat, and the extension of pressure drop and filtration theories to reduced pressures are discussed in this paper.

#### DESCRIPTION OF TEST APPARATUS

A survey of the literature will disclose numerous experimental apparatus (14, 15) for determining efficiency and pressure drop through filters. However, none of these test methods function at reduced pressures. The test



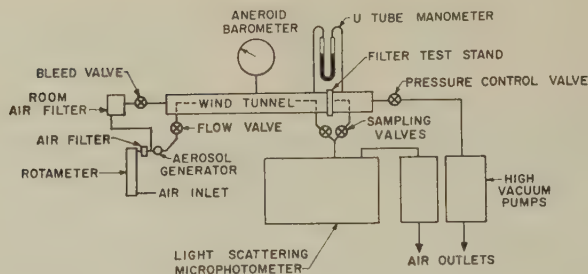


FIG. 1. Schematic diagram of test equipment for determining collection efficiency and pressure drop of filter mats.

apparatus developed in our laboratory is unique in the sense that filter efficiency and pressure drop as a function of free stream velocity can be determined in a wind tunnel at simulated air densities between 1000 and 17 millibars pressure.

A schematic diagram of the test equipment is shown in Fig. 1. The major components are (1) an aerosol generator;<sup>2</sup> (2) a wind tunnel section which houses a filter test stand, (3) a vacuum system, and (4) a light-scattering microphotometer for assaying aerosol concentrations.<sup>3</sup>

The aerosol generator is an all-glass, filtered air-operated Vaponefrin nebulizer which produces from a hydrosol aqueous droplets which are initially about 0.5 to 2.5  $\mu$  diameter. Monodispersed homogeneous aerosols are produced by the dispersion and subsequent evaporation of these aqueous droplets which contain, in the main, a single particle. The chance of two particles being present simultaneously in a single evaporating water droplet is 1 in 100, owing to dilution of the hydrosol concentration. Dilutions are made with double-distilled, "particle-free" water. The generated aerosol concentrations are about  $10^6$  particles per cubic centimeter and aerosol homogeneity is checked by electron microscopic measurement of the size of particles impacted at reduced pressure on a wire mesh grid supporting a collodion substrate. Six discrete aerosol sizes between 0.088  $\mu$  and 1.171  $\mu$  in diameter are obtained by nebulizing dilute suspensions of polystyrene latex spheres.<sup>4</sup> A 35 m $\mu$  homogeneous aerosol is generated by aerosolizing a dilute aqueous suspension of T-3 *E. coli* phage. A 26 m $\mu$  diameter homogeneous aerosol is produced by dispersion of a dilute dialyzed suspension of inactivated Type 3 poliomyelitic virus obtained by processing Salk polio vaccine (16).

<sup>2</sup> Vaponefrin Nebulizer No. 166, Vaponefrin Co., P.O. Box 24, Upper Darby, Pa.

<sup>3</sup> Model 4-6001, American Instrument Co., Silver Springs, Md. (equipped with quartz optics).

<sup>4</sup> Polystyrene spheres furnished by the Physical Research Laboratory, Dow Chemical Co., Midland, Michigan.



The wind tunnel filter test facility (Fig. 1) is fabricated from two pieces of 4-inch diameter aluminum tubing. One piece, which is 48 inches long, has a Stairmand diffuser on an aerosol inlet tube located ten pipe diameters upstream of a filter test stand and an axially centered aerosol sampling tube located 4 inches upstream of the filter. The second section of the tunnel is 16 inches in length and has an axially centered aerosol sampling tube located 4 inches downstream of the filter.

A filter test stand is located between the two sections of the wind tunnel. It consists of a solid rubber gasket, cut to the size of the inside diameter of the wind tunnel, which is sandwiched between two smaller phenolic rings. These rings have matched in-line circular cross-sectional openings. The filter mat is placed taut between the phenolic rings and rubber gasket to fill the opening. A fine mesh screen is placed behind the filter mat for support purposes. The rubber gasket and phenolic ring are bolted together so that the outer rim of the filter mat is constantly under compression. This prevents the aerosol stream from bypassing the mat. The filter test stand is placed between the two wind tunnel sections with the rubber gasket bearing against end plates on the pipe ends. Under vacuum the gasket serves as an air seal and holds the two pipe sections together.

As shown in Fig. 1, three pressure taps are located in the wind tunnel sections. One tap is connected to a Wallace and Tiernan microbarometer which measures absolute pressure in the wind tunnel. The other taps are connected to a differential manometer to measure pressure drop across the filter paper.

The vacuum system serves several purposes. It is used to reduce and maintain a desired air density in the wind tunnel concurrent with providing air flow through the wind tunnel section. An auxiliary vacuum system is used to bleed aerosol samples upstream and downstream of the filter into a highly illuminated viewing volume of a quartz window aerosol cell which is part of a light-scattering photometer equipped with quartz optics.

In practice, the wind tunnel is first evacuated to a desired reduced pressure and an aerosol generated by admitting filtered air into the nebulizer. Sampling valves to the photometer are then opened, and air inlet and outlet control valves are adjusted so that the vacuum system maintains the desired reduced pressure and air flow through the tunnel. At least three aerosol efficiency tests are conducted for each particle size and free stream velocity. Tests are conducted in less than 2 minutes. During this period, aerosols upstream and downstream of the filter are passed sequentially through a quartz window aerosol cell in a light-scattering photometer to determine relative concentrations at either  $90^\circ$  or in a near forward position. The pressure drop across the filter mat is monitored continuously during these tests, and all data are rejected if the drop exceeds by 1.0% the initial pressure drop.

TABLE I  
Physical Properties of the Institute of Paper Chemistry (IPC) Fibrous  
Filter Mats

Material	Viscose
Mat thickness	0.084 cm.
Average fiber diameter	17 $\mu$
Fiber density	1.49 g./cm. <sup>3</sup>
Bulk density	0.189 g./cm. <sup>3</sup>
Average pore diameter	170 $\mu \pm 60$
Porosity	90%
Fiber volume	10%

The filter mat selected after test for sampling aerosols at reduced pressure was fabricated by the Institute of Paper Chemistry (IPC), Appleton, Wisconsin. Its physical properties are shown in Table I. It should be noted that the fibers of this mat had been impregnated with an organic adhesive by the manufacturer in order to prevent particle "bounce off" in the range of velocities from a few to 3000 ft./min.

#### DISCUSSION OF RESULTS

##### *Collection Efficiency at Reduced Pressures*

The aerosol filter efficiency of the filter was determined at the ambient pressure in the laboratory and at 465, 140, 53, and 24 millibars pressures. These data, in terms of aerosol collection efficiency as a function of particle size and filter face velocity for constant pressures, are plotted in Figs. 2-6. Since tests included velocities from a few to approximately 1000 ft./min., collection efficiency for the near diffusion regime and inertial impac-

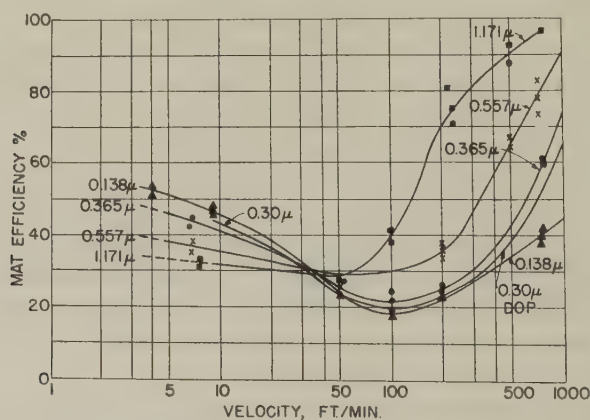


FIG. 2. Experimental collection efficiencies of the IPC filter mat for spherical polystyrene particles of density 1.05 at ambient pressure.

tion regime were obtained. In addition, the efficiency of the IPC filter for an uncharged  $0.3\mu$  liquid droplet aerosol of DOP, as determined by another laboratory, has been plotted in Fig. 2. These data permit a comparison between liquid and solid aerosol efficiencies and a qualitative estimate of any electrostatic effects.

From the test data shown in Figs. 2-6, the following conclusions can be made:

1. A minimum efficiency exists for each particle size at ambient and reduced pressures. This minimum occurs at a point in the efficiency curve where diffusion effects are at a minimum and inertial effects are beginning to dominate the mechanism of collection. This phenomenon has been

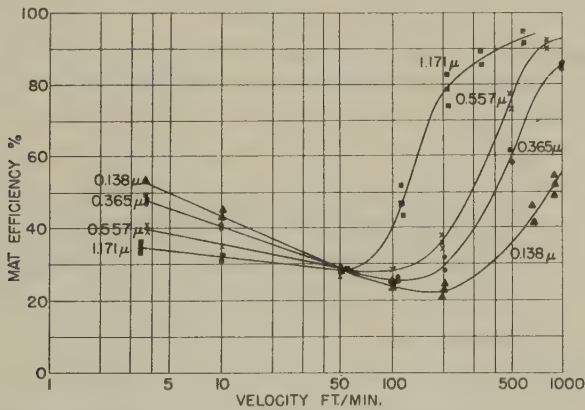


FIG. 3. Experimental collection efficiencies of the IPC filter mat for spherical polystyrene particles of density 1.05 at 465 mb. pressure.

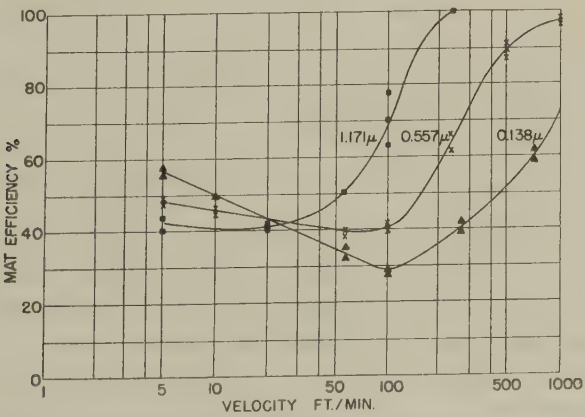


FIG. 4. Experimental collection efficiencies of the IPC filter mat for spherical polystyrene particles of density 1.05 at 140 mb. pressure.

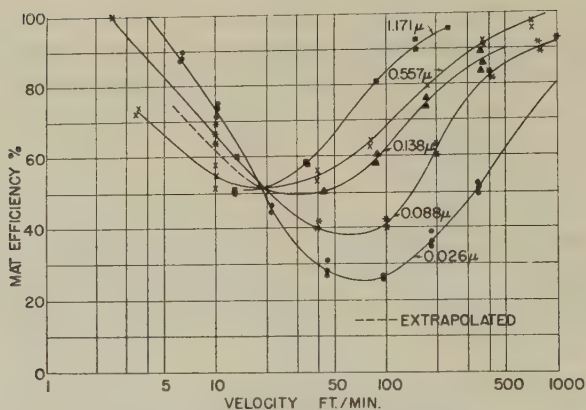


FIG. 5. Experimental collection efficiencies of the IPC filter mat for spherical polystyrene particles of density 1.05 and spherical poliomyelitic particles of density 1.23 at 53 mb. pressure.

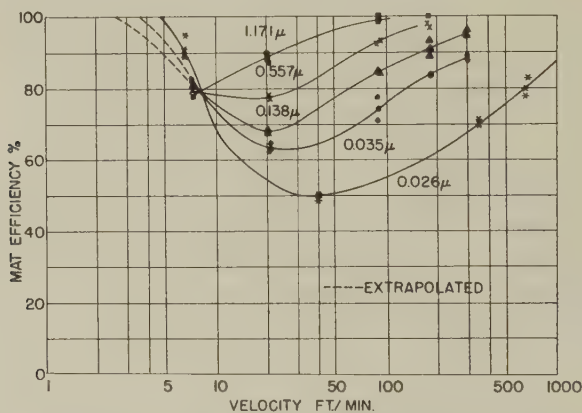


FIG. 6. Experimental collection efficiencies of the IPC filter mat for spherical polystyrene particles of density 1.05 and spherical T-3 *E. Coli* phage and poliomyelitic particles of density 1.23 at 23 mb. pressure.

reported by Smith and Surprenant (17) and Ramskill and Anderson (9) but not by La Mer (18).

2. A unique velocity exists where collection efficiency is the same for all particle sizes. This velocity shifts to lower values with reduction in pressure. The presence of an "isoefficiency" point in the efficiency curve had previously been reported by Chen (6).

3. For a given particle size and face velocity, efficiency increases with reduction in pressure.

4. In the inertial impaction regime efficiency increases with increase in particle size.

5. In the diffusion regime aerosol efficiency increases with smaller particle size.

6. At extremely low pressures (24 millibars) approximately 100% collection efficiency for millimicron particulates can be obtained by either diffusion or impaction mechanisms.

7. In the diffusion regime no particle size of maximum penetration was found to exist. This is contrary to theories proposed by Langmuir (19) and Gillespie (20) but is in substantial agreement with experimental results of other investigators (9).

8. In the impaction regime, the collection efficiency for an uncharged DOP liquid droplet aerosol of diameter  $0.3\mu$  and density 0.984 is in accordance with theory. As shown in Fig. 2, the efficiency curve for this aerosol lies just below and parallel to the efficiency curve for a polystyrene aerosol of diameter  $0.365\mu$  and density of 1.05. In the near diffusion regime (velocities  $\leq 30$  ft./min.) the efficiency for the DOP  $0.3\mu$  aerosol lies just above and parallel to the efficiency curve for the  $0.365\mu$  polystyrene aerosol; this again is in accordance with theory. From these data it is evident that the IPC filter does not discriminate between liquid and solid aerosol particulates and that if the polystyrene aerosol is charged, the role of electric forces in the filtration of this aerosol is relatively minor for this study.

The increase in collection efficiency with reduction in pressure is compatible with theory. Aerosol penetration through a filter in the diffusion regime is a function of the diffusion parameter,  $D$ , and in the impaction regime it can be shown that aerosol penetration is a function of the impaction parameter,  $\psi$ . These parameters can be expressed as follows (6):

$$D = \frac{1}{v d_f} \left( \frac{C k T}{3 \pi n d_p} \right) = \frac{D_{BM}}{v d_f}; \quad [1]$$

$$\psi = \frac{C \rho_p v d_p^2}{18 n d_f}. \quad [2]$$

Both parameters are a direct function of the Cunningham correction to the Stokes equation for the steady or terminal velocity of a sphere falling in a fluid in which slip occurs between fluid and sphere. This correction for slip may be expressed as (21):

$$C = 1 + \frac{2 \lambda}{d_p} \left[ 1.23 + 0.41 e^{-0.44 d_p / \lambda} \right], \quad [3]$$

when

$$0.1 < \frac{2 \lambda}{d_p} < 134.$$

A reduction in pressure results in an increase in the mean free path,  $\lambda$ , a corresponding increase in the absolute value of  $D$  and  $\psi$ , and a subse-



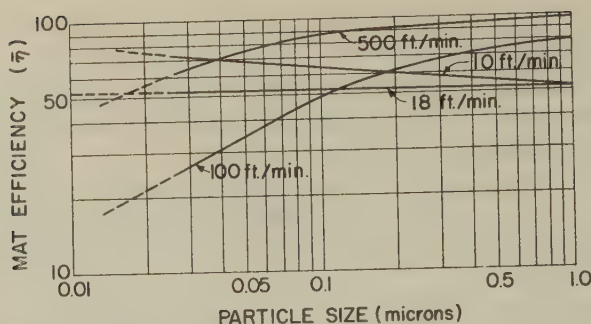


FIG. 7. Collection efficiencies of the IPC filter mat at 53 mb. in the near diffusion, transition, and impaction regimes for spherical particles of densities 1.05 and 1.23.

quent decrease in aerosol penetration. It can be seen from Eq. [3] that for constant values of  $\lambda$  large particles are affected far less by the phenomenon of slip than small particles.

The test data obtained at 53 millibars pressure have been replotted in Fig. 7 to illustrate collection efficiency as a function of particle size for free stream velocities of 10, 18, 100, and 500 ft./min., a range covering diffusion, transition, and impaction regimes. From these data it can be seen that at the two higher velocities efficiency decreases as the particle size decreases, efficiency is constant at 18 ft./min., and efficiency increases at 10 ft./min. with decrease in particle size. Plotting the data in this way makes it possible to predict the collection efficiency of aerosols larger and smaller than those actually tested.

#### *Comparison of Theoretical and Experimental Efficiencies*

The major objective in theoretical studies of aerosol collection by fibrous mats is the development of a mathematical expression to predict efficiency from physical characteristics of the mat and the nature of the aerodynamic flow through the filter. The solution of this problem requires the calculation of the efficiency of a single fiber imbedded in a filter and the use of single fiber efficiency to calculate overall filter efficiency.

If the efficiency of a single fiber imbedded in a mat of known porosity is  $\eta_\alpha$ , it can be shown that overall mat efficiency  $\bar{\eta}$  is:

$$\bar{\eta} = 1 - \exp \left\{ - \frac{4}{\pi} \frac{\alpha}{d_f} \frac{h}{d_f} \eta_\alpha \right\}. \quad [4]$$

The numerical value for  $\eta_\alpha$  should differ from  $\eta_0$ , the isolated single fiber efficiency, mainly because of the different flow conditions existing in the fibrous mat and certain physical and geometrical characteristics of the filter such as fiber orientation and fiber size distribution.

In the diffusion regime, Langmuir (19) has proposed that  $\eta_\alpha$  can be calculated from the expression:

$$\eta_\alpha = \frac{1}{2(2.0 - \ln Re)} \left[ 2 \left( 1 + \frac{2x_0}{d_f} \right) \ln \left( 1 + \frac{2x_0}{d_f} \right) - \left( 1 + \frac{2x_0}{d_f} \right) + \frac{1}{1 + \frac{2x_0}{d_f}} \right], \quad [5]$$

where

$$\frac{x_0}{d_f} = \frac{1}{2} \frac{1}{d_f} \left[ \frac{35.8 D \alpha n h}{\Delta p} \right]^{1/3}.$$

On sound theoretical grounds Torgeson (22) has recently shown that  $\eta_\alpha$  in the diffusion regime can be expressed as follows:

$$\eta_\alpha = 0.755 \left( \frac{C_{D\alpha} Re}{2} \right)^{0.4} Pe^{-0.6}, \quad [6]$$

where  $C_{D\alpha}$  is the drag coefficient for a fiber imbedded in a mat and  $Re$  is  $\frac{\rho d_f v}{n}$ . The dimensionless factor  $\left( \frac{C_{D\alpha} Re}{2} \right)$  is obtained from filter pressure drop characteristics from a relationship developed by Chen (6):

$$\left( \frac{C_{D\alpha} Re}{2} \right) = \frac{\pi \Delta p}{4 v} \frac{1 - \alpha}{\alpha} \frac{d_f^2}{nh} \quad [7]$$

A comparison between experimental values for  $\eta_\alpha$  computed from Eq. [4] and theoretical values for  $\eta_\alpha$  computed from Eqs. [5] and [6] for the diffusion regime have been plotted against the nondimensional Peclet number in Fig. 8. The drag parameter  $\frac{C_{D\alpha} Re}{2}$  for IPC paper was obtained from pressure drop data.

Agreement between experimental data and Torgeson's diffusion theory is quite good. The Langmuir theory yields values for  $\eta_\alpha$  which are approximately half the values for  $\eta_\alpha$  computed from the Torgeson theory. Total mat efficiency for the diffusion regime (low Peclet numbers) computed from a value for  $\eta_\alpha$  calculated from Eqs. [6] and [7] should, therefore, yield satisfactory results for IPC paper.

In the impaction regime it has been found that single fiber efficiency,  $\eta_\alpha$ , is nearly equal to the impaction parameter  $\psi$ . This relationship was established by plotting single fiber efficiency,  $\eta_\alpha$ , against  $\psi^{1/2}$ , the classical parameter for inertial impaction of a particle on a cylindrical fiber placed crosswind to the direction of air flow. These data, obtained from Figs. 2-6,

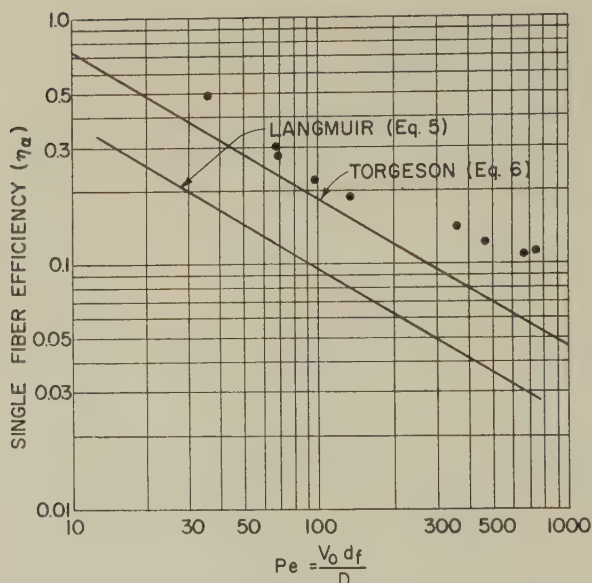


FIG. 8. Comparison of experimental and theoretical values of single fiber efficiencies in the diffusion regime.

are shown in Fig. 9, with additional values of  $\eta_\alpha$  obtained from IPC tests conducted by Ramskill and Anderson (9).

For low Reynolds numbers, i.e.,  $\simeq 0.2$ , Davies (5) has proposed the following empirical expression for  $\eta_\alpha$ , which combines the physical properties of the filter with the mechanisms of diffusion, interception, and impaction:

$$\eta_\alpha = (0.16 + 10.9\alpha - 17\alpha^2) \cdot [R + (0.5 + 0.8R)(\psi + D) - 0.1052R(\psi + D)^2]. \quad [8]$$

The diameter of the fiber used in calculating  $\psi$  and  $R$  in Eq. [8] is a virtual size obtained from Davies' (5) empirical pressure drop equation:

$$\Delta p = \frac{70 \, n v h \, \alpha^{1.5}}{d_f^2} (1 + 52 \, \alpha^{1.5}),$$

where  $d_f$  is the virtual fiber diameter.

For  $R \leq 0.1$ ,  $\alpha = 0.1$  and  $Re \leq 0.2$  (values applicable for the IPC tests at reduced pressure),  $\eta_\alpha$  has been calculated from Eq. [8] for assumed values of  $\psi$  and plotted against  $\psi^{1/2}$ . As shown in Fig. 9, the agreement between theoretical and experimental values of  $\eta_\alpha$  is satisfactory. This implies that total mat efficiency for the IPC filter can be predicted from Davies' theory. The validity of Eq. [8] has not been verified by other investigators (4) who

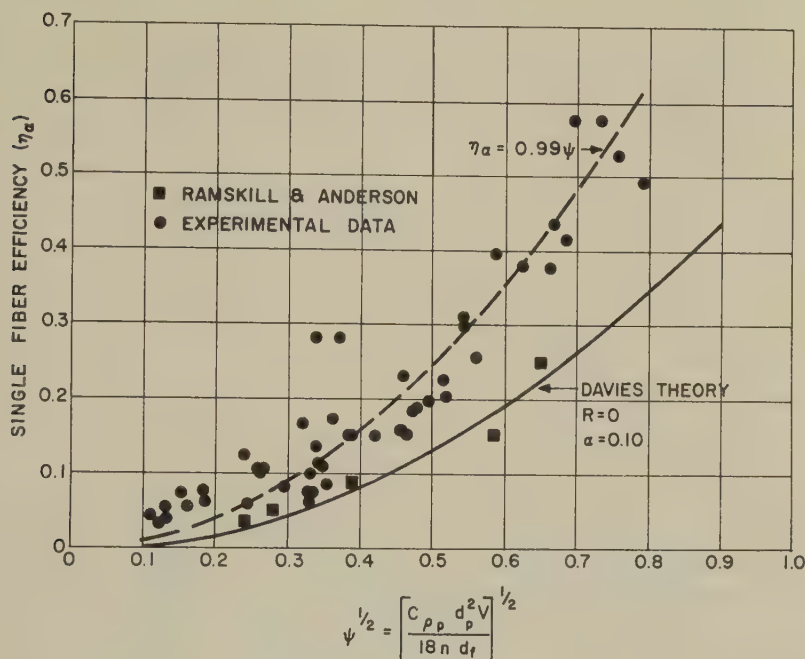


FIG. 9. Comparison of experimental and theoretical values of single fiber efficiencies in the impaction regime.

used fiber glass mats and may be due primarily to the presence of an adhesive on the fibers of the IPC mats which precludes any bounce off of impacted particles.

#### *Pressure Drop through IPC Filters at Reduced Pressures*

Using the test apparatus shown in Fig. 1, pressure drop as a function of free stream velocities was determined at reduced pressures. These experimental data of  $\Delta p$  vs.  $v$  at a constant pressure are shown in Fig. 10. For velocities  $\leq 200$  ft./min., pressure drop at constant pressure varies directly with velocity. Furthermore, as the pressure is reduced, the value of  $\Delta p/v$  decreases. These data indicate that viscous flow exists through the filter mat and that Darcy's law (12) is applicable. This law states that:

$$\Delta p = v n_0 h / B_0. \quad [9]$$

As shown by Davies (23), the specific permeability coefficient for viscous flow,  $B_0$ , is a physical property of the filter and is related to fiber diameter and bulk density of the filter. This parameter is independent of viscosity, air density, and pressure. It may be calculated from the experimental data obtained at 1000 millibars pressure.

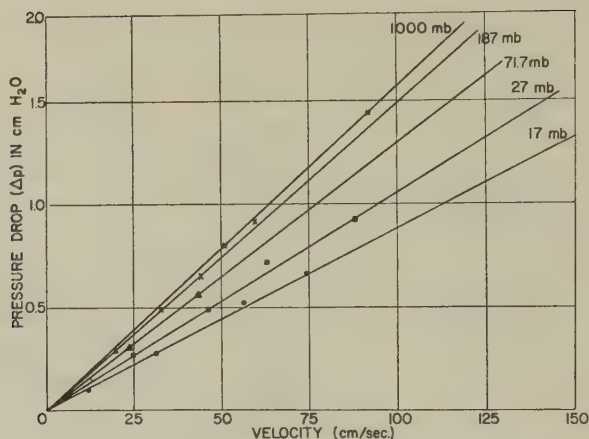


FIG. 10. Experimental pressure drop across the fiber mat.

According to kinetic theory the viscosity of a gas at constant temperature is independent of pressure. However, if a fibrous mat is considered to be an interconnected bundle of capillary channels, slip will occur at the walls of these channels when the mean free path of the rarefied gas approaches the diameter of the channel. Under these circumstances the reduction in the apparent viscosity of the rarefied gas may be responsible for the decrease in pressure drop through the mat at reduced pressure.

Equation [9] may be modified to account for slip through the filter by introducing a correction for slip flow. Equation [9] then takes the form:

$$\Delta p = \frac{v n_0 h}{C_a B_0}, \quad [10]$$

where  $C_a$  is a correction for slip, equal to  $n/n_0$ , which can be calculated from pressure drop data, and  $n$  is the apparent viscosity of the rarefied gas.

Using the experimental data for the IPC filter plotted in Fig. 10 and the physical characteristics of the filter (Table I) it can be shown that Eq. [10] may be expressed, to a high degree of accuracy, as:

$$\frac{\Delta p}{v} = \frac{0.0161}{1 + 13.75/p}, \quad [11]$$

where  $\Delta p$  is the pressure drop in centimeters of water,  $v$  is the face velocity in centimeters per second, and  $p$  is the pressure in millibars.

The modified Cunningham correction for slip,  $C_a$ , can be expressed as:

$$C_a = 1 + 13.75/p,$$

and the term  $n_0 h/B_0$  equals 0.0161. Calculated values of  $C_a$  for the IPC filter at reduced pressures are presented in Table II.



TABLE II  
*Modified Cunningham Correction Factors for IPC Filter*

Pressure (mb.)	$C_a = 1 + 13.75/p$
1000	1.0138
465.5	1.0294
187.5	1.0734
71.7	1.1916
44.5	1.309
27.4	1.509
17.07	1.810

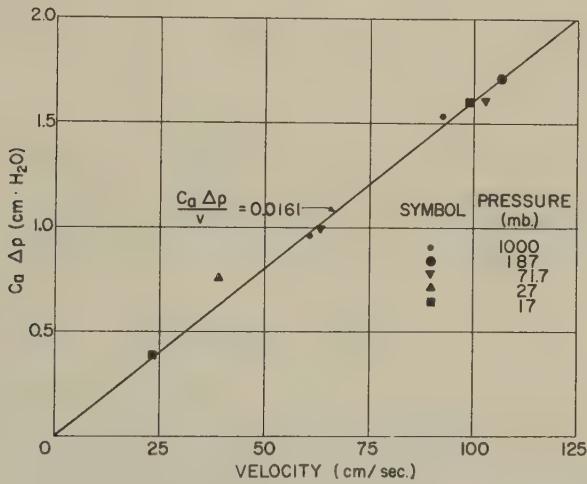


FIG. 11. Pressure drop relationship for IPC paper at reduced pressures.

From Eq. [11] it can be seen that for zero slip  $\Delta p/v$  equals 0.0161. When slip occurs,  $C_a \Delta p/v = 0.0161$ . A plot of  $C_a \Delta p$  vs.  $v$ , Fig. 11, indicates that  $C_a \Delta p$  is independent of pressure, implying that pressure drop for the IPC filter may be predicted for pressures between 1000 and 17 millibars for moderate velocities. It should be possible to extend this approach to other fibrous filter mats.

If one accepts the premise that pressure drop across a unit thickness of a filter is the total drag force on the fibers in a unit volume of the filter, then following Chen (6), pressure drop can be expressed as:

$$\Delta p = \frac{4}{\pi} \left[ \frac{C_{D\alpha} Re}{2} \right] \frac{\alpha}{1 - \alpha} \frac{n v h}{d_f^2} \tag{12}$$

The experimental pressure drop data for IPC filters have been used to compute values of  $C_{D\alpha} Re/2$ , which are plotted against  $Re$  in Fig. 12 for

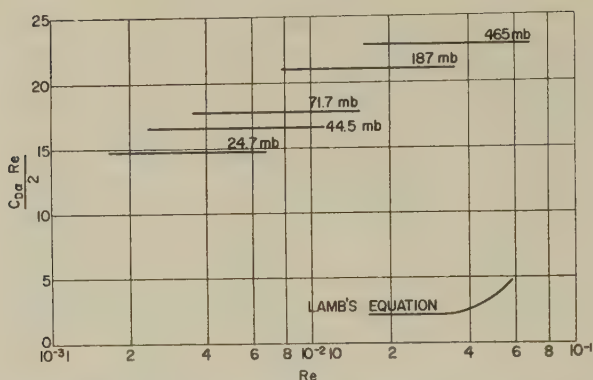


Fig. 12. Drag coefficient of a single fiber imbedded in a mat compared with Lamb's theory for a single isolated fiber.

constant values of pressure. The drag coefficient for a cylinder computed from Lamb's theory (24) for an isolated cylindrical fiber  $C_D = 8/Re(2.00 - \ln Re)$ , has also been plotted in Fig. 12 against  $Re$ . It will be noted that Lamb's theory for an isolated fiber underestimates the drag coefficient of a fiber subject to interfiber interference by factors of five (5) to ten (10).

### CONCLUSIONS

Experimental methods have been developed to determine the aerosol collection efficiency of fibrous filter mats for particles in the micron and submicron size range under simulated high-altitude conditions. The collection efficiency of an IPC fibrous mat was determined for particles ranging in size from  $0.026 \mu$  to  $1.71 \mu$  and for simulated altitudes from near sea level to 24 millibars pressure. Single fiber efficiency in the impaction regime was found to be nearly equal to the classical impaction parameter  $\psi$ . These data are in agreement with other experimental results reported in the literature. The experimental impaction data are also in good agreement with a theory proposed by Davies. Experimental collection efficiencies in the diffusion regime are in reasonably good agreement with a new diffusion theory proposed by Torgeson. A diffusion theory of Langmuir was found to underestimate single fiber collection efficiency by a factor of two.

The experimental and theoretical results of this study show clearly the dominant effects of slip flow in the filtration of very small particles at reduced pressure.

In agreement with results obtained in previous investigations, it has been found experimentally that the drag coefficient of a single fiber imbedded in a mat is considerably higher than the isolated fiber drag coefficient computed from Lamb's theory. It has also been found that a linear

relationship exists between  $C_a \Delta p$  and  $v$ , which is independent of pressure over the range of test conditions. This implies that pressure drops for IPC mats may be predicted for many reduced pressures and velocities.

### ACKNOWLEDGMENTS

The authors acknowledge gratefully the assistance of Richard Olson and Jerry Ungs for performing experimental work. We are also indebted to Lee Torgeson and Sam P. Jones for their very helpful discussions and suggestions.

### GLOSSARY

- $B_0$  = specific permeability coefficient for viscous flow.  
 $C$  = Cunningham correction factor.  
 $C_a$  = modified Cunningham correction factor computed from pressure drop data through a fibrous mat.  
 $C_D$  = drag coefficient of isolated fiber.  
 $C_{Da}$  = drag coefficient of fiber imbedded in a mat.  
 $D$  = diffusion parameter =  $\frac{1}{Pe}$ .  
 $D_{BM} = \frac{CkT}{3\pi nd_p}$  = diffusion coefficient.  
 $d_f$  = fiber diameter.  
 $d_p$  = aerosol particle diameter.  
 $h$  = thickness of fiber mat measured parallel to the direction of flow.  
 $k$  = Boltzmann constant.  
 $n$  = viscosity of the gas (poise).  
 $n_0$  = viscosity of the gas in the absence of slip flow.  
 $Pe$  = Peclet number,  $d_f v / D_{BM}$ .  
 $p$  = pressure (mb.).  
 $\Delta p$  = pressure drop across the fiber mat.  
 $R = d_p / d_f$  = interception parameter (dimensionless).  
 $Re = d_f v \rho / n$ , Reynolds number based on fiber diameter.  
 $T$  = gas temperature (degrees absolute).  
 $v$  = free stream or filter face velocity.  
 $x_0$  = effective fluid layer thickness from which particles are removed by diffusion.  
 $\alpha = \rho_b / \rho_f$ , fiber volume fraction.  
 $\bar{\eta}$  = total efficiency of aerosol collection on the mat.  
 $\eta_\alpha$  = efficiency of a single fiber imbedded in a mat.  
 $\eta_0$  = single isolated fiber efficiency.  
 $\lambda$  = mean free path of the gas molecule.  
 $\rho$  = density of the gas.  
 $\rho_b$  = bulk density of the mat.  
 $\rho_f$  = density of the fiber.  
 $\rho_p$  = density of aerosol particle.  
 $\psi = \frac{C\rho_p d_p^2}{18nd_f}$ , inertial parameter.

### REFERENCES

1. FRIEDLANDER, S. K., *et al.*, "Handbook on Air Cleaning." U. S. Government Printing Office, Washington, D. C., 1952.

2. LA MER, V. K., *et al.*, "Filtration of electrically charged aerosols." N. Y. Office, AEC-514, June 30, 1952.
3. GALLILI, I., AND LA MER, V. K., "On the behavior of liquid droplets after impinging on solid surface." *J. Phys. Chem.* **62**, 1295 (1958).
4. WONG, J. B., *et al.*, "Collection efficiency of aerosol particles and resistance to flow through fiber mats." *J. Appl. Phys.* **27**, 161-169 (1956).
5. DAVIES, C. N., "The separation of airborne dust and particles." *Inst. Mech. Engrs. (London), Proc.* **1B**, 185-213 (1952).
6. CHEN, C. Y., "Filtration of aerosols by fibrous media." *Chem. Revs.* **55**, 595-623 (1955).
7. RODEBUSH, W. H., *et al.*, "Report on filtration of aerosols and the development of filter materials." U. S. Office of Scientific Research & Development, Report No. 865 (1942) (PB 99,669).
8. FRIEDLANDER, S. K., "Mass and heat transfer to single spheres and cylinders at low Reynolds numbers." *Am. Inst. Chem. Engrs. J.* **3**, 43-48 (1957).
9. RAMSKILL, E. A., AND ANDERSON, W. L., "The inertial mechanism in the mechanical filtration of aerosols." *J. Colloid Sci.* **6**, 416-428 (1951).
10. LA MER, V. K., AND DROZIN, V. G., "Filtration of monodisperse solid aerosols." *Proc. 2nd Intern. Congr. Surface Activity, London*, 1957.
11. SULLIVAN, R. R., AND HERTEL, K. L., *J. Appl. Phys.* **11**, 761 (1940).
12. DARCY, H. P. G., "Les fontaines publiques de la ville de Dijon." Victor Dalmont, Paris, 1856.
13. TSIEN, H. S., "Superaerodynamics. Mechanics of rarefied gas." *J. Aeronaut. Sci.* **13**, 653 (1946).
14. Massachusetts Institute of Technology. CWS Development Laboratory. Test Methods conference. Group VI—Filter tests. Sept. 2, 1952, pp. 1-2, 45-63.
15. Great Britain. Chemical Defense Experimental Establishment. Porton. Memo No. 17. Standard methods of test (chemical and physical) employed in C. W. investigation. I(3) Tests on particulate filters (March 7, 1942).
16. STERN, S. C., *et al.*, "A simple technique for the generation of homogeneous aerosols." *J. Appl. Phys.* **30**, 952 (1959).
17. SMITH, W. J., AND SURPRENANT, N. F., "Properties of various filter media for atmospheric dust sampling." Presented to the American Society for Testing Materials, Philadelphia, Pa., July 1, 1953.
18. LA MER, V. K., "Studies on filtration of monodisperse aerosols." U. S. Atomic Energy Commission, N. Y. Office 512, 1951.
19. LANGMUIR, I., Office Scientific Research & Development, Report 865, Sept. 14, 1942.
20. GILLESPIE, T., "The role of electric forces in the filtration of aerosols by fiber filters." *J. Colloid Sci.* **10**, 299-313 (1955).
21. RANZ, W. E., and WONG, J. B., Technical Report No. 4, AEC Contract No. AT(30-3)-28, July 31, 1951.
22. STERN, S. C., *et al.*, General Mills Report No. 1890. Upper Atmosphere Monitoring Program, AEC Contract No. AT(11-1)-401, Jan. 1, 1959.
23. DAVIES, C. N., *Discussions Faraday Soc.* **3**, 127 (1948).
24. LAMB, H., "Hydrodynamics," 6th ed., pp. 609-616. Cambridge University Press, London, 1932.

## EMULSION PARTICLE SIZE II. DETERMINATION OF THE DISTRIBUTION FUNCTION USING THE ULTRACENTRIFUGE<sup>1</sup>

John G. Brodnyan

*Research Laboratories, Rohm & Haas Company, Philadelphia, Pennsylvania*

*Received November 6, 1959; revised February 9, 1960*

### ABSTRACT

The electron microscope has been the only instrument widely used in the determination of the particle size distribution of synthetic latices, although the use of an ordinary laboratory centrifuge has been investigated. In this report the use of a Spinco Model L ultracentrifuge in determining the particle size distributions of several acrylic latices is examined.

It is shown that latices of poly (*n*-butyl methacrylate) and poly ethyl acrylate give experimentally a log radius-normal probability distribution. However, latices of poly (methyl methacrylate) are shown to have their radii distributed normally in one case and log-normally in a second case.

It is also shown that the electron microscope data of Ewart and Carr on polystyrene can fit both the distributions reasonably well. The data of French on poly (vinyl acetate), which are also electron microscope data, indicate that the particle radii are distributed log-normally.

### INTRODUCTION

The latex particles formed by emulsion polymerization are usually of varying sizes, i.e., poly disperse, and the physical properties of the emulsions very often depend upon the size and distribution of the sizes of the particles. Therefore it is important to know how these particle sizes are distributed.

The principal method employed in measuring the particle size distribution of emulsion latices has been that of counting particles on electron micrographs. However, there has also been described in the literature (1) a method based on Stokes' law, involving the use of an ordinary laboratory centrifuge. This use of centrifugal sedimentation in determining particle size is well known in the analysis of such disperse systems as clays, pigments, etc. (2, 3).

The determination of the cumulative distribution function by such a sedimentation method has been critically analyzed by C. Brown (4). He

<sup>1</sup> Presented before the Division of Colloid Chemistry, 136th National Chemical Society Meeting at Atlantic City, September, 1959.



has shown mathematically that sufficiently accurate results can be obtained if the ratio of the length of the centrifuge arm to the distance of travel of the particles to the sampling point is greater than 4.

An ordinary laboratory centrifuge produces rather small centrifugal forces and can sediment only large particles or particles having densities much different from the density of water. Therefore, to determine the particle size distributions of latices having rather small sizes a Spinco Model L ultracentrifuge was used in the work reported here.

### *Description of the Method*

When a sedimenting force acts on spherical particles such as those in latices, data can be correctly analyzed on the assumption that the fractional loss in solids content at a given point in the vessel, after a measurable time interval, corresponds to the weight fraction of dispersed solids consisting of particles larger than a certain calculated radius  $r_c$  (1, 4). For particles with a density greater than water, the case for all the acrylics investigated, this radius is that of a particle which will just reach the point of sampling from the top of the vessel during the experiment. The values of  $r_c$  can be calculated by Stokes' law from the experimental variables using the following equation:

$$r_c^2 = \frac{9}{2} \frac{\eta \ln \frac{(S + X)}{(S)}}{(\rho - \rho_0)\omega^2 t} \quad [1]$$

Here  $\eta$  is the viscosity of the solvent,  $\rho$  and  $\rho_0$  are the densities of the solute and solvent, respectively,  $\omega$  is the angular velocity,  $t$  is the time of centrifugation,  $S$  is the distance of the top of the cell from the axis of rotation, and  $S + X$  is the distance of the point of sampling from the axis of rotation.

The length of the centrifuge arm is approximately 4.6 cm. and the distance of travel of the particles is approximately 0.68 cm. This gives a ratio of 6.8, which, according to C. Brown (4), is sufficient to obtain accurate results.

The density of the solid is calculated from the density of the solution measured with a pycnometer, the density of water, and the solids content, assuming additivity of the volumes.

The emulsions to be centrifuged are diluted to approximately 3% solids with deionized water. The exact concentration  $C_0$  is determined. The centrifuge tubes are filled to a predetermined and reproducible spot, a distance  $S$  from the axis of rotation, and centrifuged for a given time at a measured speed. The centrifuge is then stopped and samples are taken from duplicate tubes by inserting a hypodermic syringe into the tubes a constant distance corresponding to  $S + X$ . The liquid is evaporated to

dryness and the average concentration of the duplicates recorded as  $C_{\omega,t}$ . The ratio  $C_{\omega,t}/C_0$  gives the weight fraction of particles with a radius of  $r_c$  or less.

When the ratio  $C_{\omega,t}/C_0$  is plotted as a function of  $r_c$  a cumulative curve (ogive) is obtained from which one can evaluate the weight-fraction of material between  $r_i$  and  $r_i + \Delta r$ . If the distribution function is a known one, this can be done analytically but for any other function it must be done graphically. This can be done by first dividing the radius axis into a number of small intervals,  $\Delta r$ , starting from the radius at which  $C_{\omega,t}/C_0$  is equal to zero and ending at the radius where  $C_{\omega,t}/C_0$  equals unity. Then the radius at the center of the interval,  $r_i + \Delta r/2$ , is assumed to represent all the particles in the interval and compose the weight fraction calculated by subtracting the value of  $C_{\omega,t}/C_0$  at  $r_i$  from the value of  $C_{\omega,t}/C_0$  at  $r_i + \Delta r$ . In this manner a histogram representing the distribution can be determined. This derived distribution can then be used to derive the weight-average radius,  $r_w$ , the surface-average radius,  $r_s$ , the number-average radius,  $r_n$ , or the number of particles per gram of solid,  $N$ , etc. The radii mentioned are defined by the following equations (5):

$$\begin{aligned} r_n &= \sum_i n_i r_i \\ r_s &= \sum_i s_i r_i = \frac{\sum_i n_i r_i^3}{\sum_i n_i r_i^2} \\ r_w &= \sum_i w_i r_i = \frac{\sum_i n_i r_i^4}{\sum_i n_i r_i^3} \end{aligned}$$

where  $n_i$ ,  $s_i$ , and  $w_i$  are the number, surface, and weight fractions, respectively, of particles of radius,  $r_i$ .

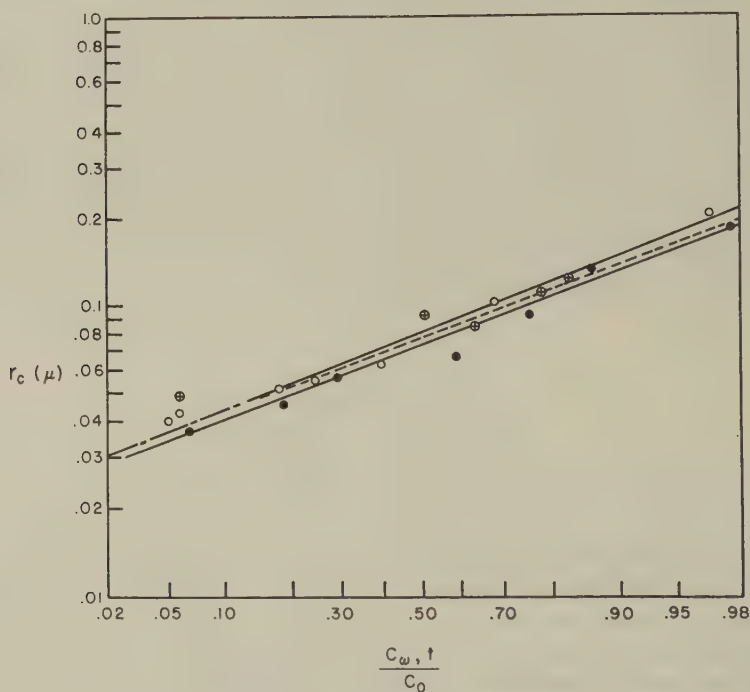
Since the weight fraction,  $w_i$ , is determined directly from the ultracentrifuge analysis, the weight-average radius is given most accurately by the use of that instrument. The number-average radius is determined most accurately by the electron microscope since that instrument determines directly the number fraction. The surface-average radius is determined directly by soap titration (6, 7).

#### Calibration

As a check on the accuracy of the particle sizes determined by the ultracentrifuge a known distribution was made by combining four samples of monodisperse polystyrene latices. The kindness of Dr. J. W. Vanderhoff of Dow Chemical Co. in supplying these samples is appreciated. From the known sizes and weights the arithmetic weight and number-average radii were calculated. These were then compared with the radii computed by the method outlined above using the experimental data obtained from the ultracentrifuge. The comparison is given below:

TABLE I

	Calculated	Experimental	Error (%)
$r_w (\mu)$	0.160	0.163	1.9
$r_n (\mu)$	0.0517	0.046	9.4
$N \frac{(\text{number})}{(\text{g. solid})} \times 10^{-14}$	6.7	7.4	11.0

FIG. 1. Poly (*n*-butyl methacrylate).

The agreement is seen to be good, although the number of particles per gram of solid and the number-average radius are not determined as well as the weight-average radius.

#### *Reproducibility of the Technique*

In order to estimate the reproducibility of the ultracentrifuge a sample of poly (*n*-butyl methacrylate) was investigated three different times by two different operators. The data are indicated by different symbols on Fig. 1. There the data have been plotted on graph paper which has a probability grid for the *x*-axis and a logarithmic scale on the *y*-axis, i.e., log-normal paper. The experimental values of the cumulative weight frac-

tion are plotted on the probability scale versus the radii on the logarithmic scale and a straight line is obtained. Therefore, the distribution is said to be log-normal and the distribution function is of the type (5):

$$w_i = \frac{4\pi\rho \sum_i n_i r_i^3}{3 \log \sigma (2\pi)^{1/2} \int_{r_1/\log}^{r_2/\log} \exp \left[ - \frac{(\log r - \log r_g)^2}{2 \log^2 \sigma} \right] d \log r. \quad [2]$$

In the above equation  $w_i$  is the weight fraction between radii  $r_1$  and  $r_2$  where  $r_g$  and  $\sigma$  are the weight geometric mean and the standard deviation, respectively. Only two sets of data cover a sufficient range to calculate the average radii accurately, and these two are compared below. The surface-average radius is also included in the table below.

TABLE II

	$r_w(\mu)$	$r_s(\mu)$	$r_n(\mu)$	$N \times 10^{-15}$
1st set	0.090	0.071	0.045	1.08
2nd set	0.082	0.066	0.044	1.04
Average	$0.086 \pm .004$	$0.068 \pm .0025$	$0.044_5 \pm 0.0005$	$1.06 \pm .02$
Error (%)	4.7	3.6	1.1	1.9

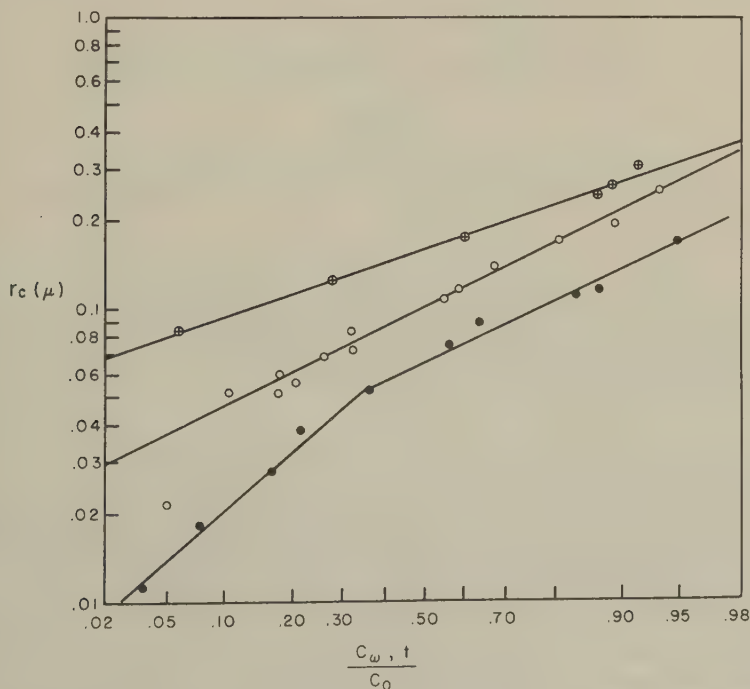


FIG. 2. Acrylic emulsions. ● MMA, anionic soap; ⊕ MMA, nonionic soap; ○ EA, nonionic soap.

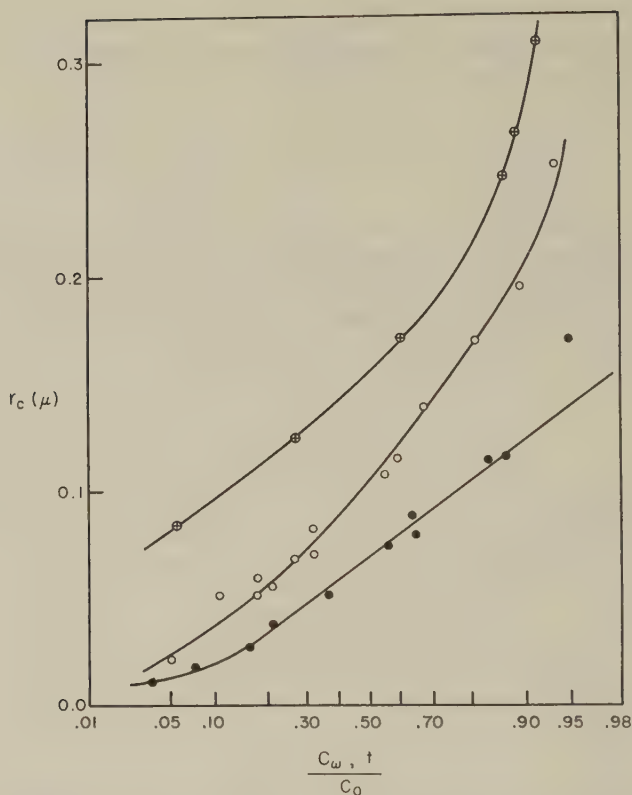


FIG. 3. Acrylic emulsions. ● MMA, anionic soap; ⊕ MMA, nonionic soap; ○ EA, nonionic soap.

Here again the agreement is quite good. The average difference from the mean is taken as the estimate of error. The middle line on Fig. 1 was drawn in to represent all the data, and the average radii predicted by the line agrees with the average values tabulated.

#### *Distribution Functions of Other Acrylic Latices*

Several other acrylic emulsions were investigated: (1) a poly (methyl methacrylate) latex prepared using an anionic emulsifier, (2) a poly (methyl methacrylate) latex prepared using a nonionic emulsifier, and (3) a poly (ethyl acrylate) latex prepared using a nonionic emulsifier.

The experimental data for all three have been plotted on log-normal probability paper in Fig. 2. Rajagopal (8) argues that one can put only limited confidence in points outside the 0.15 to 0.85 region of a normal distribution or log-normal distribution. With the use of this criterion, it appears that (1) does not have a log-normal distribution, i.e., it doesn't



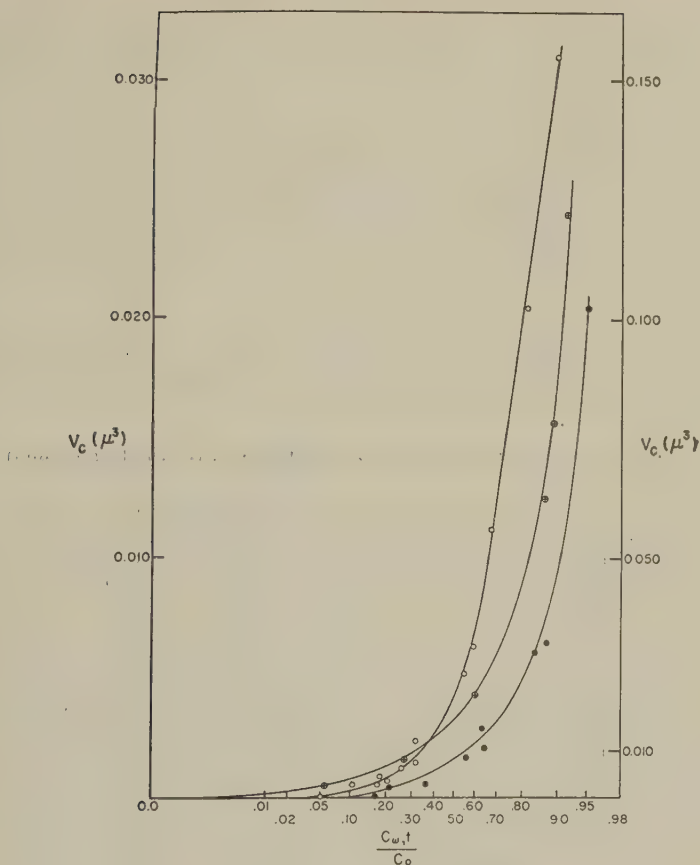


FIG. 4. Acrylic emulsions.

- MMA, anionic soap } left side scale
- EA, nonionic soap } left side scale
- ⊕ MMA, nonionic soap—right side scale

give a straight line, whereas (2) and (3) appear to have this type of distribution.

In Fig. 3 the ultracentrifuge data have been plotted on normal probability paper, i.e., the  $y$ -axis now has a linear scale. Again with the use of the criterion of Rajagopal it appears that (1) is normally distributed while (2) and (3) are not. In Fig. 4 the data have been plotted as volume versus the normal probability function and none of the three have their volumes normally distributed. The above comparisons, although qualitative, seem to be valid.

#### *Nonacrylic Emulsions*

No nonacrylic emulsions were investigated using the ultracentrifuge. However, there are available in the literature electron microscope data on

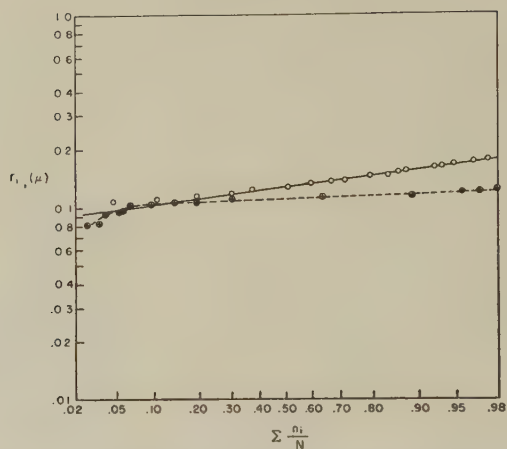


FIG. 5. Nonacrylic emulsions. ○ Poly (vinyl acetate); ⊕ poly (styrene).

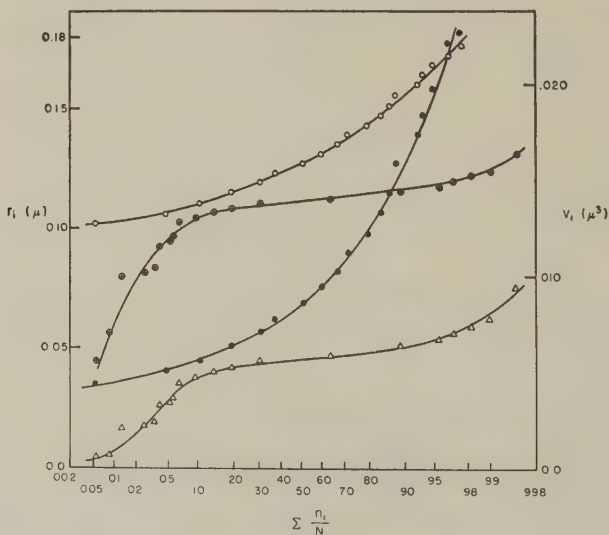


FIG. 6. Nonacrylic emulsions.

	<i>p</i> -VAC	<i>p</i> -STY
$r_i$	○	⊕
$v_i$	●	△

polystyrene (9) and poly (vinyl acetate) (10). Since numbers of particles were counted, cumulative number fraction must be plotted on the probability scale. The data for these two materials are plotted on a log-normal probability graph in Fig. 5. Both sets of data seem to fit this function quite

well. In Fig. 6 both sets of data have been plotted as radius and volume on normal probability paper versus number fraction. The poly (vinyl acetate) data definitely do not fit these distributions and, therefore, we may conclude that this set also has a log-normal distribution. The polystyrene data indicate that the volume may not be normally distributed. However, using Rajagopal's criterion one could say the radius fits a normal distribution. This may be because the distribution is so narrow, since in that case a normal distribution and a log-normal one look very much alike.

### DISCUSSION

It has been shown (11) that if the rate of change of volume of polymer in a polymerizing particle is given by Eq. [3]:

$$\frac{dv}{dt} = \text{constant } r^n, \quad [3]$$

then the type of distribution obtained depends upon the value of the exponent  $n$ . For  $n = 0$  the volumes are distributed normally, for  $n = 2$  the radii are distributed normally, and for  $n = 3$  the logarithms of the radii are distributed normally.

The experimental work presented in the preceding sections indicates that  $n$  equals 3 for poly (vinyl acetate) and 2 to 3 for the poly acrylates and poly methacrylates. However, it was not possible to determine the value of  $n$  accurately by this method for polystyrene. Other data by Vanderhoff *et al.* (12) obtained from competitive growth experiments indicate that  $n = 2.5$  for polystyrene. Ewart and Carr's (9) data can be interpreted (11) to give  $n \simeq 2$ .

At the present time the theory of Smith and Ewart (13) is the only quantitative theory explaining most of the results of emulsion polymerization. It predicts that the rate of polymerization depends upon the number of particles present. They also derived the dependence of this particle number on the initial emulsifier and initiator concentrations. One of the basic assumptions of their derivation of the number dependence is that  $n = 0$ . Since in no case is it possible to show that the volume is definitely normally distributed, one must re-examine this assumption. The fact that a log-normal distribution is usually obtained should be taken into account.

It must be realized, however, that the particle numbers, sizes, and distributions are usually determined on finished emulsions for comparison with rate data gathered at much lower conversions.

### ACKNOWLEDGMENTS

The author wishes to thank Dr. B. E. Larsson for many of the emulsion samples, Mr. E. L. Kelley and Mr. M. Gregory for making many of the measurements, and Mr. J. A. Cala and Dr. G. L. Brown for their continued advice and encouragement.

## REFERENCES

1. NISONOFF, A., MESSER, W. E., AND HOWLAND, L. H., *Anal. Chem.* **26**, 856 (1954).
2. MARSHALL, C. E., *Proc. Roy Soc. (London)* **A126**, 427 (1930).
3. JACOBSEN, A. E., AND SULLIVAN, W. F., *Ind. Eng. Chem. (Anal. Ed.)* **18**, 360 (1946).
4. BROWN, C., *J. Phys. Chem.* **48**, 246 (1944).
5. HERDAN, G., "Small Particle Statistics." Elsevier, New York, N. Y., 1953.
6. MARON, S. H., ELDER, M. E., AND ULEVITCH, I. N., *J. Colloid Sci.* **9**, 89 (1954).
7. BRODNYAN, J. G., AND BROWN, G. L., *J. Colloid Sci.* **15**, 76 (1960).
8. RAJAGOPAL, E. S., *Kolloid-Z.* **162**, 85 (1959).
9. EWART, R. H., AND CARR, C. I., *J. Phys. Chem.* **58**, 640 (1954).
10. FRENCH, D. M., *J. Polymer Sci.* **32**, 395 (1958).
11. BRODNYAN, J. G., *J. Colloid Sci.* **15**, 573 (1960).
12. VANDERHOFF, J. W., VITKUSKE, J. F., BRADFORD, E. B., AND ALFREY, T., JR., *J. Polymer Sci.* **20**, 225 (1956).
13. SMITH, W. V., AND EWART, R. H., *J. Chem. Phys.* **16**, 592 (1948).

### EMULSION PARTICLE SIZE III. PARTICLE SIZE DISTRIBUTIONS DETERMINED BY VARIOUS GROWTH MECHANISMS

John G. Brodnyan

*Research Laboratories, Rohm & Haas Company, Philadelphia, Pennsylvania*

*Received June 24, 1960*

#### ABSTRACT

In a treatment of emulsion polymerization as a stochastic process, the effect of the mechanism of growth of an emulsion polymer particle on the final particle size distribution is examined. If the rate of change of polymer volume is given by:

$$dV/dt = kr^\alpha,$$

where  $k$  is a constant and  $r$  is the radius of the polymer sphere, then it can be shown that for  $\alpha$  equal to 0 the volumes are distributed normally, for  $\alpha$  equal to 2 the radii are distributed normally, and for  $\alpha$  equal to 3 the logarithms of the radii are distributed normally.

The Smith-Ewart theory has  $\alpha$  equal to 0 as a basic assumption in the derivation of the dependence of the number of particles per milliliter of water on soap and initiator concentration. Since the acrylic latices and a poly (vinyl acetate) latex that have been examined do not have their volumes distributed normally, caution must be used in extending the Smith-Ewart results.

#### INTRODUCTION

Such physical properties of a latex as viscosity (1) and minimum film formation temperature (2) have been found to depend on the size and size distributions of the latex particles, indicating the importance of knowledge of latex particle size. This paper is the third in a series investigating the size and size distributions of the latex particles. The first two described a soap titration technique (3) for determining the surface average radius and an ultracentrifuge technique (4) for determining the distribution of particle sizes. This paper investigates the use of a statistical technique in relating the particle size distribution to the mechanism of growth.

The use of a statistical approach in solving this problem theoretically is very inviting since there are of the order of  $10^{14}$  particles per milliliter of water in a latex and the complete randomness required is probably found. In fact, Ewart and Carr (5) developed such a statistical theory, relating

<sup>1</sup> Presented before the Division of Colloid Chemistry, 137th National American Chemical Society Meeting at Cleveland, April, 1960.



the size distribution to fluctuations in the time that a particle contains a free radical, which predicted a normal distribution of the diameters. However, there is no apparent way to modify their theory to explain other distributions.

An analogous problem is that of breaking solids or liquids into smaller sizes. This latter problem has been solved for the grinding of coal (6) and the formation of suspensions and emulsions by dispersion (7) by treating the breaking process as a stochastic one, i.e., one in which the variable quantity (size) has a definite range of values, each one of which, depending on chance, can be attained with a definite probability. The application of the Central Limit theorem then solves the problem. This approach is more general than that of Ewart and Carr and is used below to predict the type of distributions to be expected from various growth processes.

### *Rate of Growth*

The rate of volume increase of polymer in a particle can be expressed by an equation of the following type:

$$dV/dt = k^\alpha; \quad [1]$$

the radius of the sphere containing the polymer is  $r$  and  $k$  is a constant. The exponent  $\alpha$  depends upon the process of growth. Smith and Ewart (8) assumed that  $\alpha$  equals 0 in their derivation of the dependence of the number of polymer particles formed per milliliter of water on soap and initiator concentrations. In an experimental investigation of the emulsion polymerization of styrene Ewart and Carr (5) found that  $d_i - \bar{d}$  ( $d_i$  is the diameter of the  $i$ th particle and  $\bar{d}$  is the average diameter) was approximately constant. This indicated that  $dr/dt$  is approximately constant or  $\alpha$  is approximately equal to 2. In some competitive growth experiments with monodisperse polystyrene latices Vanderhoff *et al.* (9) found that  $\alpha$  is approximately equal to  $2\frac{1}{2}$ .

In the derivation below it will be assumed that  $\alpha$  takes on integral values equal to 0, 2, and 3. This is a simplifying assumption although setting  $\alpha$  equal to 2 or 3 is equivalent to saying that the increase of mass of polymer per unit time, i.e., the rate of conversion, is proportional to the surface of the particle or its volume, respectively.

### *Derivation of the Distribution Functions*

To use the statistical method, it must be assumed that growth takes place in discrete time intervals by completely random processes. The intervals must be long enough to permit some growth but short enough to have a large number of intervals. The probability of growth in an interval must be independent of size (6). This quantity, whether it be volume, radius, or logarithm of the radius, which has a probability independent of size is determined by the rate of growth process.

It is assumed that there is an original cumulative size distribution  $F_0(r)$  composed of monomer droplets and micelles, and in the first growth step a distribution  $F_1(r)$  is formed. In the second step a distribution  $F_2(r)$  is formed and so on until by growth in  $N$  steps the final cumulative size distribution  $F_n(r)$  is formed.

When  $\alpha$  equals zero,  $dV/dt$  is constant, and therefore the probability of the growth of the volume is independent of the size of the particles. Going from time interval  $n$  to time interval  $n + 1$ , there is a change independent of the size of the particle expressed by:

$$V_{n+1} = V_n + \beta_n = V_{n-1} + \beta_{n-1} + \beta_n = V_0 + \sum_{j=0}^n \beta_j. \quad [2]$$

The growth of a single particle in the  $j$  time interval,  $\beta_j$ , is assumed to be a random event with an average value  $\bar{\beta}$  and a variance,  $\sigma_j$ . The average value  $\bar{\beta}$  must be such that for the whole distribution the differential equation stating that  $dV/dt$  be constant is satisfied. Since  $\beta_j$  is independent of size and when  $n$  approaches  $N$  there are a large number of time intervals, one can apply the Central Limit theorem (6).

The Central Limit theorem states that a random variable, which is the resultant of a large number of random events, will have a normal distribution, subject to some general conditions.

This means that the random variable, volume, which is the resultant of a large number of random events,  $\beta_j$ , will have a normal distribution provided  $\alpha$  equals 0.

For  $\alpha$  equal to 2,  $dr/dt$  is constant and the probability of the growth of the radius is independent of size. Therefore, going from time interval  $n$  to time interval  $n + 1$ , we have:

$$r_{n+1} = r_n + \gamma_n = r_0 + \sum_{j=0}^n \gamma_j. \quad [3]$$

Again applying the Central Limit theorem one obtains that for  $\alpha$  equal to 2 the radii are normally distributed.

For  $\alpha$  equal to 3  $dr/dt$  is proportional to  $r$  on  $d \ln r/dt$  is constant. Therefore for the change from time interval  $n$  to  $n + 1$  one obtains:

$$\ln r_{n+1} = \ln r_n + \delta_n = \ln r_0 + \sum_{j=0}^n \delta_j.$$

Applying the Central Limit theorem to this result shows that the logarithms of the radii are distributed normally for  $\alpha$  equal to 3.

#### DISCUSSION

The available experimental data can be used to check the applicability of the results of the analysis presented here. Data on the distribution functions of acrylic and poly (vinyl acetate) latices (4) indicate that in no case

are the volumes distributed normally and in all cases investigated, except one, the logarithms of the radii appear to be normally distributed. Since the Smith-Ewart theory has  $\alpha$  equal to 0 as a basic assumption in the derivation of the dependence of number of particles per milliliter of water on soap and initiator concentration, and this requires the volumes to be normally distributed, caution must be used in extending the Smith-Ewart result to water-soluble monomers.

The polystyrene latex data of Ewart and Carr (5) seemed to fit all three distributions although the volume-normal probability distribution doesn't fit the data as well as the other. This result was probably caused by the narrow distribution. However, their evaluation that indicated  $\alpha$  is approximately equal to 2 means that the Smith-Ewart number relationship must be used with caution even with polystyrene.

A process which may be analogous to emulsion polymerization is that of the formation and growth of sulfur hydrosols. La Mer *et al.* (10, 11) have shown that after nucleation the variation of  $r^2$  with time is linear, i.e.,  $dr^2/dt$  is constant or  $\alpha$  is approximately equal to 1. By means of the method outlined in this report, it can be shown that  $r^2$  should be normally distributed. However, the uniform growth by diffusion (11, 12) after the first nuclei are formed creates a "monodisperse" colloid (12, 13), obviating the need for a distribution function.

Since La Mer's results show that  $dr^2/dt$  should be constant if diffusion is the rate-controlling step (11, 12) and it is found experimentally (4) that either  $dr/dt$  or  $d \log r/dt$  is constant in the growth of emulsion polymer particles, diffusion is eliminated as the rate-controlling step in the emulsion polymerization studied. This is in agreement with the conclusion of Flory (14) based on estimates of the ease of supply of monomer from the aqueous phase to the growing particle.

It appears that the analysis of the type of particle size distribution obtained in emulsion polymerization can now be used as another tool in the investigation of the mechanism of polymerization supplementing the usual studies of the rate of polymerization and the number of particles formed.

#### ACKNOWLEDGMENTS

The author wishes to express his thanks to Dr. Serge Gratch and Mr. J. A. Cala for their interest in this work and for their many helpful suggestions.

#### REFERENCES

1. JOHNSON, P. H., AND KELSEY, R. H., *Rubber World* **138**, 877 (1958).
2. BROWN, G. L., *J. Polymer Sci.* **22**, 423 (1956).
3. BRODNYAN, J. G., AND BROWN, G. L., *J. Colloid Sci.* **15**, 76 (1960).
4. BRODNYAN, J. G., *J. Colloid Sci.* **15**, 563 (1960).
5. EWART, R. H., AND CARR, C. I., *J. Phys. Chem.* **58**, 690 (1954).
6. EPSTEIN, B., *Ind. Eng. Chem.* **40**, 2289 (1948).

7. RAJAGOPAL, E. S., *Kolloid-Z.* **162**, 85 (1959).
8. SMITH, W. V., AND EWART, R. H., *J. Chem. Phys.* **16**, 592 (1948).
9. VANDERHOFF, J. W., VITKUSKE, J. F., BRADFORD, E. G., AND ALFREY, T., JR.,  
*J. Polymer Sci.* **20**, 225 (1956).
10. ZAISER, E. M., AND LA MER, V. K., *J. Colloid Sci.* **3**, 571 (1948).
11. REISS, H., AND LA MER, V. K., *J. Chem. Phys.* **18**, 1 (1950).
12. REISS, H., *J. Chem. Phys.* **19**, 482 (1951).
13. WILSON, I. B., AND LA MER, V. K., *J. Ind. Hyg. Toxicol.* **30**, 265 (1948).
14. FLORY, P. J., "Principles of Polymer Chemistry," p. 210. Cornell University Press, Ithaca, New York, 1953.



## THE ZERO POINT OF CHARGE OF TOBERMORITE

H. N. Stein

*Central Laboratory TNO, Julianalaan 134, Delft, Netherlands*

*Received January 12, 1960; revised April 27, 1960*

### ABSTRACT

Synthetic tobermorite with a molar ratio  $\text{CaO/SiO}_2 = 1.08$  was studied as a model substance for the hydration products of Portland cement. By electrophoresis measurements it was found that at hydroxyl ion concentrations ranging from  $10^{-3}$  to  $2 \cdot 10^{-2} M$  the sign of the surface charge is negative at low Ca concentrations and positive at high Ca concentrations. The zero point of charge is situated at  $4 \times 10^{-3} M \text{ Ca}^{++}$ , independent of the hydroxyl ion concentration. Under conditions prevailing in hardening normal cements, the resulting Ca hydrosilicate probably has a positive surface charge.

### INTRODUCTION

In the course of an investigation on the influence of polar organic materials, e.g., cationic or anionic detergents, on hardened Portland cement, knowledge was desired about the sign of the surface charge on the cement particles, enabling one to predict the adsorption of the said materials.

Pertinent measurements have been reported by Reshetnikov (1) and by Zhuravlev and Tikhonov (2). Both groups of investigators found that the solid particles in Portland cement have a positive surface charge. Their data, however, do not permit drawing a conclusion about the sign of the surface charge of unhydrated material as distinct from hydration products; in their communications, no reference is made to the time having passed between mixing the paste and measuring. Pike and Hubbard (3) concluded from adsorption measurements of  $\text{Ag}(\text{NH}_3)_2^+$  and  $\text{Br}^-$  in concentrated ammonia on hydrated Portland cements, that the latter have a positive surface charge under these conditions. We thought it worth while to study the surface charge of model substances for hydration products of Portland cement more directly by electrophoresis, especially since a positive surface charge is quite unexpected for silicate materials at the high pH existing in hardening cement pastes (higher than 12), unless  $\text{Ca}^{++}$ , present in high concentration in the water phase of hardening cement pastes, reverses the sign of the surface charge through its adsorption on the solid particles.

As a model for cement hydration products we took synthetic tobermorite. The idea that the most important product of hardening cement pastes,



the Ca hydrosilicate, resembles a product of hydrothermal reaction between CaO and SiO<sub>2</sub> (identical with the mineral tobermorite (4)), was first put forward by Taylor (5-7) and Bernal (8). The phase identity of the two substances has been questioned by Kalousek (9, 10), but most authors seem to be inclined to think that the Ca hydrosilicate formed at room temperature is a badly crystallized and rather disordered form of the Ca hydrosilicate prepared by hydrothermal synthesis (see, for example, references 11 and 12) especially since Roentgen analytical evidence points that way (13).

The surface charge of synthetic tobermorite has been examined by Pike and Hubbard (3), using their adsorption method in concentrated ammonia (see above). They concluded that tobermorite itself has a negative surface charge under these conditions but a positive surface charge if treated beforehand with a saturated Ca(OH)<sub>2</sub>-solution. Indeed one expects a negative surface charge for tobermorite at the pH prevailing in the water phase of hardening cement pastes; the question may be considered whether Ca ions might reverse this sign. We therefore carried out electrophoresis measurements in media of various NaOH and CaCl<sub>2</sub> concentrations.

The synthetic tobermorite investigated was prepared by hydrothermal synthesis from CaO and SiO<sub>2</sub>, since a homogeneous product can be obtained conveniently (5) in this way. From the range of compositions possible for tobermorite, we arbitrarily chose a molar ratio CaO/SiO<sub>2</sub> = 1.08; it was felt that the use of higher CaO/SiO<sub>2</sub> ratios (which correspond to the conditions also present in cement pastes) would greatly enhance the risk of obtaining also other Ca hydrosilicates or Ca(OH)<sub>2</sub>, especially since the range of compositions possible for tobermorite seems to be smaller at the temperature of hydrothermal synthesis than at room temperature (10).

## EXPERIMENTAL METHODS

### *Synthesis of Tobermorite*

Tobermorite was synthesized from CaO (C.P. ex Merck, freed from CO<sub>2</sub> by heating to 1000°C. shortly before use) and from quartz which had the following characteristics: loss on heating—0.5%; residue on treating with HF and H<sub>2</sub>SO<sub>4</sub>—0.4%; 94% had an equivalent radius smaller than 20μ (determined by sedimentation in 0.06% Na-oxalate solution).

10.18 g. CaO and 10.07 g. SiO<sub>2</sub> were suspended in 1700 ml. boiled distilled water, using Kalousek's "wet mix" method (9). The mixture was heated at 150°C. for 4 days in an autoclave the inner surface of which had been lined with stainless steel. The resulting product was filtered off in an atmosphere of nitrogen and washed with boiled distilled water until the filtrate contained no detectable amount of Ca<sup>++</sup> (reaction with NH<sub>4</sub>-oxalate). The product was kept wet in an atmosphere of nitrogen in order to minimize any contamination with CO<sub>2</sub>. Its thermogravimetric analysis showed a form typical for tobermorite (14) with the exception of extra weight losses at 480°–520°C. (indicating the presence of about 1.5% Ca(OH)<sub>2</sub>) and at 630°–660°C. (corresponding to 0.7% CaCO<sub>3</sub>). The electron micrograph of the material, shown in Fig. 1,



FIG. 1. Electron micrograph of the tobermorite investigated.

closely resembles analogous micrographs published by Kalousek (10) (sheets and rod-shaped particles).

Roentgen analytical examination (15), in agreement with the thermogravimetric data, showed a diagram typical for tobermorite (it could be indexed completely on the basis of an orthorhombic unit cell of dimensions  $a = 11.26 \text{ \AA}$ ,  $b = 7.36 \text{ \AA}$ ,  $c = 22.4 \text{ \AA}$ ), with traces of  $\text{Ca}(\text{OH})_2$ ,  $\text{CaCO}_3$ , and  $\alpha\text{-}2 \text{ CaO} \cdot \text{SiO}_2$  as sole contaminants.

#### PROCEDURE

Some tobermorite was dispersed in  $\text{NaOH}$  solution containing  $\text{Ca}(\text{OH})_2$ . The concentration of  $\text{Ca}(\text{OH})_2$  was about 1% of the  $\text{NaOH}$  concentration, the latter varied according to the conditions investigated. Dispersion was accomplished by covering the tobermorite with this  $\text{NaOH}$  solution and keeping the system, for 10 minutes, in the focus of a crystal generator (1 mc./sec., total output 30 watt; sometimes another crystal generator producing vibrations of frequency 1 kc./sec., total output 75 watt was used too.)

Five milliliters of this solution were pipetted into 50 ml. of a solution containing the same  $\text{NaOH}$  concentration as the suspension and varying amounts of  $\text{CaCl}_2$  (C.P., Merck). The diluted suspension was kept in a polyethylene bottle, well protected from contact with air.

One day after preparation, electrophoresis in this suspension was carried out,

using an instrument for microscopical observation of electrophoresis, at the Van't Hoff Laboratory, Utrecht. The design of this instrument is described, for example, in reference 16. The particular cell used in this investigation had a depth of 0.98 mm. and a breadth of about 11 mm. Ag/AgCl electrodes were used, surrounded by NaCl solutions of the same molar concentration as the NaOH concentration in the suspension concerned.

Before the instrument was filled, the suspension of tobermorite, having flocculated and settled since its preparation, was redispersed by shaking.

Some difficulties were encountered in performing electrophoresis, caused by the very rapid flocculation of tobermorite, necessitating frequent refilling of the cell. At higher NaOH concentrations, convection currents also became disturbing factors; convection was promoted by the greater amount of heat, generated by a current through a medium of higher specific conductance with about equal field strength, as compared with experiments at lower concentrations. These convection currents prohibited measurements at concentrations higher than 0.02 *N* NaOH.

One day after the electrophoresis experiments, electrical conductivity was measured in the suspensions. The suspensions were filtered, and Ca concentrations were determined in the filtrates. Determination of  $\text{Ca}^{++}$  was carried out in the more concentrated solutions (higher than about 0.003 *M*) by titration with EDTA as titrant and calcon (Eriochrome Blue Black R) as indicator, after addition of  $\text{MgSO}_4$ ; in the more dilute ones by titration with EDTA as titrant and Eriochrome Black T as indicator, after addition of Mg-EDTA complex.

In general, the final pH was not measured. However, separate tests with tobermorite suspensions in NaOH solutions of concentrations comparable with those employed in the electrophoresis experiments showed only insignificant differences (not exceeding 0.1 pH unit) between the pH of the suspension and the pH of the solution used for preparing the suspension.

## RESULTS AND DISCUSSION

The electrophoretic velocities in the stationary layer of the electrophoresis cell were found by extrapolating measurements taken at different heights in the cell, as described in reference (16). The results are reproduced in Fig. 2; the electrophoretic velocity in the stationary layer is plotted against the final Ca concentration as found by titration. An electrophoretic velocity, directed towards the negative electrode, is called positive.

Volume changes due to electrode reactions were found to be negligible, according to computations based on the cells Ag/AgCl/NaCl-solution/NaOH-solution/NaCl-solution/AgCl/Ag and Ag/AgCl/NaCl-solution/ $\text{CaCl}_2$ -solution/NaCl-solution/AgCl/Ag for cases of low and high Ca concentrations, respectively. The calculated volume changes amounted to 2% of the observed electrophoretic velocities at the most, the highest relative values being found for measurements in the region of the zero point of charge, at high electrolyte concentrations.

From the results we see clearly that the zero point of charge of tobermorite lies at 0.004 *M*  $\text{Ca}^{++}$ , independent of the hydroxyl ion concentration, within the precision of the results. This zero point of charge, being found by electrophoresis, is related to the slipping plane between the stationary layer near the tobermorite surface and the moving bulk liquid;

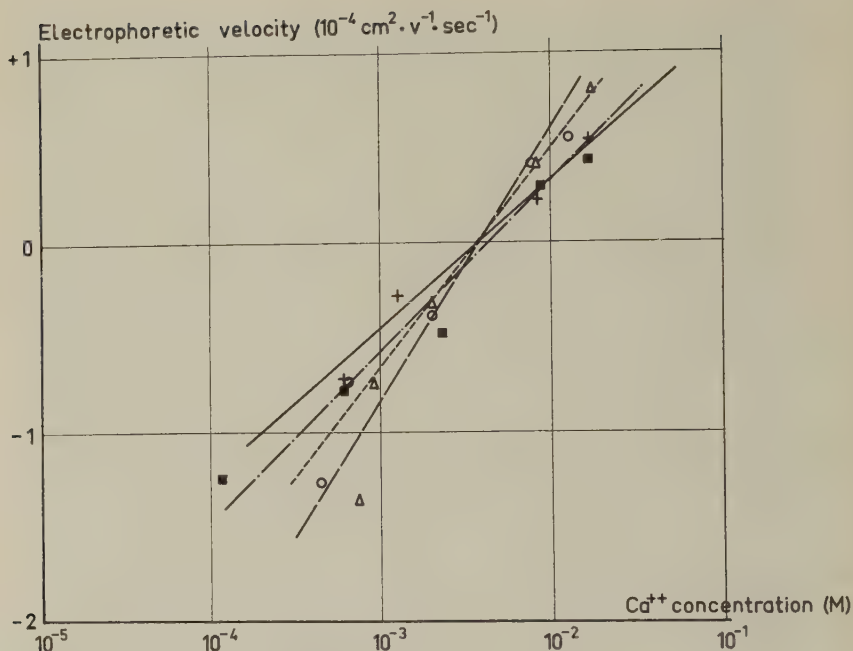


FIG. 2. Electrophoretic velocity as a function of Ca concentration at different hydroxyl ion concentrations. —■— Initial  $\text{OH}^-$  concentration = 0.001  $N$ . —+— Initial  $\text{OH}^-$  concentration = 0.005  $N$ . —△— Initial  $\text{OH}^-$  concentration = 0.01  $N$ . —○— Initial  $\text{OH}^-$  concentration = 0.02  $N$ . —□— Initial  $\text{OH}^-$  concentration = 0.05  $N$ .

all Ca ions within the stationary layer count as if they were adsorbed on the solid particles.

In hardening Portland cement pastes, values for Ca concentration are reported ranging from  $3 \times 10^{-3} M$  to  $8 \times 10^{-2} M$  (17–21), depending somewhat on the time of hardening and on the type of cement used, especially on its alkali and gypsum contents. Most values reported, however, are higher than  $1 \times 10^{-2} M$ , lower values being found in cements with high alkali content (18) and in general during later stages of hydration (21). The hydroxyl ion concentration in cement pastes is higher than could be realized in this investigation; there are also differences related to sulfate as anion in cement pastes as against  $\text{Cl}^-$  in this investigation and to a higher general electrolyte content in cement.

Extrapolating our results to the higher hydroxyl ion concentrations concerned and neglecting the influence of other ions, we conclude that tobermorite has a positive surface charge under conditions prevailing in normal hardening cement; in high alkali cements and during the later stages of hydration, the zero point of charge is approached. Only one reference (20) could be found mentioning a value for Ca concentration lower than the one corresponding to the zero point of charge.



Assuming a fundamental similarity of the Ca hydrosilicate formed at room temperature with the product of hydrothermal reaction (*cf.* Megaw and Kelsey's interpretation of Roentgen analytical data (13)), the same conclusion as to the sign of the surface charge should hold true for the Ca hydrosilicate formed by hydrating cement.

However, after this paper had been accomplished, the author's attention was drawn to measurements by J. A. Gard, J. W. Howison, and H. F. W. Taylor (*Magazine of Concrete Research* **11**, No. 33, November, 1959, p. 151) indicating a considerable difference between Ca hydrosilicates formed at room temperature and the corresponding autoclaved products. The difference has been tentatively explained as being due to a lack of homogeneity (perhaps on a very small scale) in room temperature preparations. These results may cast some doubt on the validity of the figure for the zero point of charge (as found in this investigation) in the case of Ca hydrosilicate in hydrating cement.

#### SUMMARY

1. The zero point of charge of tobermorite lies at  $4 \times 10^{-3} M \text{ Ca}^{++}$ , independent of hydroxyl ion concentration in the range studied (0.001 *N*–0.02 *N*).

2. Under conditions prevailing in normal hardening cements the resulting Ca hydrosilicate probably has a positive surface charge.

#### ACKNOWLEDGMENTS

The author wishes to express his gratitude to Prof. Dr. J. Th. G. Overbeek and Drs. J. Broekema, of the Van't Hoff Laboratory, Utrecht, for facilities, to Drs. Ch. A. Kruissink for many discussions, and to Miss C. van Harberden for assistance.

#### REFERENCES

1. RESHETNIKOV, M. A., *Kolloid. Zhur.* **1**, 525 (1935); *Chem. Zentr.* **1937**, **I**, 404.
2. ZHURAVLEV, V. F., AND TIKHONOV, V. A., *Zhur. Priklad. Khim.* **25**, 1256 (1952).
3. PIKE, R. G., AND HUBBARD, D., *Natl. Research Council Natl. Acad. Sci. U. S.* No. 531, 16–33 (1958); *Chem. Abstr.* **53**, 1669 d; *Highway Research Board Proc.* **37**, 256 (1958); *Chem. Abstr.* **53**, 22818 i.
4. CLARINGBULL, G. F., AND HEY, M. H., *Mineralog. Mag.* **29**, 960 (1952).
5. TAYLOR, H. F. W., *J. Chem. Soc.* **1950**, 3682.
6. HELLER, L., AND TAYLOR, H. F. W., *J. Chem. Soc.* **1951**, 2397.
7. TAYLOR, H. F. W., *Proc. 3rd Intern. Symposium Chem. Cement, London, 1952*, p. 362.
8. BERNAL, J. D., *Proc. 3rd Intern. Symposium Chem. Cement, London, 1952*, p. 216.
9. KALOUSEK, G. L., *J. Am. Concrete Inst.* **26**, 989 (1955).
10. KALOUSEK, G. L., AND PREBUS, A. F., *J. Am. Ceram. Soc.* **41**, 124 (1958).
11. BUCKLE, E. R., AND TAYLOR, H. F. W., *J. Appl. Chem. (London)* **9**, 163 (1959).
12. BRUNAUER, S., KANTRO, D. L., AND COPELAND, L. E., *J. Am. Chem. Soc.* **80**, 761 (1958).
13. MEGAW, H. D., AND KELSEY, C. H., *Nature* **177**, 390 (1956).
14. GREENBERG, S. A., *J. Phys. Chem.* **58**, 362 (1954).
15. VISSER, J. W., personal communication.



16. OVERBEEK, J. TH. G., in H. R. Kruyt, ed., "Colloid Science," Vol. 1, p. 218. Elsevier, Amsterdam, 1952.
17. STEINHERZ, A. R., AND WELCMAN, N., *Rev. matériaux construction et trav. publ.* **517**, 265 (1958).
18. HEDIN, R., "Chemical processes in the hardening of Portland cement," *Svensk Forskningsinst. Cement Betong vid Kgl. Tek. Högskol. Stockholm Handl.* **1945**, No. 3, 115, 123.
19. HÄNSEL, P., STEINHERZ, R., AND WAGNER, C. L., *Zement* **22**, 625 (1933).
20. STEIN, S., *Zement* **19**, 240 (1930).
21. STRELKOV, M. I., *Proc. Symposium Chem. Cement, Moscow*, **1956**, p. 183; *Chem. Abstr.* **52**, 6748 e.

## BOOK REVIEW

**Soap Films, Studies of Their Thinning and a Bibliography.** By KAROL J. MYSELS, KOZO SHINODA, AND STANLEY FRANKEL, Pergamon Press, 116 pp. 1959. Price \$7.50.

The main text of this small volume (88 pages subdivided in seven chapters) is based on an experimental study by one of the authors (K. Shinoda) during his stay at the University of Southern California, Los Angeles, 1955-56. Part of the work has been reported at two A.C.S. meetings in 1957, but its publication in scientific journals encountered difficulties because of the length and detail of the presentation and, also, because of the presence of some color illustrations. The publication in its present form, excellently executed, is due to Pergamon Press. As the authors state in the preface: "The reader should be warned not to expect the completeness and coherence of a fully completed investigation." No one acquainted with the subject will be surprised by this statement, but one should regret that the authors, as they also state in their preface "(. . .) have not attempted to prepare a survey of existing knowledge concerning film thinning, let alone the many related subjects." An extensive bibliography containing 324 items in chronological order and an author's index have been added to the book but in the text reference to the work of others is mostly absent; the authors seem even to ignore some of the work cited in the bibliography.

This publication has to be considered not as a textbook or as an introduction but as a report on an experimental study and an attempt to explain the obtained results. The experiments are concerned mostly with the thickness changes in lamellae composed of dilute aqueous solutions of pure and commercial detergents. The lamellae formed by dipping glass frames of varying size and shape into the solution were preserved in closed bottles containing the solution, and their thickness changes were measured by observation of the color of interference fringes or, for very small thicknesses, by determination of the intensity of locally reflected monochromatic light. In an introductory chapter a detailed description of the experimental procedure is given. Chapter II starts with a morphological classification of soap films based on the difference in rate and regularity of the thinning process that may be observed depending on the composition and on the external conditions. Some color plates give a clear presentation of these differences. A qualitative discussion of different thinning mechanisms is given with special reference to the fundamental work of Gibbs. The greater part of this chapter is clearly presented, as is the next one treating viscous flow and evaporation in vertical films, but now in a quantitative way. The observed parabolic profile of the colored part of a slowly draining vertical film is satisfactorily explained by a model of viscous flow between two flexible planes. The difference between theoretical and experimental values of the rate of thickness change may be accounted for by evaporation of solvent. Evaporation will lead to direct thinning of a film element but also to its stretching (if the volume and surface concentrations are to remain constant); this reduces the thickness still further. The possible effect of temperature variations due to solvent evaporation is not considered by the authors. The combined effects of viscous flow and solvent evaporation are not sufficient, however, to explain the rapid and irregular thinning of mobile films, nor the formation of a very thin, rapidly growing, region in the upper part and near the borders of a

rigid soap film. This thinning is due to capillary suction into the so-called Plateau-borders that are much thicker than the film itself. The resulting change of curvature near the edges is responsible for a pressure gradient in the liquid which, according to the well-known Laplace's equation, is proportional to the surface tension. In their discussion of this phenomenon the authors fail to make a clear distinction between causes (intermolecular forces and gravity) and effect (motion of liquid). In order to explain a certain number of observations, they propose a new mechanism which they call marginal regeneration and which is based on a continuous generation and consumption of liquid film along the borders. It is difficult to imagine how such a process might take place spontaneously. A series of interesting experiments concerning the influence of the height and width of the frame, described in Chapter IV, show clearly the importance of the borders but they do not prove anything about the plausibility of the proposed mechanism of thinning. The same is true for the mathematical treatment in Chapter V; the derived relationship between film thickness and speed of film drawing is of interest for the problem of film and foam formation but does not tell us much about the mechanism of spontaneous film thinning. The other derived relationships are, according to the authors, in clear conflict with observations.

In Chapter VI measurements are recorded of the decrement of thickness at the silver-black boundary as a function of detergent concentration. The authors have found that the thickness of the black film decreases with increasing detergent concentration in a range of concentrations above the C.M.C., whereas the thickness of the silvery film varies in the opposite direction. Somewhat further in the text they state, however, that the thickness of the black film decreased gradually with time to about 90 Å, independent of the concentration between 0.4% and 2% sodium lauryl sulfate. This seems to suggest that the reported values are more or less instantaneous nonequilibrium values, but this is not made clear in the text. Equilibrium thicknesses of about 100 Å. have been frequently reported in the literature, whereas higher values may be found if the ionic strength is very low, in agreement with the theory of colloid stability based on double layer repulsion and London-van der Waals' attraction. This theory is not discussed by the authors, who seem to suppose that the presence of micelles is necessary for the formation of black film. No explanation, however, is offered for this supposed influence of micelles.

In the last chapter an interesting attempt is made to treat quantitatively the motion of thin region (e.g., a black spot) under the influence of gravity. If the equation for the drag on a cylinder moving transversely through a fluid is applied to the motion of a circular spot in a thicker film, after replacing density by mass/unit area and viscosity by a two-dimensional film viscosity, reasonable values for the latter quantity are found. The found values are much lower than the values of surface viscosity determined on the surface of bulk liquid but they are comparable to the values of film viscosity determined by Trapeznikow's method. It will be worth while to explore the possibilities of this original method.

Though the book does not offer a comprehensive treatment of the thinning of soap films, many readers of this journal should find it interesting and stimulating.

A. J. DE VRIES, Paris, France

*Compagnie de Saint-Gobain  
Services de Recherche  
Centre de la Villette*

### Erratum

Volume 15, Number 4 in the Letter to the Editor entitled "A Bar Viscometer with Conical Annulus" by D. Tollenaar, pp. 381-383:

On page 382, Figure 1 has been printed upside down.

# AUTHOR INDEX

<b>A</b>		HIGUCHI, W. I.,	14
ALBERS, W.,	489	HOERR, CHARLES W.,	427
ALEXANDER, A. E.,	155, 168	HUGHES, WILLIAM H.,	307
<b>B</b>		<b>I</b>	
BEATTIE, WILLARD H.,	183	INOUE, H.,	268
BLEI, IRA,	209, 370	<b>J</b>	
BONDI, A.,	531	JOANES, ANN A.,	193
BOTTY, M. C.,	83	<b>K</b>	
BOUCEK, ROBERT J.,	97	KAWASAKI, KOJI,	402
BRADLEY, R. S.,	525	KEITH, C. H.,	340
BRODNYAN, J. G.,	76, 563, 573	KITANI, SUSUMU,	287
BROWN, CHARLES A.,	418	KURIYAMA, K.,	268
BROWN, G. L.,	76	<b>L</b>	
BURCIK, EMIL J.,	383	LAKSHMANAN, A. S.,	205
BURSH, T. P.,	361	LA MER, VICTOR K.,	123
<b>C</b>		LANGER, G.,	357
CALLAHAN, JAMES L.,	418	LIEBERMAN, A.,	357
CARROLL, BENJAMIN,	209	<b>M</b>	
CHARLES, G. E.,	105, 236	MASON, S. G.,	105, 236
COUMOU, D. J.,	408	MATHIESON, A. R.,	387
<b>D</b>		MATHUR, PREM BEHARI,	205
DERRICK, J. C.,	340	MAZUR, J.,	437
DUNELL, B. A.,	193	MEEHAN, E. J.,	183
<b>E</b>		MILLER, M. L.,	83
ELDEN, HARRY R.,	97	MILLER, ROBERT S.,	232
<b>F</b>		MURAKAMI, K.,	282
FERRY, JOHN D.,	294	<b>N</b>	
FISHMAN, MYER M.,	232	NAKAGAWA, T.,	268
FLETCHER, G. E.,	485	NEWLIN, THOMAS E.,	294
FOWKES, F. M.,	531	NEWMAN, ROBERT C.,	383
<b>G</b>		<b>O</b>	
GAINES, GEORGE L., JR.,	321	O'KONSKI, C. T.,	14
GILLESPIE, THOMAS,	219, 313	OTTEWILL, R. H.,	512
GORING, D. A. I.,	452, 472	OVERBEEK, J. TH. G.,	489
<b>H</b>		<b>P</b>	
HARROLD, S. P.,	280	PADDAY, J. F.,	503
HECKLER, GEORGE E.,	294	PETRUCCI, RALPH H.,	418
HELFFERICH, FRIEDRICH,	483	PLAZEK, DONALD J.,	50

R				
RAUHUT, C. E.,	83	TOLLENAAR, D.,		381
REZANOWICH, A.,	452, 472	TRURNIT, H. J.,		1
ROBBINS, MAX L.,	123	TSCHOEGL, N. W.,		155, 168
RUSSELL, D. R.,	503	TSUBOMURA, MICHU,		278
RYE, R. T. B.,	193		V	
S		VEIS, ARTHUR,		427
SAITO, SHUJI,	283		W	
SCHEKMAN, A. I.,	546			
SCHICK, M. J.,	531	WILKINS, D. J.,		512
SIEGLAFF, C. L.,	437	WITT, JERRY R.,		294
SISKO, A. W.,	89		Y	
SLABAUGH, W. H.,	485			
STEIN, H. N.,	578			
STERN, DONALD M.,	294	YABE, AKIHIKO,		278
STERN, S. C.,	546	YOUNG, G. J.,		361
STRATTON, ROBERT A.,	294		Z	
T				
TACHIBANA, TARO,	278			
TOBOLSKY, A. V.,	282	ZELLER, H. W.,		546



## SUBJECT INDEX

### A

Aerosol, filter for aerosols, STERN *et al.*,  
546

### C

Calcium, self-diffusion of ions, FLETCHER  
AND SLABAUGH, 485  
Cellulose nitrate, properties of a  
solution, PLAZEK, 50  
Cigarette smoke, distribution and con-  
centration, KEITH AND DERRICK, 340  
Coalescence, of drops, CHARLES AND  
MASON, 105, 236  
Collagen, extraction from hide powder,  
ELDEN AND BOUCEK, 97  
Colloids, flocculation, GILLESPIE, 313;  
particle counting, OTTEWILL AND  
WILKINS, 512  
Copolymers, surface-active, FOWKES  
*et al.*, 531  
Emulsion, particle size, BRODNYAN AND  
BROWN, 76; BRODNYAN, 563, 573; sta-  
bility of water in oil, ALBERS AND  
OVERBEEK, 489

### L

Latex, electrochemistry, SIEGLAFF AND  
MAZUR, 437  
Liesegang rings, spacing law, MATHUR  
AND LAKSHMANAN, 205  
Light scattering, measurement, COUMOU,  
408  
Lignin sulfonate, expansion, REZANO-  
WICH AND GORING, 452

### M

Micellar weight, of nonionic surfactants,  
NAKAGAWA *et al.*, 268  
Micelle formation, free energy, VEIS  
AND HOERR, 427

Molybdena, growth of whiskers, CAL-  
LAHAN *et al.*, 418

### N

Nucleation, kinetics, HIGUCHI AND  
O'KONSKI, 14; at high pressures,  
BRADLEY, 525  
Nylon, monofilaments, viscoelasticity,  
DUNELL *et al.*, 193

### P

Particle size, measurement, KITANI,  
287  
Polyacrylic acid, crystalline, MILLER  
*et al.*, 83  
Polymer, viscosities of concentrated  
solutions, HECKLER *et al.*, 294  
Polystyrene, precipitation titration,  
MATHIESON, 387  
Polystyrene latex, aerosol, LANGER AND  
LIEBERMAN, 357  
Protein(s), spreading of monolayers,  
TURNIT, 1; denatured, BLEI AND  
CARROLL, 209; solubilization of pro-  
tein-detergent complex, BLEI, 370

### R

Relaxation, and chain length, TOBOLSKY  
AND MURAKAMI, 282

### S

Silica, surfaces, and water, YOUNG AND  
BURSH, 361  
Silver bromide, electron microscopy,  
MEEHAN AND BEATTIE, 183  
Soap, damping of vibratory motion by  
soap films, BURCIK AND NEWMAN,  
383  
Sodium dodecyl sulfate, purification,  
HARROLD, 280

Spreading solvent, effect on monolayers,  
 ROBBINS AND LA MER, 123  
 Starch, and ammonium compounds,  
 FISHMAN AND MILLER, 232  
 Stearic acid, monolayers, GAINES, 321  
 Strontium, diffusion, HELFFERICH, 483  
 Surface tension, of liquids, PADDAY AND  
 RUSSELL, 503  
 Surfactants, and polymers, SAITO, 283

## T

Thermal force, on particulate material,  
 HUGHES, 307  
 Tobermorite, zero point of charge,  
 STEIN, 578

## V

Viscometer, capillary, SISCO, 89; bar  
 viscometer, TOLLENAAR, 381, 586  
 Viscosity, of pseudoplastic systems,  
 GILLESPIE, 219; for a polyelectrolyte,  
 GORING AND REZANOWICH, 472

## W

Washing efficiency, of a detergent,  
 TACHIBANA *et al.*, 278  
 Wettability, of polymers, KAWASAKI,  
 402  
 Wheat gluten, surface chemistry,  
 TSCHOEGL AND ALEXANDER, 155, 168

## INDEX OF BOOK REVIEWS

ASTON, J. C., AND FRITZ, J. J., Thermo-  
 dynamics and Statistical Thermo-  
 dynamics (LA MER, V. K.), 190  
 BENESCH, R., *et al.* (eds.), Sulfur in  
 Proteins (STEINHARDT, J.), 86  
 DE JUHASZ, K. J. (ed.), Spray Literature  
 Abstracts (BIKERMAN, J. J.), 188  
 EVERETT, D. H., AND STONE, F. S.  
 (eds.), The Structure and Properties  
 of Porous Materials (EMMETT, P. H.),  
 87

JANZ, G. J., Estimation of Thermo-  
 dynamic Properties of Organic Com-  
 pounds (McCULLOUGH, J. P.), 86  
 MYSELS, K. J., *et al.*, Soap Films, Studies  
 of Their Thinning and a Bibliography  
 (DE VRIES, A. J.), 585  
 ORR, C., JR., AND DALLAVALLE, J. M.,  
 Fine Particle Measurement (LA MER,  
 V. K.), 188  
 STACEY, K. A., Light Scattering in Phys-  
 ical Chemistry (LA MER, V. K.), 189

# JOURNAL OF COLLOID SCIENCE

*Editor-in-Chief*

VICTOR K. LA MER, Columbia University, New York

*Advisory Board*

A. E. ALEXANDER

STEPHEN BRUNAUER

J. A. CHRISTIANSEN

P. J. W. DEBYE

B. DERJAGUIN

D. G. DERVICHIAN

JOHN T. EDSALL

I. FANKUCHEN

JOHN D. FERRY

J. J. HERMANS

L. G. LONGSWORTH

S. G. MASON

KAROL J. MYSELS

J. TH. G. OVERBEEK

J. H. SCHULMAN

LEO SHEDLOVSKY

THEODORE SHEDLOVSKY

ROBERT SIMHA

R. H. SMELLIE

HARRY SOBOTKA

JACINTO STEINHARDT

TORSTEN TEORELL

A. C. ZETTMEOYER

BRUNO H. ZIMM

W. A. ZISMAN



VOLUME 15

1960

ACADEMIC PRESS  
New York and London

COPYRIGHT ©, 1960, BY ACADEMIC PRESS INC.

ALL RIGHTS RESERVED

NO PART OF THIS VOLUME MAY BE REPRODUCED IN ANY  
FORM, BY PHOTOSTAT, MICROFILM, OR ANY OTHER MEANS,  
WITHOUT WRITTEN PERMISSION FROM THE PUBLISHERS.

*Made in the United States of America*

## Contents of Volume 15

### NUMBER 1, FEBRUARY 1960

H. J. TRURNIT. A Theory and Method for the Spreading of Protein Monolayers.....	1
W. I. HIGUCHI AND C. T. O'KONSKI. A Test of the Becker-Doering Theory of Nucleation Kinetics.....	14
DONALD J. PLAZEK. Dynamic Mechanical and Creep Properties of a 23 % Cellulose Nitrate Solution; Andrade Creep in Polymeric Systems.....	50
J. G. BRODNYAN AND G. L. BROWN. Emulsion Particle Size. I. The Soap Titration of Acrylic Emulsions.....	76
LETTER TO THE EDITOR	
M. L. MILLER, M. C. BOTTY, AND C. E. RAUHUT. Crystalline Polyacrylic Acid.....	83
BOOK REVIEWS	
JOHN P. McCULLOUGH. Estimation of Thermodynamic Properties of Organic Compounds.....	86
JACINTO STEINHARDT. Sulfur in Proteins.....	86
PAUL H. EMMETT. The Structure and Properties of Porous Materials.....	87

### NUMBER 2, APRIL 1960

A. W. SISCO. Capillary Viscometer for Non-Newtonian Liquids.....	89
HARRY R. ELDEN AND ROBERT J. BOUCEK. The Successive-Extraction of Collagen from Hide Powder.....	97
G. E. CHARLES AND S. G. MASON. The Mechanism of Partial Coalescence of Liquid Drops at Liquid/Liquid Interfaces.....	105
MAX L. ROBBINS AND VICTOR K. LA MER. The Effect of the Spreading Solvent on the Properties of Monolayers.....	123
N. W. TSCHOEGL AND A. E. ALEXANDER. The Surface Chemistry of Wheat Gluten. I. Surface Pressure Measurements.....	155
N. W. TSCHOEGL AND A. E. ALEXANDER. The Surface Chemistry of Wheat Gluten. II. Measurements of Surface Viscoelasticity.....	168
E. J. MEEHAN AND WILLARD H. BEATTIE. Preparation of Replicas of Silver Bromide for Electron Microscopy.....	183
BOOK REVIEWS	
VICTOR K. LA MER. Fine Particle Measurement.....	188
J. J. BIKERMAN. Spray Literature Abstracts.....	188



VICTOR K. LA MER. Light-Scattering in Physical Chemistry . . .	189
VICTOR K. LA MER. Thermodynamics and Statistical Thermodynamics . . . . .	190

## NUMBER 3, JUNE 1960

B. A. DUNELL, ANN A. JOANES, AND R. T. B. RYE. Viscoelastic Behavior of Nylon 6-6 Monofilaments below Room Temperature . . . . .	193
PREM BEHARI MATHUR AND A. S. LAKSHMANAN. A Spacing Law for Liesegang Rings. Mercurous Iodate System . . . . .	205
IRA BLEI AND BENJAMIN CARROLL. The Characterization of Denatured Proteins by Adsorption Indicators . . . . .	209
THOMAS GILLESPIE. An Extension of Goodeve's Impulse Theory of Viscosity to Pseudoplastic Systems . . . . .	219
MYER M. FISHMAN AND ROBERT S. MILLER. The Interaction of Quaternary Ammonium Compounds with Starch . . . . .	232
G. E. CHARLES AND S. G. MASON. The Coalescence of Liquid Drops with Flat Liquid/Liquid Interfaces . . . . .	236
T. NAKAGAWA, K. KURIYAMA, AND H. INOUE. Micellar Weights of Nonionic Surfactants in the Presence of <i>n</i> -Decane or <i>n</i> -Decanol . . . . .	268

## LETTERS TO THE EDITOR

TARO TACHIBANA, AKIHIKO YABE, AND MICHU TSUBOMURA. The Existence of a Maximum in the Curve of Washing Power vs. Concentration of Detergent . . . . .	278
S. P. HARROLD. Purification of Sodium Dodecyl Sulfate . . . . .	280
A. V. TOBOLSKY AND K. MURAKAMI. Relation Between Maximum Relaxation Time and Chain Length . . . . .	282
SHUJI SAITO. The Binding of Surfactants by Polymers . . . . .	283

## NUMBER 4, AUGUST 1960

SUSUMU KITANI. Measurement of Particle Sizes by Higher Order Tyndall Spectra ( $\theta_1$ Method) . . . . .	287
GEORGE E. HECKLER, THOMAS E. NEWLIN, DONALD M. STERN, ROBERT A. STRATTON, JERRY R. WITT, AND JOHN D. FERRY. Viscosities of Concentrated Polymer Solutions. V. Two Polyelectrolytes . . . . .	294
WILLIAM H. HUGHES. Thermal Force on Particulate Material at High Knudsen Numbers in the Absence of a Thermal Gradient . . . . .	307
THOMAS GILLESPIE. The Limited Flocculation of Colloidal Systems . .	313
GEORGE L. GAINES, JR. Some Observations on Monolayers of Carbon-14 Labeled Stearic Acid . . . . .	321
C. H. KEITH AND J. C. DERRICK. Measurement of the Particle Size	

Distribution and Concentration of Cigarette Smoke by the "Conifuge" .....	340
G. LANGER AND A. LIEBERMAN. Anomalous Behavior of Aerosol Produced by Atomization of Monodisperse Polystyrene Latex .....	357
G. J. YOUNG AND T. P. BURSH. Immersion Calorimetry Studies of the Interaction of Water with Silica Surfaces .....	361
IRA BLEI. The Solubilizing Properties of the Protein-Detergent Complex .....	370
LETTERS TO THE EDITOR	
D. TOLLENAAR. A Bar Viscometer with Conical Annulus .....	381
EMIL J. BURCIK AND ROBERT C. NEWMAN. The Damping of Vibratory Motion by Soap Films .....	383

## NUMBER 5, OCTOBER 1960

A. R. MATHIESON. The Turbidimetric Precipitation Titration of Polystyrene .....	387
KOJI KAWASAKI. Study of Wettability of Polymers by Sliding of Water Drop .....	402
D. J. COUMOU. Apparatus for the Measurement of Light Scattering in Liquids. Measurement of the Rayleigh Factor of Benzene and of Some Other Pure Liquids .....	408
JAMES L. CALLAHAN, RALPH H. PETRUCCI, AND CHARLES A. BROWN. The Hydrothermal Growth of Molybdena Whiskers on $\text{MoO}_3$ - $\text{SiO}_2$ Substrate .....	418
ARTHUR VEIS AND CHARLES W. HOERR. An Evaluation of the Electrostatic Free Energy of Micelle Formation .....	427
C. L. SIEGLAFF AND J. MAZUR. Electrophoretic Mobility and Electrochemistry of Latex Systems .....	437
A. REZANOWICH AND D. A. I. GORING. Polyelectrolyte Expansion of a Lignin Sulfonate Microgel .....	452
D. A. I. GORING AND A. REZANOWICH. The Huggins Viscosity Coefficient for a Polyelectrolyte Microgel .....	472
LETTER TO THE EDITOR	

FRIEDRICH HELFFERICH. Comment on the Paper "Diffusion of Strontium in Ion-Exchange Membranes" by J. de Lopez-Gonzales and H. Jenny .....	483
--	-----

## NUMBER 6, DECEMBER 1960

G. E. FLETCHER AND W. H. SLABAUGH. Self-Diffusion of Calcium Ions in Calcium Montmorillonite Gels .....	485
W. ALBERS AND J. TH. G. OVERBEEK. Stability of Emulsions of Water in Oil. III. Flocculation and Redispersion of Water Droplets Covered by Amphipolar Monolayers .....	489

J. F. PADDAY AND D. R. RUSSELL. The Measurement of the Surface Tension of Pure Liquids and Solutions.....	503
R. H. OTTEWILL AND D. J. WILKINS. Studies on a Flow Method for Particle Counting in Colloidal Systems.....	512
R. S. BRADLEY. The Rate of Nucleation at High Pressures.....	525
F. M. FOWKES, M. J. SCHICK, AND A. BONDI. Oil-Soluble Surface-Active Copolymers of Alkenes and Polar Monomers.....	531
S. C. STERN, H. W. ZELLER, AND A. I. SCHEKMAN. The Aerosol Efficiency and Pressure Drop of a Fibrous Filter at Reduced Pressures.....	546
JOHN G. BRODNYAN. Emulsion Particle Size. II. Determination of the Distribution Function Using the Ultracentrifuge.....	563
JOHN G. BRODNYAN. Emulsion Particle Size. III. Particle Size Distributions Determined by Various Growth Mechanisms.....	573
H. N. STEIN. The Zero Point of Charge of Tobermorite.....	578
BOOK REVIEW	
A. J. DE VRIES. Soap Films, Studies of Their Thinning and a Bibliography.....	585
Erratum.....	586
Author Index.....	587
Subject Index.....	589
Index of Book Reviews.....	590



# Modern Materials

## Advances in Development and Applications

Edited by **Henry H. Hausner**

*Consulting Engineer, New York; Polytechnic Institute of Brooklyn*

**Advisory Board:** J. A. HEDVALL, E. C. JAHN, IVOR JENKINS, HERMAN MARK,  
J. T. NORTON, T. A. SOLBERG, W. R. WILLETS

### CONTENTS

**Volume 1, 1958, 402 pp., illus., \$12.50**  
**Some New Developments in Wood as a Material**

By CARL DE ZEEUW, State University  
College of Forestry at Syracuse  
University

**Synthetic Rubbers for Special Service Conditions**

By F. A. BOVEY, Minnesota Mining and  
Manufacturing Company, St. Paul

**Fiber Materials**

By T. D. CALLINAN, International  
Business Machines Corporation,  
Poughkeepsie, New York

**High Voltage Insulation Papers**

By WM. A. DEL MAR, Consulting  
Engineer, Phelps Dodge Copper  
Products Corporation, Yonkers, New  
York

**Special Glasses for Nuclear Engineering Applications**

By N. J. KREIDL and J. R. HENSLER,  
Bausch and Lomb Optical Company,  
Rochester, New York

**Characteristic Properties of Modern Ceramics**

By JOHN H. KOENIG and EDWARD J.  
SMOKE, School of Ceramics, College of  
Engineering, Rutgers—The State  
University, New Brunswick, New Jersey

**Germanium and Silicon**

By GUSTAV SZEKELEY, Sylvania Electric  
Products, Inc., Flushing, New York

**Zirconium**

By G. L. MILLER, Murex Limited,  
Rainham, Essex, England

AUTHOR INDEX—SUBJECT INDEX.

**Volume 2, December, 1960, about 450 pp., illus. approx. \$13.00**

**Polymer Modified Papers**

By EDWIN C. JAHN and V. STANNETT,  
Syracuse University

**Ceramics for Cutting Purposes**

By W. M. WHEILDON, Norton Company,  
Worcester, Massachusetts

**Modern Flame-Sprayed Ceramic Coatings**

By N. N. AULT and W. M. WHEILDON,  
Norton Company, Worcester,  
Massachusetts

**Borides, Part A: Basic Factors**

By BERTIL ARONSSON, University of  
Uppsala, Sweden

**Borides, Part B: Fabrication, Properties, and Applications**

By ROBERT STEINITZ, General Telephone  
and Electronics Laboratories, New  
York

**Welding Materials**

By CLARENCE E. JACKSON, Linde  
Company, Division of Union Carbide  
Corporation, Newark

**Titanium Metallurgy**

By HAROLD MARGOLIN and JOHN P.  
NIELSEN, New York University

**Soldering Materials: Their Production, Properties, and Application**

By DAVID M. BORCINA, Lead Industries  
Association, New York

AUTHOR INDEX—SUBJECT INDEX.

### Review of Volume 1:

"This volume is the first of a new series on modern materials. It has been prepared especially for the engineer with broad interests and for the specialist who wants information on materials other than those in his own field of specialization. In these days of rapid development of new materials the engineer has had to become more materials-minded and must therefore acquaint himself with the properties and commercial applications of the many new Materials that come on the market.

"In spite of the great diversity of the subjects covered, this first volume should prove to be extremely valuable and interesting to the development engineer and to the student. The appearance of succeeding volumes will eagerly be awaited."

—*Science*



**ACADEMIC PRESS** New York and London

111 Fifth Avenue, New York 3, New York

17 Old Queen Street, London, S. W. 1

# ACTIVATION ANALYSIS HANDBOOK

by **R. C. KOCH**

*Nuclear Science and  
Engineering Corporation  
Pittsburgh, Pennsylvania*

*October 1960, 8¼ x 10½", 219 pp., illus., \$8.00*

ACTIVATION ANALYSIS may be defined as a method of measuring concentrations of constituents in a given sample by measuring the characteristic radiations emitted by the radioactive nuclides resulting from selected nuclear transformations. The unique combination of chemical and nuclear properties of each activation product provides a specific method for its identification and measurement. The great number of applications both actual and potential in activation analysis will assure this book an important place on the desk of every analyst who is faced by difficult problems of analysis of minor constituents. Here he will find, besides extensive tables and references to the literature through mid-1959, discussions of many of the principal factors involved.

## **Contents:**

### **Introduction**

Purpose and Scope

History and Growth of Activation Analysis

Activation Analysis: The General Technique

### **Activation Analysis:**

#### **Theoretical Considerations**

Basic Concepts

Sources of Nuclear Data

Sources of Experimental Methods

Selection of Activation Reactions

General Considerations

Suitability of Activation Products

Sensitivity Estimates

Interfering Reactions

Competing Reactions

Experimental Feasibility

### **Activation Analysis: Experimental Methods**

Irradiation Facilities

Sources of Neutrons

Sources of Charged Particles and Photons

Selection of an Irradiation Facility

### **Preparation and Encapsulation of Samples**

Neutron Irradiations

Charged Particle Irradiations

Photon Irradiations

Comparator or Monitor Samples

Irradiations

Post-Irradiation Assays

Evaluation of the Data

### **The Tabulation**

Introduction

Directory to the Tabulation

Table I: The Elements and Their Atomic Numbers

Table II: The Key to the Tabulation

Table III: A Tabulation of Nuclear Data and  
Experimental Methods for Activation Analysis

### **Glossary**

Part I: Definitions

Part II: Examples of Nuclear Reactions

### **Bibliography**

#### **Addendum to the Bibliography**

### **Index.**



**ACADEMIC PRESS** *New York and London*

111 Fifth Avenue, New York 3, New York

17 Old Queen Street, London, S. W. 1





